Design and Synthesis of Tris-Heteroleptic Bis-Cyclometalated Chiral-at-Rhodium Catalysts for Application in Asymmetric Catalysis

Dissertation

zur Erlangung des Doktorgrades

der Naturwissenschaften

(Dr. rer. nat.)

dem Fachbereich Chemie

der Philipps-Universität Marburg

vorgelegt von

Yvonne Grell

aus Seligenstadt

Marburg/Lahn 2021

Die vorliegende Dissertation wurde in der Zeit von September 2017 bis Dezember 2021 am Fachbereich Chemie der Philipps-Universität Marburg unter der Anleitung von Prof. Dr. Eric Meggers angefertigt.

Vom Fachbereich Chemie der Philipps-Universität Marburg (Hochschulkennziffer: 1180) als Dissertation angenommen am: 13.01.2022

Erstgutachter: Prof. Dr. Eric Meggers
Zweitgutachter: Prof. Dr. Armin Geyer

Eingereicht am: 17.12.2021
Tag der mündlichen Prüfung: 02.02.2022

Acknowledgement

First and foremost, I want to thank Prof. Dr. Eric Meggers for the great supervision over the past four years. Thank you for the excellent support during this time, for your inspiring and motivating spirit, for always being understanding and having an open door for the concerns of your students, no matter what it is about, for giving us the freedom to realize our own ideas to help us grow into better scientists and for the invaluable feedback on our research every week.

I would also like to thank Prof. Dr. Armin Geyer, Prof. Dr. Jörg Sundermeyer and Prof. Dr. Andreas Seubert for their willingness to attend the examination commission, as well as Prof. Geyer for his considerate acceptance to act as second assessor for the present work.

I also want to thank all service divisions in the chemistry department for their fast and reliable work. In particular the employees of the departments for NMR spectroscopy, mass spectrometry and crystal structure analysis. Special thanks go to Dr. Xiulan Xie for her excellent expertise on all NMR issues and for the good cooperation in recent years on almost all of my projects.

Furthermore, I want to give a warm thanks to Ina Pinnschmidt and Dr. Lilu Zhang for their helpfulness during the course of my Ph.D. and for handling all the administrative and organizational matters, which have made our everyday laboratory life so much easier.

In this context, I would also like to thank Marcel Hemming for always taking care of organizational matters in the laboratory and, in particular, for his active support in setting up my laboratory section at the beginning of my Ph.D. In addition, I want to thank him and Tim Ohlenburger for their occasional help with the synthesis of substrates.

At this point, I also want to thank all other members of the Meggers group, namely Xin Nie, Tianjiao Cui, Xiang Shen, Chen-Xi Ye, Han Feng, Peng Xiong, Zijun Zhou, Yubiao Hong, Chenhao Zhang, Philipp Steinlandt, Erik Winterling, Frank Abendroth, Nemrud Demirel and Dominik Baran for the always pleasant working atmosphere in the lab, the good collegial cooperation and all the constructive discussions about chemistry. I would especially like to thank my direct laboratory partners Philipp, Erik, Frank, Nemrud and Dominik for the great time we spent together, for the motivated atmosphere in our lab, with good and sometimes bad music, for the one or other coffee and chocolate break, the constant mutual support, for always sharing high hopes together and for all the fruitful brainstorming sessions on our projects. In addition, I would

like to thank Yubiao for patiently teaching me the art of making crystals using all different kinds of techniques, and Zijun for all the helpful discussions about chemistry. I also want to say thank you to all of the former members of the Meggers group, Lucie Jarrige, Sebastian Brunen, Long Li, Guanghui Wang, Tatsuya Jamahira, Takuya Mochizuki, Kenichi Endo, Nikita Ankudinov, Naifu Hu and, in particular, to Jiajia Ma, Jie Qin, Xiaoqiang Huang, Qi Zhang, Francisco Fávaro de Assis, Yu Zheng, Shipeng Luo and Yuqi Tan for your warm and friendly welcome at the beginning of my Ph.D., for your willingness to help me at any time and your priceless professional advice, you gave me a good start. It has been a pleasure for me to work with all of you and I wish you all the best for your future.

Moreover, I want to appreciate all of my Master students Philipp Steinlandt, Maike Klüppel, Carolin Kalff, Nemrud Demirel, Veronika Schmalz and Chun-Ho Ip for their dedicated synthetic support and the good cooperation.

In addition, I want to thank Matthias Tripp, Philipp Steinlandt, Nemrud Demirel and Dominik Baran for the quick and conscientious proofreading of this work.

Special thanks also go to my parents, who supported me unreservedly at all times during my studies and beyond.

And finally, I would like to express my deepest gratitude to my boyfriend Matthias Tripp. I want to thank you for your constant encouragement, the moral support and for always being by my side, in good times as in bad. I am very grateful to have you.

Dedicated to my father

Parts of the research results presented in this dissertation have already been published:

- Y. Grell, Y. Hong, X. Huang, T. Mochizuki, X. Xie, K. Harms, E. Meggers, Chiral-at-Rhodium Catalyst Containing Two Different Cyclometalating Ligands. *Organometallics* **2019**, *38*, 3948–3954.
- Y. Grell, N. Demirel, K. Harms, E. Meggers, Chiral Bis(oxazoline) Ligands as C_2-Symmetric Chiral Auxiliaries for the Synthesis of Enantiomerically Pure Bis-Cyclometalated Rhodium(III) Complexes. *Organometallics* **2019**, *38*, 3852–3859.
- Y. Grell, X. Xie, S. I. Ivlev, E. Meggers, Enantioselective α-Fluorination and α-Chlorination of *N*-Acyl Pyrazoles Catalyzed by a Non-C_2-Symmetric Chiral-at-Rhodium Catalyst. *ACS Catal.* **2021**, *11*, 11396–11406.

Abstract

Chiral transition metal complexes represent a powerful class of catalysts for the asymmetric synthesis of optically active compounds. In recent years, Meggers and co-workers introduced a new class of iridium(III)- and rhodium(III)-based Lewis acid catalysts, in which the overall chirality exclusively originates from a stereogenic metal center, with all coordinating ligands being achiral. This thesis provides a synthetic approach to a previously elusive class of tris-heteroleptic bis-cyclometalated chiral-at-rhodium(III) complexes and demonstrates their application as chiral catalysts in asymmetric catalysis.

Chapter 3.1 and 3.2. A method for the synthesis of a bis-cyclometalated rhodium complex containing two different cyclometalating ligands is developed. Preparation of this previously inaccessible family of tris-heteroleptic bis-cyclometalated rhodium catalysts was accomplished by a stepwise protocol that relies on the formation of an isolable mono-cyclometalated rhodium(III) species in the first step, which provided the opportunity to introduce a different second ligand in a subsequent second cyclometalation step. Resolution of the racemic complex into its individual Λ- and Δ-enantiomers was achieved using an established chiral auxiliary-mediated approach. The final chiral-at-metal rhodium complex contains a cyclometalated 5-*tert*-butyl-1-methyl-2-phenylbenzimidazole, a cyclometalated 5-*tert*-butyl-2-phenylbenzothiazole, and two labile acetonitrile ligands, complemented by a hexafluorophosphate counterion, and was demonstrated to be a highly efficient catalyst for asymmetric [2+2] photocycloadditions.

Chapter 3.3. An application of chiral bis(oxazoline) ligands as C_2-symmetric chiral auxiliaries for the synthesis of enantiopure bis-cyclometalated rhodium(III) complexes is described. Bis(oxazolines) are versatile chiral ligands for asymmetric catalysis, but have not been used for the resolution of racemic mixtures of transition metal complexes. Due to their C_2-symmetry, chiral bis(oxazolines) are particularly useful for the synthesis of nonracemic transition metal complexes with lower symmetry and this is demonstrated for the synthesis of an enantiomerically pure rhodium(III) complex containing two different cyclometalated ligands.

Chapter 3.4. The developed synthetic method for the preparation of bis-cyclometalated rhodium(III) complexes with two different cyclometalating ligands was further improved and the modularity of the procedure demonstrated by the addition of two new catalyst derivatives which, in addition to a cyclometalated 5-*tert*-butyl-1-methyl-2-phenylbenzimidazole, contained a cyclometalated 3,5-diphenyl-1*H*-pyrazole or a sterically more demanding 1-mesityl-3,5-diphenyl-1*H*-pyrazole ligand. Both catalysts were readily accessible in an enantiomerically pure fashion (>99% ee) via the previously established chiral bis(oxazoline) mediated strategy.

Chapter 3.5. A non-C_2-symmetric and sterically demanding chiral-at-rhodium(III) catalyst is demonstrated to efficiently catalyze the highly enantioselective α-fluorination (12 examples, up to >99% ee) and α-chlorination (12 examples, up to 98% ee) of *N*-acyl pyrazoles in high yields. Comparison of the catalytic performance with related C_2-symmetric rhodium catalysts revealed the clear superiority of the non-C_2-symmetric design for the presented α-halogenation reactions, which are generally featured by a very simple synthetic protocol. Conversion of the α-halogenated products into the corresponding esters with almost no epimerization was achieved and allowed the synthesis of valuable chiral compounds for subsequent chemical transformations.

Kurzdarstellung

Chirale Übergangsmetallkomplexe stellen eine leistungsstarke Klasse von Katalysatoren für die asymmetrische Synthese optisch aktiver Verbindungen dar. In den letzten Jahren stellten Meggers und Mitarbeiter eine neue Klasse von Iridium(III)- und Rhodium(III)-basierten Lewis-Säure Katalysatoren vor, die aus vollständig achiralen Liganden bestehen und deren Gesamtchiralität ausschließlich von einem stereogenen (*chiral-at-metal*) Metallzentrum stammt. In dieser Arbeit wird ein synthetischer Zugang zu einer bisher unzugänglichen Klasse von tris-heteroleptischen bis-cyclometallierten *chiral-at*-Rhodium(III)-Komplexen geschaffen und ihre Anwendung als chirale Katalysatoren in der asymmetrischen Katalyse demonstriert.

Kapitel 3.1 und 3.2. Eine Methode zur Synthese eines bis-cyclometallierten Rhodiumkomplexes mit zwei verschiedenen cyclometallierenden Liganden wird entwickelt. Die Herstellung dieser bisher nicht zugänglichen Familie tris-heteroleptischer bis-cyclometallierter Rhodiumkatalysatoren wurde durch ein schrittweises Verfahren ermöglicht, das auf der Bildung einer isolierbaren monocyclometallierten Rhodium(III)-Spezies im ersten Schritt beruht, welche die Möglichkeit bot, einen anderen zweiten Liganden in einem nachfolgenden zweiten Cyclometallierungsschritt einzuführen. Die Racematspaltung des racemischen Komplexes in seine entsprechenden Λ- und Δ-Enantiomere wurde mit einem etablierten chiralen Auxiliar-vermittelten Ansatz erreicht. Der finale *chiral-at-metal*-Rhodiumkomplex enthält ein cyclometalliertes 5-*tert*-Butyl-1-methyl-2-phenylbenzimidazol, ein cyclometalliertes 5-*tert*-Butyl-2-phenylbenzothiazol und zwei labile Acetonitrilliganden, ergänzt durch ein Hexafluorphosphat-Gegenion, und erwies sich als hocheffizienter Katalysator für asymmetrische [2+2]-Photocycloadditionen.

Kapitel 3.3. Die Anwendung chiraler Bis(oxazolin)-Liganden als C_2-symmetrische chirale Auxiliare für die Synthese enantiomerenreiner bis-cyclometallierter Rhodium(III)-Komplexe wird beschrieben. Bis(oxazoline) sind vielseitige chirale Liganden für die asymmetrische Katalyse, sie wurden jedoch noch nicht für die Synthese von enantiomerenreinen Übergangsmetallkomplexen verwendet. Aufgrund ihrer C_2-Symmetrie sind chirale Bis(oxazoline) besonders nützlich für die Synthese nicht-racemischer Übergangsmetallkomplexe mit niedrigerer Symmetrie, was anhand der Synthese eines enantiomerenreinen Rhodiumkomplexes mit zwei verschiedenen cyclometallierten Liganden demonstriert wird.

Kapitel 3.4. Die entwickelte Synthesemethode zur Herstellung von bis-cyclometallierten Rhodium(III)-Komplexen mit zwei verschiedenen cyclometallierenden Liganden wurde weiter verbessert und die Modularität des Verfahrens mittels der Erweiterung um zwei neue Katalysatorderivate erwiesen, welche neben einem cyclometallierten 5-*tert*-Butyl-1-methyl-2-

phenylbenzimidazol, einen cyclometallierten 3,5-Diphenyl-1*H*-pyrazol oder einen sterisch anspruchsvolleren 1-Mesityl-3,5-diphenyl-1*H*-pyrazol-Liganden enthalten. Beide Katalysatoren waren über die zuvor etablierte chirale Bis(oxazolin)-vermittelte Strategie leicht in enantiomerenreiner Form (>99% ee) zugänglich.

Kapitel 3.5. Ein nicht-C_2-symmetrischer und sterisch anspruchsvoller chiraler Rhodium(III)-Komplex katalysiert effizient die hoch enantioselektive α-Fluorierung (12 Beispiele, bis zu >99% ee) und α-Chlorierung (12 Beispiele, bis zu 98% ee) von *N*-Acylpyrazolen in hohen Ausbeuten. Der Vergleich der katalytischen Leistung mit verwandten C_2-symmetrischen Rhodiumkatalysatoren zeigte die klare Überlegenheit des nicht-C_2-symmetrischen Designs für die vorgestellten α-Halogenierungsreaktionen, die sich im Allgemeinen durch ein sehr einfaches Syntheseprotokoll auszeichnen. Die Umwandlung der α-halogenierten Produkte in die entsprechenden Ester wurde fast ohne Epimerisierung erreicht und ermöglichte somit die Synthese wertvoller chiraler Verbindungen für nachfolgende chemische Transformationen.

Table of Contents

1. C_2 *vs.* C_1-Symmetry in Asymmetric Transition Metal Catalysis

1.1 Introduction

The catalytic asymmetric synthesis of enantiomerically enriched chiral compounds is one of the most active areas of modern chemical research due to the increasing demand for optically active molecules from the pharmaceutical, flavors and fragrances, and agrochemical industries.[1,2] An attractive approach for effectively creating new stereocenters is the application of chiral transition metal complexes, which can mainly be attributed to two reasons. A direct coordination of a substrate or reagent to a reactive metal center can strongly activate it towards a chemical transformation, while a sophisticated chiral environment around the central metal can ensure an efficient asymmetric induction.[3] An ongoing endeavor in the field of enantioselective synthesis with chiral transition metal complexes thus constitutes the design of suitable chiral ligands and metal catalysts for novel applications.[4,5]

Enzymes, the catalysts evolved by nature, are characterized by complex structures and in most cases by the absence of symmetry.[6] In contrast, symmetry is often considered as a guiding principle for the design of new synthetic catalysts. In particular, the presence of rotational symmetry in chiral ligands and metal complexes has been recognized to have beneficial effects on the reaction outcome of asymmetric reactions.[5] Generally, the rotation about an *n*-fold axis of symmetry is specified by the symbol C_n (point group), in which the angle of rotation is 360°/*n*. For example, the rotation of a C_2-symmetric molecule through 180° generates a representation of the structure that is indistinguishable from, and superimposable on, the original configuration, while molecules which are devoid of any symmetry are denoted with the symbol C_1.[7] Rotational symmetry, such as C_2-symmetry, creates homotopic reaction sites which are related by proper rotation. Coordination of a prochiral substrate to any of the vacant coordination sites of a complex having a C_2-symmetry axis therefore leads to identical catalyst-substrate arrangements (Figure 1a), which would be diastereomeric in a related nonsymmetrical complex (Figure 1b). Consequently, in a reaction that is performed with a C_2-symmetric catalyst, the amount of possible reaction intermediates is effectively halved compared to a complex with C_1-symmetry.[8,5]

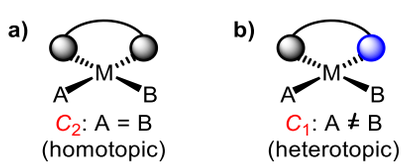

Figure 1: Schematic example of a square planar complex containing a) a C_2-symmetric ligand with two homotopic coordination sites; b) a C_1-symmetrical ligand with heterotopic reaction sites.[5]

In this way, two-fold rotational symmetry reduces the amount of competing diastereomeric transition states and reaction pathways that may lead to enantiomeric products, and therefore C_2-symmetric catalysts are frequently observed to provide higher levels of enantioselectivity.[9]

Despite these advantages, there is no fundamental reason why complexes of lower symmetry should necessarily be inferior to their related symmetrical counterparts.[10] In this sense, the following two chapters aim to, firstly, provide a short overview of a range of popular C_2-symmetric ligand families, and secondly, to give a few representative examples of catalytic asymmetric reactions, in which non-C_2-symmetric catalysts outperform their structurally related C_2-symmetrical analogues. However, a direct cross comparison between reactions with and without symmetry is usually not straightforward, since symmetry does not represent the only feature that determines the stereochemical course of a reaction.[9] Distorting the symmetry of a given ligand structure is inevitably accompanied by structural changes, and whether improved selectivities can be ascribed to the reduced symmetry or, for example, to the altered steric or electronic properties of the resulting catalytic intermediates is often difficult to evaluate.[5] Due to the complexity of most catalytic asymmetric processes, new chiral ligands and catalysts are still often discovered empirically, by chance, and through screening and comparison of a variety of different ligand structures for a particular transformation. Whereas a more tailored ligand design is enabled for reactions having a well-known mechanism.[4] Both types of examples will be presented and reasons for the improved selectivities with nonsymmetrical catalysts will be given when they were discussed and not found by coincidence. In the latter cases, the comparison was made formally.

1.1.1 *C*$_2$-Symmetric Ligands

C_2-symmetric ligands have dominated in the field of asymmetric catalysis for a long time.[4] Among the plethora of ligands, a few ligand classes stand out because of their broad applicability. Chiral ligands and catalysts which provide high enantioselectivities over a wide range of mechanistically unrelated reactions are also termed “privileged structures” and many of these structures possess two-fold axes of symmetry.[11] Some of the most recognized chiral ligands are shown in Figure 2 and include, for example, axially chiral BINAPs and BINOLs, salens, bis(oxazolines) (BOX), tartaric acid derived ligands such as TADDOL and DIOP, phospholanes such as DuPhos, or cinchona alkaloid based ligands.[11–13] A common feature of these ligands is their ready accessibility and the modular nature of their design, allowing the ligand structure to be optimized for a specific application.[4,12]

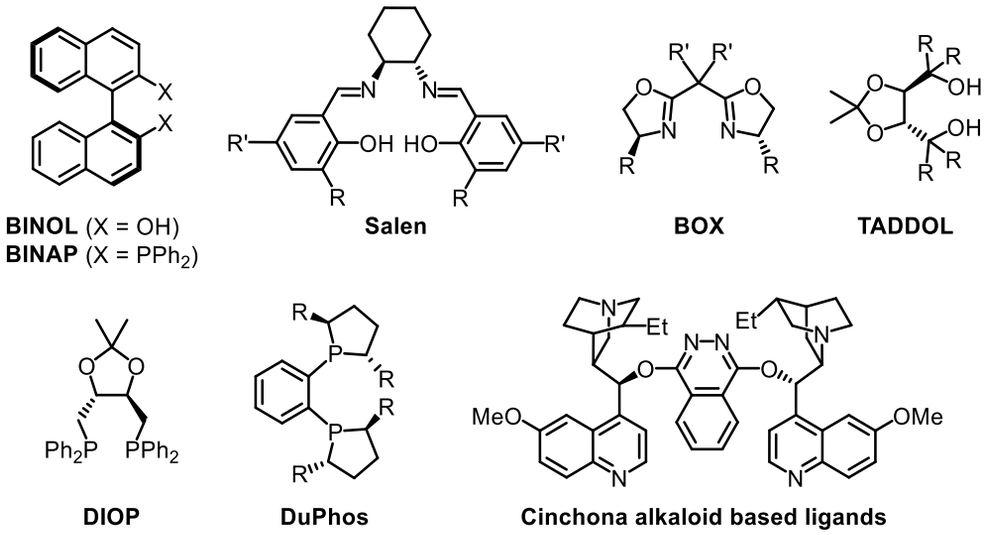

Figure 2: Examples of privileged chiral C_2-symmetric ligand families.

An important landmark for the concept of C_2-symmetry within the field of ligand design constituted the introduction of the C_2-symmetric ligand DIOP by Dang and Kagan in 1971.[14,9] As a consequence of this influential work, a large number of chiral bidentate diphosphines of this type were investigated in the years that followed.[4] Inspired by the design principle of DIOP, Nobel laureate Knowles, for example, introduced a dimeric version of one of his chiral monophosphine ligands, which he called DiPAMP (Scheme 1).[15] Based on this ligand structure, a cationic rhodium complex was discovered to efficiently catalyze the enantioselective hydrogenation of enamides. An instructive example provides the hydrogenation of the cinnamic acid derivative **1**, which was hydrogenated in the presence of catalytic amounts of [Rh((*R*,*R*)-(DiPAMP)(COD)]BF_4 (**2**) to give a protected precursor of the drug L-DOPA (3,4-dihydroxy-L-phenylalanine (**3**)) in quantitative yield and in 95% ee. An acid-catalyzed hydrolysis in the subsequent step provided the desired amino acid **3**, which proved to be effective in the treatment of Parkinson's disease.[16,17]

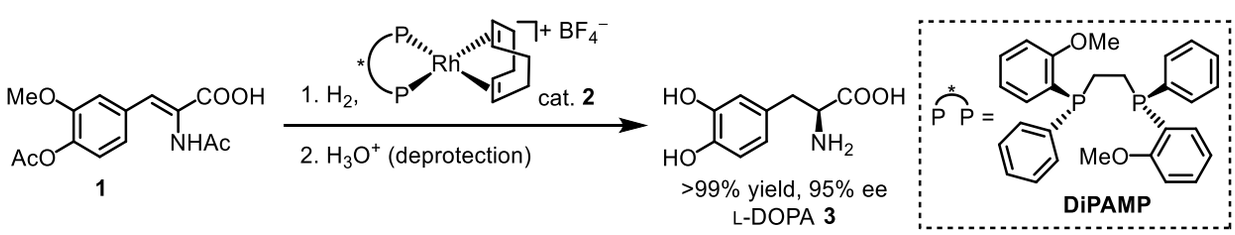

Scheme 1: Key step of the synthesis of L-DOPA (**3**) via asymmetric rhodium-catalyzed hydrogenation.

Developed at Monsanto, this process represented the first commercialized catalytic asymmetric synthesis using a chiral transition metal complex and significantly contributed to the rapid growth of this research area in subsequent years.[17]

Another great impact on stereoselective organic synthesis had the discovery of the C_2-symmetric and atropisomeric chiral diphosphine ligand BINAP by Noyori in 1980.[18] His ruthenium(II)-based BINAP catalysts proved to be highly efficient asymmetric hydrogenation catalysts for a range of substrates, such as α,β- and β,γ-unsaturated carboxylic acids.[19] An example is illustrated in Scheme 2, and shows the hydrogenation of the aryl substituted acrylic acid **4** in the presence of catalytic amounts of [Ru((*S*)-BINAP)$(OAc)_2$] (**5**), which produced the anti-inflammatory agent (*S*)-naproxen (**6**) in high yield and stereoselectivity (92% yield, 97% ee).

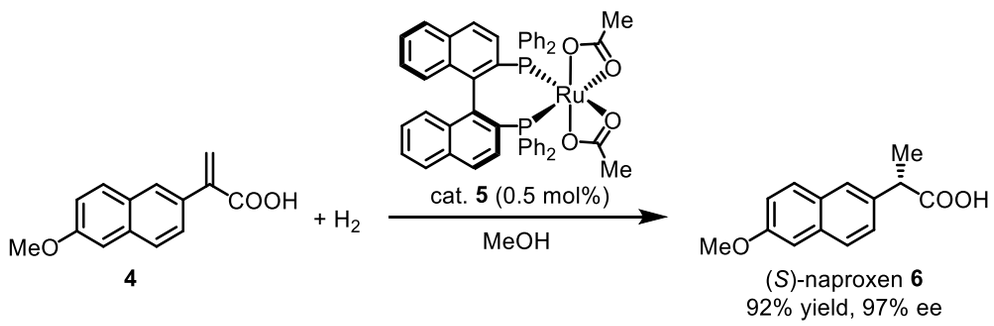

Scheme 2: Synthesis of (*S*)-naproxen (**6**) via ruthenium(II)-catalyzed enantioselective hydrogenation.[19]

Besides functionalized olefins, related catalysts also provided excellent stereocontrol in the asymmetric hydrogenation of functionalized ketones, which is exploited, for example, in the industrial syntheses of synthetic intermediates of antibiotic carbapenems and antibacterial levofloxacin.[20,21,17] Another major advance was achieved by combining the previous catalyst system with a chiral diamine. In the presence of 2-propanol and a strong base such as KOH, the corresponding ruthenium(II)-BINAP-diamine catalysts displayed a greatly enhanced reactivity, which enabled the enantioselective hydrogenation of simple ketones that lack a second heteroatom functionality.[22] Remarkably, the same catalytic system also allowed the highly enantioselective and chemoselective hydrogenation of α,β-unsaturated ketones.[23] In contrast to most conventional hydrogenation methods, the reduction selectively proceeded at the carbonyl moiety and left the carbon-carbon double bond intact, thereby expanding the scope considerably.

In view of these achievements, Knowles,[15] Noyori,[24] as well as Sharpless[25] were awarded the Nobel prize in 2001 for their pioneering contributions to the development of catalytic asymmetric synthesis, which at the same time highlights the importance of chiral transition metal complexes as chiral catalysts.

1.1.2 *C*$_2$ *versus* *C*$_1$-Symmetry

Although rotational symmetry can often have beneficial properties, an increasing number of reports exist, in which nonsymmetrical ligands give higher enantioselectivities than the best known C_2-symmetric ligands. In particular, for reactions for which the mechanistic scenario has been well understood, a more rational ligand design is possible, which can enable the development of more efficient chiral catalysts.

As an instructive example serves the design concept developed by Achiwa and co-workers for the generation of more effective chiral diphosphine ligands for rhodium-catalyzed asymmetric hydrogenation (Figure 3a).[26] Since the catalytic intermediates are of a nonsymmetrical nature, Achiwa pointed out that the two phosphine moieties of the bidentate ligand interact in a sterically and electronically distinct fashion with a rhodium-bound substrate. In a catalyst-substrate complex, such as the one shown in Figure 3a, the interaction between the coordinated substrate and P_1, which is oriented *cis* to the prochiral group, was expected to be mainly steric in nature and thus particularly important for providing a high asymmetric induction. Whereas P_2, oriented *trans* to the prochiral unit, was considered to primarily have an electronic influence. Conceptually, the design of a diphosphine ligand with two sterically and electronically nonequivalent phosphine moieties should therefore provide a more efficient chiral ligand. In particular, the incorporation of a more electron-rich phosphine group was believed to enhance the overall catalyst performance. An increased electron density at the rhodium center was, on the one hand, rationalized to strengthen the dσ*-interaction between the metal and the hydrogen molecule in the rate-determining step and thus to accelerate the oxidative addition of molecular hydrogen to the rhodium-substrate complex, which would be reflected in an improved catalytic activity. On the other hand, the dπ*-back donative effect from an electron-rich rhodium to an electron deficient olefin or ketone would be enhanced and lead to a more rigid chelation of metal and substrate, resulting in an increased enantioselectivity.[26]

Based on these considerations, they developed a nonsymmetrical derivative of the known C_2-symmetric ligand DIOP **7**, in which one of the two diphenylphosphine groups was replaced by a more electron-rich dicyclohexylphosphine residue (Figure 3b).[27] Indeed, the C_1-symmetrical ligand **8** proved to be more efficient in the catalytic asymmetric hydrogenation of ketopantolactone (**9**) than the corresponding DIOP-based rhodium catalyst. As anticipated, the catalyst derived from **8** showed a significantly higher catalytic activity and provided the product **10** with an increased enantioselectivity under the same reaction conditions. Due to these results, it was assumed that the prochiral keto group coordinates selectively *trans* to the electron-rich phosphine moiety, and selectively *cis* to the diphenylphosphine group, thus being consistent

with their design concept. Since this preferred orientation of the substrate to the nonsymmetrical complex reduces the number of diastereomeric intermediates in the catalytic cycle, C_2-symmetry does not offer any advantages here.[27,26]

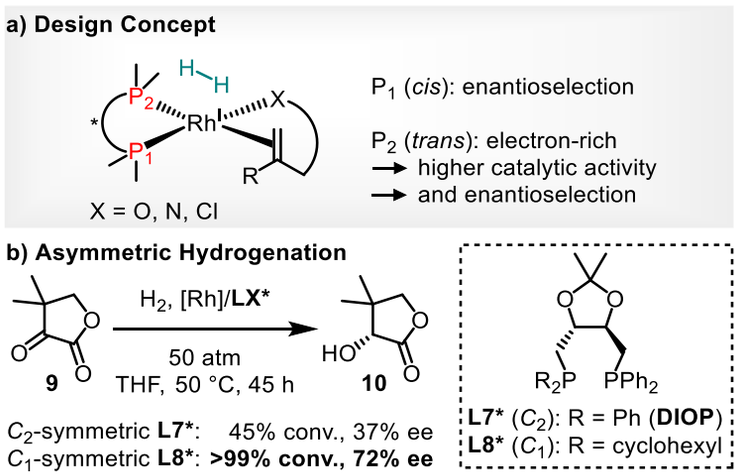

Figure 3: a) Achiwa's design concept for the development of more efficient chiral diphosphine ligands; b) Asymmetric hydrogenation with desymmetrized DIOP ligand.[27,26]

Another effective approach to steric and electronic ligand desymmetrization represents the design of heterobidentate ligands. For certain reactions, such as palladium-catalyzed allylic substitutions, conclusive arguments can be made as to why nonsymmetrical ligands with two different coordinating heteroatoms should allow better enantiocontrol than C_2-symmetrical ligands.[10] An example is shown in Figure 4a.[10,4] For symmetrically substituted allyl systems, such as the racemic mixture of allyl acetate **11** and *ent*-**11**, an allyl complex **I** is formed. Since both enantiomers of the starting material are converted into the same catalytic intermediate, the stereochemical information is lost in this step. Consequently, the regioselectivity of the subsequent nucleophilic attack is decisive for the ratio of the two enantiomeric products. A nucleophilic attack at C1 would lead to product **12**, while an attack at C3 would produce the other enantiomer *ent*-**12**. For π-allyl intermediates, in which the metal center is coordinated by two different donor atoms X and Y, the two allylic termini become electronically dissimilar and are therefore expected to exhibit different reactivity. In contrast to C_2-symmetrical allyl complexes, which are structurally precluded from taking advantage of different *trans*-influences, the complexation of heterobidentate ligands should, in principle, enable a more efficient regiocontrol.[4] In this context, a large variety of P,N-ligands such as the shown phosphinooxazolines (PHOX) have been developed (Figure 4b).[28,4] Introduced by Pfaltz, and independently by the groups of Helmchen and Williams,[29–31] the Pd-PHOX complexes proved to be highly reactive and selective catalysts for allylic substitution reactions, with the observed

selectivities being rationalized by a preferential nucleophilic attack at the allylic carbon atom *trans* to the phosphino group.[4] Due to the modular nature of the oxazoline group, the backbone, and the phosphine moiety, the application range of the PHOX ligands could be extended to include various other metal-catalyzed reactions, such as Heck reactions, copper-catalyzed 1,4-additions, ruthenium-catalyzed transfer hydrogenation, iridium-catalyzed asymmetric hydrogenations, and many more.[32,33,28,34] Chiral PHOX ligands have therefore emerged as a highly versatile and prominent C_1-symmetrical ligand class, which in many cases outperformed symmetric homobidentate P,P- or N,N-ligands.[4]

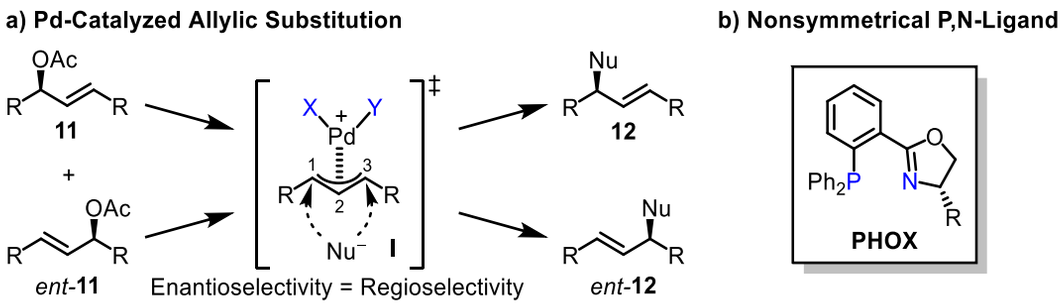

Figure 4: a) Mechanism of Pd-catalyzed enantioselective allylic substitution of symmetrical allyl systems; b) Common structure of a phosphinooxazoline (PHOX) ligand.[10,4]

Electronic differentiation of this type has also been demonstrated by Faller and co-workers. In 2001, they reported a highly enantioselective Diels-Alder reaction with the half-sandwich complex **13**, in which the ruthenium center is chiral, due to the non-C_2-symmetry of the coordinated chiral bisphosphine monoxide ligand (*S*)-BINPO (Figure 5a).[35] Conversion of the corresponding bidentate ligand with $[(\eta^6\text{-cymene})RuCl_2]_2$ in the presence of $NaSbF_6$ in CH_2Cl_2 provided the stereogenic-at-metal complex (R_{Ru})-[(η^6-cymene)Ru((*S*)-BINPO))Cl]SbF_6 (**13**) in a highly diastereoselective manner as a single diastereomer in 85% yield. In the presence of a slight excess of $AgSbF_6$, the precatalyst **13** can *in situ* be converted into the catalytically active Lewis acid, in which the coordinated chloride ligand is replaced by a more labile water molecule, originating from traces of water in the solvent. As confirmed by ^1H and $^{31}P\{^1H\}$ NMR spectroscopy, the resulting aqua complex (R_{Ru})-[(η^6-cymene)Ru((*S*)-BINPO))(OH_2)]$(SbF_6)_2$ is also obtained in a diastereomerically pure fashion. In the Diels-Alder reaction of methacrolein (**14**) and cyclopentadiene (**15**) with 11 mol% of the catalyst precursor **13** and 10 mol% of the silver salt at –78 °C, the conversion was completed after 12 hours and the desired cycloaddition product **16** was obtained with an excellent enantioselectivity of 99% ee (*S*) and *exo*-diastereoselectivity (93% de) (Figure 5a). In contrast, when the identical reaction was performed with the related complex containing the C_2-symmetric ligand analogue (*S*)-BINAP, in which the central

ruthenium is consequently not chiral, the Diels-Alder cycloadduct **16** was obtained with a much lower enantioselectivity of only 19% ee (82% de) at –78 °C and the opposite enantiomer (*R*) was formed. At –24 °C, the selectivity could be increased but still remained modest (50% ee and 93% de). Although these differences may, to a certain extent, be due to the change of the chelate ring size, the authors considered that the pronounced enhancement of the enantioselectivity with the nonsymmetrical catalyst can be attributed to the presence of the electronically asymmetric stereogenic ruthenium center in **13**. Figure 5b shows the two possible *anti-s-trans* conformations of the ruthenium-substrate complex, which were adduced to explain the observed stereochemical reaction outcome. In these conformations, the substrate **14** can adopt the two different orientations (**A**) or (**B**), which differ in terms of their steric hindrance. In conformation (**A**), the steric bulk of the η^1-coordinated aldehyde points towards the diphenylphosphine moiety of the chiral ligand, resulting in a considerable steric repulsion. Whereas in conformer (**B**) the substrate is more favorably oriented towards the cavity created by the sterically less crowded PPh_2=O group. For this reason, conformer (**B**) was supposed to represent the actual conformation in solution. This preferential orientation of the metal-bound substrate gives rise to a well-defined catalyst-substrate arrangement which is likely to account for the high enantioselectivity achieved. Figure 5c depicts the proposed transition state **II**, in which the approach of the cyclopentadiene (**15**) from the Cα *Re*-diastereoface is blocked by the binaphthyl and aryl groups of the chiral heterobidentate ligand, whereas a controlled approach from the Cα *Si*-diastereoface is enabled, giving the (*S*)-enantiomer of **16**. Correspondingly, a less organized transition state was expected to form for the C_2-symmetric BINAP derived catalyst and thus, as experimentally confirmed, to result in much lower enantioselectivities.[35]

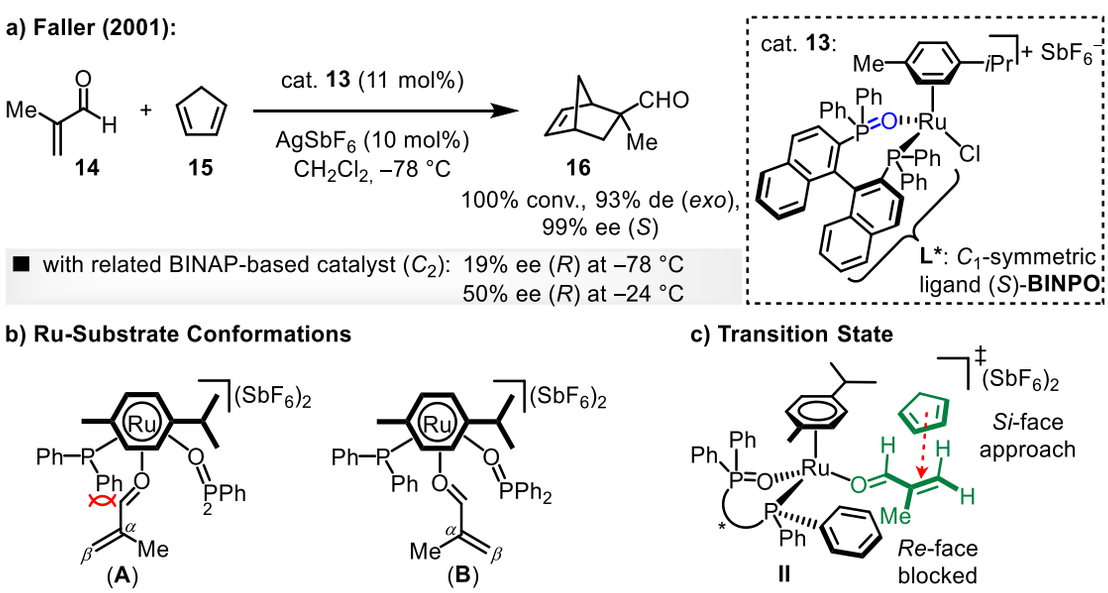

Figure 5: a) Enantioselective Diels-Alder reaction catalyzed by a non-C_2-symmetric Ru-catalyst; b) Possible Ru-substrate conformations (**A**) (disfavored) and (**B**) (favored); c) Proposed transition state.[35]

Beyond such highly selective heterobidentate ligands, numerous reports exist on chiral ligand structures, which are based on nonsymmetrical substitution patterns. Many of these ligands have been used successfully in asymmetric catalysis and often performed similarly or even gave better results than their closely related C_2-symmetric counterparts.

In recent years, for example, C_1-symmetric BINOL derived ligands and catalysts[36–42] with different functional groups at the 3,3'-positions of the chiral binaphthyl moiety have been found to induce superior enantioselectivities in some asymmetric transformations than the corresponding symmetrical catalysts.[43] An example is presented in Scheme 3. In 2013, Endo and Shibata reported the highly enantioselective, multinuclear copper/aluminum-catalyzed conjugate addition of trimethylaluminum to acyclic, α,β-unsaturated and β,β-disubstituted enones for the respective construction of tertiary and quaternary stereocenters.[44] For both substrate classes, the nonsymmetrical BINOL ligand **18**, containing only a single diphenylphosphine group at the 3-position, gave higher selectivities than the C_2-symmetric analogue **17**. Starting with an initial screening of conditions, the conversion of chalcone (**19**) with 2 equivalents of Me_3Al in the presence of $CuCl_2 \cdot 2\ H_2O$ (5 mol%) and the corresponding chiral ligand **17** or **18** (5 or 10 mol%) conveniently yielded the methylated product **20** (Scheme 3a). For each ligand, the best results were achieved when a 2:1 ratio of the chiral ligand and the copper salt was employed (55% ee (C_2) *versus* 71% ee (C_1)), while a 1:1 ratio gave slightly reduced selectivities (49% ee (C_2) *versus* 63% ee (C_1)). Replacement of the diarylphosphine moiety of the C_1-symmetrical ligand by a sterically more demanding 3,5-$(CF_3)_2C_6H_3$-group further raised the selectivity to 95% ee, demonstrating that C_2-symmetry is not required to achieve high levels of enantiocontrol. Subsequently, the application of BINOL **18** also enabled the more challenging installation of a small methyl group on β,β-disubstituted enones for the formation of all-carbon quaternary stereocenters. For the reaction of (*E*)-**21**, for example, the product **22** was obtained with excellent yield and stereoselectivity (>98%, >98% ee) with conversion being complete after only 1 hour (Scheme 3b).[44]

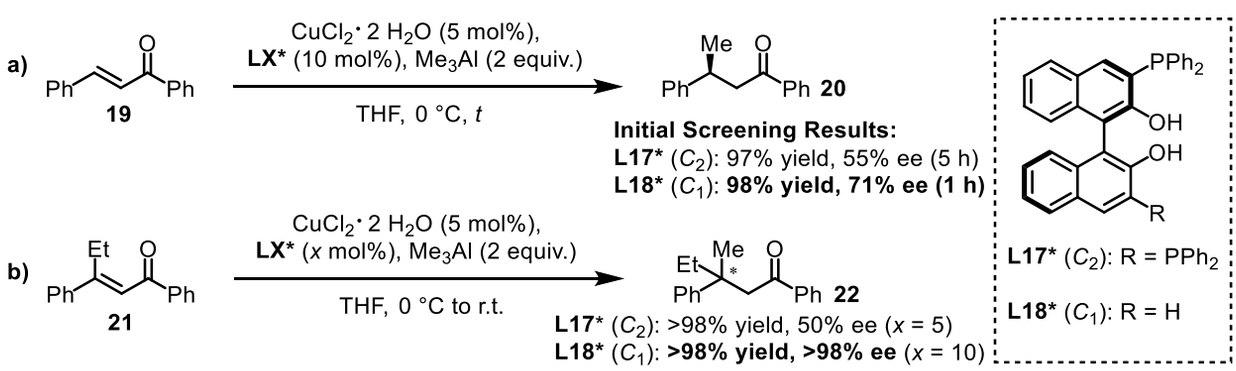

Scheme 3: Cu/Al-catalyzed asymmetric conjugate additions with C_1-symmetric BINOL-based ligands for the construction of a) tertiary; and b) all-carbon quaternary stereocenters.[44]

In 2011, Ohshima and Mashima developed a catalytic asymmetric alkynylation of α-ketoesters with a diverse set of aryl- and alkyl-substituted terminal alkynes using C_1- and C_2-symmetric rhodium/Phebox complexes (Scheme 4).[45] In general, compared to the progress that has been achieved with aldehydic substrates, the corresponding alkynylation of ketones had been much less advanced due to their lower reactivity and the difficulty to obtain sufficient enantiofacial differentiation. In the presence of 3 mol% of the corresponding rhodium catalysts, the alkynylation of the CF_3-substituted α-ketoester **23** with acetylenes **24** smoothly proceeded at room temperature to give the desired tetrasubstituted propargylic alcohols **25** in high yields and enantioselectivities. In most cases, the C_1-symmetric complexes gave better results than the symmetrical congeners, whereby the indanyl-based systems **26** (C_2) and **27** (C_1) were found to be the most efficient catalysts. While the nonsymmetrical catalyst **27** afforded the products in 88–99% yield with enantioselectivities ranging from 90–95% ee, the C_2-symmetric catalyst **26** proved to be less effective, giving the products in 78–86% yield and 80–95% ee. Moreover, they found that the synthesized rhodium complexes displayed a unique chemoselectivity, leading to the exclusive alkynylation of the ketone in the presence of an aldehyde function. Electronic modification of the *para*-position of the cyclometalated phenyl moiety of complex **27** with a nitro-substituent subsequently also enabled the alkynylation of **23** with less reactive alkyl-substituted alkynes with high selectivities (up to >99% ee). For these substrates, however, no comparison has been made with a C_2-symmetric catalyst.[45]

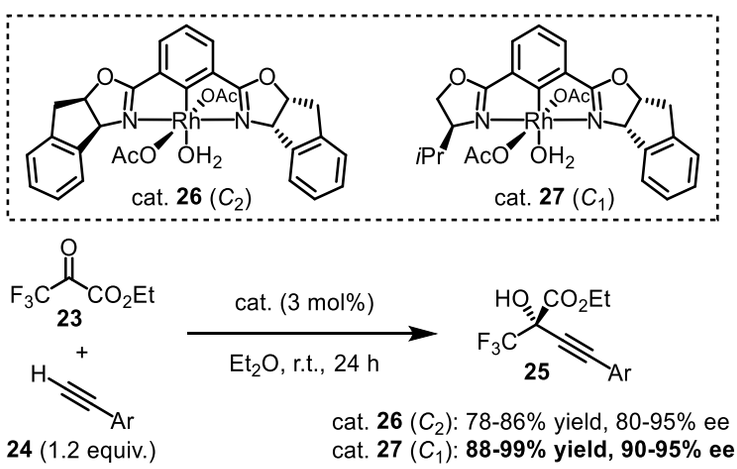

Scheme 4: C_1-symmetric Rh/Phebox-catalyzed enantioselective alkynylation of α-ketoesters.[45]

A striking example, in which the catalytic performance of a non-C_2-symmetric catalyst plainly exceeded that of the related C_2-symmetrical derivatives has been described by Guiry and co-workers.[46,47] In 2009, they reported the first regio- and enantioselective chromium-catalyzed Nozaki Hiyama-Kishi (NHK) homoallenylation of aldehydes using a number of symmetrically

and non-symmetrically substituted tridentate bis(oxazoline) ligands, in which the two oxazoline rings are linked by an *N*-phenylaniline backbone (Scheme 5a).[46] Previously, they had introduced a synthetic access to this novel class of ligands and demonstrated their successful application in asymmetric NHK allylation, crotylation and methallylation of aldehydes.[48–51] For the shown homoallenylation of homoallenyl bromide **29** with benzaldehyde (**28**) a range of seven bis(oxazolines) with different substitution patterns were investigated. In the absence of a chiral ligand, the reaction gave a mixture of the regioisomeric products, the desired *β*-allenol **30** and the butadiene **31**, in a ratio of about 3:1. While the results obtained in the presence of the bis(oxazolines) proved to be highly dependent on the oxazoline substitution pattern, which significantly influenced the reactivity, regioselectivity, and also the extent of the asymmetric induction. Clearly the best results were achieved with the C_1-symmetric ligand **34**, containing both an isopropyl and *tert*-butyl substituent, which afforded the *β*-allenol **30** as the only reaction product in 51% yield with 96% ee (*R*). In contrast, the sterically more congested C_2-symmetric di-*tert*-butyl ligand **32** provided a mixture of the two regioisomers **30** and **31** and yielded the desired product **30** in a reduced yield of 39% with poor stereoselectivity (8% ee) for the opposite enantiomer (*S*). Although the isopropyl-derivative **33** showed excellent regioselectivity, the product **30** was obtained with a decreased enantioselectivity of 84% ee (*R*), and both the conversion and the product yield were considerably lower compared to the results obtained with the C_1-symmetric ligand.[46]

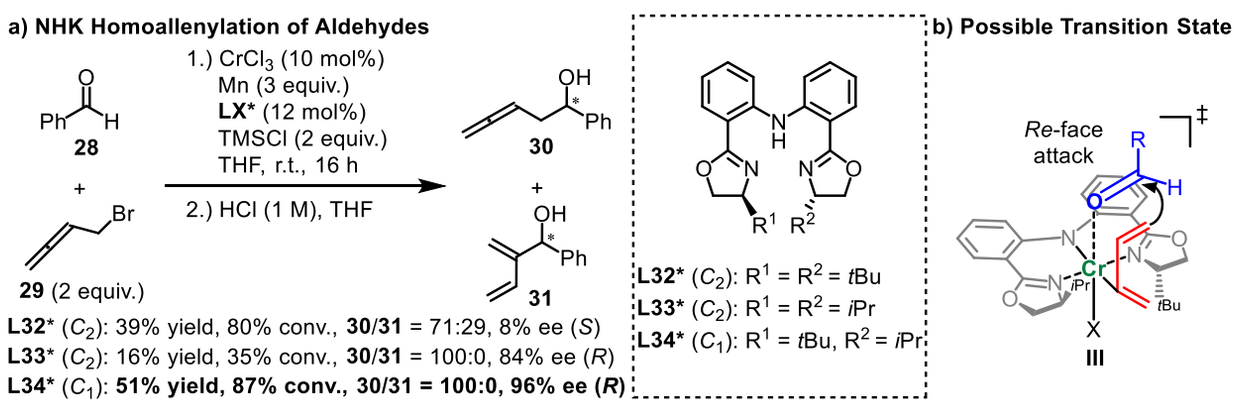

Scheme 5: a) Asymmetric Cr-catalyzed homoallenylation of aldehydes using tridentate bis(oxazolines); b) Possible transition state.[46]

With the optimal ligand **34** in hand, the substrate scope was further expanded to include different aromatic and aliphatic aldehydes reaching enantiomeric excesses of up to 98% ee. Scheme 5b shows their proposed transition state **III**.[46] In theory, the interaction of the homoallenyl bromide **29** with the chromium catalyst can lead to the formation of an homoallenyl and an 1,3-butadien-2-yl chromium(III) intermediate. The authors suggest, that the regioselectivity of

this addition may be rationalized by a fast equilibration of both complexes, with the 1,3-butadien-2-yl chromium(III) species apparently being more favored. In **III**, the 1,3-butadien-2-yl entity is thus supposed to be bonded to the metal center in the equatorial position, while the aldehyde coordinates at the apical position through an *anti*-geometry to diminish the steric interference between the isopropyl-group and the oxazoline ring,[46] similar to models that have been proposed by Nakada and co-workers.[52,53] In this transition state, an attack from the *Re*-face would be preferred. Although reasons for the improved stereorecognition with the C_1-symmetrical catalyst were not discussed, the stereogenicity of the central chromium ion in **III** might represent a critical factor and could give rise to a superior chiral site than the related C_2-symmetric complexes, in which the metal center is not chiral. However, the authors concluded that intermolecular reaction pathways or the involvement of dinuclear complexes cannot be ruled out, requiring further studies of the mechanism.[46]

Moreover, examples of powerful ligand scaffolds of even higher denticity with nonsymmetrical chiral backbones have been described. For instance, Sun and co-workers reported the asymmetric C–H oxidation of spirocyclic compounds by non-heme manganese(II) catalysts, which are based on linear tetradentate bis(benzimidazolylmethyl)diamine ligands, containing both symmetrical and nonsymmetrical chiral diamine linkers (Scheme 6).[54,55] In all four complexes **35**–**37**, the chiral N4 ligands adopt a helical *cis*-α conformation around the central metal, in which the nitrogen atoms of the benzimidazole ligands are *trans* to each other and occupy the apical positions of the octahedral complex, while the two labile, equatorially coordinated triflate anions are oriented *cis* to each other.[56] In this coordination geometry, the complexes feature a stereogenic metal center and, in the case of complex **36** and **37**, possess an overall C_2-symmetric topology. In contrast to the chiral cyclohexanediamine-based framework of the coordinated N4 ligand in **37**, the L-proline derived diamine and the dipyrrolidine moiety in **35a**/**b** and **36** provide a more rigid chiral backbone, and therefore ligands of this type have often been found to induce higher stereoselectivity.[55] For the investigated enantioselective oxidative desymmetrization of spirocyclic tetralone and indanone derivatives **38** to the corresponding chiral diketones **39**, the catalytic performances of all four catalysts were compared. Starting with the oxidation of the methylene C–H bond of tetralone **38a**, the non-C_2-symmetric proline-based catalyst **35a** proved to be the best choice. In the presence of 0.5 mol% of **35a**, 14 equivalents of 2,2-dimethylbutanoic acid (DMBA) and using 5 equivalents of H_2O_2 as the terminal oxidant, the *β,β'*-diketone **39a** was obtained in 80% yield and 94% ee (*S*) after 4 hours at –30 °C. Exchanging the *N*-ethyl substituent of the benzimidazole moiety of **35a** by a methyl group (**35b**) still led to a high, but slightly decreased enantioselectivity of 92% ee (*S*). In contrast to catalyst **35a**, complex **36** bearing the symmetrical dipyrrolidine backbone afforded the desired product **39a**

with a significantly reduced enantiomeric excess of 80% ee (*R*) in 78% yield. Compared with the more rigidly chelated catalysts, the C_2-symmetric complex **37** was indeed found to furnish the spirocyclic product **39a** with the lowest stereoselectivity (75% ee (*R*)) in 75% yield. Following the optimized conditions with the best catalyst **35a**, a variety of tetralone and indanone substrates were oxidized selectively, providing the chiral diketones in moderate to high yields with high enantioselectivities of up to 98% ee. Furthermore, the synthetic utility of the catalytic system was demonstrated by the gram-scale conversion of tetralone **38a** into **39a**, which was obtained in 70% yield and 92% ee, and in >99% ee after recrystallization.[54]

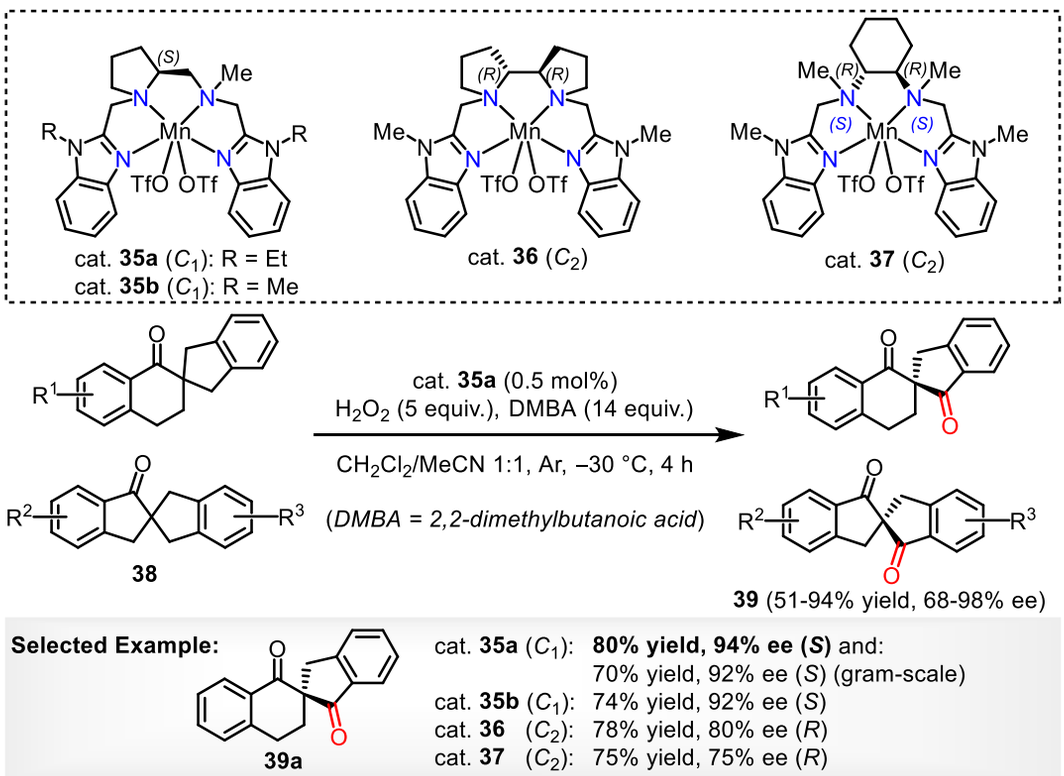

Scheme 6: Enantioselective oxidative desymmetrization of spirocyclic compounds catalyzed by a non-C_2-symmetric bioinspired Mn-complex.[54]

Although the consideration of molecular symmetry constitutes an important element for the design of novel catalysts, rotational symmetry such as C_2-symmetry does not always guarantee the key to high stereoselectivity. Besides symmetry, the examples given in this section also reveal that electronic and steric factors play a crucial role for an efficient stereorecognition, and these factors often surpass the benefits gained from symmetry.[8,5] Consequently, many more reports of highly effective catalysts of lower symmetry[57–68] can be found in the literature and this thesis includes an additional example.

2. Aim of this Work

Chiral transition metal complexes represent a powerful class of catalysts for the asymmetric synthesis of optically active compounds.[2] Metal-based chiral catalysts typically contain at least one chiral organic ligand within their coordination sphere to implement the overall chirality of the metal complexes. In recent years, Meggers and co-workers and others have demonstrated that nonracemic transition metal complexes composed of entirely achiral ligands are highly versatile catalysts for the realization of a wide variety of asymmetric transformations,[69–71] such as conjugate additions,[3,72–75] enolate chemistry[76–78] and asymmetric transfer hydrogenations[79] in addition to unique visible-light-induced asymmetric reactions.[80–83] In these chiral-at-metal catalysts the overall chirality exclusively originates from a stereogenic metal center (metal-centered chirality[84–87]), which arises from the asymmetric coordination of the otherwise achiral ligands, as it is here exemplary shown for the new class of stereogenic-at-metal Lewis acid catalysts introduced by the Meggers laboratory (Figure 6).[88]

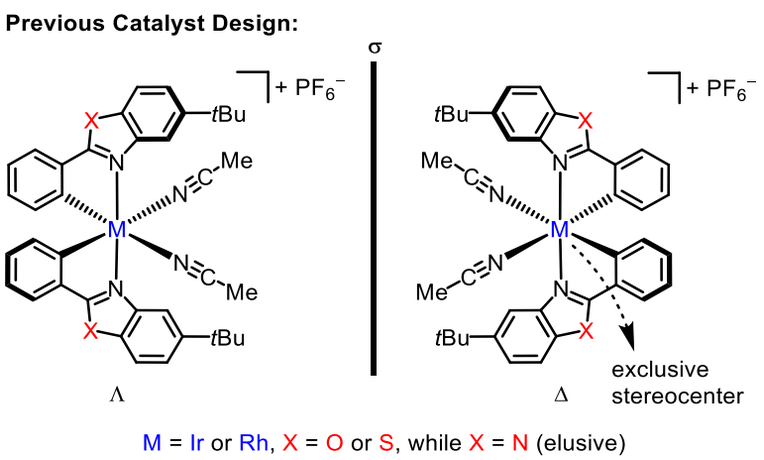

Figure 6: Overview of reactive chiral-at-metal iridium and rhodium catalysts.

In this basic design, iridium(III)[3] or rhodium(III)[77] is cyclometalated by two substitutionally and configurationally inert bidentate ligands which create a C_2-symmetrical propeller-type geometry with either a left-handed (Λ-enantiomer) or right-handed (Δ-enantiomer) helical twist. The octahedral coordination sphere is supplemented by a hexafluorophosphate counterion and two substitutionally labile acetonitrile ligands which generate vacant coordination sites for the direct catalytic activation of a substrate or reagent. Such reactive chiral-at-metal catalysts are attractive since the close proximity of the stereogenic metal center and the metal-coordinated substrate offers the prospect for a particularly effective transfer of chirality from the catalyst to the reaction product in the course of the asymmetric induction, and due to their structural

simplicity, as they are composed only of achiral ligands. Without the requirement for chiral motifs in the ligand sphere, untapped opportunities emerge for expanding the chemical space of chiral metal complexes with the potential to discover chiral metal catalysts with new electronic and structural properties for the exploration of novel catalytic asymmetric transformations. For example, previous chiral iridium or rhodium catalysts developed by Meggers and co-workers typically contained two 5-*tert*-butyl-2-phenylbenzoxazole ligands (further referred to as **IrO**[3,89] or **RhO**[76,77]) or the analogous benzothiazole derivatives (**IrS**[80,90,91] or **RhS**[92,93]), while the development of the structurally related benzimidazole complexes (X = N, **IrN** or **RhN**) has been elusive. In particular, the synthesis of the corresponding rhodium complexes is of substantial interest, as previous studies have revealed that the bis-cyclometalated rhodium catalysts proved to be superior to their iridium congeners for many catalytic applications, which can mainly be attributed to their significantly faster ligand exchange kinetics.[94–96]

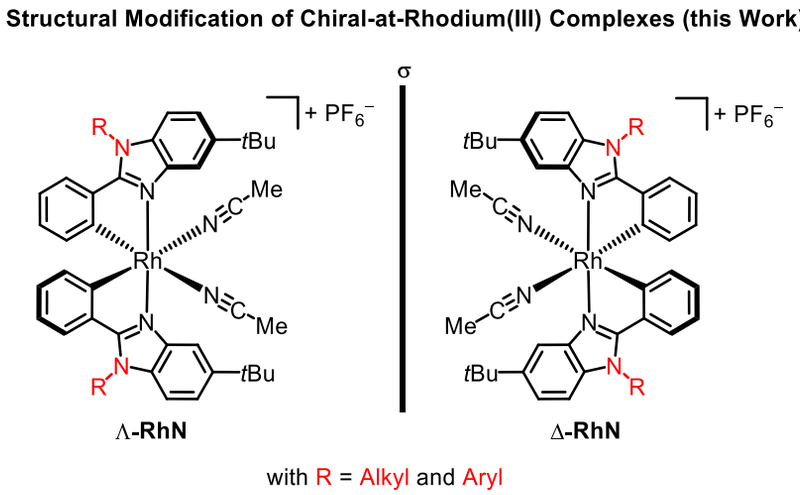

Figure 7: Intended extension of previous chiral-at-rhodium catalysts by a bis-benzimidazole derivative.

Along these lines, the aim of this work was to elaborate synthetic access to the respective bis-cyclometalated rhodium(III) complexes with two cyclometalated 5-*tert*-butyl-2-phenylbenz-imidazoles, as shown in Figure 7. An important feature of this ligand scaffold is the possibility of further expanding the structural diversity of this class of chiral Lewis acids, as it intrinsically permits the introduction of different substituents on the nitrogen atom of the imidazole moiety and thus allows the design of a large number of sterically and electronically modified chiral-at-rhodium catalysts, whose catalytic and photochemical properties should be investigated in the context of this thesis.

3. Results and Discussion

3.1 Expanding the Family of Bis-Cyclometalated Chiral-at-Rhodium(III) Catalysts with a Benzimidazole Derivative

3.1.1 Auxiliary-Mediated Synthesis of Enantiomerically Pure Rhodium Complexes

Over the past several years, Meggers and co-workers established an auxiliary-mediated strategy for the asymmetric synthesis of nonracemic chiral-at-metal complexes which is based on the application of tailored chiral bidentate ligands.[97–99] In this strategy, the coordination of a chiral bidentate chelate to the metal center assists in a first step the efficient implementation of the absolute metal-centered configuration, and in a second step the chiral auxiliary can be removed in a traceless fashion with complete retention of the stereochemical information. Although, this approach was originally developed for the synthesis of enantiomerically pure tris-heteroleptic ruthenium(II) polypyridyl complexes,[99] it later also proved to be a viable synthetic method for the preparation of enantiopure bis-cyclometalated iridium(III) and rhodium(III) complexes, as shown here, for example, on the basis of the synthesis of Λ- and Δ-**RhS**.[93,100]

In a first step, heating of rhodium trichloride hydrate and 2 equivalents of 5-*tert*-butyl-2-phenylbenzothiazole (**40**) in a 3:1 mixture of 2-ethoxyethanol and water provides a racemic bis-cyclometalated chloro-bridged rhodium(III) dimer [Rh(μ-Cl)(**40**-H^+)$_2$]$_2$ as an intermediate product, which is subsequently converted into the corresponding racemic acetonitrile complex *rac*-**RhS** with $AgPF_6$ in acetonitrile (Scheme 7).

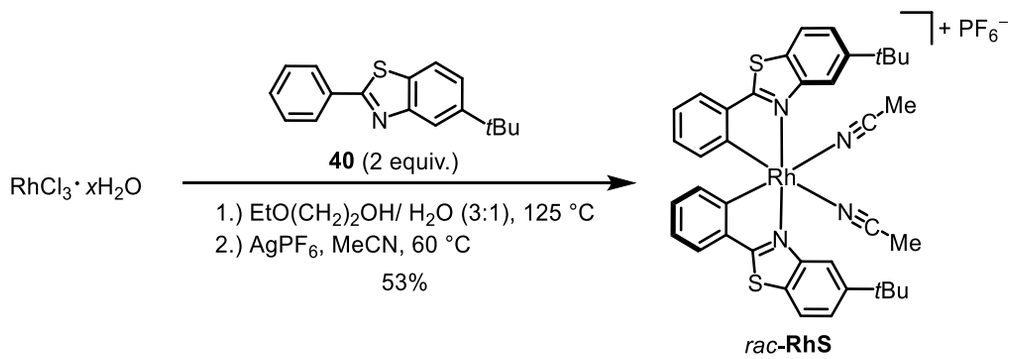

Scheme 7: Synthesis of the racemic complex *rac*-**RhS**.[100]

For the resolution of the racemic complex into its individual Λ- and Δ-enantiomers, *rac*-**RhS** is reacted with the fluorinated salicyloxazoline (*S*)-**41**, which was first reported by Monari, Bandini

and Ceroni[101] and later became the chiral auxiliary of choice for the synthesis of enantiomerically pure bis-cyclometalated rhodium(III) complexes in the Meggers laboratory.[93] An essential feature of this auxiliary is the fluorine substitution of the phenol moiety, as this supplies rhodium auxiliary complexes with an increased acidity, which therefore exhibit optimal stability in solution and when exposed to silica gel. Accordingly, the conversion of *rac*-**RhS** with (*S*)-**41** in the presence of K_2CO_3 results in the formation of two diastereomers in which the bidentate chiral ligand in its monodeprotonated form is coordinated as a six-membered chelate, and thus provides the corresponding stereoisomers Λ- and Δ-(*S*)-**42** as neutral complexes, which can either be separated based on their different solubilities in EtOH or via regular silica gel column chromatography, or a combination thereof (Scheme 8).

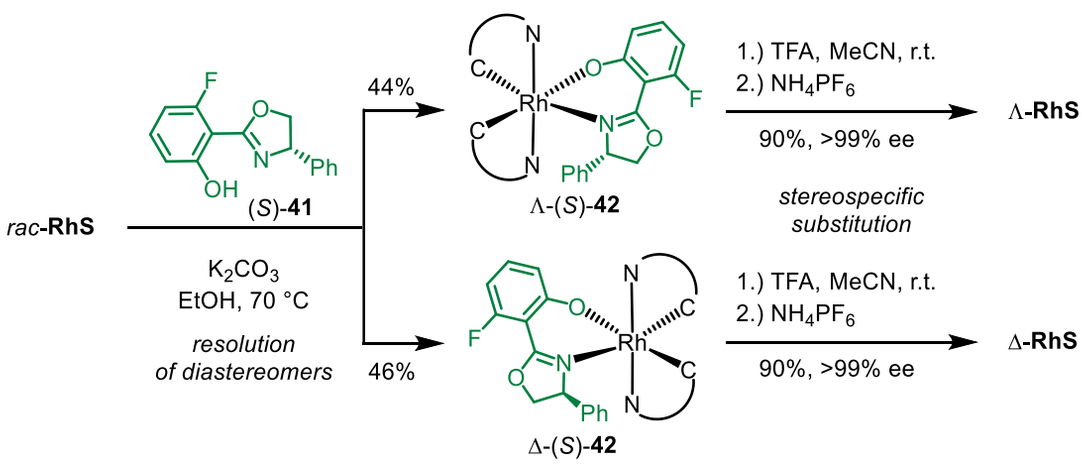

Scheme 8: Auxiliary-based synthesis of enantiomerically pure Λ- and Δ-**RhS**.[100]

Importantly, the binding strength of the coordinated phenolate can be weakened by protonation, which makes the coordination reversible and thus enables a stereospecific substitution of the chiral auxiliary for an achiral ligand without compromising the chiral information. In a final step, the two diastereomerically pure complexes Λ- and Δ-(*S*)-**42** are therefore individually reacted with trifluoroacetic acid (TFA) in the presence of acetonitrile as the solvent to replace the coordinated auxiliary ligand, as depicted in Scheme 8. Subsequent anion exchange with NH_4PF_6 then affords the single enantiomers Λ- and Δ-**RhS**, in which the octahedral metal center constitutes the sole source of chirality, with an essentially complete enantioselectivity (>99% ee) for each complex.

The procedure described here is considered to be generally applicable for the preparation of chiral-at-rhodium catalysts and was applied in the following to the synthesis of the analogous benzimidazole complexes.

3.1.2 Synthesis of the Benzimidazole Ligands and Initial Cyclometalation Experiments

In order to expand the family of bis-cyclometalated chiral-at-rhodium(III) catalysts with a benzimidazole derivative and to further diversify this new class of chiral Lewis acids, it was envisioned to prepare a number of complexes with different substituents on the imidazole nitrogen, including aromatic as well as alkyl residues (Figure 7). Initially, it was therefore decided to begin with the synthesis of two corresponding benzimidazole ligands, one of which should have an *N*-methyl residue and the second one a phenyl-substituent.

Scheme 9 illustrates the synthetic procedure for the synthesis of the benzimidazole ligands, on the basis of the synthesis of the methyl-substituted derivative **47a**.[102] Following a reported protocol from Beaulieu and co-workers,[103] the desired cyclometalating ligands could conveniently be accessed via the shown four-step synthesis.

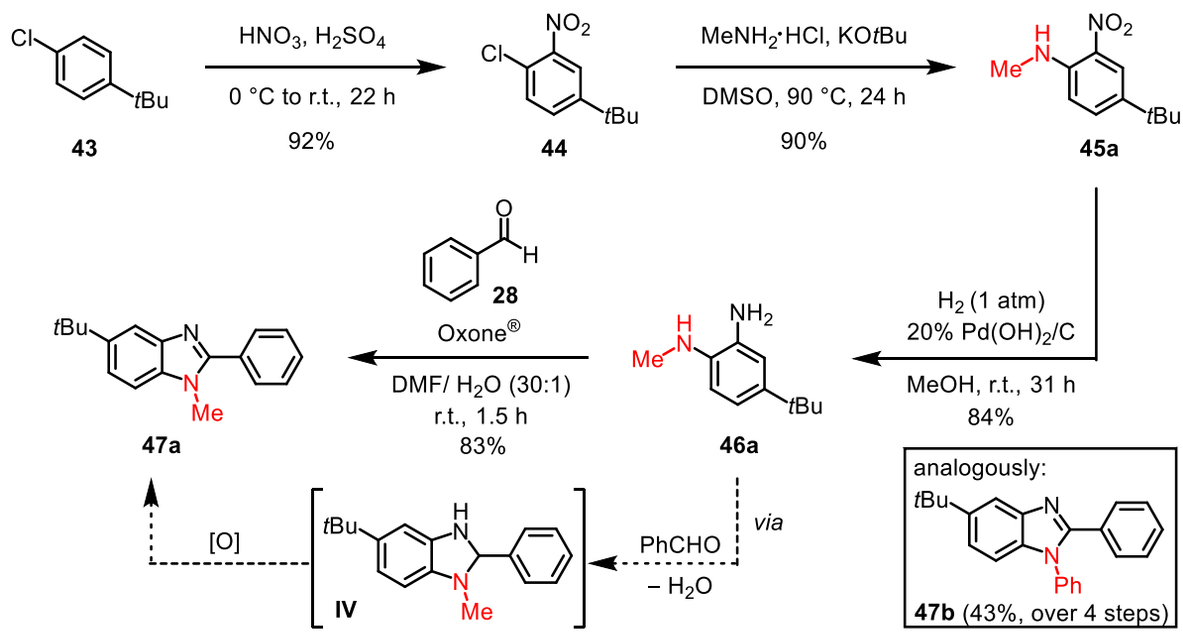

Scheme 9: Synthesis route for the preparation of the benzimidazole ligands **47**, exemplified for the synthesis of the methyl-substituted derivative (**47a**[102]).

Accordingly, starting from commercially available 1-(*tert*-butyl)-4-chlorobenzene (**43**), nitration afforded the corresponding 1-chloro-2-nitrobenzene **44** in 92% yield. Subsequent nucleophilic aromatic substitution of the chloro-substituent of **44** with methylamine in the presence of potassium *tert*-butoxide as the base in the second step provided the desired nitroaniline **45a** in 90% yield. Reduction of the nitro group of **45a** by a catalytic palladium-catalyzed hydrogenolysis in the following step gave the corresponding 1,2-phenylenediamine **46a** in 84% yield, which could be converted into the desired ligand 5-*tert*-butyl-1-methyl-2-phenylbenzimidazole (**47a**) in the last step via a condensation–dehydration sequence with benzaldehyde (**28**) and subsequent

oxidation of the intermediately formed benzimidazoline **IV** with Oxone® (2 $KHSO_5 \cdot KHSO_4 \cdot K_2SO_4$) in a one-pot process. Correspondingly, the final benzimidazole ligand **47a** was obtained in 83% yield, with an overall yield of 58% over four steps, and the analogously prepared phenyl-substituted derivative **47b** was accessible with an overall yield of 43% via the synthetic route presented.

With a synthesis of the cyclometalating ligands in hand, the corresponding cyclometalation of rhodium was next performed following the conditions previously introduced in Section 3.1.1 for the synthesis of related bis-cyclometalated rhodium(III) complexes.[100] Accordingly, rhodium trichloride hydrate and 2 equivalents of the respective benzimidazole ligand **47a** or **47b** were initially refluxed in a 3:1 mixture of 2-ethoxyethanol and water for 6 hours at 125 °C, and then reacted with $AgPF_6$ in acetonitrile (Scheme 10).

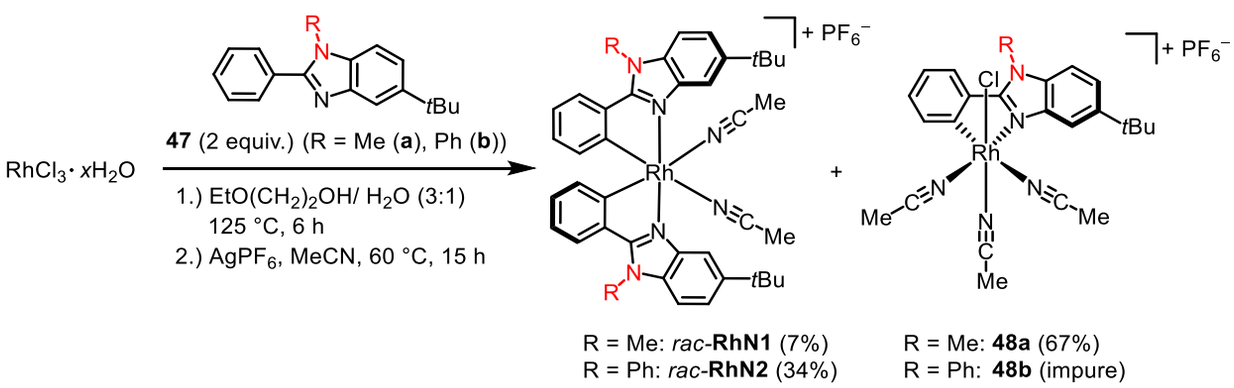

Scheme 10: Initial cyclometalation experiments of $RhCl_3 \cdot xH_2O$ with benzimidazoles **47a** and **b**.

However, for the cyclometalation with 5-*tert*-butyl-1-methyl-2-phenylbenzimidazole (**47a**), the anticipated bis-cyclometalated complex *rac*-**RhN1** was only obtained in a low yield of 7%, while a corresponding mono-cyclometalated rhodium(III) species **48a** was surprisingly formed as the major product of the reaction in 67% isolated yield. A crystal structure of **48a** is shown in Figure 8 and clearly confirmed the structure of this unexpected complex.[102] When the analogous cyclometalation reaction of rhodium trichloride was performed with benzimidazole ligand **47b** bearing an *N*-phenyl moiety, the formation of several products was observed. The bis-benzimidazole complex *rac*-**RhN2** was obtained with a comparatively higher yield of 34%, but in addition to the formation of a related mono-cyclometalated rhodium complex, other side products with the same R_f value were formed, which prevented a clean isolation of complex **48b**, whose formation therefore remained an assumption based on the evaluation of the obtained ^{1}H NMR spectrum of the isolated mixture of complexes (see Section 5.3.2, Figure 35 for more details). It is interesting to note, that in the course of this dissertation the related bis-cyclometalated iridium benzimidazole complex with ligand **47a** could smoothly be obtained by this route.[104]

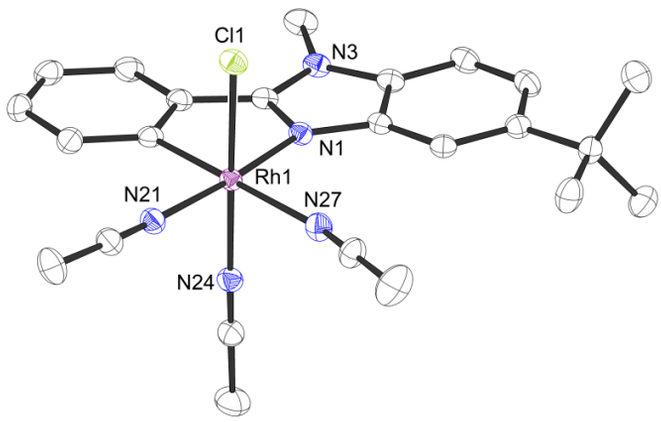

Figure 8: Crystal structure of mono-cyclometalated rhodium(III) complex **48a** as an ORTEP drawing with 50% probability thermal ellipsoids. The PF_6^- counterion and solvent molecules are omitted for clarity.

Since the previously performed cyclometalation reactions of rhodium with the related phenylbenzoxazole[77] and benzothiazole[93] ligands have always yielded the respective bis-cyclometalated rhodium complexes as the exclusive reaction products, the formation of a stable mono-cyclometalated rhodium species such as **48a** is of high interest, as this would potentially allow the introduction of a different second cyclometalating ligand in a subsequent second cyclometalation step. Hence, the newly discovered mono-cyclometalation of rhodium with *N*-alkyl substituted benzimidazole ligands should be investigated more closely in the further context of this work.

3.1.3 Condition Screening and Scope of the Mono-Cyclometalation Reaction

In the following section, the mono-cyclometalation was further examined on the basis of the cyclometalation of rhodium with 5-*tert*-butyl-1-methyl-2-phenylbenzimidazole (**47a**) and the formation of complex **48a**, since more promising results were achieved with this ligand scaffold compared to the analogous cyclometalation with the *N*-phenyl substituted derivative **47b**.

Table 1 summarizes the conditions which were tested in order to optimize the yield of the cyclometalation with respect to the formation of the mono-cyclometalated rhodium(III) species **48a**.[102] Entry 1 again shows the initial reaction conditions, which correspond to the conditions discussed in Section 3.1.2 (Scheme 10) and aimed at providing the bis-cyclometalated complex *rac*-**RhN1** using 2 equivalents of the cyclometalating ligand **47a**. In a second experiment with 2 equivalents of **47a**, extending the reaction time of the first step to 24 hours and increasing the reaction temperature to 140 °C essentially did not improve the yield for the bis-

cyclometalated complex *rac*-**RhN1**, while the mono-cyclometalation to **48a** still occurred predominantly, albeit with a reduction in yield to 57% (entry 2).[102]

Table 1: Optimization of the Reaction Conditions of the Cyclometalation with Benzimidazoles.[a]

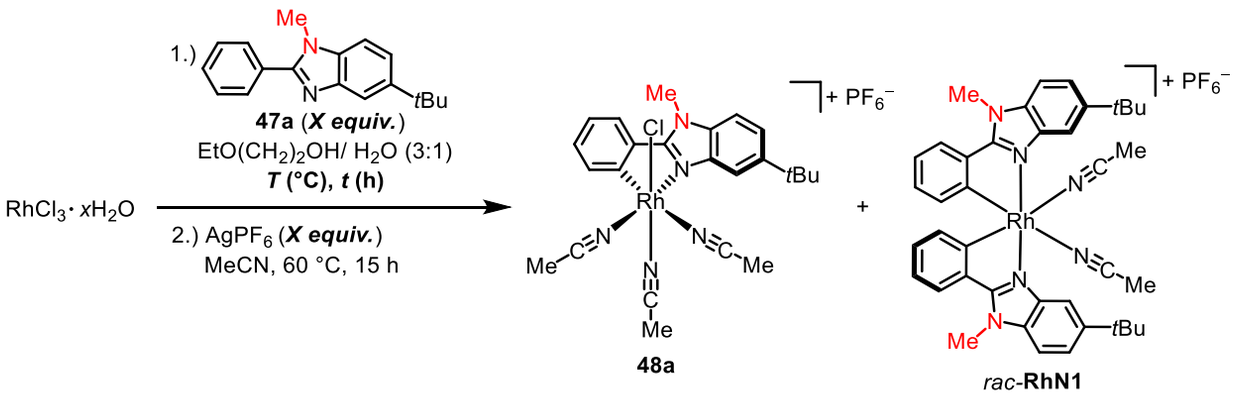

entry	*T*, *t* (1st step)	47a (equiv.)	$AgPF_6$ (equiv.)	yield of 48a[b]	yield of *rac*-RhN1[c]
1	125 °C, 6 h	2.00	2.00	67%	7%
2	140 °C, 24 h	2.00	2.00	57%	8%
3	125 °C, 6 h	1.00	2.00	78%	n.f.
4	140 °C, 7 h	1.00	1.50	82%	n.f.
5	150 °C, 7 h	1.10	1.30	79%	n.f.
6	150 °C, 7 h	1.10	1.80	86%	n.f.

[a]Reaction conditions: **First step:** $RhCl_3{\cdot}xH_2O$ and benzimidazole ligand **47a** (indicated equiv.) were stirred in a 3:1 mixture of 2-ethoxyethanol and H_2O (0.05 M) at the indicated temperature for the indicated time under an atmosphere of nitrogen. **Second step:** After thorough removal of the solvent under reduced pressure, $AgPF_6$ (indicated equiv.) and MeCN (0.05 M) were added and the resulting suspension was stirred for 15 h at 60 °C under exclusion of light. [b]Isolated yield after the second step. [c]Determined by ^{1}H NMR analysis of the crude reaction mixture. n.f. = not formed.

When only 1 equivalent of the cyclometalating ligand **47a** was employed and the reaction was otherwise performed under the same conditions as in entry 1, the yield of the desired complex **48a** could be increased to 78% (entry 3). Importantly, no formation of the bis-cyclometalated complex *rac*-**RhN1** was observed at all under these reaction conditions. A further screening of the reaction temperature of the first step and application of different equivalents of $AgPF_6$ in the subsequent second step (entry 4–6) revealed that the best results were achieved, when the cyclometalation step was performed at 150 °C for 7 hours in the presence of a slight excess of the ligand **47a**, and if the following step was executed with 1.8 equivalents of the silver

salt (entry 6). Via optimization of the initial conditions, the desired mono-cyclometalated complex **48a** could thus be obtained in a high yield of 86% as the sole product of the reaction.

In order to test the generality of the mono-cyclometalation with regard to the incorporation of benzimidazole ligands with different *N*-alkyl substituents, two derivatives of **48** were prepared which contained an *n*-butyl chain and a cyclohexyl-group. Following the synthetic procedure introduced in Section 3.1.2, the corresponding ligands **47c** and **47d** were obtained in an overall yield over four steps of 54% and 43%, respectively (Figure 9).

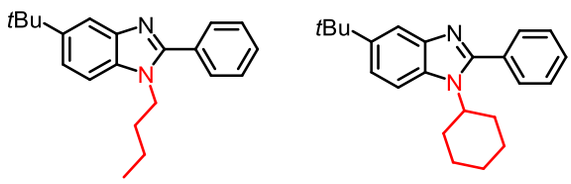

47c (54%) **47d** (43%)

Figure 9: Synthesized phenylbenzimidazole derivatives with different *N*-alkyl groups (total yield over four steps).

According to the previously optimized conditions for the cyclometalation, both ligands **47c** and **47d** were subsequently reacted with rhodium trichloride hydrate, which smoothly and exclusively provided the respective mono-cyclometalated analogues **48c** and **48d** in 85% and 83% yield, respectively, and thus proved the validity of the reaction for this class of cyclometalating ligands (Scheme 11).

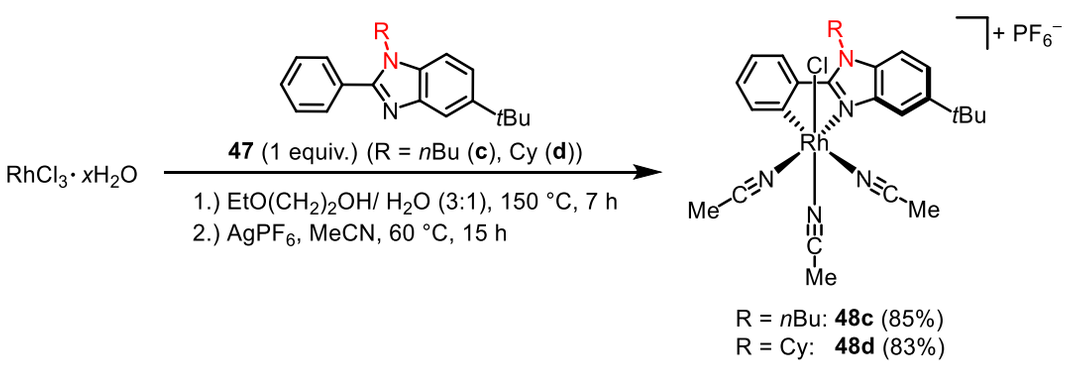

Scheme 11: Synthesis of mono-cyclometalated complexes **48** with different *N*-alkyl groups.

Moreover, crystals of the *n*-butyl derivative **48c** suitable for single crystal X-ray diffraction were obtained, as shown in the evaluated structure in Figure 10.

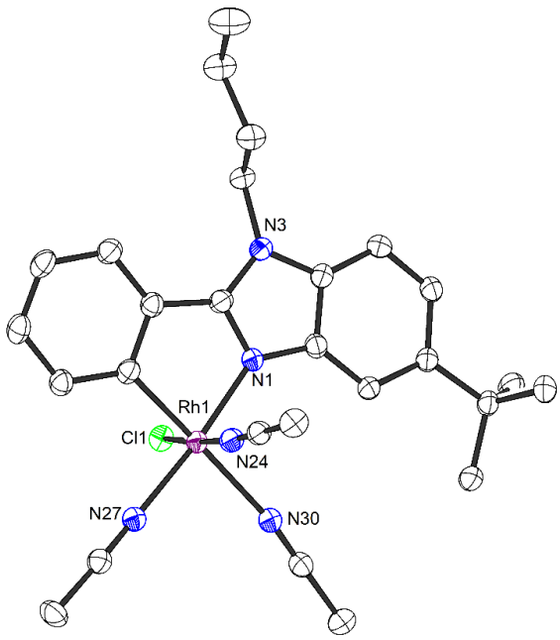

Figure 10: Crystal structure of the mono-cyclometalated rhodium complex **48c** containing an *n*-butyl side chain. Shown as an ORTEP drawing with 50% probability thermal ellipsoids. The PF_6^- counterion and solvent molecules are omitted for clarity.

In analogy to the structure of the *N*-methyl complex **48a** obtained before, the complex **48b** contains, in addition to the cyclometalated benzimidazole, three acetonitrile ligands and a chloride and thus the resulting rhodium(III) complex is obtained as a monocationic salt, which is complemented by a hexafluorophosphate counterion. However, depending on the nature of the second ligand whose incorporation should be attempted in a subsequent step, it could be advantageous to start from a corresponding complex in which all of the four labile ligands are the same, as this could reduce the number of complexes that can result from the second coordination step. Accordingly, the synthesis of a tetra-acetonitrile derivative of the mono-cyclometalated complexes was envisaged.

3.1.4 Synthesis of a Mono-Cyclometalated Tetra-Acetonitrile Rhodium Derivative

In an extension of the developed method for the synthesis of mono-cyclometalated rhodium complexes with a cyclometalated benzimidazole ligand, it was also investigated whether the remaining chloro-ligand of **48a** can be removed and replaced by another acetonitrile molecule to give a corresponding dicationic rhodium(III) complex, in which all of the four substitutionally labile ligands are represented by acetonitrile solvent molecules.

In order to remove the chloride, complex **48a** was treated again with $AgPF_6$ in acetonitrile under various reaction conditions, which were subsequently evaluated by analyzing the obtained ^1H NMR spectra of the respective crude reaction mixtures. Scheme 12 exhibits the varied reaction parameters as well as three exemplary crude ^1H NMR spectra that visualize the most important parameters for the reaction outcome. Shown is the aliphatic region which contains the singlet of the *N*-methyl group of the desired product **49**, in addition to a corresponding signal of a formed side product and of the remaining starting material **48a** (from left to right). As opposed to the conditions applied before for the synthesis of the monocationic complex **48a** (Table 1, entry 6), the removal of the residual chloride was attempted under slightly harsher conditions. Accordingly, the reaction was performed with an increased amount of $AgPF_6$ of 5 equivalents in acetonitrile, and the resulting solution was stirred at an elevated temperature of 70 °C (Scheme 12a). However, even after a reaction time of two days, only a low conversion of the starting material was observed and the desired product **49** was formed in a ratio of almost 1:1 with a side product which could not be identified, as it was not isolable via regular silica gel column chromatography, most likely due to decomposition. Importantly, the solvent concentration for this attempt was reduced from 0.05 M (Table 1, entry 6) to 0.03 M, since initial experiments have revealed that higher concentrations lead to an even increased formation of the by-product. A further screening of conditions disclosed that the added equivalents of $AgPF_6$ had almost no influence on the reaction result. Hence, the following reactions were carried out with only 2 equivalents of the silver salt, the concentration was further reduced to 0.025 M, and the temperature raised to 80 °C in order to accelerate the conversion (Scheme 12b). After 72 hours, TLC indicated almost complete consumption of the starting material, but analysis of the crude reaction mixture by ^1H NMR showed that the side product was formed as the predominant product under these conditions. In contrast, the same conditions conducted for only 48 hours provided the desired product **49** as the major product of the reaction with still almost complete conversion and with only little by-product formation being observed, and thus conditions 3 represented an optimal compromise between a high conversion of complex **48a** and an acceptable product-to-by-product ratio (about 10:1, see Scheme 12c).

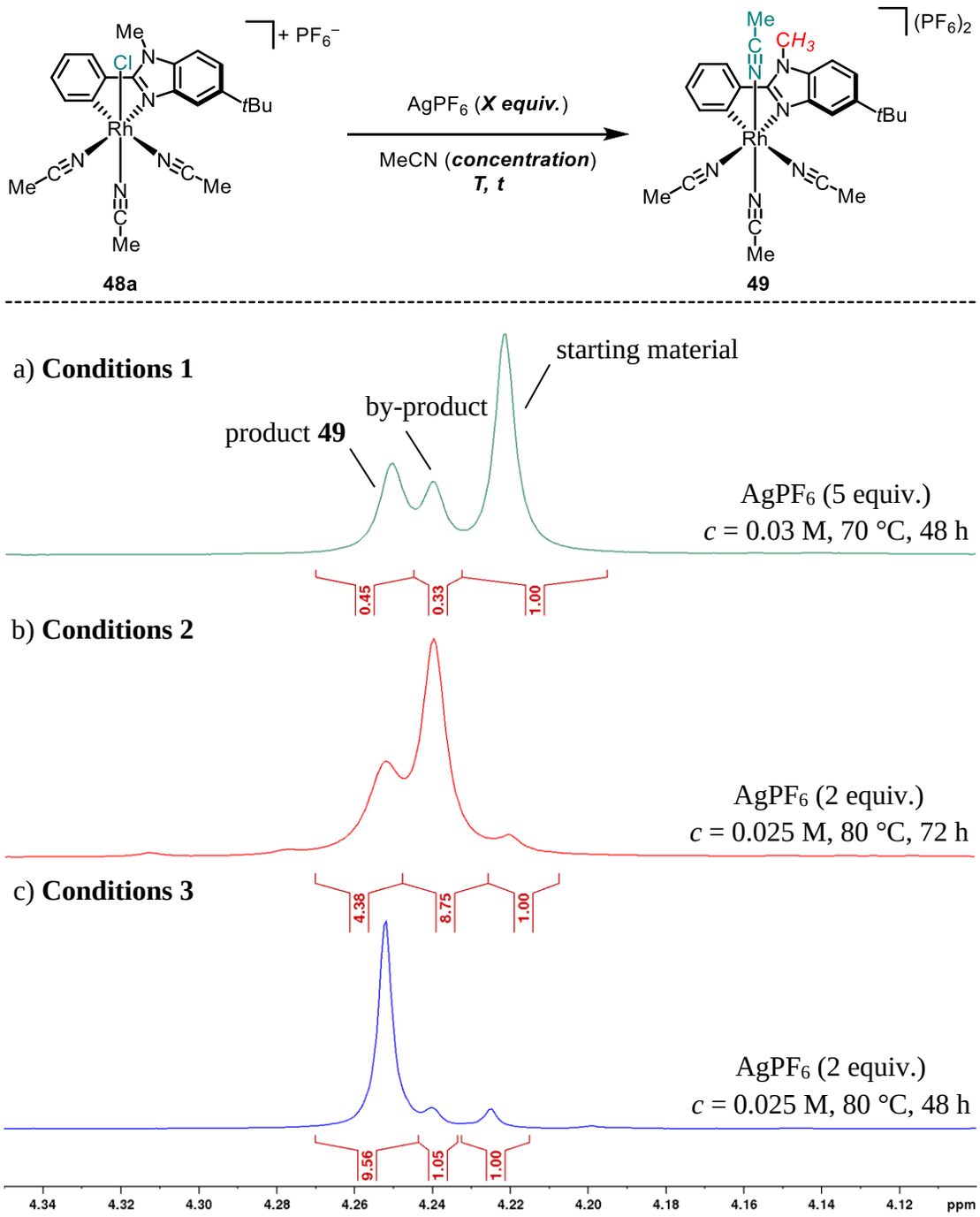

Scheme 12: Condition screening for the synthesis of the tetra-acetonitrile complex **49** and selected crude ^{1}H NMR spectra of three different reaction conditions (a–c) showing the aliphatic section of the respective spectra with the *N*-C*H*$_3$ singlet of the desired product (300 MHz, 300 K, CD_3CN).

Following the optimized conditions, the desired tetra-acetonitrile complex **49** could conveniently be generated and was obtained as a colorless salt in a high isolated yield of 91% after regular column chromatographic purification (Scheme 13).

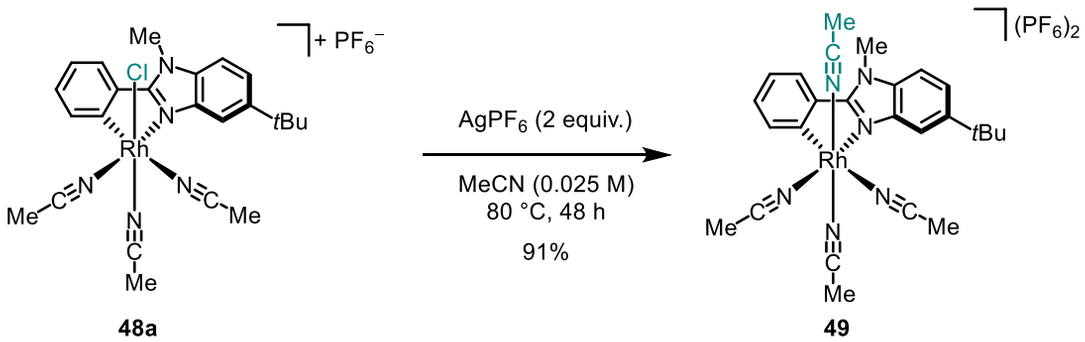

Scheme 13: Optimized conditions for the synthesis of tetra-acetonitrile complex **49**.

A crystal structure of the complex is shown in Figure 11 and demonstrates the successful substitution of the remaining chloride by another acetonitrile ligand.

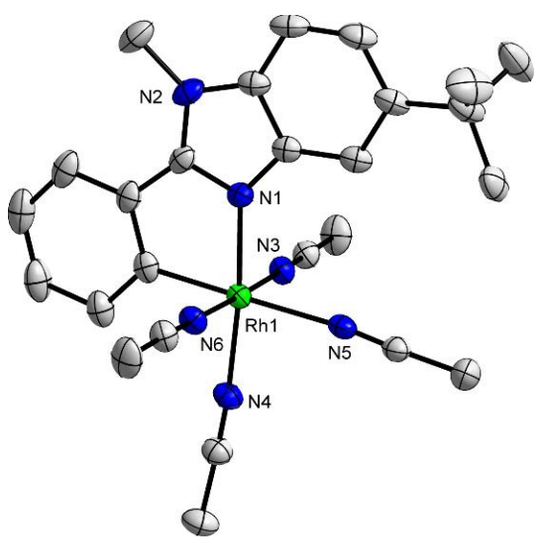

Figure 11: Crystal structure of tetra-acetonitrile complex **49** as an ORTEP drawing with 50% probability thermal ellipsoids. The two PF_6^- counterions and the hydrogen atoms are omitted for clarity.

A synthetic access to this dicationic derivative of complex **48a** could thus be established in an overall reaction sequence of three steps starting from rhodium trichloride hydrate and provided the complex in a total yield of 78%. To shorten the reaction sequence by one step, it was also possible to synthesize the tetra-acetonitrile complex directly via the two-step procedure described in Section 3.1.3., simply by adjusting the reaction conditions of the second step (Scheme 14).

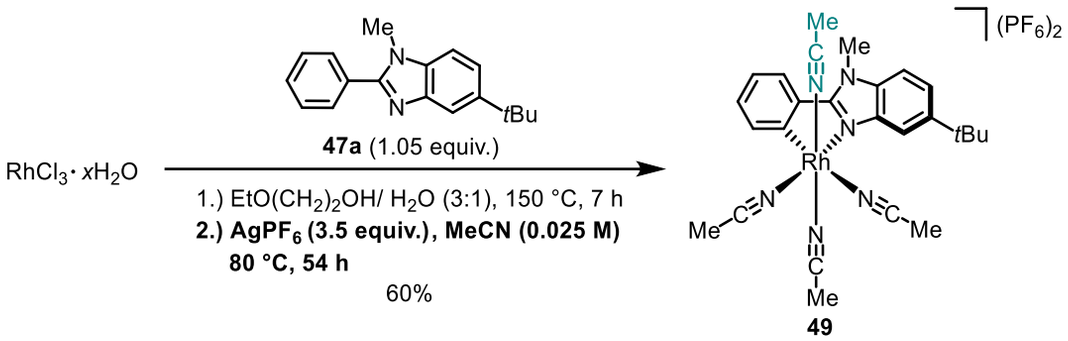

Scheme 14: Direct synthesis of the tetra-acetonitrile derivative **49** from $RhCl_3 \cdot xH_2O$.

Correspondingly, the initial cyclometalation step with benzimidazole ligand **47a** was executed following the previously introduced conditions. For the second step, the equivalents of $AgPF_6$ were increased to 3.5 equivalents, and as in the previously performed three-step synthesis of **49**, the solvent concentration was lowered to 0.025 M and the resulting suspension stirred for 54 hours at 80 °C, which furnished the desired complex in an isolated yield of 60% in a more time-efficient manner, albeit with a slightly reduced overall yield.

3.1.5 Conclusions

An unprecedented mono-cyclometalation of rhodium trichloride hydrate was discovered at the beginning of this thesis, when it was intended to expand the class of bis-cyclometalated rhodium catalysts with a phenylbenzimidazole derivative. Previous cyclometalation reactions of rhodium typically yielded the corresponding bis-cyclometalated rhodium complexes containing either two 5-*tert*-butyl-2-phenylbenzoxazoles[77] or the analogous benzothiazole ligands,[93] whereas the cyclometalation with a related benzimidazole derivative unexpectedly resulted in the formation of an isolable mono-cyclometalated rhodium(III) species.[102] As opposed to the respective cyclometalation with an *N*-phenyl group containing benzimidazole ligand **47b**, which proceeded rather sluggishly, the mono-cyclometalation with the *N*-alkyl substituted relatives **47a**, **c** and **d** performed reliably, and a small range of in total three complexes with different alkyl residues on the imidazole moiety was prepared (**48a**, **c**, **d**). Following the optimized conditions, all three complexes were formed as the exclusive reaction products in high yields (83–86%). Furthermore, it was demonstrated that the remaining chloro-substituent of the mono-cyclometalated complexes, exemplified for complex **48a**, could be removed and substituted by a fourth acetonitrile molecule, which enabled the synthesis of a corresponding tetra-acetonitrile derivative **49**.

Conclusively, the formation of these stable complexes opened up for the first time the prospect to design chiral-at-rhodium catalysts, in which the two cyclometalating ligands are not identical, with the possibility of starting from either a respective mono- or dicationic rhodium complex. In the following course of this work, further efforts should therefore be entirely addressed to the development of a synthetic method for the synthesis of such a new and intriguing class of chiral complexes.

3.2 Chiral-at-Rhodium Catalyst with Two Different Cyclometalating Ligands

3.2.1 Strategies for the Synthesis of Bis-Cyclometalated Tris-Heteroleptic Complexes

Over the past several years, Meggers and co-workers introduced a new class of chiral Lewis acids based on bis-cyclometalated iridium(III) and rhodium(III) complexes,[88] which exclusively derive their absolute configuration from a stereogenic metal center[84–87] (see Chapter 2 for more details). The first synthetic method for the preparation of a bis-cyclometalated complex of iridium(III) was reported by Nonoyama[105] in 1974. Based on this original protocol, the standard synthesis typically involves heating iridium trichloride hydrate with a ligand of choice in 2-ethoxyethanol to provide the corresponding bis-cyclometalated, μ-chloro-bridged iridium(III) dimers as individual diastereomers, which then serve as versatile intermediates for subsequent chemical transformations. In an analogous manner, the same procedure can also be used for the synthesis of the related rhodium complexes starting from the respective rhodium(III) halide. Despite the convenience of this chemistry, the obvious limitation is that it only provides bis-cyclometalated complexes in which both cyclometalating ligands are identical (Figure 12).

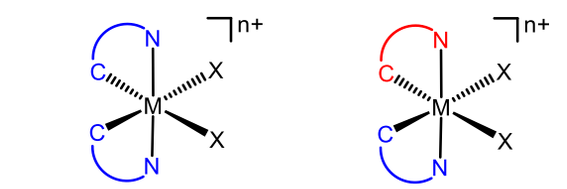

Figure 12: Comparison of bis-cyclometalated bis-heteroleptic (established, left) and bis-cyclometalated tris-heteroleptic (elusive, right) rhodium(III) complexes.[102]

However, for the modification of photophysical and catalytic applications the synthesis of bis-cyclometalated complexes of iridium(III) and rhodium(III) with two different cyclometalating ligands would be attractive. In particular, the design of structurally modified bis-cyclometalated rhodium complexes for the development of a new type of chiral-at-rhodium(III) catalysts with novel properties is appealing, since previous studies in the Meggers laboratory have already shown that in many catalytic reactions the rhodium catalysts gave better results than their isostructural iridium congeners.[94–96] In large part, this catalytic superiority of the rhodium catalysts can be ascribed to their much faster acetonitrile (≙ **X**) exchange rates.[77] Since the substrate coordination and/or release is supposed to be the rate-determining step in most light-

and heat-induced catalytic cycles, the higher coordinative lability of the acetonitrile ligands in the rhodium complexes permits higher turnover frequencies and turnover numbers.

Synthetic strategies for the preparation of bis-cyclometalated tris-heteroleptic complexes are rare and the majority of reported protocols for the synthesis of bis-cyclometalated iridium complexes with two distinct cyclometalating ligands are based on statistical methods,[106–112] which have the disadvantage of leading to statistical mixtures of complexes and therefore often result in low product yields for the desired tris-heteroleptic complexes. As one of the first examples, Edkins and co-workers[107] presented a synthetic procedure for the synthesis of three different bis-cyclometalated tris-heteroleptic iridium complexes, which is outlined in Scheme 15 for one of these complexes containing a cyclometalated 2-phenylpyridine (ppy) and a 2,4-diphenylpyridine (dppy) ligand. In the first step, iridium trichloride hydrate was refluxed in a mixture of water and 2-ethoxyethanol with the two cyclometalating ligands, which provided the desired complex $[Ir(ppy)(dppy)(\mu\text{-}Cl)]_2$ as part of a complex mixture of dinuclear species that contained at least seven combinations of ligands. Subsequently, the mixture of dimers obtained was reacted with acetylacetone (acac) in the presence of a base without further purification, leading to a statistical mixture of the three mononuclear complexes $IrL_2(acac)$, $IrL'_2(acac)$ and the desired complex IrLL'(acac), which were separated by column chromatography to give the tris-heteroleptic complexes in isolated yields of 7 to 11%.

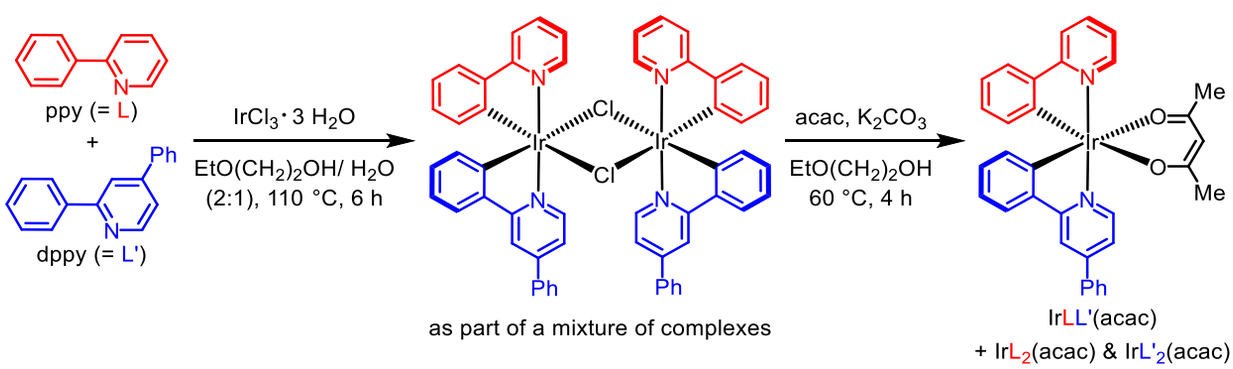

Scheme 15: Statistical synthesis of a bis-cyclometalated tris-heteroleptic iridium complex by Edkins.[107]

While a few reports have recently been published on strategies that circumvent such a combinatorial approach,[113–115] no method for the controlled synthesis of related bis-cyclometalated rhodium(III) complexes has existed. Hence, the following sections of this chapter aim to disclose the first method for the stepwise synthesis of an enantiomerically pure bis-cyclometalated rhodium(III) complex containing two different cyclometalating ligands and, furthermore, to demonstrate the high catalytic performance of the newly developed catalyst in asymmetric [2+2] photocycloaddition reactions.[102]

3.2.2 Synthesis of a Racemic Bis-Cyclometalated Tris-Heteroleptic Rhodium(III) Complex

The synthetic route for the synthesis of enantiopure catalysts consists of two main stages: first, the synthesis of the racemic catalyst and, second, the auxiliary-mediated synthesis of the individual enantiomerically pure Λ- and Δ-enantiomers of the catalysts (see Section 3.1.1).

In this first section, the step-by-step synthesis of a racemic rhodium(III) complex containing two different cyclometalating ligands is presented, which is based on a serendipitous finding.[102] While previous bis-cyclometalated rhodium complexes developed by the Meggers laboratory typically contained either two 5-*tert*-butyl-2-phenylbenzoxazole[77] ligands or two of the analogous benzothiazole[93] derivatives, it was found that the reaction stopped after the first cyclometalation, when the class of bis-cyclometalated rhodium catalysts should be expanded to include a related benzimidazole complex. As a result, a stable and isolable mono-cyclometalated rhodium(III) species **48a** was obtained in high yield (86%) and as the only product of the first cyclometalation step after optimization of the initial reaction conditions (discussed in detail in Chapter 3.1). In order to further expand the scope of bis-cyclometalated chiral-at-rhodium(III) catalysts, the incorporation of a different second ligand in a subsequent second cyclometalation step was envisioned. For this purpose, the related 5-*tert*-butyl-2-phenylbenzothiazole ligand (**40**) was initially selected as a suitable candidate, which is accessible via the reported two-step synthesis from Meggers and co-workers, shown in Scheme 16.[100]

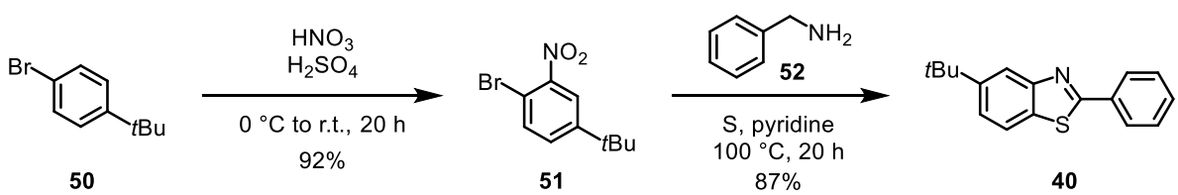

Scheme 16: Synthetic route to 5-*tert*-butyl-2-phenylbenzothiazole (**40**).[100]

Accordingly, nitration of commercially available 1-bromo-4-(*tert*-butyl)benzene (**50**) in the first step gave the corresponding 1-bromo-2-nitrobenzene **51** in 92% yield.[100] Based on a reported protocol from Nguyen and coworkers,[116] the redox condensation of **51** with benzylamine (**52**) and elemental sulfur in pyridine as the solvent in the subsequent step provided the desired cyclometalating ligand **40** in 87% yield.[100]

With the benzothiazole ligand **40** in hand, the second cyclometalation step was attempted next. Gratifyingly, the addition of the corresponding ligand **40** to a suspension of the mono-cyclometalated rhodium complex **48a** in a 3:1 mixture of 2-ethoxyethanol and water led to the formation of the coveted tris-heteroleptic complex *rac*-**RhNS1**. However, in addition to the

desired product, these initial conditions also resulted in the formation of the two bis-heteroleptic complexes having two identical cyclometalating ligands. Accordingly, in addition to the formation of *rac*-**RhNS1**, **RhS** and, to a smaller extent, **RhN1** were obtained as side products of the reaction (Table 2, entry 1).

Table 2: Optimization of the Reaction Conditions for the Second Cyclometalation Step.[a]

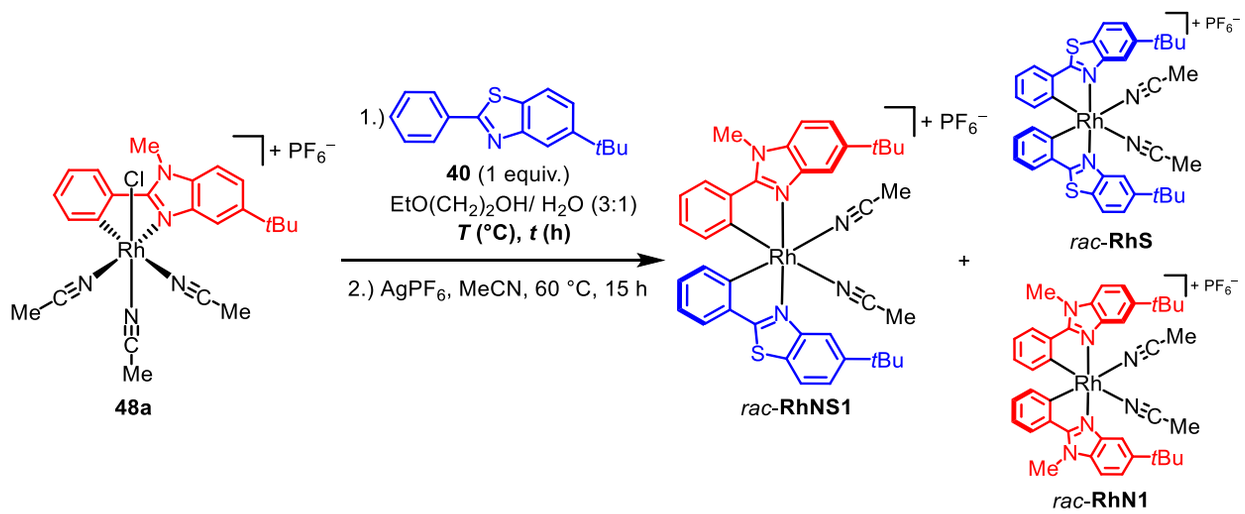

entry	conditions (1st step)		overall yield (%)[b]	ratio *rac*-RhNS1
	T (°C)	*t* (h)		to RhS/RhN1[c]
1	125	5	60	1.7:1
2	80	23	29	4.6:1
3	80	48	44	5.3:1
4	80	72	56	5.6:1
5[d]	80	48	21	0:1

[a]Reaction conditions of the first step: **48a** and **40** (1.00 equiv.) were stirred in 2-ethoxyethanol and water (3:1) (0.05 M) at the indicated temperature for the indicated time under an atmosphere of nitrogen. [b]Isolated yield after the second step. The product was isolated as a mixture of *rac*-**RhNS1** and the bis-heteroleptic complexes **RhS** and **RhN1**. [c]Determined by analysis of the ^{1}H NMR of the isolated mixture of complexes. [d]Sequential addition of ligands. After stirring $RhCl_3 \cdot xH_2O$ with ligand **47a** for 7 h at 150 °C (as shown in Table 1, entry 6), the benzothiazole ligand **40** was added to the same reaction mixture, and the resulting suspension was further stirred at the indicated temperature for the indicated time. Exclusive formation of **RhS**.

Since all three complexes had the same R_f value, they were isolated as a mixture by standard silica gel chromatography, and therefore overall yields are given in Table 2, which were calculated with the molar mass of *rac*-**RhNS1**, as this also represents the average molecular weight of all three bis-cyclometalated complexes. By analyzing the ^{1}H NMR spectra of the

isolated mixtures obtained, the relative amount of each complex was determined via integration of significant signals. Since the corresponding signals of **RhS** and **RhN1** were not baseline separated, only ratios of the tris-heteroleptic target complex to both bis-heteroleptic complexes are reported. For entry 1, the ratio of 1.7:1 corresponds to an approximate by-product yield of 22%. Subsequently, various reaction conditions for the second cyclometalation step were tested in order to improve the yield with respect to the desired complex *rac*-**RhNS1**. Reducing the reaction temperature from 125 °C to 80 °C could significantly enhance the product-to-by-product ratio (entry 2–4) and afforded *rac*-**RhNS1** in a reasonable yield after a prolonged reaction time (entry 4). It is noteworthy, that the desired tris-heteroleptic complex was always formed as the major product of the reaction and thus the formation of a statistical distribution of the complexes was not observed. In an attempt to shorten the reaction sequence by one step, the synthesis of *rac*-**RhNS1** was also investigated via a sequential addition of the two cyclometalating ligands, first of **47a**, followed by the addition of **40**, to a suspension of the rhodium(III) halide. Contrary to expectations, this one-pot approach completely abolished the formation of the desired complex. Instead, only **RhS** was generated and isolated in 21% yield, demonstrating the necessity of the stepwise introduction of ligands starting from rhodium trichloride hydrate and ligand **47a**, as summarized in Scheme 17.

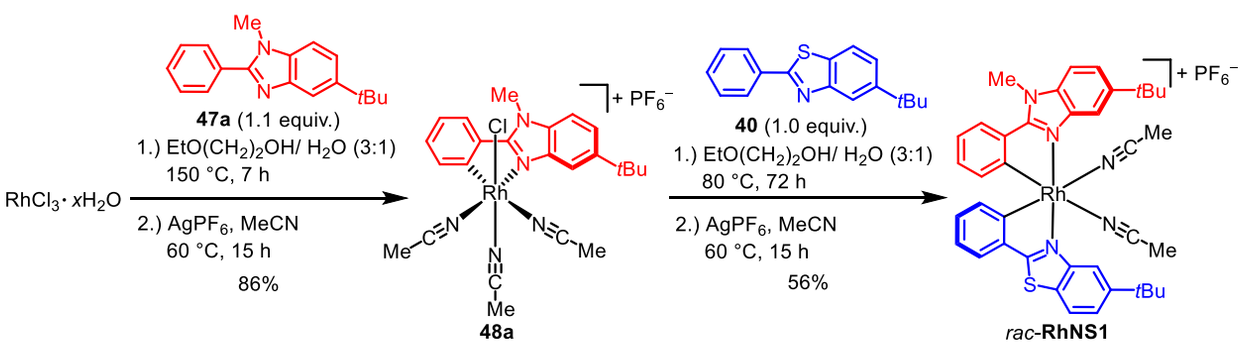

Scheme 17: Optimized conditions for the stepwise synthesis of *rac*-**RhNS1**.

Having established conditions for the synthesis of the racemic catalyst, the next step was to engage in the preparation of the single enantiomers.

3.2.3 Synthesis of an Enantiomerically Pure Tris-Heteroleptic Chiral-at-Rh(III) Catalyst

With *rac*-**RhNS1** in hand, the synthesis of the individual Λ- and Δ-enantiomers was assailed as the next task, following a previously established chiral auxiliary-mediated approach.[98,101,99][117–120] In analogy to the procedure described in Section 3.1.1,[93,100] *rac*-**RhNS1** was first converted with the chiral salicyloxazoline (*S*)-**41**,[101] whose synthesis is depicted in Scheme 18. According to the conditions published by Meggers *et al.*,[100] the condensation of commercially available 2-fluoro-6-hydroxybenzonitrile (**53**) and (*S*)-2-phenylglycinol (*S*)-**54** in toluene under reflux in the presence of a catalytic amount of anhydrous zinc dichloride provided the chiral auxiliary ligand (*S*)-**41** in 95% yield.[100]

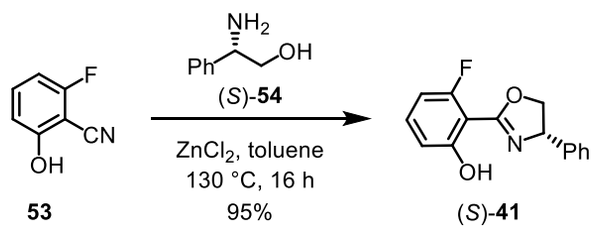

Scheme 18: Synthesis of (*S*)-3-fluoro-2-(4-phenyl-4,5-dihydrooxazol-2-yl)phenol ((*S*)-**41**).[100]

As shown in Scheme 19, the reaction of the racemic catalyst with (*S*)-**41** resulted in the formation of a mixture of four diastereomers. As a consequence of the unsymmetrical nature of the chiral auxiliary, in theory the four stereoisomers Λ-(*S*)-**55a**, Λ-(*S*)-**55b**, Δ-(*S*)-**55a**, and Δ-(*S*)-**55b** can form. Indeed, the diastereomers Λ-(*S*)-**55a**, Λ-(*S*)-**55b** and Δ-(*S*)-**55a** could be resolved by regular silica gel column chromatography to furnish the corresponding diastereomerically pure complexes, while Δ-(*S*)-**55b** was not isolated most likely because it was only formed in trace amounts.

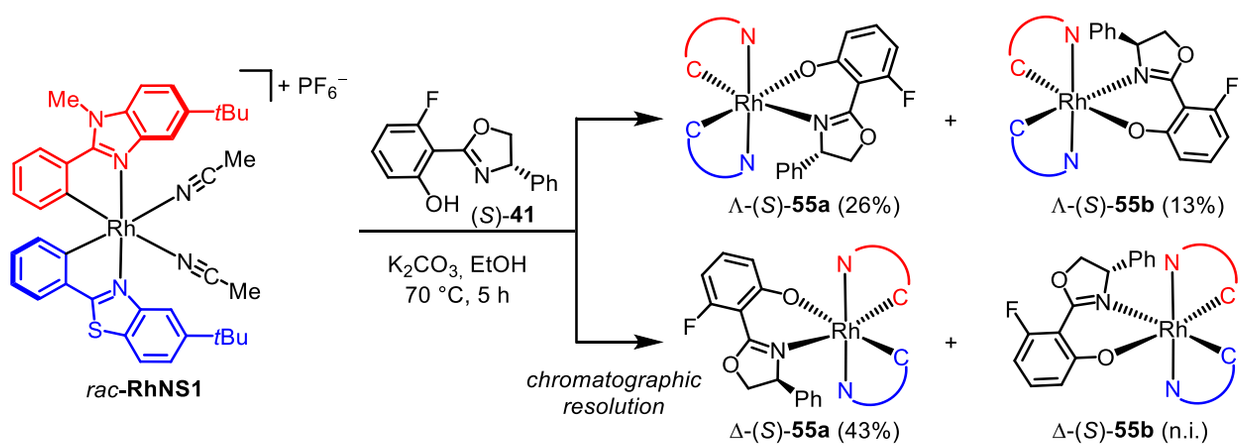

Scheme 19: Synthesis and chromatographic resolution of the chiral auxiliary complexes of *rac*-**RhNS1** with (*S*)-**41** (n.i. = not isolated).

Importantly, the corresponding auxiliary complexes generated from the racemic complexes **RhS** and **RhN1** could easily be separated from the stereoisomers of the desired tris-heteroleptic complex at this stage of the catalyst synthesis. The absolute configurations of the four complexes were assigned on the basis of the obtained crystal structure of Δ-(*S*)-**55a** (Figure 13).

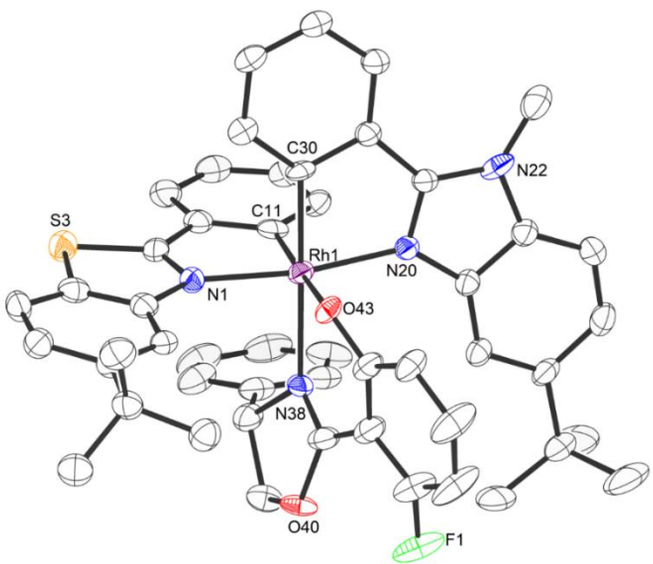

Figure 13: Crystal structure of auxiliary complex Δ-(*S*)-**55a** as an ORTEP drawing with 50% probability thermal ellipsoids. Solvent molecules are omitted for clarity.

The structure of Δ-(*S*)-**55a**, in which the oxazoline nitrogen of (*S*)-**41** is arranged *trans* to the phenyl moiety of phenylbenzimidazole **47a** and the oxygen of (*S*)-**41** *trans* to the phenyl group of phenylbenzothiazole ligand **40**, thus revealed the apparently more favorable orientation of the coordinated chiral auxiliary in **55a** compared to the opposite orientation in **55b**, which consequently was almost not formed. ^{1}H–^{1}H 2D NOESY experiments could additionally confirm the structure obtained for Δ-(*S*)-**55a** in solution and subsequently also helped to elucidate the structure of the predominantly formed complex with metal-centered Λ-configuration (see Section 5.4.2 for more details). Accordingly, the analogous NMR measurements performed for the more stable stereoisomer Λ-(*S*)-**55a** clearly disclosed that the chiral auxiliary possesses the same connectivity as in Δ-(*S*)-**55a**. A similar NOESY experiment for the minor stereoisomer Λ-(*S*)-**55b**, whose configuration was initially only an assumption, could not be performed, since the complex isomerized rapidly to Λ-(*S*)-**55a** in CD_2Cl_2, as confirmed by comparison of the ^{1}H NMR spectra of both compounds, indicating an equilibrium between the two diastereomers (Scheme 20).

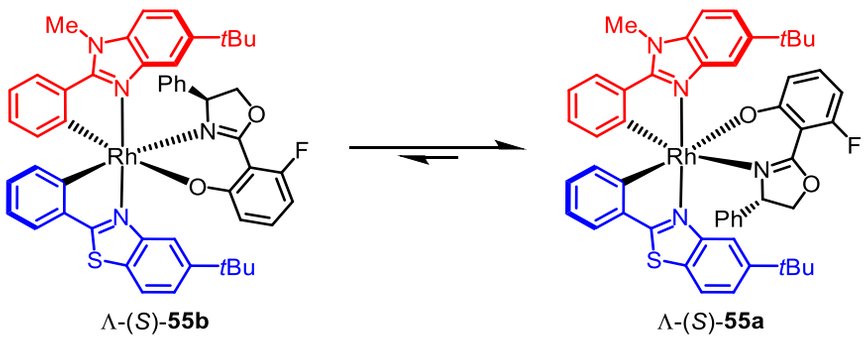

Scheme 20: Equilibrium between Λ-(*S*)-**55b** and Λ-(*S*)-**55a**.

Moreover, the isomerization of Λ-(*S*)-**55b** to Λ-(*S*)-**55a** at room temperature was monitored by recording several ^{19}F NMR spectra of an initially pure sample of Λ-(*S*)-**55b** in CD_2Cl_2 after certain time intervals, as exhibited in Figure 14.

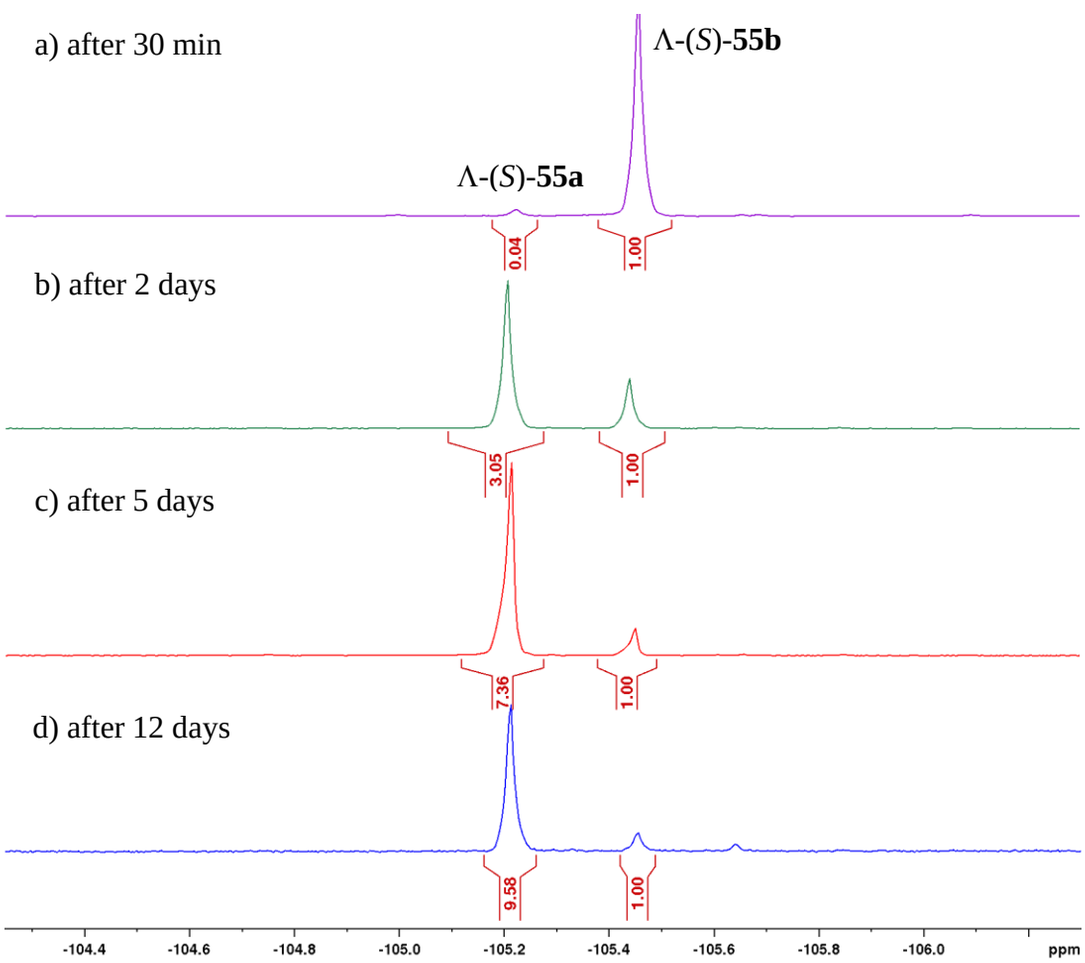

Figure 14: Isomerization of Λ-(*S*)-**55b** to Λ-(*S*)-**55a** traced by ^{19}F NMR spectroscopy (235 MHz, 300 K, CD_2Cl_2). Shown is the comparison of four ^{19}F NMR spectra of the same (and initially pure) sample of Λ-(*S*)-**55b** in CD_2Cl_2, which was repeatedly measured after the specified time intervals (a–d).

Accordingly, traces of the isomerization of Λ-(*S*)-**55b** to Λ-(*S*)-**55a** were already observed after 30 minutes (Figure 14a), while after two days, Λ-(*S*)-**55a** was the predominant species in solution (Figure 14b) with a steadily increasing diastereomeric ratio in favor of the more stable stereoisomer **55a** (Figure 14c and d).

A second experiment which confirmed that both complexes had the same metal-centered configuration was circular dichroism (CD) spectroscopy. Consistently, the CD spectra obtained for the purely separated stereoisomers Λ-(*S*)-**55a** and Λ-(*S*)-**55b**, after each complex had previously been subjected to an acidic cleavage of the coordinated chiral auxiliary (*S*)-**41**, showed that Λ-**RhNS1** was obtained as the product in both cases (Figure 15).

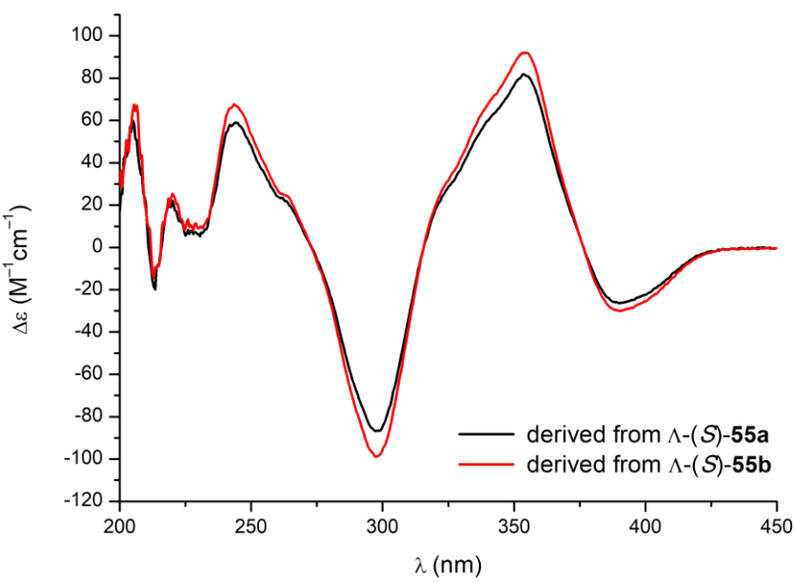

Figure 15: CD spectra (0.2 mM in MeOH) of Λ-(*S*)-**55a** and Λ-(*S*)-**55b** after cleavage of the chiral auxiliary ligand display that both diastereomers have the same metal-centered configuration and consequently led to the formation of Λ-**RhNS1**.

Consequently, Λ-(*S*)-**55a** and Λ-(*S*)-**55b** do not have to be separated from each other and can be isolated as a mixture, which greatly facilitates the resolution of the diastereomeric complexes.

Finally, with the well-resolved and structurally elucidated auxiliary complexes in hand, the second step of the auxiliary-mediated synthesis could be performed. Accordingly, the acid induced substitution of the chiral auxiliary by two acetonitrile ligands with trifluoroacetic acid at slightly elevated temperatures and subsequent counterion exchange with NH_4PF_6 provided the individual enantiomers Λ-**RhNS1** (93%) and Δ-**RhNS1** (>99%) with complete retention of the metal-centered configuration, as shown in Scheme 21. HPLC performed on a chiral stationary phase validated the high enantiomeric purity (>99% ee for each complex) of the tris-heteroleptic rhodium complexes (see Chapter 6.2).

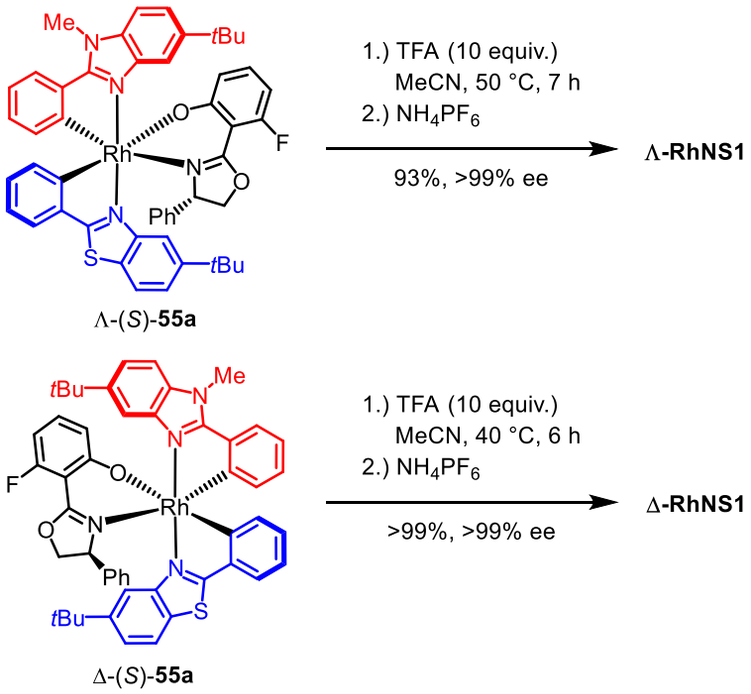

Scheme 21: Acid induced replacement of the chiral auxiliary ligand.

Furthermore, the CD spectra of Λ- and Δ-**RhNS1** could verify their mirror-image structures, as shown in Figure 16.

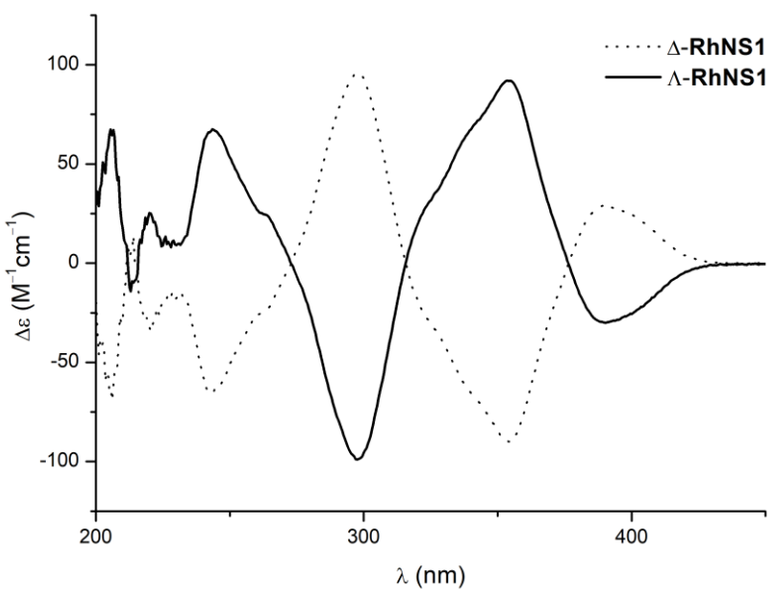

Figure 16: CD spectra (0.2 mM in MeOH) of Λ- and Δ-**RhNS1**.

Conclusively, single crystals of Δ-**RhNS1** suitable for X-ray diffraction could be obtained and the evaluated structure of the final enantiomerically pure tris-heteroleptic complex, whose catalytic properties will be examined in the following section, is depicted in Figure 17.

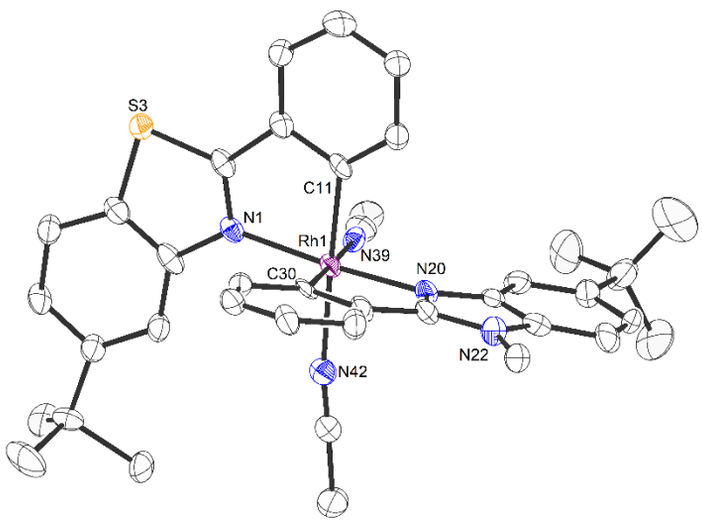

Figure 17: Crystal structure of Δ-**RhNS1** as an ORTEP drawing with 50% probability thermal ellipsoids. The PF_6^- counterion and solvent molecules are omitted for clarity.

3.2.4 Catalytic Application of Λ- and Δ-RhNS1 in Asymmetric [2+2] Photocycloadditions

After an initial screening of diverse catalytic asymmetric transformations, the newly developed chiral complexes Λ- and Δ-**RhNS1** proved to be powerful catalysts for the asymmetric [2+2] photocycloaddition between *α,β*-unsaturated *N*-acyl pyrazoles and alkenes,[96][121,122] and thus this reaction was investigated more closely. As shown in Figure 18, two different reactions were examined and the catalytic performances of the new rhodium complexes Λ- and Δ-**RhNS1** compared with the established bis-heteroleptic catalysts Λ- and Δ-**RhS**.[93] Accordingly, the reaction of *α,β*-unsaturated *N*-acyl pyrazole **56** with 2-phenylpropene (**57**) under irradiation with blue LEDs in the presence of 4 mol% of Λ-**RhNS1** gave the corresponding [2+2] photocycloaddition product **58** in 94% yield and with an essentially complete enantioselectivity of 99% ee. In a control experiment, in which Δ-**RhNS1** was employed as the catalyst instead, the opposite enantiomer of the product was obtained with an identical enantiomeric excess of 99%. Since these results were comparable to those previously reported for Λ- and Δ-**RhS**,[96] a second [2+2] photocycloaddition between the *α,β*-unsaturated *N*-acyl pyrazole **59** and the aliphatic internal alkene cycloheptene (**60**), which had not been reported before, was executed with

Δ-**RhNS1** as the catalyst and provided the desired cyclobutane **61** in a high yield of 98%, with a satisfactory diastereoselectivity and with an excellent enantioselectivity of 99% ee.

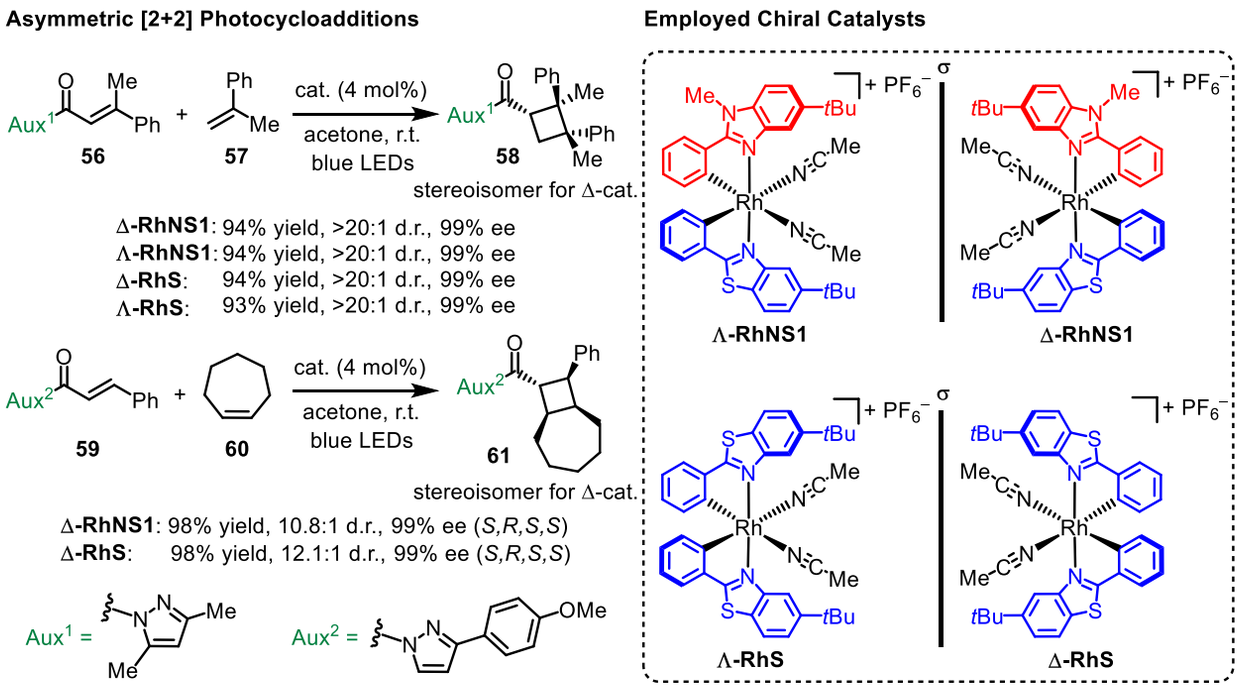

Figure 18: Comparison of the catalytic activities of the catalysts **RhNS1** and **RhS** for the two intermolecular [2+2] photocycloadditions of *α,β*-unsaturated *N*-acyl pyrazoles and alkenes.

The relative and absolute configuration of the cycloaddition product **61** was determined from the corresponding X-ray structure (Figure 19).

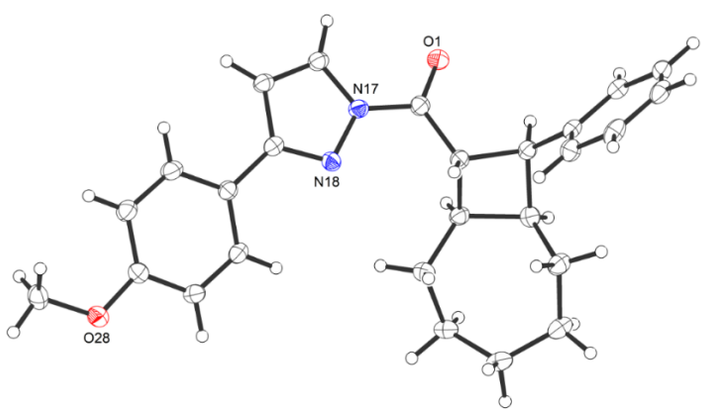

Figure 19: Crystal structure of **61** as an ORTEP drawing with 50% probability thermal ellipsoids.

3.2.5 Conclusions

In conclusion, the first method for the synthesis of a bis-cyclometalated rhodium(III) complex having two different cyclometalating ligands was introduced. The synthesis of this previously inaccessible class of chiral-at-rhodium catalysts is based on a stepwise introduction of the two cyclometalating ligands, which is enabled by the formation of an isolable mono-cyclometalated rhodium(III) species instead of the expected bis-cyclometalated complex in the first step, when a phenylbenzimidazole ligand was employed (see also Chapter 3.1). The stability of this intermediate allowed the incorporation of a different second cyclometalating ligand in a subsequent additional cyclometalation step, thereby providing access to this novel type of tris-heteroleptic bis-cyclometalated rhodium complexes and offering ample opportunities to further expand the structural diversity of chiral-at-metal catalysts in the future. The final enantiomerically pure rhodium catalyst **RhNS1** could be prepared using an established chiral auxiliary-based approach, which afforded the individual Λ- and Δ-enantiomers with excellent enantiomeric purities (>99% ee). Moreover, the high efficiency of the newly developed catalyst for two different [2+2] photocycloadditions could be demonstrated, as the desired cyclobutanes were obtained in high yields (up to 98%) and stereoselectivities (99% ee).

3.3 Chiral Bis(oxazoline) Ligands as C_2-Symmetric Chiral Auxiliaries for the Synthesis of Enantiopure Bis-Cyclometalated Rhodium(III) Complexes

3.3.1 Preparation of Enantiomerically Pure Octahedral Transition Metal Complexes

More than 100 years after Alfred Werner's pioneering contributions to the chemistry and theory of octahedral coordination complexes,[123] extensive research efforts have been devoted to the development of synthetic strategies for the synthesis of nonracemic octahedral transition metal complexes, which occupy a pivotal role as chiral catalysts for the asymmetric synthesis of highly requested optically active compounds in academia and industry.[2] Such chiral catalysts are typically constructed by assembling chiral ligands around a central metal to control the overall chirality of the metal complexes. However, the stereoselective synthesis of the previously introduced class of reactive chiral-at-metal complexes poses a different challenge, as the overall chirality is exclusively the consequence of a stereogenic metal center, with all coordinating ligands being achiral (see Chapter 2 for more details).

While synthetic methods to control the metal-centered configuration with carefully tailored chiral ligands have been well-established,[84–87,124,125] different or modified strategies have to be applied for the preparation of stereogenic-at-metal complexes being devoid of any chirality in the organic ligand sphere. An emerging strategy in this field is the application of chiral auxiliaries to influence the relative and absolute stereochemistry at octahedral metal centers.[98] Reported chiral auxiliary-mediated approaches for the preparation of enantiomerically pure octahedral metal complexes typically exploit one of the following three strategies: diastereoselective crystallization techniques using chiral counterions, the attachment of cleavable chiral linkers to the periphery of coordinating ligands, and the temporary coordination of a monodentate or bidentate chiral ligand whose coordinative strength can be altered.[84–86,98,87,124,125] Meggers and co-workers[99,88] as well as other research groups[117,101,119,126,127] successfully developed and applied such temporarily coordinating chiral bidentate ligands as chiral auxiliaries for the synthesis of nonracemic complexes. A selection of chiral auxiliaries employed for the resolution of metal-centered stereoisomers of bis-cyclometalated iridium and rhodium complexes is exemplarily shown in Figure 20.[88]

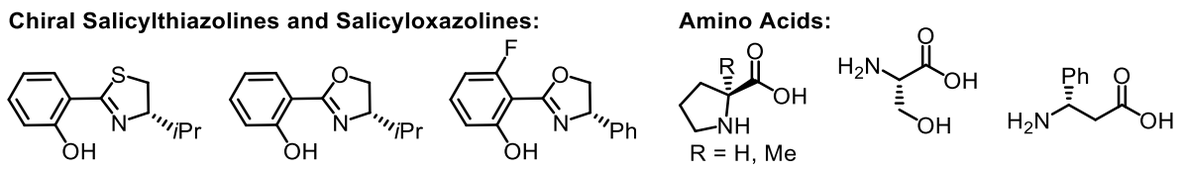

Figure 20: Collection of chiral auxiliaries used for asymmetric coordination chemistry.[88]

In a first step, the bidentate auxiliary ligand coordinates to the central metal thereby either implementing the metal-centered configuration or creating a mixture of two diastereomers that can be resolved. Finally, the chiral ligand can be removed from the metal without leaving a chemical trace, typically by labilization with a Brønsted acid, to give the enantiomerically pure metal complexes without any loss of chiral information, as depicted schematically in Figure 21.

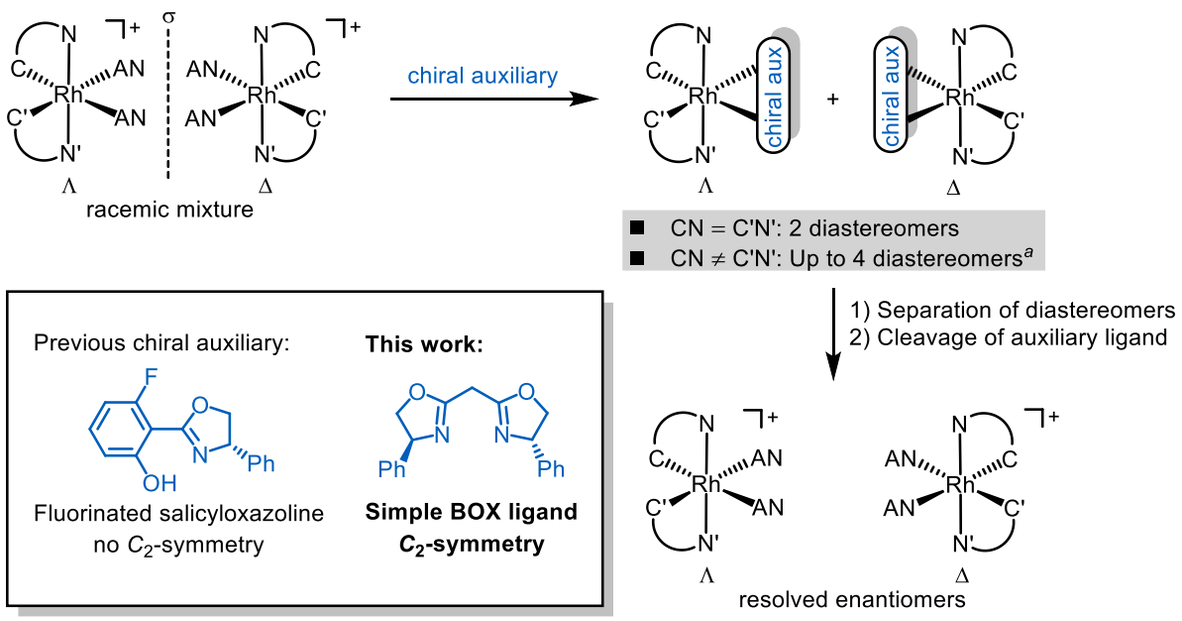

Figure 21: Chiral auxiliaries for the resolution of stereoisomers of bis-cyclometalated rhodium(III) complexes. AN = acetonitrile, CN and C'N' = cyclometalated ligands. [a]Formation of four diastereomers possible with a non-C_2-symmetrical chiral auxiliary such as the shown salicyloxazoline, while only two diastereomers can be formed with a C_2-symmetric chiral auxiliary such as the shown bis(oxazoline) (BOX) ligand.

Previously, a fluorinated salicyloxazoline[101] has been the auxiliary of choice for the preparation of enantiopure bis-cyclometalated rhodium complexes (see also Section 3.1.1 for a detailed example).[93,100] Although this auxiliary proved to be a suitable tool for the synthesis of the corresponding nonracemic bis-heteroleptic complexes, a limitation of its practicability was disclosed for the synthetic method introduced in Chapter 3.2 for the synthesis of bis-cyclometalated rhodium(III) catalysts containing two different cyclometalating ligands, which resulted in the formation of complexes with lower symmetry (CN ≠ C'N').[102] Due to the non-C_2-symmetry of the chiral salicyloxazoline, four diastereomers were obtained upon coordination of the auxiliary to the bis-cyclometalated rhodium complex, two having metal-centered Λ-configuration and two Δ-configuration, which considerably complicated the separation of the stereoisomers. In order to render the preparation of this class of complexes more straightforward, a C_2-symmetric chiral auxiliary was conceived to solve this inconvenience.

Herein, this chapter comprises the development of a corresponding chiral auxiliary-mediated synthesis of bis-cyclometalated rhodium(III) complexes using simple chiral bis(oxazoline) (BOX) ligands as C_2-symmetric chiral auxiliaries.[128] Chiral bis(oxazolines) represent one of the most popular classes of chiral ligands for the synthesis of chiral transition metal complexes, which are used as chiral catalysts for a large variety of asymmetric transformations. On the one hand, this can be attributed to their easy and flexible synthesis and, on the other hand, to their C_2-symmetric scaffold, which reduces the possible number of competing transition states throughout a catalytic cycle.[129–137] However, despite the extensive use of chiral bis(oxazolines) within the realm of asymmetric catalysis, the application of these bidentate ligands as chiral auxiliaries for the synthesis of enantiomerically pure metal complexes has not been reported before.

3.3.2 Chiral Bis(oxazoline) Mediated Synthesis of the C_2-Symmetric Catalysts Λ-/Δ-RhS

In order to determine the suitability of chiral bis(oxazolines) as chiral auxiliaries for the preparation of nonracemic complexes, their application was first investigated for the synthesis of the standard bis-cyclometalated and C_2-symmetric rhodium(III) catalysts Λ- and Δ-**RhS**,[93,82] the synthesis of which was previously introduced in Section 3.1.1 using the chiral salicyloxazoline (*S*)-**41** as the auxiliary ligand.

At the beginning of these studies, the C_2-symmetric chiral bis(oxazoline) ligands (*S*,*S*)-**64** and (*S*,*S*)-**65** were easily prepared in one step by a reported procedure[138] from the respective and readily available β-amino alcohols ((*S*)-**63** or (*S*)-**54**) by condensation with the symmetrically disubstituted diethyl malonimidate dihydrochloride **62**, as shown in Scheme 22.[128]

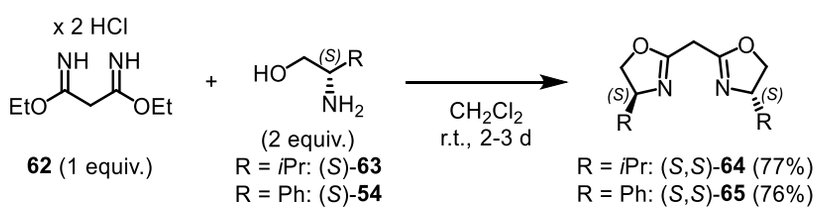

Scheme 22: Synthesis of the chiral bis(oxazoline) ligands (*S*,*S*)-**64** and (*S*,*S*)-**65**.

With the two bis(oxazolines) in hand, the preparation of the corresponding rhodium auxiliary complexes was first explored with the isopropyl-substituted BOX ligand (*S*,*S*)-**64**. Encouragingly, the reaction of *rac*-**RhS** with 1.10 equivalents of this ligand in EtOH in the presence of 3 equivalents of K_2CO_3 gave the anticipated Λ- and Δ-configured auxiliary complexes after only 1 hour of reaction time at room temperature (Scheme 23).

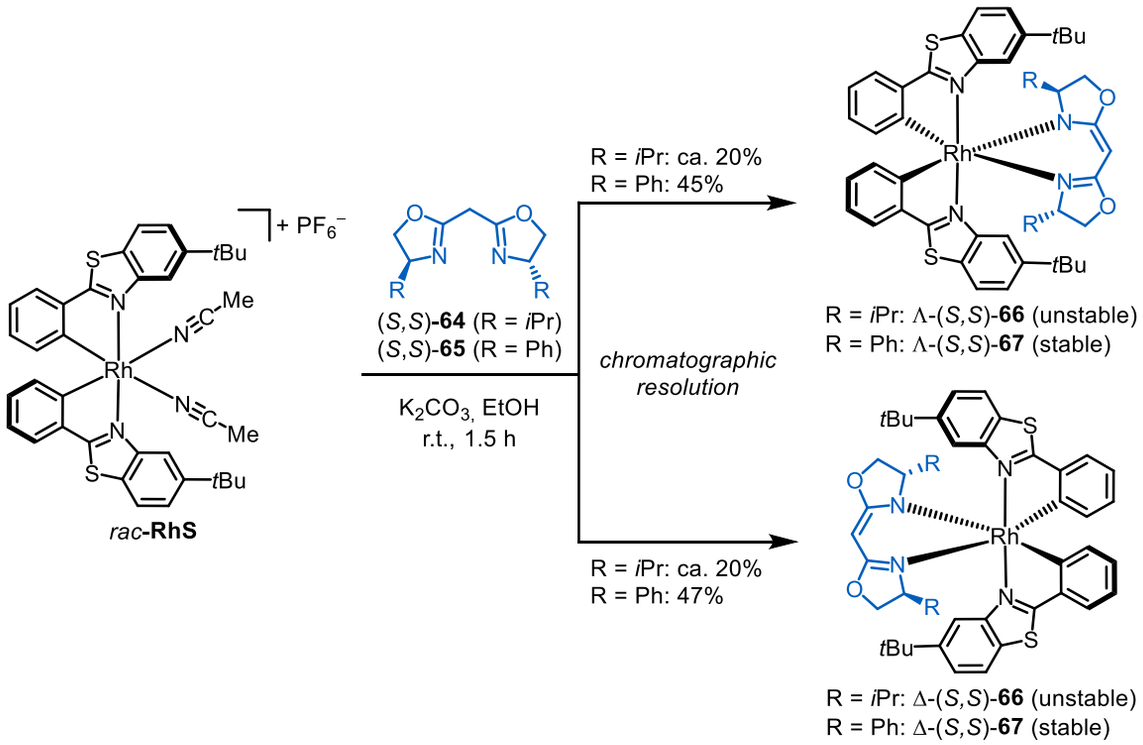

Scheme 23: Application of chiral bis(oxazolines) as chiral auxiliaries for the resolution of metal-centered stereoisomers of the C_2-symmetric catalyst **RhS**.

Analysis of the ^{1}H NMR of the crude material confirmed the formation of a 1:1 mixture of two diastereomers by showing the combination of two different sets of signals and the complete conversion of the racemic starting material (see Section 5.5.2.2). However, when it was attempted to separate the two diastereomeric complexes by column chromatography on previously deactivated silica gel (1% of Et_3N), both complexes largely decomposed during purification, thus resulting in only low isolated yields of about 20% for each of the two stereoisomers Λ- and Δ-(*S*,*S*)-**66** after chromatographic resolution. Hence, the phenyl-substituted BOX ligand (*S*,*S*)-**65** was envisioned to be a promising alternative, as stabilizing π-π-stacking interactions between the phenyl moieties of the bis(oxazoline) and the cyclometalated ligands of the rhodium complex were expected. Following the previously applied conditions, the addition of the respective chiral ligand (*S*,*S*)-**65** to a suspension of *rac*-**RhS** conveniently provided the two phenyl analogues Λ- and Δ-(*S*,*S*)-**67** with conversion being complete after only 1.5 hours. And indeed, the diastereomeric mixture of Λ- and Δ-(*S*,*S*)-**67** could chromatographically be purified on deactivated silica gel without resulting in any degradation of the auxiliary complexes. Accordingly, the individual diastereomers Λ- and Δ-(*S*,*S*)-**67** could be obtained in high yields of 45% and 47%, respectively. Based on the crystal structure of Λ-(*S*,*S*)-**67** presented in Figure 22, the absolute configurations of the complexes could be assigned. As intended, the chiral BOX ligand coordinates as a 6-membered chelate in its monodeprotonated form to give a neutral

rhodium complex. Moreover, the structure shows the anticipated π-π stacking interactions between the two phenyl groups of the BOX ligand (*S*,*S*)-**65** and the benzothiazole moieties of the bis-cyclometalated rhodium complex.

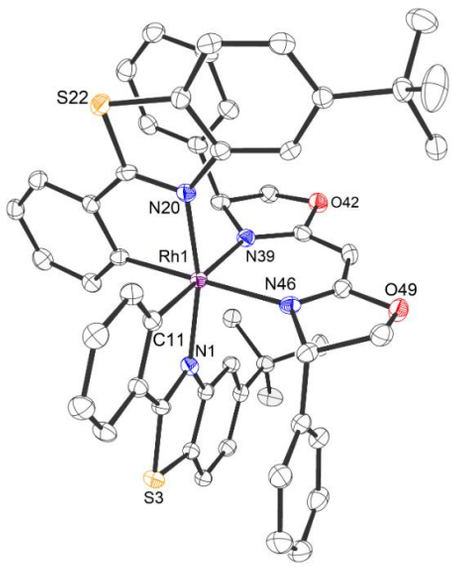

Figure 22: Crystal structure of auxiliary complex Λ-(*S*,*S*)-**67** as an ORTEP drawing with 50% probability thermal ellipsoids. Solvent molecules are omitted for clarity.

For the synthesis of the individual Λ- and Δ-enantiomers of **RhS** from the purely separated stereoisomers, the stereospecific replacement of the chiral bis(oxazoline) by two acetonitrile molecules was examined next. Previously, a coordinated, deprotonated phenolate warranted the reversibility of the auxiliary coordination to the central metal, as its substitution for an achiral ligand could smoothly be mediated in the presence of a strong acid, such as trifluoroacetic acid (TFA). In contrast, the protonation of the here coordinated, monoanionic bis(oxazolinate) ligand could not necessarily trigger its dissociation from the metal center, since these ligands can also bind strongly as a neutral bidentate chelate. With this in mind, the acid induced substitution of the coordinated bis(oxazoline) by two acetonitrile ligands and the subsequent counterion exchange with NH_4PF_6 were initially performed using the previously established conditions. Accordingly, 10 equivalents of trifluoroacetic acid were added to a suspension of either Λ- or Δ-(*S*,*S*)-**67** in acetonitrile and the resulting mixture was stirred at room temperature (Table 3, entry 1). Although TLC indicated completion of the reaction after 1 hour, the ^{1}H NMR of the isolated compound after performance of the subsequent anion exchange and purification of the crude material by regular silica gel chromatography revealed that indeed correspondingly Λ- or Δ-(*S*,*S*)-**67-H** was obtained as the main product of the reaction, while the desired complex Λ- or Δ-**RhS** was only formed in trace amounts (see Section 5.5.2.4 for more details). Since both

monocationic complexes had the same R_f value, they were isolated as a mixture. The relative amount of **RhS** compared to (*S*,*S*)-**67-H** was determined by ^{1}H NMR of the isolated mixture and showed that **RhS** was only formed in a ratio of 1:5.5 under these initial reaction conditions (Table 3, entry 1). Hence, to improve the reaction result with respect to the target complex, various reaction conditions were then tested, which are resumed in Table 3.

Table 3: Optimization of the Acid Induced Cleavage of the Coordinated Auxiliary Ligand.[a]

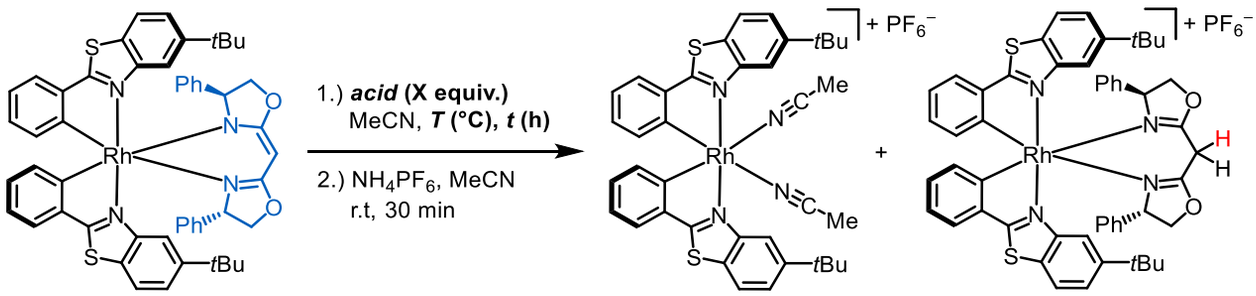

entry	acid (equiv.)	conditions (1st step)		ratio RhS to (*S*,*S*)-67-H[b]
		T (°C)	*t* (h)	
1[c]	TFA (10)	r.t.	1	1:5.5
2	TFA (20)	40	15	1.5:1
3	TFA (20)	50	22	>20:1 (81%)[d]
4	MsOH (5)	0 to r.t.	5	5.2:1
5[e]	MsOH (5)	r.t.	6	14:1
6[e]	MsOH (10)	r.t.	6	>20:1 (98%)[d]

[a]Reaction conditions of the first step: Λ- or Δ-(*S*,*S*)-**67** was dissolved in MeCN (0.04 M), the indicated acid (indicated equiv.) was added in one portion and the resulting solution was stirred at the indicated temperature for the indicated time under an atmosphere of nitrogen. [b]Ratios were determined by ^{1}H NMR after column chromatographic purification of the crude material obtained after the second step. Isolated yields are only provided, if the conversion to Λ-/Δ-**RhS** was complete. [c]Λ-(*S*,*S*)-**69** was employed (synthesis see Section 3.3.3). [d]Isolated yields of **RhS** are provided in brackets. [e]MsOH was added at 0 °C and the resulting solution was stirred for further 15 min at 0 °C before the ice bath was removed.

Notably, increasing the amount of TFA to 20 equivalents in addition to an extension of the reaction time and performance of the reaction at elevated temperature could significantly enhance the obtained ratio in favor of the desired complex, with **RhS** now being formed as the major product (entry 2). Finally, conduction of the reaction at 50 °C for 22 hours led to a complete dissociation of the coordinated bis(oxazoline) ligand from the central metal, thus providing **RhS**

as the only product of the reaction in 81% isolated yield after chromatographic purification. Alternatively, the application of 5 equivalents of methanesulfonic acid (MsOH) instead of TFA already allowed the transformation to proceed at room temperature in a considerably shorter reaction time thereby also resulting in reasonable product to by-product ratios (entry 4 and 5). By adjusting the amount of MsOH added to 10 equivalents, the individual enantiomers Λ-**RhS** (entry 6) and Δ-**RhS** could be obtained after 6 hours with complete retention of the absolute configuration in excellent yields of 98% and 99%, respectively, as summarized in Scheme 24.

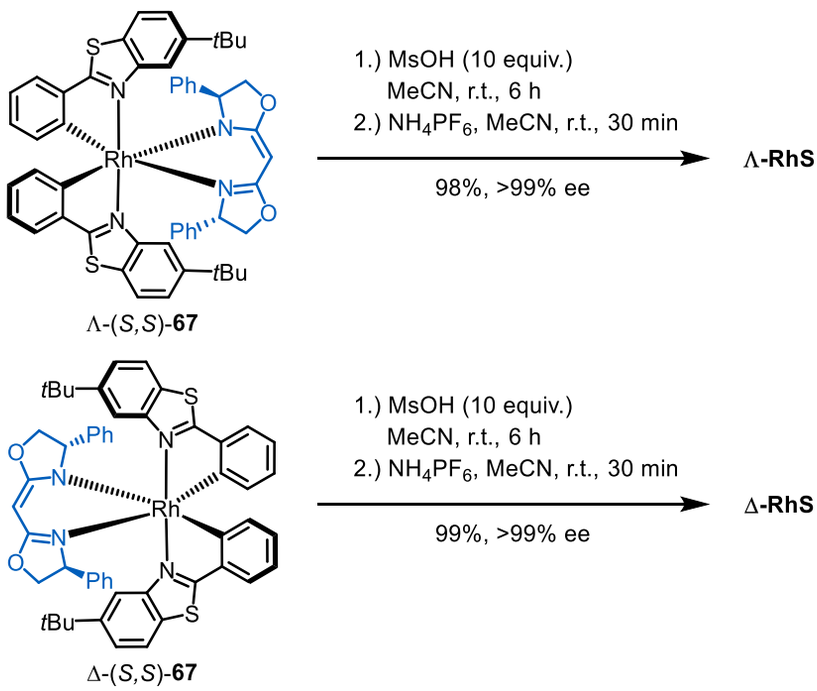

Scheme 24: Optimized conditions for the stereospecific auxiliary removal.

Enantiomeric excess was established by HPLC analysis on a chiral stationary phase and validated the high enantiopurity of more than 99% ee for each of the two enantiomers, as illustrated in Figure 23.

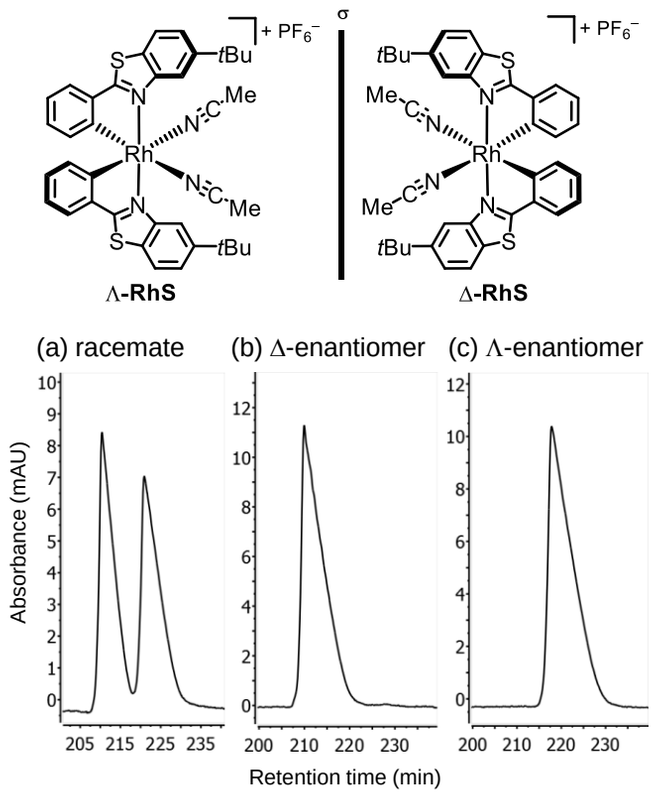

Figure 23: HPLC traces on a chiral stationary phase: a) Racemic complex **RhS** as a reference; b) Δ-Enantiomer of **RhS** synthesized using (*S*,*S*)-**65** as the chiral auxiliary; c) Λ-Enantiomer of **RhS** synthesized using (*S*,*S*)-**65** as the chiral auxiliary. HPLC conditions: Daicel Chiralpak® IB-N5 column, 250 × 4.6 mm, absorbance at 254 nm, H_2O + 0.1% TFA/MeCN = 60:40 to 50:50 in 180 min, 50:50 maintained until 240 min, gradient elution, flow rate 0.6 mL/min, 25 °C.

3.3.3 Bis(oxazoline) Mediated Synthesis of the Non-*C*$_2$-Symmetric Catalysts Λ-/Δ-RhNS2

Having established the conditions for the chiral bis(oxazoline) mediated synthesis of nonracemic rhodium(III) catalysts on the basis of the bis-cyclometalated and *C*$_2$-symmetric complex **RhS**, the viability of the new strategy for the related synthesis of an enantiomerically pure non-*C*$_2$-symmetric rhodium complex containing two different cyclometalating ligands was then investigated. In the previous Chapter 3.2, the synthesis of such a complex was introduced, which contained in addition to a cyclometalated 5-*tert*-butyl-1-methyl-2-phenylbenzimidazole, an analogous 5-*tert*-butyl-2-phenylbenzothiazole ligand as the second cyclometalating component.[102] As a variation of this initial design, the synthesis of a sterically more demanding derivative was envisioned, in which the *tert*-butyl group of the priorly employed benzothiazole ligand should be replaced by a more bulky adamantyl group, thus providing a complex with different steric demand in close proximity to the substrate coordination sites. To this end, 5-(adamantan-1-yl)-2-phenylbenzothiazole (**68**) was prepared in five steps following a previously

reported synthetic route by Meggers and co-workers (see Section 5.5.1 for more details).[139] Subsequently, the second cyclometalation step of the mono-cyclometalated rhodium complex **48a** with the synthesized ligand **68** was carried out according to the elaborated conditions in Chapter 3.2, whereby the desired racemic complex *rac*-**RhNS2** was formed smoothly and was isolated as before along with the corresponding bis-heteroleptic by-products in an overall yield of 66% yield (Scheme 25).

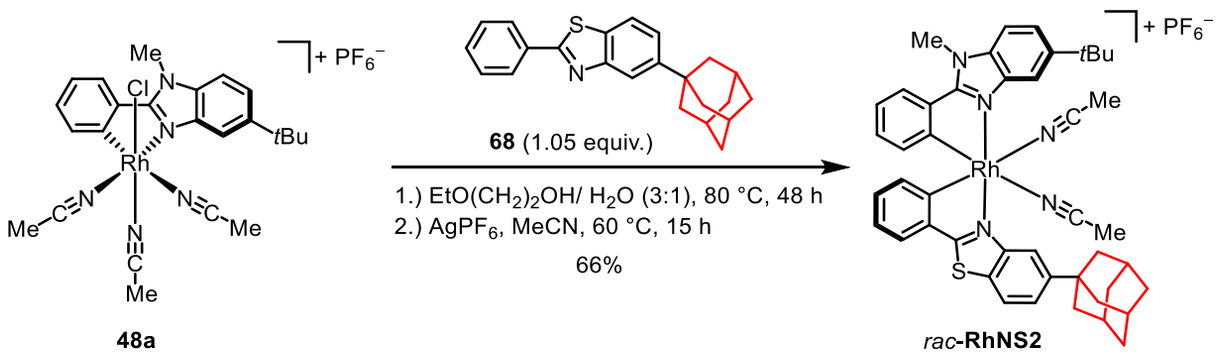

Scheme 25: Synthesis of the sterically more encumbered rhodium complex *rac*-**RhNS2**.

With the racemic catalyst in hand, the chiral bis(oxazoline) based synthesis of the respective single enantiomers of **RhNS2** was endeavored next. Thus, *rac*-**RhNS2** was reacted with BOX ligand (*S*,*S*)-**65**, which, as expected, led to the formation of only two diastereomeric complexes due to the C_2-symmetry of the chiral auxiliary ligand (Scheme 26a). Resolution of the two complexes by silica gel chromatography conveniently furnished the pure diastereomers Λ-(*S*,*S*)-**69** (44%) and Δ-(*S*,*S*)-**69** (45%), whereby it is important to note that the corresponding auxiliary complexes, which were formed from the bis-heteroleptic by-products of the previous step with (*S*,*S*)-**65**, were readily separable from the stereoisomers of the desired complex **RhNS2**, since they greatly differed in their R_f values. In addition, Scheme 26b images the chromatographic resolution of the desired tris-heteroleptic stereoisomers by showing two distinct and well pre-separated bands on the silica gel column, with the Λ-isomer eluting first as a pale yellow band, followed by the elution of Δ-(*S*,*S*)-**69** as the second and clearly visible, darker yellow band, thus highlighting the convenience of the present methodology.

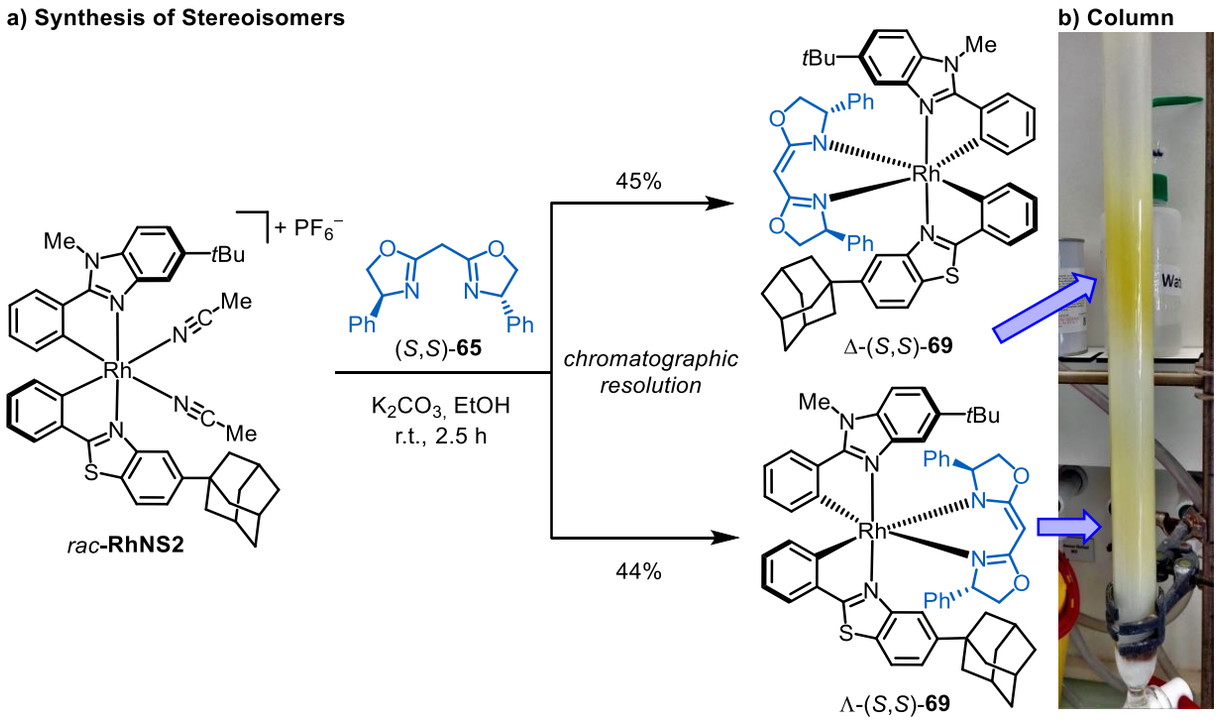

Scheme 26: a) Chiral bis(oxazoline) mediated synthesis of chromatographically separable stereoisomers of the non-C_2-symmetric catalyst **RhNS2**; b) Column chromatographic separation of the two diastereomers.

Configurations of the complexes obtained were assigned with reference to the obtained crystal structure of Λ-(*S*,*S*)-**69**, which is exhibited in Figure 24.

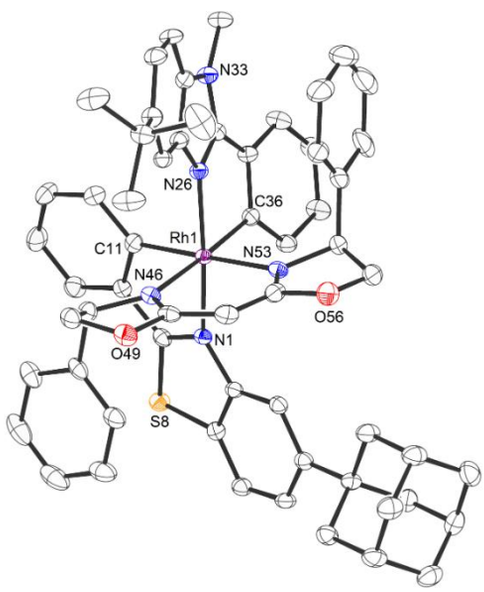

Figure 24: Crystal structure of auxiliary complex Λ-(*S*,*S*)-**69** as an ORTEP drawing with 50% probability thermal ellipsoids. Solvent molecules are omitted for clarity.

In the final step, the acid induced replacement of the coordinated bis(oxazoline) ligand with MsOH, followed by counterion exchange with NH_4PF_6 according to the optimized conditions of Section 3.3.2 afforded the enantiomerically pure tris-heteroleptic complexes Λ-**RhNS2** and Δ-**RhNS2** in high yields of 95% for each complex with retention of the metal-centered configuration (Scheme 27). As expected, both enantiomers exhibit mirror-image circular dichroism (CD) spectra, as shown in Figure 106 (Chapter 6.3). Since a satisfactory separation of the two enantiomers Λ- and Δ-**RhNS2** could not be achieved by HPLC analysis on a chiral stationary phase, the individual enantiomers were converted back into Λ- and Δ-(*S*,*S*)-**69**, respectively, to verify the enantiomeric purity via determination of the diastereomeric ratio from the ^{1}H NMR of the crude materials. Hereby, Λ- as well as Δ-(*S*,*S*)-**69** were obtained with a d.r. of more than 20:1 (see Section 5.5.2.5, Figure 50).

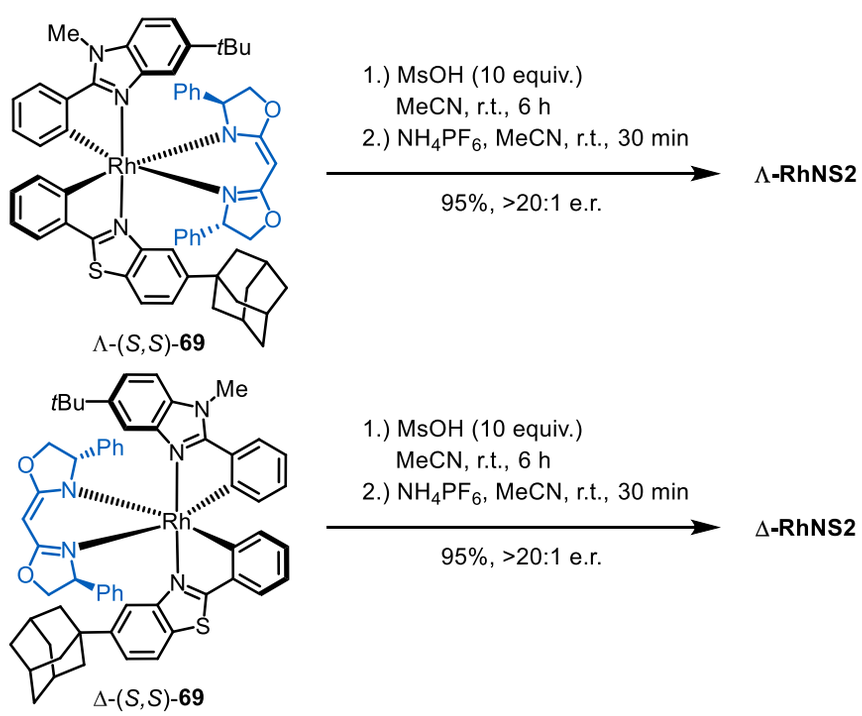

Scheme 27: MsOH-induced dissociation of the coordinated chiral auxiliary.

3.3.4 Conclusions

In summary, the first auxiliary-mediated strategy for the preparation of nonracemic bis-cyclometalated rhodium(III) catalysts was developed which is based on the application of a simple chiral bis(oxazoline) ligand as the chiral auxiliary. Chiral bis(oxazolines) were readily accessible via a single step procedure and the feasibility of the new auxiliary approach was then

first demonstrated for the synthesis of the established C_2-symmetrical benzothiazole complex Λ- and Δ-**RhS**. Accordingly, a pair of two chromatographically stable and separable diastereomers was generated in the first step, by reacting the racemic complex *rac*-**RhS** with a phenyl-substituted BOX ligand. In the subsequent second step, the critical acid-mediated dissociation of the coordinated bis(oxazoline) succeeded despite the ability of the bidentate ligand to bind in its neutral form, when methanesulfonic acid was employed as the proton source. Hereby, the final catalysts Λ- and Δ-**RhS** could efficiently be obtained with excellent optical purities (>99% ee for each enantiomer) and in high isolated yields (95% for each complex). Having evidenced the workability of the elaborated method with the C_2-symmetric catalyst, the studies were finally complemented by the preparation of a new derivative of a bis-cyclometalated and non-C_2-symmetric rhodium complex Λ- and Δ-**RhNS2** bearing in addition to the previously employed 5-*tert*-butyl-1-methyl-2-phenylbenzimidazole, a sterically highly hindered 5-(adamantan-1-yl)-2-phenylbenzothiazole as the second cyclometalating ligand. Since these tris-heteroleptic complexes are inherently of lower symmetry, the particular advantage of the C_2-symmetrical auxiliary is revealed. It reduces the number of possible diastereomers upon coordination to the metal complex to only two, which substantially simplifies the resolution of the metal-centered stereoisomers and renders the preparation of this sort of catalysts less time-consuming. Consequently, the newly developed auxiliary-based protocol using chiral bis(oxazolines) constitutes a considerable improvement of the synthetic method presented in Chapter 3.2 and also demonstrates that chiral BOX ligands represent an economical tool for the synthesis of enantiomerically pure bis-cyclometalated rhodium complexes that have extensively been applied as chiral transition metal catalysts in recent years.[73–77,81,82,88,139–148]

3.4 Supplementing the Class of Bis-Cyclometalated Tris-Heteroleptic Chiral-at-Rhodium(III) Catalysts with a Pyrazole Derivative

3.4.1 Motivation for the Structural Modification with a Cyclometalated Pyrazole Ligand

Progress in asymmetric catalysis benefits from the development of new types of chiral catalysts with potentially novel catalytic properties. In recent years, Meggers and co-workers have disclosed the merit of chiral-at-metal catalysts, in which two inert and achiral cyclometalating ligands implement a stereogenic metal center (see Chapter 2). In particular, the developed bis-cyclometalated rhodium(III) complexes were found to be excellent chiral Lewis acid catalysts.[77,88,82] However, in almost all reports by the Meggers group and others, the two cyclometalating ligands are identical and thus create a C_2-symmetrical geometry.[77,88,82,148–150]

In the course of this thesis, access was granted to a previously elusive class of chiral-at-rhodium(III) catalysts containing two different cyclometalating ligands, which was enabled by the cyclometalation of a single phenylbenzimidazole ligand in the first step, followed by the incorporation of a second cyclometalating ligand of the same basic structure in the second step, namely a related phenylbenzothiazole (see Chapter 3.2 and 3.3).[102][128] Thus, the overall topology of the synthesized complexes still closely resembled that of previous chiral rhodium complexes introduced by the Meggers laboratory.[77,93] However, in order to discover chiral metal complexes with new structural and electronic features, the development of structurally more diverse or even bifunctional chiral catalysts is desirable and the methodology for the synthesis of tris-heteroleptic bis-cyclometalated rhodium(III) complexes presented in the previous chapters potentially provides numerous possibilities to expand the chemical space of this type of chiral catalysts, relying only on the initial introduction of a benzimidazole ligand, whereas the second ligand can be of a completely different nature. Along these lines, the focus of this chapter is directed towards the design of two new tris-heteroleptic rhodium complexes containing in addition to the cyclometalated benzimidazole ligand either a cyclometalated 3,5-diphenylpyrazole ligand or a related but sterically demanding derivative bearing a 2,4,6-trimethylphenyl (mesityl) moiety on the pyrazole nitrogen, which is supposed to create a considerable steric hindrance on one side of the catalyst active site (Figure 25). As an inspiration for these designs served the complexes displayed in Figure 26. Meggers and co-workers have had great success with coordinated pyrazole ligands in the past.[151–155] Figure 26a shows an example of a member of the previously developed generation of rigid and substitutionally inert chiral-at-metal complexes.[152] In these non-covalent catalysts, catalysis is entirely mediated by the organic ligand sphere, while the central metal serves as a structural anchor point and provides octahedral centrochirality as the

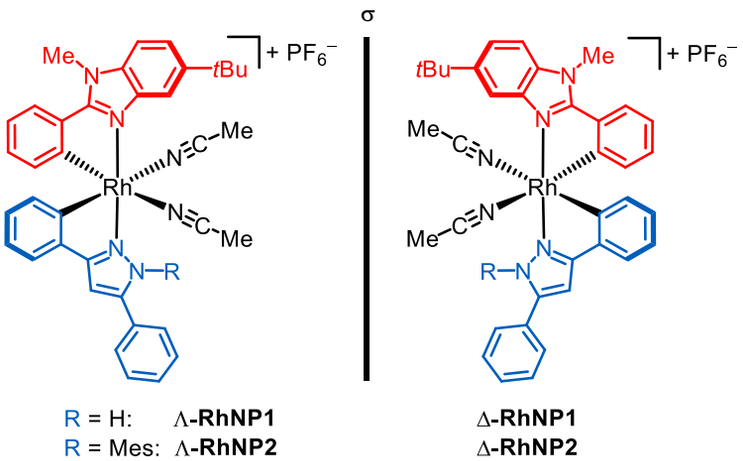

Figure 25: Envisaged synthesis of bis-cyclometalated chiral-at-rhodium catalysts bearing a phenylpyrazole ligand (with R = H, Mes) as the second cyclometalating ligand.

exclusive source of chirality.[156] In this design, the bis-cyclometalated iridium(III) complexes contain a bidentate, non-cyclometalated pyrazole ligand as a third chelating ligand, which can activate a substrate by double hydrogen-bonding.[151,152,155] Alternatively, a corresponding deprotonated pyrazolato complex was demonstrated to serve as a highly effective chiral Brønsted base/H-bonding dual activation asymmetric catalyst, thus operating in a bifunctional mode of action.[153,154] An iridium-based metal-ligand cooperative bifunctional catalyst **71** has been reported by Ikariya and Kuwata in 2010,[157] in which a cyclometalated 3,5-diphenyl-1*H*-pyrazole ligand (**70**) provides a protic NH-functionality in *β*-position to the metal, thus having the ability to either donate a proton or an H-bond (Figure 26b).[158] Ligand deprotonation thereby affords a corresponding Brønsted basic pyrazolato complex (**B**), which can reversibly become protonated to the pyrazole complex (**A**), which thus represent an interconvertible couple.

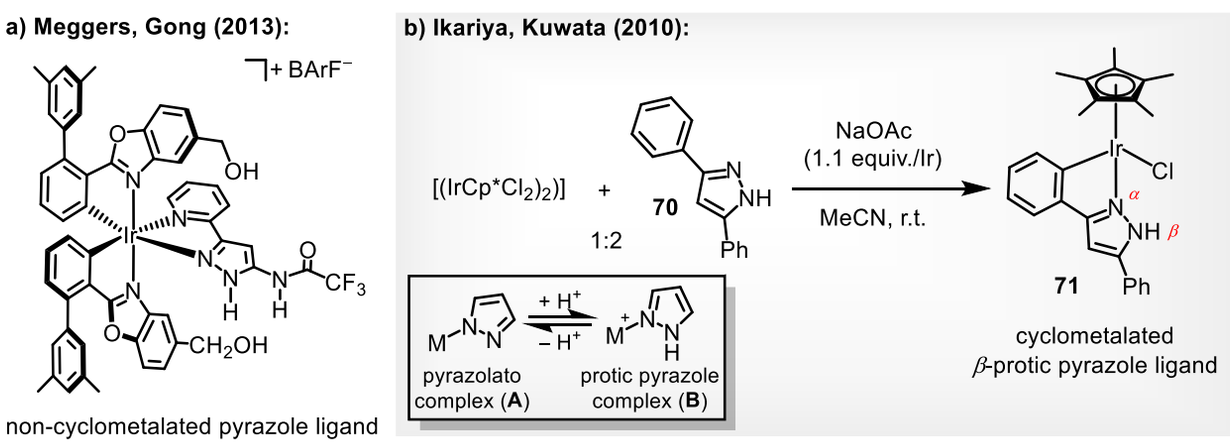

Figure 26: a) Substitutionally inert chiral-at-iridium(III) catalyst containing a non-cyclometalated pyrazole ligand; b) Synthesis of a cyclometalated *β*-protic pyrazole complex and reversible protonation of the *β*-nitrogen. BArF = tetrakis[(3,5-bis(trifluoromethyl)phenyl]borate.

3.4.2 Synthesis of the Enantiomerically Pure Protic Pyrazole Complex RhNP1

Motivated by these works and with the intention of further broadening the scope of tris-heteroleptic bis-cyclometalated chiral-at-rhodium(III) catalysts, the synthesis of a corresponding derivative containing a 3,5-diphenylpyrazole ligand (**70**) as the second cyclometalating ligand was attempted first.

Following the conditions previously established for the synthesis of the catalysts **RhNS1/2**, the mono-cyclometalated rhodium complex **48a** was initially heated with 1.2 equivalents of the commercially available ligand **70** in a 3:1 mixture of 2-ethoxyethanol and water at different temperatures (60/80/100 °C), followed by reaction with $AgPF_6$ in acetonitrile in the second step (Scheme 28, Conditions 1). Although the target complex *rac*-**RhNP1** was formed, the reaction proceeded rather sluggishly, resulting in the formation of considerable amounts of by-products and leading to non-reproducible yields of the desired tris-heteroleptic complex. Hence, the subsequent cyclometalation was performed according to a different protocol, involving heating **48a** and **70** at 80 °C in the presence of 1.1 equivalents of NaOAc in acetonitrile for 24 hours, which smoothly provided the coveted complex *rac*-**RhNP1** in 68% isolated yield, without the requirement of the subsequent addition of a silver salt to ensure removal of the residual coordinated chloride ligand (Scheme 28, Conditions 2). Notably, the bis-cyclometalated bis-heteroleptic rhodium complexes containing either only the phenylbenzimidazole or the phenylpyrazole ligand were not formed using these conditions. Moreover, an extension of the reaction time to 48 hours under otherwise identical reaction conditions gave *rac*-**RhNP1** in a similar yield of 67%, thus revealing no benefit of prolonged reaction times.

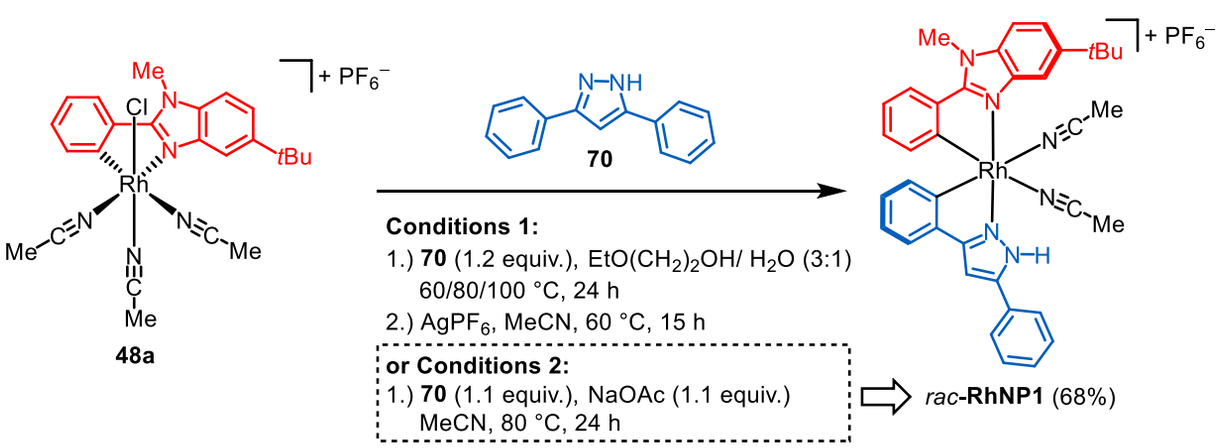

Scheme 28: Cyclometalation of **48a** with 3,5-diphenylpyrazole (**70**) using different conditions.

As illustrated in Figure 27, a crystal structure of the racemic complex *rac*-**RhNP1** could be obtained and confirmed the successful incorporation of the protic pyrazole ligand, which shows a

low-field NH-singlet at 11.81 ppm in the ^{1}H NMR spectrum that is comparable to the corresponding chemical shift of 11.58 ppm[157] exhibited by Ikariya's complex **71** (Section 3.4.1).

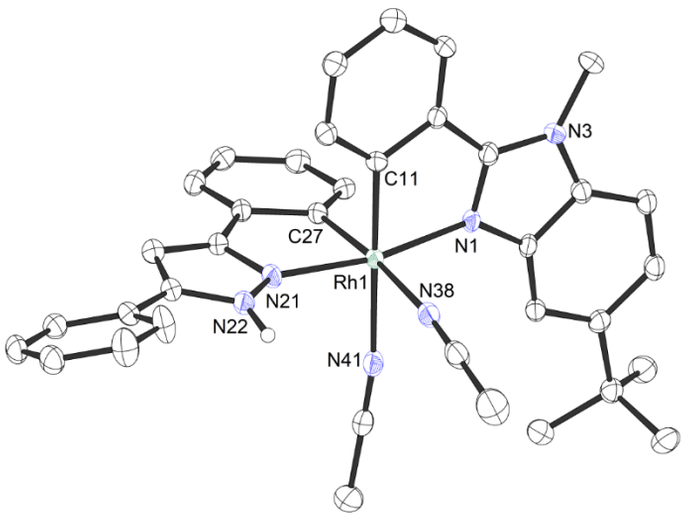

Figure 27: Crystal structure of *rac*-**RhNP1** as an ORTEP drawing with 50% probability thermal ellipsoids. The PF_6^- counterion and solvent molecules are omitted for clarity.

For the subsequent step, the previously elaborated chiral bis(oxazoline) mediated strategy was applied to the synthesis of the single Λ- and Δ-enantiomers of the catalyst. Accordingly, *rac*-**RhNP1** was first reacted with the phenyl-substituted BOX ligand (*S*,*S*)-**65** in the presence of an excess of K_2CO_3 (Scheme 29, Conditions 1). Since TLC showed no conversion of the racemic starting material after 1 hour at room temperature, the reaction mixture was further stirred at a slightly elevated temperature of 40 °C. However, the formation of a diastereomeric mixture of complexes could still not be observed. Instead, analysis of the ^{1}H NMR of the crude material revealed the decomposition of the complex by showing a complicated mixture of species. Noticeably, the ^{1}H spectrum no longer contained a characteristic low-field shifted singlet for the protic NH-group, indicating the deprotonation of the cyclometalated pyrazole ligand. In a second attempt, the reaction was thus initially performed in the absence of a base, which conveniently provided a 1:1 mixture of two diastereomers (Λ- and Δ-(*S*,*S*)-**72-H**), with the conversion of the racemic starting material being complete, as confirmed by ^{1}H NMR of the crude reaction mixture (Scheme 29, Conditions 2). In order to generate a neutral pair of stereoisomers (Λ- and Δ-(*S*,*S*)-**72**) in the second step, the mixture obtained was redissolved in EtOH and only 1.05 equivalents of K_2CO_3 were added to deprotonate the coordinated bis(oxazoline) ligand. But as before, this only resulted in the decomposition of the two complexes, thus revealing the addition of the base as the critical parameter of the reaction as well as the apparently higher

acidity of the NH-group of the cyclometalated pyrazole ligand compared to the coordinated auxiliary (*S*,*S*)-**65**.

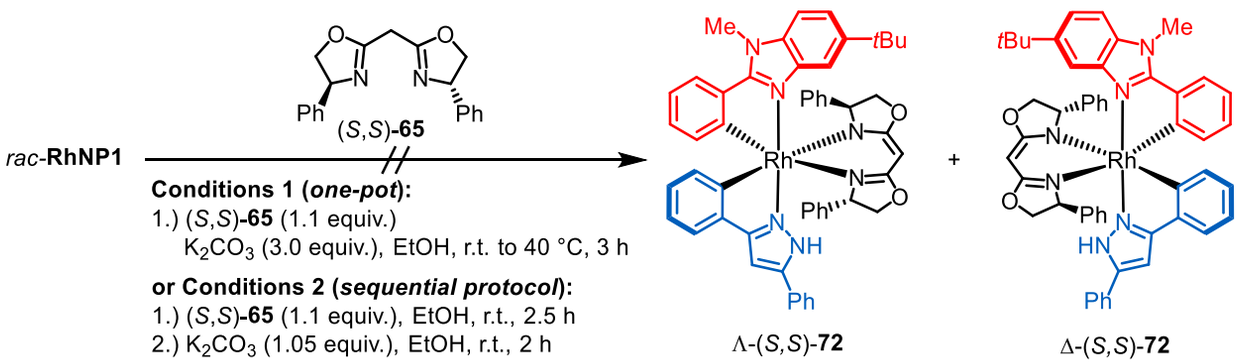

Scheme 29: Synthesis of rhodium auxiliary complexes using (*S*,*S*)-**65** as the chiral auxiliary.

Since the chromatographic resolution of neutral stereoisomers is much more feasible for practical reasons, the preparation of a more acidic chiral bis(oxazoline) was sought to solve this problem. In 1993, Corey and Wang first reported the synthesis of more acidic cyanobisoxazolines,[159] which were readily accessible from the non-substituted, methylene-bridged bis(oxazolines) by treatment with *n*-butyllithium in the presence of tetramethylethylenediamine (TMEDA) in the first step, followed by the subsequent addition of *p*-toluenesulfonyl cyanide (*p*TosCN) to the same reaction mixture. Inspired by this work, (*S*,*S*)-**65** was converted into the corresponding nitrile-substituted ligand (*S*,*S*)-**73** in 91% yield, as shown in Scheme 30.

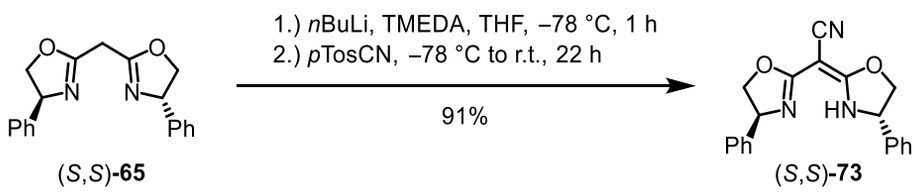

Scheme 30: Sequential synthesis of the more acidic cyanobisoxazoline ligand (*S*,*S*)-**73**.

Fortunately, the addition of 1.1 equivalents of this ligand and equimolar amounts of K_2CO_3 to a suspension of *rac*-**RhNP1** in EtOH led to the formation of the desired Λ- and Δ-configured auxiliary complexes with conversion being complete after 6 hours at room temperature (Scheme 31). ^{1}H NMR of the crude mixture affirmed the complete consumption of the racemic complex as well as the 1:1 generation of the two stereoisomers Λ- and Δ-(*S*,*S*)-**74**. Both complexes exhibit a low-field singlet at 12.63 ppm (Λ) and 9.57 ppm (Δ) for the intact NH-functionality of the pyrazole ligand, accordingly the modified auxiliary ligand could meet the expectations. Subsequent resolution of the diastereomeric mixture of complexes by regular silica gel chromatography conveniently gave the respective diastereomers Λ-(*S*,*S*)-**74** (50%) and

Δ-(*S*,*S*)-**74** (45%). Importantly, the assignment of the absolute metal-centered configurations in this section remains an assumption based on the experience, that the Λ-stereoisomer previously always eluted from the silica gel column first when auxiliaries with (*S*)-configuration were used. However, this has yet to be confirmed by a crystal structure of one of the auxiliary complexes or one of the final enantiomerically pure complexes Λ- or Δ-**RhNP1**.

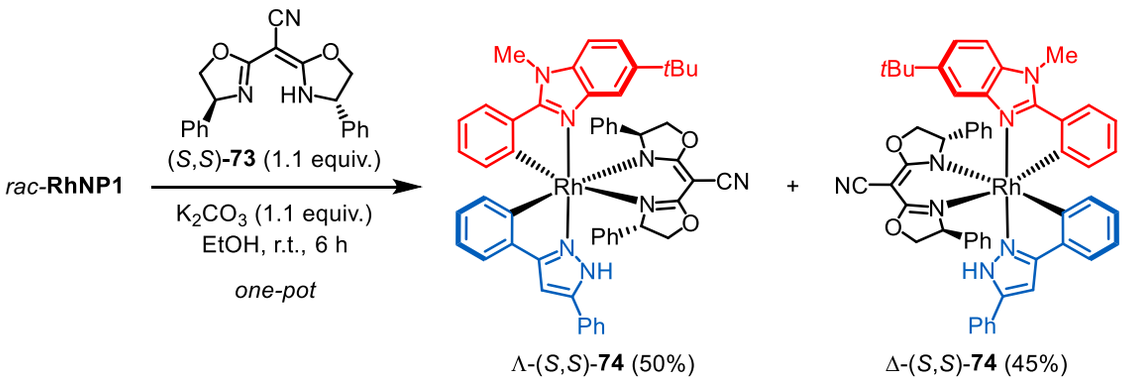

Scheme 31: Synthesis of metal-centered stereoisomers of **RhNP1** with nitrile-modified (*S*,*S*)-**73** as the chiral auxiliary.

With the individual diastereomers in hand, the next step was to proceed with the acid induced cleavage of the cyanobisoxazoline ligand (*S*,*S*)-**73**, followed by counterion exchange with NH_4PF_6. To this end, 20 equivalents of TFA were added to a suspension of Λ- or Δ-(*S*,*S*)-**74** in acetonitrile and the resulting reaction mixture was stirred for 17 hours at room temperature (Table 4, entry 1). Since the desired complex Λ-/Δ-**RhNP1** and Λ-/Δ-(*S*,*S*)-**74-H** have the same R_f value, the progress of the reaction could not be monitored by TLC (compare with the procedure described in Section 3.3.2). Instead, the reaction result was validated after performance of the second step and chromatographic purification of the crude material. Analysis of the ^{1}H NMR then revealed whether the coordinated auxiliary ligand could successfully be removed or whether a mixture of the two complexes was isolated. Determination of the relative amount of each complex by integration of baseline separated signals in the ^{1}H NMR thus showed, that the target complex **RhNP1** was only formed in a ratio of 1.3:1 under these initial conditions. Instead, following the previously optimized conditions for the acid-mediated substitution of the standard methylene-bridged BOX ligand (*S*,*S*)-**65**, namely by adding 10 equivalents of MsOH, the product ratio could only slightly be improved to 1.6:1 (entry 2), thus revealing the necessity to adjust the former conditions in order to also achieve the complete dissociation of the more acidic chiral auxiliary. Correspondingly, the amount of MsOH was next doubled to 20 equivalents, which, however, still yielded **RhNP1** along with considerable amounts of the by-product Λ-/Δ-(*S*,*S*)-**74-H** and other impurities that could not be separated by column chromatography (entry 3).

Table 4: Optimization of the Acid Induced Cleavage of the Coordinated Auxiliary Ligand.[a]

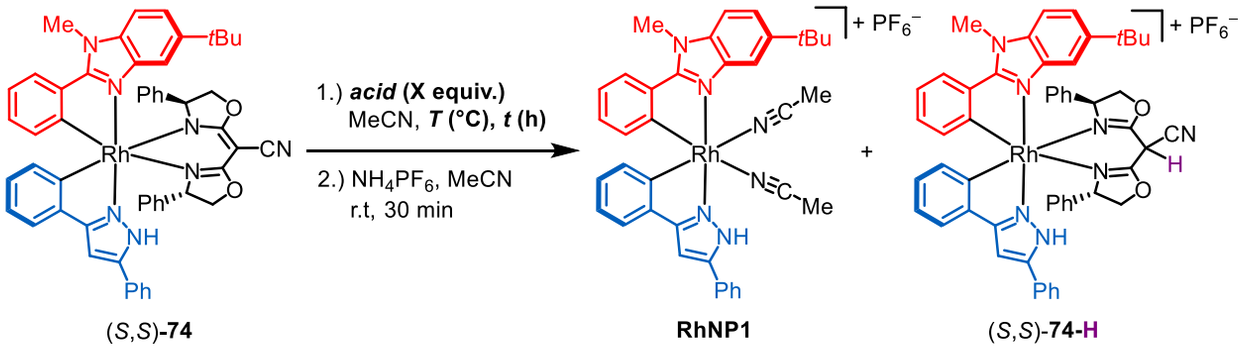

entry	acid (equiv.)	conditions (1st step)		ratios RhNP1 to (*S*,*S*)-74-H[b]
		T (°C)	*t* (h)	
1	TFA (20)	r.t.	17	1.3:1
2[c]	MsOH (10)	r.t.	16	1.6:1
3[c]	MsOH (20)	r.t.	22	5.7:1
4[c,d]	MsOH (20)	r.t.	22	>20:1 (79%)[e]
5[c]	TFA (10)/ MsOH (10)	r.t.	15	>20:1 (77%)[e]
6[c]	TFA (20)/ MsOH (10)	r.t.	15	>20:1 (95%)[e]

[a]Reaction conditions: **First step**: Λ- or Δ-(*S*,*S*)-**74** was dissolved in MeCN (0.04 M), the indicated acid (indicated equiv.) was added in one portion and the resulting solution was stirred at the indicated temperature for the indicated time under an atmosphere of nitrogen. **Second step:** After thorough removal of the solvent under reduced pressure, NH_4PF_6 (15.0 equiv.) and MeCN (0.02 M) were added and the resulting suspension was stirred for 30 min at room temperature. [b]Ratios were determined by ^{1}H NMR after column chromatographic purification of the crude material obtained after the second step. Isolated yields are only provided, if the conversion to Λ-/Δ-**RhNP1** was complete. [c]The indicated acid was added at 0 °C and the resulting solution was stirred for further 15 min at 0 °C before the ice bath was removed. [d]**1-step procedure:** The first step was performed as described under *a*. Afterwards, the reaction mixture was not concentrated, but instead the whole solution was transferred to a silica gel column, NH_4PF_6 (15.0 equiv.) was added atop of the sea sand and the column was flushed with CH_2Cl_2/MeCN (1:1) to exchange the counterion. [e]Isolated yields of **RhNP1** are provided in brackets.

Importantly, when the reaction was conducted in a one-step manner by performing the subsequent anion exchange with NH_4PF_6 on the silica gel column, the product ratio could significantly be improved (>20:1) under otherwise identical reaction conditions (Table 4, entry 4). Inferior results of the previous two-step protocol could therefore be rationalized by the re-coordination of the dissociated auxiliary to the bis-cyclometalated complex, presumably during concentration of the crude reaction mixture after the first step, before the subsequent counterion exchange is carried out. But even though the changed reaction process could enhance the product ratio, several column chromatographic purifications were necessary to obtain pure **RhNP1** in 79% isolated yield, since these conditions still led to the formation of other by-

products with similar R_f values. Notably, the successive addition of MsOH and TFA to a suspension of Λ- or Δ-(*S*,*S*)-**74** also resulted in the complete dissociation of (*S*,*S*)-**73** in a shorter reaction time at room temperature and gave a much cleaner reaction result (entries 5 and 6). It is also noteworthy that, despite the two-step protocol, no re-coordination of the chiral auxiliary ligand could be observed. In previous work it has already been noticed that different acids can lead to poorer reaction results, thus revealing the importance of the effect of the conjugate base on the reaction outcome.[160] Here, the best results were even achieved using an excess of TFA over MsOH (entry 6). Hence, executing the reaction in the presence of TFA and MsOH in a 2:1 ratio conveniently and reproducibly provided the individual enantiomers Λ-**RhNP1** (86%) and Δ-**RhNP1** (95%, entry 6) without racemization in high yields, as resumed in Scheme 32. HPLC performed on a chiral stationary phase verified the high enantiomeric purity (99% ee) of the two enantiomers (see Chapter 6.2).

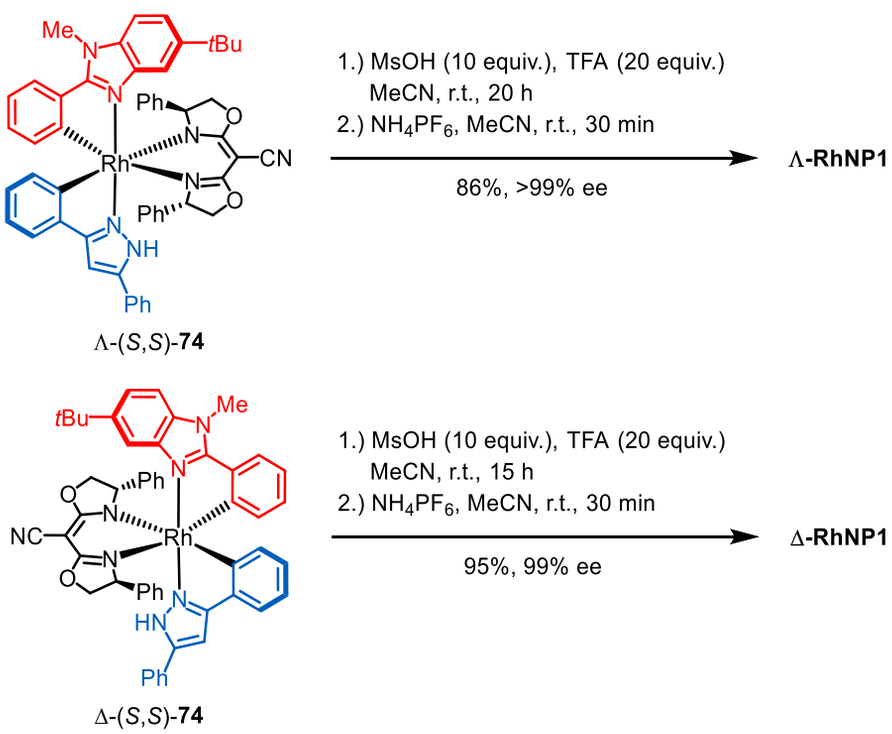

Scheme 32: Optimized acid promoted substitution of the coordinated cyanobisoxazoline ligand.

3.4.3 Synthesis of the Enantiopure and Sterically Demanding Pyrazole Complex RhNP2

Having established conditions for the synthesis of the protic pyrazole complex **RhNP1**, the development of a sterically demanding derivative containing a 2,4,6-trimethylphenyl (mesityl) residue on the pyrazole nitrogen was pursued next.[161] A design that was prompted by the idea to create a chiral catalyst, in which the steric hindrance of both cyclometalated ligands differs significantly from one another.

According to a reported procedure from Gonda and Novák, the corresponding ligand 1-mesityl-3,5-diphenyl-1*H*-pyrazole (**78**) was first synthesized via the short two-step procedure shown in Scheme 33.[162] In the first step, the diaryliodonium salt **77** was prepared from iodobenzene (**75**) and mesitylene (**76**), which was then further reacted with the commercially available diphenylpyrazole **70** under basic conditions to give the desired *N*-arylated pyrazole ligand **78**.

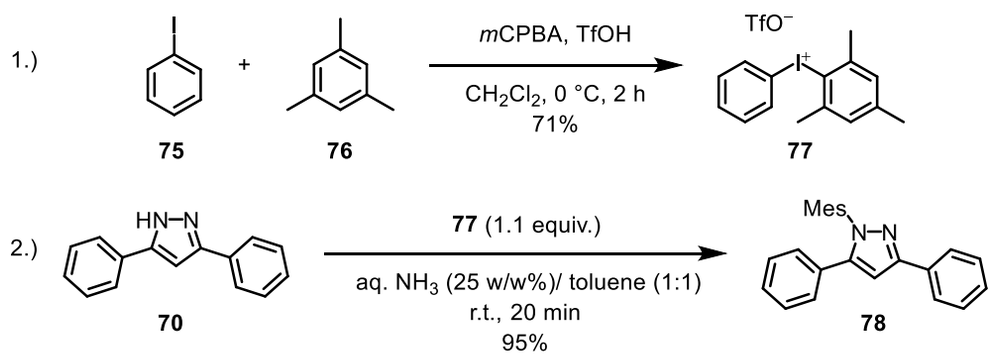

Scheme 33: Synthetic route to 1-mesityl-3,5-diphenyl-1*H*-pyrazole (**78**) as reported by Gonda *et al*.[162]

As already proven for the synthesis of **RhNP1**, the acetate assisted cyclometalation of 1.2 equivalents of the synthesized pyrazole ligand **78** with the mono-cyclometalated complex **48a** at 80 °C in the presence of 1.1 equivalents of NaOAc also reliably provided the related racemic complex *rac*-**RhNP2** after a reaction time of 25 hours in 74% isolated yield (Scheme 34a). Importantly, the formation of a mixture of complexes was again not observed using this method. Furthermore, a crystal structure of the racemic complex was obtained that reveals the anticipated high steric congestion in immediate proximity to the active site of the non-C_2-symmetric catalyst, in which the two substitutionally labile acetonitrile ligands are placed directly above the plane mesityl moiety (Scheme 34b).

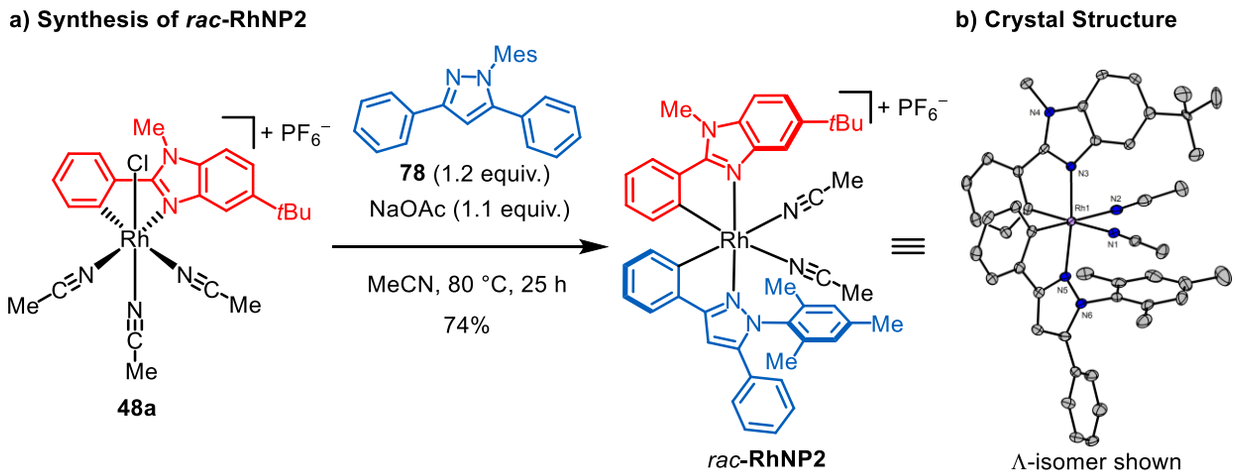

Scheme 34: a) Acetate promoted cyclometalation of 1-mesityl-3,5-diphenyl-1*H*-pyrazole (**78**); b) Crystal structure of *rac*-**RhNP2** as an ORTEP drawing with 50% probability thermal ellipsoids (only the Λ-isomer is shown). The PF_6^- counterion and solvent molecules are omitted for clarity.

For the synthesis of the nonracemic catalyst, the racemic complex *rac*-**RhNP2** was further reacted with the standard methylene-bridged BOX ligand (*S*,*S*)-**65** and K_2CO_3 according to the synthesis protocol described in Chapter 3.3 (Scheme 35). Analysis of the ^{1}H NMR of the crude reaction mixture confirmed the formation of a 1:1 mixture of Λ- and Δ-(*S*,*S*)-**79**. However, when the separation of the two diastereomers via silica gel column chromatography on previously deactivated silica gel (1% of Et_3N) was attempted, the Δ-isomer completely decomposed on the

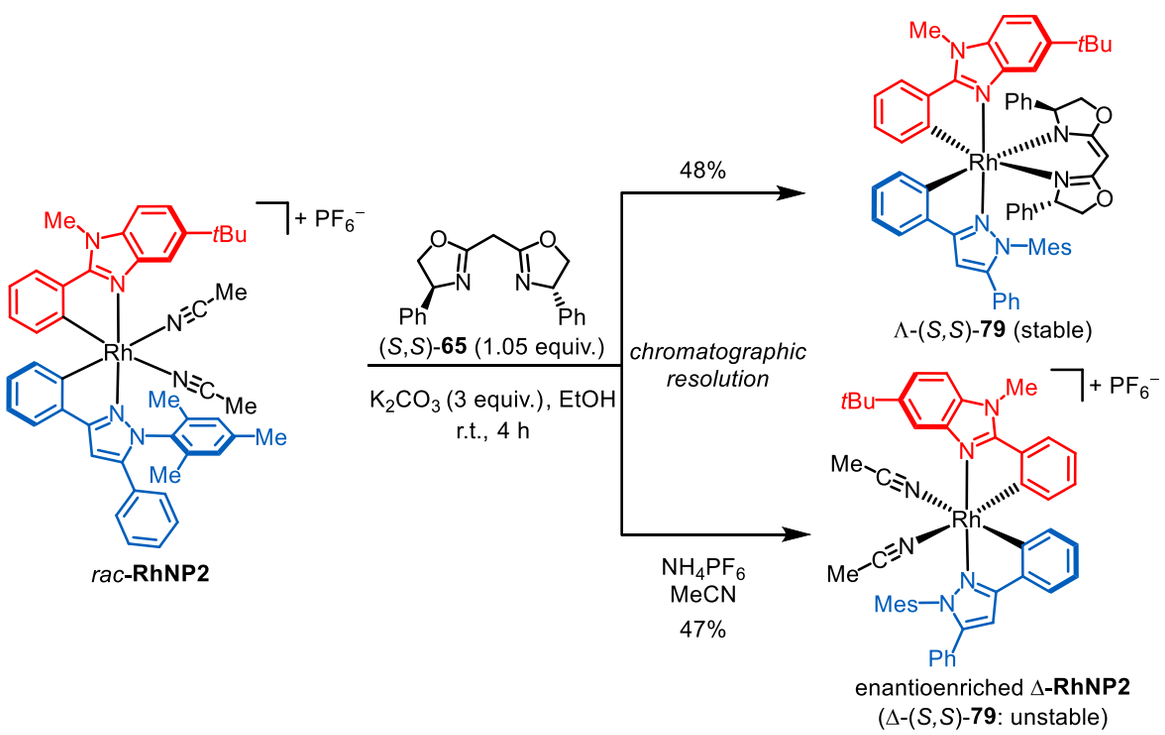

Scheme 35: Reaction of *rac*-**RhNP2** with the chiral bis(oxazoline) ligand (*S*,*S*)-**65**.

column, while Λ-(*S*,*S*)-**79** could be isolated, although only in around 30% yield, thus indicating a limited stability of the Λ-stereoisomer as well. Taking advantage of the different stability of the two diastereomers on silica, it was found that a simple filtration of the crude mixture of complexes through a short silica gel column, performed in less than 15 minutes, could afford 48% of diastereomerically pure Λ-(*S*,*S*)-**79**, whereas the rapidly degraded Δ-stereoisomer remained stuck on top of the column. Nevertheless, the enantioenriched Δ-isomer Δ-**RhNP2** could also be eluted from the short column with NH_4PF_6 in acetonitrile, which gave the corresponding complex in 47% yield.

Continuing with Λ-(*S*,*S*)-**79**, the stereospecific replacement of the coordinated bis(oxazoline) (*S*,*S*)-**65** by two acetonitrile ligands was performed using a slightly modified version of the conditions established in the previous Section 3.4.2 for removal of the nitrile-containing analogue (*S*,*S*)-**73**. Accordingly, instead of solely using MsOH, the auxiliary ligand was cleaved with a 2:1 mixture of TFA and MsOH. Due to the less acidic nature of (*S*,*S*)-**65**, the acid equivalents have been halved to 10 and 5 equivalents, respectively. Following this adapted protocol, the complete dissociation of (*S*,*S*)-**65** was achieved after a comparably short reaction time of 4.5 hours, after which the Λ-enantiomer Λ-**RhNP2** was obtained in 95% isolated yield and with an essentially complete enantioselectivity (>99% ee) (Scheme 36).

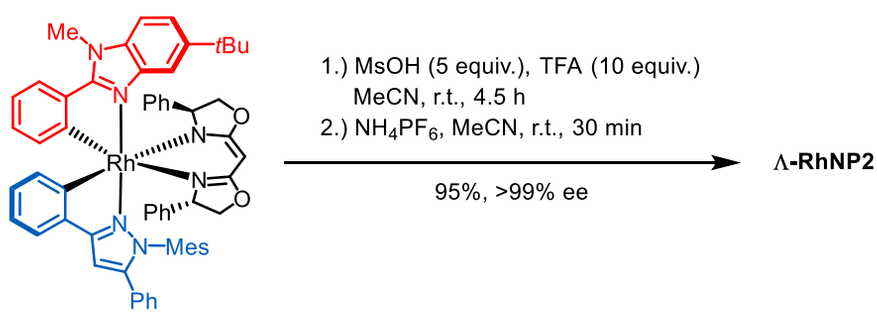

Λ-(*S*,*S*)-**79**

Scheme 36: Stereospecific substitution of (*S*,*S*)-**65** using a mixture of acids.

In order to obtain the Δ-catalyst in an enantiomerically pure fashion as well, the recovered and enantioenriched complex Δ-**RhNP2** was subsequently reacted with the previously synthesized cyanobisoxazoline ligand (*S*,*S*)-**73**, since the formation of a more stable rhodium auxiliary complex was expected as a result of the increased acidity of this modified ligand (Scheme 37). In this way, Δ-(*S*,*S*)-**80** was readily generated along with traces of the corresponding Λ-isomer. A diastereomeric ratio of 10:1 was determined by analyzing the ^{1}H NMR of the crude material obtained. As expected, Δ-(*S*,*S*)-**80** displayed a significantly enhanced stability on silica gel and less sensitivity to different solvents, thus enabling further purification of the complex via simple

recrystallization of the crude material, which provided pure Δ-(*S*,*S*)-**80** in 86% yield with a d.r. of more than 20:1. Finally, the acid-induced cleavage of the coordinated auxiliary ligand in acetonitrile was performed as in Section 3.4.2 with 10 equivalents of MsOH and 20 equivalents of TFA. After 17 hours, the second enantiomer Δ-**RhNP2** could also smoothly be obtained in 96% yield without loss of its stereogenic integrity (Scheme 37). The high enantiomeric purity of the individual enantiomers Λ- and Δ-**RhNP2** (>99% ee for each complex) as well as their mirror-image nature were validated and confirmed by chiral HPLC analysis and CD spectroscopy, respectively (see Chapter 6.2 and 6.3).

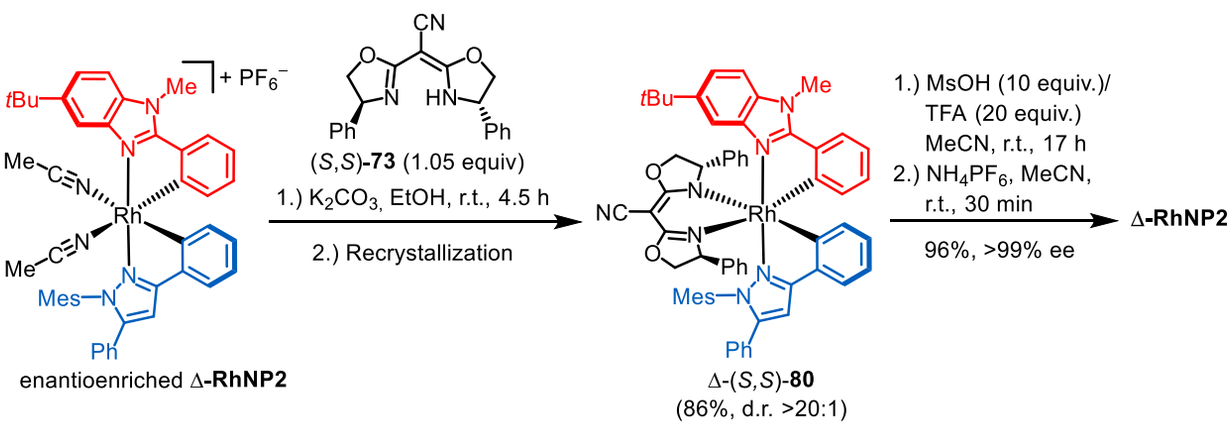

Scheme 37: Chiral cyanobisoxazoline mediated synthesis of enantiomerically pure Δ-**RhNP2**.

Absolute configurations were assigned based on the crystal structure of Δ-(*S*,*S*)-**80** (Figure 28).

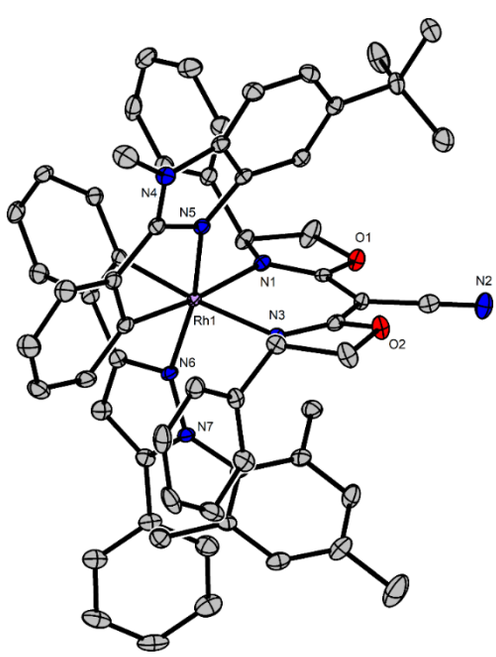

Figure 28: Crystal structure of the rhodium cyanobisoxazoline complex Δ-(*S*,*S*)-**80** (ORTEP drawing with 50% probability thermal ellipsoids). Solvent molecules are omitted for clarity.

In an attempt to shorten the catalyst synthesis by one step, *rac*-**RhNP2** was also directly converted with the nitrile-modified ligand (*S*,*S*)-**73** into the corresponding 1:1 mixture of Λ- and Δ-(*S*,*S*)-**80** (see Section 5.6.3 for more details). However, this alternative approach proved less practical as the column chromatographic separation of the two now silica gel-stable diastereomers became a tedious and time-consuming task due to their very close R_f values, which at the same time emphasizes the convenience of the previous synthetic procedure.

3.4.4 Conclusions

In conclusion, the structural diversity of the new family of bis-cyclometalated tris-heteroleptic rhodium complexes was expanded by two additional chiral catalysts containing either a 3,5-diphenylpyrazole (**RhNP1**) or an *N*-mesitylated derivative (**RhNP2**[161]) as the respective second cyclometalating ligand. Hereby, the previously developed synthetic protocol from Chapter 3.2 and 3.3 was further revised. In the first step, the subsequent second cyclometalation of the mono-cyclometalated rhodium complex with the corresponding pyrazole ligand was performed via an acetate-mediated route, which permitted the application of non-toxic and cheaper reagents and reduced the previous reaction sequence by one step. While long reaction times of two to three days were previously necessary to provide the desired complexes in reasonable yields, the two pyrazole derivatives were obtained with significantly improved results after only 24 hours. Importantly, the formation of mixtures of complexes was completely abolished using this method, yielding the pure racemic complexes after chromatographic purification. For the subsequent synthesis of the single Λ- and Δ-enantiomers of the non-C_2-symmetric catalysts, the chiral bis(oxazoline) mediated strategy was used. For the protic complex **RhNP1**, the synthesis of a pair of two diastereomers was enabled by reaction with a modified chiral bis(oxazoline) containing a nitrile-substituted backbone. A valuable complement, which subsequently also proved to be a viable tool to modulate the stability of metal-centered stereoisomers of the sterically demanding complex **RhNP2**, thus allowing the straightforward synthesis of both catalyst enantiomers. Final removal of the more acidic chiral cyanobisoxazoline was accomplished by using a mixture of two Brønsted acids. Since this protocol generally led to cleaner and more reproducible reaction results, it was also implemented as the new method of choice for the substitution of the standard methylene-bridged BOX ligand, and efficiently afforded both catalysts with high enantiomeric purities (>99% ee). This final draft thus offers a straightforward synthetic pathway to enantiomerically pure bis-cyclometalated rhodium(III) catalysts having two different cyclometalated ligands, with all improvements contributing to the practicality of the current procedure and ultimately rendering this class of catalysts as conveniently accessible as their C_2-symmetrical counterparts.

3.5 Enantioselective α-Fluorination and α-Chlorination of *N*-Acyl Pyrazoles

3.5.1 Asymmetric α-Fluorination and α-Chlorination of Carboxylic Acid Derivatives

Catalytic asymmetric methods for the construction of carbon–halogen bonds provide access to valuable chiral building blocks with important physical and chemical properties. Since the introduction of fluorine into a small molecule can greatly affect a number of variables, such as the metabolic stability, the bioavailability and polarity of a bioactive molecule, the stereoselective formation of carbon–fluorine bonds has increasingly gained medical and pharmaceutical relevance,[163–165] while the stereoselective introduction of carbon–chlorine bonds is of eminent interest because of their versatility as synthetic intermediates for the synthesis of more complex chiral compounds.[166–168] So far, catalytic enantioselective concepts that enable the synthesis of α-halogenated carbonyl compounds have mainly been based on organocatalytic methods that include cinchona alkaloid and secondary amine catalysis, or on transition metal-based strategies using electrophilic halogenation reagents.[169–173] Carbonyl substrates are typically limited to relatively acidic carbonyl compounds such as aldehydes,[174–177] ketones,[178,179] β-ketoesters[180–185] and 3-substituted oxindoles,[186,187] the majority of which have substituents in α-position and are therefore structurally precluded from product epimerization. Contrary to this, synthetically more challenging conversions of α-nonbranched and less acidic carboxylic acid derivatives remain scarce and only a few methods have been reported.[188–194][195–199] Correspondingly, and with regard to asymmetric α-fluorination reactions, Ishihara and co-workers recently disclosed an impressive catalytic approach for the enantioselective synthesis of α-fluorinated *N*-acyl pyrazoles using a chiral copper(II) Lewis acid catalyst, that provided a variety of substrates with high enantioselectivities of up to 97% ee for individual examples under cryostat conditions (Scheme 38).[200]

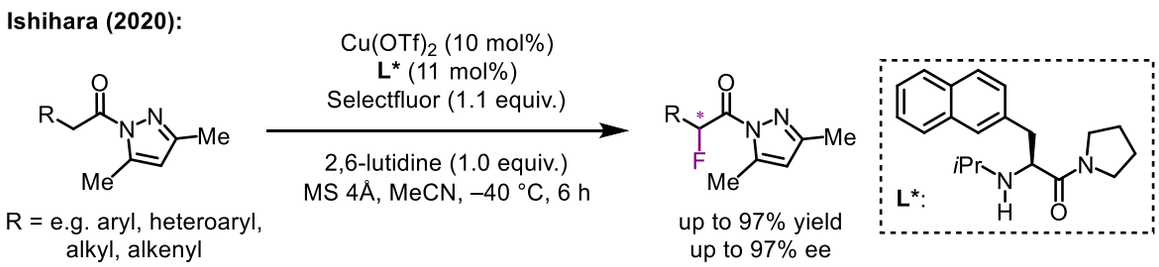

Scheme 38: Asymmetric α-fluorination of *N*-acyl pyrazoles with a chiral Cu(II) catalyst.[200]

However, the analogous enantioselective α-chlorination of *N*-acyl pyrazoles has been elusive. Generally, and in contrast to α-fluorinations, the corresponding development of catalytic and highly enantioselective chlorination methods for the efficient synthesis of α-chloro carboxylic acid derivatives is even less advanced and not many successful examples have been published. Scheme 39 provides an overview of the existing methods. In 2001, Lectka reported a cinchona alkaloid catalyzed α-chlorination of highly reactive acid chlorides **81** with a polyhalogenated quinone **82** which proceeded via the formation of intermediate ketene enolates and gave optically enriched secondary α-chloroesters **83** with enantioselectivities of up to 99% ee in moderate to good yields (43–81%), with the lower yields being mainly due to the formation of a non-chlorinated by-product generated from the starting material and the electrophilic chlorinating reagent (Scheme 39a).[195,196] In 2007, Fu reported the catalytic enantioselective chlorination of isolated ketenes **84** (Scheme 39b).[197] A planar chiral 4-(pyrrolidino)pyridine derivative (**PPY***) was employed as the catalyst for the asymmetric construction of tertiary chlorides from aryl alkylketenes **84** and 2,2,6,6-tetrachlorocyclohexanone (**85**) as the electrophilic chlorine source, which produced the corresponding products **86** with moderate to high stereoselectivities of up to 95% ee. Smith presented a similar strategy in 2010 with a chiral *N*-heterocyclic carbene (NHC) catalyst, which, however, mediated the enantioselective chlorination of ketenes **84** to the corresponding chloroesters **87** with only moderate enantioselectivities of up to 61% ee (Scheme 39c).[198] In 2009, Toru and Shibata provided a single example of a DBFOX/nickel(II) catalyzed enantioselective α-chlorination of 3-(2-phenylacetyl)thiazolidin-2-one (**88**) as part of their studies on the corresponding α-fluorination reaction.[191] The product **89** was obtained in 97% yield and with a high enantioselectivity of 93% ee, but three days of reaction time at –60 °C were required and removal of the thiazolidinone moiety has not been ascertained (Scheme 39d). In 2011, as an extension of their pioneering work on enantioselective α-fluorination of carboxylic acid derivatives,[188] Sodeoka and co-workers published a modification of their original procedure for the enantioselective α-chlorination of 3-acyloxazolidin-2-ones **90** (Scheme 39e).[199] The products **91** were obtained in high yields and with enantioselectivities of 75% to 89% ee for a range of aryl-substituted substrates, achieving 72% ee for a crotonyl derivative.

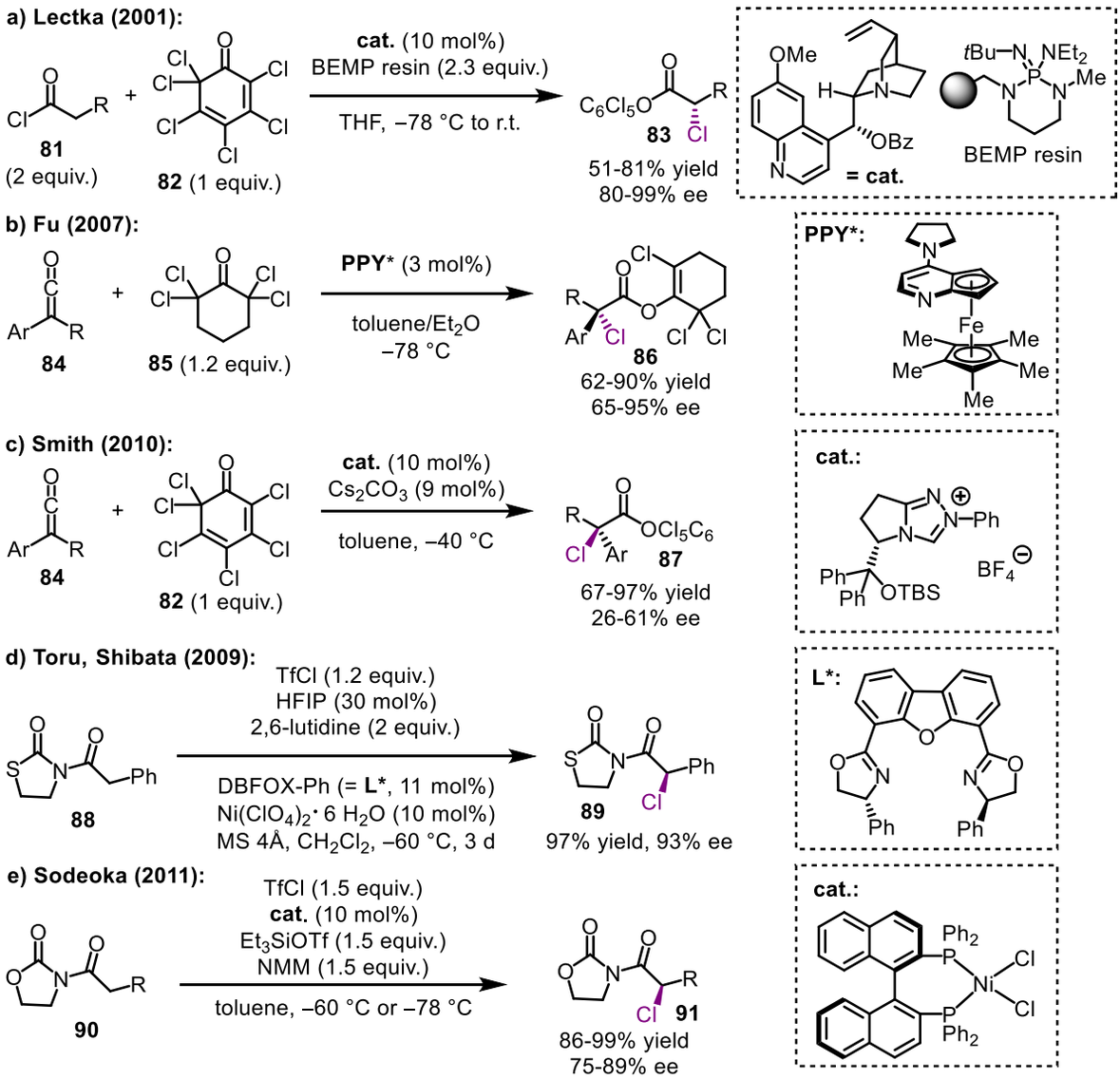

Scheme 39: Previous examples of catalytic enantioselective α-chlorination of carboxylic acid derivatives.

Despite these advances, there are still limitations which make the preparation of this class of optically active α-chloro carbonyl compounds less feasible, such as long reaction times, the use of expensive or non-commercially available chlorinating agents, or the dependence of all of these approaches on low temperature conditions. Application of highly reactive starting materials or the involvement of unstable intermediates additionally implies the need for more complex reaction setups, including glove box manipulations, syringe pump infusions or the need for special equipment suggesting the demand for more convenient and robust catalytic methods.[161]

In view of these drawbacks and inspired by Ishihara's[200] notable work, this final chapter aims to demonstrate the high efficiency of the well-tailored non-C_2-symmetrical chiral-at-rhodium catalyst **RhNP2** for the catalytic enantioselective α-fluorination of *N*-acyl pyrazoles as well as the successful extension of the developed strategy to the corresponding α-chlorination reaction (Figure 29).[161]

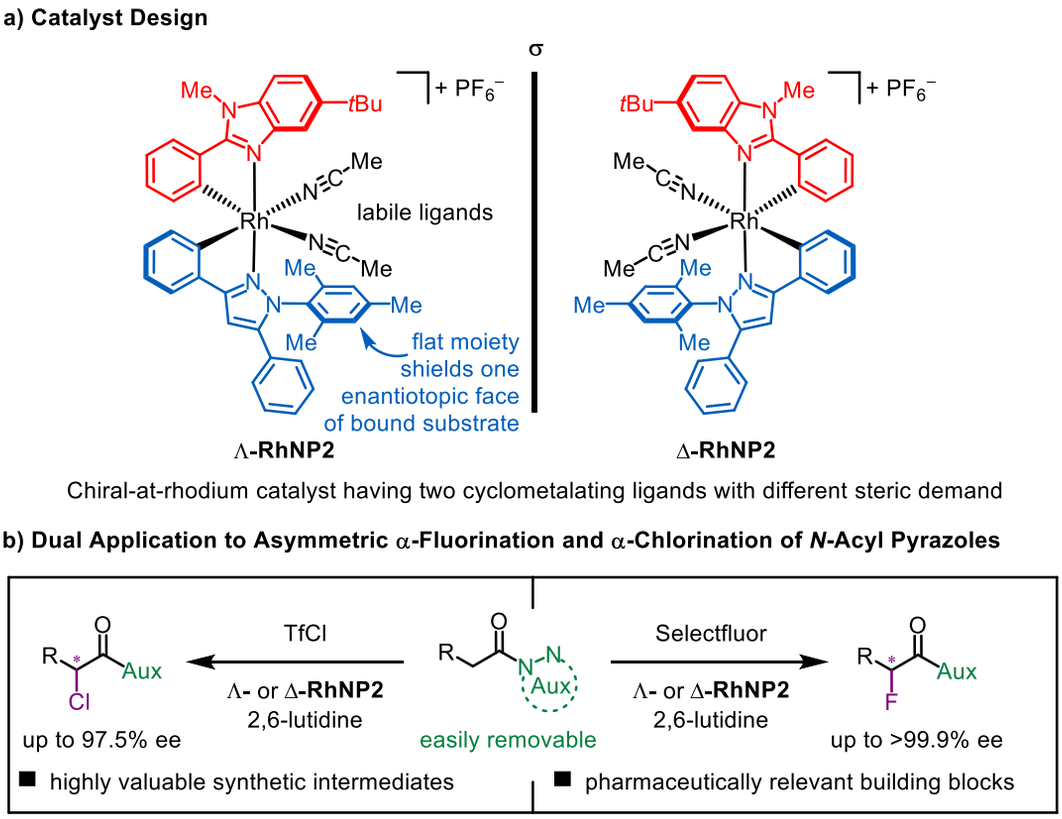

Figure 29: Dual application of the non-C_2-symmetric rhodium catalyst Λ-/Δ-**RhNP2** to asymmetric α-fluorination and α-chlorination of *N*-acyl pyrazoles.[161]

3.5.2 Initial Catalytic α-Fluorination Experiments

With a synthesis of the two novel tris-heteroleptic complexes **RhNP1** and **RhNP2** in hand, extensive work was then dedicated to the screening of a wide variety of different catalytic asymmetric transformations. In this context, **RhNP2** was found to be a highly effective catalyst for enantioselective α-halogenations.[161] Confirming the hypothesis that the newly developed and sterically highly demanding complex could be a particularly promising catalyst for asymmetric conversions which are based on the addition of either very small nucleophiles or electrophiles to a rhodium-bound substrate, for which high stereoselectivities due to insufficient steric discrimination are otherwise difficult to achieve.

Studies were started with the investigation of the α-fluorination of *N*-acyl pyrazoles **92** with different electrophilic fluorinating reagents **93** and with Λ-**RhNP2** as catalyst (Table 5). Gratifyingly, the reaction of the 3,5-dimethylpyrazole substrate **92a** with Selectfluor **93a** in the presence of 2,6-lutidine and 2 mol% of the rhodium catalyst gave the desired fluorinated product **94a**, but only with a moderate enantioselectivity of 57% ee and in 33% yield with incomplete conversion after 16 hours (entry 1). Afterwards, the influence of different substituents

within the pyrazole moiety was examined, whereby it was found that a sole substitution at the 3-position of the pyrazole auxiliary leads to considerably improved results (entries 2–4). Best results were achieved with substrate **92d**, containing a 3-(4-fluorophenyl) pyrazole residue, as it smoothly provided spot-to-spot α-fluorinated **94d** in almost quantitative yield with high stereoselectivity (>99% NMR yield, 98% isolated yield, 99.4% ee) and thus emerged as the best choice (entry 4). It is noteworthy that the fluorination can be executed at room temperature and therefore differs from most of the other methods reported, which depend on low reaction temperature conditions.[188–192] Although easy removability of the pyrazole auxiliary is desirable, it was noticed that product yields decreased with prolonged exposure to silica gel due to pyrazole cleavage during chromatographic purification. However, since the reaction proceeded without the formation of by-products, pure products could easily be obtained in high yield by simply filtering the crude material through a short pad of silica gel, which further emphasizes the simplicity of the developed procedure. Continuing with the investigation of the influence of various parameters on the reaction result, the application of a different base was explored next. Correspondingly, when triethylamine was used as the base instead, the conversion was low and the enantioselectivity decreased to 92% ee (entry 5). In contrast to the reaction with commercially available Selectfluor **93a**, which can be purchased as tetrafluoroborate salt, the reaction with the hexafluorophosphate analogue was not complete after 16 hours and **94d** was formed with a somewhat poorer stereoselectivity of 96% ee (entry 6). Other fluorinating reagents, such as *N*-fluorobenzenesulfonimide (NFSI, **93b**) resulted in an even lower conversion of the starting material and provided the fluorinated product with a reduced ee of 88% (entry 7). No product formation at all was observed using the *N*-fluoropyridinium salts **93c** (entries 8 and 9), whereas 1-fluoro-2,4,6-trimethylpyridinium triflate **93d** afforded **94d** with a good enantioselectivity of 97% ee, albeit with very poor conversion (entry 10). Importantly, the catalyst loading could be reduced down to 1 mol% while maintaining a high yield and excellent stereoselectivity of 98.8% ee (entry 11). Almost no conversion was observed in the absence of a base, but a small amount of product was formed (entry 12). Notably, the fluorination could be carried out in the presence of residual water and under air without significantly affecting the reaction outcome (entries 13 and 14). Finally, the catalytic performance of the new non-C_2-symmetric catalyst **RhNP2** was compared with that of the two established bis-cyclometalated rhodium complexes **RhO**[77] and **RhS**,[93] in which rhodium is cyclometalated by two 5-*tert*-butyl-2-phenylbenz-oxazoles or by the related benzothiazole ligands, but which are otherwise structurally identical to **RhNP2** (see Chapter 2, Figure 6). At first, the C_2-symmetric catalyst **RhO** was tested, which also gave the α-fluorinated product **94d** in high yield (96% NMR yield), but with a substantially lower enantioselectivity of only 85% ee with incomplete conversion after 16 hours (entry 15).

Table 5: Initial α-Fluorination Experiments and Optimization of Reaction Conditions.[a]

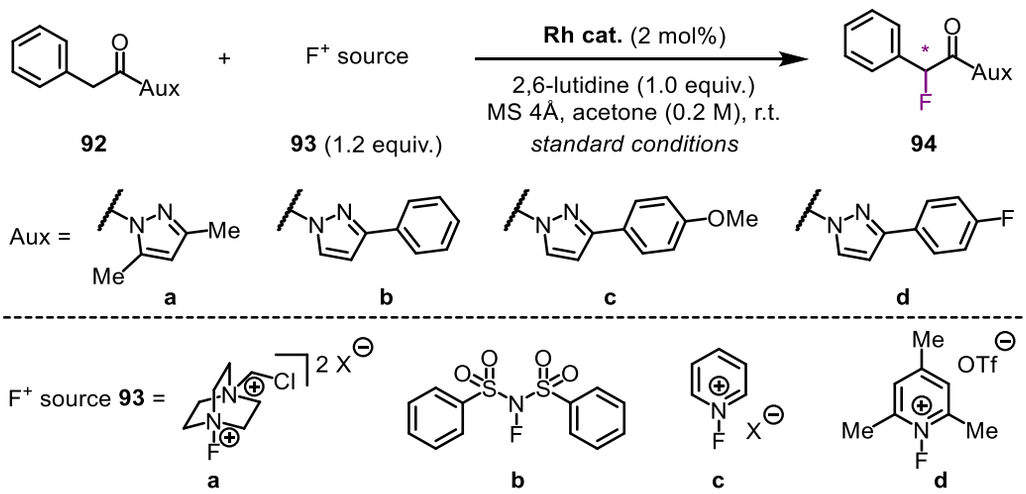

	catalyst	Aux	F^+ source	X	conditions[b]	*t* (h)	conv. (%)[c]	yield (%)[d]	ee (%)[e]
1	Λ-**RhNP2**	**92a**	**93a**	BF_4	standard	16	41	33	56.9 (*R*)
2	Λ-**RhNP2**	**92b**	**93a**	BF_4	standard	16	>99	>99	98.7 (*R*)
3	Λ-**RhNP2**	**92c**	**93a**	BF_4	standard	16	88	87	97.6 (*R*)
4	Λ-**RhNP2**	**92d**	**93a**	BF_4	standard	16	>99	>99 (98)[f]	99.4 (±0.1)[g] (*R*)
5	Λ-**RhNP2**	**92d**	**93a**	BF_4	Et_3N (1.0 eq)	16	10	8	91.7 (*R*)
6	Λ-**RhNP2**	**92d**	**93a**	PF_6	standard	16	82	82	95.7 (*R*)
7	Λ-**RhNP2**	**92d**	**93b**	–	standard	16	39	36	88.2 (*R*)
8	Λ-**RhNP2**	**92d**	**93c**	OTf	standard	16	1	–	–
9	Λ-**RhNP2**	**92d**	**93c**	BF_4	standard	16	4	–	–
10	Λ-**RhNP2**	**92d**	**93d**	OTf	standard	16	8	7	97.4 (*R*)
11	Λ-**RhNP2**	**92d**	**93a**	BF_4	1 mol% catalyst	16	>99	99	98.8 (*R*)
12	Λ-**RhNP2**	**92d**	**93a**	BF_4	without base	16	11	8	93.7 (*R*)
13	Λ-**RhNP2**	**92d**	**93a**	BF_4	without MS 4Å	16	97	96	98.2 (*R*)
14	Λ-**RhNP2**	**92d**	**93a**	BF_4	under air	16	>99	>99	98.8 (*R*)
15	Λ-**RhO**	**92d**	**93a**	BF_4	standard	16	97	96	85.3 (*R*)
16	Δ-**RhS**	**92d**	**93a**	BF_4	standard	0.25	>99	97	89.5 (*S*)
17	Δ-**RhS**	**92d**	**93a**	BF_4	standard	0.5	>99	95	91.7 (*S*)
18	Δ-**RhS**	**92d**	**93a**	BF_4	standard	5	>99	85[f]	98.8 (*S*)

[a]Standard conditions: **92** (0.05 mmol), Rh catalyst (2 mol%) and MS 4Å (powder, 20 mg) were dissolved in acetone (0.2 M) under an atmosphere of nitrogen. **93** (1.2 equiv.) was added, followed by 2,6-lutidine (1.0 equiv.) and the resulting mixture was stirred at room temperature for 16 h unless noted otherwise. [b]Deviations from standard conditions shown. [c]Determined by ^{1}H NMR of the crude products using 1,1,2,2-tetrachloroethane as the internal standard. [d]Yields based on ^{1}H NMR analysis. [e]Enantiomeric excess (ee) of crude products was determined by HPLC analysis on a chiral stationary phase. [f]Isolated yields in brackets. [g]Average ee of 3 experiments, standard deviation in brackets.

Contrary to this, **RhS** provided **94d** also in good yield (97% NMR yield) and with a reduced enantioselectivity of 89.5% ee, but the reaction was significantly faster with conversion being complete after only 15 minutes (Table 5, entry 16). Since the complex with metal-centered Δ-configuration was employed, the opposite product enantiomer was obtained. In view of the comparatively high reactivity of **RhS** for the present α-fluorination, the combination of this catalyst with the highly reactive fluorinating reagent Selectfluor **93a** was supposed to be a possible reason for the poorer enantioselectivity achieved. In a further attempt, the corresponding transformation was therefore carried out with the milder reagent NFSI **93b** and **RhS** using otherwise the standard conditions. However, this experiment could not confirm this assumption, since these conditions led to an even worse reaction result and gave the product with only 18% ee and with an incomplete conversion after 24 hours (93% conversion, 81% NMR yield).

3.5.3 Mechanistic Discussion

Mechanistically, the reaction is expected to proceed via the bidentate *N*,*O*-coordination of the *N*-acyl pyrazole substrate to the rhodium catalyst,[88,82] followed by enolate formation and subsequent stereoselective fluorination of the chiral rhodium enolate complex, analogous to the iridium-catalyzed (**IrS**) α-fluorination of 2-acyl imidazoles with Selectfluor, which was recently reported by Xu and co-workers.[193] In contrast to C_2-symmetric catalysts, complexes with lower symmetry often allow additional reaction pathways via different reaction intermediates which can result in a reduced overall enantioselectivity (see Chapter 1).[9] For the present catalytic system, owing to the non-C_2-symmetry of catalyst **RhNP2** and the unsymmetrical nature of substrate **92d**, two diastereomers (**95a** and **95b**) can theoretically be formed by coordination of **92d** to **RhNP2**, which threatens to adversely affect the result of the catalysis (Figure 30a). Interestingly, experimentally it was found that the conversion of *rac*-**RhNP2** with **92d** exclusively yielded the rhodium-substrate complex **95a** as a single diastereomer, while **95b** was not formed, probably due to unfavorable steric repulsion. ^{1}H–^{1}H 2D NOESY experiments confirmed the generation of complex **95a** and Figure 30b shows some of the decisive NOE correlations (see Section 5.7.2 for more details). Figure 30c exhibits a proposed model for the asymmetric induction in the course of the electrophilic fluorine addition to the corresponding enolate complex of diastereomer **95a**, which is in agreement with the experimental results. Accordingly, stabilizing π-π-stacking interactions between the coordinated, planar enolate and the mesityl group of the cyclometalated pyrazole ligand enable a complete shielding of the *Si*-face of the bound enolate. Consequently, only the *Re*-face of the enolate α-carbon is susceptible

to electrophilic attack by the fluorinating reagent, thereby providing an almost perfect asymmetric induction.

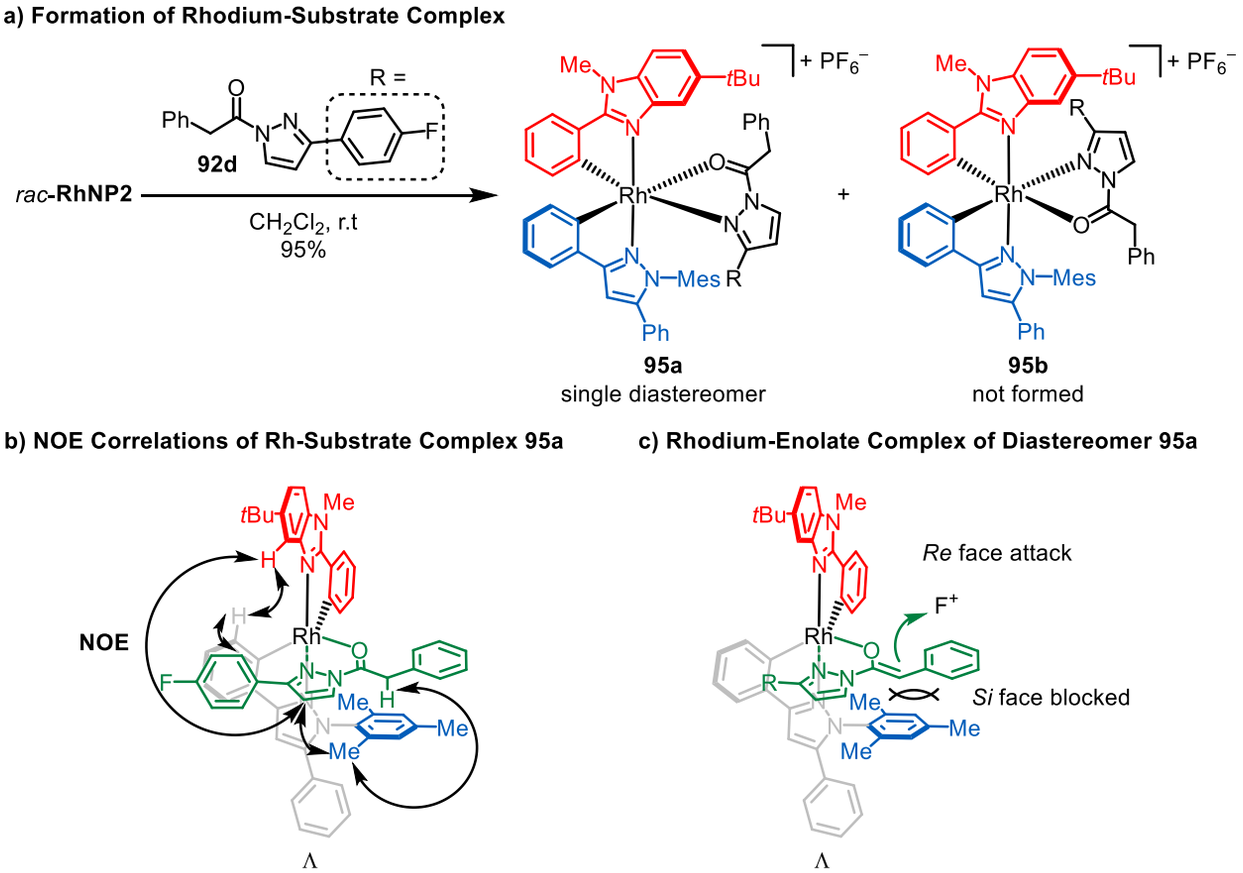

Figure 30: a) Coordination of substrate **92d** to *rac*-**RhNP2** can lead to the formation of two different diastereomers due to the non-C_2-symmetry of the catalyst (here exemplary shown for Λ-**RhNP2**); b) Selection of significant interligand long-range NOE interactions from **95a** (shown for Λ-**RhNP2**). c) Proposed model for the asymmetric induction in the transition state in which one prochiral face of the substrate is shielded by the mesityl group (shown for Λ-**RhNP2**).

In this way, the excellent shielding of one enantiotopic face of the coordinated enolate can explain the higher enantiomeric excess achieved with the non-C_2-symmetrical catalyst **RhNP2** compared to the established chiral-at-rhodium Lewis acid catalyst **RhS**. On the other hand, the inferior steric shielding in **RhS** rationalizes the faster turnover frequency of **RhS** compared to **RhNP2**. Interestingly, when **RhS** was used as the catalyst, it was also observed that the enantioselectivity increases with progressing reaction time, but that this increase is associated at the same time with a gradually decreasing product yield (Table 5, entries 17 and 18). Identification of a difluorinated by-product revealed that this is the consequence of overfluorination. Apparently, Δ-**RhS** selectively converts (*R*)-**94**, but not (*S*)-**94**, into the undesired achiral difluorinated compound. Since the formation of this side product prevented the determination of an NMR yield by integration of baseline separated signals in the ^{1}H NMR, only

an isolated yield of **94d** is given for entry 13. Formation of the α,α-difluorinated by-product was confirmed by HRMS, although it was not purely isolable due to the similarity of its R_f value to that of the mono-fluorinated product, in addition to its rapid decomposition on silica gel during chromatographic purification. Despite this fact, the desired product could only be isolated together with traces of this by-product, the formation of which does not occur with **RhNP2** as the catalyst.

3.5.4 Scope of Enantioselective α-Fluorination

With the reaction conditions optimized, the substrate scope was next assessed using either Λ- or Δ-**RhNP2** (Scheme 40). In order to ensure complete conversion within 16 hours, the amount of Selectfluor **93a** (with X = BF_4) was increased to 2 equivalents for some substrates. A variety of *N*-acyl pyrazoles with diverse substitution patterns of the phenyl moiety and of different electronic nature provided the α-fluorinated products in high yields of up to 99% with excellent to almost complete enantioselectivities (up to >99% ee) (**94d–i**). Heterocyclic entities such as naphthyl-, 3-thienyl- or Boc-protected indolyl- were also well accommodated (**94j–l)**, although the indolyl product **94l** was only obtained in moderate yield. Moreover, the unsaturated product **945m** was formed with a modest stereoselectivity of 68% ee in good yield. An NMR yield is reported, as it was formed together with a by-product which was not purely separable from the product, because it had the same R_f value and **94m** also tended to decompose rapidly upon prolonged exposure to silica gel. With **RhNP2**, almost no conversion was observed for the formation of product **94n** containing an aliphatic side chain using either 2,6-lutidine or K_2CO_3 as the base. However, small amounts of the product were formed with moderate stereoselectivity in the presence of K_2CO_3, when **RhS** was employed as the catalyst. Interestingly, it was found here that both the yield and the enantioselectivity decreased with increasing reaction time, which was attributed to a slow cleavage of the pyrazole auxiliary over time under these modified reaction conditions. Subsequently, the α-fluorination of tertiary C–H bonds was achieved with **RhNP2** as the catalyst using K_2CO_3 as the base instead of 2,6-lutidine, albeit the desired product **94o** was only obtained in 48% yield with a low enantioselectivity of 11% ee, which can be rationalized by an uncatalyzed background reaction. Consistently, a control experiment which was performed without catalyst led to the formation of a considerable amount of product (56% conversion and 56% NMR yield after 4 h). Gratifyingly, the more reactive catalyst **RhS** was able to efficiently realize the challenging construction of a quaternary stereocenter with excellent yield and high enantioselectivity (96% yield, 87% ee), with conversion being complete after only 4 hours. As

already observed for substrate **94n**, longer reaction times led to poorer results. No conversion was observed, when the ester moiety of **94o** was replaced by a methyl group (see Section 5.7.4 for more details).

Scheme 40: Substrate scope for enantioselective α-fluorination.[a]

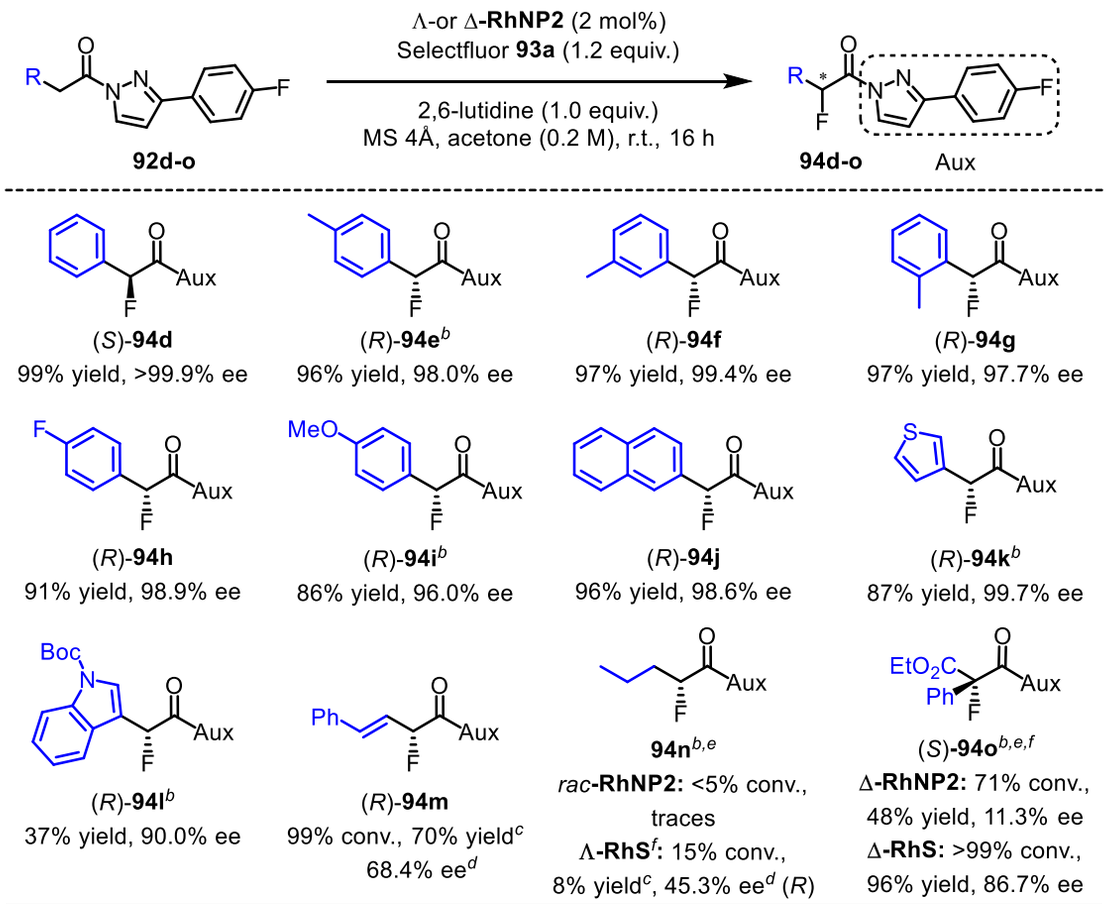

[a]Reactions were conducted on a 0.1 mmol scale of **92** according to the conditions presented in Table 5, entry 4. (*S*)-Products were obtained with Δ-**RhNP2** and (*R*)-products with Λ-**RhNP2**. See Section 5.7.4 for more details. [b]Performed with 2 equiv. Selectfluor **93a** (X = BF_4). [c]NMR yield. [d]Enantiomeric excess of the crude product. [e]Performed with 3 mol% catalyst and 1.1 equiv. K_2CO_3 instead of 2,6-lutidine. [f]Stirred for 4 h at room temperature.

3.5.5 Expansion to Catalytic α-Chlorination of *N*-Acyl Pyrazoles

With the desire to extend this practical method to other synthetically challenging α-halogenation reactions, it was decided to examine enantioselective α-chlorination. Encouragingly, starting with the conditions established for fluorination and with *N*-chlorosuccinimide (NCS, **96a**) as the initial electrophilic chlorine source, the coveted product **97d** was formed in 51% yield, albeit along with significant amounts of the α,α-dichlorinated compound as by-product, thus preventing complete conversion of the starting material when 1.2 equivalents NCS were employed (Table 6, entry 1). Subsequent evaluation of various electrophilic chlorinating reagents (entries 2–4), indicated that

they either provided the overchlorinated compound as the main product of the reaction (entry 2) or performed similarly to NCS (entry 3). Fortunately, readily available trifluoromethanesulfonyl chloride (TfCl, **96d**) provided the desired α-chlorinated product **97d** in excellent yield and with high enantioselectivity after a short reaction time at room temperature (98% NMR yield, 96% isolated yield, 96.2% ee), with only traces of double chlorination being observed (entries 4 and 5). When **RhO** was used as the catalyst instead, only little conversion of the starting material was observed and the product was produced with a poor stereoselectivity of 11% ee (entry 6). Application of **RhS** instead of **RhNP2** provided the product in 88% yield, with a modest enantioselectivity of 81% ee and with incomplete conversion after 4 hours (entry 7). Interestingly, extending the reaction time to 24 hours did not lead to a full consumption of the starting material under otherwise identical reaction conditions, nor to an increase in enantioselectivity, as it was previously observed for the α-fluorination, which could indicate a possible degradation of the catalyst under the reaction conditions.

Table 6: Initial α-Chlorination Experiments and Optimization of Reaction Conditions.[a]

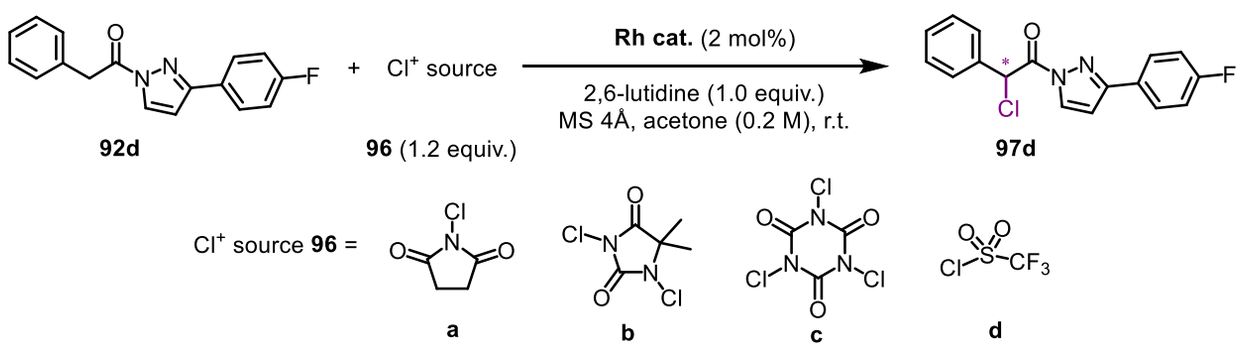

entry	catalyst	Cl^+ source	*t* (h)	conv. (%)[b]	yield (%)[c]	ee (%)[d]
1	*rac*-**RhNP2**	**96a**	3	86	51	–
2	*rac*-**RhNP2**	**96b**	3	>99	18	–
3	*rac*-**RhNP2**	**96c**	3	81	49	–
4	*rac*-**RhNP2**	**96d**	3	>99	98	–
5	Δ-**RhNP2**	**96d**	4	>99	98 (96)[e]	96.2 (*S*)
6	Λ-**RhO**	**96d**	4	33	28	10.8 (*R*)
7	Δ-**RhS**	**96d**	4	90	88	80.8 (*S*)

[a]Conditions: **92d** (0.05 mmol), Rh catalyst (2 mol%) and MS 4Å (powder, 20 mg) were dissolved in acetone (0.2 M) under an atmosphere of nitrogen. Reagent **96** (1.2 equiv.) was added, followed by 2,6-lutidine (1.0 equiv.) and the resulting mixture was stirred at room temperature for 3 h unless noted otherwise. [b]Determined by ^{1}H NMR of the crude products using 1,1,2,2-tetrachloroethane as the internal standard. [c]Yields based on ^{1}H NMR analysis. [d]Enantiomeric excess (ee) of crude products was determined by HPLC analysis on a chiral stationary phase. [e]Isolated yields in brackets.

Scheme 41 depicts the scope of the enantioselective α-chlorination. Correspondingly, *N*-acyl pyrazoles with substituents in different positions of the α-aryl moiety were well tolerated and the chlorinated products were efficiently obtained in excellent yields (99% to >99%) and stereoselectivities (95.4–97.5% ee) (**97e–g**). Substrates containing electron-donating or electron-deficient substituents within the phenyl unit were also compatible and afforded the products in high yields with slightly reduced enantioselectivities (83.8–91.1% ee), but regardless of their position (**97h–i**, **97p**). Similar results were also achieved with substrates bearing heteroaromatic residues (**97j** and **97k**). As a limitation, the unsaturated substrate **97m** only gave poor results and no conversion was observed for the aliphatic substrate **97n**.

Scheme 41: Substrate scope for enantioselective α-chlorination.[a]

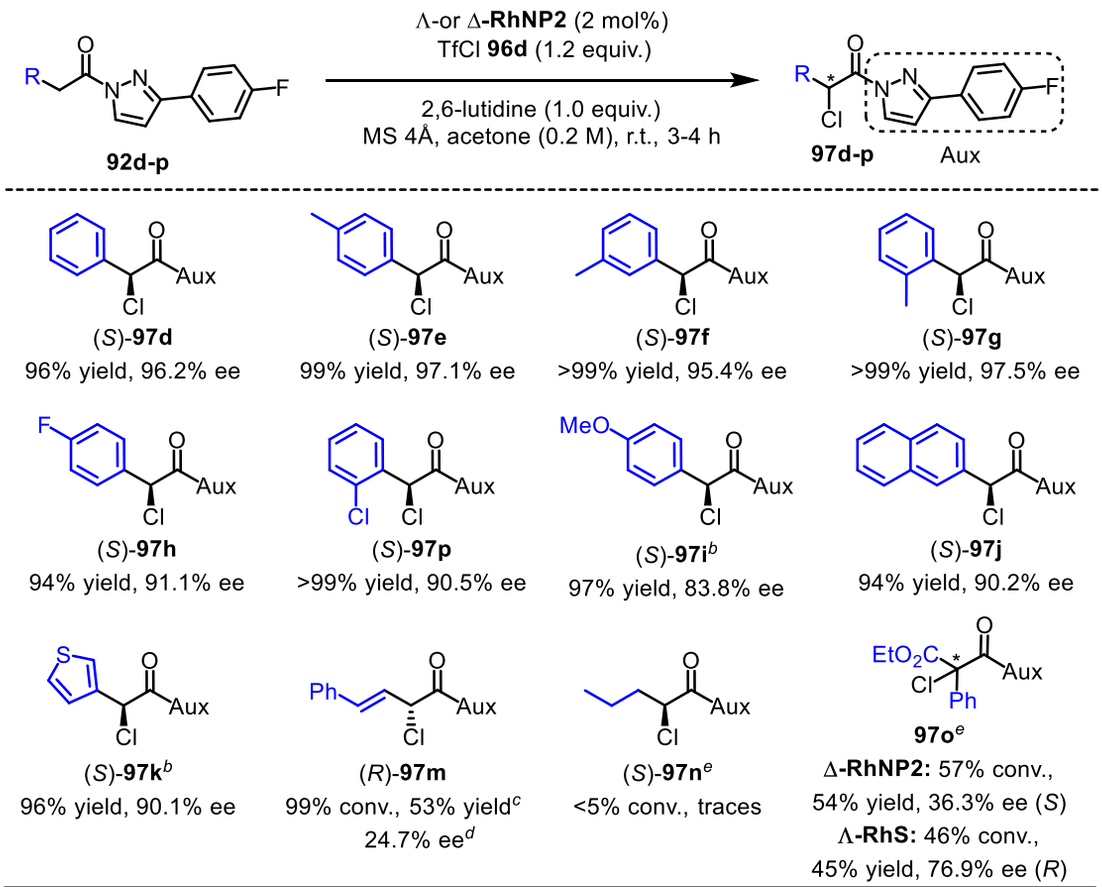

[a]Reactions were conducted on a 0.1 mmol scale of **92** according to the conditions presented in Table 6, entry 5. (*S*)-Products were obtained with Δ-**RhNP2** and (*R*)-products with Λ-**RhNP2**. See Section 5.7.5 for more details. [b]Performed with 1.3 equiv. TfCl (**96d**). [c]NMR yield. [d]Enantiomeric excess of the crude product. [e]Performed with 3 mol% catalyst, 2 equiv. TfCl and 1.1 equiv. K_2CO_3 instead of 2,6-lutidine, stirred for 16 h at room temperature.

Gratifyingly, the formation of the chiral tertiary chloride **97o** was achieved after some adaptations of the standard reaction conditions. As previously ascertained for the corresponding α-fluorination, **RhS** proved to be the more suitable catalyst for the halogenation of a tertiary C–H

bond and furnished the desired product **97o** with a reasonable enantioselectivity of 77% ee. A related control reaction in the absence of catalyst was also conducted, but revealed that only a small amount of product (3% conversion, 3% NMR yield) can be generated within 16 hours. In analogy to the corresponding α-fluorination reaction, the chlorination of a modified substrate having a methyl substituent instead of the ester group did not lead to any conversion (see Section 5.7.5 for more details).

3.5.6 Removal of the Auxiliary Pyrazole Moiety

Finally, the removal of the auxiliary pyrazole moiety was envisioned to highlight the utility of *N*-acyl pyrazoles as precursors for carboxylic acids and their derivatives.[201] Unlike the related 2-acyl imidazoles, the pyrazole moiety can typically be cleaved under mild reaction conditions. Difficulties in a synthetic transformation of the α-halogenated products arise rather due to the relatively high acidity of their α-hydrogen atoms. In order to achieve the removal of the pyrazole moiety without compromising the stereochemical information of the products, different reaction conditions were tested for the pyrazole substitution with methanol to give the corresponding α-fluoro- and α-chloroesters. Table 7 summarizes a number of conditions that have been optimized with regard to enantiomeric excess, using α-chlorinated (*S*)-**97d** as the test substrate. At first, the substitution was performed with methanol as the only solvent in the presence of molecular sieve. Although the conversion to (*S*)-**98d** was complete after only 12 minutes of reaction time, these initial conditions also resulted in a significant loss of enantiomeric purity (entry 1). Subsequently, the pyrazole removal was carried out according to a slightly modified reported procedure[154] using DMAP (30 mol%) and a 3:1 mixture of THF and methanol as solvent. Since the racemic version of this reaction was also very fast with conversion being complete in less than 15 minutes (entry 2), the amount of methanol was reduced to the addition of only 10 equivalents and only 5 mol% of DMAP were used for the subsequent conversion of the enantiomerically enriched substrate (*S*)-**97d**. Following these conditions, a considerably lower degree of epimerization was observed (entry 3). Changing the solvent from THF to CH_2Cl_2 further improved the reaction outcome (entry 4). Since the reaction still only required a short reaction time for completion, the pyrazole removal was finally executed at 0 °C under otherwise identical reaction conditions, which smoothly provided the desired α-chloroester (*S*)-**98d** with almost no racemization after 2.5 hours (entry 5).

Table 7: Optimization of the Reaction Conditions for Pyrazole Cleavage.[a]

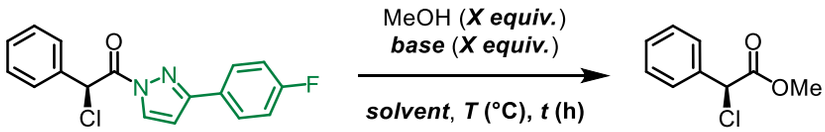

(*S*)-**97d** (*S*)-**98d**

	conditions	*T*	*t*	ee[b] (%)	loss of ee (%)
1	MeOH (0.1 M), MS 4Å (30 mg)	r.t.	12 min	72.4	–20.8
2[c]	THF/MeOH 3:1 (0.3 M), DMAP (30 mol%)	r.t.	<15 min	–	–
3	THF (0.2 M), MeOH (10 equiv.), DMAP (5 mol%)	r.t.	3 h	88.5	–5.6
4	CH_2Cl_2 (0.2 M), MeOH (10 equiv.), DMAP (5 mol%)	r.t.	2 h 15 min	92.9	–2.4
5	CH_2Cl_2 (0.2 M), MeOH (10 equiv.), DMAP (5 mol%)	0 °C	2.5 h	95.0	–0.4

[a]Reaction conditions: (*S*)-**97d** (0.05 mmol) was converted under the specified conditions. The resulting solution was stirred at the indicated temperature under nitrogen atmosphere until TLC showed completion of the reaction. Purification by silica gel chromatography (*n*-pentane/Et_2O 10:1) afforded pure (*S*)-**98d**. [b]Enantiomeric excess (ee) of isolated products was determined by HPLC analysis on a chiral stationary phase. [c]Performed with *rac*-**97d**.

An efficient strategy for cleavage of the auxiliary pyrazole moiety could thus be elaborated and proved to be generally applicable for the synthesis of both, fluorinated and chlorinated methyl esters. According to the optimized conditions, all of the methyl esters were obtained in high yields (99%) with only negligible loss of enantiomeric excess (**98d** and **98p**), as shown in Scheme 42. Remarkably, no epimerization at all was observed in the synthesis of the α-fluorinated ester **99d** and thus the complete enantioselectivity (>99.9% ee) was retained. Despite the relatively high acidic nature of the α-halogenated products, the current method provides convenient access to synthetically important chiral building blocks that offer the potential for a variety of subsequent chemical transformations,[183,171,173,200] as demonstrated, for example, by the synthesis of α-chloroester **98p**, a known[202–204] synthetic intermediate in the synthesis of the antiplatelet drug (*S*)-Clopidogrel.

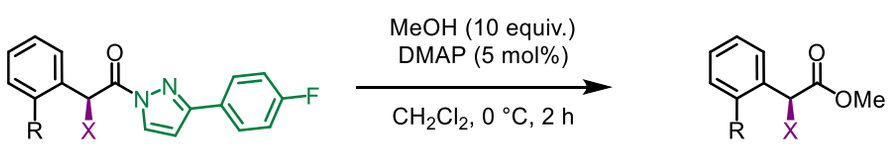

94d: R = H, X = F (>99.9% ee)
97d: R = H, X = Cl (95.4% ee)
97p: R = Cl, X = Cl (90.5% ee)

99d: R = H, X = F (99% yield, >99.9% ee)
98d: R = H, X = Cl (99% yield, 95.0% ee)
98p: R = Cl, X = Cl (>99% yield, 90.3% ee)

Scheme 42: Optimized conditions for removal of the pyrazole auxiliary.

3.5.7 Conclusions

In summary, this chapter presents a rare example in which the catalytic performance of a chiral Lewis acid catalyst with lower symmetry exceeds the performance of related standard C_2-symmetric catalysts. The non-C_2-symmetrical chiral-at-rhodium complex **RhNP2** was found to be amenable to the efficient and challenging asymmetric formation of carbon–fluorine as well as of carbon–chlorine bonds using essentially the same simple reaction conditions, thus demonstrating the versatility of the present catalytic system. For a range of different *N*-acyl pyrazoles, the corresponding α-fluorinated and α-chlorinated products were obtained in high yields and with high enantioselectivities. While the non-C_2-symmetric catalyst **RhNP2** was clearly superior in the conversion of substrates containing a secondary C–H by providing the corresponding α-halogenated products in high yields and stereoselectivities, the application of the sterically less hindered and established catalyst **RhS** could effectively fill the void for the construction of quaternary stereocenters for the generation of enantioenriched tertiary fluorides and chlorides with respectable results. Hence, the developed catalytic enantioselective α-fluorination and α-chlorination represent a valuable complement to existing methods and, moreover, are based on an exceptionally simple synthetic protocol, which is characterized by mild and fast (3–16 h) reaction conditions that allow a transformation at room temperature, with the requirement of only low catalyst loadings and readily available reagents. Finally, the usefulness of the auxiliary pyrazole moiety was corroborated, as this structural motif could readily be removed in a subsequent step with almost no epimerization, thus providing access to valuable chiral building blocks for subsequent chemical modifications.

4. Summary and Outlook

4.1 Summary

For the first time, this thesis opened up access to a previously elusive class of tris-heteroleptic bis-cyclometalated chiral-at-rhodium(III) complexes, which were demonstrated to be powerful Lewis acid catalysts for asymmetric photocycloadditions and highly enantioselective α-halogenation reactions. Single Λ- and Δ-enantiomers of the final catalysts were conveniently obtained in a nonracemic fashion after the development of a novel auxiliary-mediated strategy using chiral bis(oxazolines) as the chiral auxiliary ligands for the resolution of diastereomeric mixtures of complexes.

Chapter 3.1. Synthetic access to this new and intriguing class of chiral complexes was granted by serendipity, when the expansion of the family of bis-cyclometalated rhodium catalysts with a bis-benzimidazole derivative (**RhN**) was envisaged. In contrast to previous chiral-at-metal rhodium catalysts developed by the Meggers laboratory, the corresponding cyclometalation of rhodiumtrichloride hydrate with a structurally related phenylbenzimidazole ligand **47** stopped after the first cyclometalation and surprisingly afforded an isolable and stable mono-cyclometalated rhodium(III) species **48** as the main product of the reaction, while the originally targeted bis-cyclometalated complex **RhN** was only formed in traces. Optimization of the initial reaction conditions finally provided a small range of mono-cyclometalated rhodium complexes **48** (**a**,**c**,**d**) as the exclusive reaction products in high yields (83–86%), whereby *N*-alkyl groups on the imidazole nitrogen were well tolerated whereas aromatic residues gave inferior reaction results. Removal of the residual chloride ligand was also achieved by an adjustment of the reaction conditions and enabled access to a dicationic tetra-acetonitrile derivative **49** (Scheme 43).

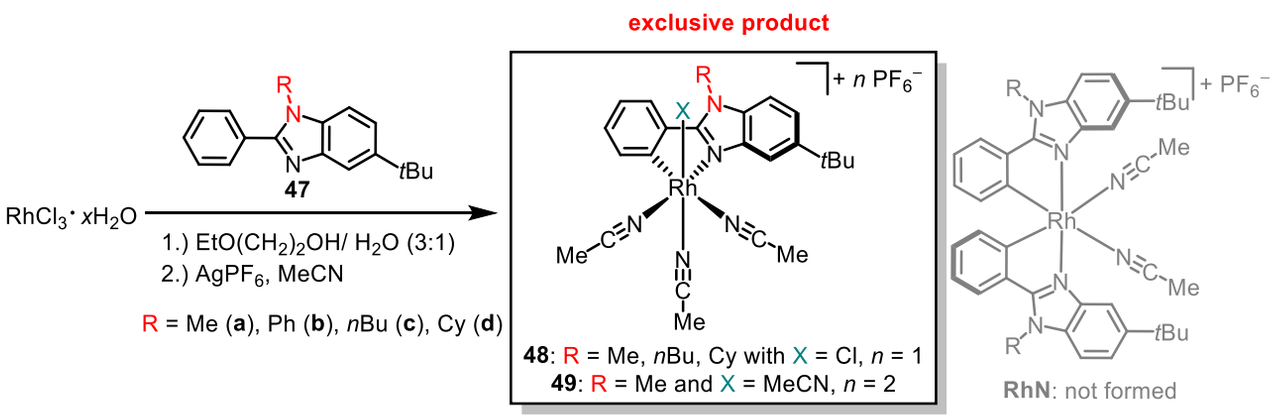

Scheme 43: Cyclometalation of $RhCl_3$ with phenylbenzimidazole ligands **47** provides stable mono-cyclometalated rhodium(III) species **48** instead of the expected bis-cyclometalated Rh-complexes **RhN**.

Chapter 3.2. A synthetic method for the preparation of chiral-at-rhodium(III) complexes containing two different cyclometalating ligands was developed. Due to the stability of the mono-cyclometalated rhodium species **48**, the introduction of a second different cyclometalating ligand in a subsequent second cyclometalation step was enabled. In this initial design, a related 5-*tert*-butyl-2-phenylbenzothiazole (**40**) was selected as the second ligand. Single Λ- and Δ-enantiomers of the catalyst were prepared using an established chiral auxiliary-mediated approach, which makes use of a chiral salicyloxazoline (*S*)-**41** as the chiral auxiliary ligand. However, due to the lower symmetry of the tris-heteroleptic complex **RhNS1** and the non-C_2-symmetry of the salicyloxazoline, a mixture of four diastereomers was obtained, which turned the resolution of the Λ- and Δ-configured stereoisomers into a rather tedious task. Nevertheless, the final catalysts Λ- and Δ-**RhNS1** were accessible with an essentially complete enantioselectivity of more than 99% ee and proved to be highly competent catalysts for intermolecular [2+2] photocycloadditions of α,β-unsaturated *N*-acyl pyrazoles and alkenes (Figure 31).[102]

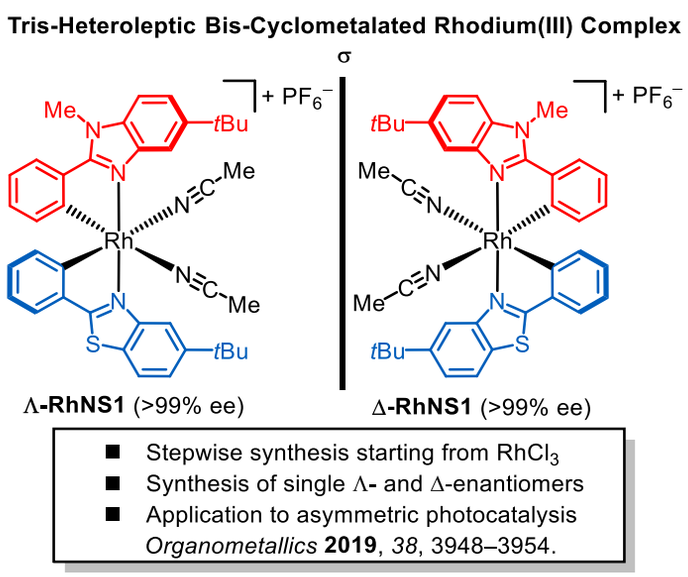

Figure 31: First method for the preparation of tris-heteroleptic bis-cyclometalated chiral-at-Rh catalysts.

Chapter 3.3. Synthetic access to the new class of tris-heteroleptic rhodium complexes was vastly improved by the introduction of a novel auxiliary-mediated strategy, which uses simple C_2-symmetric chiral bis(oxazolines) as the chiral auxiliary ligands. At first, the practicability of the new protocol was successfully demonstrated for the nonracemic synthesis of the established C_2-symmetric complexes Λ- and Δ-**RhS**, followed by the application to the synthesis of a new derivative of a bis-cyclometalated and non-C_2-symmetrical rhodium complex Λ- and Δ-**RhNS2**, whereby the particular benefit of the bis(oxazoline) auxiliary was disclosed. Due to its C_2-symmetry, only two diastereomers can form upon its coordination to a complex with lower

symmetry, which considerably simplified the chromatographic separation of the stereoisomers and thus convincingly solved the bottle-neck of the previous synthesis method (Figure 32).[128]

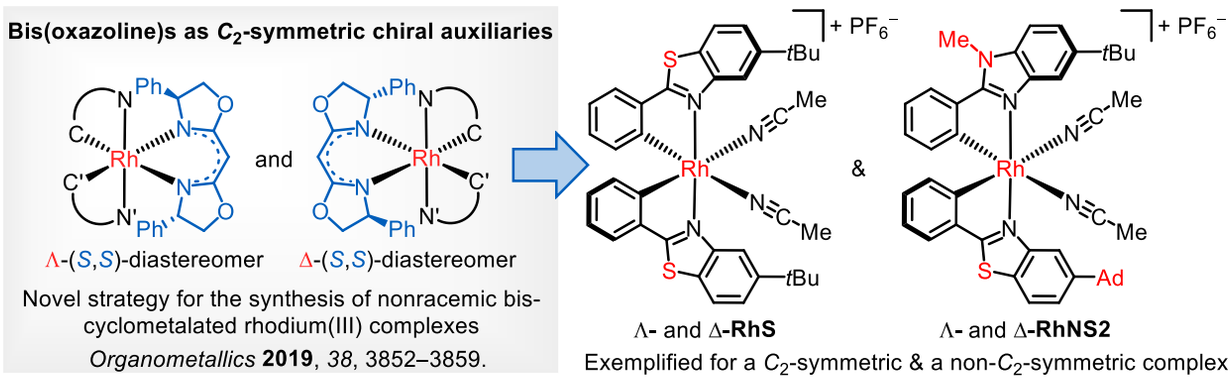

Figure 32: Synthesis of enantiomerically pure bis-cyclometalated rhodium(III) complexes using a simple chiral bis(oxazoline) ligand as the chiral auxiliary (no precedence). Only Λ-**RhS** and Λ-**RhNS2** are shown.

Chapter 3.4. In this chapter, the structural diversity of the new family of bis-cyclometalated rhodium catalysts with two different cyclometalating ligands was further expanded to include two phenylpyrazole derivatives. In this context, the elaborated synthetic method for the preparation of these complexes was subjected to a third revision cycle. Advantageously, the cyclometalating ligands were either commercially available or readily accessible via a short synthesis route and both ligands could be incorporated more efficiently according to an acetate promoted cyclometalation method. Introduction of a modified cyanobisoxazoline as chiral auxiliary further complemented the toolbox for the efficient synthesis of enantiomerically pure metal complexes and proved to be a useful lever to improve the stability of diastereomeric rhodium auxiliary complexes. Concluding with a more reliable acid mediated substitution of the coordinated bis(oxazolines), both catalysts **RhNP1** and **RhNP2** were conveniently accessible in a nonracemic fashion (>99% ee), thus proving the modularity of the present synthetic method (Figure 33).

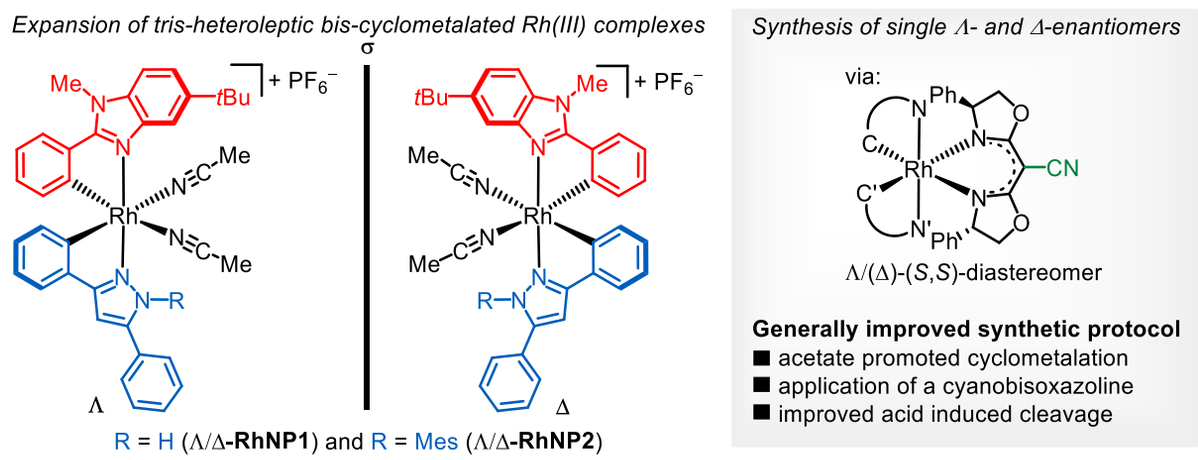

Figure 33: Supplementation of the new class of complexes by two phenylpyrazole catalysts and optimization of the previous synthetic method. Only the Λ-(*S*,*S*)-isomer is shown.

On account of all these appreciable improvements, a valid and straightforward synthetic approach to this novel class of tris-heteroleptic bis-cyclometalated chiral-at-rhodium(III) Lewis acid catalysts was ultimately developed and provides the corresponding complexes as reliably as their C_2-symmetric counterparts.

Chapter 3.5. An application of the non-C_2-symmetric and sterically demanding chiral-at-rhodium catalyst **RhNP2** to a highly enantioselective and high yielding α-fluorination (up to >99% ee and 99% yield) and α-chlorination (up to 98% ee and >99% yield) of *N*-acyl pyrazoles is introduced (Scheme 44). Both reactions are characterized by an exceptionally simple synthetic protocol, which at the same time represents a rare example in which a non-C_2-symmetrical catalyst design clearly outperforms the catalytic performance of related C_2-symmetric rhodium catalysts. A mild and convenient cleavage of the auxiliary pyrazole moiety moreover provides access to important chiral α-halogenated building blocks for subsequent chemical conversions.[161]

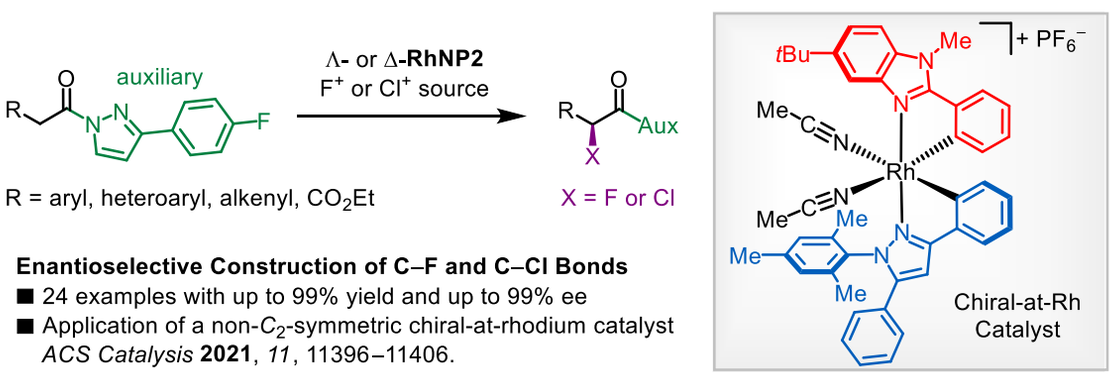

Scheme 44: Rhodium-catalyzed enantioselective α-fluorination and α-chlorination of *N*-acyl pyrazoles.

4.2 Outlook

In past and present work of the Meggers laboratory, the merit of chiral-at-metal complexes in a variety of different asymmetric conversions has been convincingly demonstrated and has at the same time entailed the continuous interest in the development of further sophisticated and structurally diverse catalyst designs for the realization of novel and intricate catalytic asymmetric transformations. Conceptually, the synthetic method for the preparation of tris-heteroleptic bis-cyclometalated rhodium complexes developed in this thesis, offers almost infinite possibilities to expand the structural diversity of chiral-at-rhodium(III) catalysts and to further exploit the structural richness of the octahedral coordination geometry by only being reliant on the introduction of a cyclometalating phenylbenzimidazole ligand in the first cyclometalation step. A

first demonstration of the versatility of this catalyst design has been exposed with the catalysts **RhNS1** and **RhNP2**, while a catalytic application of the sterically demanding catalyst **RhNS2** and the *β*-protic complex **RhNP1** remained elusive. Further efforts could thus be devoted to ascertain appropriate conversions for these two catalysts. Concerning the developed auxiliary-mediated strategy, chiral bis(oxazolines) have proven to be economical tools for the successful synthesis of enantiomerically pure rhodium complexes, but further investigations could be directed towards the elucidation of the generality of the developed approach for the synthesis of chiral transition metal catalysts, which differ from rhodium.

In terms of catalyst diversification, this thesis mainly concentrated on the synthesis of chiral-at-rhodium catalysts containing two different cyclometalating ligands according to the schematically illustrated **Design A** in Figure 34. Another appealing and potentially bifunctional version thereof represents **Example A**. Instead of a cyclometalated phenylbenzothiazole, the cyclometalation of a related phenylthiazolo[4,5-*b*]pyridine ligand as the second cyclometalating component could implement an internal Brønsted basic function in close proximity to the active site of the catalyst, whereby the basicity of the pyridine unit could be modulated by the introduction of electron-donating groups at R^2, while sterically demanding groups at R^1 could serve for an efficient asymmetric induction.

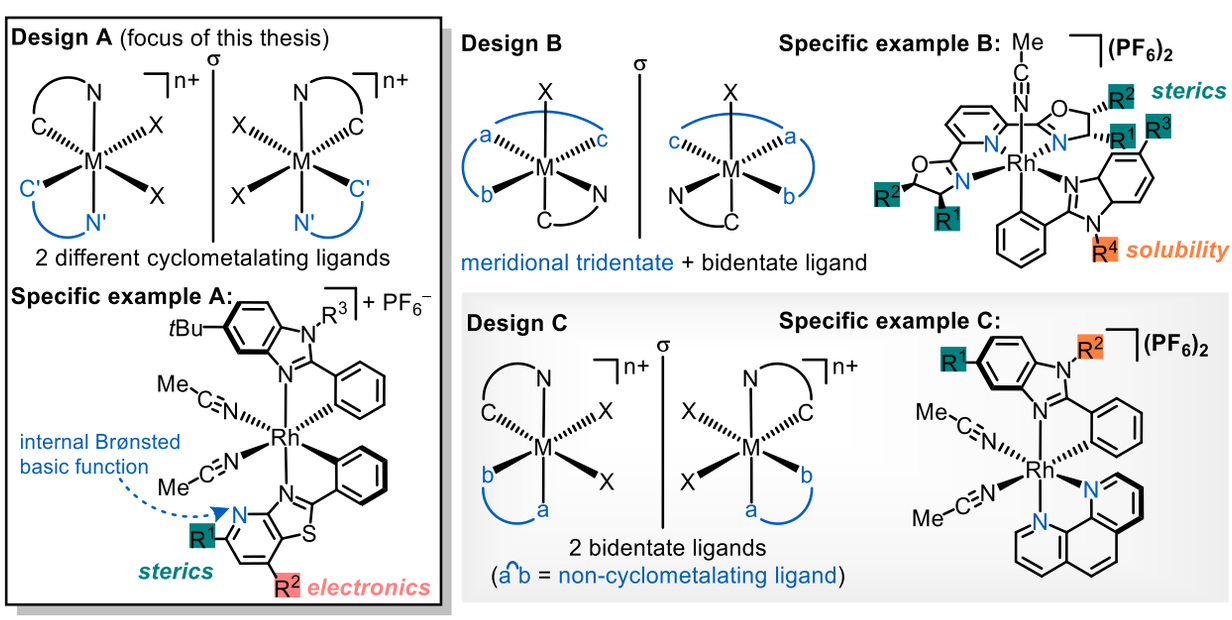

Figure 34: Suggestions for subsequent tris-heteroleptic catalyst designs based on the established key structure of the mono-cyclometalated rhodium benzimidazole complexes.

Apart from the design of bis-cyclometalated rhodium complexes, the incorporation of a second but non-cyclometalating ligand could be attractive, as the resulting dicationic complexes should be superior Lewis acid catalysts and could also serve as stronger oxidants in their photoexcited

states. While the monocationic mono-cyclometalated species **48** experimentally proved to be suitable starting materials for the introduction of a subsequent second cyclometalating ligand, the dicationic tetra-acetonitrile complex **49** and derivatives thereof would be the complexes of choice to attempt the introduction of a second non-cyclometalating ligand, since the equivalence of all four labile ligands could potentially reduce the number of isomeric complexes, that can result from the second coordination step. In theory, the incorporation of a second tridentate or bidentate ligand could be considered, thus generating another multitude of options for structural catalyst modifications (Figure 34, **Design B** and **C**). For example, Meggers and co-workers recently reported the synthesis and application of a ruthenium catalyst that contained, in addition to a cyclometalated bidentate *N*-heterocyclic carbene, a coordinated chiral pyridine-2,6-bis(oxazoline) (pybox) ligand,[205] which could be employed here in a similar way to complement the mono-cyclometalated rhodium(III) fragment, as shown in **Example B** (Figure 34). Considering the incorporation of a second bidentate chelating ligand, one could for example imagine to attempt the introduction of a phenanthroline (**Example C**, Figure 34), an *N*-heterocyclic carbene, or a phenylpyridine (ppy) ligand with different substitution patterns to modulate the steric environment of the reactive site, while the ability to synthesize mono-cyclometalated rhodium complexes with different *N*-alkyl residues on the imidazole nitrogen would generally provide a useful handle for the modulation of the solubility of the dicationic complexes.

5. Experimental Section

5.1 General Methods

All reactions were carried out under nitrogen atmosphere in oven-dried glassware unless otherwise noted. Reagents that were purchased from commercial suppliers were used without further purification. All solvents were distilled off from higher-boiling impurities on a rotary evaporator at 40 °C under reduced pressure prior to use. Solvents for non-aqueous reactions were dried and freshly distilled under nitrogen atmosphere from calcium hydride (CH_2Cl_2, MeCN and MeOH), phosphorus pentoxide ($CHCl_3$), sodium/benzophenone (THF) or sodium (toluene and Et_2O). Unless otherwise mentioned, HPLC Grade solvents including EtOH, DMF, 2-ethoxyethanol and DMSO were employed without further purification or further drying measures.

5.2 Instruments and Materials

Thin Layer Chromatography (TLC)

Reactions were monitored by TLC on glass TLC plates (TLC Silica gel 60 F_{254}) from Merck KGaA and either visualized via fluorescence quenching under UV-light (λ = 254 nm) and/or stained with a potassium permanganate solution (3 g $KMnO_4$, 20 g Na_2CO_3 and 1 NaOH pellet dissolved in 240 mL H_2O).

Flash Chromatography

Chromatographic purification of products was performed with silica gel 60 M from Macherey-Nagel (irregular shaped, 230–400 mesh, pH 6.8, pore volume: 0.81 mL · g^{-1}, mean pore size: 66 Å, specific surface: 492 $m^2 \cdot g^{-1}$, particle size distribution: 0.5% < 25 µm and 1.7% > 71 µm, water content: 1.6%) or aluminum oxide 90 neutral from Macherey-Nagel (activity 1). For loading the crude product onto the column, the sample was either dissolved in a minimum amount of solvent or it was adsorbed onto a small amount of silica gel. Unless otherwise specified, liquid sample loading was performed.

High-Performance Liquid Chromatography (HPLC)

Enantiomeric excess was established by HPLC analysis on a chiral stationary phase on an Agilent 1200 or 1260. Reversed phase HPLC measurements were performed on a Shimadzu LC-2030C or on an Agilent 1200 with an Agilent 6120 Series Quadrupole LC/MS System with multimode source. The HPLC conditions are detailed in the individual procedures.

Nuclear Magnetic Resonance Spectroscopy (NMR)

^{1}H, $^{13}C\{^{1}H\}$ and $^{19}F\{^{1}H\}$ NMR spectra were recorded on a Bruker AVIII HD 250 MHz or AVII 300 MHz spectrometer in automation or on a Bruker AVIII HD 300 MHz, AVIII 500 MHz, AVIII HD 500 MHz or AVII 600 MHz spectrometer by the members of the NMR service department of the Philipps-Universität Marburg. All measurements were performed at ambient temperature (300 K) unless otherwise stated. Chemical shifts δ are referenced against tetramethylsilane (TMS, $\delta = 0$ ppm) and reported in ppm with the residual solvent resonance as internal standard ($CDCl_3$ (^{1}H and ^{13}C): $\delta = 7.26$ ppm and 77.16 ppm; CD_2Cl_2 (^{1}H and ^{13}C): $\delta = 5.32$ ppm and 53.84 ppm; CD_3CN (^{1}H and ^{13}C): $\delta = 1.94$ ppm and 1.32/118.26 ppm; DMSO-d_6 (^{1}H and ^{13}C): $\delta = 2.50$ ppm and 39.52 ppm).[206] $^{19}F\{^{1}H\}$ NMR spectra were calibrated to trichlorofluoromethane ($CFCl_3$, $\delta = 0$ ppm) as the external standard. The information on the signal shapes is phenomenological and therefore does not describe the theoretically expected multiplicity. Multiplicities are described as follows: s = singlet, brs = broad singlet, d = doublet, t = triplet, q = quartet, m = multiplet and combinations thereof. All coupling constants *J* are given in Hertz (Hz) and refer to H–H or H–F (^{1}H NMR), F–F or F–P (^{19}F NMR) or C–F and C–Rh couplings (^{13}C NMR). H–F, C–F and C–Rh coupling interactions are only indicated for unambiguously assignable signals.

High Resolution Mass Spectrometry (HRMS)

Mass spectra were recorded by the mass service department of the Philipps-Universität Marburg. HR-ESI and APCI mass spectra were acquired with an LTQ-FT Ultra mass spectrometer from Thermo-Fischer Scientific. The resolution was set to 100.000. HR-EI mass spectra were acquired with an AccuTOF GCv 4G (JEOL) Time of Flight (TOF) mass spectrometer. An internal or external standard was used for drift time correction. The ion masses m/z are given in unit (u).

Infrared Spectroscopy (IR)

IR spectra were recorded on a Bruker Alpha FT-IR spectrometer. The absorption bands are given in wave numbers $\tilde{\nu}$ (cm^{-1}). Intensities are reported as follows: s = strong, m = medium, w = weak.

Melting Points

Melting points were determined on a Mettler Toledo MP70 using one end closed capillary tubes.

Circular Dichroism Spectroscopy (CD)

CD spectra were acquired with a JASCO J-810 CD spectropolarimeter with the following parameters: 600–200 nm, data pitch 0.5 nm, bandwidth 1 nm, response 1 second, sensitivity standard, scanning speed 50 nm/min, accumulation of 3 scans. Measurements were performed in a quartz cuvette (1.00 mm light path) with a sample concentration of 0.20 mM. CD spectra are reported as ellipticity θ and measured in units of mdeg but were converted into molar absorptivity $\Delta\varepsilon$ ($M^{-1}cm^{-1}$), which normalizes the circular dichroism spectra based on concentration and cell path length.

Optical Rotation

Optical rotations were determined at 22 °C for the Na-D wavelength (λ = 589 nm) on a Krüss P8000-T polarimeter with $[\alpha]_D^{22}$ values reported in degrees and concentrations in g/100 mL.

Light Source

Photochemical reactions were performed in 10 mL Synthware™ storage vessels made of borosilicate glass with a high vacuum valve and with a PTFE-O-ring on top. Reactions were placed 5–10 cm away from the irradiation source. Irradiation was performed with a 24 W blue LED (company: Hongchangzhaoming, website: https://hongchang-led.taobao.com) and reaction setups were covered with aluminum foil.

X-Ray Crystallography

Single crystal X-ray diffraction measurements were performed on a STOE STADIVARI or a Bruker AXS D8 Quest diffractometer by the members of the department for crystal structure analysis of the Philipps-Universität Marburg. Collected diffraction data were evaluated and crystal structures were solved and refined by Dr. Klaus Harms or Dr. (RUS) Sergei Ivlev.

5.3 Expanding the Family of Bis-Cyclometalated Chiral-at-Rhodium(III) Catalysts with a Benzimidazole Derivative

5.3.1 Synthesis of Cyclometalating Ligands

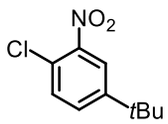

4-(*tert*-Butyl)-1-chloro-2-nitrobenzene (44)

According to a slightly modified procedure from Wegner *et al.*,[207] concentrated H_2SO_4 (7.56 mL, 135 mmol, 2.25 equiv.) was added slowly to concentrated HNO_3 (4.91 mL, 71.9 mmol, 1.20 equiv.) at 0 °C under air. 1-(*tert*-Butyl)-4-chlorobenzene (**43**, 10.0 mL, 59.9 mmol, 1.00 equiv.) was added dropwise to the cold mixture. The resulting solution was allowed to reach room temperature and was stirred vigorously for 22 h. The reaction mixture was poured into ice water (200 mL) and the aqueous phase was extracted with Et_2O (3 x 50 mL). The combined organic phases were dried over Na_2SO_4, filtered and the solvent was removed under reduced pressure. The crude product was adsorbed onto silica gel and then purified via column chromatography (*n*-pentane/EtOAc 50:1 → 45:1) to afford 4-(*tert*-butyl)-1-chloro-2-nitrobenzene (**44**, 11.7 g, 54.9 mmol, 92%) as a yellow oil.

TLC: R_f = 0.69 (*n*-pentane/EtOAc 20:1).

^{1}H NMR: 300 MHz, $CDCl_3$; δ = 7.86 (d, J = 2.3 Hz, 1H), 7.53 (dd, J = 8.5, 2.3 Hz, 1H), 7.46 (d, J = 8.5 Hz, 1H), 1.34 (s, 9H) ppm.

^{13}C NMR: 75 MHz, $CDCl_3$; δ = 151.9, 147.9, 131.5, 130.6, 124.0, 122.7, 35.1, 31.1 (3C) ppm.

IR: film, $\tilde{\nu}$ = 2965 (m), 2908 (w), 2872 (w), 1604 (w), 1531 (s), 1481 (w), 1351 (m), 1284 (w), 1256 (w), 1204 (w), 1167 (w), 1146 (w), 1116 (w), 1045 (m), 892 (w), 829 (m), 760 (m), 707 (w), 672 (w), 644 (w), 586 (w), 523 (w), 477 (w) cm^{-1}.

HRMS: EI; m/z calcd. for $C_{10}H_{12}ClNO_2$ [M]: 213.05566, found: 213.05568.

General Procedure A: S_NAr of 1-Chloro-2-nitroarenes with Amines

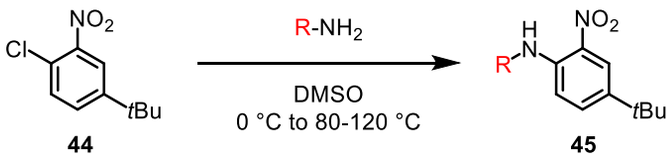

According to a slightly modified procedure from Beaulieu *et al.*,[103] 4-(*tert*-butyl)-1-chloro-2-nitrobenzene (**44**, 1.00 equiv.) and the specified primary amine (3.00–4.00 equiv.) were dissolved in DMSO (1 M), and the resulting solution was stirred at the indicated temperature for the indicated time. H_2O was added and the aqueous phase was extracted three times with EtOAc. The combined organic extracts were washed once with brine, dried over Na_2SO_4, and filtered. The solvent was removed under reduced pressure and the crude product was adsorbed onto silica gel. Purification by column chromatography (*n*-pentane/EtOAc 0:1 → 50:1) yielded the desired nitroanilines **45**.

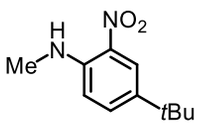

4-(*tert*-Butyl)-*N*-methyl-2-nitroaniline (45a)

Following the general procedure A, 4-(*tert*-butyl)-1-chloro-2-nitrobenzene (**44**, 311 mg, 1.46 mmol, 1.00 equiv.) and methylamine hydrochloride (295 mg, 4.37 mmol, 3.00 equiv.) were dissolved in DMSO (1.40 mL) under air. At 0 °C, KO*t*Bu (506 mg, 4.51 mmol, 3.10 equiv.) was added in small portions (exothermic reaction!). After 15 min, the ice bath was removed and the resulting black suspension was stirred at 90 °C for 24 h. Purification by column chromatography afforded 4-(*tert*-butyl)-*N*-methyl-2-nitroaniline (**45a**, 272 mg, 1.31 mmol, 90%) as an orange solid. For bigger approaches (>1 g of **44**), the reaction mixture was heated to 120 °C and stirred until TLC confirmed completion of the reaction. Typically, prolonged reaction times were then necessary to ensure complete conversion of the starting material. Sometimes, methylamine hydrochloride (0.50 equiv.) and KO*t*Bu (0.60 equiv.) were added again after a reaction time of 24 h in order to accelerate the reaction progress.

TLC: R_f = 0.21 (*n*-pentane/EtOAc 50:1).

^{1}H NMR: 300 MHz, $CDCl_3$; δ = 8.15 (d, J = 2.4 Hz, 1H), 7.94 (brs, 1H), 7.54 (dd, J = 9.0, 2.4 Hz, 1H), 6.81 (d, J = 9.0 Hz, 1H), 3.02 (d, J = 5.0 Hz, 3H), 1.30 (s, 9H) ppm.

^{13}C NMR: 126 MHz, $CDCl_3$; δ = 144.7, 138.6, 134.6, 131.5, 122.6, 113.4, 34.0, 31.2 (3C), 29.9 ppm.

IR: neat, $\tilde{\nu}$ = 3390 (m), 2955 (m), 2907 (w), 2865 (w), 1632 (m), 1564 (m), 1520 (s), 1464 (w), 1413 (w), 1391 (w), 1351 (m), 1316 (w), 1280 (w), 1255 (w), 1230 (m), 1180 (s), 1135 (w), 1113 (w), 1082 (w), 1046 (m), 1021 (w), 910 (w), 899 (w), 827 (w), 809 (m), 765 (m), 708 (m), 660 (w), 547 (s), 515 (w) cm^{-1}.

HRMS: ESI; m/z calcd. for $C_{11}H_{17}N_2O_2$ $[M+H]^+$: 209.1285, found: 209.1285.

m.p.: 52 °C (EtOAc).

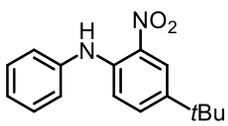

4-(*tert*-Butyl)-2-nitro-*N*-phenylaniline (45b)

The following procedure has not been optimized. According to the general procedure A, 4-(*tert*-butyl)-1-chloro-2-nitrobenzene (**44**, 200 mg, 0.94 mmol, 1.00 equiv.) was dissolved in DMSO (0.86 mL) under air. Subsequently, aniline (0.34 mL, 3.74 mmol, 4.00 equiv.) was added. At 0 °C, KO*t*Bu (210 mg, 1.87 mmol, 2.00 equiv.) was added portionwise. After 15 min, the ice bath was removed and the resulting reaction mixture was stirred at 80 °C for 24 h. Purification by column chromatography gave 4-(*tert*-butyl)-2-nitro-*N*-phenylaniline (**45b**, 193 mg, 0.71 mmol, 76%) as an orange oil along with some impurities which could not be completely separated from the product. However, the compound **45b** obtained was used for the subsequent step without further purification.

TLC: R_f = 0.30 (*n*-pentane/EtOAc 50:1).

^{1}H NMR: 500 MHz, $CDCl_3$; δ = 9.40 (brs, 1H), 8.17 (d, J = 2.4 Hz, 1H), 7.44 (dd, J = 9.0, 2.4 Hz, 1H), 7.42-7.38 (m, 2H), 7.28-7.26 (m, 2H), 7.22 (d, J = 8.9 Hz, 2H), 1.31 (s, 9H) ppm.

^{13}C NMR: 126 MHz, $CDCl_3$; δ = 141.1, 141.0, 139.2, 135.6, 133.9, 129.8 (2C), 125.4, 124.1 (2C), 122.5, 116.2, 34.3, 31.1 (3C) ppm.

HRMS: ESI; m/z calcd. for $C_{16}H_{18}N_2O_2Na$ $[M+Na]^+$: 293.1260, found: 293.1262.

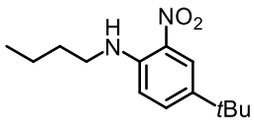

4-(*tert*-Butyl)-*N*-butyl-2-nitroaniline (45c)

Following the general procedure A, 4-(*tert*-butyl)-1-chloro-2-nitrobenzene (**44**, 1.00 g, 4.68 mmol, 1.00 equiv.) was dissolved in DMSO (4.70 mL) under nitrogen atmosphere. Subsequently, *N*-butylamine (1.85 mL, 18.7 mmol, 4.00 equiv.) was added and the resulting solution was stirred at 80 °C for 26 h. Purification by column chromatography afforded 4-(*tert*-butyl)-*N*-butyl-2-nitroaniline (**45c**, 1.15 g, 4.59 mmol, 98%) as a red oil.

TLC: R_f = 0.15 (*n*-pentane).

^{1}H NMR: 500 MHz, DMSO-d_6; δ = 8.03 (t, J = 5.5 Hz, 1H), 7.96 (d, J = 2.4 Hz, 1H), 7.64 (ddd, J = 9.0, 2.3, 0.1 Hz, 1H), 7.01 (d, J = 9.1 Hz, 1H), 3.36-3.32 (m, 2H), 1.63-1.57 (m, 2H), 1.42-1.34 (m, 2H), 1.25 (s, 9H), 0.92 (t, J = 7.4 Hz, 3H) ppm.

^{13}C NMR: 126 MHz, DMSO-d_6; δ = 143.5, 137.5, 134.8, 130.0, 121.1, 114.6, 41.9, 33.5, 30.6 (3C), 30.5, 19.6, 13.6 ppm.

IR: film, $\tilde{\nu}$ = 3384 (w), 2958 (m), 2932 (w), 2868 (w), 1738 (w), 1631 (m), 1564 (m), 1519 (s), 1467 (w), 1424 (w), 1404 (w), 1349 (m), 1306 (w), 1281 (w), 1252 (w), 1233 (s), 1205 (w), 1164 (m), 1135 (w), 1114 (w), 1064 (w), 953 (w), 912 (w), 897 (w), 814 (m), 765 (w), 710 (w), 663 (w), 521 (m) cm^{-1}.

HRMS: ESI; m/z calcd. for $C_{14}H_{23}N_2O_2$ $[M+H]^+$: 251.1754, found: 251.1762.

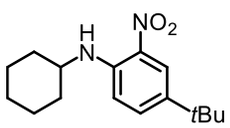

4-(*tert*-Butyl)-*N*-cyclohexyl-2-nitroaniline (45d)

Following the general procedure A, 4-(*tert*-butyl)-1-chloro-2-nitrobenzene (**44**, 0.20 g, 0.94 mmol, 1.00 equiv.) was dissolved in DMSO (0.90 mL) under nitrogen atmosphere. Subsequently, cyclohexylamine (0.43 mL, 3.74 mmol, 4.00 equiv.) was added and the resulting solution was stirred at 120 °C for 25 h. Purification by column chromatography afforded 4-(*tert*-butyl)-*N*-cyclohexyl-2-nitroaniline (**45d**, 0.25 g, 0.89 mmol, 95%) as an orange solid.

TLC: R_f = 0.11 (*n*-pentane).

^{1}H NMR: 300 MHz, DMSO-d_6; δ = 7.96 (d, J = 2.4 Hz, 1H), 7.93 (brs, 1H), 7.63 (dd, J = 9.1, 2.4 Hz, 1H), 7.01 (d, J = 9.2 Hz, 1H), 3.68-3.59 (m, 1H), 1.96-1.93 (m, 2H), 1.71-1.67 (m, 2H), 1.61-1.55 (m, 1H), 1.49-1.30 (m, 5H), 1.25 (s, 9H) ppm.

^{13}C NMR: 75 MHz, DMSO-d_6; δ = 142.7, 137.6, 135.0, 129.9, 121.2, 115.1, 50.0, 33.6, 32.1 (2C), 30.6 (3C), 25.1, 24.0 (2C) ppm.

IR: neat, $\tilde{\nu}$ = 3357 (w), 2929 (m), 2857 (w), 1632 (w), 1565 (w), 1513 (s), 1467 (w), 1450 (w), 1426 (w), 1398 (w), 1365 (w), 1346 (m), 1303 (w), 1285 (w), 1261 (w), 1241 (m), 1224 (w), 1187 (w), 1156 (m), 1110 (w), 1065 (w), 914 (w), 892 (w), 817 (s), 766 (m), 727 (w), 664 (w), 556 (s), 522 (w), 469 (w) cm^{-1}.

HRMS: ESI; m/z calcd. for $C_{16}H_{24}N_2O_2Na$ $[M+Na]^+$: 299.1730, found: 299.1739.

m.p.: 95 °C (EtOAc).

General Procedure B: Synthesis of 1,2-Phenylenediamines

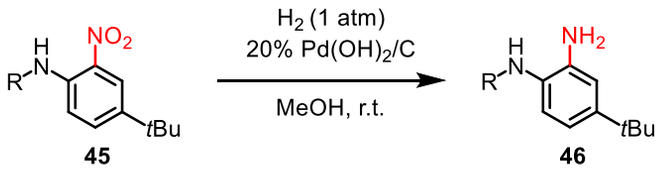

45 **46**

According to a slightly modified procedure from Beaulieu *et al.*,[103] the corresponding nitroaniline **45** (1.00 equiv.) and 20% $PdOH_2$ on charcoal (3 mol%) were suspended in MeOH (0.2 M) and hydrogenated (1 atm H_2 gas) for the indicated time at room temperature under vigorous stirring. Subsequently, the reaction mixture was filtered over a short plug of celite and rinsed with MeOH. The solvent was removed under reduced pressure and the crude product was adsorbed onto silica gel. Purification by column chromatography (*n*-pentane/EtOAc with a gradient) provided pure 1,2-phenylenediamines **46**.

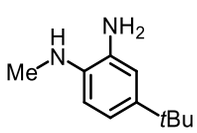

4-(*tert*-Butyl)-*N*^{1}-methylbenzene-1,2-diamine (46a)

Following the general procedure B, 4-(*tert*-butyl)-*N*-methyl-2-nitroaniline (**45a**, 359 mg, 1.72 mmol, 1.00 equiv.) and 20% $PdOH_2$ on charcoal (36.0 mg, 0.05 mmol, 3 mol%) were suspended in MeOH (9.00 mL) and hydrogenated (1 atm H_2 gas) for 31 h at room temperature

under vigorous stirring. Purification by column chromatography (*n*-pentane/EtOAc 4:1 → 2:1) gave 4-(*tert*-butyl)-N^1-methylbenzene-1,2-diamine (**46a**, 259 mg, 1.45 mmol, 84%) as a dark purple solid.

TLC: R_f = 0.20 (*n*-pentane/EtOAc 2:1).

^{1}H NMR: 500 MHz, DMSO-d_6; δ = 6.60 (d, J = 2.3 Hz, 1H), 6.52 (dd, J = 8.1, 2.3 Hz, 1H), 6.29 (d, J = 8.2 Hz, 1H), 4.35 (brs, 2H), 2.67 (d, J = 2.2 Hz, 3H), 1.19 (s, 9H) ppm.

^{13}C NMR: 126 MHz, DMSO-d_6; δ = 138.9, 134.9, 134.7, 113.9, 111.4, 108.9, 33.4, 31.6 (3C), 30.4 ppm.

IR: neat, $\tilde{\nu}$ = 3338 (m), 3208 (w), 2954 (s), 2901 (w), 2865 (w), 2805 (w), 1621 (w), 1590 (m), 1519 (s), 1477 (w), 1458 (w), 1419 (w), 1391 (w), 1360 (w), 1330 (w), 1284 (s), 1259 (w), 1219 (m), 1202 (w), 1169 (m), 1132 (w), 1090 (w), 1046 (w), 935 (w), 865 (m), 801 (s), 767 (w), 738 (w), 686 (m), 653 (w), 626 (s), 578 (w), 535 (w), 495 (m), 456 (m), 426 (w) cm^{-1}.

HRMS: ESI; m/z calcd. for $C_{11}H_{19}N_2$ $[M+H]^+$: 179.1543, found: 179.1543.

m.p.: 49 °C (EtOAc).

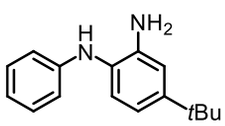

4-(*tert*-Butyl)-N^1-phenylbenzene-1,2-diamine (46b)

Following the general procedure B, 4-(*tert*-butyl)-2-nitro-*N*-phenylaniline (**45b**, 240 mg, 0.89 mmol, 1.00 equiv.) and 20% $PdOH_2$ on charcoal (18.7 mg, 0.03 mmol, 3 mol%) were suspended in MeOH (4.67 mL) and hydrogenated (1 atm H_2 gas) for 22 h at room temperature under vigorous stirring. Purification by column chromatography (*n*-pentane/EtOAc 10:1 → 8:1) gave 4-(*tert*-butyl)-N^1-phenylbenzene-1,2-diamine (**46b**, 162 mg, 0.67 mmol, 76%) as a colorless solid.

TLC: R_f = 0.24 (*n*-pentane/EtOAc 10:1).

^{1}H NMR: 500 MHz, DMSO-d_6; δ = 7.11-7.07 (m, 2H), 7.00 (brs, 1H), 6.91 (d, J = 8.2 Hz, 1H), 6.79 (d, J = 2.3 Hz, 1H), 6.69-6.67 (m, 2H), 6.64-6.60 (m, 1H), 6.57 (d, J = 8.2, 2.3 Hz, 1H), 4.62 (brs, 2H), 1.25 (s, 9H) ppm.

^{13}C NMR: 126 MHz, DMSO-d_6; δ = 146.8, 146.4, 142.1, 128.8 (2C), 124.9, 123.5, 117.2, 114.1 (2C), 113.4, 112.3, 33.9, 31.3 (3C) ppm.

HRMS: ESI; m/z calcd. for $C_{16}H_{21}N_2$ $[M+H]^+$: 241.1699, found: 241.1700.

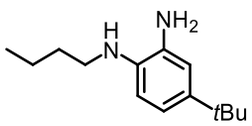

4-(*tert*-Butyl)-N^1-butylbenzene-1,2-diamine (46c)

Following the general procedure B, 4-(*tert*-butyl)-*N*-butyl-2-nitroaniline (**45c**, 1.15 g, 4.59 mmol, 1.00 equiv.) and 20% $PdOH_2$ on charcoal (96.8 mg, 0.14 mmol, 3 mol%) were suspended in MeOH (30.0 mL) and hydrogenated (1 atm H_2 gas) for 24 h at room temperature under vigorous stirring. Purification by column chromatography (*n*-pentane/EtOAc 5:1 → 2:1) afforded 4-(*tert*-butyl)-N^1-butylbenzene-1,2-diamine (**46c**, 1.01 g, 4.58 mmol, >99%) as a brown solid.

TLC: R_f = 0.60 (*n*-pentane/EtOAc 2:1).

^{1}H NMR: 250 MHz, DMSO-d_6; δ = 6.59 (d, J = 2.3 Hz, 1H), 6.49 (dd, J = 8.1, 2.3 Hz, 1H), 6.32 (d, J = 8.2 Hz, 1H), 4.38 (brs, 2H), 4.12 (brs, 1H), 3.00-2.94 (m, 2H), 1.61-1.50 (m, 2H), 1.47-1.32 (m, 2H), 1.18 (s, 9H), 0.92 (t, J = 7.2 Hz, 3H) ppm.

^{13}C NMR: 75 MHz, DMSO-d_6; δ = 138.9, 134.6, 133.9, 113.8, 111.6, 109.4, 43.3, 33.4, 31.6 (3C), 31.1, 20.0, 13.9 ppm.

IR: neat, $\tilde{\nu}$ = 3378 (w), 3297 (w), 3049 (w), 2953 (s), 2930 (w), 2865 (w), 1619 (m), 1583 (w), 1520 (s), 1469 (w), 1422 (w), 1361 (w), 1329 (w), 1280 (s), 1251 (w), 1220 (w), 1157 (m), 1134 (w), 1097 (w), 1028 (w), 990 (w), 935 (w), 905 (w), 865 (m), 796 (s), 753 (w), 720 (w), 697 (m), 636 (w), 619 (w), 575 (w), 529 (w), 455 (m) cm^{-1}.

HRMS: ESI; m/z calcd. for $C_{14}H_{25}N_2$ $[M+H]^+$: 221.2012, found: 221.2018.

m.p.: 137 °C (EtOAc).

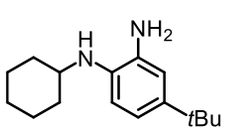

4-(*tert*-Butyl)-N^1-cyclohexylbenzene-1,2-diamine (46d)

Following the general procedure B, 4-(*tert*-butyl)-*N*-cyclohexyl-2-nitroaniline (**45d**, 5.29 g, 19.1 mmol, 1.00 equiv.) and 20% $PdOH_2$ on charcoal (0.40 g, 0.57 mmol, 3 mol%) were suspended in MeOH (98.5 mL) and hydrogenated (1 atm H_2 gas) for 36 h at room temperature under vigorous stirring. Purification by column chromatography (*n*-pentane/EtOAc 10:1 → 6:1

→ 4:1) yielded 4-(*tert*-butyl)-N^1-cyclohexylbenzene-1,2-diamine (**46d**, 3.77 g, 15.3 mmol, 80%) as a purple solid.

TLC: R_f = 0.27 (*n*-pentane/EtOAc 5:1).

^{1}H NMR: 500 MHz, DMSO-d_6; δ = 6.60 (d, J = 2.3 Hz, 1H), 6.47 (dd, J = 8.2, 2.3 Hz, 1H), 6.36 (d, J = 8.3 Hz, 1H), 4.37 (brs, 2H), 3.88 (brs, 1H), 3.11 (brs, 1H), 1.95-1.92 (m, 2H), 1.73-1.69 (m, 2H), 1.62-1.59 (m, 1H), 1.36-1.27 (m, 2H), 1.20-1.10 (m, 3H), 1.18 (s, 9H) ppm.

^{13}C NMR: 126 MHz, DMSO-d_6; δ = 138.8, 134.9, 132.5, 113.8, 112.0, 110.7, 51.2, 33.3, 33.0 (2C), 31.5 (3C), 25.7, 24.7 (2C) ppm.

IR: neat, $\tilde{\nu}$ = 3386 (w), 3325 (m), 3048 (w), 2926 (s), 2854 (m), 2659 (w), 1616 (w), 1584 (w), 1515 (s), 1477 (w), 1450 (w), 1423 (w), 1391 (w), 1363 (w), 1328 (w), 1306 (w), 1282 (s), 1257 (w), 1240 (w), 1216 (w), 1203 (w), 1161 (w), 1128 (w),1106 (w), 1073 (w), 1026 (w), 978 (w), 937 (w), 887 (m), 860 (w), 846 (w), 821 (w), 797 (s), 772 (w), 728 (w), 631 (w), 586 (m), 517 (w), 455 (m), 427 (w) cm^{-1}.

HRMS: ESI; m/z calcd. for $C_{16}H_{27}N_2$ $[M+H]^+$: 247.2169, found: 247.2175.

m.p.: 66 °C (EtOAc).

<u>General Procedure C:</u> Oxone®-Mediated Synthesis of Benzimidazoles

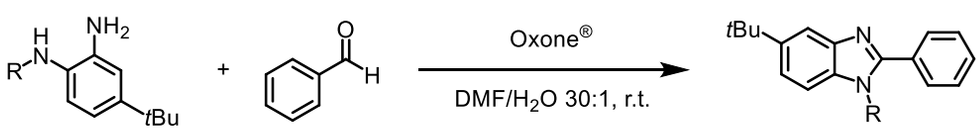

46 + **28** → **47**

According to a slightly modified procedure from Beaulieu *et al.*,[103] the specified 1,2-phenylenediamine (**46**, 1.00 equiv.) was dissolved in a 30:1 mixture of DMF and H_2O (0.62 M) under air. Subsequently, benzaldehyde (**28**, 1.10 equiv.) was added dropwise, followed by addition of Oxone® (0.65 equiv.) in one portion. The resulting solution was stirred for the indicated time at room temperature, before it was poured into H_2O. Some K_2CO_3 (aq., 1 M) was added and the aqueous phase was extracted three times with EtOAc. The combined organic phases were washed once with brine, dried over Na_2SO_4 and filtered. The solvent was removed under reduced pressure and the crude product was adsorbed onto silica gel. Purification by column chromatography (*n*-pentane/EtOAc with a gradient) afforded the corresponding

benzimidazole **47**. Since a high purity of the final ligands is important for the subsequent cyclometalation step with rhodium, the benzimidazole ligands obtained were recrystallized from hot *n*-hexane every time they were isolated as off-white or pale yellow solids after chromatographic purification. Recrystallization provided the benzimidazole ligands **47** as colorless crystalline solids.

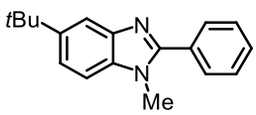

5-(*tert*-Butyl)-1-methyl-2-phenyl-1*H*-benzo[*d*]imidazole (47a)

Following the general procedure C, 4-(*tert*-butyl)-N^1-methylbenzene-1,2-diamine (**46a**, 201 mg, 1.13 mmol, 1.00 equiv.) was dissolved in DMF (1.77 mL) and H_2O (59.0 µL) under air. Benzaldehyde (**28**, 125 µL, 1.24 mmol, 1.10 equiv.) was added dropwise, followed by addition of Oxone® (225 mg, 0.73 mmol, 0.65 equiv.) in one portion, and the resulting solution was stirred for 1.5 h at room temperature. Purification by column chromatography (*n*-pentane/EtOAc 5:1 → 3:1) gave 5-*tert*-butyl-1-methyl-2-phenylbenzimidazole (**47a**, 246 mg, 0.93 mmol, 83%) as a colorless solid. Recrystallization from hot *n*-hexane afforded **47a** as a colorless crystalline solid.

TLC: R_f = 0.52 (*n*-pentane/EtOAc 2:1).

^{1}H NMR: 500 MHz, $CDCl_3$; δ = 7.87 (dd, J = 1.8, 0.6 Hz, 1H), 7.77-7.75 (m, 2H), 7.54-7.50 (m, 3H), 7.42 (dd, J = 8.6, 1.8 Hz, 1H), 7.33 (dd, J = 8.2, 0.3 Hz, 1H), 3.85 (s, 3H), 1.42 (s, 9H) ppm.

^{13}C NMR: 126 MHz, $CDCl_3$; δ = 153.9, 146.0, 143.1, 134.7, 130.5, 129.7, 129.5 (2C), 128.8 (2C), 121.0, 116.2, 109.1, 34.9, 32.0 (3C), 31.8 ppm.

IR: neat, $\tilde{\nu}$ = 3059 (w), 2947 (m), 2898 (w), 2865 (w), 2343 (w), 2183 (w), 2073 (w), 1967 (w), 1903 (w), 1852 (w), 1826 (w), 1781 (w), 1738 (w), 1723 (w), 1619 (w), 1600 (w), 1522 (w), 1485 (w), 1467 (s), 1417 (w), 1379 (m), 1363 (w), 1323 (m), 1281 (w), 1260 (w), 1228 (w), 1205 (w), 1156 (w), 1108 (w), 1078 (w), 1057 (w), 1022 (m), 999 (w), 931 (w), 868 (w), 850 (w), 818 (w), 800 (m), 772 (s), 714 (w), 700 (s), 652 (m), 609 (w), 576 (w), 522 (w), 489 (w), 457 (w), 432 (w) cm^{-1}.

HRMS: ESI; m/z calcd. for $C_{18}H_{21}N_2$ $[M+H]^+$: 265.1699, found: 265.1698.

m.p.: 111 °C (EtOAc).

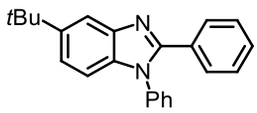

5-(*tert*-Butyl)-1,2-diphenyl-1*H*-benzo[*d*]imidazole (47b)

Following the general procedure C, 4-(*tert*-butyl)-N^1-phenylbenzene-1,2-diamine (**46b**, 138 mg, 0.57 mmol, 1.00 equiv.) was dissolved in DMF (0.91 mL) and H_2O (30.2 µL) under air. Benzaldehyde (**28**, 63.8 µL, 0.63 mmol, 1.10 equiv.) was added dropwise, followed by addition of Oxone® (115 mg, 0.37 mmol, 0.65 equiv.) in one portion, and the resulting solution was stirred for 2 h at room temperature. Purification by column chromatography (*n*-pentane/EtOAc 10:1 → 9:1) afforded **47b** (149 mg, 0.46 mmol, 80%) as colorless needles.

TLC: R_f = 0.25 (*n*-pentane/EtOAc 10:1).

^{1}H NMR: 500 MHz, $CDCl_3$; δ = 7.93 (d, J = 1.8 Hz, 1H), 7.58-7.55 (m, 2H), 7.51-7.44 (m, 3H), 7.37-7.33 (m, 2H), 7.31-7.28 (m, 4H), 7.19 (d, J = 8.6 Hz, 1H), 1.42 (s, 9H) ppm.

^{13}C NMR: 126 MHz, $CDCl_3$; δ = 152.6, 146.6, 143.2, 137.4, 135.3, 130.3, 129.9 (2C), 129.5 (2C), 129.4, 128.5, 128.4 (2C), 127.5 (2C), 121.5, 116.3, 109.9, 35.0, 32.0 (3C) ppm.

IR: neat, $\tilde{\nu}$ = 3047 (w), 2961 (w), 2866 (w), 1872 (w), 1742 (w), 1614 (w), 1594 (w), 1520 (w), 1496 (w), 1474 (w), 1449 (w), 1422 (w), 1381 (m), 1325 (w), 1308 (w), 1284 (m), 1231 (w), 1202 (w), 1184 (w), 1111 (w), 1074 (w), 1025 (w), 1002 (w), 977 (w), 939 (w), 920 (w), 875 (m), 846 (w), 808 (m), 769 (s), 689 (s), 655 (w), 637 (w), 615 (w), 581 (w), 543 (w), 502 (w), 462 (w) cm^{-1}.

HRMS: ESI; m/z calcd. for $C_{23}H_{23}N_2$ $[M+H]^+$: 327.1856, found: 327.1857.

m.p.: 141 °C (EtOAc).

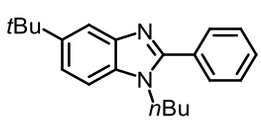

5-(*tert*-Butyl)-1-butyl-2-phenyl-1*H*-benzo[*d*]imidazole (47c)

Following the general procedure C, 4-(*tert*-butyl)-N^1-butylbenzene-1,2-diamine (**46c**, 4.73 g, 21.4 mmol, 1.00 equiv.) was dissolved in DMF (47.0 mL) and H_2O (1.4 mL) under air. Benzaldehyde (**28**, 2.38 mL, 23.6 mmol, 1.10 equiv.) was added dropwise, followed by addition of Oxone® (4.28 g, 13.9 mmol, 0.65 equiv.) in one portion, and the resulting solution was stirred for 1 h at room temperature. Purification by column chromatography (*n*-pentane/EtOAc 10:1 →

7:1 → 5:1) afforded **47c** as a brown solid. Subsequent recrystallization from hot *n*-hexane gave 5-*tert*-butyl-1-butyl-2-phenylbenzimidazole (**47c**, 3.92 g, 12.8 mmol, 60%) as a colorless crystalline solid.

TLC: R_f = 0.45 (*n*-pentane/EtOAc 5:1).

^{1}H NMR: 300 MHz, $CDCl_3$; δ = 7.86-7.85 (m, 1H), 7.74-7.68 (m, 2H), 7.55-7.46 (m, 3H), 7.42-7.33 (m, 2H), 4.23-4.18 (m, 2H), 1.86-1.76 (m, 2H), 1.42 (s, 9H), 1.35-1.23 (m, 2H), 0.87 (t, *J* = 7.4 Hz, 3H) ppm.

^{13}C NMR: 126 MHz, DMSO-d_6; δ = 152.9, 144.6, 142.6, 133.5, 130.8, 129.4, 129.0 (2C), 128.7 (2C), 120.3, 115.1, 110.1, 43.7, 34.4, 31.7 (3C), 31.2, 19.2, 13.2 ppm.

IR: neat, $\tilde{\nu}$ = 3059 (w), 2958 (m), 2934 (w), 2865 (w), 2080 (w), 2032 (w), 1987 (w), 1893 (w), 1851 (w), 1748 (w), 1621 (w), 1600 (w), 1523 (w), 1485 (w), 1463 (s), 1422 (w), 1389 (m), 1360 (w), 1325 (m), 1280 (w), 1258 (w), 1230 (w), 1203 (w), 1175 (m), 1151 (w), 1116 (w), 1073 (w), 1024 (w), 970 (w), 933 (w), 876 (w), 853 (w), 821 (w), 800 (m), 776 (m), 739 (w), 698 (s), 670 (w), 650 (m), 625 (w), 578 (w), 491 (w), 458 (w) cm^{-1}.

HRMS: ESI; m/z calcd. for $C_{21}H_{27}N_2$ $[M+H]^+$: 307.2169, found: 307.2176.

m.p.: 93 °C (EtOAc).

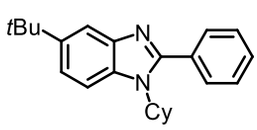

5-(*tert*-Butyl)-1-cyclohexyl-2-phenyl-1*H*-benzo[*d*]imidazole (47d)

Following the general procedure C, 4-(*tert*-butyl)-N^1-cyclohexylbenzene-1,2-diamine (**46d**, 1.41 g, 5.72 mmol, 1.00 equiv.) was dissolved in DMF (8.95 mL) and H_2O (0.30 mL) under air. Benzaldehyde (**28**, 0.64 mL, 6.30 mmol, 1.10 equiv.) was added dropwise, followed by addition of Oxone® (1.14 g, 3.72 mmol, 0.65 equiv.) in one portion, and the resulting solution was stirred for 1 h at room temperature. Purification by column chromatography (*n*-pentane/EtOAc 10:1 → 6:1 → 4:1) afforded **47d** (1.35 g, 4.06 mmol, 71%) as a pale yellow solid. After recrystallization from hot *n*-hexane 5-*tert*-butyl-1-cyclohexyl-2-phenylbenzimidazole (**47d**, 1.15 g, 3.47 mmol, 61%) was obtained as a colorless crystalline solid.

TLC: R_f = 0.22 (*n*-pentane/EtOAc 5:1).

^{1}H NMR: 500 MHz, $CDCl_3$; δ = 7.85 (d, J = 1.6 Hz, 1H), 7.64-7.61 (m, 2H), 7.59 (d, J = 8.7 Hz, 1H), 7.54-7.51 (m, 3H), 7.34 (dd, J = 8.7, 1.8 Hz, 1H), 4.37-4.30 (m, 1H), 2.36-2.29 (m, 2H), 1.97-1.91 (m, 4H), 1.76-1.75 (m, 1H), 1.41 (s, 9H), 1.37-1.27 (m, 3H) ppm.

^{13}C NMR: 126 MHz, $CDCl_3$; δ = 153.9, 145.5, 143.9, 132.0, 131.5, 129.6, 129.6 (2C), 128.8 (2C), 120.3, 116.6, 112.1, 57.0, 34.8, 31.9 (3C), 31.7 (2C), 26.1 (2C), 25.5 ppm.

IR: neat, $\tilde{\nu}$ = 3060 (w), 2948 (m), 2928 (w), 2855 (w), 1522 (w), 1471 (w), 1446 (m), 1425 (w), 1390 (w), 1368 (s), 1328 (w), 1282 (w), 1202 (w), 1175 (w), 1155 (w), 1117 (w), 1076 (w), 1022 (w), 991 (w), 940 (w), 880 (m), 842 (w), 801 (m), 768 (s), 719 (m), 695 (s), 677 (w), 654 (w), 635 (w), 581 (w), 474 (w) cm^{-1}.

HRMS: ESI; m/z calcd. for $C_{23}H_{29}N_2$ $[M+H]^+$: 333.2325, found: 333.2334.

m.p.: 132 °C (EtOAc).

5.3.2 Synthesis of Mono-Cyclometalated Rhodium(III) Complexes

General Procedure D:

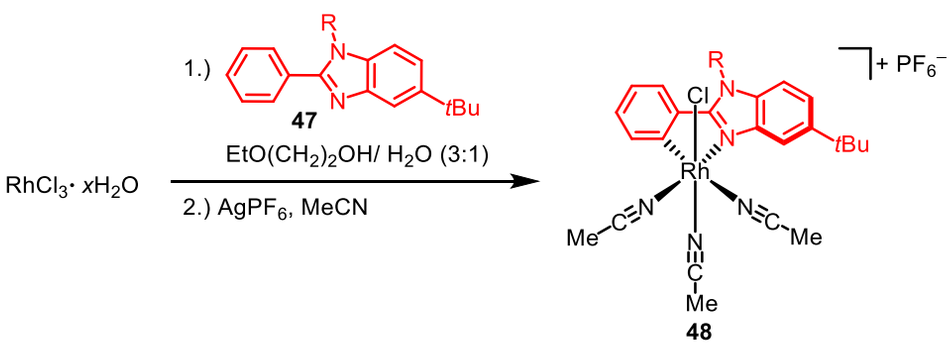

Based on a previously published protocol by the Meggers group,[100] the synthesis of mono-cyclometalated rhodium complexes **48** was carried out with some modifications. Accordingly, a suspension of rhodium(III) trichloride hydrate (40% Rh content, 1.00 equiv.) and the specified benzimidazole ligand (**47**, 1.00–1.10 equiv.) in a 3:1 mixture of 2-ethoxyethanol and H_2O (0.05 M) was stirred at 140–150 °C for 7 h. The reaction mixture was cooled to room temperature, and the solvent was thoroughly removed under reduced pressure (water bath of rotary evaporator set to 60 °C). $AgPF_6$ (1.80 equiv.) and MeCN (0.05 M) were added, successively, and the resulting suspension was stirred at 60 °C for the indicated time under exclusion of light. The mixture was allowed to reach room temperature, before it was filtered over a short plug of celite and rinsed with MeCN. After removal of the solvent under reduced

pressure, the yellow oil obtained was purified via column chromatography (CH_2Cl_2/MeCN with a gradient) to give the respective complex **48**.

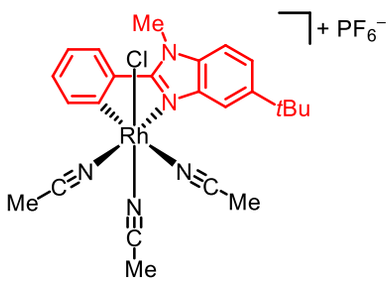

Synthesis of Mono-Cyclometalated Rhodium Complex 48a

Following the general procedure D, a suspension of rhodium(III) trichloride hydrate (100 mg, 0.39 mmol, 1.00 equiv.) and 5-*tert*-butyl-1-methyl-2-phenylbenzimidazole (**47a**, 113 mg, 0.43 mmol, 1.10 equiv.) in 2-ethoxyethanol (5.85 mL) and H_2O (1.95 mL) was stirred at 150 °C for 7 h. For the second step, $AgPF_6$ (177 mg, 0.70 mmol, 1.80 equiv.) and MeCN (7.80 mL) were added successively to the brown residue obtained, and the resulting suspension was stirred at 60 °C for 15 h in the dark. Purification by column chromatography (CH_2Cl_2/MeCN 40:1 → 20:1 → 15:1 → 10:1 → 5:1) (Ø = 3 cm, H = 30 cm) afforded **48a** (223 mg, 0.33 mmol, 86%) as a yellow solid. A crystal structure of complex **48a** is available. Detailed information and the corresponding crystallographic data can be found in Chapter 6.4.

TLC: R_f = 0.33 (CH_2Cl_2/MeCN 5:1).

^{1}H NMR: 500 MHz, CD_3CN; δ = 8.13 (dd, J = 1.7, 0.6 Hz, 1H), 8.01 (dd, J = 7.7, 1.5 Hz, 1H), 7.97 (dd, J = 7.8, 1.1 Hz, 1H), 7.61 (dd, J = 8.8, 1.8 Hz, 1H), 7.57 (d, J = 8.8 Hz, 1H), 7.42-7.39 (m, 1H), 7.36-7.33 (m, 1H), 4.21 (s, 3H), 2.63 (s, 3H), 2.10 (s, 3H), 1.47 (s, 9H) ppm.

^{13}C NMR: 126 MHz, CD_3CN; δ = 157.9 (d, $J_{C,Rh}$ = 2.5 Hz, 1C), 157.1 (d, $J_{C,Rh}$ = 25.2 Hz, 1C), 148.8, 140.0, 136.7, 135.7, 134.2, 131.1, 126.6, 125.9, 123.6, 123.5 (d, $J_{C,Rh}$ = 5.9 Hz, 1C), 123.0 (d, $J_{C,Rh}$ = 6.2 Hz, 1C), 112.6, 111.8, 35.7, 33.2, 31.9 (3C), 4.49, 3.92 ppm.

^{19}F NMR: 282 MHz, CD_3CN; δ = –72.9 (d, $J_{P,F}$ = 707 Hz, 6F) ppm.

IR: neat, $\tilde{\nu}$ = 2958 (w), 2332 (w), 1621 (w), 1584 (w), 1523 (w), 1485 (w), 1428 (w), 1366 (w), 1335 (w), 1295 (w), 1262 (w), 1161 (w), 1027 (w), 831 (s), 769 (w), 733 (w), 695 (w), 651 (w), 556 (m), 453 (w) cm^{-1}.

HRMS: APCI; m/z calcd. for $C_{24}H_{27}N_5Rh$ $[M–HCl]^+$: 488.1316, found: 488.1329 and APCI; m/z calcd. for $C_{22}H_{25}ClN_4Rh$ $[M–MeCN]^+$: 483.0817, found: 483.0830.

m.p.: 214 °C decomposition (CH_2Cl_2).

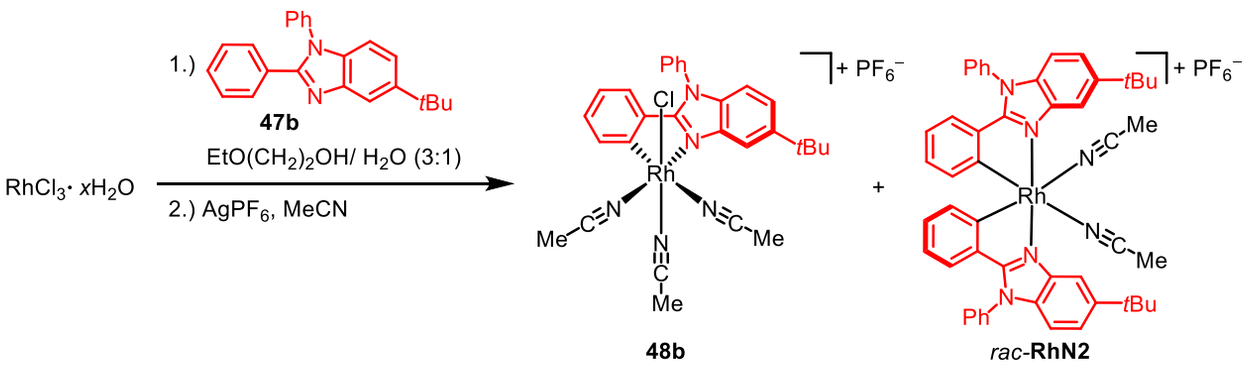

Synthesis of *rac*-RhN2/Mono-Cyclometalated Rhodium Complex 48b

For the following synthesis, the general procedure D was followed with some modifications. As one of the first experiments, the cyclometalation of rhodium with benzimidazole ligand **47b** was attempted with the aim of obtaining the corresponding bis-cyclometalated rhodium complex *rac*-**RhN2**. Accordingly, a suspension of rhodium(III) trichloride hydrate (110 mg, 0.43 mmol, 1.00 equiv.) and 2 equivalents of 5-*tert*-butyl-1,2-diphenylbenzimidazole (**47b**, 279 mg, 0.86 mmol) in 2-ethoxyethanol (6.42 mL) and H_2O (2.14 mL) was stirred at 125 °C for 5 h. For the second step, $AgPF_6$ (216 mg, 0.86 mmol, 2.00equiv.) and MeCN (8.56 mL) were added successively to the brown residue obtained, and the resulting suspension was stirred at 60 °C for 15 h under exclusion of light. TLC indicated the formation of several products. Purification by column chromatography (CH_2Cl_2/MeCN 25:1 → 20:1 → 15:1 → 10:1 → 5:1 → 3:1) (Ø = 3 cm, H = 30 cm) afforded the desired bis-cyclometalated complex *rac*-**RhN2** in about 34% yield as a pale yellow solid. Due to similar R_f values of the target bis-cyclometalated complex and residual ligand **47b** only 8% (32.0 mg, 32.6 µmol) of the complex were purely isolated, whereas the rest was isolated as a mixture of *rac*-**RhN2** and **48b** (188 mg). The overall yield of 34% was calculated by integration of baseline separated signals from the ^{1}H NMR of the mixture obtained. Furthermore, a mixture of two or more complexes started to elute with more polar solvent mixtures (CH_2Cl_2/MeCN 5:1). Analysis of the ^{1}H NMR of the isolated brown solid (202 mg) revealed that it most likely contained the mono-cyclometalated species **48b**, but also a significant amount of side products (Figure 35).

Analytical data of purely isolated *rac*-**RhN2**:

TLC: R_f = 0.71 (CH_2Cl_2/MeCN 5:1).

^{1}H NMR: 500 MHz, $CDCl_3$; δ = 8.15 (brs, 2H), 7.77-7.64 (m, 8H), 7.52 (dd, J = 8.7, 1.1 Hz, 2H), 7.47 (d, J = 7.8 Hz, 2H), 7.17 (d, J = 8.7 Hz, 2H), 6.76-6.73 (m, 2H), 6.66-6.63 (m, 2H), 6.56 (dd, J = 7.8, 1.3 Hz, 2H), 6.30 (brs, 2H), 2.35 (brs, 6H), 1.46 (s, 18H) ppm.

^{13}C NMR: 126 MHz, $CDCl_3$; δ = 163.0 (2C), 157.7 (2C), 148.9 (2C), 139.8 (2C), 135.3 (2C), 134.9 (2C), 134.3 (2C), 133.5 (2C), 130.8 (2C), 130.7 (2C), 130.6 (2C), 129.5 (2C), 128.2 (2C), 128.0 (2C), 124.8 (2C), 123.0 (2C), 122.9 (2C), 121.1 (2C), 113.0 (2C), 110.6 (2C), 35.3 (2C), 31.8 (6C), 3.47 (2C) ppm.

^{19}F NMR: 282 MHz, $CDCl_3$; δ = –73.0 (d, $J_{P,F}$ = 712 Hz, 6F) ppm.

HRMS: APCI; m/z calcd. for $C_{50}H_{48}N_6Rh$ $[M]^+$: 835.2990, found: 835.3019.

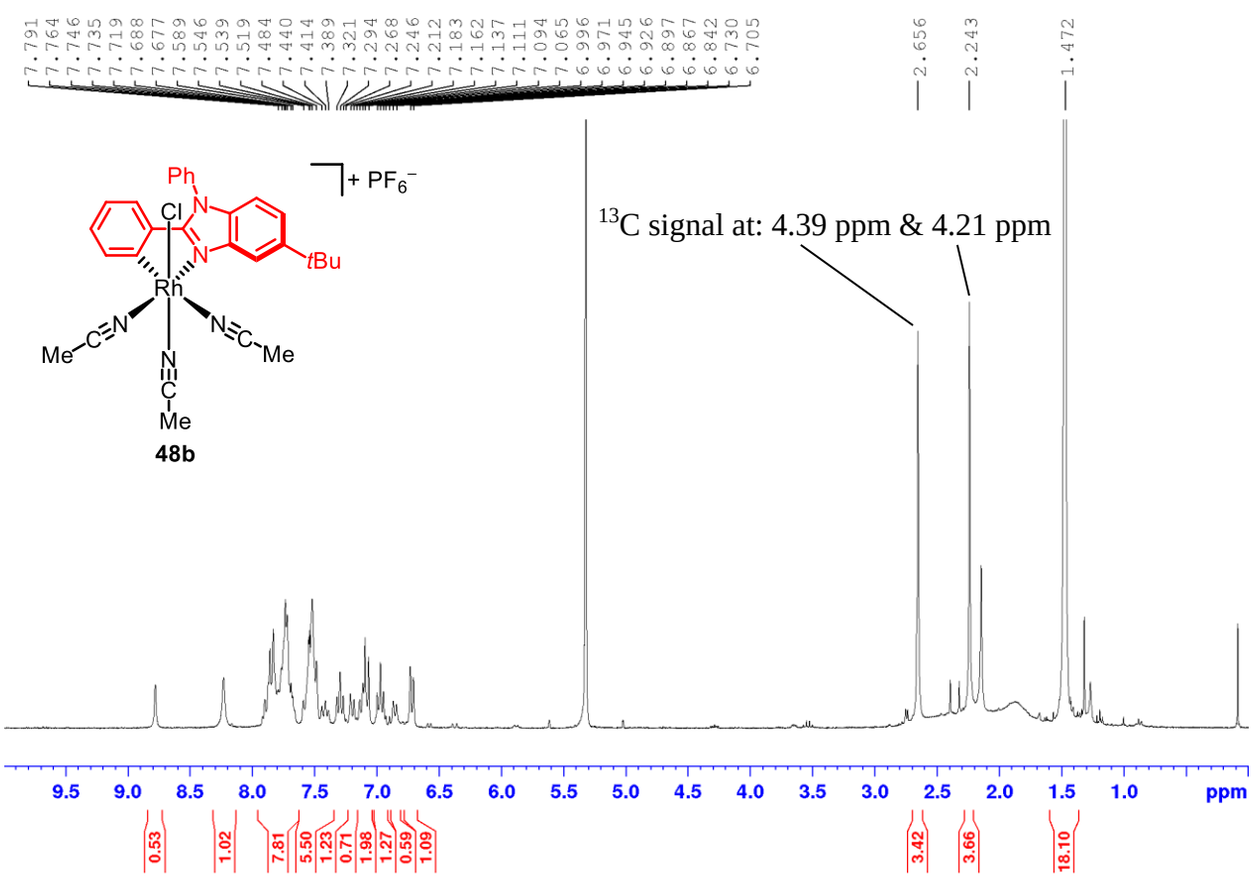

Figure 35: ^{1}H NMR (300 MHz, 300 K, CD_2Cl_2) spectrum of the isolated mixture of complexes. The chemical shifts of the two singlets at 2.66 and 2.24 ppm and their respective ^{13}C signals are very similar to those of the previously synthesized complexes **48a**,**c**,**d** and therefore the mixture obtained most likely contains the mono-cyclometalated rhodium species **48b**, in addition to other complexes with the same R_f value.

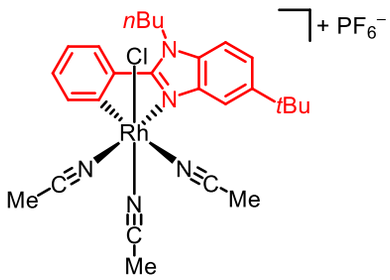

Synthesis of Mono-Cyclometalated Rhodium Complex 48c

Following the general procedure D, a suspension of rhodium(III) trichloride hydrate (150 mg, 0.58 mmol, 1.00 equiv.) and 5-*tert*-butyl-1-butyl-2-phenylbenzimidazole (**47c**, 179 mg, 0.58 mmol, 1.00 equiv.) in 2-ethoxyethanol (8.75 mL) and H_2O (2.92 mL) was stirred at 140 °C for 7 h. For the second step, $AgPF_6$ (265 mg, 1.05 mmol, 1.80 equiv.) and MeCN (11.7 mL) were added successively to the brown residue obtained, and the resulting suspension was stirred at 60 °C for 19 h in the dark. Purification by column chromatography (CH_2Cl_2/MeCN 40:1 → 20:1 → 10:1 → 5:1 → 3:1) (Ø = 3.5 cm, H = 30 cm) yielded **48c** (351 mg, 0.49 mmol, 85%) as a yellow solid. A crystal structure of complex **48c** is available. Detailed information and the corresponding crystallographic data can be found in Chapter 6.4.

TLC: R_f = 0.61 (CH_2Cl_2/MeCN 5:1).

^{1}H NMR: 300 MHz, CD_3CN; δ = 8.15 (brs, 1H), 7.98 (dd, J = 7.5, 1.5 Hz, 1H), 7.89 (dd, J = 7.4, 1.8 Hz, 1H), 7.60 (d, J = 1.1 Hz, 2H), 7.43-7.33 (m, 2H), 4.64 (dd, J = 8.2, 7.0 Hz, 2H), 2.62 (s, 3H), 2.11 (s, 3H), 1.92-1.87 (m, 2H), 1.53-1.41 (m, 2H), 1.47 (s, 9H), 0.96 (t, J = 7.4 Hz, 3H) ppm.

^{13}C NMR: 75 MHz, CD_3CN; δ = 157.4 (d, $J_{C,Rh}$ = 25.0 Hz, 1C), 157.3, 149.0, 140.1, 136.7, 135.4, 133.8, 131.2, 126.4, 126.1, 123.7, 123.5 (d, $J_{C,Rh}$ = 5.9 Hz, 1C), 123.1 (d, $J_{C,Rh}$ = 6.2 Hz, 1C), 112.8, 111.9, 46.0, 35.7, 32.5, 31.9 (3C), 20.7, 14.0, 4.47, 3.94 ppm.

^{19}F NMR: 282 MHz, CD_3CN; δ = –73.0 (d, $J_{P,F}$ = 706 Hz, 6F) ppm.

IR: neat, $\tilde{\nu}$ = 2954 (w), 2310 (w), 1618 (w), 1582 (w), 1516 (w), 1481 (w), 1428 (w), 1367 (w), 1335 (w), 1295 (w), 1189 (w), 1029 (w), 830 (s), 770 (w), 733 (w), 698 (w), 653 (w), 555 (s), 457 (w) cm^{-1}.

HRMS: APCI; m/z calcd. for $C_{27}H_{33}N_5Rh$ $[M–HCl]^+$: 530,1791, found: 530.1789 and APCI; m/z calcd. for $C_{25}H_{31}ClN_4Rh$ $[M–MeCN]^+$: 525.1287, found: 525.1290.

m.p.: 130 °C decomposition (CH_2Cl_2).

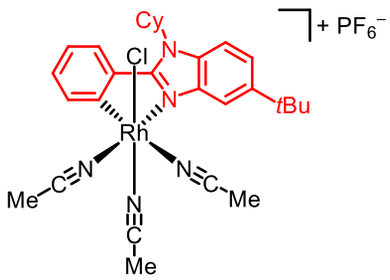

Synthesis of Mono-Cyclometalated Rhodium Complex 48d

Following the general procedure D, a suspension of rhodium(III) trichloride hydrate (150 mg, 0.58 mmol, 1.00 equiv.) and 5-*tert*-butyl-1-cyclohexyl-2-phenylbenzimidazole (**47d**, 194 mg, 0.58 mmol, 1.00 equiv.) in 2-ethoxyethanol (8.75 mL) and H_2O (2.92 mL) was stirred at 150 °C for 7 h. For the second step, $AgPF_6$ (265 mg, 1.05 mmol, 1.80 equiv.) and MeCN (11.7 mL) were added successively to the brown residue obtained, and the resulting suspension was stirred at 60 °C for 14 h in the dark. Purification by column chromatography (CH_2Cl_2/MeCN 80:1 → 60:1 → 40:1 → 30:1 → 20:1 → 10:1 → 5:1 → 3:1) (Ø = 3.5 cm, H = 30 cm) yielded **48d** (356 mg, 0.48 mmol, 83%) as a yellow solid.

TLC: R_f = 0.23 (CH_2Cl_2/MeCN 10:1).

^{1}H NMR: 500 MHz, CD_3CN; δ = 8.20 (d, J = 1.7 Hz, 1H), 7.99 (dd, J = 7.6, 1.3 Hz, 1H), 7.92 (dd, J = 7.6, 1.0 Hz, 1H), 7.84 (d, J = 8.9 Hz, 1H), 7.52 (dd, J = 8.9, 1.9 Hz, 1H), 7.41-7.34 (m, 2H), 5.21-5.14 (m, 1H), 2.63 (s, 3H), 2.45-2.35 (m, 2H), 2.11 (s, 3H), 2.08-1.99 (m, 3H), 1.84-1.80 (m, 1H), 1.71-1.60 (m, 2H), 1.52-1.42 (m, 2H), 1.46 (s, 9H) ppm.

^{13}C NMR: 126 MHz, CD_3CN; δ = 157.8 (d, $J_{C,Rh}$ = 24.8 Hz, 1C), 157.3 (d, $J_{C,Rh}$ = 3.0 Hz, 1C), 148.7, 141.1, 136.8, 135.7, 132.0, 131.0, 126.8, 126.0, 123.4 (d, $J_{C,Rh}$ = 5.8 Hz, 1C), 123.2, 123.0 (d, $J_{C,Rh}$ = 6.0 Hz, 1C), 115.3, 113.3, 59.4, 35.6, 32.0, 31.9, 31.8 (3C), 26.5, 26.5, 25.7, 4.50, 3.99 ppm.

^{19}F NMR: 282 MHz, CD_3CN; δ = –72.9 (d, $J_{P,F}$ = 706 Hz, 6F) ppm.

IR: neat, $\tilde{\nu}$ = 2928 (w), 2855 (w), 2336 (w), 2173 (w), 1618 (w), 1581 (w), 1513 (w), 1469 (w), 1426 (w), 1367 (w), 1281 (w), 1257 (w), 1185 (w), 1028 (w), 830 (s), 769 (w), 732 (w), 699 (w), 684 (w), 652 (w), 556 (m), 455 (w), 426 (w) cm^{-1}.

HRMS: APCI; m/z calcd. for $C_{29}H_{35}N_5Rh$ $[M–HCl]^+$: 556.1948, found: 556.1959.

m.p.: 184 °C (CH_2Cl_2).

5.3.3 Synthesis of the Dicationic Tetra-Acetonitrile Rhodium Complex 49

Method A (3-Step Synthesis):

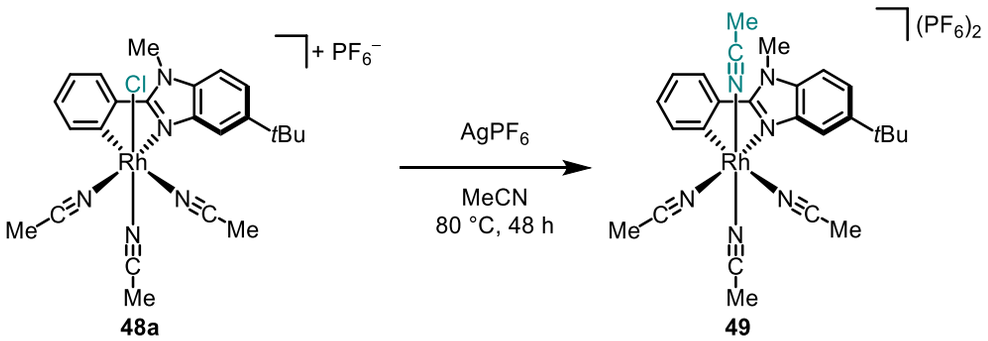

Synthesis of Tetra-Acetonitrile Complex 49 Starting from Complex 48a

A solution of mono-cyclometalated rhodium complex **48a** (20.0 mg, 0.03 mmol, 1.00 equiv.) (prepared via the 2-step synthesis described in Section 5.3.2) and $AgPF_6$ (15.1 mg, 0.06 mmol, 2.00 equiv.) in MeCN (1.20 mL) was stirred for 48 h at 80 °C under careful exclusion of light. The mixture was cooled to room temperature, and filtered over a short plug of celite which was rinsed with MeCN. After removal of the solvent under reduced pressure, the residue obtained was purified via column chromatography (CH_2Cl_2/MeCN 20:1 → 10:1 → 5:1 → 2:1) (Ø = 2 cm, H = 15 cm) to give tetra-acetonitrile complex **49** (22.3 mg, 27.2 µmol, 91%) as a colorless solid. A crystal structure of the complex is available. Detailed information and the corresponding crystallographic data can be found in Chapter 6.4.

TLC: R_f = 0.21 (CH_2Cl_2/MeCN 5:1).

^{1}H NMR: 300 MHz, CD_3CN; δ = 8.11-8.08 (m, 2H), 8.00-7.97 (m, 1H), 7.69-7.62 (m, 2H), 7.53-7.47 (m, 2H), 4.25 (s, 3H), 2.68 (s, 3H), 2.17 (s, 6H), 1.47 (s, 9H) ppm.

^{13}C NMR: 126 MHz, CD_3CN; δ = 157.6 (d, $J_{C,Rh}$ = 2.0 Hz, 1C), 152.2 (d, $J_{C,Rh}$ = 23.7 Hz, 1C), 149.5, 139.5, 136.3, 135.2, 134.2, 132.2, 127.6, 127.4, 125.2 (2C), 125.2, 124.3, 112.5, 112.1, 35.8, 33.4, 31.8 (3C), 4.59, 4.23 (2C) ppm.

^{19}F NMR: 235 MHz, CD_3CN; δ = –72.9 (d, $J_{P,F}$ = 706 Hz, 6F) ppm.

IR: neat, $\tilde{\nu}$ = 3640 (w), 3571 (w), 2945 (w), 2343 (w), 2311 (w), 2281 (w), 1628 (w), 1588 (w), 1533 (w), 1487 (w), 1432 (w), 1365 (w), 1339 (w), 1296 (w), 1264 (w), 1233 (w), 1161 (w), 1123 (w), 1029 (w), 827 (s), 771 (w), 732 (m), 696 (w), 651 (w), 610 (w), 556 (s), 452 (w) cm^{-1}.

Method B (2-Step Synthesis):

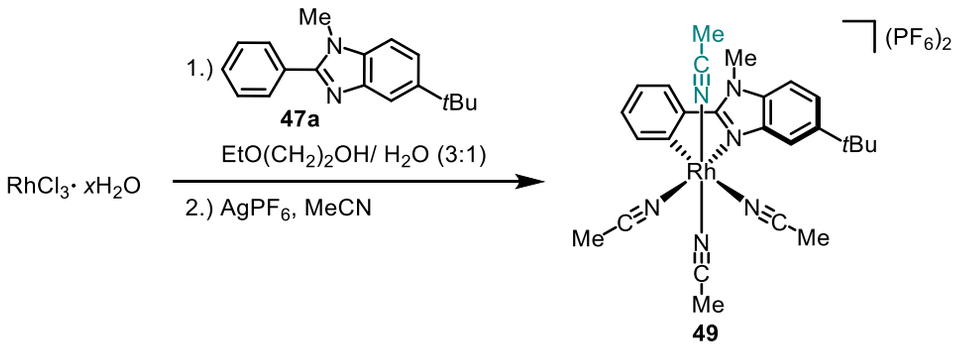

Direct Synthesis of Tetra-Acetonitrile Complex 49 Starting from $RhCl_3 \cdot xH_2O$

A suspension of rhodium(III) trichloride hydrate (50.0 mg, 0.19 mmol, 1.00 equiv.) and 5-*tert*-butyl-1-methyl-2-phenylbenzimidazole (**47a**, 53.9 mg, 0.20 mmol, 1.05 equiv.) in 2-ethoxyethanol (2.91 mL) and H_2O (0.97 mL) was stirred at 150 °C for 7 h. The reaction mixture was cooled to room temperature, and the solvent was thoroughly removed under reduced pressure (water bath of rotary evaporator set to 60 °C). For the second step, $AgPF_6$ (172 mg, 0.68 mmol, 3.5 equiv.) and MeCN (7.76 mL) were added, successively, and the resulting suspension was stirred at 80 °C for 54 h under careful exclusion of light. The mixture was allowed to reach room temperature, before it was filtered over a short plug of celite and rinsed with MeCN. After removal of the solvent under reduced pressure, the yellow oil obtained was purified by column chromatography (CH_2Cl_2/MeCN 40:1 → 20:1 → 10:1 → 5:1 → 2:1) (Ø = 2,5 cm, H = 38 cm). Via this route, tetra-acetonitrile complex **49** was obtained in 60% yield (95.4 mg, 0.12 mmol) over two steps as a colorless solid. Analytical data were in agreement with the spectroscopic data obtained from Method A.

5.4 Chiral-at-Rhodium Catalyst with Two Different Cyclometalating Ligands

5.4.1 Catalyst Synthesis

5-*tert*-Butyl-2-phenylbenzothiazole (**40**), chiral fluorinated salicyloxazoline (*S*)-**41** and **RhS** were synthesized according to previously published procedures by the Meggers group.[100] 5-*tert*-Butyl-1-methyl-2-phenylbenzimidazole (**47a**) and mono-cyclometalated rhodium complex **48a** were prepared as described in Chapter 5.3.

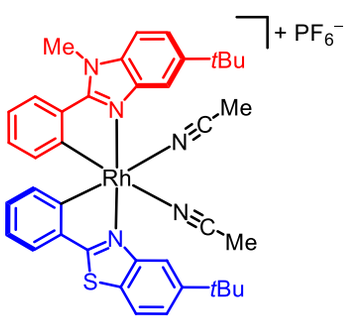

Synthesis of *rac*-RhNS1

A suspension of mono-cyclometalated rhodium species **48a** (100 mg, 0.15 mmol, 1.00 equiv.) and 5-*tert*-butyl-2-phenylbenzothiazole (**40**, 40.0 mg, 0.15 mmol, 1.00 equiv.) in 2-ethoxyethanol (2.25 mL) and H_2O (0.75 mL) was stirred at 80 °C for 72 h in the dark. The reaction mixture was cooled to room temperature, and the solvent was thoroughly removed under reduced pressure (water bath of rotary evaporator set to 60 °C). $AgPF_6$ (68.0 mg, 0.27 mmol, 1.80 equiv.) and MeCN (3.00 mL) were added, successively, and the resulting suspension was stirred at 60 °C for 14 h in the dark. The mixture was allowed to reach room temperature, before it was filtered over a short plug of celite and rinsed with MeCN. The solvent was removed under reduced pressure and the obtained residue was purified by column chromatography (CH_2Cl_2/MeCN 60:1 → 40:1 → 20:1) to afford *rac*-**RhNS1** (72.0 mg, 0.08 mmol, 56%, ratio of *rac*-**RhNS1** to **RhS**/**RhN1** = 5.6:1) as a pale yellow solid.

TLC: R_f = 0.40 (CH_2Cl_2/MeCN 20:1).

^{1}H NMR: 300 MHz, CD_2Cl_2; δ = 8.52 (d, J = 1.6 Hz, 1H), 8.03 (d, J = 8.6 Hz, 1H), 7.99 (d, J = 1.1 Hz, 1H), 7.82 (dd, J = 7.8, 1.1 Hz, 1H), 7.72 (dd, J = 8.6, 1.8 Hz, 1H), 7.68-7.64 (m, 2H), 7.61 (d, J = 8.7 Hz, 1H), 7.05 (dt, J = 7.6, 1.0 Hz, 1H), 7.00 (dt,

J = 7.5, 1.0 Hz, 1H), 6.84-6.78 (m, 2H), 6.27 (d, J = 7.8 Hz, 1H), 6.15 (d, J = 7.8 Hz, 1H), 4.29 (s, 3H), 2.18 (brs, 6H), 1.47 (s, 9H), 1.46 (s, 9H) ppm.

^{13}C NMR: 126 MHz, CD_2Cl_2; δ = 176.6, 161.7, 158.3, 158.2, 152.5, 150.5, 148.5, 140.4, 139.7, 135.1, 134.1, 134.0, 133.5, 131.0, 129.9, 129.3, 126.1, 125.3, 125.0, 124.1, 124.0, 123.1, 122.8, 121.4 (2C), 117.1, 112.6, 110.4, 35.6, 35.4, 32.8, 31.8 (3C), 31.6 (3C), 3.64 (2C) ppm.

^{19}F NMR: 282 MHz, CD_2Cl_2; δ = –74.0 (d, $J_{P,F}$ = 711 Hz, 6F) ppm.

IR: neat, $\tilde{\nu}$ = 2957 (w), 2868 (w), 2282 (w), 1580 (w), 1555 (w), 1513 (w), 1480 (w), 1440 (w), 1419 (w), 1364 (w), 1330 (w), 1294 (w), 1257 (w), 1160 (w), 1122 (w), 1026 (w), 993 (w), 933 (w), 835 (s), 760 (w), 729 (w), 699 (w), 671 (w), 651 (w), 611 (w), 555 (m), 458 (w) cm^{-1}.

HRMS: APCI; m/z calcd. for $C_{39}H_{41}N_5RhS$ $[M]^+$: 714.2132, found: 714.2135.

m.p.: 213 °C (CH_2Cl_2).

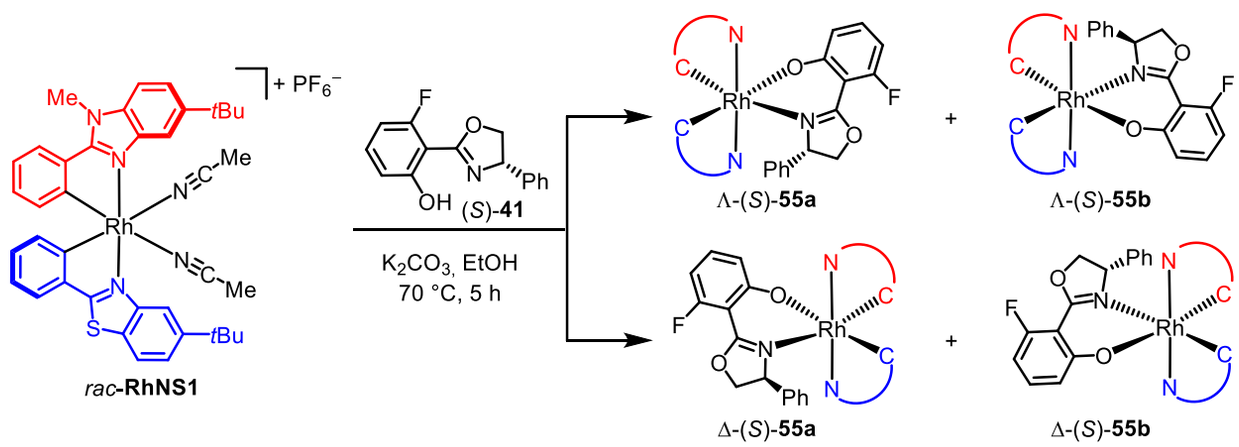

Synthesis of Λ- and Δ-(*S*)-55

Rac-**RhNS1** (93.0 mg, 0.11 mmol, 1.00 equiv.), K_2CO_3 (45.0 mg, 0.33 mg, 3.00 equiv.) and chiral auxiliary (*S*)-**41** (31.0 mg, 0.12 mmol, 1.10 equiv.) were dissolved in EtOH (4.60 mL, absolute) and stirred for 5 h at 70 °C. The reaction mixture was cooled to room temperature, diluted with CH_2Cl_2 and filtered over a short plug of celite. The solvent was removed under reduced pressure and the mixture of four diastereomers was purified by column chromatography (*n*-pentane/EtOAc 10:1 → 8:1 → 6:1 → 5:1 → 4:1 → 3:1, plus 1% Et_3N) to give Λ-(*S*)-**55a** (25.0 mg, 0.03 mmol, 26%), Λ-(*S*)-**55b** (12.0 mg, 0.01 mmol, 13%) and Δ-(*S*)-**55a** (42.0 mg, 0.05 mmol, 43%) as yellow solids. Complex Δ-(*S*)-**55b** could not be isolated, most likely due to formation only in trace amounts. If necessary, the individual diastereomers have to be purified again by column chromatography in order to provide the final catalysts Λ- and Δ-**RhNS1** with

high enantiomeric purities. For precise assignments of ^{1}H and ^{13}C signals see Section 5.4.2 (Figures 37–46). Furthermore, a crystal structure of Δ-(*S*)-**55a** is available. Detailed information and the corresponding crystallographic data can be found in Chapter 6.4.

Analytical data of Λ-(*S*)-**55a**:

TLC: R_f = 0.38 (*n*-pentane/EtOAc 2:1, plus 1% Et_3N).

^{1}H NMR: 600 MHz, CD_2Cl_2; δ = 8.98 (d, *J* = 1.6 Hz, 1H), 7.73 (dd, *J* = 7.8, 1.1 Hz, 1H), 7.63 (d, *J* = 8.5 Hz, 1H), 7.59 (d, *J* = 1.3 Hz, 1H), 7.48-7.46 (m, 2H), 7.39 (d, *J* = 8.8 Hz, 1H), 7.34 (dd, *J* = 7.6, 1.1 Hz, 1H), 6.95-6.92 (m, 2H), 6.89-6.85 (m, 1H), 6.82-6.79 (m, 1H), 6.78 (dt, *J* = 7.4, 1.4 Hz, 1H), 6.72 (dt, *J* = 7.5, 1.3 Hz, 1H), 6.55 (d, *J* = 7.8 Hz, 1H), 6.43 (d, *J* = 8.7 Hz, 1H), 6.28 (d, *J* = 7.4 Hz, 2H), 6.60 (d, *J* = 7.9 Hz, 1H), 5.87 (ddd, *J* = 13.0, 7.8, 1.1 Hz, 1H), 4.84-4.80 (m, 2H), 4.10 (s, 3H), 4.01 (dd, *J* = 6.7, 2.3 Hz, 1H), 1.45 (s, 9H), 1.30 (s, 9H) ppm.

^{13}C NMR: 126 MHz, CD_2Cl_2; δ = 175.5 (d, $J_{C,Rh}$ = 3.3 Hz, 1C), 174.9 (d, $J_{C,F}$ = 3.4 Hz, 1C), 171.1 (d, $J_{C,Rh}$ = 30.6 Hz, 1C), 169.6 (d, $J_{C,Rh}$ = 32.4 Hz, 1C), 165.8 (d, $J_{C,F}$ = 3.4 Hz, 1C), 164.0 (d, $J_{C,F}$ = 257.2 Hz, 1C), 159.6 (d, $J_{C,Rh}$ = 3.3 Hz, 1C), 151.7, 151.6, 147.5, 141.9, 141.5, 140.6, 136.2, 134.9, 134.1, 134.0, 132.6 (d, $J_{C,F}$ = 14.1 Hz, 1C), 129.7, 129.5, 128.9, 128.0 (2C), 127.5 (2C), 125.8, 124.6, 123.7, 122.5, 122.2, 121.7, 121.3, 121.1 (d, $J_{C,F}$ = 2.4 Hz, 1C), 119.8, 112.6, 109.7, 100.9 (d, $J_{C,F}$ = 6.2 Hz, 1C), 98.4 (d, $J_{C,F}$ = 24.1 Hz, 1C), 75.3, 69.5, 60.7, 35.4, 35.3, 32.7, 31.9 (3C), 31.8 (3C) ppm.

^{19}F NMR: 235 MHz, CD_2Cl_2; δ = –105.3 (s, 1F) ppm.

IR: neat, $\tilde{\nu}$ = 3048 (w), 2952 (w), 2865 (w), 2328 (w), 1617 (s), 1579 (w), 1528 (w), 1510 (w), 1476 (w), 1445 (s), 1364 (w), 1321 (w), 1280 (w), 1250 (w), 1216 (m), 1156 (w), 1093 (w), 1031 (m), 989 (w), 951 (w), 925 (w), 864 (w), 817 (w), 792 (w), 754 (w), 729 (m), 696 (m), 672 (w), 651 (w), 612 (w), 579 (w), 530 (w), 461 (w) cm^{-1}.

HRMS: APCI; m/z calcd. for $C_{50}H_{47}F_1N_4O_2Rh_1S_1$ $[M+H]^+$: 889.2453, found: 889.2460.

m.p.: 305 °C decomposition (EtOAc).

CD: MeOH; λ, nm (Δε, $M^{-1}cm^{-1}$) 397 (–16), 347 (+57), 300 (–55), 243 (+48), 229 (–23), 218 (+13), 206 (+42).

Analytical data of Λ-(*S*)-**55b**:

TLC: R_f = 0.50 (*n*-pentane/EtOAc 2:1, plus 1% Et_3N).

^{1}H NMR: 250 MHz, CD_2Cl_2; δ = 8.15 (s, 1H), 8.03 (s, 1H), 7.83 (d, *J* = 8.5 Hz, 1H), 7.59 (d, *J* = 7.5 Hz, 1H), 7.53 (d, *J* = 8.6 Hz, 1H), 7.42-7.37 (m, 2H), 7.15 (d, *J* = 8.6 Hz, 1H), 6.97-6.88 (m, 5H), 6.80-6.68 (m, 4H), 6.46 (d, *J* = 8.7 Hz, 1H), 6.16 (d, *J* = 6.0 Hz, 2H), 5.90-5.82 (m, 2H), 4.93-4.79 (m, 2H), 3.98-3.95 (m, 1H), 3.74 (s, 3H), 1.45 (s, 9H), 1.28 (s, 9H) ppm.

^{13}C NMR: Could not be measured due to rapid isomerization to Λ-(*S*)-**55a**.

^{19}F NMR: 235 MHz, CD_2Cl_2; δ = –105.5 (s, 1F) ppm.

IR: neat, $\tilde{\nu}$ = 3052 (w), 2954 (w), 2922 (s), 2853 (w), 1616 (s), 1579 (m), 1528 (m), 1509 (w), 1477 (w), 1444 (s), 1378 (w), 1364 (w), 1323 (w), 1280 (w), 1250 (w), 1216 (m), 1157 (w), 1095 (m), 1026 (s), 988 (w), 950 (w), 927 (w), 866 (w), 791 (m), 755 (w), 728 (s), 695 (m), 670 (w), 651 (w), 612 (w), 580 (w), 531 (m), 461 (m) cm^{-1}.

HRMS: APCI; m/z calcd. for $C_{50}H_{47}F_1N_4O_2Rh_1S_1$ $[M+H]^+$: 889.2453, found: 889.2474.

m.p.: 254 °C decomposition (CH_2Cl_2).

Analytical data of Δ-(*S*)-**55a**:

TLC: R_f = 0.23 (*n*-pentane/EtOAc 2:1, plus 1% Et_3N).

^{1}H NMR: 600 MHz, CD_2Cl_2; δ = 9.11 (d, *J* = 1.6 Hz, 1H), 7.93 (d, *J* = 8.5 Hz, 1H), 7.83 (d, *J* = 1.4 Hz, 1H), 7.71 (dd, *J* = 7.8, 1.1 Hz, 1H), 7.56 (dd, *J* = 8.6, 1.9 Hz, 1H), 7.42 (dd, *J* = 8.8, 1.7 Hz, 1H), 7.38 (dd, *J* = 7.6, 1.1 Hz, 1H), 8.76 (d, *J* = 8.8 Hz, 1H), 6.95 (dt, *J* = 7.5, 1.2 Hz, 1H), 6.92-6.89 (m, 1H), 6.86-6.82 (m, 4H), 6.79-6.75 (m, 2H), 6.62 (dt, *J* = 7.4, 1.1 Hz, 1H), 6.40 (d, *J* = 7.7 Hz, 1H), 6.29-6.25 (m, 2H), 5.91 (d, *J* = 7.8 Hz, 1H), 5.87 (ddd, *J* = 11.7, 7.9, 1.0 Hz, 1H), 4.22 (dd, *J* = 8.9, 7.7 Hz, 1H), 4.12 (s, 3H), 4.07-4.00 (m, 2H), 1.39 (s, 9H), 1.23 (s, 9H) ppm.

^{13}C NMR: 126 MHz, CD_2Cl_2; δ = 176.1 (d, $J_{C,Rh}$ = 3.7 Hz, 1C), 174.4 (d, $J_{C,F}$ = 3.6 Hz, 1C), 170.7 (d, $J_{C,Rh}$ = 32.5 Hz, 1C), 169.7 (d, $J_{C,Rh}$ = 31.5 Hz, 1C), 166.0, 163.2 (d, $J_{C,F}$ = 253.9 Hz, 1C), 159.1 (d, $J_{C,Rh}$ = 3.1 Hz, 1C), 152.3, 151.4, 147.0, 140.6, 140.5, 140.4, 135.8, 135.4, 134.1, 133.6, 132.3 (d, $J_{C,F}$ = 13.4 Hz, 1C), 129.3, 129.0, 128.9, 128.3 (2C), 127.4, 127.4 (2C), 125.8, 124.5, 124.2, 122.5, 121.9, 121.8, 121.7, 119.7 (d, $J_{C,F}$ = 1.9 Hz, 1C), 119.2, 113.6, 109.4, 103.3 (d, $J_{C,F}$ =

7.8 Hz, 1C), 98.3 (d, $J_{C,F}$ = 22.7 Hz, 1C), 75.3, 70.0, 35.4, 35.3, 32.5, 31.9 (3C), 31.4 (3C) ppm.

^{19}F NMR: 282 MHz, CD_2Cl_2; δ = –107.5 (s, 1F) ppm.

IR: neat, $\tilde{\nu}$ = 3049 (w), 2954 (m), 2864 (w), 1733 (w), 1618 (s), 1579 (m), 1530 (w), 1508 (w), 1476 (w), 1446 (s), 1418 (w), 1361 (m), 1327 (w), 1281 (w), 1261 (w), 1220 (s), 1156 (w), 1118 (w), 1093 (w), 1027 (s), 988 (w), 952 (w), 867 (w), 842 (w), 788 (m), 753 (w), 725 (m), 695 (s), 672 (w), 650 (w), 613 (w), 582 (w), 529 (m), 460 (m) cm^{-1}.

HRMS: APCI; m/z calcd. for $C_{50}H_{47}F_1N_4O_2Rh_1S_1$ $[M+H]^+$: 889.2464, found: 889.2476.

m.p.: 267 °C (EtOAc).

CD: MeOH; λ, nm (Δε, M^{-1}cm^{-1}) 391 (+15), 359 (–14), 351 (–10), 333 (–29), 300 (+39), 265 (–12), 246 (–34), 230 (+19), 219 (–11), 215 (+4), 205 (–82).

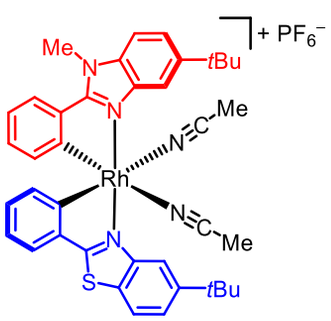

Synthesis of Λ-RhNS1

To a solution of Λ-(*S*)-**55a** (20.0 mg, 0.02 mmol, 1.00 equiv.) in MeCN (0.55 mL) was added trifluoroacetic acid (17.0 µL, 0.22 mmol, 10.0 equiv.) in one portion and the reaction was stirred for 7 h at 50 °C. The mixture was cooled to room temperature and the solvent was removed under reduced pressure. The obtained yellow oil was transferred to a column with few CH_2Cl_2, and CH_2Cl_2/MeCN 100:1, plus 0.1% trifluoroacetic acid was used as the first eluent to prevent the auxiliary from re-coordinating to the metal center. By using CH_2Cl_2/MeCN 20:1 → 10:1 residual trifluoroacetic acid and the auxiliary ligand (dark purple band) were eluted, before an excess NH_4PF_6 (20.0 equiv.) was added atop of the sea sand. The residual pale yellow band was then eluted with CH_2Cl_2/MeCN 1:1. After removal of the solvent under reduced pressure, the obtained yellow solid was subjected to a short silica pad (ca. 1 cm) using CH_2Cl_2/MeCN 50:1 as eluent to remove the excess NH_4PF_6 to yield Λ-**RhNS1** (18.0 mg, 0.02 mmol, 93%) as a pale yellow solid. Enantiomeric excess was established by HPLC analysis on a chiral stationary phase: ee = 99.6%, HPLC conditions: Daicel Chiralpak® IB-N5 column, 250 x 4.6 mm, absorbance at 254 nm,

H_2O + 0.1% TFA/MeCN = 60:40 to 50:50 in 180 min, 50:50 maintained until 240 min, gradient elution, flow rate 0.6 mL/min, 25 °C, t_r (Δ-**RhNS1**) = 195.7 min, t_r (Λ-**RhNS1**) = 205.3 min).

CD: MeOH; λ, nm (Δε, $M^{-1}cm^{-1}$) 391 (–30), 354 (+92), 298 (–99), 244 (+67), 228 (+10), 220 (+23), 213 (–12), 205 (+65).

All other spectroscopic data were in agreement with *rac*-**RhNS1**.

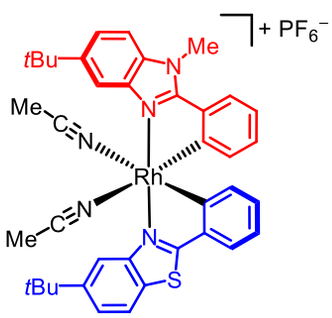

Synthesis of Δ-RhNS1

To a solution of Δ-(*S*)-**55a** (43.0 mg, 0.05 mmol, 1.00 equiv.) in MeCN (1.20 mL) was added trifluoroacetic acid (37.0 µL, 0.48 mmol, 10.0 equiv.) in one portion and the reaction was stirred for 6 h at 40 °C. Workup was performed as described for Λ-**RhNS1**. Δ-**RhNS1** (42.0 mg, 0.05 mmol, >99%) was obtained as a pale yellow solid. A crystal structure of Δ-**RhNS1** is available. Detailed information and the corresponding crystallographic data can be found in Chapter 6.4. Enantiomeric excess was established by HPLC analysis on a chiral stationary phase: ee = 99.4%, HPLC conditions: Daicel Chiralpak® IB-N5 column, 250 x 4.6 mm, absorbance at 254 nm, H_2O + 0.1% TFA/MeCN = 60:40 to 50:50 in 180 min, 50:50 maintained until 240 min, gradient elution, flow rate 0.6 mL/min, 25 °C, t_r (Δ-**RhNS1**) = 193.7 min, t_r (Λ-**RhNS1**) = 208.8 min).

CD: MeOH; λ, nm (Δε, $M^{-1}cm^{-1}$) 389 (+29), 354 (–90), 297 (+95), 242 (–64), 230 (–18), 220 (–32), 214 (+14), 206(–69).

All other spectroscopic data were in agreement with *rac*-**RhNS1**.

5.4.2 NMR Studies of Λ- and Δ-(*S*)-RhNS1 Auxiliary Complexes

It has already been shown that the configuration of tris-heteroleptic metal complexes can be determined by careful analysis of the long-range NOE interactions between the ligands.[208] Hence, to confirm the structure of Δ-(*S*)-**55a** and to elucidate the structure of the more stable stereoisomer Λ-(*S*)-**55a** (compared to Λ-(*S*)-**55b**), both with regard to the orientation of the bound chiral fluorinated auxiliary (*S*)-**41** and the metal-centered configuration of the complexes, ^{1}H–^{1}H 2D NOESY experiments were performed. The structure determination of the diastereomeric rhodium auxiliary complexes and the implementation of the corresponding NMR experiments were carried out by Dr. Xiulan Xie, head of the NMR department at the Philipps-Universität Marburg.

Sample Preparation and Experimental Setup

About 15 to 30 mg of substance were dissolved in CD_2Cl_2 (0.60 mL), the resulting solutions were degassed and filled in J-Young tubes under inert gas (nitrogen). NMR measurements were performed on a Bruker AVII 600 MHz spectrometer equipped with a 5 mm TXI probe with z-gradient. NOESY experiments were performed with mixing times of 1.5 and 2.5 s.

Results and Discussion

The two diastereomeric complexes shown in Figure 36 were examined by NMR spectroscopy. A crystal structure was available for Δ-(*S*)-**55a**, whereas the configuration of Λ-(*S*)-**55a** was an assumption. Signal assignment was fulfilled with the standard experiments ^{1}H, ^{13}C, DQF-COSY, HSQC and HMBC. ^{1}H and ^{13}C NMR spectra labeled with assignments and the corresponding NOESY spectra are given in Figure 37–Figure 41 and Figure 42–Figure 46.

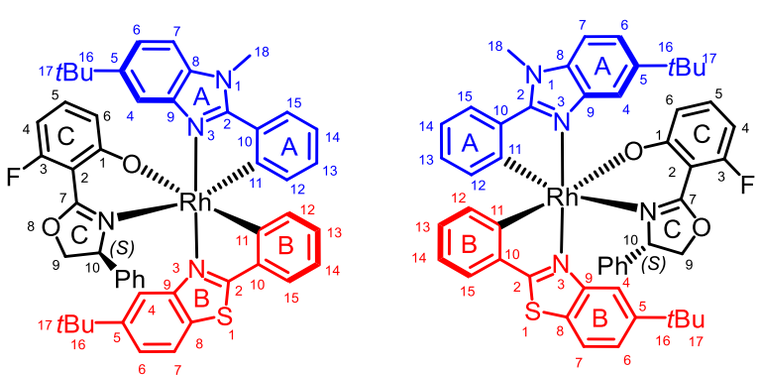

Δ-(*S*)-**55a** Λ-(*S*)-**55a**

Figure 36: Investigated compounds.

The observed NOE interactions are given in Table 8. Δ-(*S*)-**55a** is referred to as Δ-**Rh1** and Λ-(*S*)-**55a** is referred to as Λ-**Rh1.**

Table 8: Significant Interligand Long-Range NOE Correlations.

complex	NOEs between LA – LB	NOEs between LA – LC	NOEs between LB – LC
Δ-**Rh1**	A4 – B4	A4 – C9β, A4 – Cph	B4 – C6, B4 – C10
	A18 – B12	A17 – C4, A17 – Cph	B12 – Cph
			B15 – Cph
			B17 – C6
Λ-**Rh1**	A12 – B4	A4 – C9β, A4 – C10	B4 – C6, B4 – Cph
		A17 – C9β, A17 – C10	B12 – C10
			B15 – Cph

A close inspection of the observed NOE interactions revealed that the chiral center C10 of the auxiliary ligand C could contribute to the differentiation of the Δ- and Λ-configuration. While maintaining a constant chirality at C10, a change in the configuration at the metal center resulted in a corresponding change in the absolute orientation of the phenyl group of ligand C. This change in orientation led to a difference in the spatial proximity between ligands B and C, which was reflected in the various NOE interactions between these two ligands, as depicted in Table 8. In this way, the observed interligand long-range NOE contacts could unequivocally confirm and determine the configuration of Δ-(*S*)-**55a** and Λ-(*S*)-**55a** to be as shown in Figure 36.

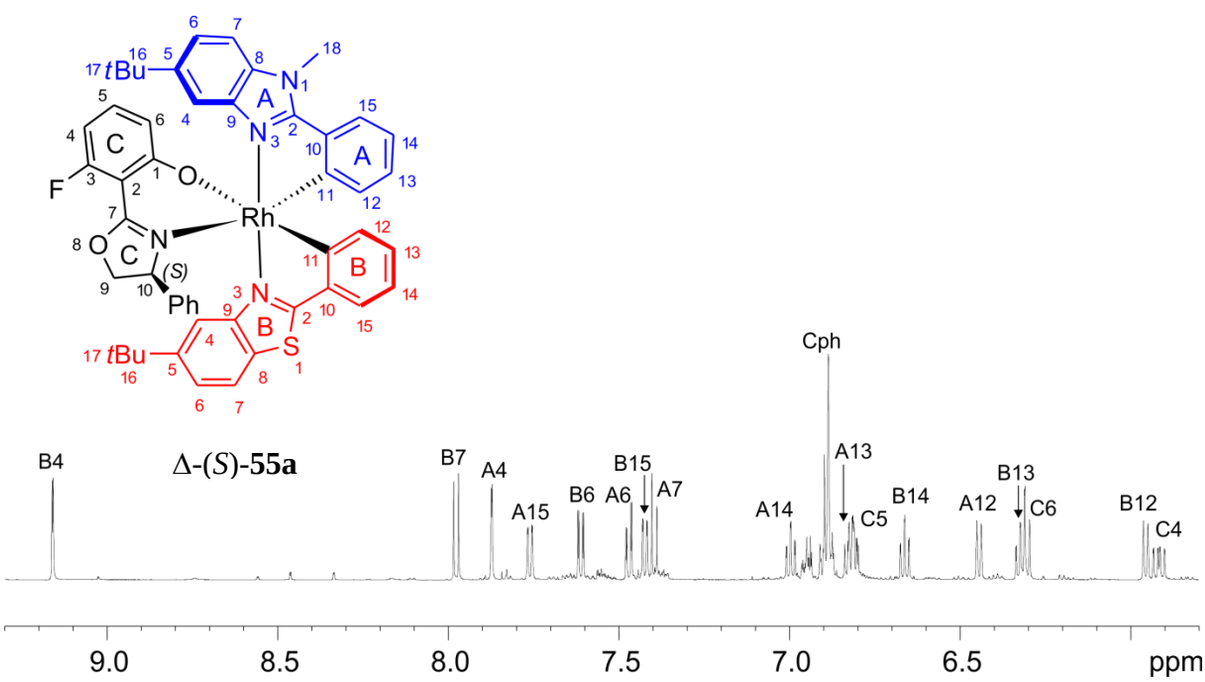

Figure 37: Aromatic region of the ^{1}H NMR spectrum of Δ-(*S*)-**55a** in CD_2Cl_2 at 300 K.

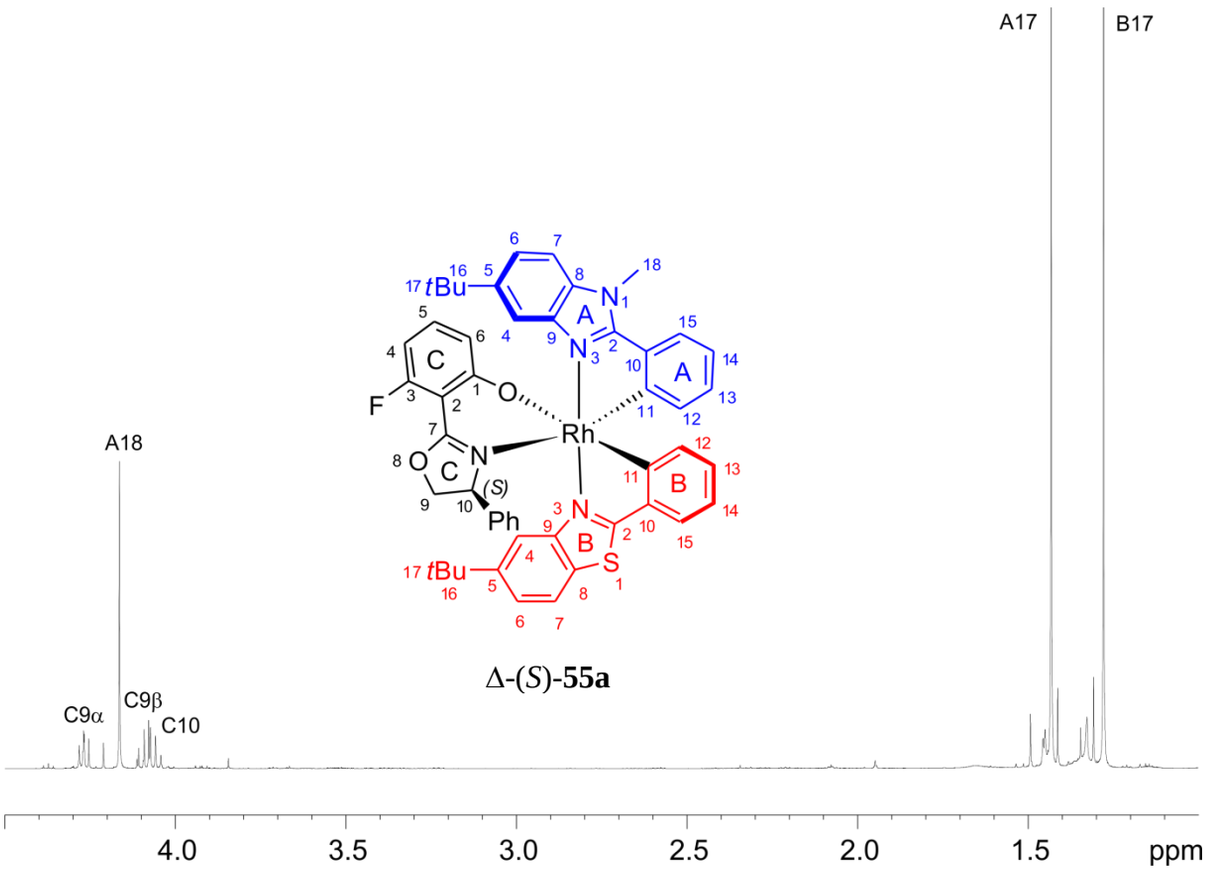

Figure 38: Aliphatic region of the ^{1}H NMR spectrum of Δ-(*S*)-**55a** in CD_2Cl_2 at 300 K.

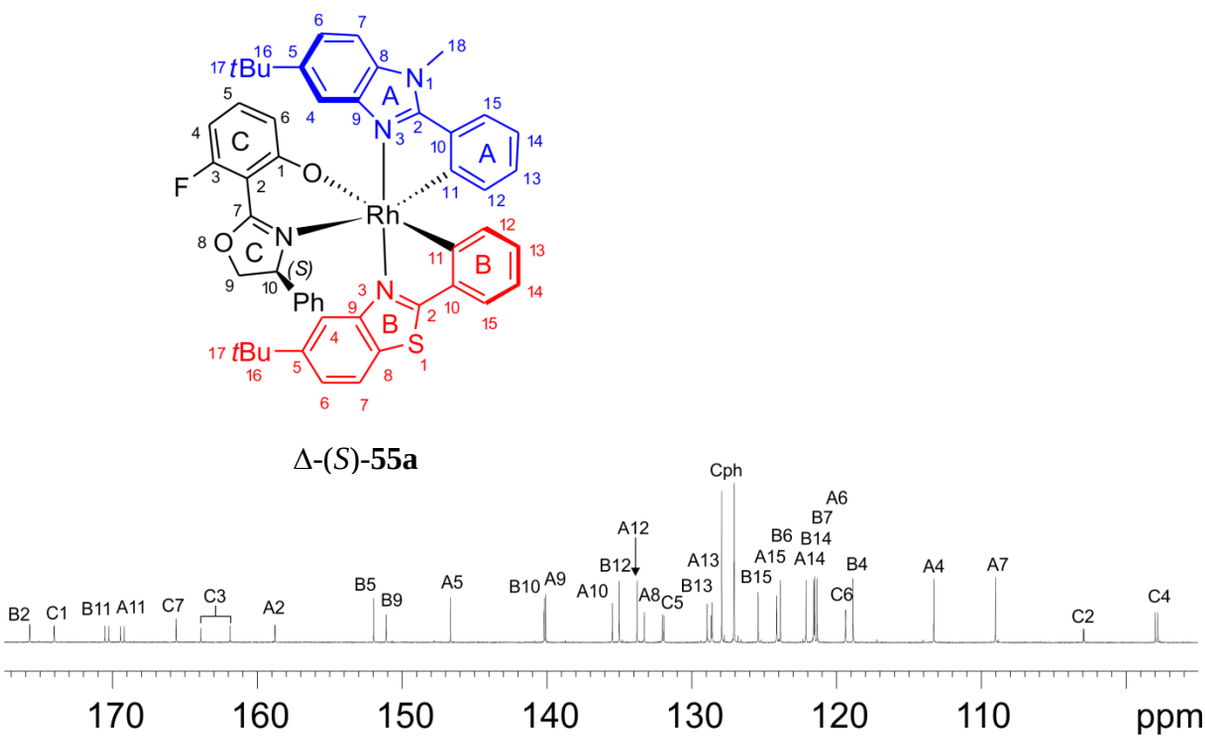

Figure 39: Aromatic region of the ^{13}C NMR spectrum of Δ-(*S*)-**55a** in CD_2Cl_2 at 300 K.

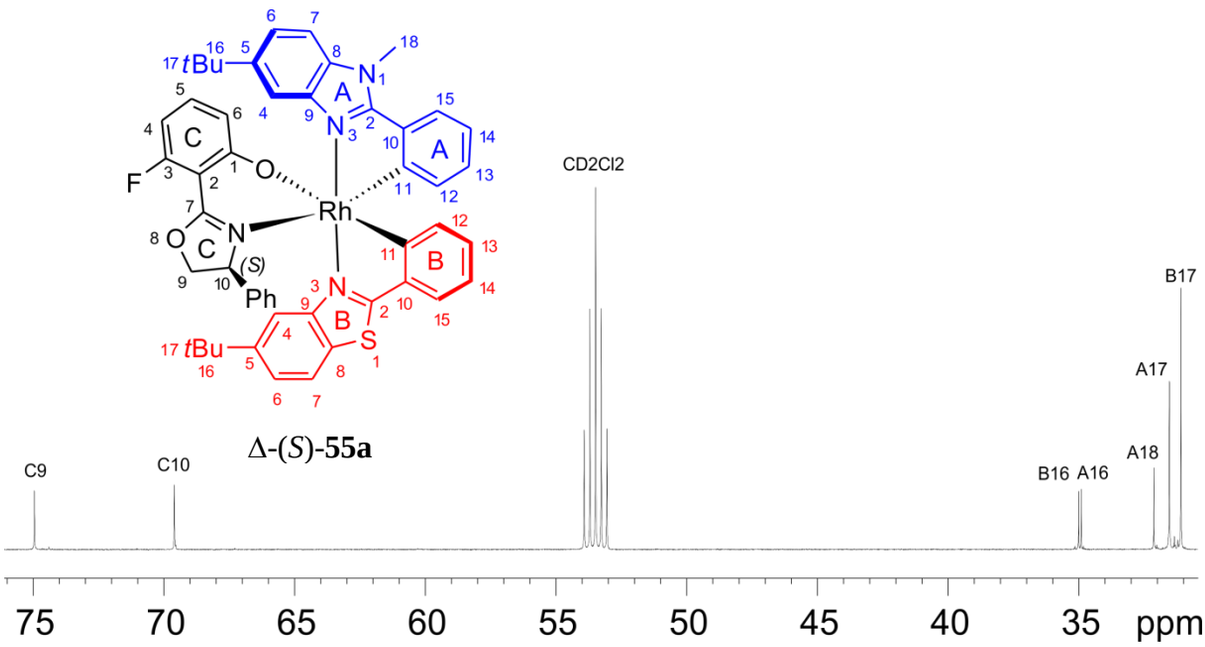

Figure 40: Aliphatic region of the ^{13}C NMR spectrum of Δ-(*S*)-**55a** in CD_2Cl_2 at 300 K.

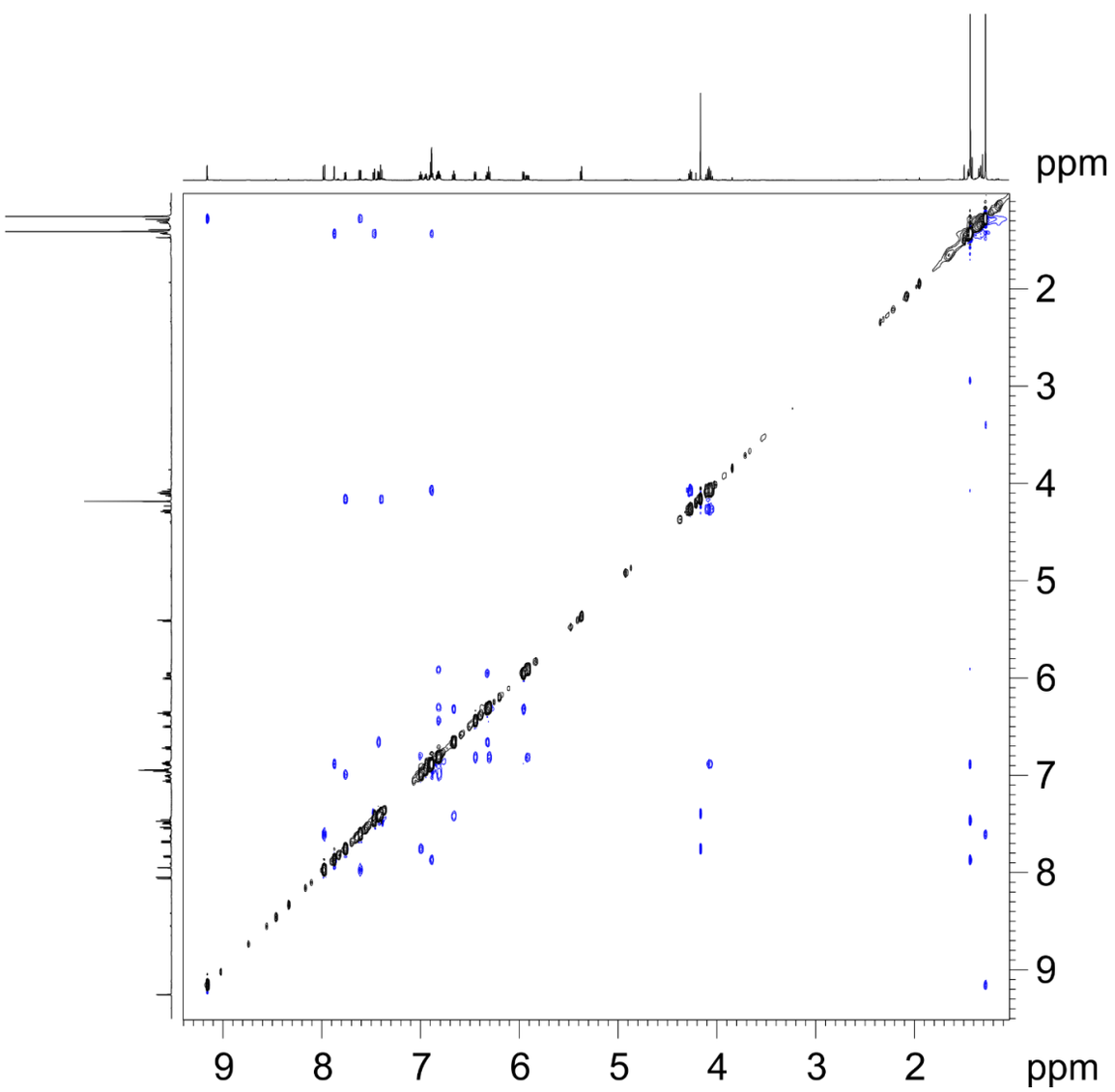

Figure 41: NOESY spectrum of Δ-(*S*)-**55a** in CD_2Cl_2 at 300 K (mixing time = 1.5 s).

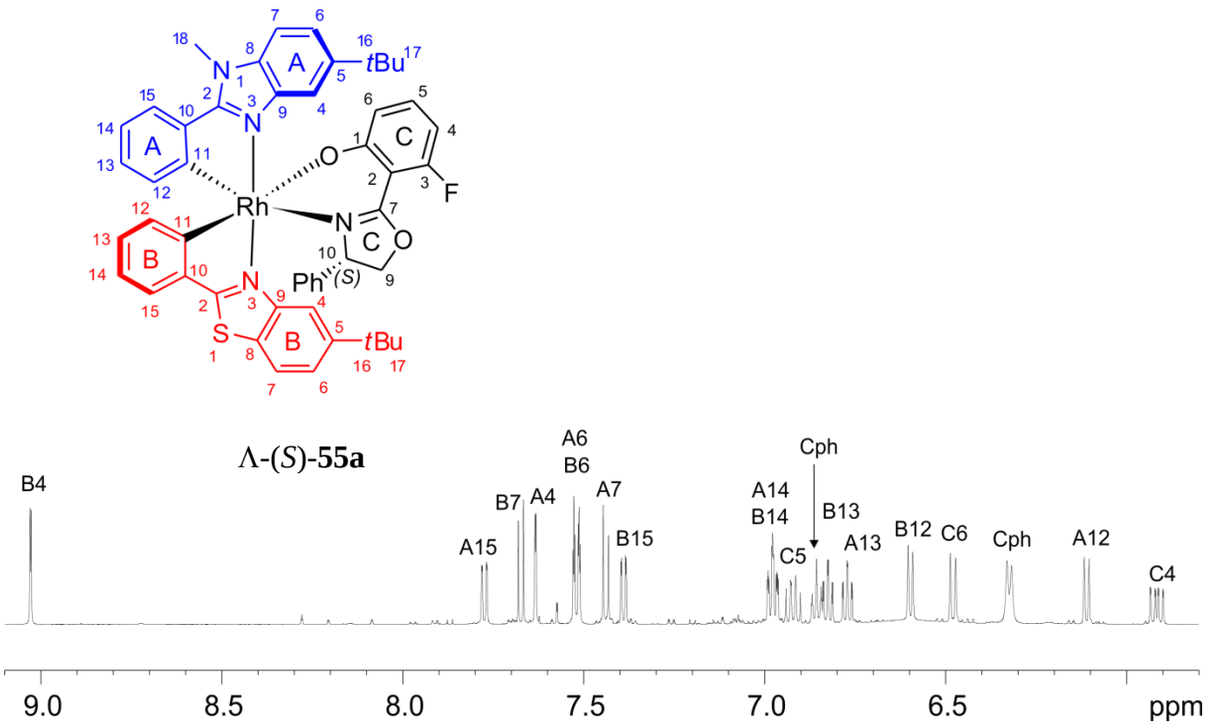

Figure 42: Aromatic region of the ^{1}H NMR spectrum of Λ-(*S*)-**55a** in CD_2Cl_2 at 300 K.

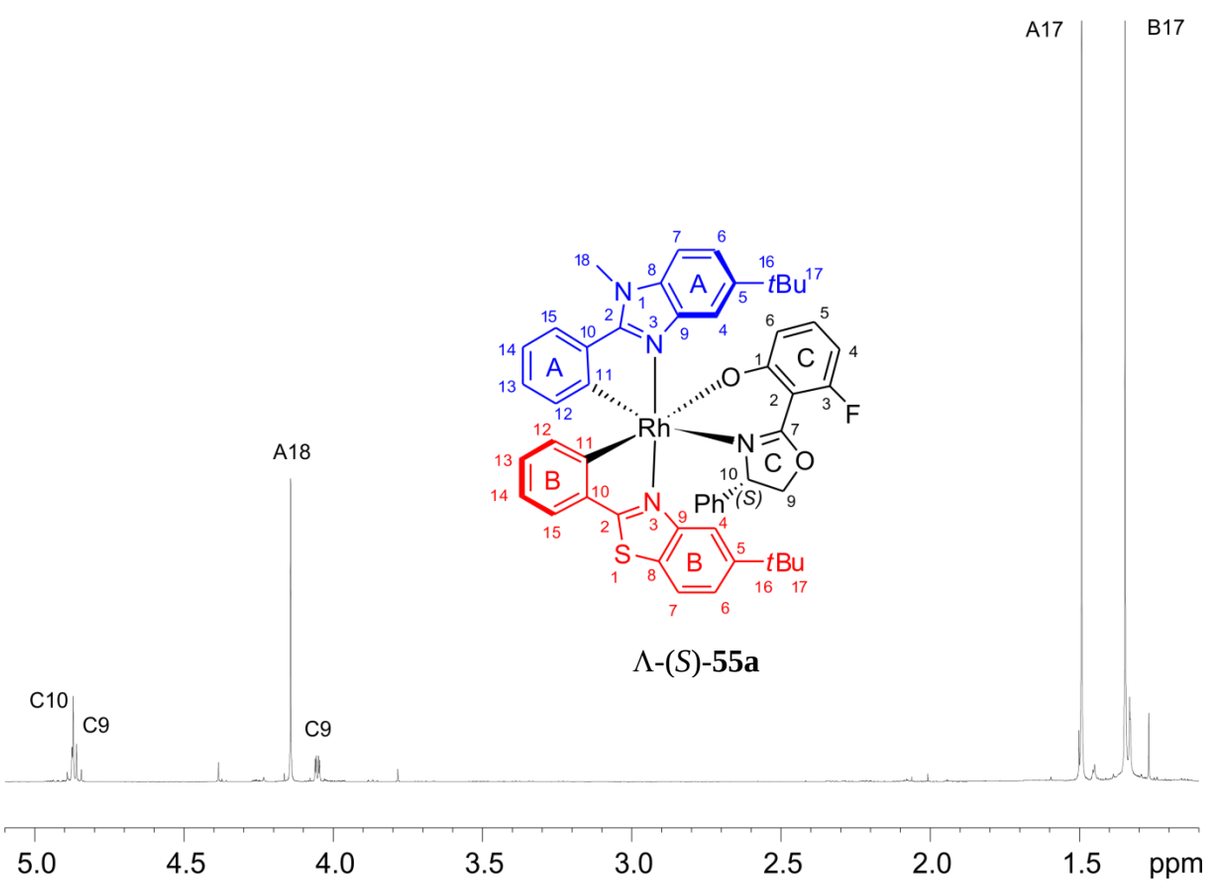

Figure 43: Aliphatic region of the ^{1}H NMR spectrum of Λ-(*S*)-**55a** in CD_2Cl_2 at 300 K.

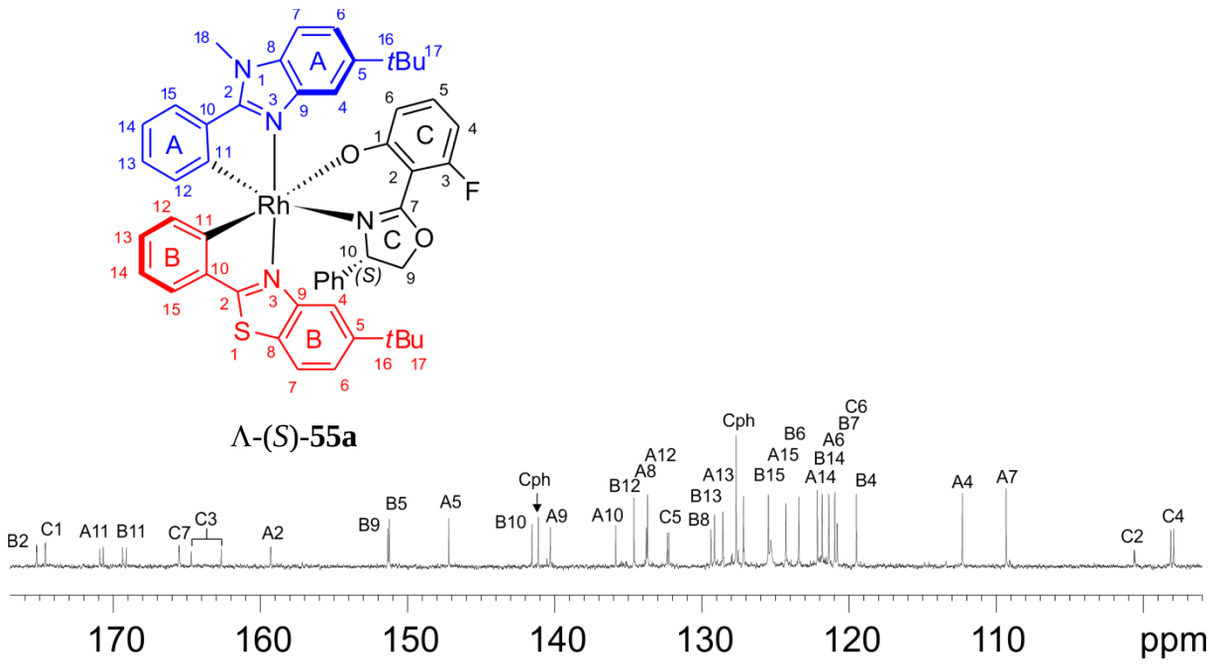

Figure 44: Aromatic region of the ^{13}C NMR spectrum of Λ-(*S*)-**55a** in CD_2Cl_2 at 300 K.

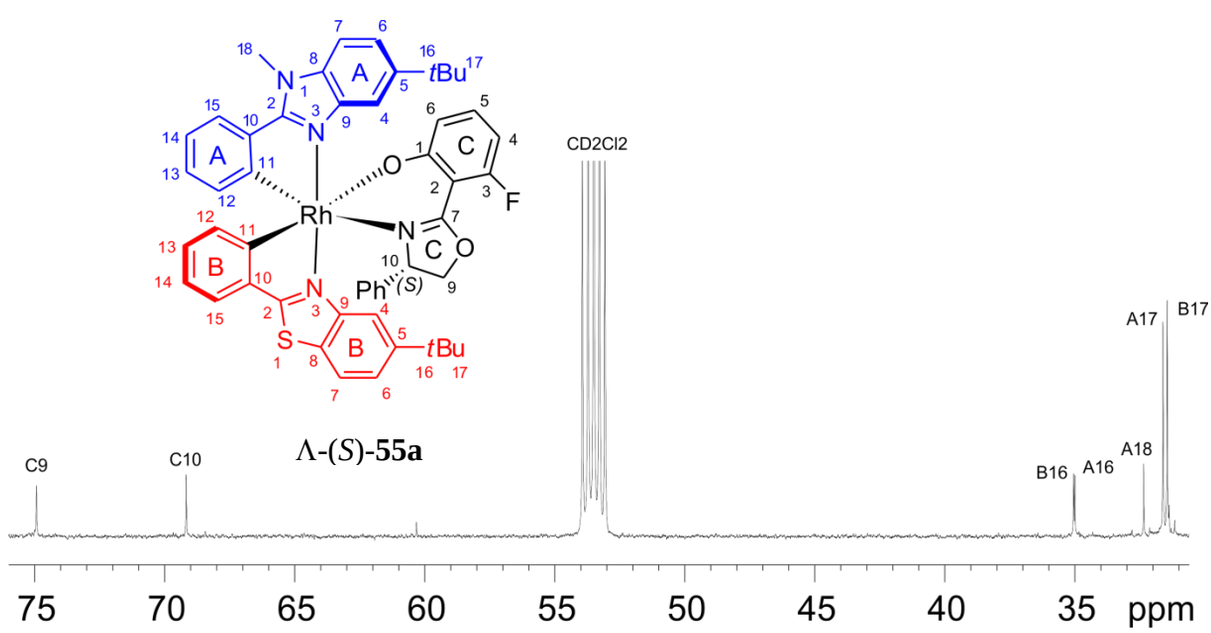

Figure 45: Aliphatic region of the ^{13}C NMR spectrum of Λ-(*S*)-**55a** in CD_2Cl_2 at 300 K.

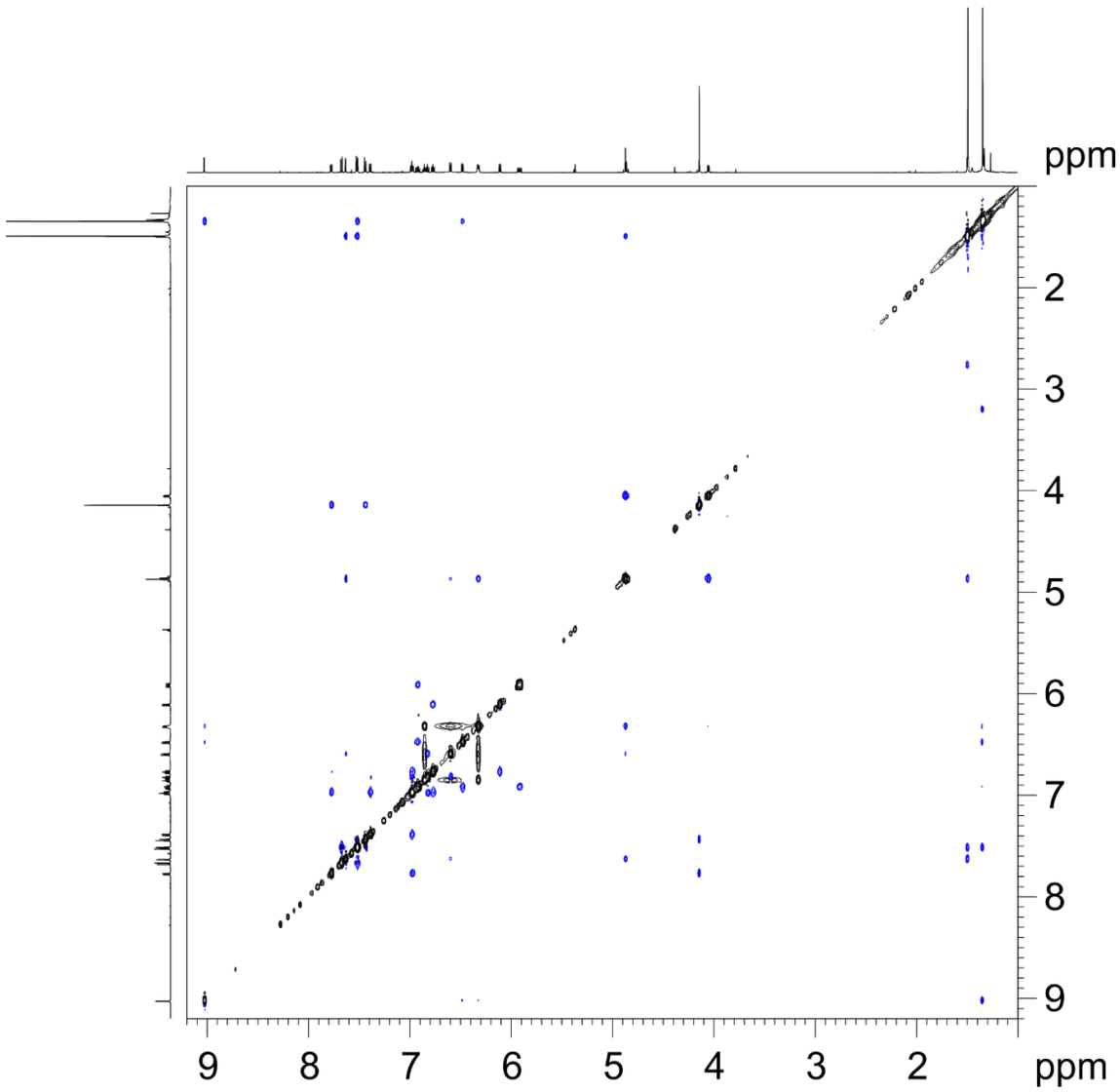

Figure 46: NOESY spectrum of Λ-(*S*)-**55a** in CD_2Cl_2 at 300 K (mixing time = 1.5 s).

5.4.3 [2+2] Photocycloaddition Reactions

5.4.3.1 <u>General Procedure E:</u> [2+2] Photocycloaddition with 2-Phenylpropene

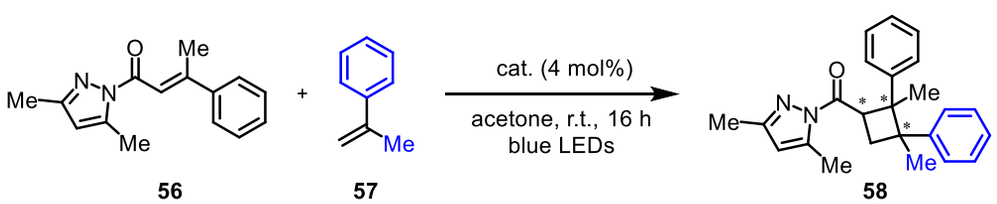

56 **57** **58**

According to a slightly modified reported procedure,[96] an oven-dried 10 mL Schlenk tube was charged with α,β-unsaturated *N*-acyl pyrazole **56** (24.0 mg, 0.10 mmol, 1.00 equiv.) and the indicated catalyst (3.4 mg, 4 mol%) under nitrogen atmosphere. Acetone (HPLC Grade, 0.50 mL,

0.2 M) was added, followed by 2-phenylpropene (**57**, 130 µL, 1.00 mmol, 10.0 equiv.). Subsequently, the resulting reaction solution was thoroughly degassed via freeze-pump-thaw for three cycles, then the vial was sealed and placed 5 cm away from a 24 W blue LED lamp. After stirring for 16 h at room temperature, the mixture was diluted with CH_2Cl_2, and the solvent was removed under reduced pressure. Diastereomeric ratios were determined by ^{1}H NMR analysis of the crude reaction mixtures. Purification by column chromatography (*n*-pentane/EtOAc 50:1) afforded pure product **58**. Enantiomeric excess was established by HPLC analysis on a chiral stationary phase. Racemic samples were obtained by performing the reaction with *rac*-**RhS**.

5.4.3.2 Experimental Procedures and Characterization Data of Substrates and Products

N-acyl pyrazole **56** was prepared following a published procedure.[92] Analytical data were consistent with reported data.[92]

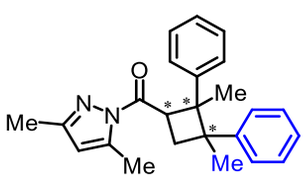

(3,5-Dimethyl-1*H*-pyrazol-1-yl)(2,3-dimethyl-2,3-diphenylcyclobutyl)methanone (58)

Following the general procedure E, compound **58** was obtained as a colorless oil. The results achieved with Λ- and Δ-**RhNS1** and Λ- and Δ-**RhS** are summarized in Table 9. Enantiomeric excess was established by HPLC analysis on a chiral stationary phase, HPLC conditions: Daicel Chiralcel® OD-H column, 250 x 4.6 mm, absorbance at 254 nm, *n*-hexane/isopropanol = 100:0, isocratic flow, flow rate 0.4 mL/min, 25 °C, t_r = 44.7 min, t_r = 59.9 min. Analytical data were in agreement with published data and absolute configurations were assigned accordingly.[96]

Table 9: Comparison of the Catalytic Performance of Λ- and Δ-Catalysts.

entry	catalyst	results
1	Δ-**RhS**	94% yield, >20:1 d.r., 99% ee (1*S*,2*S*,3*S*)[96]
2	Λ-**RhS**	93% yield, >20:1 d.r., 99% ee (1*R*,2*R*,3*R*)
3	Δ-**RhNS1**	94% yield, >20:1 d.r., 99% ee (1*S*,2*S*,3*S*)
4	Λ-**RhNS1**	94% yield, >20:1 d.r., 99% ee (1*R*,2*R*,3*R*)

5.4.3.3 General Procedure F: [2+2] Photocycloaddition with Cycloheptene

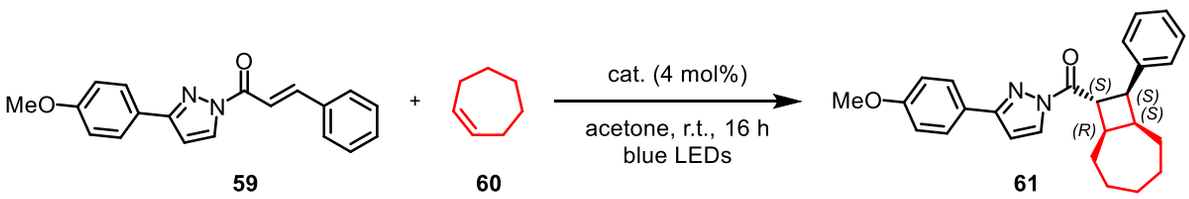

According to a slightly modified reported procedure,[96] an oven-dried 10 mL Schlenk tube was charged with α,β-unsaturated *N*-acyl pyrazole **59** (30.4 mg, 0.10 mmol, 1.00 equiv.) and Δ-**RhNS1** (3.4 mg, 4 mol%) under nitrogen atmosphere. Acetone (HPLC Grade, 1.00 mL, 0.1 M) was added, followed by cycloheptene (**60**, 360 µL, 3.00 mmol, 30.0 equiv.). Subsequently, the resulting reaction solution was thoroughly degassed via freeze-pump-thaw for three cycles, then the vial was sealed and placed 10 cm away from a 24 W blue LED lamp. After stirring for 16 h at room temperature, the mixture was diluted with CH_2Cl_2, and the solvent was removed under reduced pressure. Diastereomeric ratios were determined by ^{1}H NMR analysis of the crude reaction mixtures. Purification by column chromatography (*n*-pentane/EtOAc 12:1) afforded pure product **61** as a mixture of two diastereomers. Enantiomeric excess was established by HPLC analysis on a chiral stationary phase. Racemic samples were obtained by performing the reaction with *rac*-**RhS**.

5.4.3.4 Experimental Procedures and Characterization Data of Substrates and Products

N-acyl pyrazole **59** was synthesized following a published procedure.[121] Analytical data were consistent with reported data.[121]

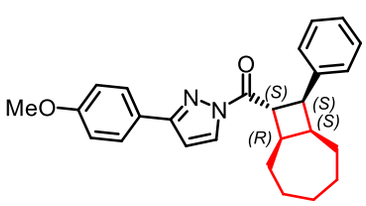

(3-(4-Methoxyphenyl)-1*H*-pyrazol-1-yl)((1*S*,7*R*,8*S*,9*S*)-9-phenylbicyclo[5.2.0]nonan-8-yl)methanone (61)

Following the general procedure F using Δ-**RhNS1** as catalyst, compound **61** (39.0 mg, 0.10 mmol, 98%) was obtained as a colorless solid with a diastereomeric ratio of 10.8:1. The

absolute configuration was assigned on the basis of a crystal structure of product **61**. Detailed information and the corresponding crystallographic data can be found in Chapter 6.4. Enantiomeric excess of the major diastereomer was established by HPLC analysis on a chiral stationary phase: ee = 99.4%, HPLC conditions: Daicel Chiralpak® IG column, 250 x 4.6 mm, absorbance at 254 nm, *n*-hexane/isopropanol = 98:2, isocratic flow, flow rate 0.6 mL/min, 25 °C, t_r (minor) = 23.7 min, t_r (major) = 32.3 min.

With Δ-**RhS**, **61** was obtained in 98% yield (39.0 mg, 0.10 mmol) with a d.r. of 12.1:1 and in 99.3% ee.

TLC: R_f = 0.61 (*n*-pentane/EtOAc 5:1).

^{1}H NMR: 300 MHz, $CDCl_3$; δ = 8.22 (d, *J* = 2.7 Hz, 1H), 7.72 (d, *J* = 8.6 Hz, 2H), 7.27 (m, 2H), 7.23-7.14 (m, 2H), 6.94 (d, *J* = 8.7 Hz, 2H), 6.67 (d, *J* = 2.7 Hz, 1H), 4.56 (t, *J* = 9.2 Hz, 1H), 4.07 (t, *J* = 9.7 Hz, 1H), 3.84 (s, 3H), 2.95-2.83 (m, 1H), 2.78-2.67 (m, 1H), 2.14-2.05 (m, 1H), 1.89-1.74 (m, 3H), 1.66-1.51 (m, 2H), 1.37-0.98 (m, 5H) ppm.

^{13}C NMR: 75 MHz, $CDCl_3$; δ = 177.3, 160.5, 155.0, 139.8, 129.7, 128.2 (2C), 128.1 (2C), 127.8 (2C), 126.1, 124.9, 114.3 (2C), 107.3, 55.5, 45.2, 41.9, 41.2, 40.0, 33.2, 32.0, 30.5, 27.9, 27.3 ppm.

IR: neat, $\tilde{\nu}$ = 2915, 2846, 1705, 1610, 1512, 1433, 1401, 1342, 1286, 1243, 1175, 1094, 1026 cm^{-1}.

$[\alpha]_D^{22}$: –41.0° (*c* = 1.0, CH_2Cl_2).

HRMS: ESI; m/z calcd. for $C_{26}H_{28}N_2O_2Na$ $[M+Na]^+$ 423.2039, found: 423.2043.

m.p.: 118 °C (EtOAc).

5.5 Chiral Bis(oxazoline) Ligands as C_2-Symmetric Chiral Auxiliaries

5.5.1 Synthesis of Cyclometalating Ligands and Chiral Bis(oxazolines)

5-*tert*-Butyl-1-methyl-2-phenylbenzimidazole (**47a**) was synthesized as described in Section 5.3.1 and the analogous benzothiazole[100] ligand **40** was prepared according to a previously published synthetic protocol.

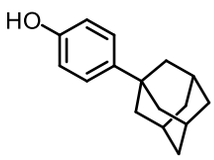

4-(Adamantan-1-yl)phenol

According to a slightly modified procedure from Stepakov *et al.*,[209] to a solution of phenol (1.00 g, 10.7 mmol, 1.00 equiv.) in trifluoroacetic acid (32.0 mL) was added 1-adamantanol (1.62 g, 10.7 mmol, 1.00 equiv.). The suspension was stirred for 6 h at room temperature, then it was diluted with H_2O (50 mL). The precipitate was filtered off, washed with an aqueous solution of Na_2CO_3 (until pH = 7) and dried to give 4-(adamantan-1-yl)phenol (2.43 g, 10.6 mmol, >99%) as a colorless solid. Analytical data were in agreement with published data.[209]

^{1}H NMR: 300 MHz, $CDCl_3$; δ = 7.24-7.20 (m, 2H), 6.83-6.75 (m, 2H), 4.74 (brs, 1H), 2.08 (brs, 3H), 1.88-1.87 (m, 6H), 1.76-1.75 (m, 6H) ppm.

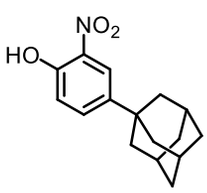

4-(Adamantan-1-yl)-2-nitrophenol

According to a slightly modified procedure from Osyanin *et al.*,[210] to a suspension of 4-(adamantan-1-yl)phenol (2.43 g, 10.6 mmol, 1.00 equiv.) in glacial acetic acid (37.0 mL) was added dropwise a solution of HNO_3 (0.79 mL, 13.0 mmol, 1.20 equiv.) in glacial acetic acid (3.70 mL) at room temperature. The reaction mixture was stirred vigorously for 30 min at room temperature, before it was poured into ice water (100 mL). The aqueous phase was extracted with

EtOAc (3 x 50 mL). The combined organic phases were washed with a saturated aqueous solution of $NaHCO_3$ (1 x 50 mL) and brine (1 x 50 mL), dried over Na_2SO_4 and filtered. The solvent was removed under reduced pressure and the crude product was adsorbed onto silica gel. Purification by column chromatography (*n*-pentane/EtOAc 20:1) provided 4-(adamantan-1-yl)-2-nitrophenol (2.04 g, 7.47 mmol, 70%) as a yellow solid. Analytical data were consistent with reported data.[210]

^{1}H NMR: 300 MHz, $CDCl_3$; δ = 10.46 (s, 1H), 8.03 (d, *J* = 2.4 Hz, 1H), 7.63 (dd, *J* = 8.8, 2.4 Hz, 1H), 7.10 (d, *J* = 8.8 Hz, 1H), 2.12 (brs, 3H), 1.89 (m, 6H), 1.83-1.72 (m, 6H) ppm.

Starting from 4-(adamantan-1-yl)-2-nitrophenol the corresponding benzothiazole ligand **68** was prepared according to a previously published method by the Meggers group,[139] as shown in Scheme 45. Analytical data were in agreement with published data.[139]

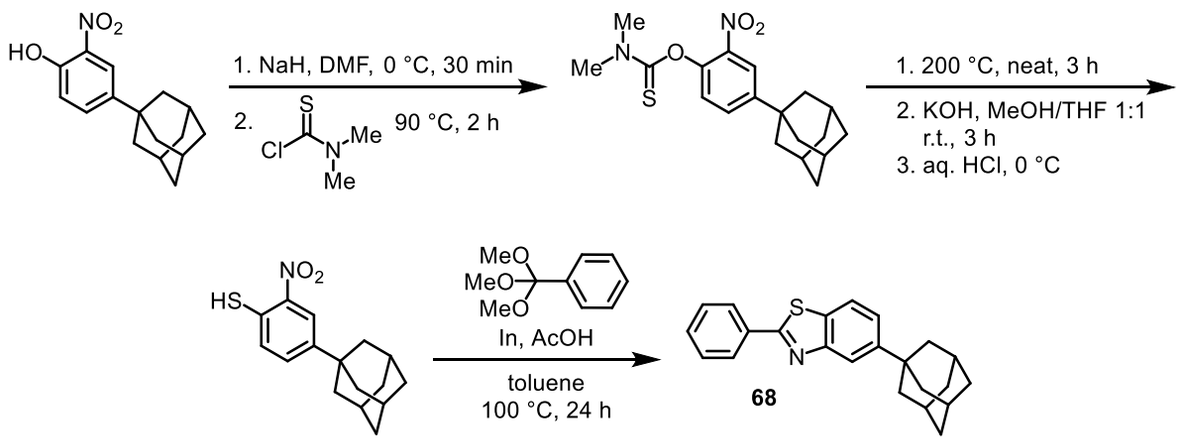

Scheme 45: Synthesis of 5-(adamantan-1-yl)-2-phenylbenzothiazole (**68**).[139]

<u>General Procedure G:</u> Synthesis of Chiral Bis(oxazoline) Ligands

According to a slightly modified procedure from Denmark *et al.*,[138] to a solution of the β-amino alcohol (2.00 equiv.) in CH_2Cl_2 (0.1 M) was added diethyl malonimidate dihydrochloride (**62**, 1.00 equiv.). The resulting cloudy solution was stirred at room temperature until TLC confirmed full consumption of the starting materials. The reaction mixture was diluted with H_2O and extracted three times with CH_2Cl_2. The combined organic layers were washed once with brine, dried over Na_2SO_4, and the solvent was removed under reduced pressure. Purification of the

obtained oily residue by bulb-to-bulb distillation (Kugelrohr distillation, 150 °C at 0.2 mbar) afforded the respective bis(oxazoline).

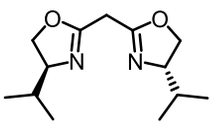

Bis((*S*)-4-isopropyl-4,5-dihydrooxazol-2-yl)methane (*S*,*S*)-64.

Following the general procedure G, to a solution of L-valinol (**63**, 893 mg, 8.65 mmol, 2.00 equiv.) in CH_2Cl_2 (43.3 mL) was added diethyl malonimidate dihydrochloride (**62**, 1.00 g, 4.33 mmol, 1.00 equiv.) and the resulting solution was stirred for 45 h at room temperature. Bulb-to-bulb distillation gave bis((*S*)-4-isopropyl-4,5-dihydrooxazol-2-yl)methane (*S*,*S*)-**64** (797 mg, 3.34 mmol, 77%) as a white waxy solid. Analytical data were consistent with reported data.[211]

^{1}H NMR: 300 MHz, $CDCl_3$; δ = 4.25 (dd, *J* = 8.9, 7.6 Hz, 2H), 4.01-3.88 (m, 4H), 3.33 (s, 2H), 1.80-1.69 (m, 2H), 0.94 (d, *J* = 6.8 Hz, 6H), 0.86 (d, *J* = 6.8 Hz, 6H) ppm.

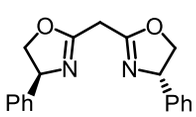

Bis((*S*)-4-phenyl-4,5-dihydrooxazol-2-yl)methane (*S*,*S*)-65.

Following the general procedure G, to a solution of (*S*)-2-phenylglycinol (**54**, 1.19 g, 8.65 mmol, 2.00 equiv.) in CH_2Cl_2 (43.3 mL) was added diethyl malonimidate dihydrochloride (**62**, 1.00 g, 4.33 mmol, 1.00 equiv.) and the resulting solution was stirred for 68 h at room temperature. Purification by bulb-to-bulb distillation yielded bis((*S*)-4-phenyl-4,5-dihydrooxazol-2-yl)methane (*S*,*S*)-**65** (1.01 g, 3.30 mmol, 76%) as a yellow oil. Analytical data were in agreement with published data.[64]

^{1}H NMR: 300 MHz, CD_2Cl_2; δ = 7.37-7.25 (m, 10H), 5.26-5.20 (m, 2H), 4.68 (dd, *J* = 10.2, 8.4 Hz, 2H), 4.14 (t, *J* = 8.2 Hz, 2H), 3.53 (s, 2H) ppm.

5.5.2 Catalyst Synthesis

5.5.2.1 Synthesis of Racemic Catalyst

Mono-cyclometalated rhodium complex **48a** was prepared as described in Section 5.3.2.

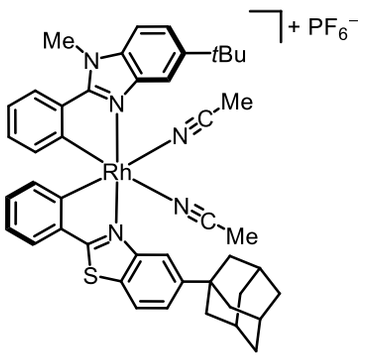

Synthesis of *rac*-RhNS2

A suspension of mono-cyclometalated rhodium(III) complex **48a** (153 mg, 0.23 mmol, 1.00 equiv.) and 5-(adamantan-1-yl)-2-phenylbenzothiazole (**68**, 83.0 mg, 0.24 mmol, 1.05 equiv.) in 2-ethoxyethanol (3.43 mL) and H_2O (1.14 mL) was stirred at 80 °C for 48 h in the dark. The reaction mixture was cooled to room temperature, and the solvent was thoroughly removed under reduced pressure (water bath of rotary evaporator set to 60 °C). $AgPF_6$ (104 mg, 0.41 mmol, 1.80 equiv.) and MeCN (4.57 mL) were added, successively, and the resulting suspension was stirred at 60 °C for 15 h in the dark. The mixture was cooled to room temperature, then it was filtered over a short plug of celite and rinsed with MeCN. The solvent was removed under reduced pressure, and the obtained residue was purified by column chromatography (CH_2Cl_2/MeCN 60:1 → 40:1 → 20:1) to afford *rac*-**RhNS2** (141 mg, 0.15 mmol, 66%, ratio of *rac*-**RhNS2** to **RhS(Ad)**/**RhN1** 1.65:1) as a pale yellow solid. As previously reported for *rac*-**RhNS1**,[102] the ratio of the target complex *rac*-**RhNS2** to both bis-heteroleptic complexes [Rh(**68**-H)$_2$(MeCN)$_2$]PF_6 (**RhS(Ad)**) and [Rh(**47a**-H)$_2$(MeCN)$_2$]PF_6 (**RhN1**) was determined by ^{1}H NMR analysis of the isolated mixture after chromatographic purification.

TLC: R_f = 0.41 (CH_2Cl_2/MeCN 20:1).

^{1}H NMR: 300 MHz, CD_2Cl_2; δ = 8.47 (brs, 1H), 8.03 (d, J = 8.6 Hz, 1H), 8.00 (brs, 1H), 7.81 (dd, J = 7.8, 0.9 Hz, 1H), 7.72-7.59 (m, 4H), 7.08-6.98 (m, 2H), 6.80 (dt, J = 7.6, 1.2 Hz, 2H), 6.27 (d, J = 7.7 Hz, 1H), 6.15 (d, J = 7.8 Hz, 1H), 4.29 (s, 3H),

2.20 (brs, 6H), 3.21 (brs, 3H), 2.05-2.04 (m, 6H), 1.88-1.78 (m, 6H), 1.45 (s, 9H) ppm.

^{13}C NMR: 126 MHz, CD_2Cl_2; δ = 176.5, 161.7, 158.3, 158.2, 152.7, 150.6, 148.6, 140.5, 139.8, 135.2, 134.2, 133.6, 133.5, 130.9, 129.9, 129.3, 126.1, 125.0, 124.8, 124.1, 124.0, 123.1, 122.8, 121.4, 121.3, 117.1, 112.7, 110.4, 43.8 (3C), 37.2, 37.0 (3C), 35.4, 32.8, 31.9 (3C), 29.5 (3C), 3.65 (2C) ppm.

IR: neat, $\tilde{\nu}$ = 2903 (w), 2848 (w), 1580 (w), 1555 (w), 1513 (w), 1481 (w), 1441 (w), 1421 (w), 1365 (w), 1317 (w), 1294 (w), 1263 (w), 1160 (w), 1104 (w), 1026 (w), 993 (w), 934 (w), 836 (s), 760 (w), 727 (w), 698 (w), 669 (w), 651 (w), 611 (w), 556 (m), 458 (w) cm^{-1}.

HRMS: APCI; m/z calcd. for $C_{45}H_{47}N_5Rh_1S_1$ $[M]^+$: 792.2602, found: 792.2617.

m.p.: 186 °C decomposition (CH_2Cl_2).

5.5.2.2 General Procedure H: Synthesis of Chiral Bisoxazolinato Rh(III) Complexes

Racemic rhodium complex (1.00 equiv.), K_2CO_3 (3.00 equiv.) and BOX ligand (*S*,*S*)-**64** or (*S*,*S*)-**65** (1.10 equiv.) were suspended in EtOH (25 mM, absolute) and stirred at room temperature until TLC indicated completion of the reaction. The reaction mixture was diluted with EtOAc and filtered over a short plug of celite. After removal of the solvent under reduced pressure, the resulting mixture of two diastereomers was transferred to a silica gel column with EtOAc and a few drops of CH_2Cl_2 (HPLC Grade) for dissolution and purified by column chromatography (*n*-pentane/EtOAc with a gradient, plus 1% Et_3N). The silica gel employed for chromatographic purification was deactivated prior to use by stirring in the initial solvent mixture together with 1% of Et_3N for about 10 min.

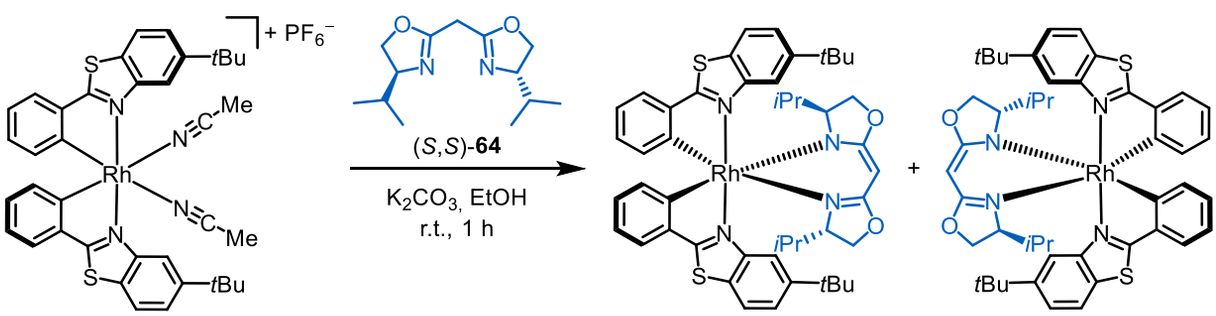

Synthesis of Λ- and Δ-(*S*,*S*)-66 with BOX Ligand (*S*,*S*)-64

Following the general procedure H, *rac*-**RhS**[100] (84.0 mg, 97.4 µmol, 1.00 equiv.), K_2CO_3 (40.4 mg, 0.29 mmol, 3.00 equiv.) and (*S*,*S*)-**64** (25.5 mg, 0.11 mmol, 1.10 equiv.) were

suspended in EtOH (3.90 mL, absolute) and stirred for 1 h at room temperature. TLC indicated full conversion of the racemic starting material and the formation of two diastereomers was confirmed by analysis of the ^{1}H NMR spectrum of the crude material (Figure 47 and Figure 48). Purification of the diastereomeric mixture by silica gel column chromatography (*n*-pentane/EtOAc 25:1 → 20:1 → 15:1, plus 1% Et_3N) afforded Λ-(*S*,*S*)-**66** and Δ-(*S*,*S*)-**66** as red solids. However, a significant amount of decomposition material was isolated along with the desired products. The yields of about 20% for each diastereomer were estimated based on the ^{1}H NMR spectra of the isolated compounds.

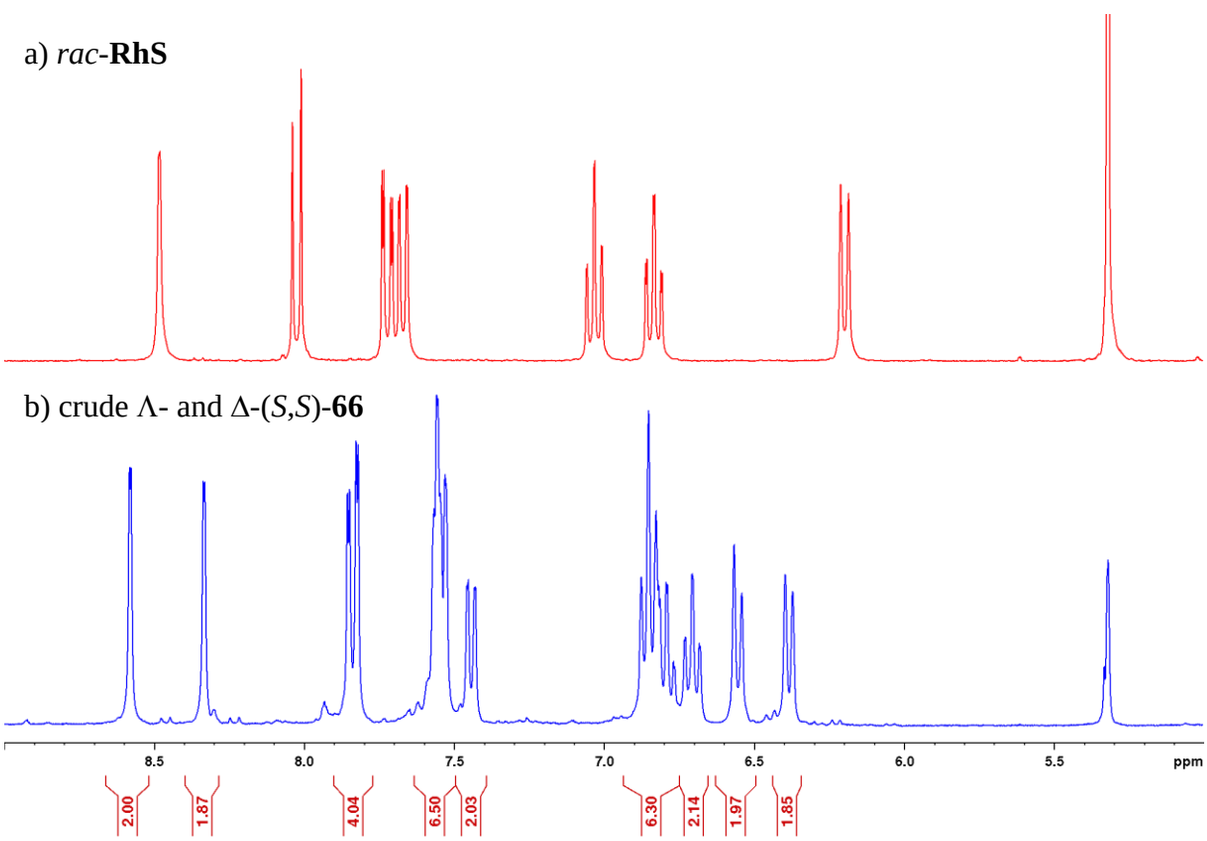

Figure 47: Comparison of the aromatic range of the ^{1}H NMR spectra (300 MHz, 300 K CD_2Cl_2) of a) *rac*-**RhS** and; b) crude Λ- and Δ-(*S*,*S*)-**66** revealing the complete conversion of the starting material as well as the formation of a 1:1 mixture of two diastereomers (28 aromatic proton signals as expected).

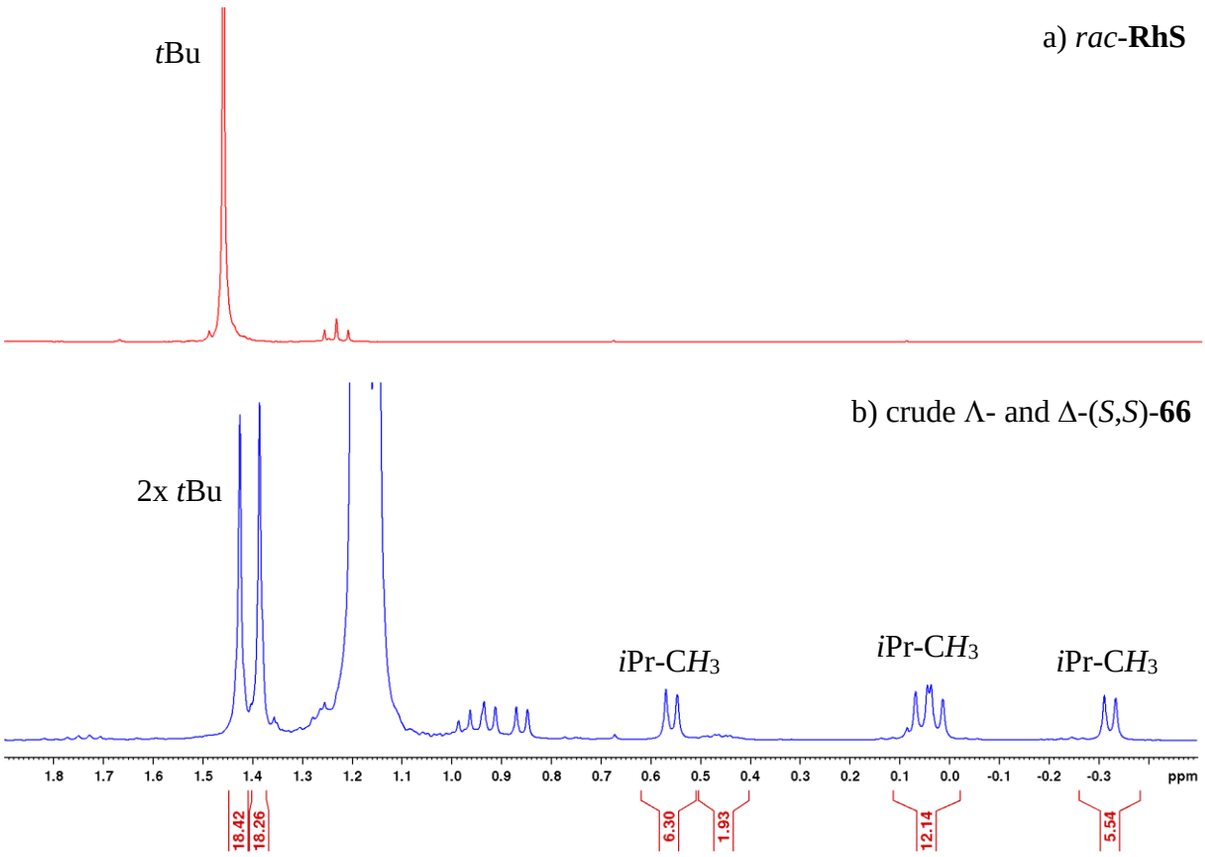

Figure 48: A comparison of a part of the aliphatic area of the ^{1}H NMR spectra (300 MHz, 300 K, CD_2Cl_2) of a) *rac*-**RhS** and; b) crude Λ- and Δ-(*S*,*S*)-**66** confirms the coordination of BOX ligand (*S*,*S*)-**64** and exhibits two new singlets for the *tert*-butyl-groups, one for each diastereomer.

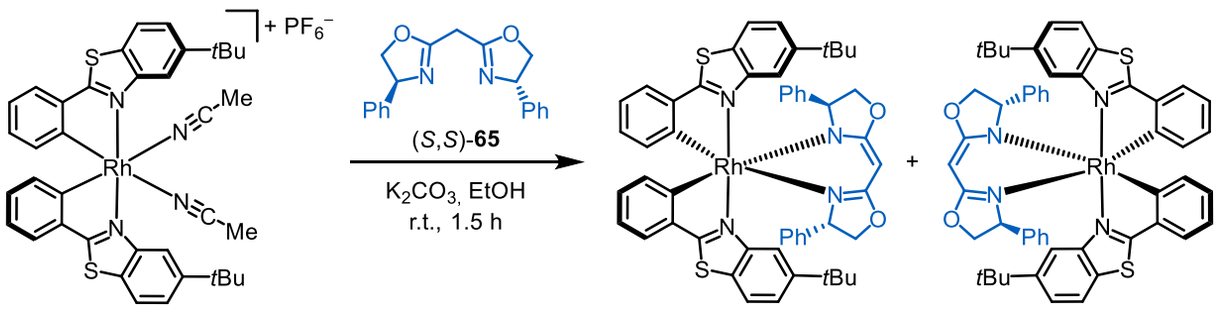

Synthesis of Λ- and Δ-(*S*,*S*)-67 with BOX Ligand (*S*,*S*)-65

Following the general procedure H, *rac*-**RhS**[100] (80.0 mg, 92.7 µmol, 1.00 equiv.), K_2CO_3 (38.4 mg, 0.28 mmol, 3.00 equiv.) and BOX ligand (*S*,*S*)-**65** (31.2 mg, 0.10 mmol, 1.10 equiv.) were suspended in EtOH (3.78 mL, absolute) and stirred for 1.5 h at room temperature. Purification by column chromatography (*n*-pentane/EtOAc 100:1 → 80:1 → 60:1, plus 1% Et_3N) afforded Λ-(*S*,*S*)-**67** (39.4 mg, 41.9 µmol, 45%) and Δ-(*S*,*S*)-**67** (40.9 mg, 43.5 µmol, 47%) as yellow solids. A crystal structure of Λ-(*S*,*S*)-**67** is available. Detailed information and the corresponding crystallographic data can be found in Chapter 6.4.

Analytical data of Λ-(*S*,*S*)-**67**:

TLC: R_f = 0.30 (*n*-pentane/EtOAc 30:1, plus 1% Et_3N).

^{1}H NMR: 300 MHz, CD_2Cl_2; δ = 8.44 (d, *J* = 1.2 Hz, 2H), 7.76 (d, *J* = 8.5 Hz, 2H), 7.59 (dd, *J* = 8.5, 1.8 Hz, 2H), 6.90-6.87 (m, 2H), 6.77-6.68 (m, 6H), 6.36 (brs, 3H), 6.18-6.15 (m, 3H), 5.95 (brs, 4H), 4.59 (dd, *J* = 8.6, 2.9 Hz, 2H), 4.50 (t, *J* = 8.3 Hz, 2H), 4.40 (s, 1H), 3.69 (dd, *J* = 7.9, 3.0 Hz, 2H), 1.55 (s, 18H) ppm.

^{13}C NMR: 126 MHz, CD_2Cl_2; δ = 176.9 (d, $J_{C,Rh}$ = 2.9 Hz, 2C), 172.9 (d, $J_{C,Rh}$ = 29.2 Hz, 2C), 169.9 (2C), 151.9 (2C), 151.6 (2C), 145.3 (2C), 142.3 (2C), 133.0 (2C), 129.7 (4C), 127.3 (4C), 126.4 (2C), 125.7 (2C), 125.5 (2C), 123.3 (2C), 121.9 (2C), 121.7 (2C), 118.9 (2C), 74.9 (2C), 70.1 (2C), 53.7, 35.6 (2C), 32.0 (6C) ppm.

IR: neat, $\tilde{\nu}$ = 3043 (w), 2958 (w), 2924 (w), 2855 (w), 1737 (w), 1607 (w), 1578 (w), 1529 (m), 1471 (w), 1439 (w), 1412 (w), 1360 (w), 1344 (w), 1319 (w), 1286 (w), 1261 (w), 1239 (w), 1201 (w), 1146 (w), 1100 (w), 1063 (w), 1032 (w), 990 (w), 959 (w), 931 (w), 892 (w), 875 (w), 846 (w), 813 (w), 755 (w), 723 (m), 697 (w), 669 (w), 647 (w), 581 (w), 543 (w), 462 (w) cm^{-1}.

HRMS: APCI; m/z calcd. for $C_{53}H_{50}N_4O_2Rh_1S_2$ $[M+H]^+$: 941.2425, found: 941.2416.

m.p.: 273 °C decomposition (EtOAc).

CD: CH_2Cl_2; λ, nm (Δε, $M^{-1}cm^{-1}$) 411 (–48), 369 (+110), 352 (+91), 339 (+54), 329 (+87), 304 (–41), 268 (+73), 250 (+110), 220 (–131), 207 (–24).

Analytical data of Δ-(*S*,*S*)-**67**:

TLC: R_f = 0.23 (*n*-pentane/EtOAc 30:1, plus 1% Et_3N).

^{1}H NMR: 500 MHz, CD_2Cl_2; δ = 9.00 (d, *J* = 1.7 Hz, 2H), 7.91 (d, *J* = 8.6 Hz, 2H), 7.64 (dd, *J* = 8.6, 1.8 Hz, 2H), 7.27 (dd, *J* = 7.1, 0.4 Hz, 2H), 6.77 (m, 6H), 6.61 (m, 4H), 6.45 (m, 2H), 5.90 (dd, *J* = 7.5, 0.8 Hz, 2H), 5.47 (d, *J* = 7.8 Hz, 2H), 4.39 (s, 1H), 4.11-4.07 (m, 2H), 3.72 (dd, *J* = 10.7, 9.1 Hz, 2H), 3.52 (dd, *J* = 10.9, 8.3 Hz, 2H), 1.54 (s, 18H) ppm.

^{13}C NMR: 126 MHz, CD_2Cl_2; δ = 176.8 (d, $J_{C,Rh}$ = 3.2 Hz, 2C), 173.5 (d, $J_{C,Rh}$ = 30.2 Hz, 2C), 171.6 (2C), 151.6 (2C), 151.1 (2C), 143.9 (2C), 139.5 (2C), 134.3 (2C), 128.9 (2C), 127.7 (4C), 127.2 (4C), 126.0 (2C), 124.6 (2C), 124.1 (2C), 121.9 (2C), 121.5 (2C), 120.0 (2C), 74.7 (2C), 70.1 (2C), 57.3, 35.8 (2C), 31.7 (6C) ppm.

IR: neat, $\tilde{\nu}$ = 3055 (w), 2959 (w), 2885 (w), 1730 (w), 1602 (w), 1580 (w), 1538 (m), 1461 (w), 1438 (w), 1413 (w), 1356 (w), 1312 (w), 1291 (w), 1279 (w), 1252 (w),

1233 (w), 1203 (w), 1154 (w), 1123 (w), 1102 (w), 1059 (w), 1039 (m), 989 (w), 959 (w), 932 (w), 888 (w), 845 (w), 809 (w), 778 (w), 750 (w), 721 (w), 695 (w), 670 (w), 647 (w), 607 (w), 585 (w), 536 (w), 459 (w) cm^{-1}.

HRMS: APCI; m/z calcd. for $C_{53}H_{50}N_4O_2Rh_1S_2$ $[M+H]^+$: 941.2425, found: 941.2439.

m.p.: 167 °C (EtOAc).

CD: CH_2Cl_2; λ, nm (Δε, $M^{-1}cm^{-1}$) 417 (+43), 377 (–47), 361 (–46), 332 (+80), 312 (–99), 283 (+21), 270 (+33), 248 (–33), 228 (+27), 221 (–9), 217 (+115), 207 (+30).

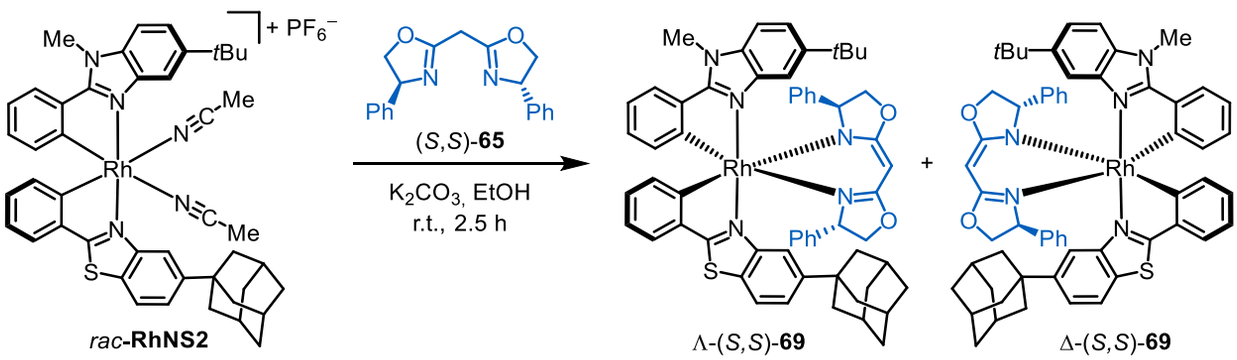

Synthesis of Λ- and Δ-(*S*,*S*)-69.

Following the general procedure H, *rac*-**RhNS2** (36.9 mg, 39.3 µmol, 1.00 equiv.), K_2CO_3 (16.3 mg, 0.12 mmol, 3.00 equiv.) and BOX ligand (*S*,*S*)-**65** (13.3 mg, 0.04 mmol, 1.10 equiv.) were suspended in EtOH (1.60 mL, absolute) and stirred for 2.5 h at room temperature. Purification by column chromatography (*n*-pentane/EtOAc 20:1 → 15:1 → 10:1 → 7:1, plus 1% Et_3N) afforded Λ-(*S*,*S*)-**69** (17.7 mg, 17.4 µmol, 44%) and Δ-(*S*,*S*)-**69** (18.0 mg, 17.7 µmol, 45%) as yellow solids. A crystal structure of Λ-(*S*,*S*)-**69** is available. Detailed information and the corresponding crystallographic data can be found in Chapter 6.4.

Analytical data of Λ-(*S*,*S*)-**69**:

TLC: R_f = 0.40 (*n*-pentane/EtOAc 5:1, plus 1% Et_3N).

^{1}H NMR: 500 MHz, CD_2Cl_2; δ = 8.46 (d, *J* = 1.6 Hz, 1H), 7.97 (d, *J* = 1.6 Hz, 1H), 7.76 (d, *J* = 8.6 Hz, 1H), 7.54 (dd, *J* = 8.5, 1.8 Hz, 1H), 7.51 (dd, *J* = 8.7, 1.8 Hz, 1H), 7.23 (d, *J* = 8.7 Hz, 1H), 6.97 (dd, *J* = 7.1, 0.6 Hz, 1H), 6.93 (dd, *J* = 7.4, 1.3 Hz, 1H), 6.80-6.77 (m, 1H), 6.74-6.67 (m, 6H), 6.33 (brs, 2H), 6.26 (d, *J* = 7.4 Hz, 1H), 6.16 (d, *J* = 7.5 Hz, 1H), 5.96 (brs, 4H), 5.75 (brs, 1H), 4.63 (dd, *J* = 8.7, 3.2 Hz, 1H), 4.55-4.48 (m, 3H), 4.33 (s, 1H), 3.70 (dd, *J* = 8.1, 3.2 Hz, 1H), 3.63 (s, 3H),

3.61 (dd, *J* = 7.4, 2.3 Hz, 1H), 2.19-2.13 (m, 9H), 1.90-1.84 (m, 6H), 1.52 (s, 9H) ppm.

^{13}C NMR: 126 MHz, CD_2Cl_2; δ = 176.3 (d, $J_{C,Rh}$ = 3.5 Hz, 1C), 174.3 (d, $J_{C,Rh}$ = 30 Hz, 1C), 173.8 (d, $J_{C,Rh}$ = 29 Hz, 1C), 170.0, 169.8, 158.9 (d, $J_{C,Rh}$ = 3.1 Hz, 1C), 152.3, 151.7, 147.3, 146.2, 145.4, 142.3, 141.0, 136.6, 134.2, 133.6, 133.1, 129.9, 129.4, 128.5, 127.2 (2C), 126.8 (2C), 126.5 (2C), 126.1, 125.6 (2C), 125.3, 125.1, 123.9, 122.5, 121.6, 121.5, 121.3, 120.9, 118.8, 114.4, 108.7, 74.8, 74.7, 70.2, 70.1, 53.0, 43.8 (3C), 37.1 (3C), 37.1, 35.4, 32.2 (3C), 31.9, 29.6 (3C) ppm.

IR: neat, $\tilde{\nu}$ = 2900 (m), 2848 (w), 1612 (w), 1580 (w), 1531 (w), 1476 (w), 1451 (w), 1414 (w), 1347 (w), 1322 (w), 1288 (w), 1260 (w), 1207 (w), 1111 (w), 1064 (w), 1034 (w), 992 (w), 962 (w), 933 (w), 867 (w), 797 (w), 758 (w), 724 (w), 696 (w), 668 (w), 637 (w), 615 (w), 542 (w), 460 (w) cm^{-1}.

HRMS: APCI; m/z calcd. for $C_{60}H_{59}N_5O_2Rh_1S_1$ $[M+H]^+$: 1016.3439, found: 1016.3464.

m.p.: 141 °C decomposition (EtOAc).

CD: MeOH; λ, nm (Δε, $M^{-1}cm^{-1}$) 388 (–13), 353 (+60), 299 (–42), 269 (+29), 260 (+25), 245 (+57), 216 (–69), 202 (–18).

Analytical data of Δ-(*S*,*S*)-**69**:

TLC: R_f = 0.27 (*n*-pentane/EtOAc 5:1, plus 1% Et_3N).

^{1}H NMR: 500 MHz, CD_2Cl_2; δ = 9.05 (d, *J* = 1.5 Hz, 1H), 8.54 (d, *J* = 1.4 Hz, 1H), 7.92 (d, *J* = 8.6 Hz, 1H), 7.59 (dd, *J* = 8.6, 1.7 Hz, 1H), 7.56 (dd, *J* = 8.7, 1.7 Hz, 1H), 7.47 (d, *J* = 8.7 Hz, 1H), 7.42 (d, *J* = 7.7 Hz, 1H), 7.31 (d, *J* = 7.6 Hz, 1H), 6.76-6.72 (m, 4H), 6.69 (d, *J* = 7.3 Hz, 2H), 6.62-6.57 (m, 4H), 6.47-6.42 (m, 2H), 5.90-5.83 (m, 2H), 5.57 (d, *J* = 7.8 Hz, 1H), 5.41 (d, *J* = 7.8 Hz, 1H), 4.37 (s, 1H), 4.17 (s, 3H), 4.07-4.03 (m, 2H), 3.71 (m, 2H), 3.57 (dd, *J* = 9.9, 8.3 Hz, 1H), 3.43 (dd, *J* = 11.3, 8.3 Hz, 1H), 2.22-2.16 (m, 6H), 2.12 (m, 3H), 1.82 (m, 6H), 1.53 (s, 9H) ppm.

^{13}C NMR: 126 MHz, CD_2Cl_2; δ = 176.2 (d, $J_{C,Rh}$ = 3.1 Hz, 1C), 175.1 (d, $J_{C,Rh}$ = 31.0 Hz, 1C), 173.8 (d, $J_{C,Rh}$ = 30.3 Hz, 1C), 171.7, 171.2, 160.0 (d, $J_{C,Rh}$ = 3.7 Hz, 1C), 152.0, 151.1, 146.6, 144.4, 143.8, 140.9, 139.8, 135.2, 134.3, 134.1, 133.8, 129.1, 128.5, 127.6 (4C), 127.5, 127.3 (2C), 127.3 (2C), 125.9, 125.8, 124.6, 123.1, 122.9, 121.8, 121.3, 121.0, 120.8, 120.4, 116.1, 108.9, 74.9, 74.5, 70.1, 69.9, 56.5, 43.6 (3C), 37.4, 37.2 (3C), 35.5, 32.4, 32.0 (3C), 29.6 (3C) ppm.

IR: neat, $\tilde{\nu}$ = 2899 (m), 2847 (w), 1603 (w), 1581 (w), 1534 (w), 1504 (w), 1475 (w), 1458 (w), 1437 (w), 1415 (w), 1353 (w), 1310 (w), 1289 (w), 1256 (w), 1232 (w), 1209 (w), 1149 (w), 1103 (w), 1062 (w), 1034 (w), 989 (w), 960 (w), 865 (w), 799 (w), 751 (w), 723 (w), 695 (w), 668 (w), 650 (w), 609 (w), 536 (w), 459 (w) cm^{-1}.

HRMS: APCI; m/z calcd. for $C_{60}H_{59}N_5O_2Rh_1S_1$ $[M+H]^+$: 1016.3439, found: 1016.3468.

m.p.: 181 °C decomposition (EtOAc).

CD: MeOH; λ, nm (Δε, $M^{-1}cm^{-1}$) 393 (+19), 357 (–54), 323 (+20), 310 (+5), 295 (+27), 245 (–46), 215 (+35), 207 (–6), 203 (+7).

5.5.2.3 General Procedure I: Acid Induced Removal of Coordinated Auxiliary Ligand

To a solution of Λ- or Δ-(*S*,*S*)-**67**/**69** (1.00 equiv.) in MeCN (0.04 M) was added methanesulfonic acid (10.0 equiv.) in one portion at 0 °C. After 15 min, the ice bath was removed and the solution was stirred for further 6 h at room temperature. Alternatively, the reaction can be stirred for 16 h without affecting the ee of the final catalyst. The solvent was removed under reduced pressure (250–50 mbar, for a maximum of 10 min), NH_4PF_6 (15.0 equiv.) was added to the residual yellow oil, and MeCN (0.02 M) was added. The resulting suspension was stirred for 30 min at room temperature, before the solvent was removed under reduced pressure. Purification by column chromatography (CH_2Cl_2/MeCN 20:1) provided the enantiomerically pure rhodium(III) complexes.

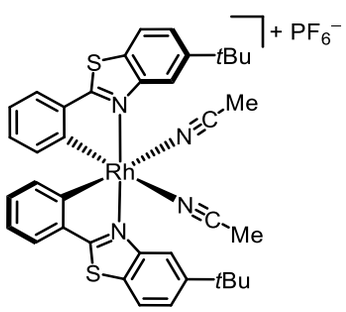

Synthesis of Λ-RhS

Following the general procedure I with Λ-(*S*,*S*)-**67** (20.0 mg, 21.3 µmol, 1.00 equiv.), Λ-**RhS** (18.0 mg, 20.9 µmol, 98%) was obtained as a pale yellow solid after column chromatographic purification. Enantiomeric excess was established by HPLC analysis on a chiral stationary phase: ee = >99.9%, HPLC conditions: Daicel Chiralpak® IB-N5 column, 250 x 4.6 mm, absorbance at 254 nm, H_2O + 0.1% TFA/MeCN = 60:40 to 50:50 in 180 min, 50:50 maintained until 240 min,

gradient elution, flow rate 0.6 mL/min, 25 °C, t_r (Δ-**RhS**) = 210.5 min, t_r (Λ-**RhS**) = 217.8 min). Analytical data were consistent with reported data.[93]

^{1}H NMR: 300 MHz, CD_2Cl_2; δ = 8.50 (brs, 2H), 8.02 (d, *J* = 8.6 Hz, 2H), 7.72 (dd, *J* = 8.6, 1.7 Hz, 2H), 7.67 (dd, *J* = 7.6, 1.2 Hz, 2H), 7.03 (dt, *J* = 7.5, 0.8 Hz, 2H), 6.83 (dt, *J* = 7.6, 1.4 Hz, 2H), 6.21 (d, *J* = 7.8 Hz, 2H), 2.18 (brs, 6H), 1.46 (s, 18H) ppm.

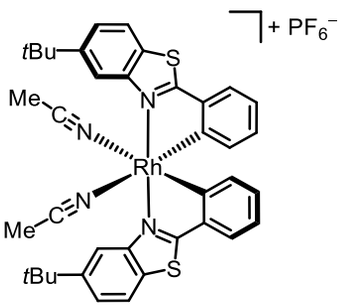

Synthesis of Δ-RhS

Following the general procedure I with Δ-(*S*,*S*)-**67** (22.0 mg, 23.4 µmol, 1.00 equiv.), Δ-**RhS** (19.9 mg, 23.1 µmol, 99%) was obtained as a pale yellow solid after column chromatographic purification. Enantiomeric excess was established by HPLC analysis on a chiral stationary phase: ee = >99%, HPLC conditions: Daicel Chiralpak® IB-N5 column, 250 x 4.6 mm, absorbance at 254 nm, H_2O + 0.1% TFA/MeCN = 60:40 to 50:50 in 180 min, 50:50 maintained until 240 min, gradient elution, flow rate 0.6 mL/min, 25 °C, t_r (Δ-**RhS**) = 210.0 min, t_r (Λ-**RhS**) = 217.8 min). Analytical data were in agreement with published data.[93]

^{1}H NMR: 300 MHz, CD_2Cl_2; δ = 8.48 (d, *J* = 1.5 Hz, 2H), 8.03 (d, *J* = 8.6 Hz, 2H), 7.72 (dd, *J* = 8.6, 1.8 Hz, 2H), 7.67 (dd, *J* = 7.6, 1.2 Hz, 2H), 7.03 (dt, *J* = 7.5, 0.9 Hz, 2H), 6.83 (dt, *J* = 7.6, 1.3 Hz, 2H), 6.20 (d, *J* = 7.8 Hz, 2H), 2.17 (brs, 6H), 1.46 (s, 18H) ppm.

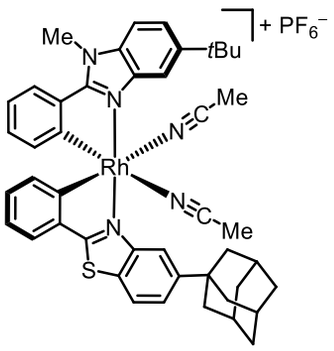

Synthesis of Λ-RhNS2

Following the general procedure I with Λ-(*S*,*S*)-**69** (20.0 mg, 19.7 µmol, 1.00 equiv.), Λ-**RhNS2** (17.5 mg, 18.7 µmol, 95%) was obtained as a pale yellow solid after column chromatographic purification. Since the enantiomeric excess of the catalyst could not be adequately established by HPLC analysis on a chiral stationary phase, Λ-**RhNS2** was reconverted into Λ-(*S*,*S*)-**69** to validate the enantiopurity via determination of the diastereomeric ratio from the ^{1}H NMR of the crude reaction mixture (see Section 5.5.2.5). Accordingly, Λ-**RhNS2** could be obtained with a d.r. of >20:1.

CD: MeOH; λ, nm (Δε, $M^{-1}cm^{-1}$) 389 (–29), 355 (+88), 298 (–95), 244 (+65), 228 (+14), 220 (+26), 214 (–17), 206 (+66).

All other spectroscopic data were in agreement with *rac*-**RhNS2.**

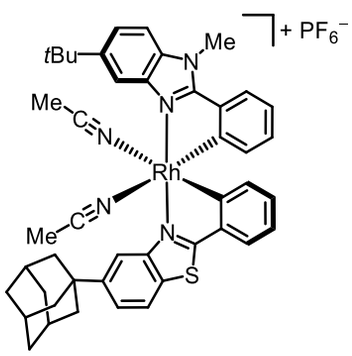

Synthesis of Δ-RhNS2

Following the general procedure I with Δ-(*S*,*S*)-**69** (30.0 mg, 29.5 µmol, 1.00 equiv.), Δ-**RhNS2** (26.2 mg, 27.9 mmol, 95%) was obtained as a pale yellow solid after column chromatographic purification. Since the enantiomeric excess of the catalyst could not be adequately established by HPLC analysis on a chiral stationary phase, Δ-**RhNS2** was reconverted into Δ-(*S*,*S*)-**69** to validate the enantiopurity via determination of the diastereomeric ratio from the ^{1}H NMR of the crude

reaction mixture (see Section 5.5.2.5). Accordingly, Λ-**RhNS2** could be obtained with a d.r. of >20:1.

CD: MeOH; λ, nm (Δε, $M^{-1}cm^{-1}$) 389 (+30), 355 (–91), 298 (+101), 244 (–65), 228 (–18), 220 (–29), 214 (+10), 206 (–67).

All other spectroscopic data were in agreement with *rac*-**RhNS2**.

5.5.2.4 Additional Data for Table 3

Formation of Λ-(*S*,*S*)-69-H

Figure 49 shows the ^{1}H NMR spectrum of isolated Λ-(*S*,*S*)-**69-H** which was obtained as the major product by following the conditions given in Scheme 46 (correspond to entry 1 in Table 3). Under these initial conditions, the desired enantiomerically pure catalyst Λ-**RhNS2** was only obtained in a ratio of 1:5.5 compared to Λ-(*S*,*S*)-**69-H**.

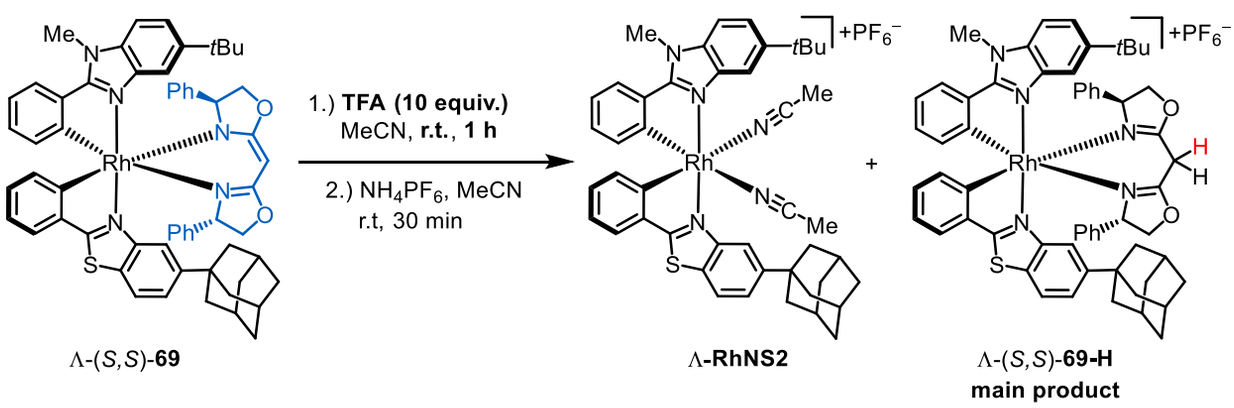

Scheme 46: Stereospecific substitution of the coordinated BOX ligand.

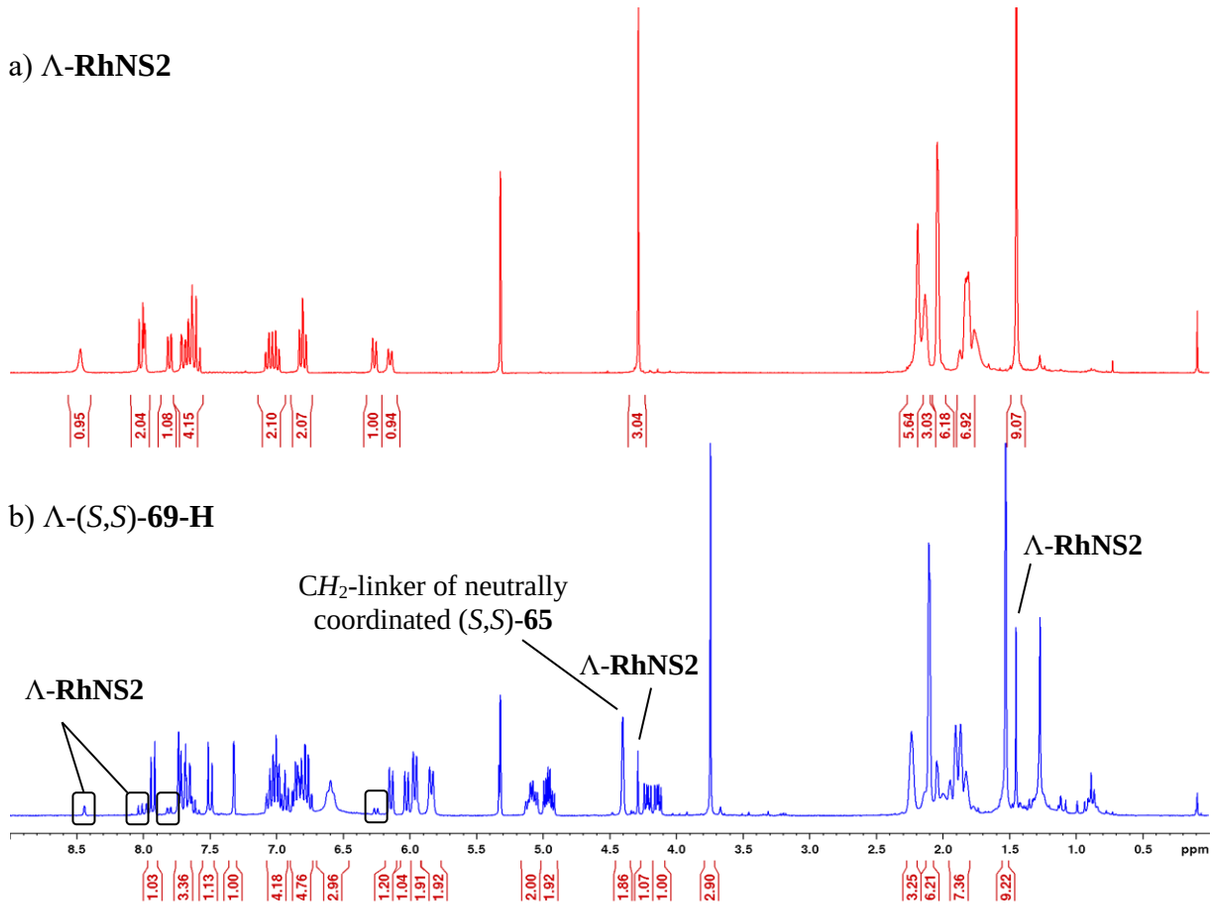

Figure 49: Comparison of a) a ^{1}H NMR spectrum (300 MHz, 300 K, CD_2Cl_2) of desired Λ-**RhNS2** and; b) the corresponding ^{1}H NMR to entry 1 of Table 3.

5.5.2.5 Determination of the Diastereomeric Ratio of Λ- and Δ-RhNS2

As shown in Scheme 47, Λ- and Δ-**RhNS2** were converted back into Λ- and Δ-(*S*,*S*)-**69**, correspondingly, in order to verify the enantiomeric purity of the final catalysts via determination of the diastereomeric ratio from the ^{1}H NMR of the crude materials. A d.r. of more than 20:1 was calculated for both stereoisomers by integration of the baseline separated doublets at 8.55 ppm (Δ) and 8.47 ppm (Λ) (Figure 50).

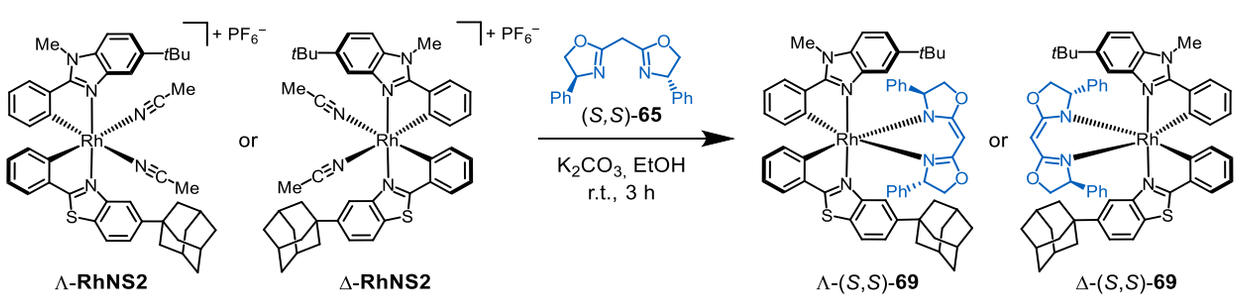

Scheme 47: Reconversion of Λ- and Δ-**RhNS2** into Λ- and Δ-(*S*,*S*)-**69**.

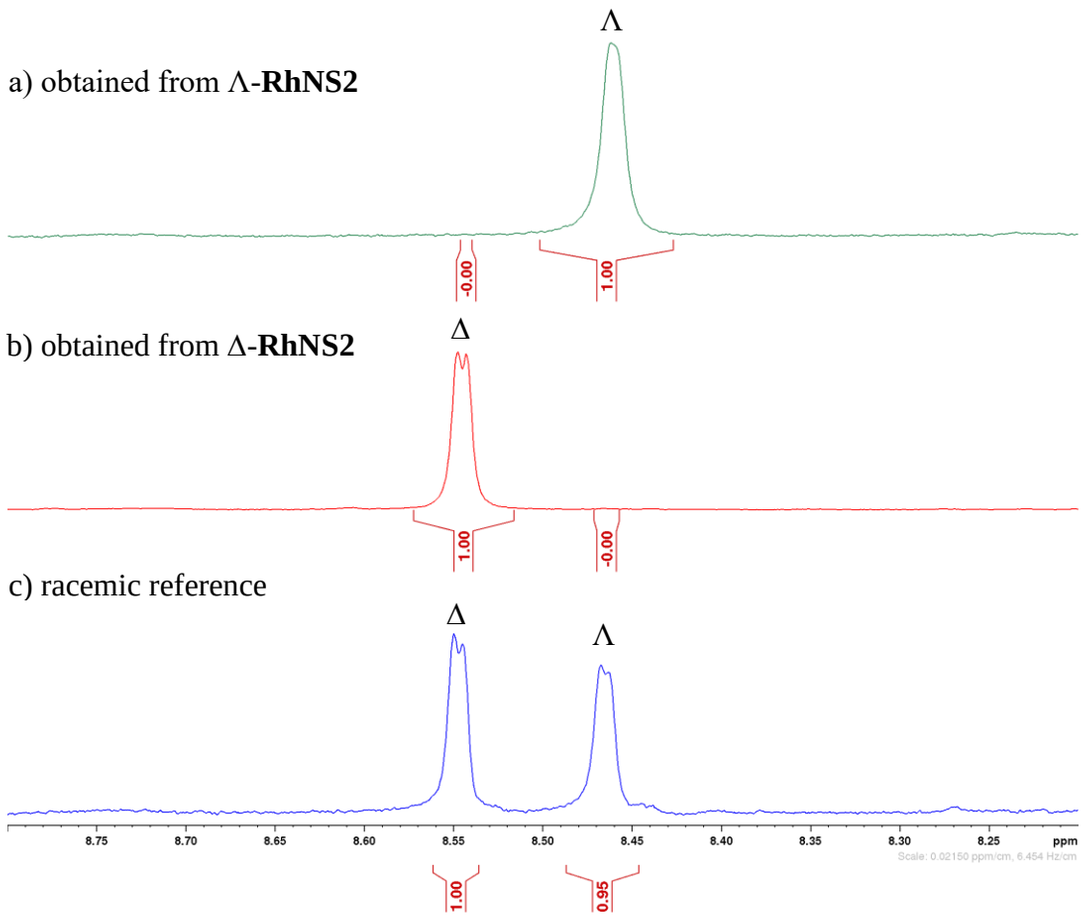

Figure 50: Region of the crude ^{1}H NMR spectra (300 MHz, 300 K, CD_2Cl_2) of a) Λ-(*S*,*S*)-**69**; b) Δ-(*S*,*S*)-**69** and; c) the racemic reference for determination of the diastereomeric ratio.

5.6 Supplementing the Class of Bis-Cyclometalated Tris-Heteroleptic Chiral-at-Rhodium(III) Catalysts with a Pyrazole Derivative

5.6.1 Synthesis of Cyclometalating Ligands and Chiral Bis(oxazolines)

5-*tert*-Butyl-1-methyl-2-phenylbenzimidazole (**47a**) was synthesized as described in Section 5.3.1. 3,5-Diphenylpyrazole (**70**), the second cyclometalating ligand for the synthesis of **RhNP1**, was purchased from commercial sources, while its derivative 1-mesityl-3,5-diphenyl-1*H*-pyrazole (**78**) for the preparation of catalyst **RhNP2** was synthesized from **70** via a short and reported two-step synthesis (Scheme 33).[162] Analytical data were in agreement with published data.[162] Chiral bis(oxazoline) auxiliary (*S*,*S*)-**65** was synthesized as specified in Section 5.5.1.

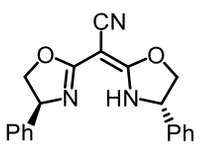

2,2-Bis((*S*)-4-phenyl-4,5-dihydrooxazol-2-yl)acetonitrile (*S*,*S*)-73

According to a slightly modified procedure from Nolin *et al.*,[212] chiral bis(oxazoline) (*S*,*S*)-**65** (69.5 mg, 0.23 mmol, 1.00 equiv.) was dissolved in THF (1.20 mL). At −78 °C, *n*BuLi (2.5 M in *n*-hexane, 0.10 mL, 0.25 mmol, 1.11 equiv.) was added dropwise to the reaction solution, followed by TMEDA (40.0 µL, 0.27 mmol, 1.17 equiv.). The solution was stirred at −78 °C for 1 h, then for 30 min at 0 °C. At −78 °C, *p*-toluenesulfonyl cyanide (46.0 mg, 0.25 mmol, 1.12 equiv.) was added and the resulting solution was allowed to slowly reach room temperature overnight. After 22 h, the reaction mixture was quenched by addition of saturated aqueous NH_4Cl solution and stirred for further 5 min. The aqueous phase was extracted with Et_2O (2 x 20 mL) and CH_2Cl_2 (2 x 20 mL). The combined organic phases were dried over Na_2SO_4, filtered and the solvent was removed under reduced pressure. The oily residue was purified via column chromatography on neutral aluminum oxide (CH_2Cl_2/MeOH 100:1 → 80:1) to afford (*S*,*S*)-**73** (68.4 g, 0.21 mmol, 91%) as a colorless foam. Analytical data were consistent with reported data.[159]

^{1}H NMR: 300 MHz, CD_2Cl_2; δ = 7.40-7.31 (m, 6H), 7.30-7.25 (m, 4H), 5.19 (dd, J = 9.2, 7.2 Hz, 2H), 4.85 (t, J = 8.9 Hz, 2H), 4.32 (dd, J = 8.6, 7.2 Hz, 2H) ppm.

5.6.2 Synthesis of Protic Pyrazole Complex RhNP1

Mono-cyclometalated rhodium complex **48a** was prepared as described in Section 5.3.2.

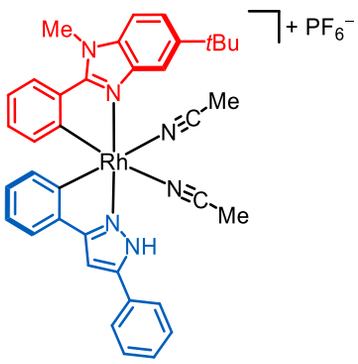

Synthesis of *rac*-RhNP1

To a solution of mono-cyclometalated rhodium(III) complex **48a** (50.0 mg, 74.6 µmol, 1.00 equiv.) and 3,5-diphenylpyrazole (**70**, 18.6 mg, 82.1 µmol, 1.10 equiv.) in MeCN (2.50 mL) was added NaOAc (6.70 mg, 82.1 µmol, 1.10 equiv.), and the resulting yellow suspension was stirred at 80 °C for 24 h in the dark. The reaction mixture was cooled to room temperature, filtered over a short plug of celite and rinsed with MeCN. After removal of the solvent under reduced pressure, the residue obtained was purified via two successive silica gel columns. Since the desired complex and residual ligand **70** have the same R_f value in CH_2Cl_2/MeCN solvent mixtures, the crude mixture was first subjected to a short silica gel column, which was rinsed with toluene/MeCN 10:1 until all of the residual ligand **70** eluted. Subsequently, *rac*-**RhNP1** was eluted with a 1:1 mixture of toluene/MeCN. After removal of the solvent under reduced pressure, the crude complex obtained was further purified via column chromatography (CH_2Cl_2/MeCN 80:1 → 60:1 → 40:1 → 20:1 → 15:1 → 10:1) (Ø = 2 cm, H = 25 cm), to afford pure *rac*-**RhNP1** (41.3 mg, 50.8 µmol, 68%) as a pale yellow solid. A crystal structure of *rac*-**RhNP1** is available. Detailed information and the corresponding crystallographic data can be found in Chapter 6.4.

TLC: R_f = 0.57 (CH_2Cl_2/MeCN 5:1).

^{1}H NMR: 300 MHz, CD_3CN; δ = 11.81 (brs, 1H), 8.00-7.94 (m, 3H), 7.86 (dd, J = 7.8, 0.9 Hz, 1H), 7.68-7.52 (m, 5H), 7.49 (dd, J = 7.4, 1.2 Hz, 1H), 7.19 (s, 1H), 7.05-7.00 (m, 1H), 6.92-6.85 (m, 2H), 6.64-6.59 (m, 1H), 6.34 (d, J = 7.8 Hz, 1H), 5.99 (d, J = 7.7 Hz, 1H), 4.24 (s, 3H), 1.44 (s, 9H) ppm.

^{13}C NMR: 126 MHz, CD_3CN; δ = 163.7 (d, $J_{C,Rh}$ = 33.1 Hz, 1C), 160.7 (d, $J_{C,Rh}$ = 2.6 Hz, 1C), 159.2 (d, $J_{C,Rh}$ = 3.8 Hz, 1C), 159.1 (d, $J_{C,Rh}$ = 33.2 Hz, 1C), 148.4, 148.3,

140.5, 139.1, 135.9, 134.9, 134.6, 133.8, 130.7, 130.2 (2C), 130.1, 129.2, 128.1, 127.4 (2C), 125.8, 124.2, 123.8, 123.2, 113.1, 111.5, 100.1, 35.6, 33.2, 32.0 (3C) ppm.

^{19}F NMR: 235 MHz, CD_3CN; $\delta = -73.0$ (d, $J_{P,F} = 706$ Hz, 6F) ppm.

IR: neat, $\tilde{\nu}$ = 3358 (w), 3041 (w), 2956 (w), 2296 (w), 1622 (w), 1585 (w), 1554 (w), 1508 (w), 1480 (w), 1425 (w), 1362 (w), 1331 (w), 1292 (w), 1264 (w), 1207 (w), 1157 (w), 1114 (w), 1023 (w), 838 (s), 819 (w), 797 (w), 753 (w), 732 (w), 683 (w), 649 (w), 596 (w), 553 (s), 450 (w), 418 (w) cm^{-1}.

HRMS: APCI; m/z calcd. for $C_{37}H_{36}N_6Rh$ $[M]^+$: 667.2051, found: 667.2051.

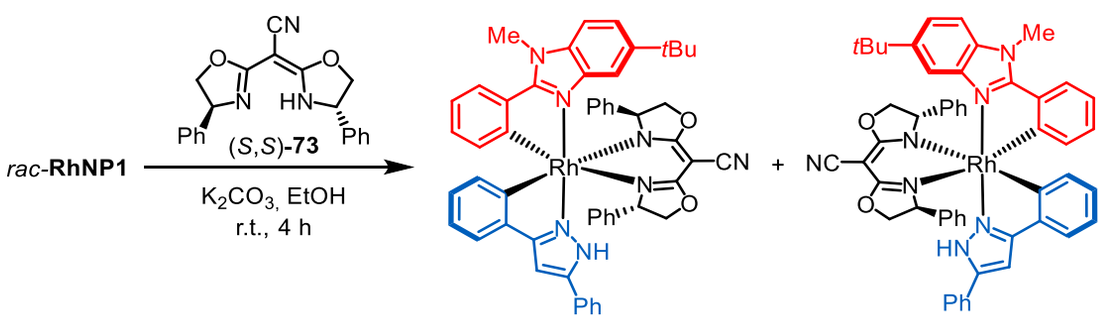

Synthesis of Λ- and Δ-(*S*,*S*)-74

Rac-**RhNP1** (60.0 mg, 73.8 µmol, 1.00 equiv.), K_2CO_3 (11.2 mg, 81.2 µmol, 1.10 equiv.) and BOX ligand (*S*,*S*)-**73** (26.9 mg, 81.2 µmol, 1.10 equiv.) were suspended in EtOH (absolute, 2.90 mL) and stirred at room temperature for 6 h. The yellow suspension was diluted with EtOAc and filtered over a short plug of celite. Removal of the solvent under reduced pressure (water bath of rotary evaporator set to 30 °C) afforded the crude mixture of Λ- and Δ-(*S*,*S*)-**74**. The silica gel employed for column chromatographic purification was deactivated prior to use by stirring in a mixture of *n*-pentane/EtOAc (10:1, plus 1% Et_3N) for about 15 min. The diastereomeric mixture was transferred to the column with the initial solvent mixture and a few drops of CH_2Cl_2 (HPLC Grade) for dissolution and purified by column chromatography (*n*-pentane/EtOAc 10:1 → 5:1 → 3:1 → 2:1 →1.5:1) (Ø = 2.5 cm, H = 28 cm) to give (Λ)-(*S*,*S*)-**74** (33.8 mg, 36.9 µmol, 50%) and (Δ)-(*S*,*S*)-**74** (30.4 mg, 33.2 µmol, 45%) as yellow solids. A crystal structure of the Λ- or Δ-complex is not yet available, but would be necessary to confirm the absolute configurations assigned here only with reservations.

Analytical data of Λ-(*S*,*S*)-**74**:

TLC: R_f = 0.41 (*n*-pentane/EtOAc 2:1).

^{1}H NMR: 300 MHz, CD_2Cl_2; δ = 12.63 (brs, 1H), 7.92 (d, J = 7.4 Hz, 2H), 7.80 (s, 1H), 7.62-7.47 (m, 4H), 7.36 (d, J = 8.7 Hz, 1H), 6.90-6.82 (m, 3H), 6.78-6.62 (m, 7H), 6.58-6.53 (m, 1H), 6.44 (brs, 2H), 6.13-6.11 (m, 2H), 6.06 (d, J = 7.4 Hz, 1H), 5.89 (d, J = 7.4 Hz, 2H), 4.76-4.66 (m, 3H), 4.51 (t, J = 8.6 Hz, 1H), 3.79 (d, J = 6.8 Hz, 1H), 3.68 (s, 3H), 3.61 (dd, J = 8.2, 3.2 Hz, 1H), 1.44 (s, 9H) ppm.

HRMS: APCI; m/z calcd. for $C_{53}H_{47}N_7O_2Rh$ $[M+H]^+$: 916.2841, found: 916.2845.

Analytical data of Δ-(*S*,*S*)-**74**:

TLC: R_f = 0.28 (*n*-pentane/EtOAc 2:1).

^{1}H NMR: 300 MHz, CD_2Cl_2; δ = 9.57 (brs, 1H), 8.27 (d, J = 1.4 Hz, 1H), 7.75 (dd, J = 7.4, 0.3 Hz, 1H), 7.62-7.47 (m, 7H), 7.25 (t, J = 7.6 Hz, 2H), 7.12 (dd, J = 7.4, 1.1 Hz, 1H), 7.04 (t, J = 7.4 Hz, 1H), 6.99-6.91 (m, 3H), 6.81-6.75 (m, 4H), 6.70-6.59 (m, 3H), 6.50-6.45 (m, 1H), 5.91-5.86 (m, 1H), 5.77 (d, J = 7.7 Hz, 1H), 5.34 (d, J = 7.7 Hz, 1H), 4.46 (dd, J = 9.9, 8.4 Hz, 1H), 4.23-4.12 (m, 4H), 4.04-3.82 (m, 4H), 1.56 (s, 9H) ppm.

HRMS: APCI; m/z calcd. for $C_{53}H_{47}N_7O_2Rh$ $[M+H]^+$: 916.2841, found: 916.2866.

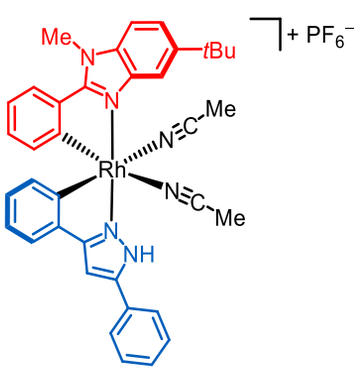

Synthesis of Λ-RhNP1

A solution of Λ-(*S*,*S*)-**74** (25 mg, 27.3 µmol, 1.00 equiv.) in MeCN (0.68 mL) was cooled to 0 °C and methanesulfonic acid (17.7 µL, 0.27 mmol, 10.0 equiv.) was added in one portion, followed by trifluoroacetic acid (42.1 µL, 0.55 mmol, 20.0 equiv.) 5 min later. After 15 min, the ice bath was removed and the solution was stirred for 20 h at room temperature. The solvent was removed under reduced pressure (water bath of rotary evaporator set to 30 °C, 250–20 mbar for a maximum of 10 min) and NH_4PF_6 (66.7 mg, 0.41 mmol, 15.0 equiv.) was added to the residual orange oil, followed by MeCN (1.37 mL). The resulting suspension was stirred for 30 min at

room temperature before the solvent was removed under reduced pressure (30 °C, 250–20 mbar). Purification by column chromatography (CH_2Cl_2/MeCN 40:1 → 20:1 → 10:1) (Ø = 2 cm, H = 20 cm) provided Λ-**RhNP1** (19.1 mg, 23.5 µmol, 86%) as a pale yellow solid. A crystal structure of Λ- oder Δ-**RhNP1** is not yet available, but would be necessary to confirm the absolute configuration assigned here only with reservations. Enantiomeric excess was established by HPLC analysis on a chiral stationary phase: ee = >99%, HPLC conditions: Daicel Chiralpak® IB-N5 column, 250 x 4.6 mm, absorbance at 254 nm, H_2O + 0.1% TFA/MeCN = 60:40 to 50:50 in 180 min, 50:50 maintained until 190 min, gradient elution, flow rate 0.6 mL/min, 25 °C, t_r (Δ-**RhNP1**) = 130.8 min, t_r (Λ-**RhNP1**) = 145.1 min).

All other spectroscopic data were in agreement with *rac*-**RhNP1**.

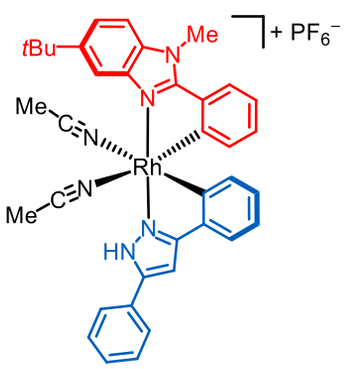

Synthesis of Δ-RhNP1

A solution of Δ-(*S*,*S*)-**74** (27.3 mg, 29.8 µmol, 1.00 equiv.) in MeCN (0.75 mL) was cooled to 0 °C and methanesulfonic acid (19.4 µL, 0.30 mmol, 10.0 equiv.) was added in one portion, followed by trifluoroacetic acid (45.9 µL, 0.60 mmol, 20.0 equiv.) 5 min later. After 15 min, the ice bath was removed and the solution was stirred for 15 h at room temperature. The solvent was removed under reduced pressure (water bath of rotary evaporator set to 30 °C, 250–20 mbar for a maximum of 10 min) and NH_4PF_6 (72.9 mg, 0.45 mmol, 15.0 equiv.) was added to the residual orange oil, followed by MeCN (1.51 mL). The resulting suspension was stirred for 30 min at room temperature before the solvent was removed under reduced pressure (30 °C, 250–20 mbar). Purification by column chromatography (CH_2Cl_2/MeCN 60:1 → 40:1 → 20:1 → 10:1) (Ø = 2 cm, H = 20 cm) provided Δ-**RhNP1** (23.1 mg, 28.4 µmol, 95%) as a pale yellow solid. A crystal structure of Λ- oder Δ-**RhNP1** is not yet available, but would be necessary to confirm the absolute configuration assigned here only with reservations. Enantiomeric excess was established by HPLC analysis on a chiral stationary phase: ee = 99%, HPLC conditions: Daicel Chiralpak®

IB-N5 column, 250 x 4.6 mm, absorbance at 254 nm, H_2O + 0.1% TFA/MeCN = 60:40 to 50:50 in 180 min, 50:50 maintained until 190 min, gradient elution, flow rate 0.6 mL/min, 25 °C, t_r (Δ-**RhNP1**) = 129.3 min, t_r (Λ-**RhNP1**) = 147.2 min).

All other spectroscopic data were in agreement with *rac*-**RhNP1**.

5.6.3 Synthesis of Mesityl Pyrazole Complex RhNP2

Mono-cyclometalated rhodium complex **48a** was prepared as described in Section 5.3.2.

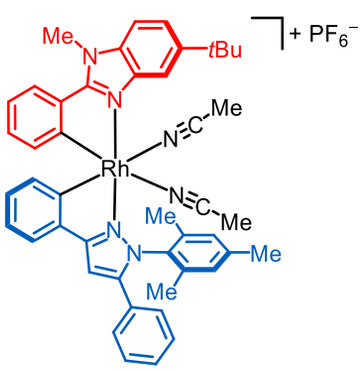

Synthesis of *rac*-RhNP2

To a solution of mono-cyclometalated rhodium(III) complex **48a** (150 mg, 0.22 mmol, 1.00 equiv.) and 1-mesityl-3,5-diphenyl-1*H*-pyrazole (**78**, 90.9 mg, 0.27 mmol, 1.20 equiv.) in MeCN (7.47 mL) was added NaOAc (20.2 mg, 0.25 mmol, 1.10 equiv.). The resulting solution was stirred at 80 °C for 25 h in the dark. The suspension was cooled to room temperature and filtered over a short plug of celite which was rinsed with MeCN. The solvent was removed under reduced pressure and the obtained residue was purified by column chromatography (CH_2Cl_2/MeCN 80:1 → 60:1 → 40:1 → 20:1 → 10:1) to afford *rac*-**RhNP2** (154 mg, 0.17 mmol, 74%) as a pale yellow solid. A crystal structure of *rac*-**RhNP2** is available. Detailed information and the corresponding crystallographic data can be found in Chapter 6.4.

^{1}H NMR: 300 MHz, CD_3CN; δ = 7.91 (s, 1H), 7.83 (dd, J = 7.8, 1.1 Hz, 1H), 7.61 (s, 2H), 7.58 (dd, J = 7.6, 1.3 Hz, 1H), 7.43-7.35 (m, 5H), 7.30 (s, 1H), 7.07-6.99 (m, 3H), 6.96-6.90 (m, 2H), 6.67-6.59 (m, 2H), 6.06 (d, J = 7.8 Hz, 1H), 4.20 (s, 3H), 2.28 (s, 6H), 1.88 (s, 3H), 1.40 (s, 9H) ppm.

^{13}C NMR: 75 MHz, CD_3CN; δ = 162.9 (d, $J_{C,Rh}$ = 33.1 Hz, 1C), 161.3 (d, $J_{C,Rh}$ = 2.4 Hz, 1C), 159.2 (d, $J_{C,Rh}$ = 3.6 Hz, 1C), 158.9 (d, $J_{C,Rh}$ = 32.3 Hz, 1C), 151.2, 148.4, 141.8, 140.3, 139.3, 139.1, 138.7, 136.1, 135.9, 135.1, 134.9, 133.8, 130.6, 130.2, 130.1, 130.0, 129.9, 129.6, 129.0, 128.5, 125.7, 124.5, 124.3, 124.2, 123.2, 112.9, 111.5, 103.4, 35.7, 33.2, 32.1 (3C), 21.2, 20.2, 18.0 ppm.

^{19}F NMR: 282 MHz, CD_3CN; δ = –74.0 (d, $J_{P,F}$ = 711 Hz, 6F) ppm.

IR: neat, $\tilde{\nu}$ = 3159 (w), 3054 (w), 2959 (w), 2924 (w), 2866 (w), 2311 (w), 2283 (w), 1584 (w), 1541 (w), 1510 (w), 1481 (m), 1450 (w), 1423 (w), 1366 (w), 1333 (w), 1286 (w), 1265 (w), 1220 (w), 1158 (w), 1118 (w), 1089 (w), 1022 (w), 986 (w), 961 (w), 871 (w), 838 (s), 766 (w), 733 (m), 692 (w), 651 (w), 613 (w), 555 (m), 455 (w) cm^{-1}.

HRMS: APCI; m/z calcd. for $C_{44}H_{43}N_5Rh$ $[M–MeCN]^+$: 744.2568, found: 744.2572.

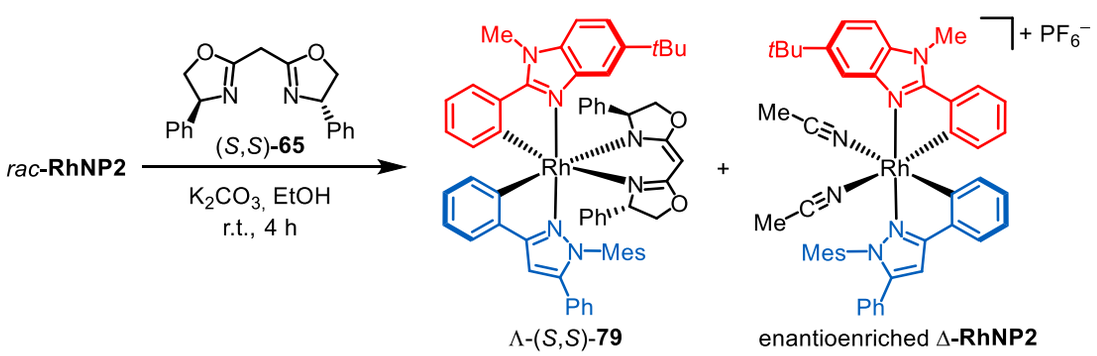

Synthesis of Λ-(*S*,*S*)-79 and Enantioenriched Δ-RhNP2

Rac-**RhNP2** (100 mg, 0.11 mmol, 1.00 equiv.), K_2CO_3 (44.5 mg, 0.32 mmol, 3.00 equiv.) and BOX ligand (*S*,*S*)-**65** (34.6 mg, 0.11 mmol, 1.05 equiv.) were suspended in EtOH (absolute, 4.28 mL) and stirred at room temperature for 4 h. The yellow suspension was diluted with EtOAc and filtered over a short plug of celite. Removal of the solvent under reduced pressure (water bath of rotary evaporator set to 30 °C) afforded the crude mixture of Λ- and Δ-(*S*,*S*)-**79**. The silica gel employed for column chromatographic purification was deactivated prior to use by stirring in a mixture of *n*-pentane/EtOAc (10:1, plus 2% Et_3N) for about 15 min. The diastereomeric mixture was transferred to the column with the initial solvent mixture and a few drops of CH_2Cl_2 (HPLC Grade) for dissolution, and was then quickly (<15min) filtered through the short silica pad (*n*-pentane/EtOAc 10:1 → 5:1, plus 0.1% Et_3N) (Ø = 3 cm, H = 5 cm) affording Λ-(*S*,*S*)-**79** (52.0 mg, 51.5 µmol, 48%) as a yellow solid, while Δ-(*S*,*S*)-**79** did not elute due to decomposition. For elution of enantiomerically enriched Δ-**RhNP2**, an excess NH_4PF_6 (263 mg, 1.61 mmol, 15.0 equiv.) was added atop of the sea sand of the same column and covered with

some additional sea sand. The residual orange band was then eluted with CH_2Cl_2/MeCN 1:1. After removal of the solvent under reduced pressure, the obtained orange solid was subjected to another short silica gel column (CH_2Cl_2/MeCN 20:1) to remove the excess of salts to yield Δ-**RhNP2** along with residual BOX ligand (*S*,*S*)-**65** which has the same R_f value. For further purification, the obtained residue was dissolved in MeCN (HPLC Grade, 1.25 mL) and trifluoroacetic acid (41.0 µL, 0.54 mmol) was added (to protonate (*S*,*S*)-**65**, which will therefore no longer elute from the column). The resulting mixture was stirred for 15 min at room temperature under air, then the solvent was removed under reduced pressure. NH_4PF_6 (123 mg, 0.75 mmol) was added, and the crude mixture redissolved in MeCN (HPLC Grade, 2.50 mL) to re-exchange the counterion. After 15 min stirring at room temperature, the solvent was removed under reduced pressure and the crude residue was filtered through a short silica gel column (CH_2Cl_2/MeCN 20:1) to afford pure enantioenriched Δ-**RhNP2** (47.0 mg, 50.5 µmol, 47%) as a pale yellow solid. Analytical data were in agreement with *rac*-**RhNP2**.

Analytical data of Λ-(*S*,*S*)-**79**:

^{1}H NMR: 300 MHz, CD_2Cl_2; δ = 7.73 (d, *J* = 1.5 Hz, 1H), 7.47 (dd, *J* = 8.7, 1.7 Hz, 1H), 7.35-7.25 (m, 5H), 7.16-7.09 (m, 3H), 6.96-6.94 (m, 1H), 6.87-6.66 (m, 9H), 6.59-6.56 (m, 1H), 6.53 (s, 1H), 6.52-6.43 (m, 4H), 5.96 (brs, 1H), 5.79 (dd, *J* = 7.1, 0.8 Hz, 1H), 5.69 (d, *J* = 7.4 Hz, 2H), 4.97 (dd, *J* = 9.0, 8.4 Hz, 1H), 4.63 (dd, *J* = 9.2, 8.4 Hz, 1H), 3.78-3.68 (m, 2H), 3.62 (s, 3H), 3.16 (dd, *J* = 8.2, 7.9 Hz, 1H), 3.07 (dd, *J* = 7.4, 3.2 Hz, 1H), 2.68 (s, 3H), 2.31 (s, 3H), 2.17 (s, 3H), 1.50 (s, 9H) ppm.

^{13}C NMR: 126 MHz, CD_2Cl_2; δ = 172.4 (d, $J_{C,Rh}$ = 30.1 Hz, 1C), 171.0, 168.6, 167.3 (d, $J_{C,Rh}$ = 29.2 Hz, 1C), 161.5 (d, $J_{C,Rh}$ = 1.4 Hz, 1C), 159.1 (d, $J_{C,Rh}$ = 3.6 Hz, 1C), 147.2, 147.1, 146.6, 145.1, 140.9, 140.3, 139.9, 139.6, 136.0, 135.9, 135.3, 134.7, 134.0, 132.0, 130.6, 130.0, 129.3, 128.8, 128.7 (2C), 128.2 (2C), 127.6 (2C), 127.3, 127.2 (2C), 126.8, 126.7, 125.4, 124.9, 123.9, 122.4, 121.6, 120.8, 120.7, 114.6, 108.4, 102.6, 75.3, 73.7, 72.2, 70.3, 35.5, 32.3 (3C), 32.0, 21.2, 20.8, 20.0 ppm.

IR: neat, $\tilde{\nu}$ = 3028 (w), 2953 (w), 2898 (w), 2028 (w), 1613 (m), 1585 (w), 1535 (s), 1510 (w), 1479 (w), 1449 (w), 1421 (w), 1359 (w), 1282 (w), 1245 (w), 1209 (w), 1152 (w), 1116 (w), 1059 (w), 1038 (m), 961 (w), 854 (w), 797 (w), 752 (w), 724 (s), 696 (m), 647 (w), 610 (w), 540 (w), 500 (w), 469 (w) cm^{-1}.

HRMS: APCI; m/z calcd. for $C_{61}H_{58}N_6O_2Rh$ $[M+H]^+$: 1009.3671, found: 1009.3695.

CD: CH_2Cl_2; λ, nm (Δε, $M^{-1}cm^{-1}$) 377 (–6), 359 (–7), 329 (+86), 281 (–16), 250 (+31), 214 (–2).

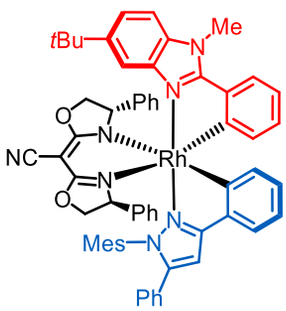

Synthesis of Δ-(*S*,*S*)-80 from Enantioenriched Δ-RhNP2

Enantiomerically enriched Δ-**RhNP2** (47.0 mg, 50.0 µmol, 1.00 equiv.), K_2CO_3 (20.9 mg, 0.15 mmol, 3.00 equiv.) and BOX ligand (*S*,*S*)-**73** (17.6 mg, 53.0 µmol, 1.05 equiv.) were suspended in EtOH (absolute, 2.00 mL) and stirred at room temperature for 4.5 h. The yellow suspension was diluted with EtOAc and filtered over a short plug of celite. Removal of the solvent under reduced pressure afforded crude Δ-(*S*,*S*)-**80** with a d.r. of 10:1. The silica gel employed for column chromatographic purification was deactivated prior to use by stirring in a mixture of *n*-pentane/EtOAc (5:1, plus 1% Et_3N) for about 15 min. To remove the salts, the crude residue was transferred to a small silica gel column with the initial solvent mixture and a few drops of CH_2Cl_2 (HPLC Grade) for dissolution and was then filtered through (*n*-pentane/EtOAc 5:1 → 2:1, plus 0.1% Et_3N) (Ø = 2 cm, H = 15 cm) to provide Δ-(*S*,*S*)-**80** along with traces of Λ-(*S*,*S*)-**80** and ligand (*S*,*S*)-**73**. For recrystallization, the mixture obtained was dissolved in CH_2Cl_2 (HPLC Grade, 2.5 mL), layered with *n*-hexane (HPLC Grade, 15 mL) and stored at –20 °C for two days to afford pure Δ-(*S*,*S*)-**80** (45 mg, 43.5 µmol, 86%, >20:1 d.r.) as yellow crystals. A crystal structure of Δ-(*S*,*S*)-**80** is available. Detailed information and the corresponding crystallographic data can be found in Chapter 6.4.

Analytical data of Δ-(*S*,*S*)-**80**:

^{1}H NMR: 500 MHz, CD_2Cl_2; δ = 8.06 (d, *J* = 1.6 Hz, 1H), 7.66 (dd, *J* = 7.8, 1.1 Hz, 1H), 7.52 (dd, *J* = 8.7, 1.8 Hz, 1H), 7.41 (d, *J* = 8.8 Hz, 1H), 7.32-7.25 (m, 4H), 7.21-7.19 (m, 2H), 7.10 (brs, 1H), 7.04-7.01 (m, 1H), 7.00 (s, 1H), 6.94 (t, *J* = 7.6 Hz, 2H), 6.91-6.88 (m, 1H), 6.82-6.79 (m, 1H), 6.72 (brs, 1H), 6.68-6.55 (m, 7H), 6.14-6.13 (m, 2H), 5.84-5.80 (m, 1H), 5.28 (d, *J* = 7.9 Hz, 1H), 4.47-4.41 (m, 2H), 4.17 (s, 3H), 3.83-3.77 (m, 1H), 3.64 (dd, *J* = 8.1, 5.1 Hz, 1H), 3.03 (dd, *J* = 9.0,

8.3 Hz, 1H), 2.90 (dd, J = 9.1, 5.1 Hz, 1H), 2.42 (s, 3H), 1.77 (s, 3H), 1.49 (s, 9H), 1.35 (s, 3H) ppm.

^{13}C NMR: 126 MHz, CD_2Cl_2; δ = 172.3 (d, $J_{C,Rh}$ = 30.7 Hz, 1C), 169.9, 168.8, 163.8 (d, $J_{C,Rh}$ = 30.9 Hz, 1C), 161.1 (d, $J_{C,Rh}$ = 1.8 Hz, 1C), 160.1 (d, $J_{C,Rh}$ = 3.7 Hz, 1C), 148.5, 147.1, 144.1, 141.4, 140.1, 139.8, 137.6, 137.5, 136.8, 136.1, 135.8, 133.9, 133.9, 133.8, 130.2, 130.0, 129.3. 129.2 (2C), 128.9 (2C), 128.2, 128.1 (2C), 127.9 (2C), 127.8 (2C), 127.5, 126.8 (2C), 126.6, 126.0, 124.4, 122.1, 122.0, 121.9, 121.9, 121.6, 114.7, 109.4, 101.3, 75.4 (2C), 70.8, 68.7, 49.6, 35.4, 32.6, 31.8 (3C), 21.4, 18.6, 17.7 ppm.

IR: neat, $\tilde{\nu}$ = 3032 (w), 2957 (w), 2921 (w), 2189 (m), 1616 (s), 1585 (w), 1537 (s), 1506 (w), 1478 (w), 1451 (w), 1414 (m), 1360 (w), 1331 (w), 1280 (w), 1259 (w), 1197 (w), 1157 (w), 1061 (s), 1044 (w), 1023 (w), 979 (w), 960 (w), 940 (w), 853 (w), 800 (m), 752 (m), 726 (m), 693 (s), 650 (w), 611 (w), 553 (m), 531 (w), 451 (w) cm^{-1}.

HRMS: APCI, m/z calcd. for $C_{62}H_{57}N_7O_2Rh$ $[M+H]^+$: 1034.3623, found: 1034.3633.

CD: CH_2Cl_2; λ, nm (Δε, M^{-1}cm^{-1}) 355 (+24), 329 (–15), 317 (–11), 298 (–34), 271 (+22), 251 (–24), 236 (–5), 231 (–7), 202 (+9).

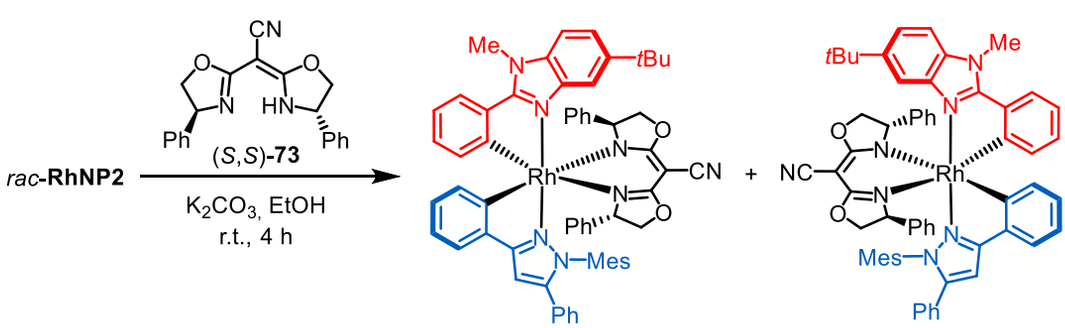

Alternative Synthetic Route: Synthesis of Λ- and Δ-(*S*,*S*)-80 from *rac*-RhNP2

Rac-**RhNP2** (97.7 mg, 0.11 mmol, 1.00 equiv.), K_2CO_3 (43.5 mg, 0.32 mmol, 3.00 equiv.) and BOX ligand (*S*,*S*)-**73** (36.5 mg, 0.32 mmol, 1.05 equiv.) were suspended in EtOH (absolute, 4.20 mL) and stirred at room temperature for 6 h. The yellow suspension was diluted with EtOAc and filtered over a short plug of celite. Removal of the solvent under reduced pressure afforded the crude 1:1 mixture of Λ- and Δ-(*S*,*S*)-**80**. The silica gel employed for column chromatographic purification was deactivated prior to use by stirring in toluene (plus 1% Et_3N) for about 15 min. The diastereomeric mixture was transferred to the column with the initial solvent mixture and was then purified several times by column chromatography until both diastereomers were purely

separated (toluene/EtOAc 50:1 → 40:1 → 35:1 → 30:1 → 20:1, plus 0.1% Et_3N) (Ø = 2.5 cm, H = 40 cm). Λ-(*S*,*S*)-**80** (30.4 mg, 29.4 µmol, 28%) and Δ-(*S*,*S*)-**80** (34.0 mg, 32.9 µmol, 31%) were obtained as yellow solids. Analytical data of Δ-(*S*,*S*)-**80** were consistent with the spectroscopic data obtained by the previously described procedure.

Analytical data of Λ-(*S*,*S*)-**80**:

^{1}H NMR: 300 MHz, CD_2Cl_2; δ = 7.43-7.41 (m, 2H), 7.25-7.16 (m, 5H), 7.05-7.03 (m, 2H), 6.93-6.90 (m, 1H), 6.83-6.78 (m, 2H), 6.74-6.66 (m, 5H), 6.58-6.39 (m, 6H), 6.34-6.32 (m, 2H), 5.90 (brs, 1H), 5.71 (d, *J* = 7.3 Hz, 1H), 5.61-5.59 (m, 2H), 4.95 (dd, *J* = 9.2, 8.3 Hz, 1H), 4.72 (t, *J* = 9.2 Hz, 1H), 3.93 (dd, *J* = 8.2, 8.2 Hz, 1H), 3.77 (dd, *J* = 8.9, 3.9 Hz, 1H), 3.54 (s, 3H), 3.34 (t, *J* = 8.5 Hz, 1H), 3.22 (dd, *J* = 7.8, 3.9 Hz, 1H), 2.48 (s, 3H), 2.27 (s, 3H), 2.11 (s, 3H), 1.43 (s, 9H) ppm.

^{13}C NMR: 126 MHz, CD_2Cl_2; δ = 170.0 (d, $J_{C,Rh}$ = 30.7 Hz, 1C), 169.7, 167.0, 165.1 (d, $J_{C,Rh}$ = 29.4 Hz, 1C), 161.4 (d, $J_{C,Rh}$ = 1.6 Hz, 1C), 158.9 (d, $J_{C,Rh}$ = 3.7 Hz, 1C), 147.8, 147.7, 144.1, 143.0, 140.7, 140.5, 139.4, 139.3, 136.2, 135.7, 134.8, 134.6, 134.0, 131.8, 130.2, 130.2, 129.7, 129.3, 129.1, 128.8 (2C), 128.2 (2C), 128.0 (2C), 127.7, 127.2 (2C), 127.1, 127.0, 126.6, 126.1, 125.6, 124.5, 124.2, 122.8, 122.2, 122.1, 121.4, 121.2, 113.1, 109.1, 102.8, 76.0, 74.7, 72.7, 70.9, 49.1, 35.5, 32.2 (3C), 32.1, 21.2, 20.3, 20.0 ppm.

IR: neat, $\tilde{\nu}$ = 3029 (w), 2956 (w), 2911 (w), 2190 (m), 1625 (s), 1585 (w), 1541 (s), 1510 (w), 1478 (m), 1451 (w), 1419 (m), 1360 (w), 1328 (w), 1280 (w), 1258 (w), 1232 (w), 1199 (w), 1158 (w), 1114 (w), 1064 (s), 1043 (w), 1022 (w), 980 (w), 958 (w), 937 (w), 858 (w), 800 (w), 754 (m), 726 (m), 695 (s), 649 (w), 610 (w), 594 (w), 555 (m), 528 (w), 458 (w) cm^{-1}.

HRMS: APCI; m/z calcd. for $C_{62}H_{57}N_7O_2Rh$ $[M+H]^+$: 1034.3623, found: 1034.3658.

CD: CH_2Cl_2; λ, nm (Δε, $M^{-1}cm^{-1}$) 362 (–8), 326 (+42), 316 (+36), 278 (–19), 253 (+24), 224 (–4), 213 (+7).

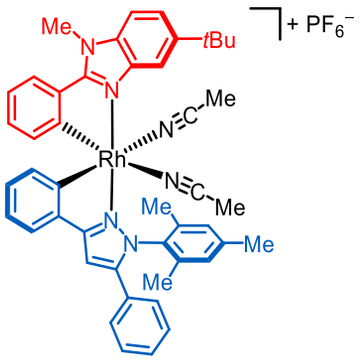

Synthesis of Λ-RhNP2

A solution of Λ-(*S*,*S*)-**79** (48.9 mg, 0.05 mmol, 1.00 equiv.) in MeCN (1.20 mL) was cooled to 0 °C and methanesulfonic acid (15.7 µL, 0.24 mmol, 5.00 equiv.) was added in one portion, followed by trifluoroacetic acid (37.3 µL, 0.50 mmol, 10.0 equiv.) 5 min later. After 15 min, the ice bath was removed and the solution was stirred for 4.5 h at room temperature. The solvent was removed under reduced pressure (water bath of rotary evaporator set to 30 °C, 250–20 mbar for a maximum of 10 min) and NH_4PF_6 (119 mg, 0.73 mmol, 15.0 equiv.) was added to the residual orange oil, followed by MeCN (2.40 mL). The resulting suspension was stirred for 30 min at room temperature before the solvent was removed under reduced pressure (30 °C, 250–20 mbar). Purification by column chromatography (CH_2Cl_2/MeCN 40:1 → 20:1) (Ø = 2 cm, H = 20 cm) provided Λ-**RhNP2** (43.0 mg, 0.05 mmol, 95%) as a pale yellow solid. Enantiomeric excess was established by HPLC analysis on a chiral stationary phase: ee = >99%, HPLC conditions: Daicel Chiralpak® IB-N5 column, 250 x 4.6 mm, absorbance at 254 nm, H_2O + 0.1% TFA/MeCN = 30:70, isocratic flow, flow rate 0.6 mL/min, 25 °C, t_r (Δ-**RhNP2**) = 14.9 min, t_r (Λ-**RhNP2**) = 28.6 min).

CD: MeOH; λ, nm (Δε, $M^{-1}cm^{-1}$) 367 (–11), 330 (+31), 286 (–32), 253 (+28), 242 (+27), 230 (+16), 225 (+22), 205 (–7).

All other spectroscopic data were in agreement with *rac*-**RhNP2**.

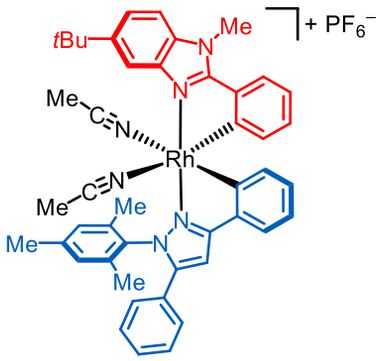

Synthesis of Δ-RhNP2

A solution of Δ-(*S*,*S*)-**80** (45.1 mg, 43.6 µmol, 1.00 equiv.) in MeCN (1.20 mL) was cooled to 0 °C and methanesulfonic acid (28.3 µL, 0.44 mmol, 10.0 equiv.) was added in one portion, followed by trifluoroacetic acid (67.2 µL, 0.87 mmol, 20.0 equiv.) 5 min later. After 15 min, the ice bath was removed and the solution was stirred for 17 h at room temperature. The solvent was removed under reduced pressure (water bath of rotary evaporator set to 30 °C, 250–20 mbar for a maximum of 10 min) and NH_4PF_6 (107 mg, 0.65 mmol, 15.0 equiv.) was added to the residual orange oil, followed by MeCN (2.40 mL). The resulting suspension was stirred for 30 min at room temperature before the solvent was removed under reduced pressure (30 °C, 250–20 mbar). Purification by column chromatography (CH_2Cl_2/MeCN 40:1 → 20:1) (Ø = 2 cm, H = 20 cm) provided Δ-**RhNP2** (39.0 mg, 41.9 µmol, 96%) as a pale yellow solid. Enantiomeric excess was established by HPLC analysis on a chiral stationary phase: ee = >99%, HPLC conditions: Daicel Chiralpak® IB-N5 column, 250 x 4.6 mm, absorbance at 254 nm, H_2O + 0.1% TFA/MeCN = 30:70, isocratic flow, flow rate 0.6 mL/min, 25 °C, t_r (Δ-**RhNP2**) = 15.3 min, t_r (Λ-**RhNP2**) = 28.7 min).

CD: MeOH; λ, nm (Δε, $M^{-1}cm^{-1}$) 367 (+12), 330 (–36), 286 (+38), 253 (–24), 242 (–21), 230 (–9), 225 (–12), 205 (+8).

All other spectroscopic data were in agreement with *rac*-**RhNP2**.

5.7 Enantioselective α-Fluorination and α-Chlorination of *N*-Acyl Pyrazoles

5.7.1 Catalyst Synthesis

RhNP2 was synthesized as described in Section 5.6.3. **RhO**[77] and **RhS**[100] were prepared according to previously published procedures by the Meggers group.

5.7.2 Synthesis and Structure Determination of Rh-Substrate Complexes 95

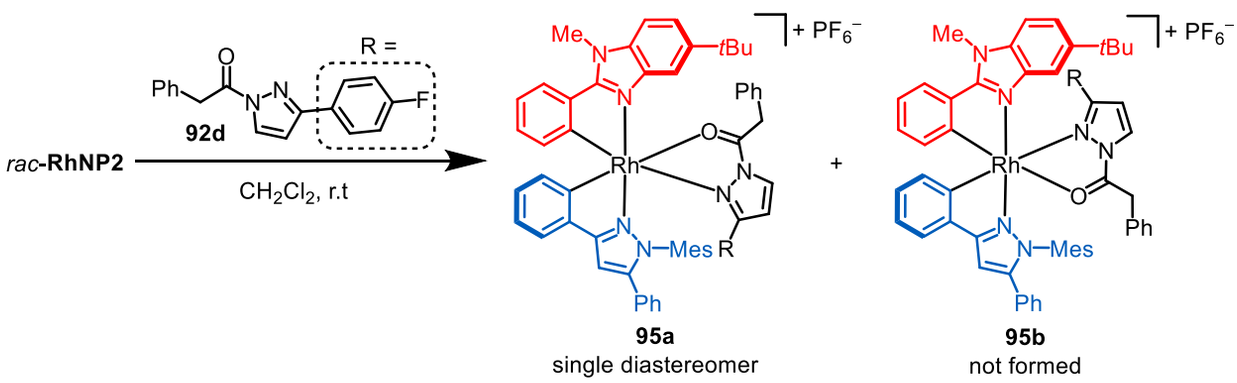

Synthesis of Rhodium-Substrate Complex 95a

Rac-**RhNP2** (15.0 mg, 16.1 µmol, 1.00 equiv.) and substrate **92d** (4.50 mg, 16.1 µmol, 1.00 equiv.) were dissolved in CH_2Cl_2 (0.22 mL) and the resulting yellow solution was stirred for 30 min at room temperature, before the solvent was removed in vacuo. CH_2Cl_2 (0.22 mL) was added and the resulting pale yellow suspension was stirred for another 10 min at room temperature, before the solvent was removed again. The last step was repeated three times to ensure complete removal of the released acetonitrile ligands. The crude material obtained after the fifth cycle, was washed with Et_2O (4 x 1 mL) and dried to give (racemic) rhodium-substrate complex **95a** (17.2 mg, 15.2 µmol, 95%) as a pale yellow solid and as a single diastereomer. For precise assignments of ^{1}H NMR signals, see Figure 52.

^{1}H NMR: 600 MHz, CD_2Cl_2; δ = 8.35 (d, J = 3.2 Hz, 1H), 7.87 (d, J = 7.9, 1.2 Hz, 1H), 7.53-7.50 (m, 2H), 7.44-7.42 (m, 2H), 7.37-7.33 (m, 2H), 7.32-7.29 (m, 2H), 7.26-7.24 (m, 2H), 7.19-7.16 (m, 1H), 7.04-6.97 (m, 5H), 6.94 (t, J = 7.5 Hz, 1H), 6.76 (brs, 1H), 6.70-6.67 (m, 3H), 6.64-6.60 (m, 3H), 6.46 (d, J = 7.9 Hz, 2H), 6.19 (d, J = 7.9 Hz, 1H), 6.12 (d, J = 1.4 Hz, 1H), 4.26 (s, 3H), 3.79 (d, J = 14.5 Hz, 1H),

3.56 (d, J = 14.4 Hz, 1H), 2.39 (s, 3H), 2.34 (s, 3H), 1.07 (s, 3H), 0.83 (s, 9H) ppm.

^{13}C NMR: 151 MHz, CD_2Cl_2; δ = 173.0, 165.3 (d, $J_{C,F}$ = 250.9 Hz, 1C), 161.8, 161.6 (d, $J_{C,Rh}$ = 34.0 Hz, 1C), 160.1 (d, $J_{C,Rh}$ = 2.2 Hz, 1C), 158.4 (d, $J_{C,Rh}$ = 3.5 Hz, 1C), 158.1 (d, $J_{C,Rh}$ = 35.4 Hz, 1C), 150.7, 148.7, 141.8, 139.1, 138.9, 137.7, 137.2, 136.4, 136.0, 135.2, 134.4, 133.8, 133.5, 130.8 (d, $J_{C,F}$ = 8.8 Hz, 2C), 130.6, 130.1, 130.0, 129.7, 129.6, 129.3 (2C), 129.3 (2C), 128.6, 128.4, 128.3, 127.9 (2C), 127.8 (2C), 125.1, 124.4, 124.4, 123.8 (d, $J_{C,F}$ = 3.3 Hz, 1C), 123.6, 122.7, 115.7 (d, $J_{C,F}$ = 22.1 Hz, 2C), 114.6, 110.6, 110.3, 102.0, 41.0, 35.0, 32.8, 31.6 (3C), 21.2, 20.2, 16.7 ppm.

^{19}F NMR: 282 MHz, CD_2Cl_2; δ = –72.7 (d, J_{P-F} = 711 Hz, 6F), –109.6 (s, 1F) ppm.

IR: neat, $\tilde{\nu}$ = 2962 (w), 1674 (w), 1602 (w), 1585 (w), 1551 (w), 1512 (m), 1481 (w), 1452 (w), 1423 (w), 1402 (w), 1361 (w), 1310 (w), 1290 (w), 1263 (w), 1233 (w), 1159 (w), 1109 (w), 1026 (w), 956 (w), 927 (w), 874 (w), 839 (s), 815 (w), 761 (w), 734 (w), 717 (m), 695 (w), 660 (w), 611 (w), 556 (m), 532 (w), 496 (w) cm^{-1}.

HRMS APCI; m/z calcd. for $C_{59}H_{53}FN_6ORh$ $[M]^+$: 983.3314, found: 983.3302.

Structure Determination by NMR Spectroscopy

The formation of rhodium-substrate complex **95a** should be verified in solution by ^{1}H–^{1}H 2D NOESY. Corresponding NMR measurements and the subsequent structure determination were again performed by Dr. Xiulan Xie.

Sample Preparation and Experimental Setup

About 17 mg of substance were dissolved in CD_2Cl_2 (0.60 mL) and the resulting solution was degassed and filled in an NMR tube under inert gas (nitrogen). NMR measurements were performed on a Bruker AVII 600 MHz spectrometer equipped with a 5 mm TXI probe with z-gradient. The NOESY spectrum was recorded with mixing times of 1.5 s.

Results and Discussion

The proposed structure is shown in Figure 51. The three bidentate ligands are referred to as L1, L2 and L3. A complete assignment of the ^{1}H signals was performed with the standard experiments ^{1}H, ^{13}C-APT, DQF-COSY, NOESY, HSQC and HMBC. The scalar couplings between F-8 and C-8, C-7/7' and C6/6' of L3 were observed to be 251 Hz, 22.1 Hz and 8.8 Hz, respectively. The scalar couplings between the rhodium metal center and C-8 of L1 and C-6 of L2 were detected to be 34.0 Hz and 35.4 Hz, respectively, and thus resemble the coupling constants $J_{C,Rh}$ previously observed for similar complexes (see Section 5.4.2). These couplings assisted the assignment to the ^{1}H signals, which were further verified by the long-range ^{1}H-^{13}C HMBC correlations. The ^{1}H NMR spectrum labeled with assignments is depicted in Figure 52.

On the basis of the assigned ^{1}H signals, the following interligand long-range NOE interactions were detected: *t*Bu – H-3 (L3), *t*Bu – H4 (L3), H-7 (L1) – H-7 (L2), H-7 (L1) – H-4 (L3), H-7 (L1) – H-6/6' (L3), H-7 (L2) – H-6/6' (L3), H-9 (L1) – $CH_3^{mes\text{-}back}$ (L2), $CH_3^{mes\text{-}front}$ (L2) – H-11 (L3), $CH_3^{mes\text{-}front}$ (L2) – H-4 (L3). This pattern of NOE interactions corresponds unambiguously to the structural arrangement shown in Figure 51.

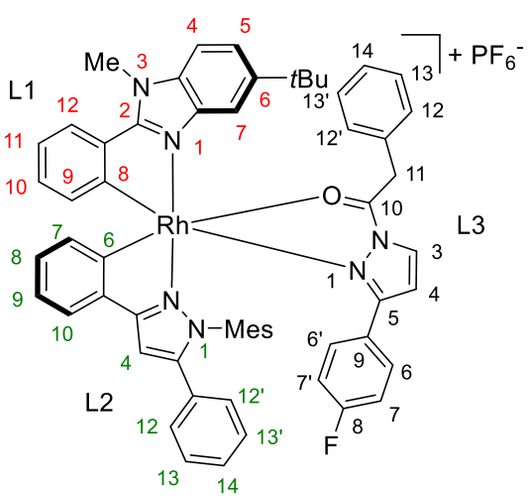

Figure 51: Investigated compound **95a**.

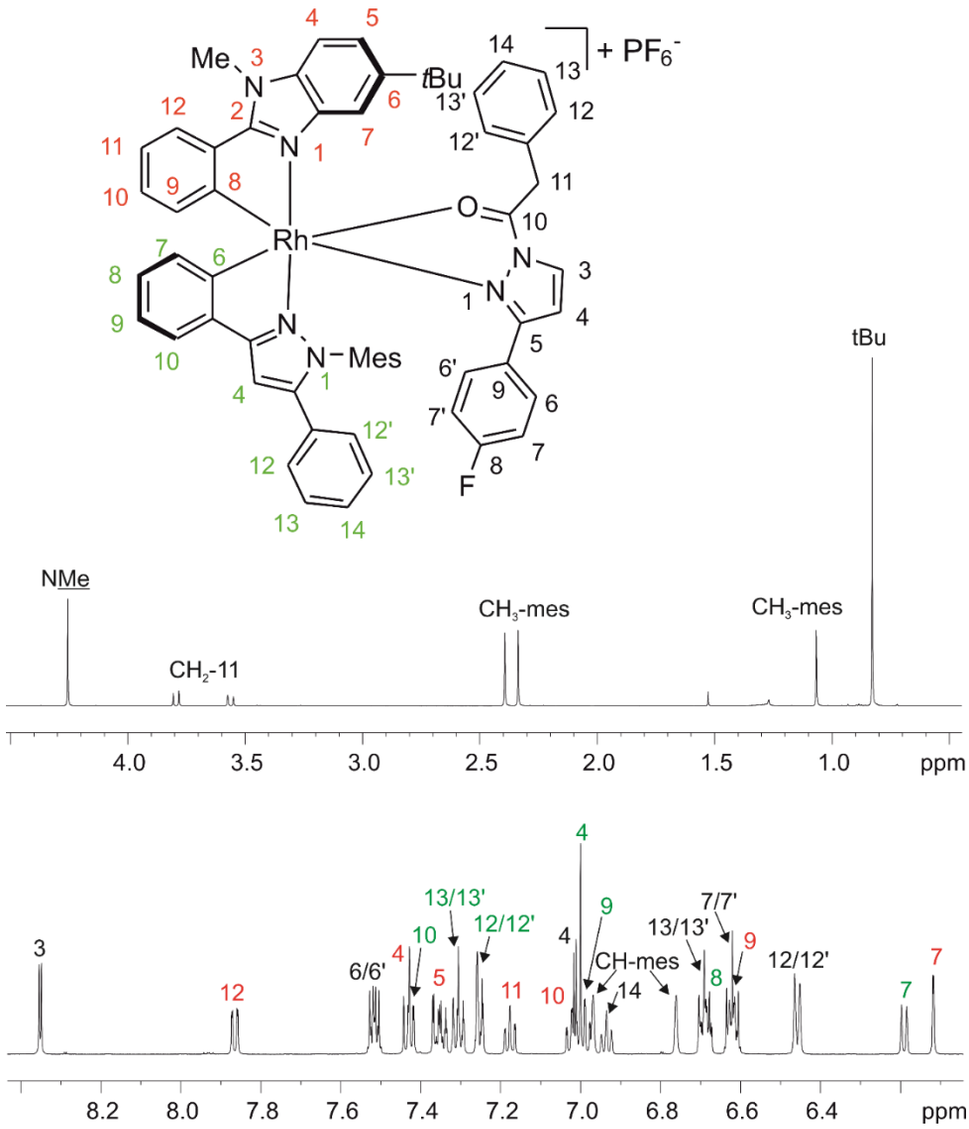

Figure 52: ^{1}H NMR spectrum of the **95a** in CD_2Cl_2 at 300 K.

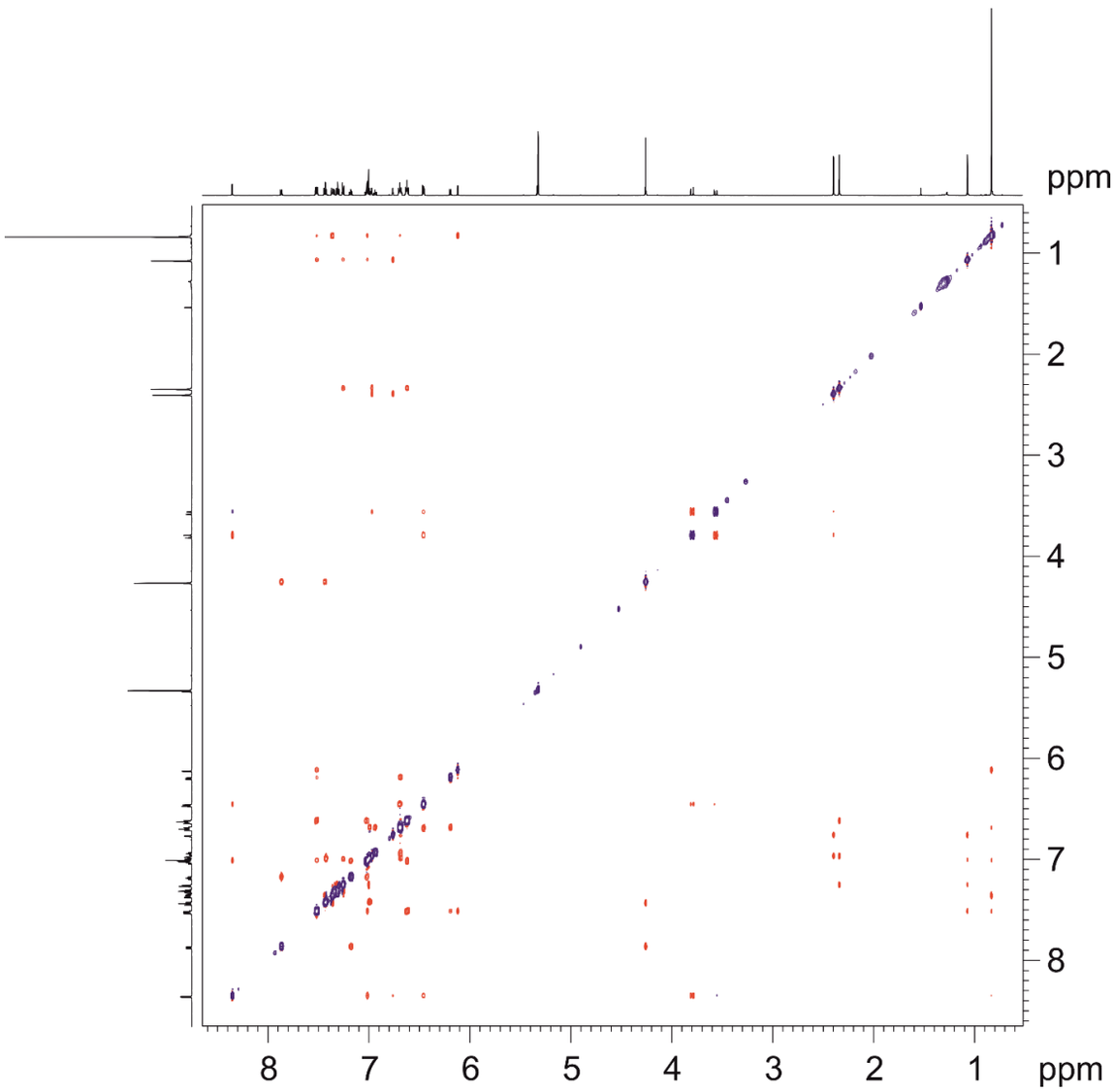

Figure 53: NOESY spectrum of **95a** in CD_2Cl_2 at 300 K (mixing time = 1.5 s).

5.7.3 Experimental Procedures and Characterization Data of Substrates

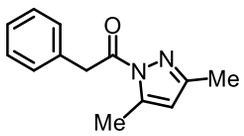

1-(3,5-Dimethyl-1*H*-pyrazol-1-yl)-2-phenylethan-1-one (92a)

Following a slightly modified reported procedure,[200] to a solution of 2-phenylacetyl chloride (500 mg, 3.17 mmol, 1.00 equiv.) in CH_2Cl_2 (10.8 mL) was added 3,5-dimethyl-1*H*-pyrazole (609 mg, 6.34 mmol, 2.00 equiv.) at 0 °C. The resulting reaction mixture was allowed to slowly reach room temperature and stirred for 19 h, then it was quenched by addition of 1 M aqueous HCl. The aqueous phase was extracted with EtOAc (3 x 50 mL) and the combined organic phases were washed with a saturated aqueous solution of $NaHCO_3$ (1 x 50 mL) and brine (1 x 50 mL). The combined organic extracts were dried over Na_2SO_4, filtered and the solvent was removed under reduced pressure. The crude product was adsorbed onto silica gel and then purified by column chromatography (*n*-pentane/EtOAc 30:1 → 20:1) to afford **92a** (624 mg, 2.91 mmol, 92%) as a colorless solid. Analytical data were consistent with reported data.[200]

^{1}H NMR 300 MHz, $CDCl_3$; δ = 7.37-7.27 (m, 5H), 5.98 (s, 1H), 4.44 (s, 2H), 2.52 (d, J = 0.8 Hz, 3H), 2.27 (s, 3H) ppm.

General Procedure J: Synthesis of Monosubstituted Pyrazoles

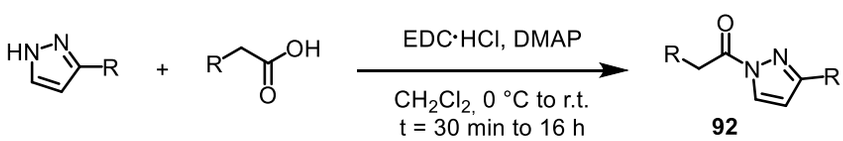

According to a slightly modified procedure from Zhang *et al*.,[213] the corresponding pyrazole (typically 100–500 mg scale reactions, 1.00 equiv.) and the corresponding carboxylic acid derivative (1.10 equiv.) were dissolved in CH_2Cl_2 (0.5 M). At 0 °C, EDC·HCl (1.10 equiv.) and DMAP (0.001 equiv.) were added and the resulting solution was stirred until TLC indicated completion of the reaction. Brine was added and the aqueous phase was extracted three times with CH_2Cl_2. The combined organic layers were dried over Na_2SO_4, filtered and the solvent was removed under reduced pressure. Purification by column chromatography (*n*-pentane/EtOAc 20:1) provided pure *N*-acyl pyrazole substrates **92**.

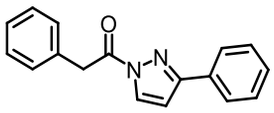

2-Phenyl-1-(3-phenyl-1*H*-pyrazol-1-yl)ethan-1-one (92b)

Following the general procedure J, **92b** was obtained as a colorless solid (98%).

^{1}H NMR: 300 MHz, $CDCl_3$; δ = 8.29 (d, J = 2.9 Hz, 1H), 7.94-7.91 (m, 2H), 7.51-7.40 (m, 5H), 7.38-7.27 (m, 3H), 6.80 (d, J = 2.9 Hz, 1H), 4.54 (s, 2H) ppm.

^{13}C NMR: 75 MHz, $CDCl_3$; δ = 170.2, 155.6, 133.6, 132.0, 130.0 (2C), 129.9, 128.4, 129.0 (2C), 128.8 (2C), 127.4, 126.5 (2C), 107.9, 40.6 ppm.

IR: neat, $\tilde{\nu}$ = 3058 (w), 3034 (w), 1726 (m), 1604 (w), 1540 (w), 1496 (w), 1452 (w), 1404 (m), 1358 (m), 1332 (w), 1304 (w), 1282 (w), 1254 (w), 1228 (m), 1195 (w), 1096 (w), 1075 (w), 1047 (w), 1028 (w), 932 (m), 878 (w), 782 (w), 765 (m), 716 (m), 690 (m), 609 (w), 579 (w), 563 (w), 539 (w), 501 (w), 470 (w), 422 (w) cm^{-1}.

HRMS: ESI; m/z calcd. for $C_{17}H_{14}N_2ONa$ $[M+Na]^+$: 285.0998, found 285.0997.

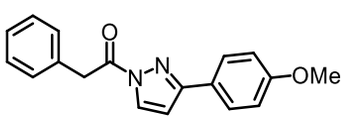

1-(3-(4-Methoxyphenyl)-1*H*-pyrazol-1-yl)-2-phenylethan-1-one (92c)

Following the general procedure J, **92c** was obtained as a colorless solid (>99%).

^{1}H NMR: 300 MHz, $CDCl_3$; δ = 8.26 (d, J = 2.9 Hz, 1H), 7.87-7.83 (m, 2H), 7.45-7.42 (m, 2H), 7.38-7.28 (m, 3H), 7.02-6.97 (m, 2H), 6.73 (d, J = 2.9 Hz, 1H), 4.52 (s, 2H), 3.87 (s, 3H) ppm.

^{13}C NMR: 75 MHz, $CDCl_3$; δ = 170.1, 160.7, 155.4, 133.8, 130.0 (2C), 129.9, 128.8 (2C), 127.8 (2C), 127.4, 124.7, 114.4 (2C), 107.6, 55.5, 40.6 ppm.

IR: neat, $\tilde{\nu}$ = 3058 (w), 3035 (w), 2989 (w), 2942 (w), 2905 (w), 2825 (w), 1724 (s), 1608 (m), 1512 (s), 1403 (s), 1358 (m), 1325 (w), 1287 (m), 1221 (m), 1201 (w), 1175 (w), 1115 (w), 1094 (m), 1049 (w), 1031 (m), 932 (s), 878 (w), 842 (m), 805 (w), 774 (s), 720 (m), 695 (m), 639 (w), 620 (m), 609 (w), 581 (w), 540 (w), 523 (m), 492 (w), 474 (w), 420 (w) cm^{-1}.

HRMS: ESI; m/z calcd. for $C_{18}H_{16}N_2O_2Na$ $[M+Na]^+$: 315.1104, found 315.1105.

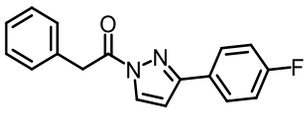

1-(3-(4-Fluorophenyl)-1*H*-pyrazol-1-yl)-2-phenylethan-1-one (92d)

Following the general procedure J, **92d** was obtained as a colorless solid (>99%).

^{1}H NMR: 300 MHz, $CDCl_3$; δ = 8.29 (d, J = 2.8 Hz, 1H), 7.89 (dd, J = 8.5, 5.4 Hz, 2H), 7.43-7.28 (m, 5H), 7.16 (t, J = 8.6 Hz, 2H), 6.75 (d, J = 2.8 Hz, 1H), 4.52 (s, 2H) ppm.

^{13}C NMR: 75 MHz, $CDCl_3$; δ = 170.1, 163.6 (d, $J_{C,F}$ = 248.8 Hz, 1C), 154.7, 133.6, 130.1, 130.0 (2C), 128.8 (2C), 128.3 (d, $J_{C,F}$ = 8.4 Hz, 2C), 128.3, 127.4, 116.0 (d, $J_{C,F}$ = 21.7 Hz, 2C), 107.6, 40.6 ppm.

^{19}F NMR: 282 MHz, $CDCl_3$; δ = –111.9 (s, 1F) ppm.

IR: neat, $\tilde{\nu}$ = 3160 (w), 3066 (w), 3035 (w), 2897 (w), 1725 (m), 1603 (m), 1512 (m), 1454 (w), 1438 (w), 1422 (w), 1401 (m), 1353 (m), 1327 (w), 1280 (w), 1251 (w), 1220 (m), 1196 (w), 1157 (w), 1094 (m), 1049 (m), 1032 (w), 1013 (w), 976 (w), 932 (m), 880 (w), 845 (m), 817 (w), 778 (m), 717 (m), 694 (m), 619 (m), 578 (m), 541 (w), 516 (m), 471 (w), 448 (w) cm^{-1}.

HRMS: ESI; m/z calcd. for $C_{17}H_{13}FN_2ONa$ $[M+Na]^+$: 303.0904, found 303.0903.

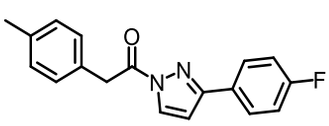

1-(3-(4-Fluorophenyl)-1*H*-pyrazol-1-yl)-2-(*p*-tolyl)ethan-1-one (92e)

Following the general procedure J, **92e** was obtained as a colorless solid (90%).

^{1}H NMR: 300 MHz, $CDCl_3$; δ = 8.28 (d, J = 2.8 Hz, 1H), 7.92-7.88 (m, 2H), 7.32 (d, J = 7.8 Hz, 2H), 7.19-7.13 (m, 4H), 6.74 (d, J = 2.8 Hz, 1H), 4.48 (s, 2H), 2.34 (s, 3H) ppm.

^{13}C NMR: 75 MHz, $CDCl_3$; δ = 170.3, 163.6 (d, $J_{C,F}$ = 248.7 Hz, 1C), 154.6, 137.1, 130.4, 130.1, 129.8 (2C), 129.5 (2C), 128.3 (d, $J_{C,F}$ = 8.3 Hz, 2C), 128.3, 116.0 (d, $J_{C,F}$ = 21.9 Hz, 2C), 107.6, 40.2, 21.2 ppm.

^{19}F NMR: 282 MHz, $CDCl_3$; δ = –111.9 (s, 1F) ppm.

IR: neat; $\tilde{\nu}$ = 1724 (m), 1603 (w), 1511 (m), 1420 (w), 1400 (m), 1352 (w), 1322 (w), 1279 (w), 1252 (w), 1220 (m), 1195 (w), 1156 (w), 1094 (w), 1048 (m), 976 (w),

932 (m), 880 (w), 843 (m), 813 (w), 774 (s), 735 (m), 700 (w), 610 (m), 554 (w), 540 (w), 513 (m), 480 (m), 447 (w) cm^{-1}.

HRMS: ESI; m/z calcd. for $C_{18}H_{15}FN_2ONa$ $[M+Na]^+$: 317.1061, found 317.1061.

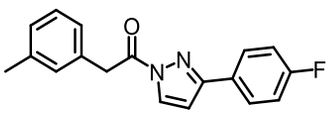

1-(3-(4-Fluorophenyl)-1*H*-pyrazol-1-yl)-2-(*m*-tolyl)ethan-1-one (92f)

Following the general procedure J, **92f** was obtained as a colorless solid (>99%).

^{1}H NMR: 300 MHz, $CDCl_3$; δ = 8.29 (d, J = 2.9 Hz, 1H), 7.94-7.87 (m, 2H), 7.28-7.20 (m, 3H), 7.20-7.10 (m, 3H), 6.75 (d, J = 2.9 Hz, 1H), 4.49 (s, 2H), 2.36 (s, 3H) ppm.

^{13}C NMR: 75 MHz, $CDCl_3$; δ = 170.2, 163.6 (d, $J_{C,F}$ = 248.9 Hz, 1C), 154.7, 138.4, 133.4, 130.7, 130.0, 128.7, 128.3 (d, $J_{C,F}$ = 8.3 Hz, 2C), 128.3 (d, $J_{C,F}$ = 3.5 Hz, 1C), 128.2, 127.0, 116.0 (d, $J_{C,F}$ = 21.7 Hz, 2C), 107.6, 40.5, 21.5 ppm.

^{19}F NMR: 282 MHz, $CDCl_3$; δ = –111.9 (s, 1F) ppm.

IR: neat, $\tilde{\nu}$ = 3158 (w), 3031 (w), 2961 (w), 2915 (w), 1728 (s), 1603 (m), 1511 (s), 1438 (w), 1421 (w), 1402 (s), 1353 (m), 1322 (m), 1296 (w), 1280 (w), 1256 (w), 1216 (s), 1158 (m), 1093 (m), 1048 (m), 936 (m), 876 (w), 843 (s), 815 (w), 774 (w), 759 (s), 732 (w), 692 (m), 619 (m), 587 (m), 543 (w), 517 (w), 434 (w) cm^{-1}.

HRMS: ESI; m/z calcd. for $C_{18}H_{15}FN_2ONa$ $[M+Na]^+$: 317.1061, found 317.1060.

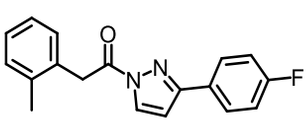

1-(3-(4-Fluorophenyl)-1*H*-pyrazol-1-yl)-2-(*o*-tolyl)ethan-1-one (92g)

Following the general procedure J, **92g** was obtained as a colorless solid (92%).

^{1}H NMR: 300 MHz, $CDCl_3$; δ = 8.31 (d, J = 2.9 Hz, 1H), 7.94-7.87 (m, 2H), 7.34-7.30 (m, 1H), 7.24-7.13 (m, 5H), 6.76 (d, J = 2.9 Hz, 1H), 4.56 (s, 2H), 2.40 (s, 3H) ppm.

^{13}C NMR: 75 MHz, $CDCl_3$; δ = 169.9, 163.6 (d, $J_{C,F}$ = 248.8 Hz, 1C), 154.7, 137.4, 132.3, 130.7, 130.6, 130.1, 128.3 (d, $J_{C,F}$ = 8.3 Hz, 2C), 128.3, 127.7, 126.3, 116.0 (d, $J_{C,F}$ = 21.7 Hz, 2C), 107.6, 38.4, 19.9 ppm.

^{19}F NMR: 282 MHz, $CDCl_3$; δ = –111.9 (s, 1F) ppm.

IR: neat, $\tilde{\nu}$ = 3134 (w), 3048 (w), 2953 (w), 2922 (w), 1731 (s), 1604 (w), 1511 (m), 1460 (w), 1436 (w), 1400 (s), 1350 (m), 1323 (m), 1287 (w), 1264 (w), 1233 (w), 1216 (s), 1154 (w), 1092 (m), 1045 (m), 940 (s), 918 (w), 888 (w), 839 (m), 807 (w), 776 (s), 741 (s), 705 (w), 686 (w), 638 (w), 620 (w), 601 (m), 544 (w), 515 (m), 444 (w) cm^{-1}.

HRMS: ESI; m/z calcd. for $C_{18}H_{15}FN_2ONa$ $[M+Na]^+$: 317.1061, found 317.1058.

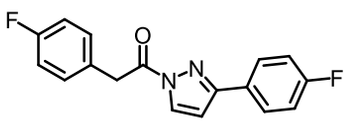

2-(4-Fluorophenyl)-1-(3-(4-fluorophenyl)-1*H*-pyrazol-1-yl)ethan-1-one (92h)

Following the general procedure J, **92h** was obtained as a colorless solid (96%).

^{1}H NMR: 300 MHz, $CDCl_3$; δ = 8.28 (d, J = 2.9 Hz, 1H), 7.92-7.86 (m, 2H), 7.41-7.36 (m, 2H), 7.20-7.12 (m, 2H), 7.07-7.00 (m, 2H), 6.75 (d, J = 2.9 Hz, 1H), 4.49 (s, 2H) ppm.

^{13}C NMR: 75 MHz, $CDCl_3$; δ = 169.9, 163.6 (d, $J_{C,F}$ = 248.9 Hz, 1C), 162.3 (d, $J_{C,F}$ = 245.9 Hz, 1C), 154.8, 131.5 (d, $J_{C,F}$ = 8.1 Hz, 2C), 130.1, 129.2 (d, $J_{C,F}$ = 3.3 Hz, 1C), 128.3 (d, $J_{C,F}$ = 8.3 Hz, 2C), 128.2 (d, $J_{C,F}$ = 3.3 Hz, 1C), 116.0 (d, $J_{C,F}$ = 21.9 Hz, 2C), 115.7 (d, $J_{C,F}$ = 21.5 Hz, 2C), 107.8, 39.8 ppm.

^{19}F NMR: 282 MHz, $CDCl_3$; δ = –111.7 (s, 1F), –115.3 (s, 1F) ppm.

IR: neat, $\tilde{\nu}$ = 2922 (w), 2853 (w), 1897 (w), 1728 (m), 1600 (m), 1507 (m), 1422 (w), 1396 (m), 1349 (w), 1320 (m), 1282 (w), 1259 (w), 1215 (m), 1194 (w), 1157 (m), 1090 (m), 1045 (m), 1013 (w), 931 (m), 861 (w), 843 (m), 824 (w), 790 (w), 772 (m), 746 (w), 694 (w), 637 (w), 609 (m), 544 (w), 518 (m), 489 (m), 416 (w) cm^{-1}.

HRMS: ESI; m/z calcd. for $C_{17}H_{12}F_2N_2ONa$ $[M+Na]^+$: 321.0810, found 321.0814.

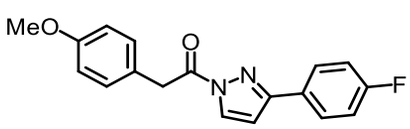

1-(3-(4-Fluorophenyl)-1*H*-pyrazol-1-yl)-2-(4-methoxyphenyl)ethan-1-one (92i)

Following the general procedure J, **92i** was obtained as a colorless solid (>99%).

^{1}H NMR: 300 MHz, $CDCl_3$; δ = 8.28 (d, J = 2.9 Hz, 1H), 7.93-7.86 (m, 2H), 7.36-7.33 (m, 2H), 7.20-7.12 (m, 2H), 6.91-6.86 (m, 2H), 6.74 (d, J = 2.9 Hz, 1H), 4.45 (s, 2H), 3.79 (s, 3H) ppm.

^{13}C NMR: 75 MHz, $CDCl_3$; δ = 170.4, 163.6 (d, $J_{C,F}$ = 248.8 Hz, 1C), 159.0, 154.6, 131.0 (2C), 130.1, 128.3 (d, $J_{C,F}$ = 8.3 Hz, 2C), 128.3, 125.5, 116.0 (d, $J_{C,F}$ = 21.7 Hz, 2C), 114.3 (2C), 107.6, 55.4, 39.8 ppm.

^{19}F NMR: 282 MHz, $CDCl_3$; δ = –111.9 (s, 1F) ppm.

IR: neat, $\tilde{\nu}$ = 3157 (w), 3018 (w), 2963 (w), 2930 (w), 2837 (w), 1724 (m), 1605 (m), 1511 (m), 1461 (w), 1439 (w), 1422 (w), 1400 (m), 1352 (w), 1322 (w), 1297 (w), 1280 (w), 1252 (w), 1219 (s), 1199 (w), 1175 (w), 1158 (w), 1094 (w), 1048 (w), 1032 (m), 932 (m), 880 (w), 846 (m), 815 (w), 777 (s), 734 (w), 702 (w), 611 (m), 555 (w), 541 (m), 515 (w), 454 (w) cm^{-1}.

HRMS: ESI; m/z calcd. for $C_{18}H_{15}FN_2O_2Na$ $[M+Na]^+$: 333.1010, found 333.1013.

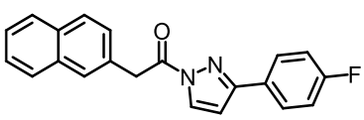

1-(3-(4-Fluorophenyl)-1*H*-pyrazol-1-yl)-2-(naphthalen-2-yl)ethan-1-one (92j)

Following the general procedure J, **92j** was obtained as a colorless solid (94%).

^{1}H NMR: 300 MHz, $CDCl_3$; δ = 8.30 (d, J = 2.9 Hz, 1H), 7.95-7.89 (m, 3H), 7.86-7.81 (m, 3H), 7.56 (dd, J = 8.5, 1.7 Hz, 1H), 7.51-7.43 (m, 2H), 7.22-7.14 (m, 2H), 6.75 (d, J = 2.9 Hz, 1H), 4.69 (s, 2H) ppm.

^{13}C NMR: 75 MHz, $CDCl_3$; δ = 170.1, 163.6 (d, $J_{C,F}$ = 248.9 Hz, 1C), 154.8, 133.6, 132.7, 131.1, 130.1, 128.8, 128.4, 128.3 (d, $J_{C,F}$ = 8.3 Hz, 2C), 128.2, 127.9, 127.9, 127.8, 126.3, 126.1, 116.0 (d, $J_{C,F}$ = 21.9 Hz, 2C), 107.7, 40.8 ppm.

^{19}F NMR: 282 MHz, $CDCl_3$; δ = –111.8 (s, 1F) ppm.

IR: neat, $\tilde{\nu}$ = 2908 (w), 2853 (w), 1740 (s), 1666 (w), 1639 (w), 1601 (w), 1508 (m), 1438 (w), 1395 (s), 1346 (m), 1328 (w), 1286 (w), 1264 (w), 1213 (s), 1160 (w), 1127 (w), 1106 (w), 1086 (m), 1043 (m), 961 (w), 941 (m), 898 (w), 875 (w), 843 (m), 799 (m), 765 (s), 747 (w), 719 (m), 686 (w), 614 (m), 537 (w), 519 (m), 497 (w), 478 (m), 447 (w) cm^{-1}.

HRMS: ESI; m/z calcd. for $C_{21}H_{15}FN_2ONa$ $[M+Na]^+$: 353.1061, found 353.1062.

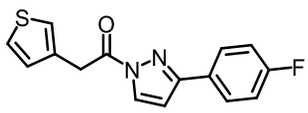

1-(3-(4-Fluorophenyl)-1*H*-pyrazol-1-yl)-2-(thiophen-3-yl)ethan-1-one (92k)

Following the general procedure J, **92k** was obtained as a colorless solid (86%).

^{1}H NMR: 300 MHz, $CDCl_3$; δ = 8.29 (d, J = 2.9 Hz, 1H), 7.92-7.87 (m, 2H), 7.33-7.30 (m, 2H), 7.19-7.13 (m, 3H), 6.75 (d, J = 2.9 Hz, 1H), 4.56 (s, 2H) ppm.

^{13}C NMR: 75 MHz, $CDCl_3$; δ = 169.5, 163.6 (d, $J_{C,F}$ = 248.9 Hz, 1C), 154.8, 132.9, 130.1, 128.9, 128.3 (d, $J_{C,F}$ = 8.3 Hz, 2C), 128.2, 125.9, 123.9, 116.0 (d, $J_{C,F}$ = 21.9 Hz, 2C), 107.7, 35.3 ppm.

^{19}F NMR: 282 MHz, $CDCl_3$; δ = –111.8 (s, 1F) ppm.

IR: neat, $\tilde{\nu}$ = 3103 (w), 1725 (m), 1602 (w), 1511 (m), 1421 (w), 1403 (m), 1350 (m), 1315 (w), 1281 (w), 1254 (w), 1216 (m), 1157 (w), 1092 (m), 1045 (m), 1014 (w), 949 (w), 932 (m), 844 (m), 819 (w), 769 (m), 691 (w), 675 (w), 616 (m), 585 (w), 549 (w), 517 (w), 446 (w) cm^{-1}.

HRMS: ESI; m/z calcd. for $C_{15}H_{11}FN_2OSNa$ $[M+Na]^+$: 309.0468, found 309.0469.

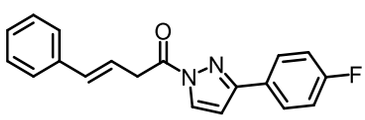

(*E*)-1-(3-(4-Fluorophenyl)-1*H*-pyrazol-1-yl)-4-phenylbut-3-en-1-one (92m)

Following the general procedure J, **92m** was obtained as a colorless solid (90%).

^{1}H NMR: 300 MHz, $CDCl_3$; δ = 8.31 (d, J = 2.9 Hz, 1H), 7.91-7.87 (m, 2H), 7.42-7.40 (m, 2H), 7.34-7.29 (m, 2H), 7.25-7.21 (m, 1H), 7.18-7.13 (m, 2H), 6.75 (d, J = 2.9 Hz, 1H), 6.66 (d, J = 16.0 Hz, 1H), 6.48 (dt, J = 15.9, 6.9 Hz, 1H), 4.14 (dd, J = 6.9, 1.0 Hz, 2H) ppm.

^{13}C NMR: 75 MHz, $CDCl_3$; δ = 170.2, 163.6 (d, $J_{C,F}$ = 248.9 Hz, 1C), 154.8, 136.9, 134.6, 129.9, 128.7 (2C), 128.3 (d, $J_{C,F}$ = 8.3 Hz, 2C), 128.2, 127.8, 126.5 (2C), 121.1, 116.0 (d, $J_{C,F}$ = 21.8 Hz, 2C), 107.6, 38.2 ppm.

^{19}F NMR: 282 MHz, $CDCl_3$; δ = –111.9 (s, 1F) ppm.

IR: neat, $\tilde{\nu}$ = 1721 (s), 1602 (w), 1510 (m), 1430 (w), 1405 (m), 1392 (w), 1363 (w), 1340 (w), 1320 (m), 1282 (w), 1253 (w), 1219 (s), 1150 (w), 1097 (w), 1045 (m),

1012 (w), 972 (m), 935 (m), 840 (s), 811 (w), 771 (s), 728 (m), 686 (m), 633 (w), 613 (w), 551 (w), 519 (m), 499 (w), 462 (w) cm^{-1}.

HRMS: ESI; m/z calcd. for $C_{19}H_{15}FN_2ONa$ $[M+Na]^+$: 329.1061, found 329.1064.

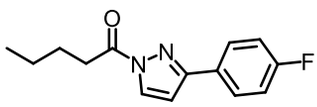

1-(3-(4-Fluorophenyl)-1*H*-pyrazol-1-yl)pentan-1-one (92n)

Following the general procedure J with some slight modifications, **92n** was obtained as a colorless solid (>99%) using 1.30 equiv. EDC·HCl and 1.30 equiv. pentanoic acid.

^{1}H NMR: 300 MHz, $CDCl_3$; δ = 8.28 (d, J = 2.9 Hz, 1H), 7.89-7.82 (m, 2H), 7.17-7.09 (m, 2H), 6.71 (d, J = 2.9 Hz, 1H), 3.19 (t, J = 7.5 Hz, 2H), 1.85-1.75 (m, 2H), 1.53-1.41 (m, 2H), 0.99 (t, J = 7.3 Hz, 3H) ppm.

^{13}C NMR: 75 MHz, $CDCl_3$; δ = 172.5, 163.5 (d, $J_{C,F}$ = 248.6 Hz, 1C), 154.4, 129.6, 128.3 (d, $J_{C,F}$ = 3.3 Hz, 1C), 128.2 (d, $J_{C,F}$ = 8.3 Hz, 2C), 115.9 (d, $J_{C,F}$ = 21.8 Hz, 2C), 107.1, 33.7, 26.7, 22.4, 13.9 ppm.

^{19}F NMR: 282 MHz, $CDCl_3$; δ = –112.2 (s, 1F) ppm.

IR: neat, $\tilde{\nu}$ = 3063 (w), 2959 (w), 2931 (w), 2869 (w), 1724 (m), 1603 (m), 1509 (m), 1466 (w), 1434 (w), 1398 (m), 1345 (w), 1325 (m), 1285 (w), 1267 (w), 1245 (w), 1214 (m), 1157 (m), 1118 (w), 1084 (m), 1042 (m), 1016 (w), 936 (m), 876 (w), 846 (m), 813 (w), 766 (m), 733 (w), 688 (w), 621 (m), 559 (w), 541 (w), 520 (m), 470 (w) cm^{-1}.

HRMS: ESI; m/z calcd. for $C_{14}H_{15}FN_2ONa$ $[M+Na]^+$: 269.1061, found 269.1058.

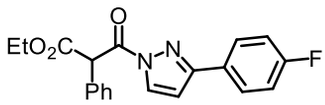

Ethyl 3-(3-(4-Fluorophenyl)-1*H*-pyrazol-1-yl)-3-oxo-2-phenylpropanoate (92o)

Following the general procedure J, **92o** was obtained as a colorless solid (91%) by converting 3-ethoxy-3-oxo-2-phenylpropanoic acid[214] with 3-(4-fluorophenyl)-1*H*-pyrazole.

^{1}H NMR: 300 MHz, $CDCl_3$; δ = 8.28 (d, J = 2.9 Hz, 1H), 7.89-7.84 (m, 2H), 7.53-7.50 (m, 2H), 7.43-7.33 (m, 3H), 7.15 (t, J = 8.7 Hz, 2H), 6.76 (d, J = 2.9 Hz, 1H), 5.97 (s, 1H), 4.31-4.14 (m, 2H), 1.22 (t, J = 7.1 Hz, 3H) ppm.

^{13}C NMR: 75 MHz, $CDCl_3$;δ = 168.1, 166.3, 163.7 (d, $J_{C,F}$ = 249.2 Hz, 1C), 154.8, 132.2, 130.3, 130.0 (2C), 128.9 (2C), 128.6, 128.3 (d, $J_{C,F}$ = 8.4 Hz, 2C), 127.9 (d, $J_{C,F}$ = 3.3 Hz, 1C), 116.0 (d, $J_{C,F}$ = 21.9 Hz, 2C), 108.0, 62.1, 56.7, 14.1 ppm.

^{19}F NMR: 282 MHz, $CDCl_3$;δ = –111.6 (s, 1F) ppm.

IR: neat, $\tilde{\nu}$ = 3153 (w), 2985 (w), 2924 (w), 2900 (w), 1722 (m), 1604 (w), 1550 (w), 1513 (m), 1489 (w), 1453 (w), 1430 (m), 1402 (m), 1351 (m), 1300 (m), 1266 (w), 1228 (m), 1191 (m), 1148 (m), 1117 (w), 1091 (m), 1042 (w), 1023 (m), 978 (w), 945 (m), 887 (w), 842 (m), 829 (w), 768 (m), 738 (m), 702 (m), 685 (w), 641 (w), 625 (m), 608 (w), 576 (m), 546 (w), 517 (m), 501 (w), 451 (w), 419 (w) cm^{-1}.

HRMS: ESI; m/z calcd. for $C_{20}H_{17}FN_2O_3Na$ $[M+Na]^+$: 375.1115, found 375.1115.

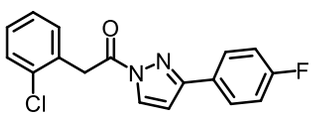

2-(2-Chlorophenyl)-1-(3-(4-fluorophenyl)-1*H*-pyrazol-1-yl)ethan-1-one (92p)

Following the general procedure J, **92p** was obtained as a colorless solid (94%).

^{1}H NMR: 300 MHz, $CDCl_3$; δ = 8.32 (d, J = 2.8 Hz, 1H), 7.90 (dd, J = 8.4, 5.5 Hz, 2H), 7.46-7.42 (m, 1H), 7.38-7.35 (m, 1H), 7.30-7.28 (m, 2H), 7.15 (t, J = 8.6 Hz, 2H), 6.77 (d, J = 2.8 Hz, 1H), 4.70 (s, 2H) ppm.

^{13}C NMR: 75 MHz, $CDCl_3$;δ = 169.0, 163.6 (d, $J_{C,F}$ = 248.8 Hz, 1C), 154.8, 135.0, 132.0, 131.9, 130.1, 129.8, 129.1, 128.3 (d, $J_{C,F}$ = 8.4 Hz, 2C), 128.2 (d, $J_{C,F}$ = 3.3 Hz, 1C), 127.1, 116.0 (d, $J_{C,F}$ = 21.8 Hz, 2C), 107.6, 38.9 ppm.

^{19}F NMR: 282 MHz, $CDCl_3$;δ = –111.9 (s, 1F) ppm.

IR: neat, $\tilde{\nu}$ = 2927 (w), 1718 (s), 1604 (w), 1574 (w), 1509 (m), 1474 (w), 1403 (s), 1356 (m), 1323 (w), 1283 (w), 1253 (w), 1215 (m), 1152 (m), 1089 (m), 1049 (m), 933 (m), 841 (m), 810 (w), 774 (m), 748 (s), 699 (w), 683 (w), 621 (m), 593 (w), 543 (w), 520 (w), 441 (w) cm^{-1}.

HRMS: ESI; m/z calcd. for $C_{17}H_{12}ClFN_2ONa$ $[M+Na]^+$: 337.0514, found 337.0519.

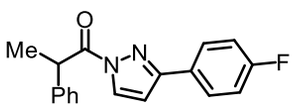

1-(3-(4-Fluorophenyl)-1*H*-pyrazol-1-yl)-2-phenylpropan-1-one (92q)

Following the general procedure J, **92q** was obtained as a colorless solid (99%) by converting (±)-2-phenylpropionic acid with 3-(4-fluorophenyl)-1*H*-pyrazole.

^{1}H NMR: 300 MHz, $CDCl_3$; δ = 8.25 (d, J = 2.9 Hz, 1H), 7.87-7.81 (m, 2H), 7.50-7.47 (m, 2H), 7.35-7.30 (m, 2H), 7.24-7.21 (m, 1H), 7.18-7.10 (m, 2H), 6.68 (d, J = 2.9 Hz, 1H), 5.27 (q, J = 7.0 Hz, 1H), 1.66 (d, J = 7.1 Hz, 3H) ppm.

^{13}C NMR: 75 MHz, $CDCl_3$; δ = 173.0, 163.5 (d, $J_{C,F}$ = 248.6 Hz, 1C), 154.3, 140.2, 130.1, 128.8 (2C), 128.3 (d, $J_{C,F}$ = 3.3 Hz, 1C), 128.2 (2C), 128.2 (d, $J_{C,F}$ = 8.1 Hz, 2C), 127.4, 115.9 (d, $J_{C,F}$ = 21.8 Hz, 2C), 107.4, 43.0, 18.7 ppm.

^{19}F NMR: 282 MHz, $CDCl_3$; δ = –112.1 (s, 1F) ppm.

IR: neat, $\tilde{\nu}$ = 3157 (w), 3131 (w), 3052 (w), 2972 (w), 2936 (w), 1718 (s), 1603 (m), 1549 (w), 1511 (m), 1457 (w), 1431 (m), 1397 (m), 1347 (s), 1319 (w), 1281 (w), 1222 (s), 1154 (w), 1106 (w), 1088 (w), 1070 (w), 1045 (m), 1019 (w), 941 (w), 914 (s), 885 (w), 843 (m), 811 (m), 772 (s), 730 (s), 696 (m), 620 (m), 600 (w), 572 (m), 545 (w), 519 (w), 498 (m), 447 (w), 416 (w) cm^{-1}.

HRMS: ESI; m/z calcd. for $C_{18}H_{16}FN_2O$ $[M+H]^+$: 295.1241, found 295.1244.

2-(1-(*tert*-Butoxycarbonyl)-1*H*-indol-3-yl)acetic acid (**100**) was synthesized according to a reported procedure,[215] as shown in Scheme 48. Analytical data were in agreement with published data.[215]

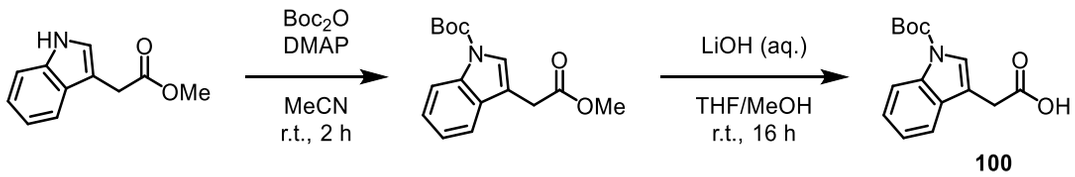

Scheme 48: Synthesis of 2-(1-(*tert*-butoxycarbonyl)-1*H*-indol-3-yl)acetic acid (**100**).

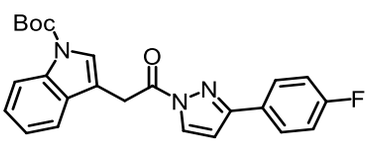

***tert*-Butyl-3-(2-(3-(4-fluorophenyl)-1*H*-pyrazol-1-yl)-2-oxoethyl)-1*H*-indole-1-carboxylate (92l)**

According to a slightly modified procedure from Tokumasu *et al.*,[216] to a solution of 2-(1-(*tert*-butoxycarbonyl)-1*H*-indol-3-yl)acetic acid (**100**, 107 mg, 0.38 mmol, 1.00 equiv.) in DMF (0.38 mL) was added EDC·HCl (87.1 mg, 0.45 mmol, 1.20 equiv.), HOBt·H_2O (71.7 mg, 0.45 mmol, 1.20 equiv.), 3-(4-fluorophenyl)-1*H*-pyrazole (67.5 mg, 0.42 mmol, 1.10 equiv.) and *N*-methylmorpholine (84.1 µL, 0.76 mmol, 2.00 equiv.) at 0 °C. The resulting solution was allowed to slowly reach room temperature and stirred for 21 h, then it was quenched by addition of a 10% aqueous solution of citric acid. The aqueous phase was extracted with EtOAc (3 x 30 mL). The combined organic extracts were washed with a saturated aqueous solution of $NaHCO_3$ (2 x 30 mL) and brine (1 x 50 mL), dried over Na_2SO_4, filtered and the solvent was removed under reduced pressure. Purification by column chromatography (*n*-pentane/EtOAc 20:1 → 10:1) gave **92l** (140 mg, 0.33 mmol, 88%) as a colorless foam.

^{1}H NMR: 300 MHz, $CDCl_3$; δ =8.30 (d, J = 2.9 Hz, 1H), 8.16 (d, J = 8.0 Hz, 1H), 7.94-7.87 (m, 2H), 7.70 (s, 1H), 7.64 (d, J = 7.3 Hz, 1H), 7.37-7.31 (m, 1H), 7.29-7.24 (m, 1H), 7.20-7.12 (m, 2H), 6.76 (d, J = 2.9 Hz, 1H), 4.62 (d, J = 0.6 Hz, 2H), 1.66 (s, 9H) ppm.

^{13}C NMR: 75 MHz, $CDCl_3$; δ = 169.3, 163.6 (d, $J_{C,F}$ = 248.8 Hz, 1C), 154.8, 149.7, 135.5, 130.4, 130.1, 128.3 (d, $J_{C,F}$ = 8.4 Hz, 2C), 128.2 (d, $J_{C,F}$ = 3.3 Hz, 1C), 125.4,

124.7, 122.8, 119.3, 116.0 (d, $J_{C,F}$ = 21.9 Hz, 2C), 115.4, 112.6, 107.7, 83.8, 30.6, 28.3 (3C) ppm.

^{19}F NMR: 282 MHz, $CDCl_3$; δ = –111.8 (s, 1F) ppm.

IR: neat, $\tilde{\nu}$ = 2974 (w), 2925 (w), 1722 (m), 1605 (w), 1513 (m), 1477 (w), 1442 (m), 1392 (m), 1366 (m), 1349 (w), 1307 (w), 1254 (m), 1218 (m), 1153 (m), 1107 (w), 1087 (m), 1048 (m), 1015 (w), 930 (m), 855 (w), 838 (m), 812 (w), 797 (w), 764 (m), 741 (m), 717 (w), 624 (m), 580 (m), 561 (w), 545 (w), 515 (w), 473 (w), 449 (w), 422 (w) cm^{-1}.

HRMS: ESI; m/z calcd. for $C_{24}H_{22}FN_3O_3Na$ $[M+Na]^+$: 442.1537, found 442.1559.

5.7.4 α-Fluorination of *N*-Acyl Pyrazoles

5.7.4.1 General Procedure K

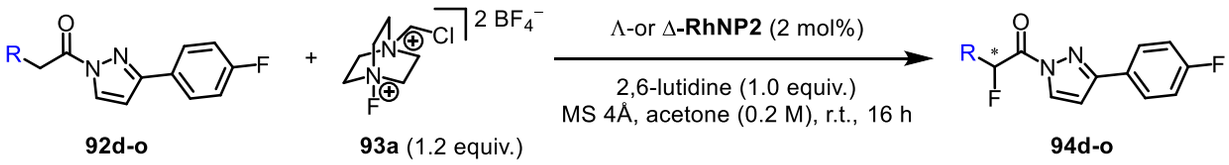

Selectfluor (**93a**, 44.2 mg, 0.12 mmol, 1.20 equiv.) and 2,6-lutidine (11.8 µL, 0.10 mmol, 1.02 equiv.) were successively added to a suspension of the corresponding *N*-acyl pyrazole substrate **92** (0.10 mmol, 1.00 equiv.), Λ- or Δ-**RhNP2** (1.9 mg, 2 mol%) and 4Å molecular sieve (powdered, 40 mg) in acetone (HPLC Grade, 0.50 mL). The resulting yellow suspension was stirred for 16 h at room temperature, unless noted otherwise. Subsequently, the solvent was removed in vacuo and the crude residue obtained was quickly filtered through a short pad of silica gel (H = 3 cm) which was rinsed with *n*-pentane/CH_2Cl_2 1:1 to afford pure α-fluorinated products **94** (Figure 54). Enantiomeric excess was established by HPLC analysis on a chiral stationary phase. Racemic samples were obtained by performing the reaction with *rac*-**RhNP2**. The absolute configuration of product **94d** was determined after pyrazole cleavage by comparison of the optical rotation with that of literature known methyl ester **99d**[217] (see Section 5.7.6). Correspondingly, (*S*)-configuration of the product was obtained when Δ-**RhNP2** was employed as the catalyst. All other products were assigned accordingly.

Figure 54: Short silica gel „column“ for purification of α-fluorinated products **94**.

5.7.4.2 Experimental Procedures and Characterization Data of Fluorinated Products

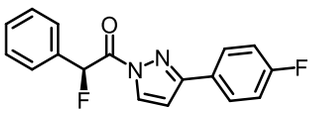

(*S*)-2-Fluoro-1-(3-(4-fluorophenyl)-1*H*-pyrazol-1-yl)-2-phenylethan-1-one (94d)

Following the general procedure K using Δ-**RhNP2** as catalyst, (*S*)-**94d** (29.5 mg, 0.10 mmol, 99%) was obtained as a colorless solid. Enantiomeric excess was established by HPLC analysis on a chiral stationary phase: ee = >99.9%, HPLC conditions: Daicel Chiralcel® OD-H column, 250 x 4.6 mm, absorbance at 254 nm, *n*-hexane/isopropanol = 95:5, isocratic flow, flow rate 1.0 mL/min, 25 °C, t_r (major) = 8.2 min, t_r (minor) = 11.2 min.

^{1}H NMR: 300 MHz, $CDCl_3$; δ = 8.26 (d, J = 2.9 Hz, 1H), 7.85-7.78 (m, 2H), 7.69-7.66 (m, 2H), 7.44-7.35 (m, 3H), 7.18-7.11 (m, 2H), 7.11 (d, $J_{H,F}$ = 47.7 Hz, 1H), 6.73 (d, J = 2.9 Hz, 1H) ppm.

^{13}C NMR: 126 MHz, $CDCl_3$; δ = 166.4 (d, $J_{C,F}$ = 28.4 Hz, 1C), 163.8 (d, $J_{C,F}$ = 249.7 Hz, 1C), 155.4, 133.9 (d, $J_{C,F}$ = 20.6 Hz, 1C), 130.5, 130.0 (d, $J_{C,F}$ = 2.0 Hz, 1C), 129.0 (2C), 128.4 (d, $J_{C,F}$ = 8.5 Hz, 2C), 128.0 (d, $J_{C,F}$ = 5.5 Hz, 2C), 127.7 (d, $J_{C,F}$ = 3.2 Hz, 1C), 116.1 (d, $J_{C,F}$ = 21.9 Hz, 2C), 108.2, 88.9 (d, $J_{C,F}$ = 180.9 Hz, 1C) ppm.

^{19}F NMR: 282 MHz, $CDCl_3$; δ = –111.2 (s, 1F), –179.4 (s, 1F) ppm.

IR: neat, $\tilde{\nu}$ = 3164 (w), 3058 (w), 2922 (w), 2852 (w), 1742 (s), 1657 (w), 1604 (w), 1548 (w), 1512 (m), 1454 (w), 1431 (m), 1408 (s), 1355 (m), 1285 (w), 1253 (w), 1232 (m), 1191 (w), 1155 (w), 1083 (m), 1045 (m), 1008 (w), 938 (m), 918 (w), 840 (w), 822 (s), 774 (m), 745 (s), 708 (w), 690 (m), 638 (w), 620 (w), 601 (m), 549 (w), 513 (m), 492 (m), 448 (w) cm^{-1}.

$[\alpha]_D^{22}$: –390.4° (*c* = 1.0, $CHCl_3$).

HRMS: ESI; m/z calcd. for $C_{17}H_{12}F_2N_2ONa$ $[M+Na]^+$: 321.0810, found 321.0807.

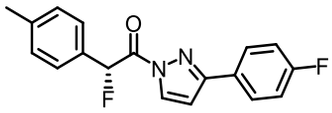

(*R*)-2-Fluoro-1-(3-(4-fluorophenyl)-1*H*-pyrazol-1-yl)-2-(*p*-tolyl)ethan-1-one (94e)

Following the general procedure K using Λ-**RhNP2** as catalyst, (*R*)-**94e** (29.9 mg, 95.7 µmol, 96%) was obtained as a colorless solid. Performed with 2.00 equiv. Selectfluor **93a**. Enantiomeric excess was established by HPLC analysis on a chiral stationary phase: ee = 98.0%, HPLC conditions: Daicel Chiralcel® OD-H column, 250 x 4.6 mm, absorbance at 254 nm, *n*-hexane/ isopropanol = 99:1, isocratic flow, flow rate 1.0 mL/min, 25 °C, t_r (minor) = 11.3 min, t_r (major) = 18.0 min.

^{1}H NMR: 500 MHz, $CDCl_3$; δ = 8.25 (d, J = 2.9 Hz, 1H), 7.82-7.79 (m, 2H), 7.57-7.55 (m, 2H), 7.21 (d, J = 8.0 Hz, 2H), 7.17-7.13 (m, 2H), 7.11 (d, $J_{H,F}$ = 47.8 Hz, 1H), 6.72 (d, J = 2.9 Hz, 1H), 2.33 (d, J = 1.5 Hz, 3H) ppm.

^{13}C NMR: 126 MHz, $CDCl_3$; δ = 166.6 (d, $J_{C,F}$ = 28.8 Hz, 1C), 163.7 (d, $J_{C,F}$ = 249.1 Hz, 1C), 155.3, 140.2 (d, $J_{C,F}$ = 2.8 Hz, 1C), 130.8 (d, $J_{C,F}$ = 21.0 Hz, 1C), 130.4, 129.7 (2C), 128.3 (d, $J_{C,F}$ = 8.4 Hz, 2C), 128.1 (d, $J_{C,F}$ = 4.9 Hz, 2C), 127.7 (d, $J_{C,F}$ = 3.0 Hz, 1C), 116.1 (d, $J_{C,F}$ = 21.8 Hz, 2C), 108.1, 88.8 (d, $J_{C,F}$ = 180.2 Hz, 1C), 21.4 ppm.

^{19}F NMR: 282 MHz, $CDCl_3$; δ = –111.4 (s, 1F), –178.1 (s, 1F) ppm.

IR: neat, $\tilde{\nu}$ = 3138 (w), 3120 (w), 1738 (s), 1679 (w), 1602 (w), 1511 (m), 1430 (w), 1409 (s), 1358 (m), 1310 (w), 1283 (w), 1236 (m), 1217 (w), 1196 (w), 1174 (w), 1155 (m), 1095 (w), 1067 (w), 1049 (m), 1010 (w), 973 (w), 935 (m), 841 (m), 812 (w), 788 (s), 726 (w), 684 (w), 621 (m), 597 (w), 564 (m), 547 (w), 516 (w), 498 (m), 449 (w) cm^{-1}.

$[\alpha]_D^{22}$: +440.5° (c = 1.0, $CHCl_3$).

HRMS: ESI; m/z calcd. for $C_{18}H_{14}F_2N_2ONa$ $[M+Na]^+$: 335.0966, found 335.0970.

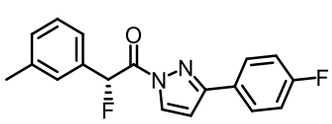

(*R*)-2-Fluoro-1-(3-(4-fluorophenyl)-1*H*-pyrazol-1-yl)-2-(*m*-tolyl)ethan-1-one (94f)

Following the general procedure K using Λ-**RhNP2** as catalyst, (*R*)-**94f** (30.2 mg, 96.7 µmol, 97%) was obtained as a colorless solid. Enantiomeric excess was established by HPLC analysis on a chiral stationary phase: ee = 99.4%, HPLC conditions: Daicel Chiralcel® OD-H column,

250 x 4.6 mm, absorbance at 254 nm, *n*-hexane/isopropanol = 95:5, isocratic flow, flow rate 1.0 mL/min, 25 °C, t_r (minor) = 7.7 min, t_r (major) = 10.1 min.

^{1}H NMR: 300 MHz, $CDCl_3$; δ = 8.26 (d, J = 2.9 Hz, 1H), 7.83-7.79 (m, 2H), 7.49-7.46 (m, 2H), 7.31-7.29 (m, 1H), 7.20-7.00 (m, 4H), 6.73 (d, J = 2.9 Hz, 1H), 2.36 (s, 3H) ppm.

^{13}C NMR: 75 MHz, $CDCl_3$; δ = 166.5 (d, $J_{C,F}$ = 28.5 Hz, 1C), 163.7 (d, $J_{C,F}$ = 249.4 Hz, 1C), 155.3, 138.8, 133.7 (d, $J_{C,F}$ = 20.5 Hz, 1C), 130.8 (d, $J_{C,F}$ = 2.6 Hz, 1C), 130.4, 128.8, 128.5 (d, $J_{C,F}$ = 5.3 Hz, 1C), 128.3 (d, $J_{C,F}$ = 8.3 Hz, 2C), 127.7 (d, $J_{C,F}$ = 3.3 Hz, 1C), 125.3 (d, $J_{C,F}$ = 5.3 Hz, 1C), 116.1 (d, $J_{C,F}$ = 21.9 Hz, 2C), 108.2, 89.0 (d, $J_{C,F}$ = 180.5 Hz, 1C), 21.5 ppm.

^{19}F NMR: 282 MHz, $CDCl_3$; δ = –111.2 (s, 1F), –178.9 (s, 1F) ppm.

IR: neat, $\tilde{\nu}$ = 3144 (w), 2922 (w), 2852 (w), 1739 (s), 1605 (w), 1512 (m), 1486 (w), 1462 (w), 1431 (w), 1406 (s), 1352 (m), 1282 (w), 1220 (m), 1154 (m), 1093 (w), 1070 (w), 1049 (m), 1008 (w), 941 (m), 898 (w), 840 (m), 814 (w), 775 (s), 707 (w), 687 (m), 606 (m), 550 (w), 516 (m), 442 (w) cm^{-1}.

$[\alpha]_D^{22}$: +362.1° (c = 1.0, $CHCl_3$).

HRMS: ESI; m/z calcd. for $C_{18}H_{14}F_2N_2ONa$ $[M+Na]^+$: 335.0966, found 335.0975.

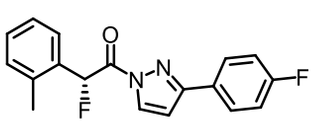

(*R*)-2-Fluoro-1-(3-(4-fluorophenyl)-1*H*-pyrazol-1-yl)-2-(*o*-tolyl)ethan-1-one (94g)

Following the general procedure K using Λ-**RhNP2** as catalyst, (*R*)-**94g** (30.2 mg, 96.7 µmol, 97%) was obtained as a colorless solid. Enantiomeric excess was established by HPLC analysis on a chiral stationary phase: ee = 97.7%, HPLC conditions: Daicel Chiralcel® OD-H column, 250 x 4.6 mm, absorbance at 254 nm, *n*-hexane/isopropanol = 95:5, isocratic flow, flow rate 1.0 mL/min, 25 °C, t_r (minor) = 8.9 min, t_r (major) = 13.7 min.

^{1}H NMR: 500 MHz, $CDCl_3$; δ = 8.37 (d, J = 3.0 Hz, 1H), 7.81-7.77 (m, 2H), 7.61 (d, J = 7.8 Hz, 1H), 7.38-7.27 (m, 4H), 7.21-7.16 (m, 2H), 6.78 (d, J = 2.9 Hz, 1H), 2.78 (d, J = 1.6 Hz, 3H) ppm.

^{13}C NMR: 126 MHz, $CDCl_3$; δ = 167.0 (d, $J_{C,F}$ = 28.5 Hz, 1C), 163.6 (d, $J_{C,F}$ = 249.2 Hz, 1C), 155.4, 137.7 (d, $J_{C,F}$ = 3.6 Hz, 1C), 132.0 (d, $J_{C,F}$ = 19.1 Hz, 1C), 131.2 (d, $J_{C,F}$ =

1.6 Hz, 1C), 130.4, 130.3 (d, $J_{C,F}$ = 3.6 Hz, 1C), 128.4, 128.3 (d, $J_{C,F}$ = 8.5 Hz, 2C), 127.7 (d, $J_{C,F}$ = 3.5 Hz, 1C), 126.6 (d, $J_{C,F}$ = 2.5 Hz, 1C), 116.1 (d, $J_{C,F}$ = 21.9 Hz, 2C), 108.2, 86.5 (d, $J_{C,F}$ = 179.3 Hz, 1C), 19.4 ppm.

^{19}F NMR: 282 MHz, $CDCl_3$; δ = –111.3 (s, 1F), –176.0 (s, 1F) ppm.

IR: neat, $\tilde{\nu}$ = 3145 (w), 3123 (w), 2920 (w), 2851 (w), 1733 (s), 1603 (w), 1548 (w), 1512 (m), 1464 (w), 1431 (w), 1407 (s), 1354 (m), 1316 (w), 1283 (w), 1239 (w), 1219 (m), 1177 (w), 1156 (w), 1100 (w), 1051 (m), 1000 (m), 958 (w), 938 (s), 895 (w), 837 (s), 783 (m), 763 (s), 725 (w), 685 (w), 610 (m), 593 (w), 560 (w), 515 (w), 497 (w), 455 (m) cm^{-1}.

$[\alpha]_D^{22}$: +217.7° (*c* = 1.0, $CHCl_3$).

HRMS: ESI; m/z calcd. for $C_{18}H_{14}F_2N_2ONa$ $[M+Na]^+$: 335.0966, found 335.0969.

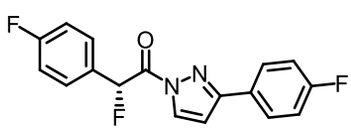

(*R*)-2-Fluoro-2-(4-fluorophenyl)-1-(3-(4-fluorophenyl)-1*H*-pyrazol-1-yl)ethan-1-one (94h)

Following the general procedure K using Λ-**RhNP2** as catalyst, (*R*)-**94h** (28.8 mg, 91.1 µmol, 91%) was obtained as a colorless solid. Enantiomeric excess was established by HPLC analysis on a chiral stationary phase: ee = 98.9%, HPLC conditions: Daicel Chiralcel® OD-H column, 250 x 4.6 mm, absorbance at 254 nm, *n*-hexane/isopropanol = 95:5, isocratic flow, flow rate 1.0 mL/min, 25 °C, t_r (minor) = 7.7 min, t_r (major) = 9.1 min.

^{1}H NMR: 300 MHz, $CDCl_3$; δ = 8.26 (d, *J* = 2.8 Hz, 1H), 7.82-7.78 (m, 2H), 7.69-7.64 (m, 2H), 7.18-7.02 (m, 5H), 6.75 (d, *J* = 2.9 Hz, 1H) ppm.

^{13}C NMR: 75 MHz, $CDCl_3$; δ = 166.2 (d, $J_{C,F}$ = 28.7 Hz, 1C), 163.8 (d, $J_{C,F}$ = 249.8 Hz, 1C), 163.7 (dd, $J_{C,F}$ = 249.7, 2.7 Hz, 1C), 155.5, 130.5, 130.1 (dd, $J_{C,F}$ = 8.6, 5.2 Hz, 2C), 129.8 (dd, $J_{C,F}$ = 21.7, 3.3 Hz, 1C), 128.4 (d, $J_{C,F}$ = 8.4 Hz, 2C), 127.6 (d, $J_{C,F}$ = 3.3 Hz, 1C), 116.2 (d, $J_{C,F}$ = 21.9 Hz, 2C), 116.1 (d, $J_{C,F}$ = 21.9 Hz, 2C), 108.4, 88.1 (d, $J_{C,F}$ = 181.2 Hz, 1C) ppm.

^{19}F NMR: 282 MHz, $CDCl_3$; δ = –110.6 (d, *J* = 4.7 Hz, 1F), –111.0 (s, 1F), –178.3 (d, *J* = 4.7 Hz, 1F) ppm.

IR: neat, $\tilde{\nu}$ = 3155 (w), 2957 (w), 2922 (w), 2852 (w), 1743 (s), 1602 (m), 1549 (w), 1506 (s), 1465 (w), 1431 (w), 1410 (m), 1354 (m), 1289 (w), 1260 (w), 1220 (s), 1189 (w), 1156 (m), 1090 (w), 1065 (w), 1046 (m), 1011 (w), 955 (w), 934 (m),

871 (w), 838 (w), 809 (w), 781 (s), 724 (w), 685 (w), 638 (w), 618 (m), 595 (w), 563 (m), 543 (w), 513 (s), 449 (w), 419 (w) cm^{-1}.

$[\alpha]_D^{22}$: +350.3° (*c* = 1.0, $CHCl_3$).

HRMS: ESI; m/z calcd. for $C_{17}H_{11}F_3N_2ONa$ $[M+Na]^+$: 339.0716, found 339.0719.

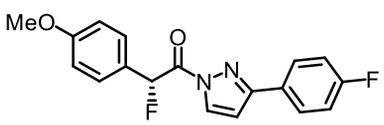

(*R*)-2-Fluoro-1-(3-(4-fluorophenyl)-1*H*-pyrazol-1-yl)-2-(4-methoxyphenyl)ethan-1-one (94i)

Following the general procedure K using Λ-**RhNP2** as catalyst, (*R*)-**94i** (28.1 mg, 85.6 µmol, 86%) was obtained as a colorless solid. Performed with 2.00 equiv. Selectfluor **93a**. Enantiomeric excess was established by HPLC analysis on a chiral stationary phase: ee = 96.0%, HPLC conditions: Daicel Chiralcel® OD-H column, 250 x 4.6 mm, absorbance at 254 nm, *n*-hexane/isopropanol = 95:5, isocratic flow, flow rate 1.0 mL/min, 25 °C, t_r (minor) = 10.0 min, t_r (major) = 12.4 min.

^{1}H NMR: 500 MHz, $CDCl_3$; δ = 8.26 (d, *J* = 3.0 Hz, 1H), 7.82-7.78 (m, 2H), 7.60-7.58 (m, 2H), 7.17-7.12 (m, 2H), 7.05 (d, $J_{H,F}$ = 47.7 Hz, 1H), 6.91 (d, *J* = 8.6 Hz, 2H), 6.72 (d, *J* = 2.9 Hz, 1H), 3.79 (s, 3H) ppm.

^{13}C NMR: 126 MHz, $CDCl_3$; δ = 166.7 (d, $J_{C,F}$ = 29.5 Hz, 1C), 163.7 (d, $J_{C,F}$ = 249.5 Hz, 1C), 160.9 (d, $J_{C,F}$ = 2.6 Hz, 1C), 155.3, 130.4, 129.7 (d, $J_{C,F}$ = 4.8 Hz, 2C), 128.3 (d, $J_{C,F}$ = 8.5 Hz, 2C), 127.7 (d, $J_{C,F}$ = 3.5 Hz, 1C), 125.8 (d, $J_{C,F}$ = 21.6 Hz, 1C), 116.1 (d, $J_{C,F}$ = 21.7 Hz, 2C), 114.4 (2C), 108.1, 88.6 (d, $J_{C,F}$ = 180.2 Hz, 1C), 55.4 ppm.

^{19}F NMR: 282 MHz, $CDCl_3$; δ = –111.4 (s, 1F), –176.1 (s, 1F) ppm.

IR: neat, $\tilde{\nu}$ = 3150 (w), 3125 (w), 3084 (w), 3005 (w), 2946 (w), 2848 (w), 1736 (s), 1604 (m), 1511 (s), 1466 (w), 1430 (m), 1408 (s), 1348 (m), 1302 (w), 1281 (w), 1240 (s), 1222 (w), 1195 (w), 1176 (m), 1154 (w), 1093 (w), 1049 (m), 1024 (m), 955 (w), 933 (m), 870 (w), 845 (m), 812 (s), 771 (s), 684 (w), 639 (w), 618 (m), 594 (w), 567 (m), 545 (w), 519 (w), 449 (w) cm^{-1}.

$[\alpha]_D^{22}$: +419.9° (*c* = 1.0, $CHCl_3$).

HRMS: ESI; m/z calcd. for $C_{18}H_{14}F_2N_2O_2Na$ $[M+Na]^+$: 351.0916, found 351.0920.

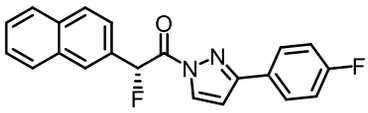

(*R*)-2-Fluoro-1-(3-(4-fluorophenyl)-1*H*-pyrazol-1-yl)-2-(naphthalen-2-yl)ethan-1-one (94j)

Following the general procedure K using Λ-**RhNP2** as catalyst, (*R*)-**94j** (33.4 mg, 95.9 µmol, 96%) was obtained as a colorless solid. Enantiomeric excess was established by HPLC analysis on a chiral stationary phase: ee = 98.6%, HPLC conditions: Daicel Chiralcel® OD-H column, 250 x 4.6 mm, absorbance at 254 nm, *n*-hexane/isopropanol = 95:5, isocratic flow, flow rate 1.0 mL/min, 25 °C, t_r (minor) = 10.3 min, t_r (major) = 12.2 min.

^{1}H NMR: 300 MHz, $CDCl_3$; δ = 8.26 (d, J = 2.9 Hz, 1H), 8.17 (s, 1H), 7.90-7.77 (m, 6H), 7.52-7.49 (m, 2H), 7.28 (d, $J_{H,F}$ = 47.7 Hz, 1H), 7.16 (t, J = 8.7 Hz, 2H), 6.71 (d, J = 2.9 Hz, 1H) ppm.

^{13}C NMR: 75 MHz, $CDCl_3$; δ = 166.4 (d, $J_{C,F}$ = 28.6 Hz, 1C), 163.7 (d, $J_{C,F}$ = 249.4 Hz, 1C), 155.4, 134.0 (d, $J_{C,F}$ = 1.7 Hz, 1C), 133.1, 131.2 (d, $J_{C,F}$ = 20.5 Hz, 1C), 130.5, 128.9, 128.5, 128.4 (d, $J_{C,F}$ = 8.4 Hz, 2C), 128.2 (d, $J_{C,F}$ = 6.4 Hz, 1C), 127.9, 127.7 (d, $J_{C,F}$ = 3.2 Hz, 1C), 127.3, 126.8, 124.8 (d, $J_{C,F}$ = 4.5 Hz, 1C), 116.1 (d, $J_{C,F}$ = 21.8 Hz, 2C), 108.2, 89.0 (d, $J_{C,F}$ = 181.0 Hz, 1C) ppm.

^{19}F NMR: 282 MHz, $CDCl_3$; δ = –111.1 (s, 1F), –178.8 (s, 1F) ppm.

IR: neat, $\tilde{\nu}$ = 3164 (w), 3056 (w), 1736 (s), 1604 (m), 1552 (w), 1512 (s), 1433 (m), 1408 (s), 1354 (s), 1318 (w), 1284 (w), 1220 (s), 1159 (m), 1125 (w), 1099 (w), 1072 (m), 1049 (m), 1013 (w), 939 (m), 905 (w), 876 (w), 842 (m), 813 (s), 772 (s), 742 (w), 687 (m), 639 (w), 618 (m), 594 (w), 568 (w), 551 (w), 516 (m), 478 (s), 449 (w) cm^{-1}.

$[\alpha]_D^{22}$: +527.5° (*c* = 1.0, $CHCl_3$).

HRMS: ESI; m/z calcd. for $C_{21}H_{14}F_2N_2ONa$ $[M+Na]^+$: 371.0966, found 371.0967.

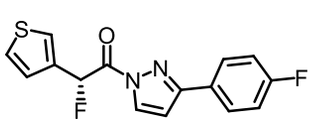

(*R*)-2-Fluoro-1-(3-(4-fluorophenyl)-1*H*-pyrazol-1-yl)-2-(thiophen-3-yl)ethan-1-one (94k)

Following the general procedure K using Λ-**RhNP2** as catalyst, (*R*)-**94k** (26.5 mg, 87.1 µmol, 87%) was obtained as a colorless solid. Performed with 2.00 equiv. Selectfluor **93a**. Enantiomeric excess was established by HPLC analysis on a chiral stationary phase: ee = 99.7%, HPLC conditions: Daicel Chiralcel® OD-H column, 250 x 4.6 mm, absorbance at 254 nm, *n*-hexane/

isopropanol = 95:5, isocratic flow, flow rate 1.0 mL/min, 25 °C, t_r (minor) = 11.5 min, t_r (major) = 13.1 min.

^{1}H NMR: 300 MHz, $CDCl_3$; δ = 8.28 (d, J = 2.9 Hz, 1H), 7.85-7.80 (m, 2H), 7.63-7.62 (m, 1H), 7.34-7.12 (m, 5H), 6.76 (d, J = 2.9 Hz, 1H) ppm.

^{13}C NMR: 75 MHz, $CDCl_3$; δ = 166.0 (d, $J_{C,F}$ = 28.2 Hz, 1C), 163.8 (d, $J_{C,F}$ = 249.7 Hz, 1C), 155.5, 134.4 (d, $J_{C,F}$ = 22.9 Hz, 1C), 130.5, 128.4 (d, $J_{C,F}$ = 8.4 Hz, 2C), 127.6 (d, $J_{C,F}$ = 3.3 Hz, 1C), 126.8, 126.5 (d, $J_{C,F}$ = 3.3 Hz, 1C), 126.1 (d, $J_{C,F}$ = 7.1 Hz, 1C), 116.1 (d, $J_{C,F}$ = 21.9 Hz, 2C), 108.3, 84.9 (d, $J_{C,F}$ = 180.0 Hz, 1C) ppm.

^{19}F NMR: 282 MHz, $CDCl_3$; δ = –111.1 (s, 1F), –178.4 (s, 1F) ppm.

IR: neat, $\tilde{\nu}$ = 3162 (w), 3114 (w), 1733 (s), 1603 (w), 1511 (m), 1431 (m), 1409 (s), 1354 (m), 1316 (w), 1283 (w), 1236 (w), 1219 (m), 1152 (m), 1097 (w), 1069 (m), 1047 (m), 1013 (w), 936 (w), 863 (w), 842 (m), 814 (w), 776 (s), 726 (w), 702 (w), 685 (w), 663 (w), 617 (w), 602 (m), 575 (w), 546 (w), 513 (m), 449 (w) cm^{-1}.

$[\alpha]_D^{22}$: +404.7° (c = 1.0, $CHCl_3$).

HRMS: ESI; m/z calcd. for $C_{15}H_{10}F_2N_2OSNa$ $[M+Na]^+$: 327.0380, found 327.0378.

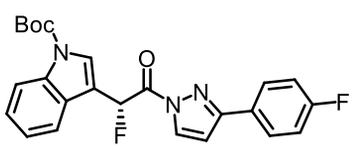

***tert*-Butyl (*R*)-3-(1-fluoro-2-(3-(4-fluorophenyl)-1*H*-pyrazol-1-yl)-2-oxoethyl)-1*H*-indole-1-carboxylate (94l)**

Following the general procedure K using Λ-**RhNP2** as catalyst, (*R*)-**94l** (16.0 mg, 36.6 µmol, 37%) was obtained as a yellow foam. Performed with 2.00 equiv. Selectfluor **93a**. Enantiomeric excess was established by HPLC analysis on a chiral stationary phase: ee = 90.0%, HPLC conditions: Daicel Chiralcel® OD-H column, 250 x 4.6 mm, absorbance at 254 nm, *n*-hexane/ isopropanol = 95:5, isocratic flow, flow rate 1.0 mL/min, 25 °C, t_r (minor) = 7.8 min, t_r (major) = 9.2 min.

^{1}H NMR: 500 MHz, $CDCl_3$; δ = 8.28 (d, J = 3.0 Hz, 1H), 8.13 (d, J = 7.6 Hz, 1H), 7.95 (d, J = 7.5 Hz, 1H), 7.90 (d, J = 3.9 Hz, 1H), 7.77-7.73 (m, 2H), 7.36 (d, $J_{H,F}$ = 47.6 Hz, 1H), 7.38-7.32 (m, 2H), 7.13-7.09 (m, 2H), 6.72 (d, J = 3.0 Hz, 1H), 1.64 (s, 9H) ppm.

^{13}C NMR: 126 MHz, $CDCl_3$; δ = 165.9 (d, $J_{C,F}$ = 29.5 Hz, 1C), 163.7 (d, $J_{C,F}$ = 249.3 Hz, 1C), 155.3, 149.3, 135.5, 130.5, 128.4 (d, $J_{C,F}$ = 8.5 Hz, 2C), 128.0, 127.6 (d, $J_{C,F}$ = 3.3 Hz, 1C), 127.2 (d, $J_{C,F}$ = 8.2 Hz, 1C), 125.3, 123.4, 120.2, 116.0 (d, $J_{C,F}$ = 21.9 Hz, 2C), 115.5, 113.7 (d, $J_{C,F}$ = 23.6 Hz, 1C), 108.2, 84.6, 83.2 (d, $J_{C,F}$ = 178.3 Hz, 1C), 28.2 (3C) ppm.

^{19}F NMR: 282 MHz, $CDCl_3$; δ = –111.3 (s, 1F), –180.9 (s, 1F) ppm.

IR: neat, $\tilde{\nu}$ = 2923 (m), 2853 (w), 1733 (s), 1606 (w), 1567 (w), 1514 (m), 1452 (m), 1432 (w), 1408 (w), 1384 (w), 1356 (s), 1310 (w), 1291 (w), 1237 (m), 1223 (w), 1152 (s), 1091 (s), 1045 (m), 1021 (w), 992 (w), 935 (m), 842 (m), 795 (w), 768 (w), 748 (s), 687 (w), 648 (w), 622 (w), 602 (w), 575 (w), 515 (w), 472 (w), 425 (w) cm^{-1}.

$[\alpha]_D^{22}$: +239.6° (*c* = 1.0, $CHCl_3$).

HRMS: ESI; m/z calcd. for $C_{24}H_{21}F_2N_3O_3Na$ $[M+Na]^+$: 460.1443, found 460.1462.

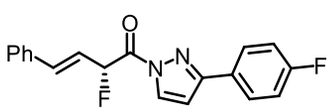

(*R*,*E*)-2-Fluoro-1-(3-(4-fluorophenyl)-1*H*-pyrazol-1-yl)-4-phenylbut-3-en-1-one (94m)

Following the general procedure K using Λ-**RhNP2** as catalyst, (*R*)-**94m** (99% conversion, 70% NMR yield) was obtained as a colorless solid after column chromatographic purification. It was isolated along with a side product which had the same R_f value and therefore could not be separated from the product. Enantiomeric excess of the crude product was established by HPLC analysis on a chiral stationary phase: ee = 68.4%, HPLC conditions: Daicel Chiralpak® IC column, 250 x 4.6 mm, absorbance at 254 nm, *n*-hexane/THF = 95:5, isocratic flow, flow rate 1.0 mL/min, 25 °C, t_r (major) = 13.3 min, t_r (minor) = 15.8 min.

^{1}H NMR: 300 MHz, $CDCl_3$; δ = 8.30 (d, *J* = 2.9 Hz, 1H), 7.88-7.83 (m, 2H), 7.41-7.26 (m, 5H), 7.18-7.12 (m, 2H), 7.04 (dd, *J* = 16.0, 1.5 Hz, 1H), 6.78 (d, *J* = 2.8 Hz, 1H), 6.74 (dd, *J* = 47.9, 6.2 Hz, 1H), 6.49 (dt, *J* = 15.6, 6.3 Hz, 1H) ppm.

^{19}F NMR: 282 MHz, $CDCl_3$; δ = –111.1 (s, 1F), –188.0 (s, 1F) ppm.

HRMS: ESI; m/z calcd. for $C_{19}H_{14}F_2N_2ONa$ $[M+Na]^+$: 347.0966, found 347.0977.

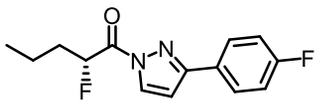

(*R*)-2-Fluoro-1-(3-(4-fluorophenyl)-1*H*-pyrazol-1-yl)pentan-1-one (94n)

Following the general procedure K with some modifications, substrate **92n** (24.6 mg, 0.10 mmol, 1.00 equiv.) was converted using 2.00 equiv. Selectfluor **93a** (73.7 mg, 0.20 mmol), 3 mol% catalyst and 1.10 equiv. of K_2CO_3 (15.2 mg, 1.10 mmol) as base. The resulting reaction mixture was stirred for the indicated time at room temperature, before it was diluted with CH_2Cl_2 and filtered through a short plug of celite. The solvent was removed under reduced pressure and 1,1,2,2-tetrachloroethane was added as internal standard to determine conversion and NMR yield by integration of baseline separated signals in the ^{1}H NMR.

With *rac*-**RhNP2** almost no conversion (<5%) was observed after 16 h reaction time and only trace amounts of product were formed.

Λ-**RhS** provided the product in 8% NMR yield, with a conversion of 15% after 4 h reaction time at room temperature. Enantiomeric excess of the crude product was established by HPLC analysis on a chiral stationary phase: ee = 45.3%, HPLC conditions: Daicel Chiralcel® OD-H column, 250 x 4.6 mm, absorbance at 254 nm, *n*-hexane/isopropanol = 99:1, isocratic flow, flow rate 1.0 mL/min, 25 °C, t_r (major) = 7.2 min, t_r (minor) = 8.0 min.

HRMS ESI; m/z calcd. for $C_{14}H_{14}F_2N_2ONa$ $[M+Na]^+$:287.0966, found 287.0977.

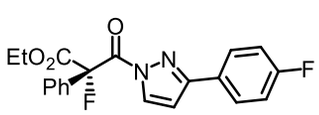

Ethyl (*S*)-2-fluoro-3-(3-(4-fluorophenyl)-1*H*-pyrazol-1-yl)-3-oxo-2-phenylpropanoate (94o)

Following the general procedure K with some modifications, substrate **92o** (35.2 mg, 0.10 mmol, 1.00 equiv.) was converted using 2.00 equiv. Selectfluor **93a** (74.5 mg, 0.20 mmol), 3 mol% catalyst and 1.10 equiv. of K_2CO_3 (15.2 mg, 1.10 mmol) as base. The resulting reaction mixture was stirred for 4 h at room temperature in dry acetone (0.50 mL).

With Δ-**RhNP2**, (*S*)-**94o** (71% conversion, 17.9 mg, 48.3 µmol, 48%) was obtained as a colorless solid after regular silica gel column chromatography (*n*-pentane/CH_2Cl_2 1:1). Enantiomeric excess was established by HPLC analysis on a chiral stationary phase: ee = 11.3%, HPLC conditions: Daicel Chiralpak® IC column, 250 x 4.6 mm, absorbance at 254 nm, *n*-hexane/THF = 96:4, isocratic flow, flow rate 1.0 mL/min, 25 °C, t_r (major) = 12.8 min, t_r (minor) = 16.1 min.

With Δ-**RhS**, (*S*)-**94o** (>99% conversion, 35.5 mg, 95.9 µmol, 96%) was obtained as a colorless solid. Since conversion of the starting material was complete, purification of the crude product was performed as described in the general procedure via filtration through a short silica pad (Figure 54). Enantiomeric excess was established by HPLC analysis on a chiral stationary phase: ee = 86.7%, HPLC conditions: Daicel Chiralpak® IC column, 250 x 4.6 mm, absorbance at 254 nm, *n*-hexane/THF = 96:4, isocratic flow, flow rate 1.0 mL/min, 25 °C, t_r (major) = 12.6 min, t_r (minor) = 16.0 min.

^{1}H NMR: 300 MHz, $CDCl_3$; δ = 8.27 (d, J = 2.9 Hz, 1H), 7.87-7.82 (m, 2H), 7.72-7.69 (m, 2H), 7.46-7.44 (m, 3H), 7.17-7.12 (m, 2H), 6.79 (d, J = 2.9 Hz, 1H), 4.30 (d, J = 7.0 Hz, 2H), 1.19 (d, J = 7.1 Hz, 3H) ppm.

^{13}C NMR: 75 MHz, $CDCl_3$; δ = 165.7 (d, $J_{C,F}$ = 24.5 Hz, 1C), 163.8 (d, $J_{C,F}$ = 249.7 Hz, 1C), 163.3 (d, $J_{C,F}$ = 26.0 Hz, 1C), 155.1, 132.5 (d, $J_{C,F}$ = 22.2 Hz, 1C), 131.1, 129.7, 128.5, 128.4, 128.4, 128.3, 127.4 (d, $J_{C,F}$ = 3.3 Hz, 1C), 126.7 (d, $J_{C,F}$ = 9.2 Hz, 2C), 116.1 (d, $J_{C,F}$ = 21.9 Hz, 2C), 108.0, 94.3 (d, $J_{C,F}$ = 197.7 Hz, 1C), 62.8, 14.0 ppm.

^{19}F NMR: 282 MHz, $CDCl_3$; δ = –111.0 (s, 1F), –155.1 (s, 1F) ppm.

IR: neat, $\tilde{\nu}$ = 3161 (w), 3064 (w), 2977 (w), 2928 (w), 1737 (s), 1606 (m), 1550 (w), 1513 (m), 1449 (w), 1432 (m), 1405 (m), 1349 (m), 1267 (w), 1209 (s), 1156 (w), 1091 (w), 1071 (w), 1045 (m), 1021 (w), 966 (w), 942 (w), 919 (w), 873 (m), 840 (s), 813 (w), 768 (w), 750 (s), 712 (w), 691 (m), 645 (w), 625 (m), 598 (w), 574 (w), 506 (m), 463 (w), 444 (w) cm^{-1}.

$[\alpha]_D^{22}$: +55.2° (*c* = 1.0, $CHCl_3$).

HRMS: ESI; m/z calcd. for $C_{20}H_{16}F_2N_2O_3Na$ $[M+Na]^+$: 393.1021, found 393.1028.

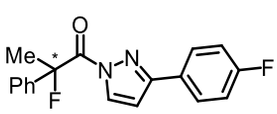

2-Fluoro-1-(3-(4-fluorophenyl)-1*H*-pyrazol-1-yl)-2-phenylpropan-1-one (94q)

Following the general procedure K with some modifications, substrate **92q** (29.4 mg, 0.10 mmol, 1.00 equiv.) was converted using 2.00 equiv. Selectfluor (**93a**, 73.7 mg, 0.20 mmol), 3 mol% catalyst and 1.10 equiv. of K_2CO_3 (15.2 mg, 1.10 mmol) as base. The resulting reaction mixture was stirred for 20 h at room temperature in acetone (0.50 mL).

However, conversion could not be observed neither with *rac*-**RhNP2** nor with *rac*-**RhS**.

5.7.5 α-Chlorination of *N*-Acyl Pyrazoles

5.7.5.1 General Procedure L

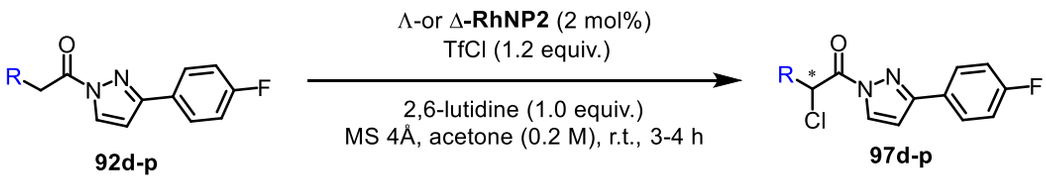

Trifluoromethanesulfonyl chloride (TfCl, 20 v/v% in acetone HPLC Grade, 64.0 µL, 0.12 mmol, 1.20 equiv.) and 2,6-lutidine (11.8 µL, 0.10 mmol, 1.02 equiv.) were successively added to a suspension of the corresponding *N*-acyl pyrazole substrate **92** (0.10 mmol, 1.00 equiv.), Λ- or Δ-**RhNP2** (1.9 mg, 2 mol%) and 4Å molecular sieve (powdered, 40 mg) in acetone (HPLC Grade, 0.44 mL). The resulting colorless to pale yellow suspension was stirred for 3–4 h at room temperature until TLC confirmed completion of the reaction. Subsequently, the solvent was removed in vacuo and the crude residue obtained was quickly filtered through a short pad of silica gel (H = 3 cm) which was rinsed with *n*-pentane/CH_2Cl_2 1:1 to afford pure α-chlorinated products **97** (Figure 54). Enantiomeric excess was established by HPLC analysis on a chiral stationary phase. Racemic samples were obtained by performing the reaction with *rac*-**RhNP2**. The absolute configuration of product **97d** was determined after pyrazole cleavage by comparison of the optical rotation with that of literature known methyl ester **98d**[199] (see Section 5.7.6). Correspondingly, (*S*)-configuration of the product was obtained when Δ-**RhNP2** was employed as the catalyst. All other products were assigned accordingly.

5.7.5.2 Experimental Procedures and Characterization Data of Chlorinated Products

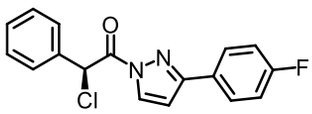

(*S*)-2-Chloro-1-(3-(4-fluorophenyl)-1*H*-pyrazol-1-yl)-2-phenylethan-1-one (97d)

Following the general procedure L using Δ-**RhNP2** as catalyst, (*S*)-**97d** (30.3 mg, 96.3 µmol, 96%) was obtained as a colorless solid. Enantiomeric excess was established by HPLC analysis on a chiral stationary phase: ee = 96.2%, HPLC conditions: Daicel Chiralcel® OD-H column, 250 x 4.6 mm, absorbance at 254 nm, *n*-hexane/isopropanol = 99.4:0.6, isocratic flow, flow rate 0.7 mL/min, 25 °C, t_r (major) = 23.5 min, t_r (minor) = 25.2 min.

^{1}H NMR: 300 MHz, $CDCl_3$; δ = 8.27 (d, J = 2.9 Hz, 1H), 7.87-7.82 (m, 2H), 7.67 (d, J = 6.5 Hz, 2H), 7.42-7.34 (m, 3H), 7.16 (t, J = 8.6 Hz, 2H), 6.94 (s, 1H), 6.76 (d, J = 2.9 Hz, 1H) ppm.

^{13}C NMR: 75 MHz, $CDCl_3$; δ = 166.1, 163.8 (d, $J_{C,F}$ = 249.4 Hz, 1C), 155.3, 135.4, 130.8, 129.5, 129.1 (2C), 128.8 (2C), 128.4 (d, $J_{C,F}$ = 8.4 Hz, 2C), 127.7 (d, $J_{C,F}$ = 3.2 Hz, 1C), 116.1 (d, $J_{C,F}$ = 21.9 Hz, 2C), 108.7, 57.2 ppm.

^{19}F NMR: 282 MHz, $CDCl_3$; δ = –111.2 (s, 1F) ppm.

IR: neat, $\tilde{\nu}$ = 3163 (w), 2921 (w), 2852 (w), 1726 (s), 1605 (m), 1551 (w), 1513 (m), 1494 (w), 1453 (w), 1432 (m), 1404 (m), 1353 (s), 1298 (w), 1251 (w), 1218 (m), 1190 (w), 1157 (m), 1106 (w), 1087 (m), 1048 (m), 1028 (w), 936 (m), 919 (w), 838 (m), 820 (w), 778 (s), 729 (s), 694 (m), 638 (w), 621 (w), 595 (w), 569 (m), 550 (w), 511 (m), 489 (w), 447 (w) cm^{-1}.

$[\alpha]_D^{22}$: –227.5° (c = 1.0, $CHCl_3$).

HRMS: ESI; m/z calcd. for $C_{17}H_{12}ClFN_2ONa$ $[M+Na]^+$: 337.0514, found 337.0520.

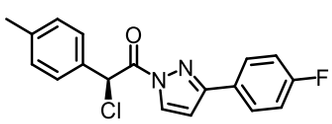

(*S*)-2-Chloro-1-(3-(4-fluorophenyl)-1*H*-pyrazol-1-yl)-2-(*p*-tolyl)ethan-1-one (97e)

Following the general procedure L using Δ-**RhNP2** as catalyst, (*S*)-**97e** (32.6 mg, 99.2 µmol, 99%) was obtained as a colorless solid. Enantiomeric excess was established by HPLC analysis on a chiral stationary phase: ee = 97.1%, HPLC conditions: Daicel Chiralcel® OJ-H column,

250 x 4.6 mm, absorbance at 254 nm, *n*-hexane/isopropanol = 85:15, isocratic flow, flow rate 1.0 mL/min, 25 °C, t_r (major) = 17.5 min, t_r (minor) = 34.1 min.

^{1}H NMR: 300 MHz, $CDCl_3$; δ = 8.27 (d, J = 2.9 Hz, 1H), 7.88-7.78 (m, 2H), 7.56 (d, J = 8.1 Hz, 2H), 7.21-7.12 (m, 4H), 6.92 (s, 1H), 6.75 (d, J = 2.9 Hz, 1H), 2.33 (s, 3H) ppm.

^{13}C NMR: 75 MHz, $CDCl_3$; δ = 166.2, 163.7 (d, $J_{C,F}$ = 249.6 Hz, 1C), 155.2, 139.6, 132.4, 130.8, 129.8 (2C), 128.7 (2C), 128.4 (d, $J_{C,F}$ = 8.3 Hz, 2C), 127.7 (d, $J_{C,F}$ = 3.3 Hz, 1C), 116.1 (d, $J_{C,F}$ = 21.9 Hz, 2C), 108.6, 57.2, 21.3 ppm.

^{19}F NMR: 282 MHz, $CDCl_3$; δ = –111.2 (s, 1F) ppm.

IR: neat, $\tilde{\nu}$ = 2921 (m), 2851 (w), 1736 (s), 1658 (w), 1604 (m), 1549 (w), 1511 (m), 1463 (w), 1429 (w), 1403 (s), 1347 (m), 1299 (w), 1282 (w), 1235 (w), 1212 (m), 1156 (m), 1114 (w), 1088 (w), 1049 (m), 937 (m), 881 (w), 839 (m), 813 (w), 775 (m), 739 (s), 701 (m), 665 (m), 616 (m), 594 (w), 551 (w), 515 (s), 484 (m), 450 (w), 416 (w) cm^{-1}.

$[\alpha]_D^{22}$: –274.3° (c = 1.0, $CHCl_3$).

HRMS: ESI; m/z calcd. for $C_{18}H_{14}ClFN_2ONa$ $[M+Na]^+$: 351.0671, found 351.0679.

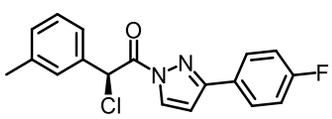

(*S*)-2-Chloro-1-(3-(4-fluorophenyl)-1*H*-pyrazol-1-yl)-2-(*m*-tolyl)ethan-1-one (97f)

Following the general procedure L using Δ-**RhNP2** as catalyst, (*S*)-**97f** (33.0 mg, 0.10 mmol, >99%) was obtained as a colorless solid. Enantiomeric excess was established by HPLC analysis on a chiral stationary phase: ee = 95.4%, HPLC conditions: Daicel Chiralcel® OJ-H column, 250 x 4.6 mm, absorbance at 254 nm, *n*-hexane/isopropanol = 85:15, isocratic flow, flow rate 1.0 mL/min, 25 °C, t_r (major) = 13.2 min, t_r (minor) = 19.1 min.

^{1}H NMR: 300 MHz, $CDCl_3$; δ = 8.27 (d, J = 2.9 Hz, 1H), 7.88-7.81 (m, 2H), 7.48-7.44 (m, 2H), 7.29-7.24 (m, 1H), 7.19-7.12 (m, 3H), 6.90 (s, 1H), 6.76 (d, J = 2.9 Hz, 1H), 2.36 (s, 3H) ppm.

^{13}C NMR: 75 MHz, $CDCl_3$; δ = 166.2, 163.7 (d, $J_{C,F}$ = 249.6 Hz, 1C), 155.2, 138.9, 135.2, 130.8, 130.3, 129.3, 128.9, 128.4 (d, $J_{C,F}$ = 8.4 Hz, 2C), 127.7 (d, $J_{C,F}$ = 3.3 Hz, 1C), 125.9, 116.1 (d, $J_{C,F}$ = 21.8 Hz, 2C), 108.6, 57.3, 21.5 ppm.

^{19}F NMR: 282 MHz, $CDCl_3$; δ = –111.2 (s, 1F) ppm.

IR: neat, $\tilde{\nu}$ = 3163 (w), 3139 (w), 3048 (w), 2921 (w), 2852 (w), 1737 (s), 1603 (m), 1548 (w), 1511 (m), 1486 (w), 1431 (m), 1400 (m), 1345 (m), 1283 (w), 1254 (w), 1216 (s), 1155 (w), 1089 (w), 1048 (m), 1012 (w), 941 (m), 917 (w), 883 (w), 843 (m), 817 (m), 774 (s), 739 (m), 691 (w), 621 (w), 598 (w), 570 (w), 547 (w), 516 (m), 489 (w), 440 (w) cm^{-1}.

$[\alpha]_D^{22}$: –247.9° (*c* = 1.0, $CHCl_3$).

HRMS: ESI; m/z calcd. for $C_{18}H_{14}ClFN_2ONa$ $[M+Na]^+$: 351.0671, found 351.0675.

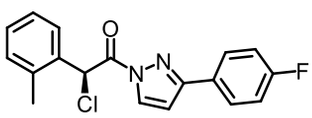

(*S*)-2-Chloro-1-(3-(4-fluorophenyl)-1*H*-pyrazol-1-yl)-2-(*o*-tolyl)ethan-1-one (97g)

Following the general procedure L using Δ-**RhNP2** as catalyst, (*S*)-**97g** (33.1 mg, 0.10 mmol, >99%) was obtained as a colorless solid. Enantiomeric excess was established by HPLC analysis on a chiral stationary phase: ee = 97.5%, HPLC conditions: Daicel Chiralcel® OJ-H column, 250 x 4.6 mm, absorbance at 254 nm, *n*-hexane/isopropanol = 85:15, isocratic flow, flow rate 1.0 mL/min, 25 °C, t_r (major) = 12.3 min, t_r (minor) = 31.2 min.

^{1}H NMR: 300 MHz, $CDCl_3$; δ = 8.30 (d, *J* = 2.9 Hz, 1H), 7.78-7.73 (m, 2H), 7.60-7.58 (m, 1H), 7.24-7.19 (m, 3H), 7.16-7.10 (m, 3H), 6.74 (d, *J* = 2.9 Hz, 1H), 2.68 (s, 3H) ppm.

^{13}C NMR: 75 MHz, $CDCl_3$; δ = 166.4, 163.7 (d, $J_{C,F}$ = 249.5 Hz, 1C), 155.3, 136.5, 134.2, 131.0, 130.8, 129.6, 128.3 (d, $J_{C,F}$ = 8.3 Hz, 2C), 128.1, 127.7 (d, $J_{C,F}$ = 3.3 Hz, 1C), 127.1, 116.1 (d, $J_{C,F}$ = 21.9 Hz, 2C), 108.5, 54.8, 19.4 ppm.

^{19}F NMR: 282 MHz, $CDCl_3$; δ = –111.2 (s, 1F) ppm.

IR: neat, $\tilde{\nu}$ = 2919 (w), 2850 (w), 1739 (s), 1604 (m), 1548 (w), 1511 (m), 1464 (w), 1430 (w), 1401 (m), 1345 (s), 1318 (w), 1284 (w), 1231 (m), 1198 (w), 1174 (w), 1155 (w), 1089 (m), 1048 (m), 1014 (w), 941 (m), 838 (m), 820 (w), 773 (m), 740 (s), 708 (w), 680 (w), 622 (m), 598 (w), 580 (w), 558 (w), 516 (w), 494 (w), 454 (w) cm^{-1}.

$[\alpha]_D^{22}$: –138.1° (*c* = 1.0, $CHCl_3$).

HRMS: ESI; m/z calcd. for $C_{18}H_{14}ClFN_2ONa$ $[M+Na]^+$: 351.0671, found 351.0675.

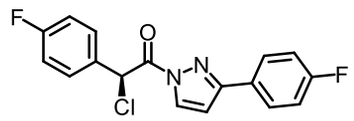

(*S*)-2-Chloro-2-(4-fluorophenyl)-1-(3-(4-fluorophenyl)-1*H*-pyrazol-1-yl)ethan-1-one (97h)

Following the general procedure L using Δ-**RhNP2** as catalyst, (*S*)-**97h** (31.4 mg, 94.4 µmol, 94%) was obtained as a colorless solid. Enantiomeric excess was established by HPLC analysis on a chiral stationary phase: ee = 91.1%, HPLC conditions: Daicel Chiralcel® OJ-H column, 250 x 4.6 mm, absorbance at 254 nm, *n*-hexane/isopropanol = 85:15, isocratic flow, flow rate 1.0 mL/min, 25 °C, t_r (major) = 16.0 min, t_r (minor) = 27.8 min.

^{1}H NMR: 300 MHz, $CDCl_3$; δ = 8.27 (d, J = 2.9 Hz, 1H), 7.87-7.80 (m, 2H), 7.69-7.63 (m, 2H), 7.20-7.12 (m, 2H), 7.11-7.03 (m, 2H), 6.93 (s, 1H), 6.77 (d, J = 2.9 Hz, 1H) ppm.

^{13}C NMR: 75 MHz, $CDCl_3$; δ = 166.0, 163.8 (d, $J_{C,F}$ = 249.8 Hz, 1C), 163.3 (d, $J_{C,F}$ = 249.5 Hz, 1C), 155.4, 131.3 (d, $J_{C,F}$ = 3.4 Hz, 1C), 130.9, 130.8, 130.7, 128.4 (d, $J_{C,F}$ = 8.5 Hz, 2C), 127.6 (d, $J_{C,F}$ = 3.3 Hz, 1C), 116.1 (d, $J_{C,F}$ = 21.9 Hz, 4C), 108.8, 56.3 ppm.

^{19}F NMR: 282 MHz, $CDCl_3$; δ = –111.0 (s, 1F), –111.4 (s, 1F) ppm.

IR: neat, $\tilde{\nu}$ = 3166 (w), 2921 (m), 2852 (w), 1740 (s), 1601 (m), 1551 (w), 1509 (s), 1463 (w), 1433 (m), 1402 (m), 1348 (m), 1291 (w), 1222 (s), 1157 (m), 1088 (w), 1049 (m), 1013 (w), 950 (w), 931 (m), 840 (m), 799 (m), 757 (s), 703 (w), 685 (w), 637 (w), 619 (m), 594 (w), 552 (w), 519 (m), 496 (s), 448 (w), 412 (w) cm^{-1}.

$[\alpha]_D^{22}$: –212.7° (c = 1.0, $CHCl_3$).

HRMS: ESI; m/z calcd. for $C_{17}H_{11}ClF_2N_2ONa$ $[M+Na]^+$: 355.0420, found 355.0427.

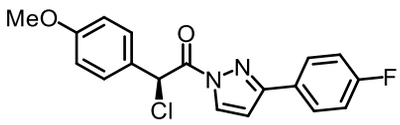

(*S*)-2-Chloro-1-(3-(4-fluorophenyl)-1*H*-pyrazol-1-yl)-2-(4-methoxyphenyl)ethan-1-one (97i)

Following the general procedure L using Δ-**RhNP2** as catalyst, (*S*)-**97i** (33.5 mg, 97.2 µmol, 97%) was obtained as a colorless solid. Performed with 1.3 equiv. TfCl. Enantiomeric excess was established by HPLC analysis on a chiral stationary phase: ee = 83.8%, HPLC conditions: Daicel Chiralcel® OJ-H column, 250 x 4.6 mm, absorbance at 254 nm, *n*-hexane/isopropanol = 85:15, isocratic flow, flow rate 1.0 mL/min, 25 °C, t_r (major) = 34.1 min, t_r (minor) = 59.7 min.

^{1}H NMR: 300 MHz, $CDCl_3$; δ = 8.27 (d, J = 2.9 Hz, 1H), 7.87-7.82 (m, 2H), 7.59 (d, J = 8.7 Hz, 2H), 7.15 (t, J = 8.6 Hz, 2H), 6.91-6.88 (m, 3H), 6.75 (d, J = 2.9 Hz, 1H), 3.79 (s, 3H) ppm.

^{13}C NMR: 75 MHz, $CDCl_3$; δ = 166.2, 163.7 (d, $J_{C,F}$ = 249.4 Hz, 1C), 160.6, 155.2, 130.8, 130.2 (2C), 128.4 (d, $J_{C,F}$ = 8.3 Hz, 2C), 127.7 (d, $J_{C,F}$ = 3.2 Hz, 1C), 127.3, 116.1 (d, $J_{C,F}$ = 21.9 Hz, 2C), 114.5 (2C), 108.6, 57.0, 55.4 ppm.

^{19}F NMR: 282 MHz, $CDCl_3$; δ = –111.2 (s, 1F) ppm.

IR: neat, $\tilde{\nu}$ = 3171 (w), 3128 (w), 3005 (w), 2920 (m), 2850 (w), 1727 (s), 1657 (w), 1604 (s), 1510 (s), 1459 (w), 1433 (m), 1404 (m), 1350 (m), 1300 (w), 1261 (m), 1226 (s), 1177 (m), 1160 (w), 1108 (w), 1088 (m), 1048 (m), 1025 (m), 928 (m), 859 (w), 838 (s), 811 (w), 774 (m), 747 (s), 706 (m), 684 (w), 638 (w), 619 (m), 593 (w), 546 (m), 514 (s), 450 (w), 416 (w) cm^{-1}.

$[\alpha]_D^{22}$: –260.7° (c = 1.0, $CHCl_3$).

HRMS: ESI; m/z calcd. for $C_{18}H_{14}ClFN_2O_2Na$ $[M+Na]^+$: 367.0620, found 367.0642.

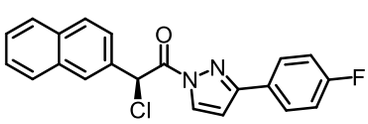

(*S*)-2-Chloro-1-(3-(4-fluorophenyl)-1*H*-pyrazol-1-yl)-2-(naphthalen-2-yl)ethan-1-one (97j)

Following the general procedure L using Δ-**RhNP2** as catalyst, (*S*)-**97j** (34.3 mg, 94.0 µmol, 94%) was obtained as a colorless solid. Enantiomeric excess was established by HPLC analysis on a chiral stationary phase: ee = 90.2%, HPLC conditions: Daicel Chiralcel® OD-H column, 250 x 4.6 mm, absorbance at 254 nm, *n*-hexane/isopropanol = 99.4:0.6, isocratic flow, flow rate 1.0 mL/min, 25 °C, t_r (minor) = 23.8 min, t_r (major) = 25.3 min.

^{1}H NMR: 300 MHz, $CDCl_3$; δ = 8.29 (d, J = 2.9 Hz, 1H), 8.11 (s, 1H), 7.89-7.77 (m, 6H), 7.52-7.47 (m, 2H), 7.16 (t, J = 8.7 Hz, 2H), 7.11 (s, 1H), 6.75 (d, J = 2.9 Hz, 1H) ppm.

^{13}C NMR: 75 MHz, $CDCl_3$; δ = 166.0, 163.7 (d, $J_{C,F}$ = 249.4 Hz, 1C), 155.3, 133.7, 133.2, 132.6, 130.8, 129.1, 128.6, 128.5, 128.4, 128.4, 127.9, 127.7 (d, $J_{C,F}$ = 3.2 Hz, 1C), 127.2, 126.8, 125.7, 116.1 (d, $J_{C,F}$ = 21.8 Hz, 2C), 108.7, 57.5 ppm.

^{19}F NMR: 282 MHz, $CDCl_3$; δ = –111.2 (s, 1F) ppm.

IR: neat, $\tilde{\nu}$ = 3158 (w), 3131 (w), 3051 (w), 3015 (w), 2921 (w), 2851 (w), 1729 (s), 1602 (m), 1551 (w), 1513 (s), 1464 (w), 1432 (m), 1406 (s), 1349 (s), 1296 (w), 1220 (s), 1156 (m), 1124 (w), 1105 (w), 1089 (m), 1050 (m), 935 (m), 895 (w), 864 (w), 841 (m), 795 (m), 778 (w), 751 (s), 681 (m), 639 (w), 619 (m), 592 (w), 554 (w), 505 (w), 473 (m), 450 (w) cm^{-1}.

$[\alpha]_D^{22}$: –314.3° (c = 0.82, $CHCl_3$).

HRMS: ESI; m/z calcd. for $C_{21}H_{14}ClFN_2ONa$ $[M+Na]^+$: 387.0671, found 387.0675.

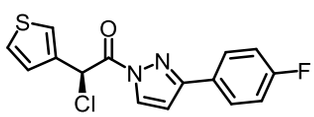

(*S*)-2-Chloro-1-(3-(4-fluorophenyl)-1*H*-pyrazol-1-yl)-2-(thiophen-3-yl)ethan-1-one (97k)

Following the general procedure L using Δ-**RhNP2** as catalyst, (*S*)-**97k** (30.7 mg, 95.7 µmol, 96%) was obtained as a colorless solid. Performed with 1.3 equiv. TfCl. Enantiomeric excess was established by HPLC analysis on a chiral stationary phase: ee = 90.1%, HPLC conditions: Daicel Chiralcel® OD-H column, 250 x 4.6 mm, absorbance at 254 nm, *n*-hexane/isopropanol = 99:1, isocratic flow, flow rate 1.0 mL/min, 25 °C, t_r (major) = 13.8 min, t_r (minor) = 15.7 min.

^{1}H NMR: 300 MHz, $CDCl_3$; δ = 8.29 (d, J = 2.9 Hz, 1H), 7.90-7.83 (m, 2H), 7.59-7.58 (m, 1H), 7.38-7.32 (m, 2H), 7.20-7.11 (m, 2H), 7.07 (s, 1H), 6.79 (d, J = 2.9 Hz, 1H) ppm.

^{13}C NMR: 75 MHz, $CDCl_3$; δ = 165.8, 163.8 (d, $J_{C,F}$ = 249.6 Hz, 1C), 155.4, 135.3, 130.9, 128.5 (d, $J_{C,F}$ = 8.4 Hz, 2C), 127.6 (d, $J_{C,F}$ = 3.3 Hz, 1C), 127.4, 126.9, 126.0, 116.1 (d, $J_{C,F}$ = 21.9 Hz, 2C), 108.9, 52.1 ppm.

^{19}F NMR: 282 MHz, $CDCl_3$; δ = –111.1 (s, 1F) ppm.

IR: neat, $\tilde{\nu}$ = 3142 (w), 3122 (w), 2919 (w), 2850 (w), 1730 (s), 1605 (m), 1549 (w), 1514 (m), 1464 (w), 1431 (m), 1404 (m), 1352 (s), 1289 (w), 1260 (w), 1217 (m),

1156 (m), 1091 (w), 1050 (m), 937 (m), 880 (w), 838 (s), 813 (w), 770 (s), 734 (m), 700 (w), 683 (w), 655 (w), 624 (m), 598 (w), 568 (w), 548 (w), 514 (m), 448 (w) cm^{-1}.

$[\alpha]_D^{22}$: –192.8° (*c* = 1.0, $CHCl_3$).

HRMS: ESI; m/z calcd. for $C_{15}H_{10}ClFN_2OSNa$ $[M+Na]^+$: 343.0079, found 343.0082.

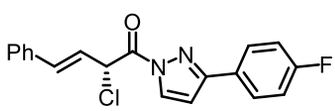

(*R*,*E*)-2-Chloro-1-(3-(4-fluorophenyl)-1*H*-pyrazol-1-yl)-4-phenylbut-3-en-1-one (97m)

Following the general procedure L using Λ-**RhNP2** as catalyst, (*R*)-**97m** (99% conversion, 53% NMR yield) was formed along with considerable amounts of *α,α*-dichlorinated byproduct and other impurities. After 4 h stirring at room temperature, the reaction mixture was diluted with CH_2Cl_2 and filtered through a short plug of celite. The solvent was removed under reduced pressure and 1,1,2,2-tetrachloroethane was added as internal standard to determine conversion and NMR yield by integration of baseline separated signals in the ^{1}H NMR. Pure (*R*)-**97m** could not be isolated due to similar R_f values of the byproducts in addition to degradation of the product upon prolonged exposure to silica gel. Enantiomeric excess of the crude product was established by HPLC analysis on a chiral stationary phase: ee = 24.7%, HPLC conditions: Daicel Chiralcel® OJ-H column, 250 x 4.6 mm, absorbance at 254 nm, *n*-hexane/isopropanol = 80:20, isocratic flow, flow rate 1.0 mL/min, 25 °C, t_r (major) = 34.0 min, t_r (minor) = 41.7 min.

HRMS: ESI; m/z calcd. for $C_{19}H_{14}ClFN_2ONa$ $[M+Na]^+$: 363.0671, found 363.0675.

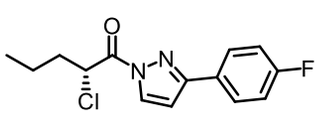

(*R*)-2-Chloro-1-(3-(4-fluorophenyl)-1*H*-pyrazol-1-yl)pentan-1-one (97n)

Following the general procedure L with some modifications, substrate **97n** (24.6 mg, 0.10 mmol, 1.00 equiv.) was converted using 2.00 equiv. TfCl (20 v/v% in acetone HPLC Grade, 106.5 µL, 0.20 mmol), 3 mol% catalyst and 1.10 equiv. of K_2CO_3 (15.2 mg, 1.10 mmol) as base. The resulting reaction mixture was stirred for the indicated time at room temperature, before it was diluted with CH_2Cl_2 and filtered through a short plug of celite. The solvent was removed under

reduced pressure and 1,1,2,2-tetrachloroethane was added as internal standard to determine conversion and NMR yield by integration of baseline separated signals in the ^{1}H NMR.

With Δ-**RhNP2** almost no conversion (<5%) was observed after 16 h reaction time and only trace amounts of product were formed.

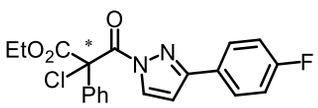

Ethyl 2-chloro-3-(3-(4-fluorophenyl)-1*H*-pyrazol-1-yl)-3-oxo-2-phenylpropanoate (97o)

Following the general procedure L with some modifications, substrate **92o** (35.2 mg, 0.10 mmol, 1.00 equiv.) was converted using 2.00 equiv. TfCl (20 v/v% in acetone HPLC Grade, 106.5 µL, 0.20 mmol), 3 mol% catalyst and 1.10 equiv. of K_2CO_3 (15.2 mg, 1.10 mmol) as base. The resulting reaction mixture was stirred for 16 h at room temperature in dry acetone (0.40 mL).

With Δ-**RhNP2**, (*S*)-**97o** (57% conversion, 21.0 mg, 54.3 µmol, 54%) was obtained as a colorless solid after regular silica gel column chromatography (*n*-pentane/CH_2Cl_2 1:1). Enantiomeric excess was established by HPLC analysis on a chiral stationary phase: ee = 36.3%, HPLC conditions: Daicel Chiralcel® OD-H column, 250 x 4.6 mm, absorbance at 254 nm, *n*-hexane/isopropanol = 99:1, isocratic flow, flow rate 1.0 mL/min, 25 °C, t_r (minor) = 13.5 min, t_r (major) = 14.8 min.

With Λ-**RhS**, (*R*)-**97o** (46% conversion, 17.2 mg, 44.5 µmol, 45%) was obtained as a colorless solid after regular silica gel column chromatography (*n*-pentane/CH_2Cl_2 1:1). Enantiomeric excess was established by HPLC analysis on a chiral stationary phase: ee = 76.9%, HPLC conditions: Daicel Chiralcel® OD-H column, 250 x 4.6 mm, absorbance at 254 nm, *n*-hexane/isopropanol = 99:1, isocratic flow, flow rate 1.0 mL/min, 25 °C, t_r (major) = 13.4 min, t_r (minor) = 14.8 min.

Analytical data of (*R*)-**97o**:

^{1}H NMR: 500 MHz, $CDCl_3$; δ = 8.28 (d, J = 2.9 Hz, 1H), 7.83-7.80 (m, 2H), 7.80-7.76 (m, 2H), 7.41-7.35 (m, 3H), 7.15-7.10 (m, 2H), 6.73 (d, J = 3.0 Hz, 1H), 4.30-420 (m, 2H), 1.09 (t, J = 7.2 Hz, 3H) ppm.

^{13}C NMR: 126 MHz, $CDCl_3$; δ = 166.0, 163.7 (d, $J_{C,F}$ = 249.6 Hz, 1C), 163.7, 154.4, 134.4, 131.3, 129.4, 128.8 (2C), 128.3 (d, $J_{C,F}$ = 8.1 Hz, 2C), 128.3 (2C), 127.4 (d, $J_{C,F}$ = 3.5 Hz, 1C), 116.1 (d, $J_{C,F}$ = 21.9 Hz, 2C), 107.5, 72.0, 63.1, 13.8 ppm.

^{19}F NMR: 282 MHz, $CDCl_3$; δ = –111.1 (s, 1F) ppm.

IR: neat, $\tilde{\nu}$ = 3159 (w), 2974 (w), 2923 (w), 2852 (w), 1761 (m), 1732 (s), 1605 (m), 1548 (w), 1512 (m), 1431 (m), 1401 (s), 1346 (s), 1288 (w), 1260 (m), 1231 (s), 1172 (m), 1155 (w), 1096 (m), 1048 (m), 1027 (m), 994 (w), 960 (w), 942 (w), 914 (w), 856 (w), 838 (m), 808 (s), 761 (s), 716 (m), 682 (s), 647 (w), 625 (w), 607 (m), 575 (w), 512 (w), 495 (m), 462 (w), 435 (w) cm^{-1}.

$[\alpha]_D^{22}$: –23.8° (*c* = 1.0, $CHCl_3$).

HRMS: ESI; m/z calcd. for $C_{20}H_{16}ClFN_2O_3Na$ $[M+Na]^+$: 409.0731, found 409.0737.

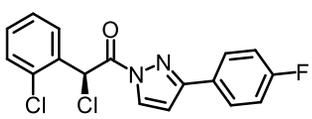

(*S*)-2-Chloro-2-(2-chlorophenyl)-1-(3-(4-fluorophenyl)-1*H*-pyrazol-1-yl)ethan-1-one (97p)

Following the general procedure L using Δ-**RhNP2** as catalyst, (*S*)-**97p** (34.9 mg, 99.9 µmol, >99%) was obtained as a colorless solid. Enantiomeric excess was established by HPLC analysis on a chiral stationary phase: ee = 90.5%, HPLC conditions: Daicel Chiralcel® OD-H column, 250 x 4.6 mm, absorbance at 254 nm, *n*-hexane/isopropanol = 99:1, isocratic flow, flow rate 1.0 mL/min, 25 °C, t_r (major) = 11.0 min, t_r (minor) = 29.3 min.

^{1}H NMR: 300 MHz, $CDCl_3$; δ = 8.21 (d, *J* = 2.9 Hz, 1H), 7.80-7.73 (m, 2H), 7.64-7.58 (m, 1H), 7.39-7.33 (m, 1H), 7.25-7.18 (m, 3H), 7.09-7.01 (m, 2H), 6.68 (d, *J* = 2.9 Hz, 1H) ppm.

^{13}C NMR: 75 MHz, $CDCl_3$; δ = 165.7, 163.7 (d, $J_{C,F}$ = 249.6 Hz, 1C), 155.3, 133.8, 133.6, 130.7 (2C), 130.0, 129.8, 128.4 (d, $J_{C,F}$ = 8.4 Hz, 2C), 127.8, 127.6 (d, $J_{C,F}$ = 3.3 Hz, 1C), 116.0 (d, $J_{C,F}$ = 21.8 Hz, 2C), 108.6, 54.5 ppm.

^{19}F NMR: 282 MHz, $CDCl_3$; δ = –111.2 (s, 1F) ppm.

IR: neat, $\tilde{\nu}$ = 3145 (w), 3126 (w), 2922 (w), 2852 (w), 1735 (s), 1606 (w), 1513 (m), 1476 (w), 1432 (m), 1402 (m), 1349 (s), 1274 (w), 1228 (s), 1206 (w), 1187 (w), 1155 (m), 1131 (w), 1089 (w), 1047 (m), 957 (w), 938 (m), 872 (w), 854 (w), 837 (m), 815 (w), 779 (w), 751 (s), 724 (w), 704 (m), 664 (w), 623 (m), 595 (w), 567 (w), 548 (w), 514 (m), 458 (w), 419 (w) cm^{-1}.

$[\alpha]_D^{22}$: –63.0° (*c* = 1.0, $CHCl_3$).

HRMS: ESI; m/z calcd. for $C_{17}H_{12}Cl_2FN_2O$ $[M+H]^+$: 349.0305, found 349.0316.

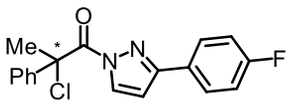

2-Chloro-1-(3-(4-fluorophenyl)-1*H*-pyrazol-1-yl)-2-phenylpropan-1-one (97q)

Following the general procedure L with some modifications, substrate **92q** (29.4 mg, 0.10 mmol, 1.00 equiv.) was converted using 2.00 equiv. TfCl (20v/v% in acetone HPLC Grade, 106.5 µL, 0.20 mmol), 3 mol% catalyst and 1.10 equiv. of K_2CO_3 (15.2 mg, 1.10 mmol) as base. The resulting reaction mixture was stirred for 16 h at room temperature in dry acetone (0.40 mL).

However, conversion could not be observed neither with *rac*-**RhNP2** nor with *rac*-**RhS**.

5.7.6 Pyrazole Cleavage

5.7.6.1 General Procedure M

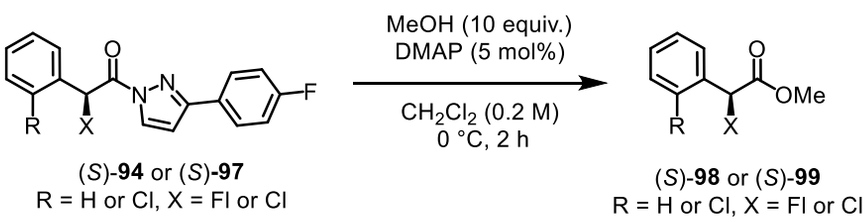

To a solution of (*S*)-**94** or (*S*)-**97** (1.00 equiv.) in CH_2Cl_2 (0.2 M) was added methanol (10.0 equiv.), followed by DMAP (0.41 M stock solution in CH_2Cl_2, 5 mol%) at 0 °C under nitrogen atmosphere. The resulting mixture was stirred for 2 h at 0 °C, before it was diluted with *n*-pentane, and the whole reaction mixture was transferred to a short silica gel column and purified (*n*-pentane/Et_2O 10:1) to give pure α-halogenated methyl esters (*S*)-**98** or (*S*)-**99**. Enantiomeric excess was established by HPLC analysis on a chiral stationary phase. The absolute configuration of (*S*)-**98d** and (*S*)-**99d** was determined by comparison of HPLC retention times and optical rotation values with published data.

5.7.6.2 Experimental Procedures and Characterization Data of Methyl Esters

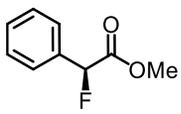

Methyl (*S*)-2-fluoro-2-phenylacetate (99d)

Following the general procedure M, (*S*)-**94d** (28.4 mg, 95.2 µmol, 1.00 equiv.) was dissolved in CH_2Cl_2 (0.48 mL). At 0 °C, methanol (38.6 µL, 0.95 mmol, 10.0 equiv.) was added, followed by DMAP (0.41 M in CH_2Cl_2, 11.6 µL, 4.76 µmol, 0.05 equiv.) and the resulting mixture was stirred for 2 h. Purification afforded (*S*)-**99d** (16.0 mg, 94.0 µmol, 99%) as a colorless oil. The absolute configuration was determined. Enantiomeric excess was established by HPLC analysis on a chiral stationary phase: ee = >99.9%, HPLC conditions: Daicel Chiralcel® OJ-H column, 250 x 4.6 mm, absorbance at 210 nm, *n*-hexane/isopropanol = 99:1, isocratic flow, flow rate 1.0 mL/min, 25 °C, t_r (minor) = 19.8 min, t_r (major) = 22.4 min. [Lit.[200] t_r (*R*) = 22.0 min, t_r (*S*) = 25.9 min]. Analytical data were consistent with reported data.[200]

^{1}H NMR: 300 MHz, $CDCl_3$; δ = 7.49-7.40 (m, 5H), 5.80 (d, *J* = 47.6 Hz, 1H), 3.79 (s, 3H) ppm.

^{19}F NMR: 282 MHz, $CDCl_3$; δ = –179.9 (s, 1F) ppm.

$[\alpha]_D^{22}$: +115.7° (*c* = 0.49, $CHCl_3$). [Lit.[217] $[\alpha]_D^{25}$ = –116° (*c* = 0.94, $CHCl_3$, 95% ee for (*R*)-enantiomer)].

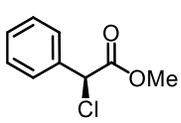

Methyl (*S*)-2-chloro-2-phenylacetate (98d)

Following the general procedure M, (*S*)-**97d** (15.0 mg, 47.7 µmol, 1.00 equiv.) was dissolved in CH_2Cl_2 (0.24 mL). At 0 °C, methanol (19.3 µL, 0.48 mmol, 10.0 equiv.) was added, followed by DMAP (0.41 M in CH_2Cl_2, 5.80 µL, 2.38 µmol, 0.05 equiv.) and the resulting mixture was stirred for 2.5 h. Purification afforded (*S*)-**98d** (9.00 mg, 47.1 µmol, 99%) as a colorless oil. The absolute configuration was determined. Enantiomeric excess was established by HPLC analysis on a chiral stationary phase: ee = 95.0%, HPLC conditions: Daicel Chiralcel® OD-H column, 250 x 4.6 mm, absorbance at 210 nm, *n*-hexane/isopropanol = 99:1, isocratic flow, flow rate

1.0 mL/min, 25 °C, t_r (minor) = 7.1 min, t_r (major) = 7.9 min. [Lit.[199] t_r (*R*) = 6.5 min, t_r (*S*) = 7.3 min]. Analytical data were consistent with reported data.[199]

^{1}H NMR: 300 MHz, $CDCl_3$; δ = 7.51-7.48 (m, 2H), 7.42-7.37 (m, 3H), 5.37 (s, 1H), 3.78 (s, 3H) ppm.

$[\alpha]_D^{22}$: +122.9° (*c* = 0.42, $CHCl_3$). [Lit.[199] $[\alpha]_D^{27}$ = –87.1° (*c* = 0.74, $CHCl_3$, 87% ee for (*R*)-enantiomer)].

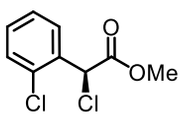

Methyl (*S*)-2-chloro-2-(2-chlorophenyl)acetate (98p)

Following the general procedure M, (*S*)-**97p** (40.0 mg, 0.12 mmol, 1.00 equiv.) was dissolved in CH_2Cl_2 (0.58 mL). At 0 °C, methanol (46.5 µL, 1.15 mmol, 10.0 equiv.) was added, followed by DMAP (0.41 M in CH_2Cl_2, 14.0 µL, 5.73 µmol, 0.05 equiv.) and the resulting mixture was stirred for 2 h. Purification afforded (*S*)-**98p** (25.0 mg, 0.11 mmol, >99%) as a colorless oil. Enantiomeric excess was established by HPLC analysis on a chiral stationary phase: ee = 90.3%, HPLC conditions: Daicel Chiralcel® OD-H column, 250 x 4.6 mm, absorbance at 210 nm, *n*-hexane/isopropanol = 98:2, isocratic flow, flow rate 1.0 mL/min, 25 °C, t_r (major) = 14.4 min, t_r (minor) = 16.3 min.

^{1}H NMR: 300 MHz, $CDCl_3$; δ = 7.66-7.61 (m, 1H), 7.42-7.38 (m, 1H), 7.37-7.27 (m, 2H), 5.89 (s, 1H), 3.80 (s, 3H) ppm.

^{13}C NMR: 75 MHz, $CDCl_3$; δ = 168.5, 134.0, 133.5, 130.6, 129.9, 129.9, 127.7, 55.5, 53.6 ppm.

IR: neat, $\tilde{\nu}$ = 2955 (w), 1751 (s), 1593 (w), 1574 (w), 1473 (w), 1436 (m), 1321 (w), 1276 (w), 1233 (w), 1193 (w), 1163 (s), 1132 (w), 1046 (w), 1000 (m), 951 (w), 906 (w), 854 (w), 799 (w), 744 (s), 697 (w), 605 (w), 572 (w), 454 (w), 425 (w) cm^{-1}.

$[\alpha]_D^{22}$: +63.0° (*c* = 0.59, $CHCl_3$).

HRMS: ESI; m/z calcd. for $C_9H_8Cl_2O_2Na$ $[M+Na]^+$: 242.9765, found 242.9766.

6. Appendix

6.1 Representative ^{1}H and ^{13}C NMR Spectra

This chapter includes all the ^{1}H and ^{13}C NMR spectra of the synthesized rhodium complexes as well as the spectroscopic data of new and unpublished compounds.

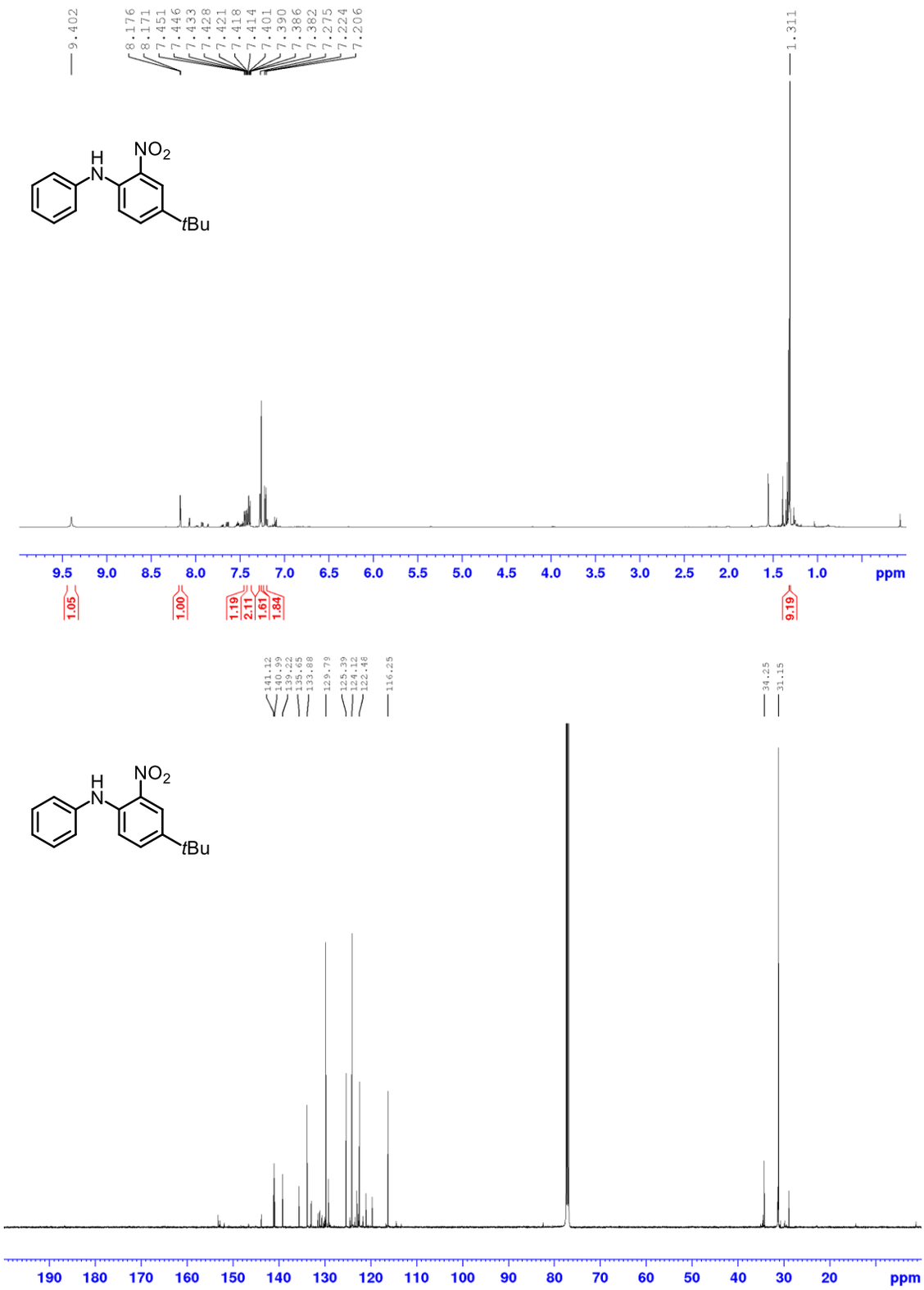

Figure 55: ^{1}H (500 MHz) and ^{13}C NMR (126 MHz) spectrum of slightly impure **45b** in $CDCl_3$.

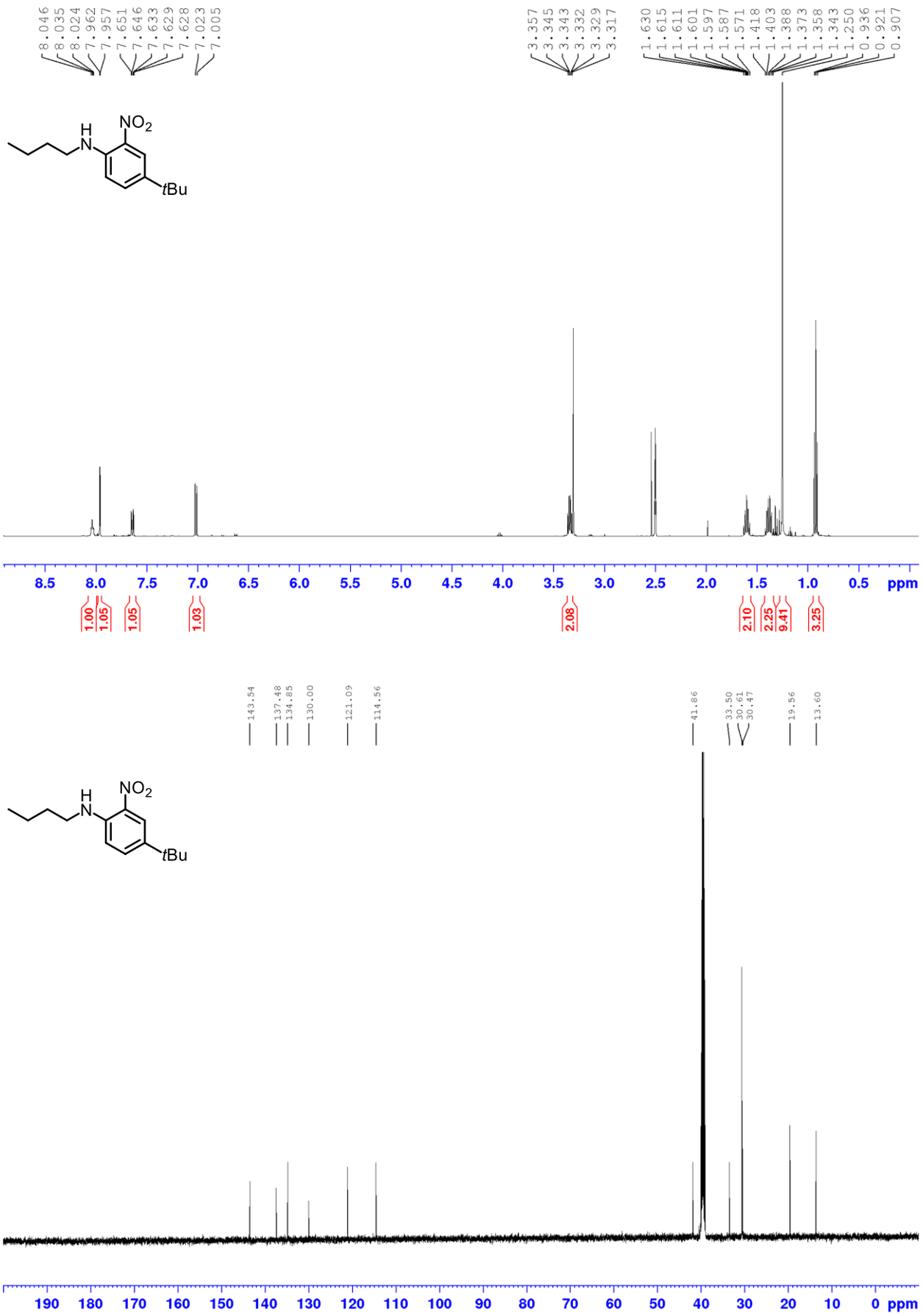

Figure 56: ^{1}H NMR (500 MHz) and ^{13}C NMR (126 MHz) spectrum of **45c** in DMSO-d_6.

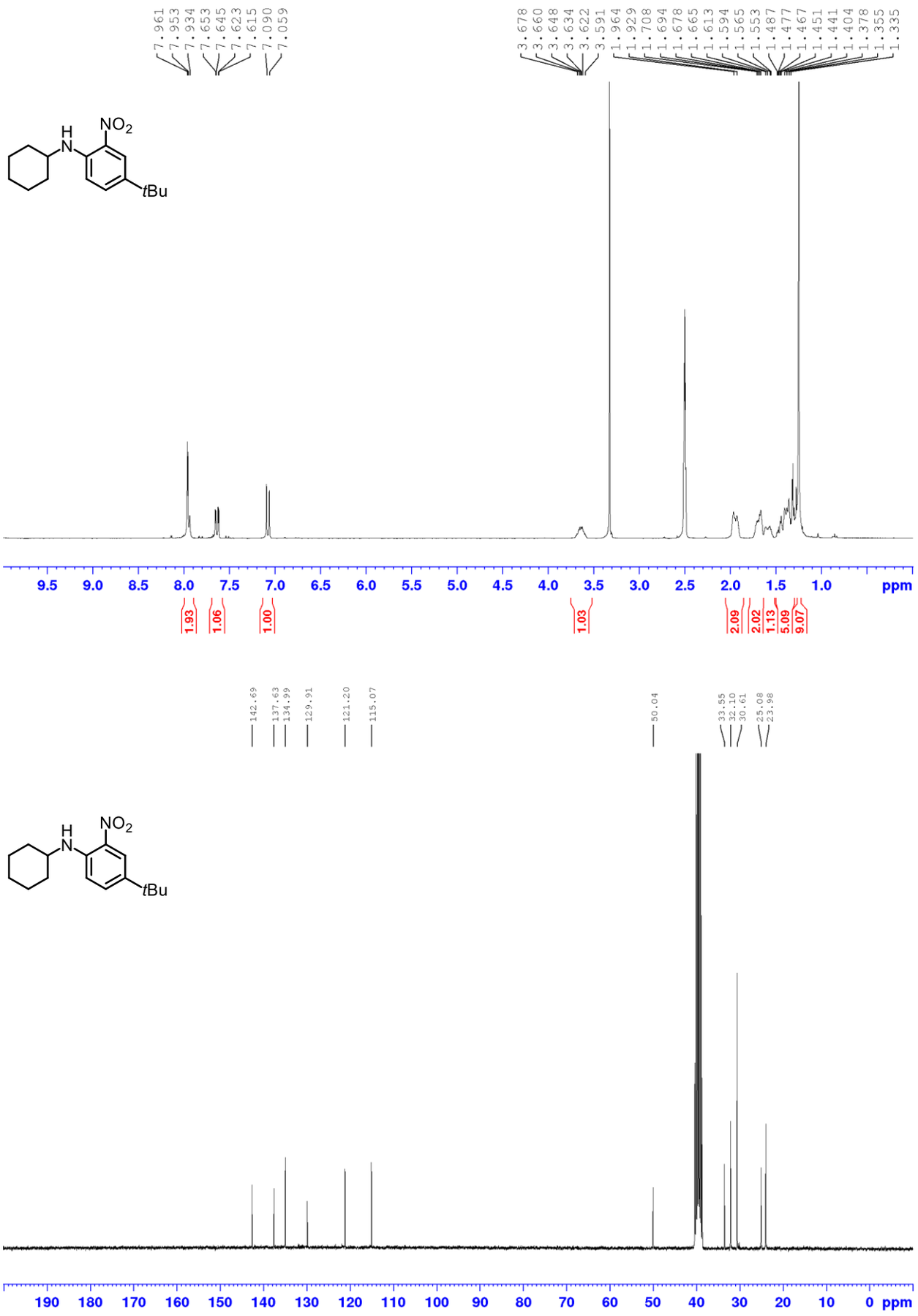

Figure 57: ^{1}H NMR (300 MHz) and ^{13}C NMR (75 MHz) spectrum of **45d** in DMSO-d_6.

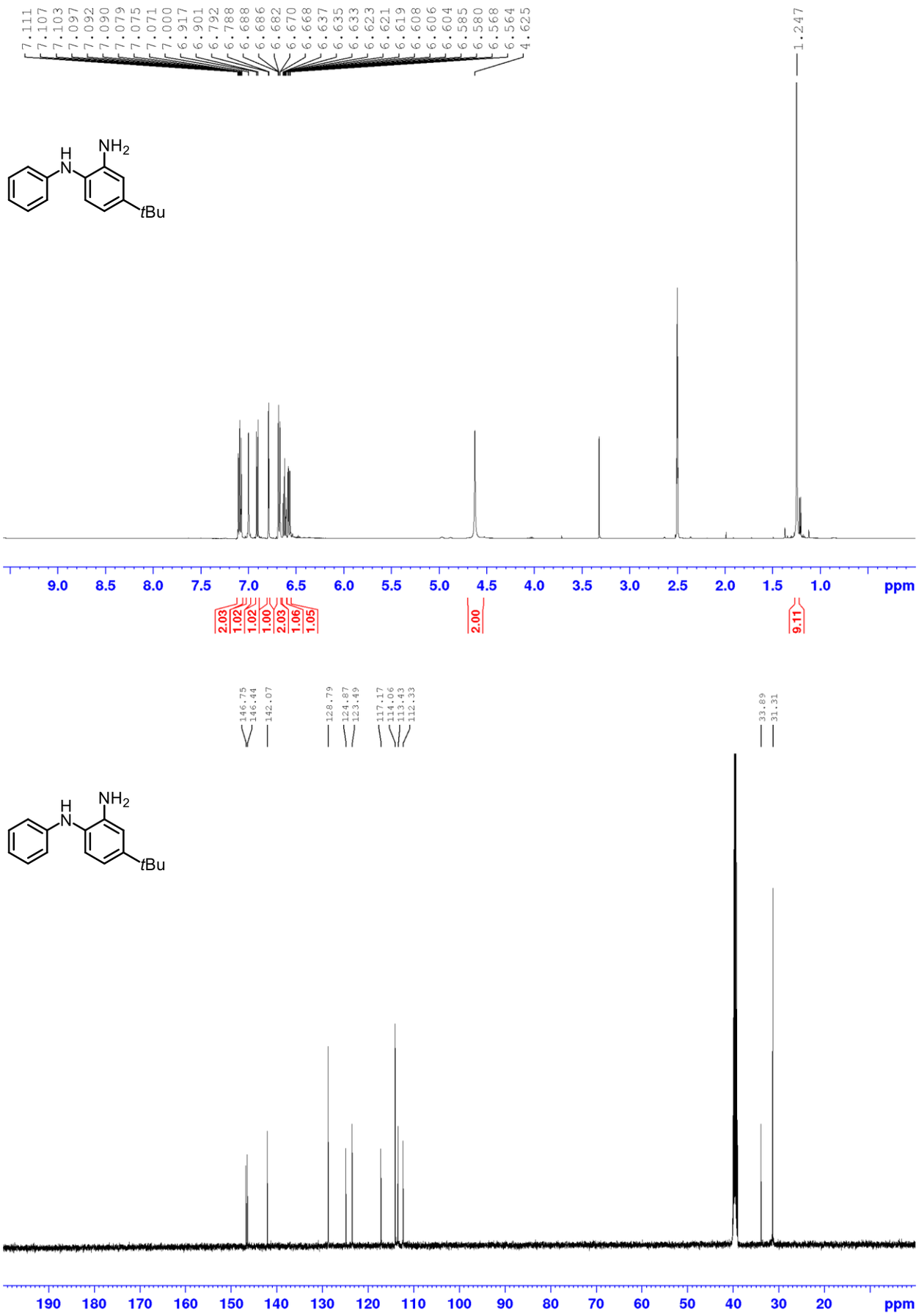

Figure 58: ^{1}H NMR (500 MHz) and ^{13}C NMR (126 MHz) spectrum of **46b** in DMSO-d_6.

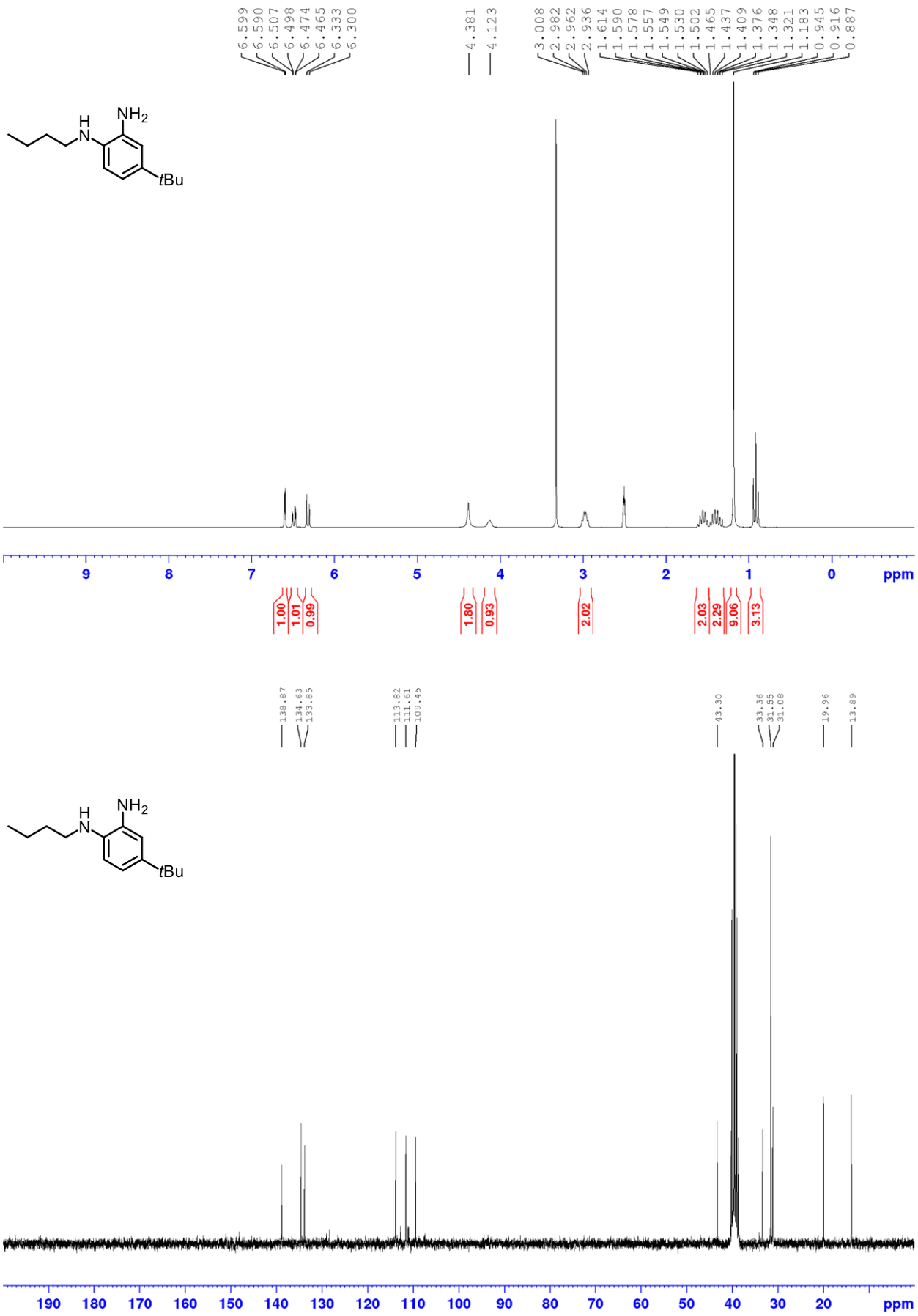

Figure 59: ^{1}H NMR (250 MHz) and ^{13}C NMR (75 MHz) spectrum of **46c** in DMSO-d_6.

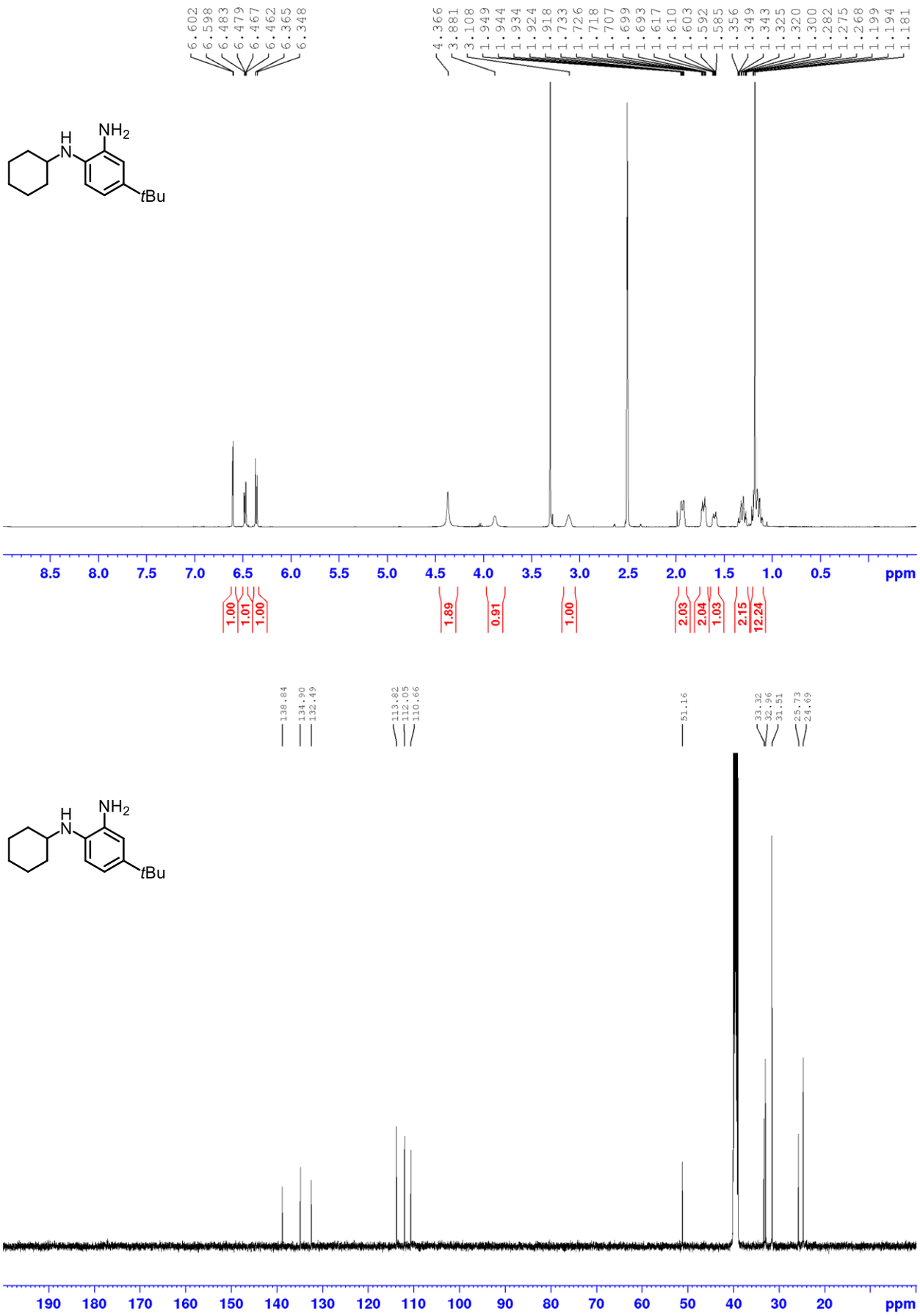

Figure 60: ^{1}H NMR (500 MHz) and ^{13}C NMR (126 MHz) spectrum of **46d** in DMSO-d_6.

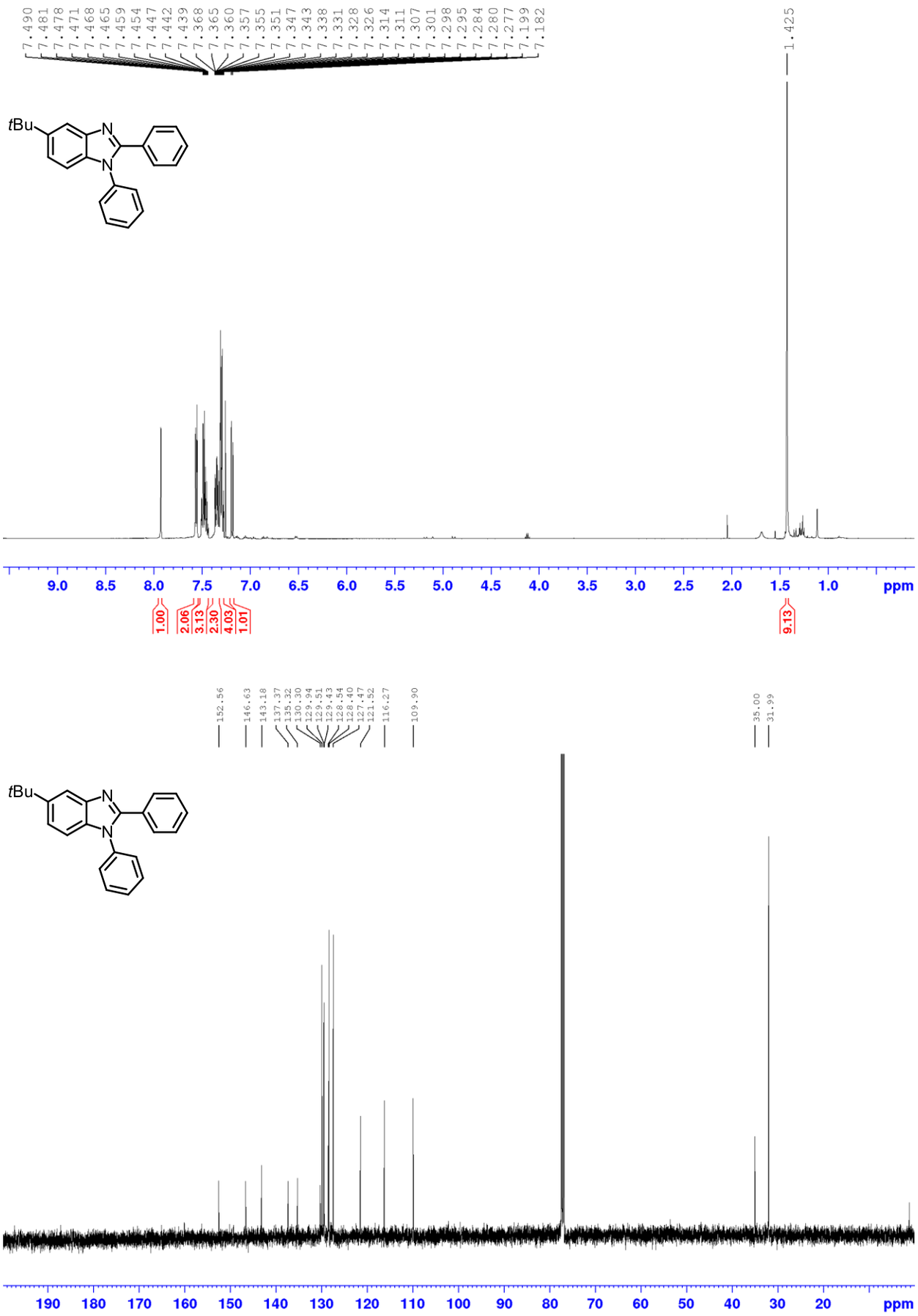

Figure 61: ^{1}H NMR (500 MHz) and ^{13}C NMR (126 MHz) spectrum of **47b** in $CDCl_3$.

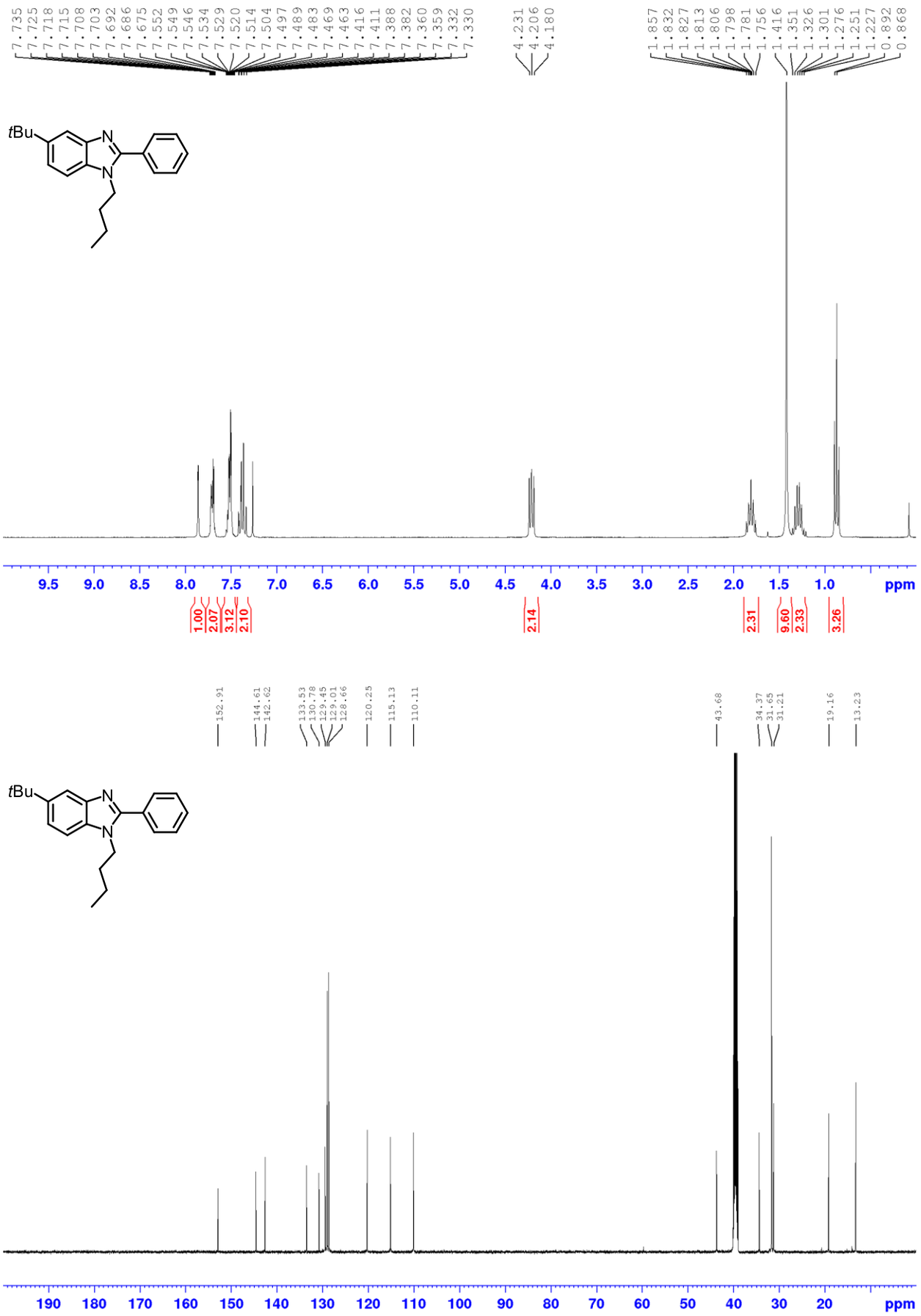

Figure 62: ^{1}H NMR (300 MHz) in $CDCl_3$ and ^{13}C NMR (126 MHz) spectrum in DMSO-d_6 of **47c**.

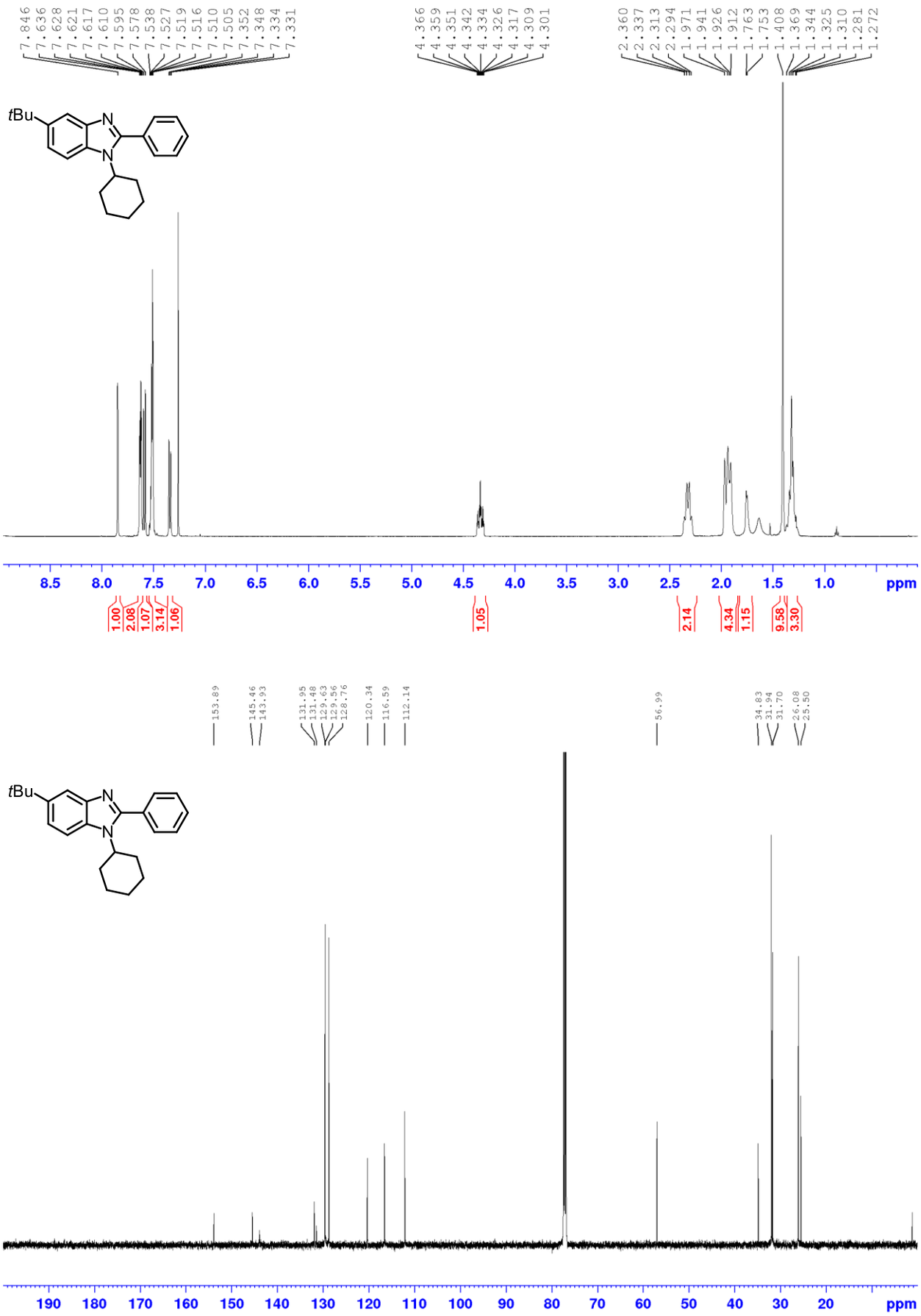

Figure 63: ^{1}H NMR (500 MHz) and ^{13}C NMR (126 MHz) spectrum of **47d** in $CDCl_3$.

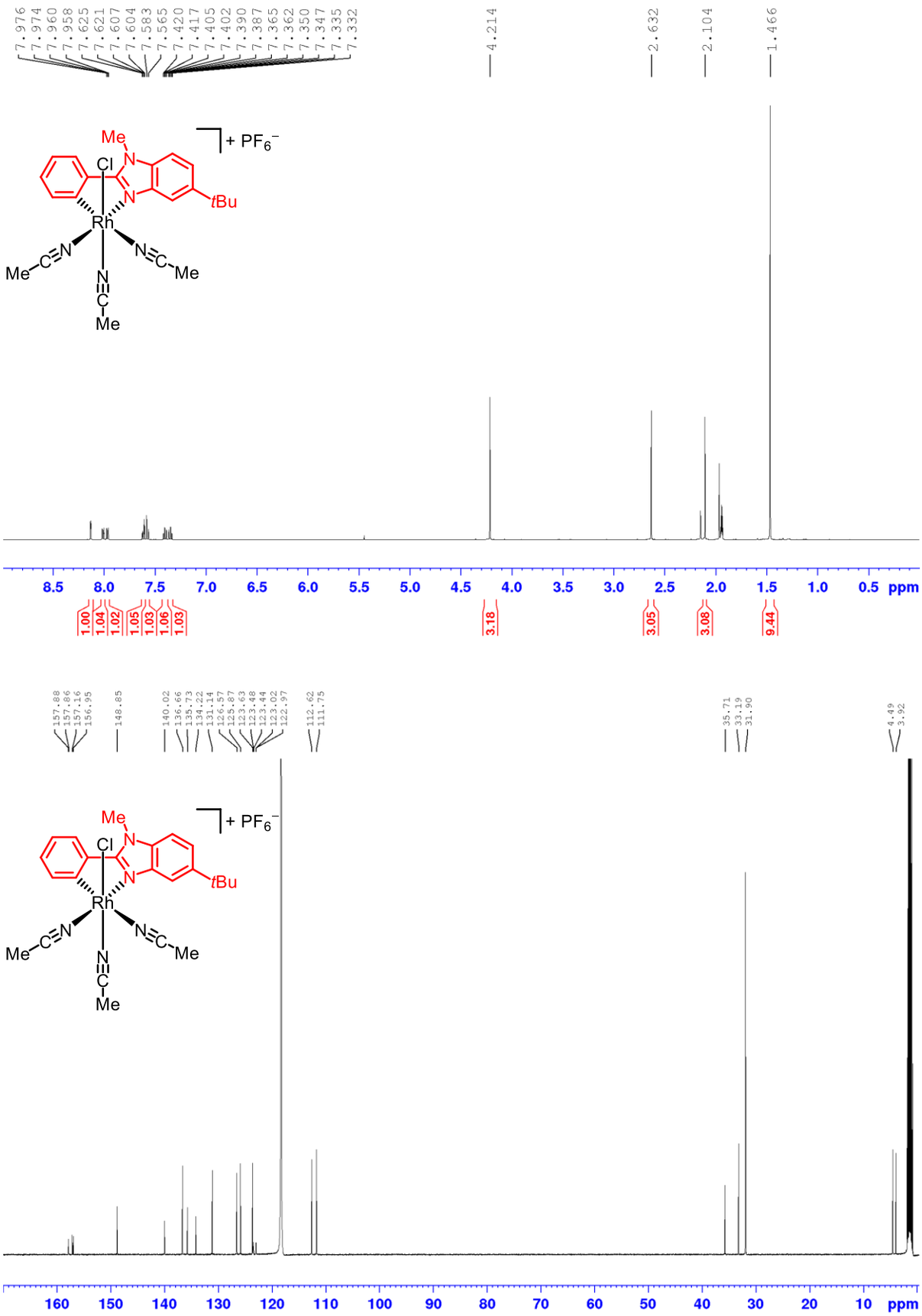

Figure 64: ^{1}H NMR (500 MHz) and ^{13}C NMR (126 MHz) spectrum of complex **48a** in CD_3CN.

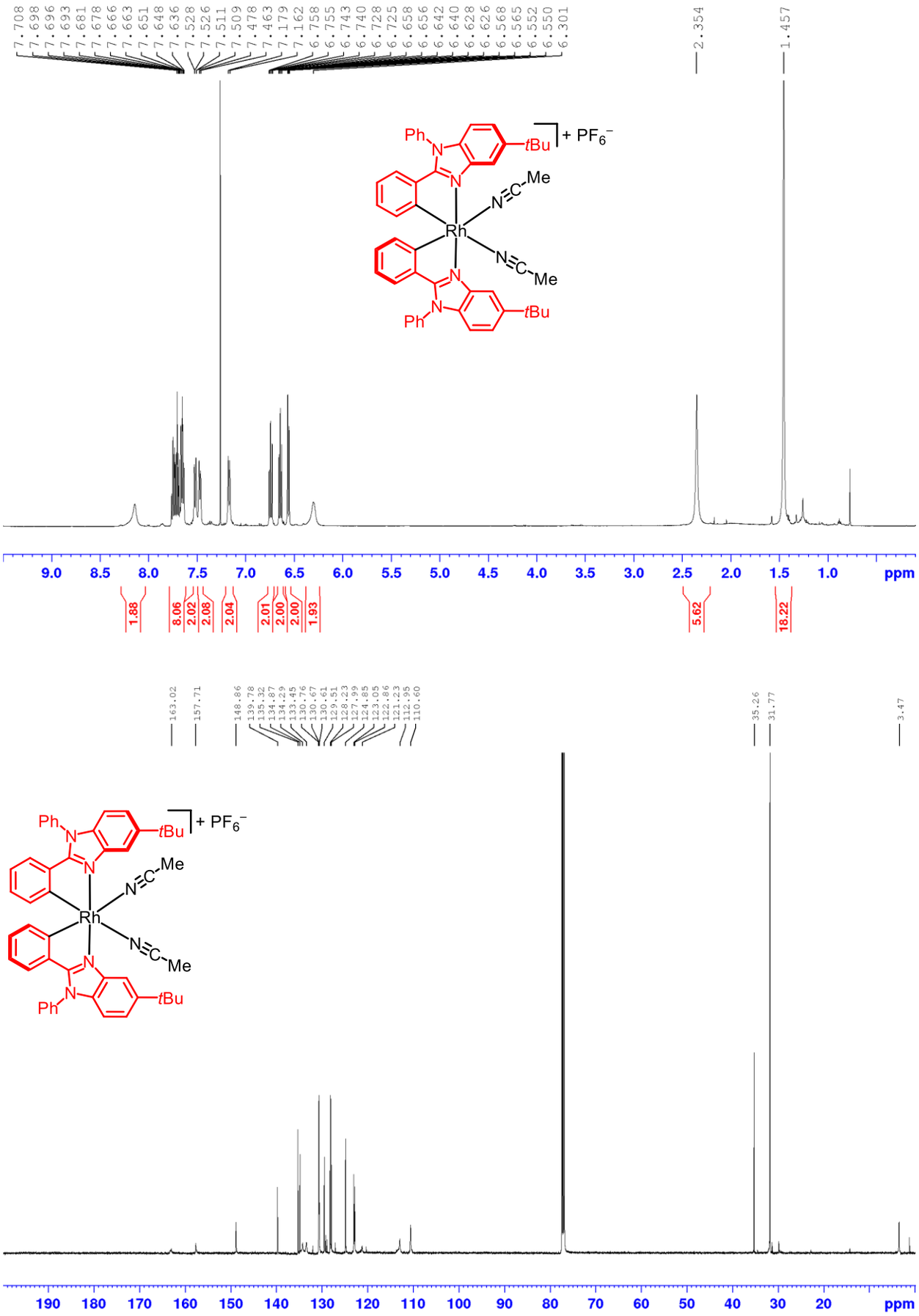

Figure 65: ^{1}H NMR (500 MHz) and ^{13}C NMR (126 MHz) spectrum of complex *rac*-**RhN2** in $CDCl_3$.

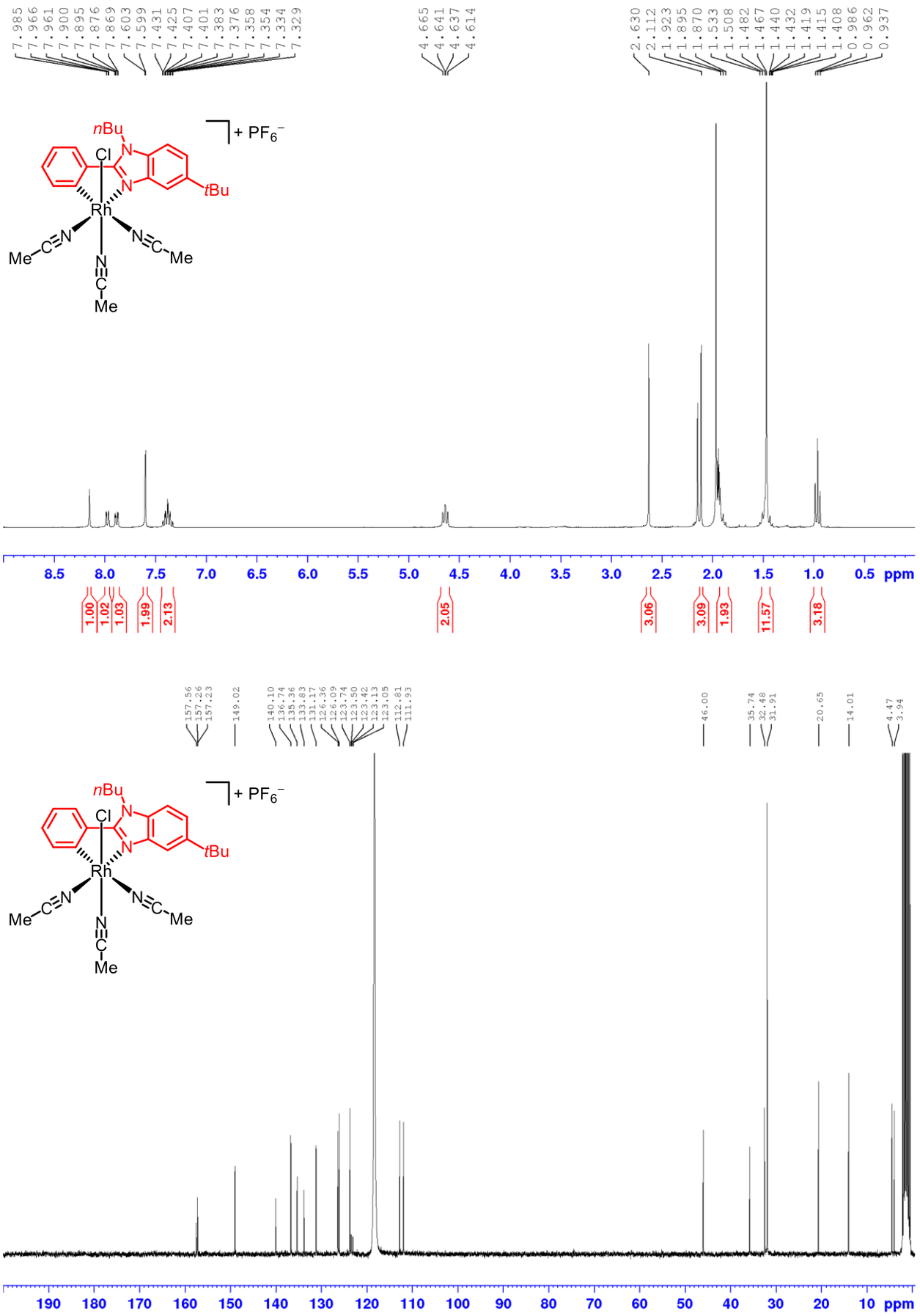

Figure 66: ^{1}H NMR (300 MHz) and ^{13}C NMR (75 MHz) spectrum of complex **48c** in CD_3CN.

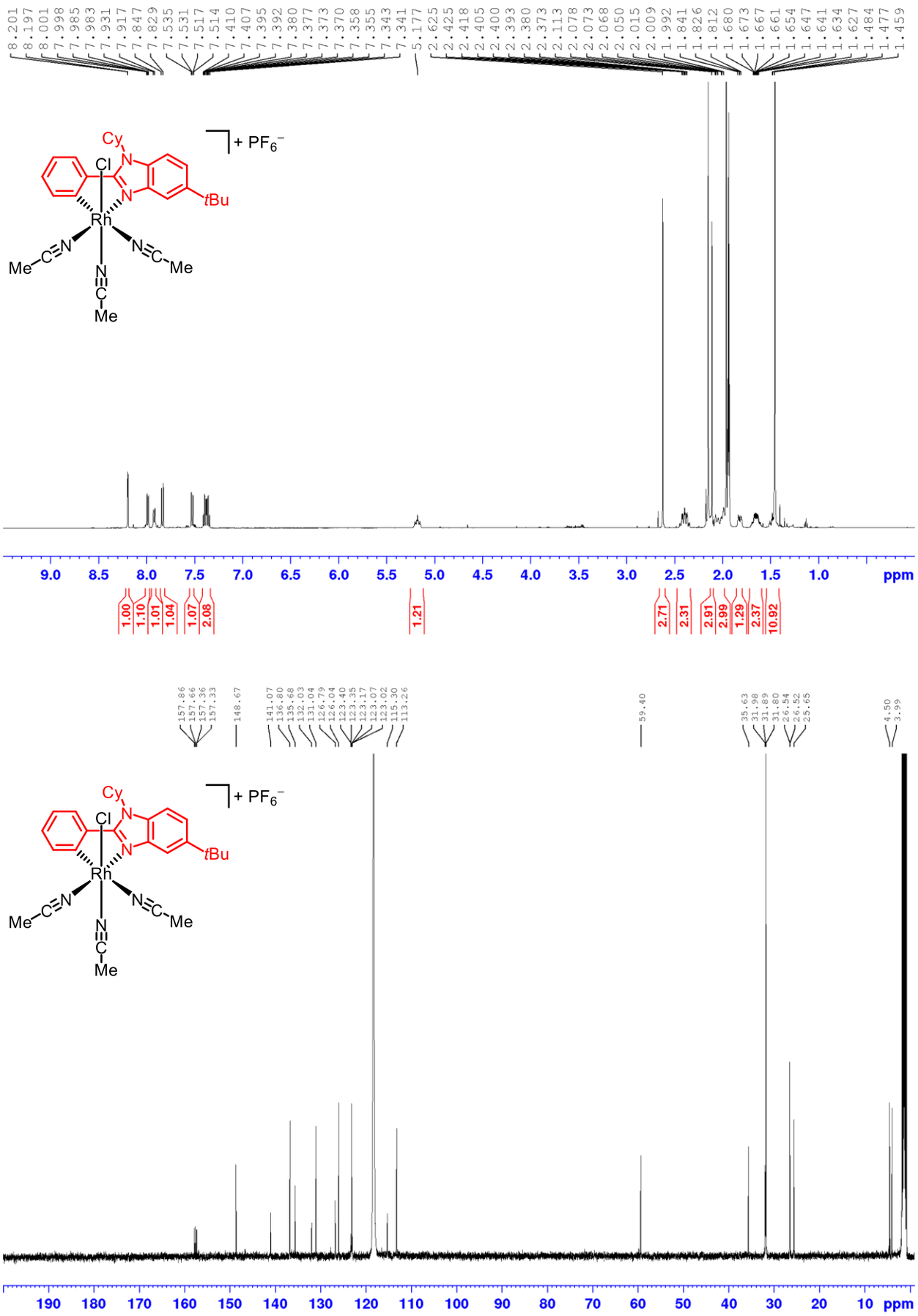

Figure 67: ^{1}H NMR (500 MHz) and ^{13}C NMR (126 MHz) spectrum of complex **48d** in CD_3CN.

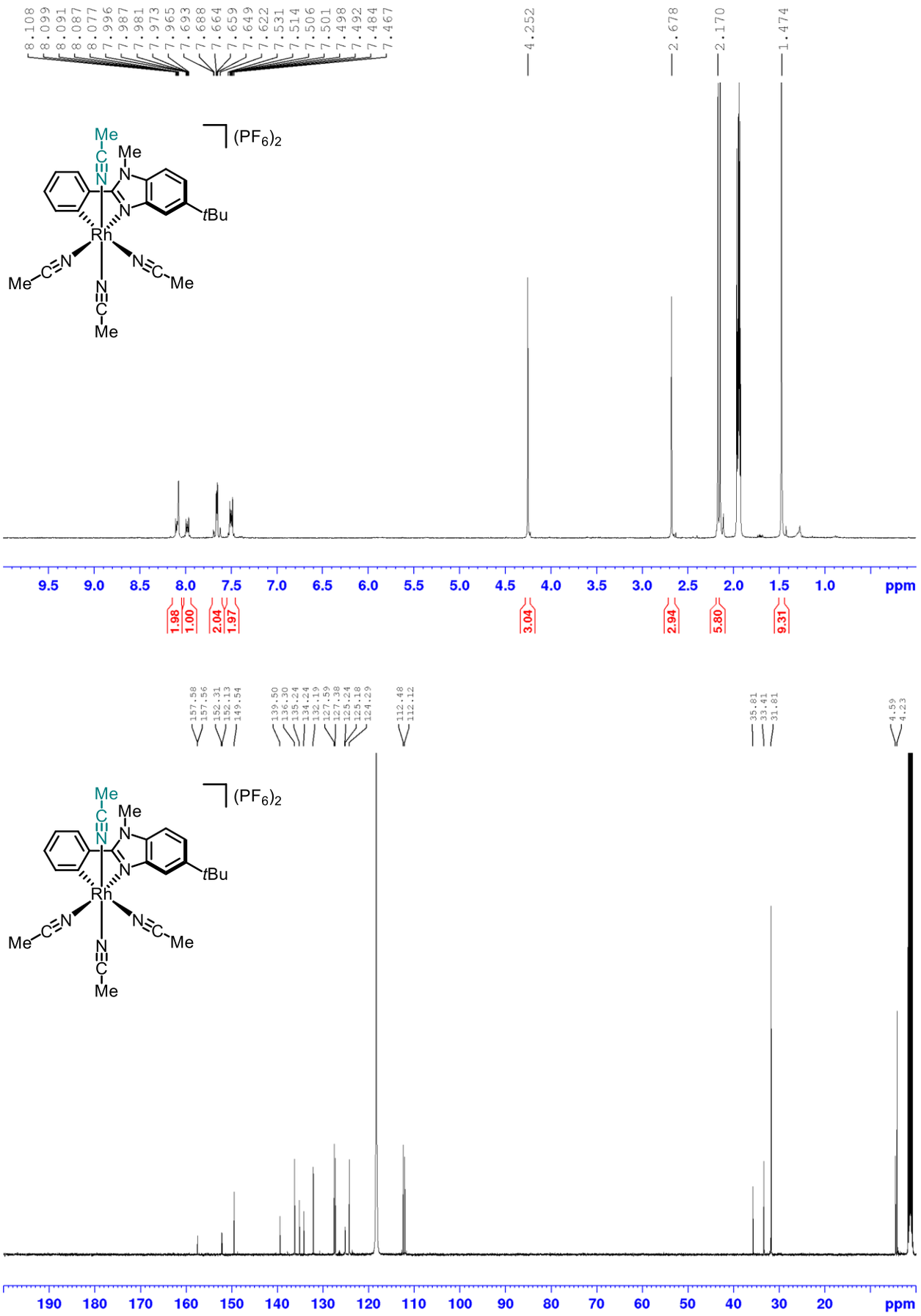

Figure 68: ^{1}H NMR (300 MHz) and ^{13}C NMR (126 MHz) spectrum of complex **49** in CD_3CN.

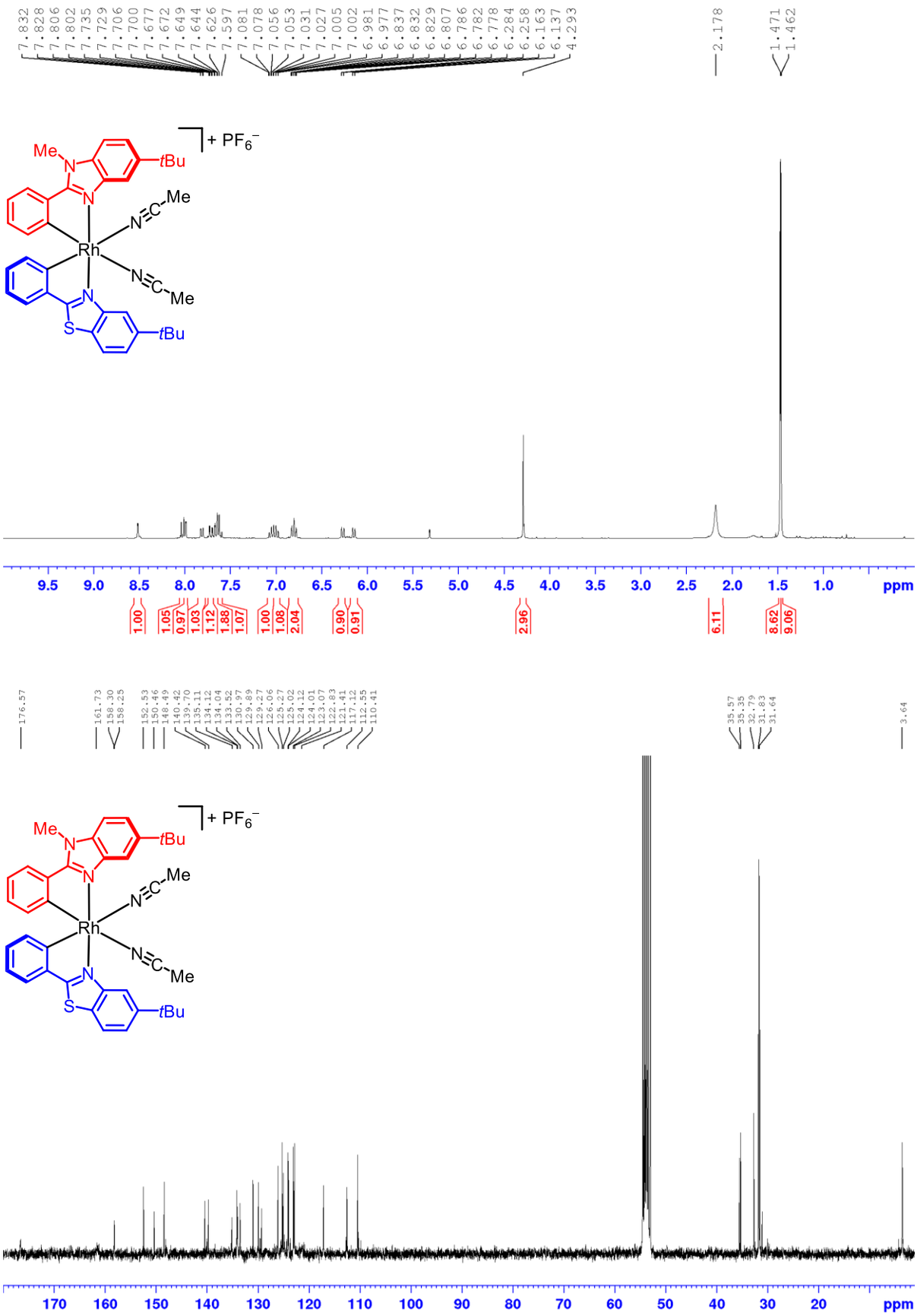

Figure 69: ^{1}H NMR (300 MHz) and ^{13}C NMR (126 MHz) spectrum of *rac*-**RhNS1** in CD_2Cl_2.

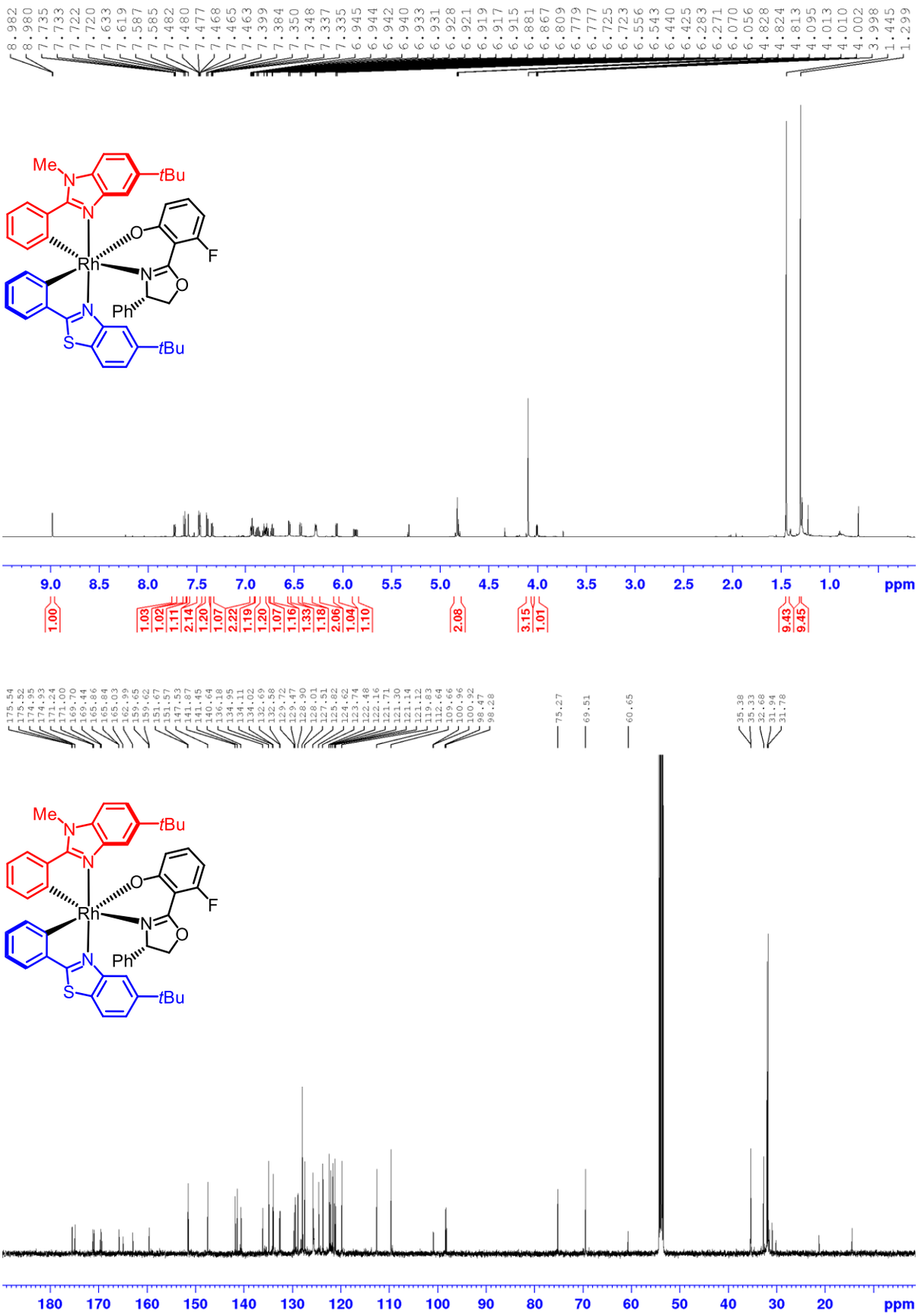

Figure 70: ^{1}H NMR (600 MHz) and ^{13}C NMR (126 MHz) spectrum of Λ-(*S*)-**55a** in CD_2Cl_2.

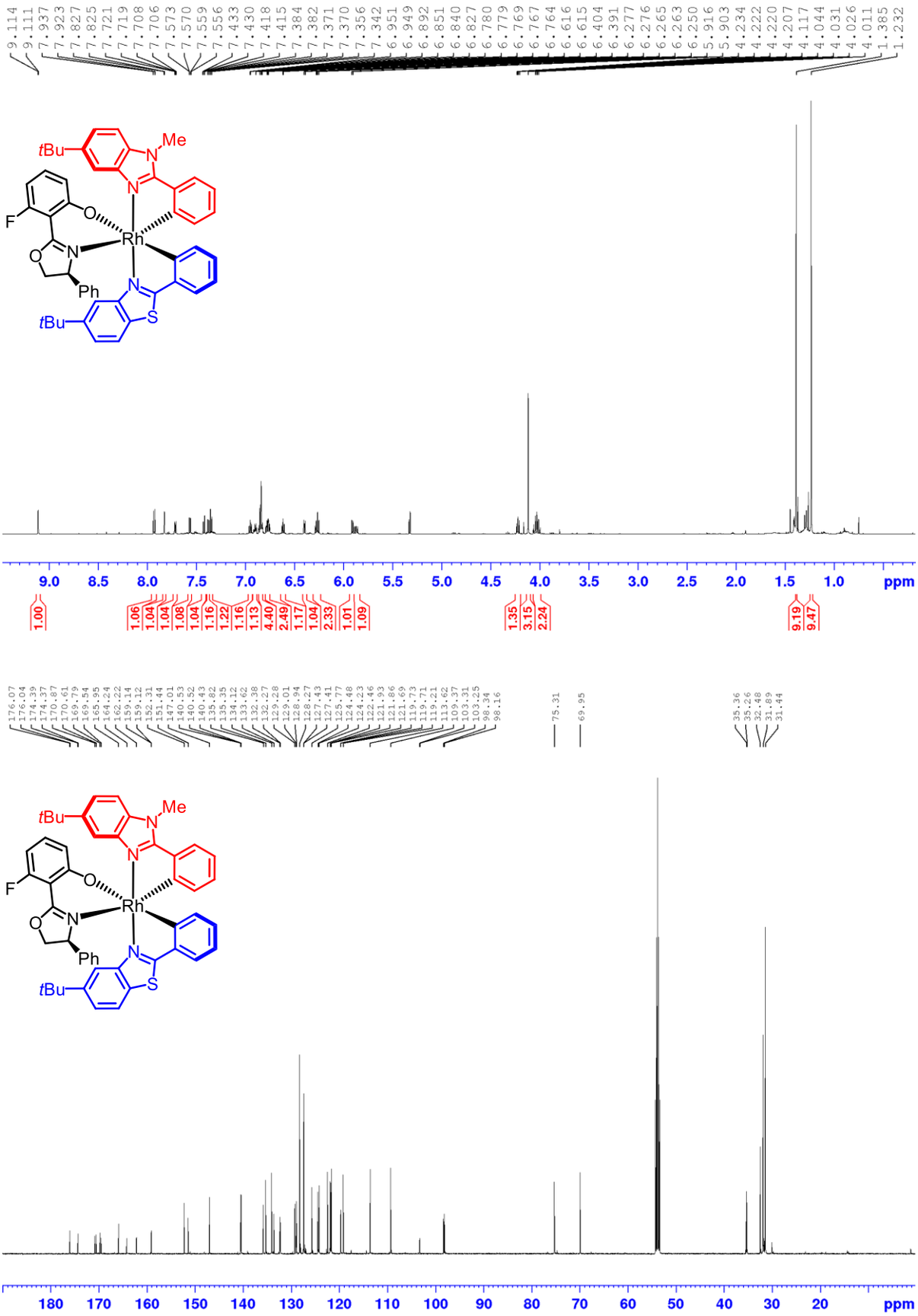

Figure 71: ^{1}H NMR (600 MHz) and ^{13}C NMR (126 MHz) spectrum of Δ-(*S*)-**55a** in CD_2Cl_2.

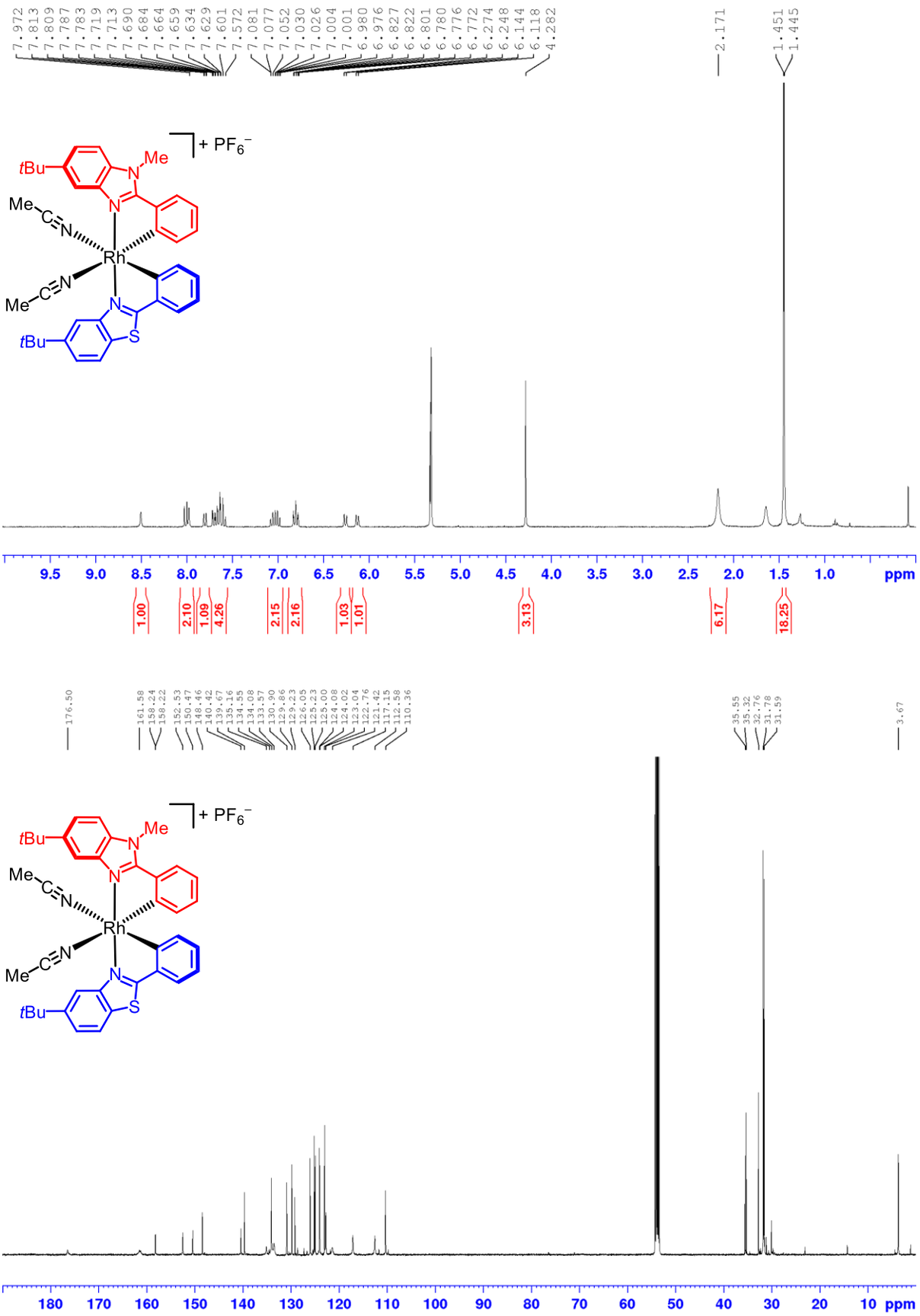

Figure 72: Representative ^{1}H NMR (300 MHz) and ^{13}C NMR (126 MHz) spectrum of the Δ-enantiomer of **RhNS1** in CD_2Cl_2.

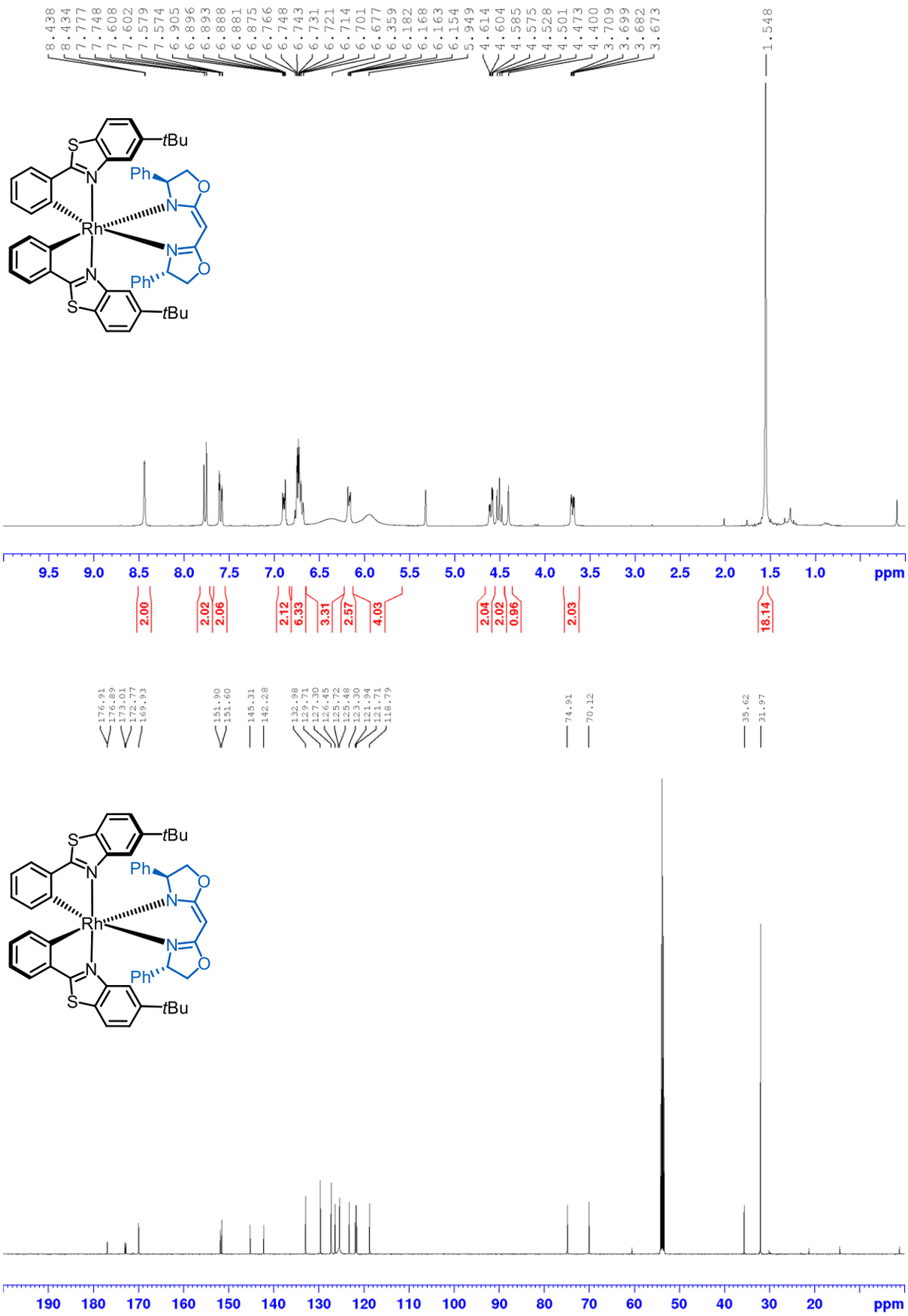

Figure 73: ^{1}H NMR (300 MHz) and ^{13}C NMR (126 MHz) spectrum of Λ-(*S*,*S*)-**67** in CD_2Cl_2.

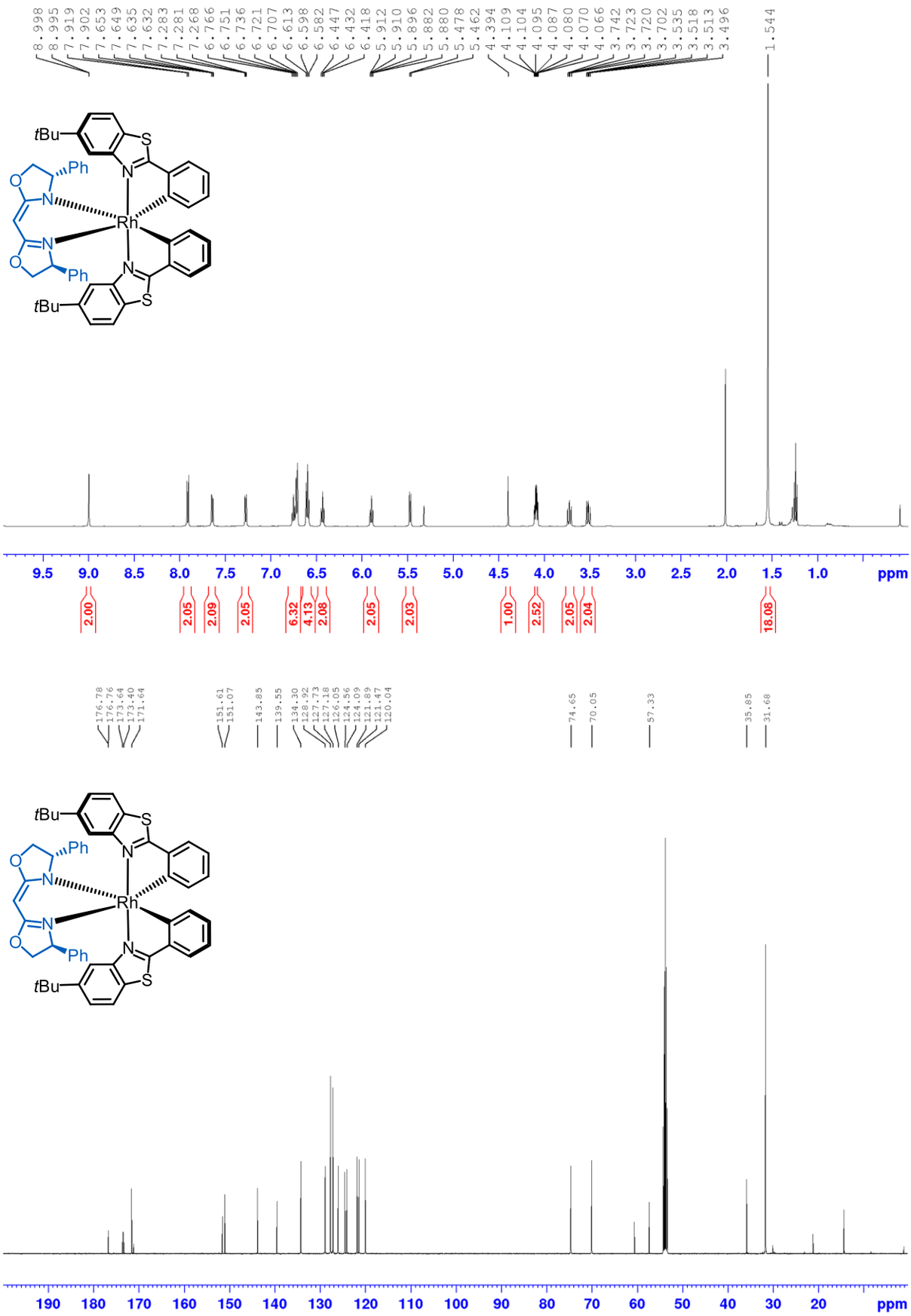

Figure 74: ^{1}H NMR (500 MHz) and ^{13}C NMR (126 MHz) spectrum of Δ-(*S*,*S*)-**67** in CD_2Cl_2.

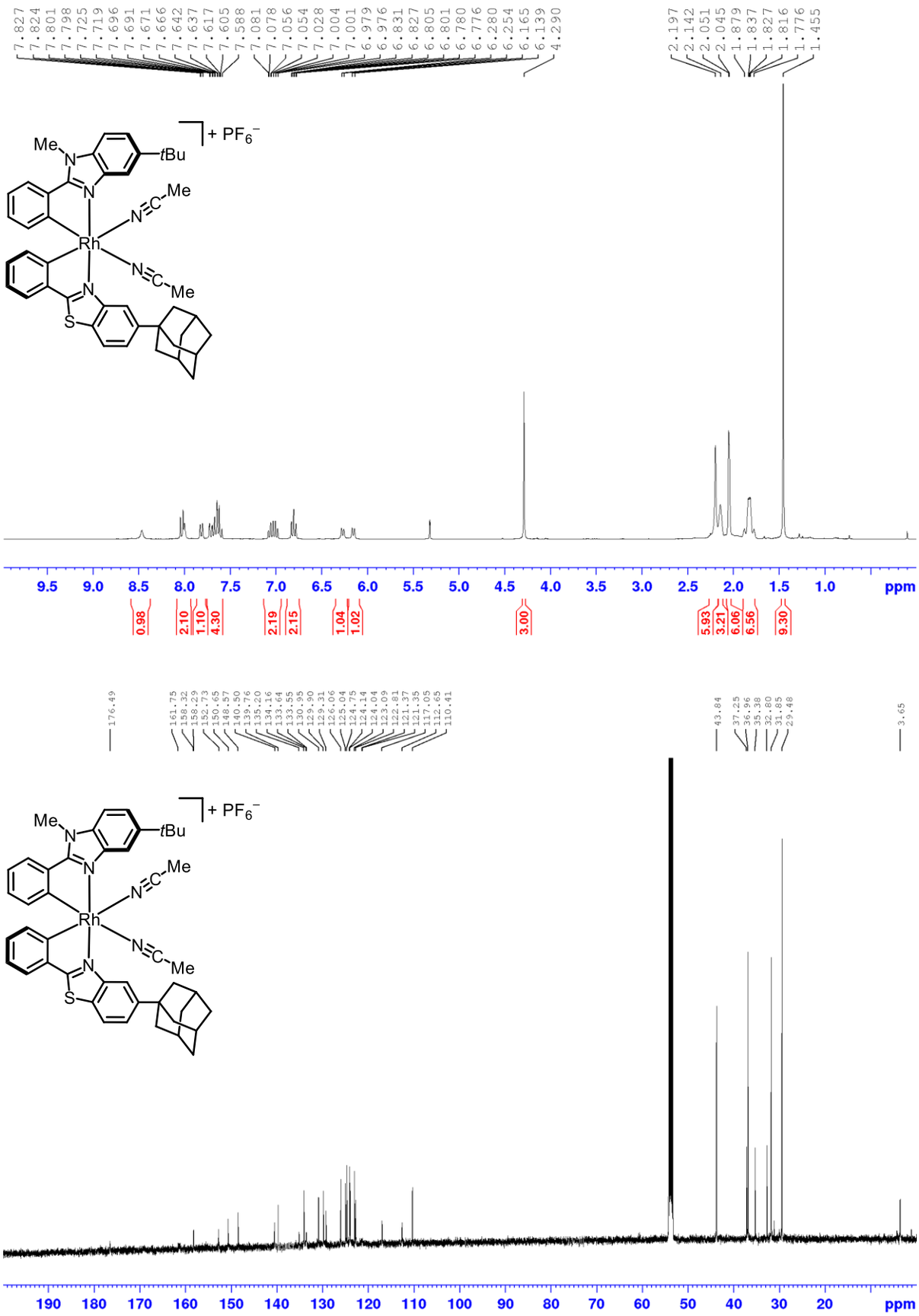

Figure 75: ^{1}H NMR (300 MHz) and ^{13}C NMR (126 MHz) spectrum of *rac*-**RhNS2** in CD_2Cl_2.

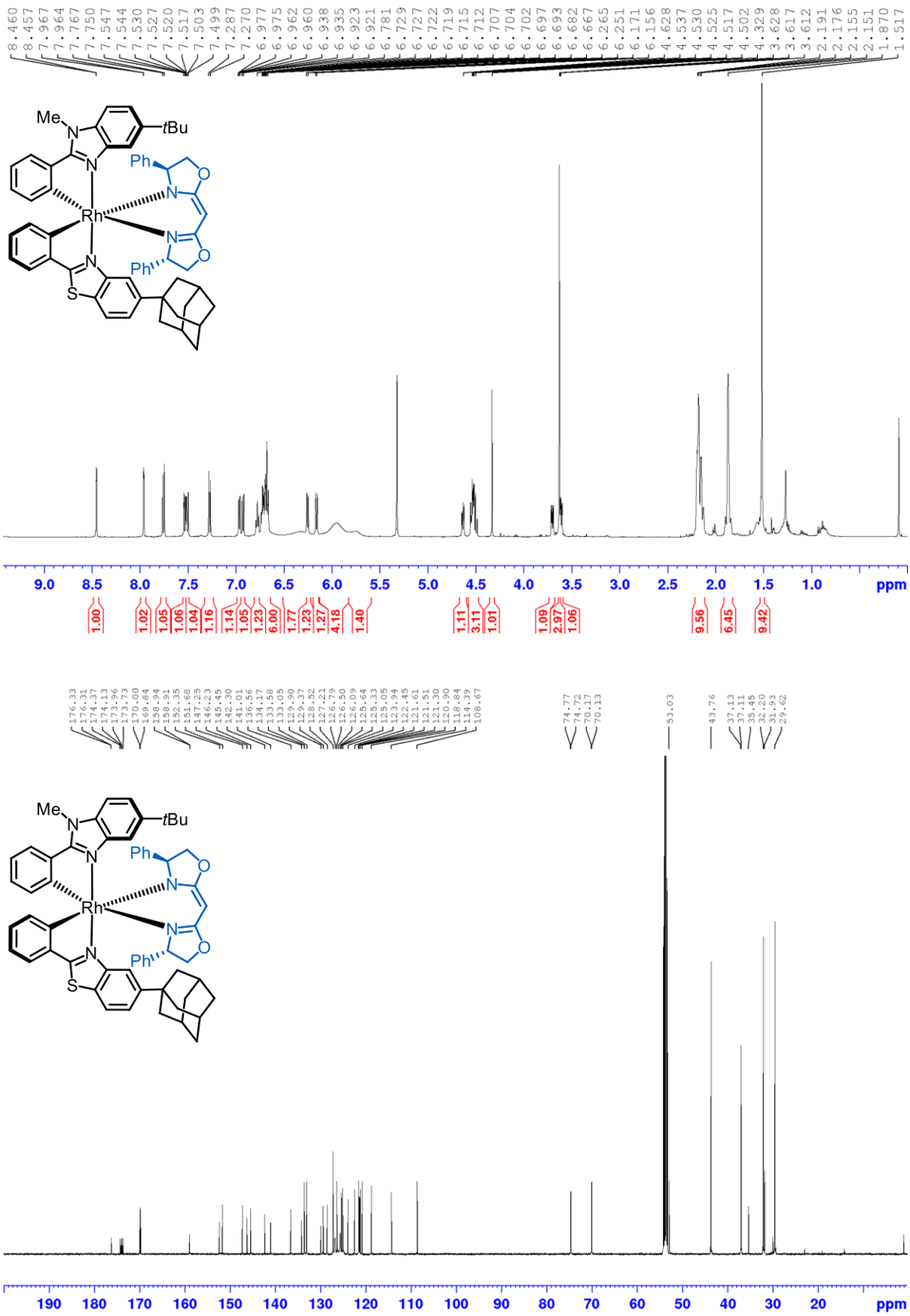

Figure 76: ^{1}H NMR (500 MHz) and ^{13}C NMR (126 MHz) spectrum of Λ-(*S*,*S*)-**69** in CD_2Cl_2.

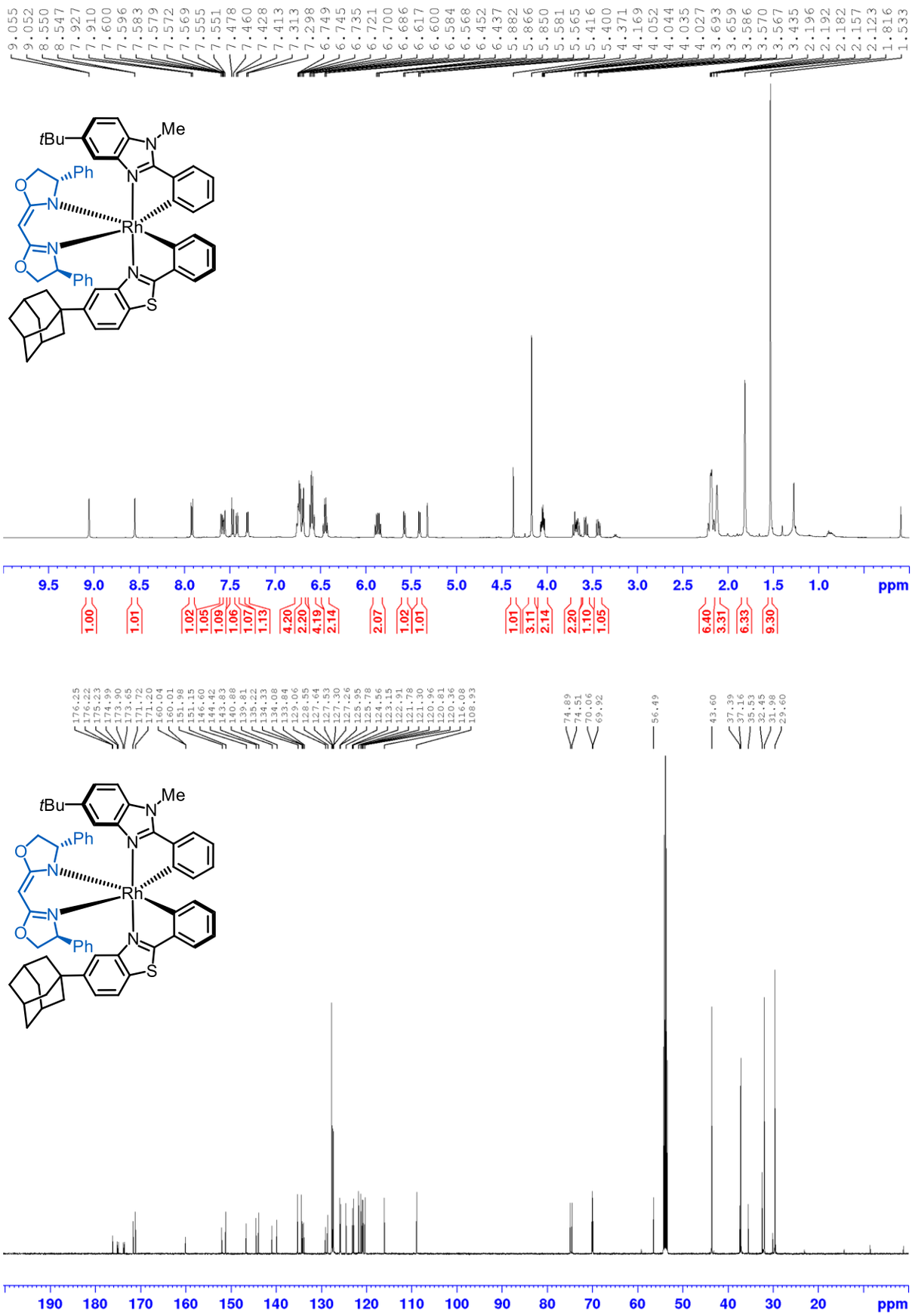

Figure 77: ^{1}H NMR (500 MHz) and ^{13}C NMR (126 MHz) spectrum of Δ-(*S*,*S*)-**69** in CD_2Cl_2.

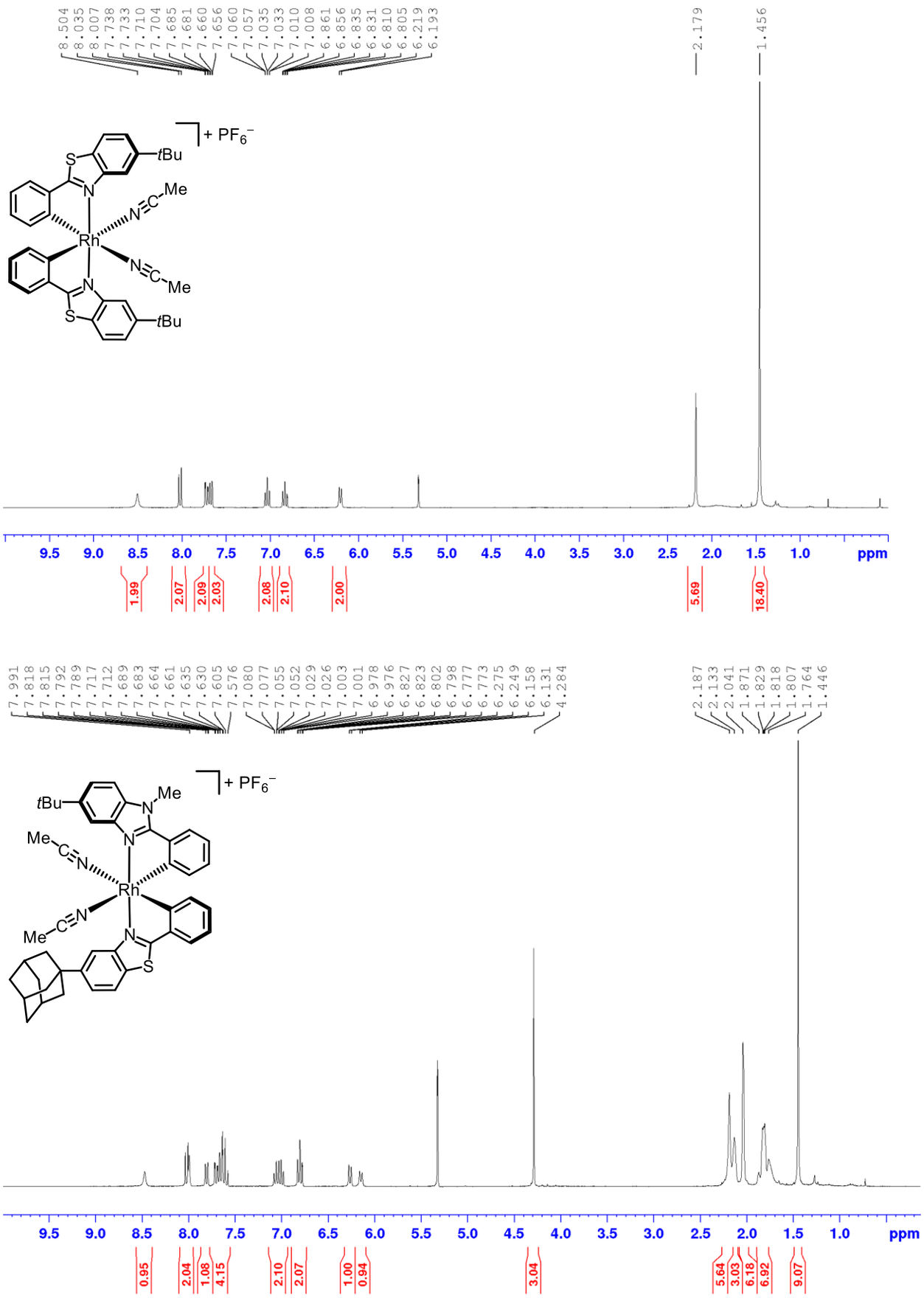

Figure 78: Representative ^{1}H NMR (300 MHz) spectra of enantiomerically pure Λ-**RhS** (top) and Δ-**RhNS2** (bottom) in CD_2Cl_2, obtained via the chiral bis(oxazoline) mediated strategy.

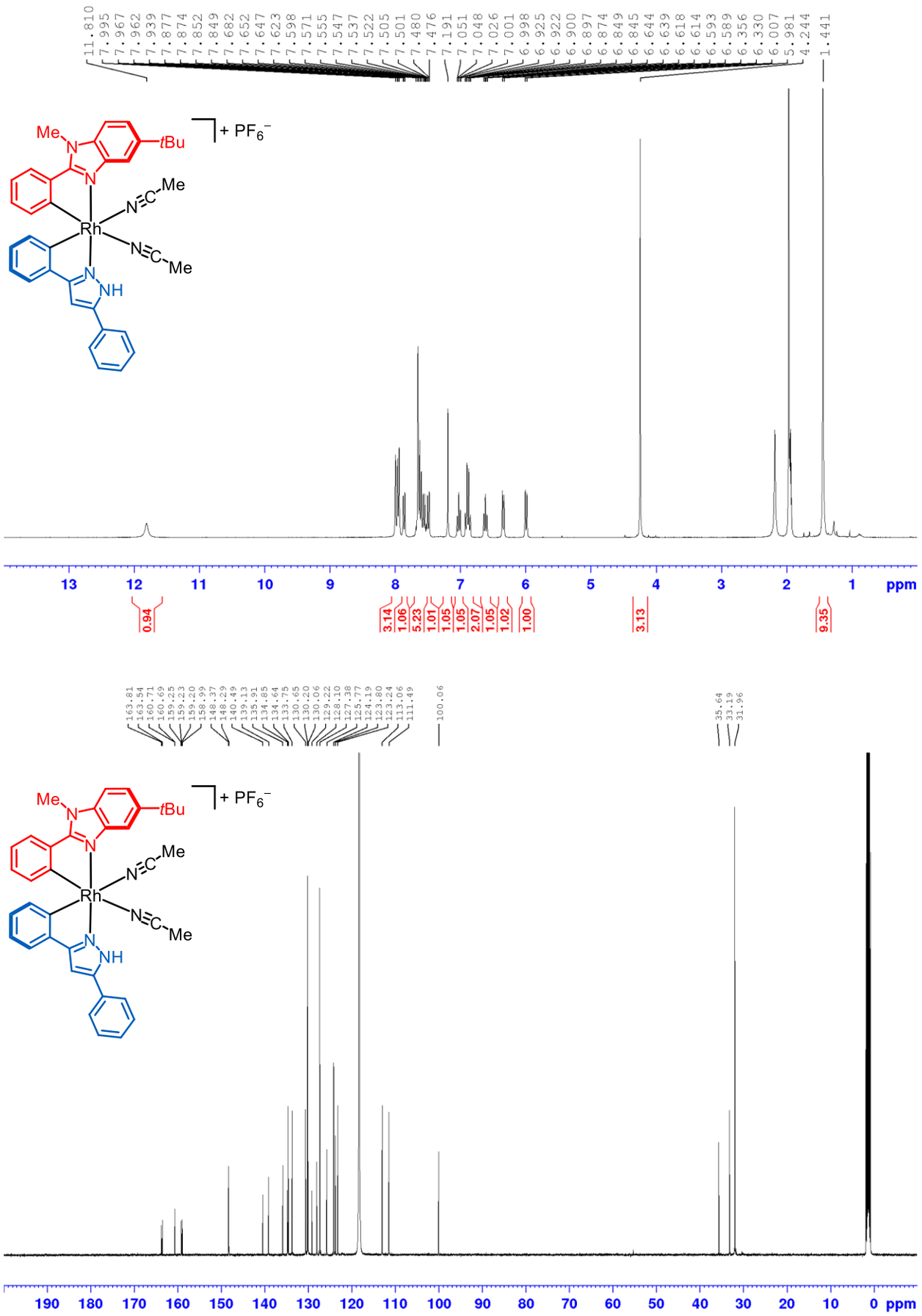

Figure 79: ^{1}H NMR (300 MHz) and ^{13}C NMR (126 MHz) spectrum of *rac*-**RhNP1** in CD_3CN.

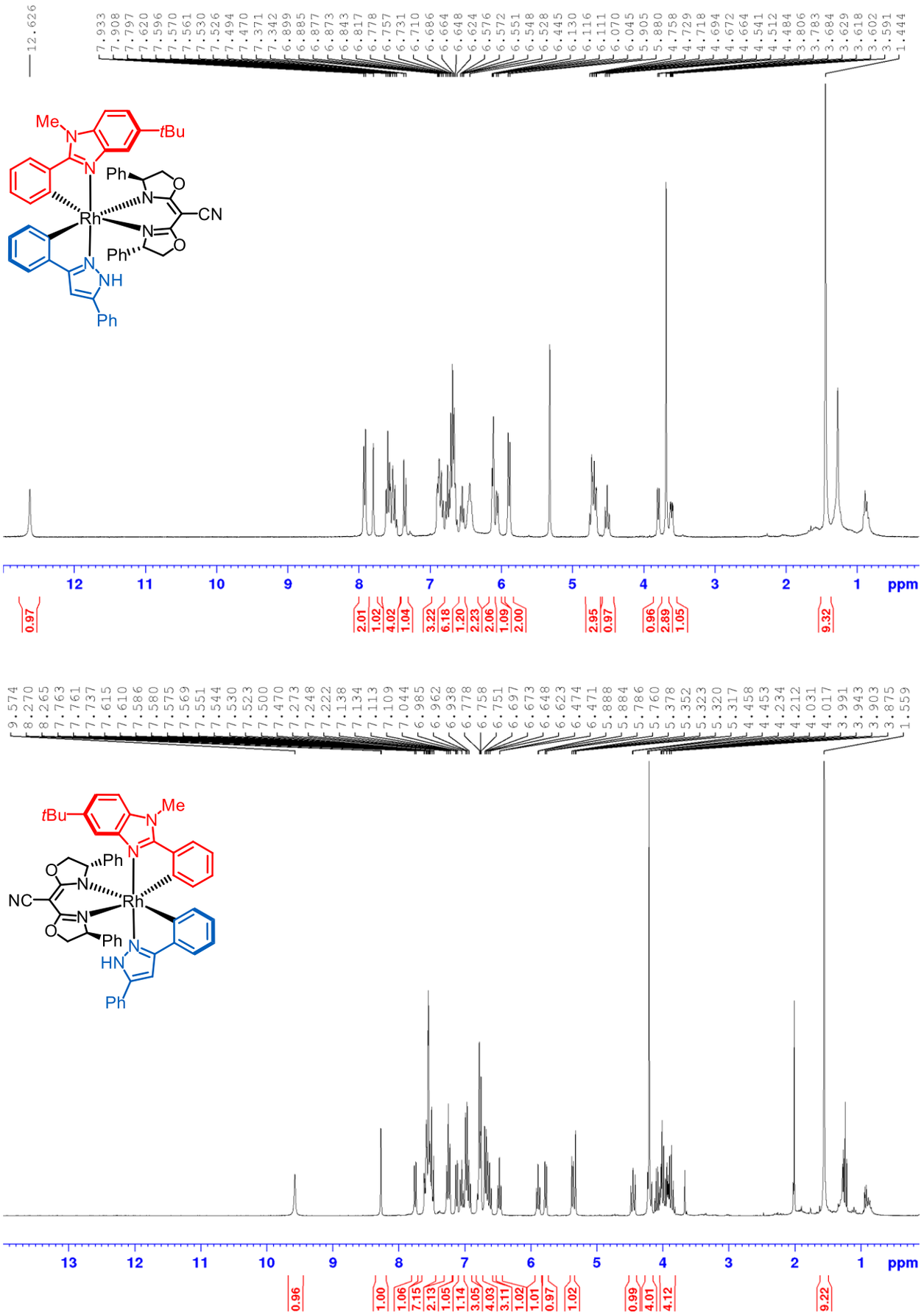

Figure 80: ^{1}H NMR (300 MHz) spectra of Λ- (top) and Δ-(*S*,*S*)-**74** (bottom) in CD_2Cl_2.

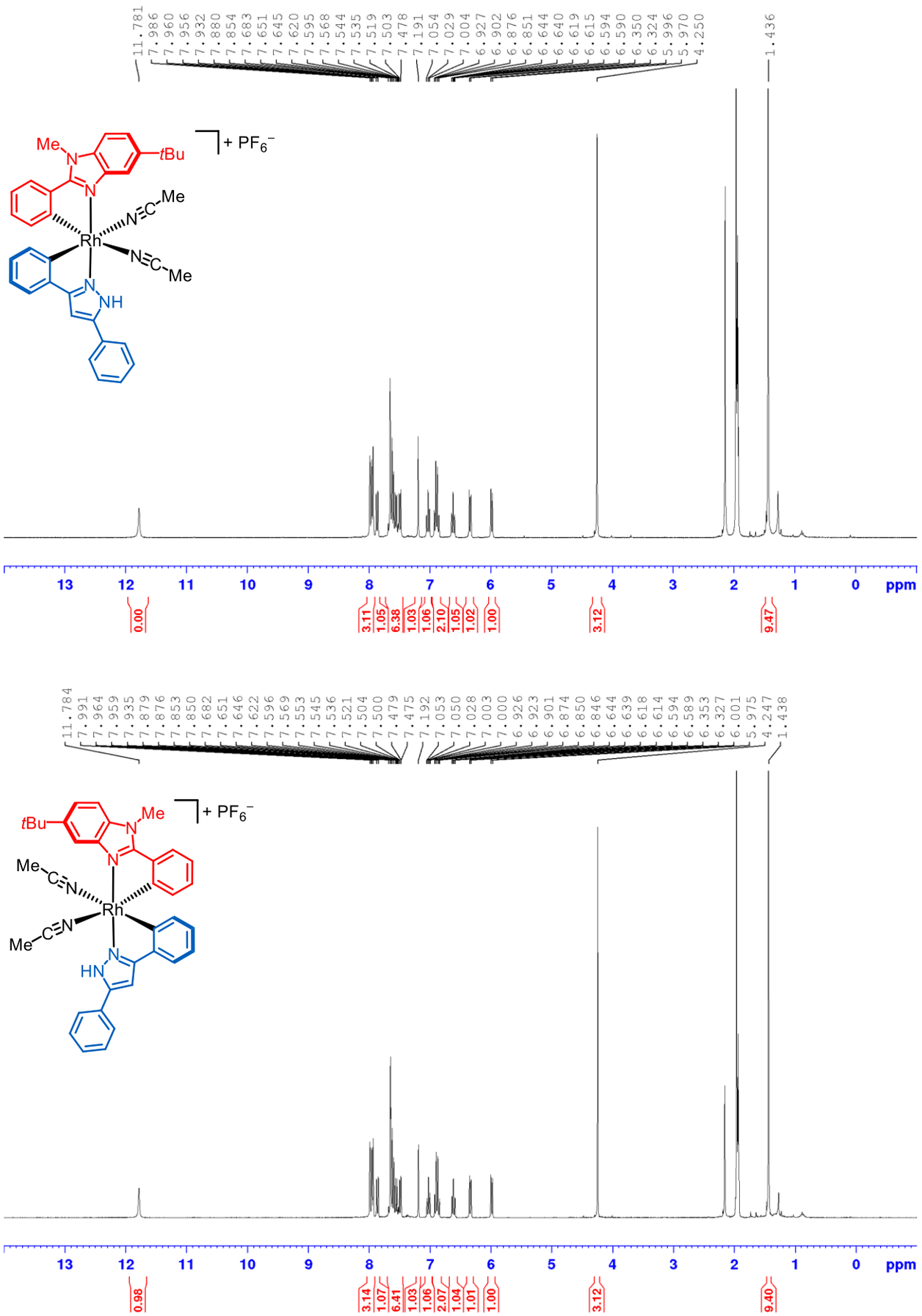

Figure 81: Representative ^{1}H NMR (300 MHz) spectra of enantiomerically pure Λ- (top) and Δ-**RhNP1** (bottom) in CD_3CN.

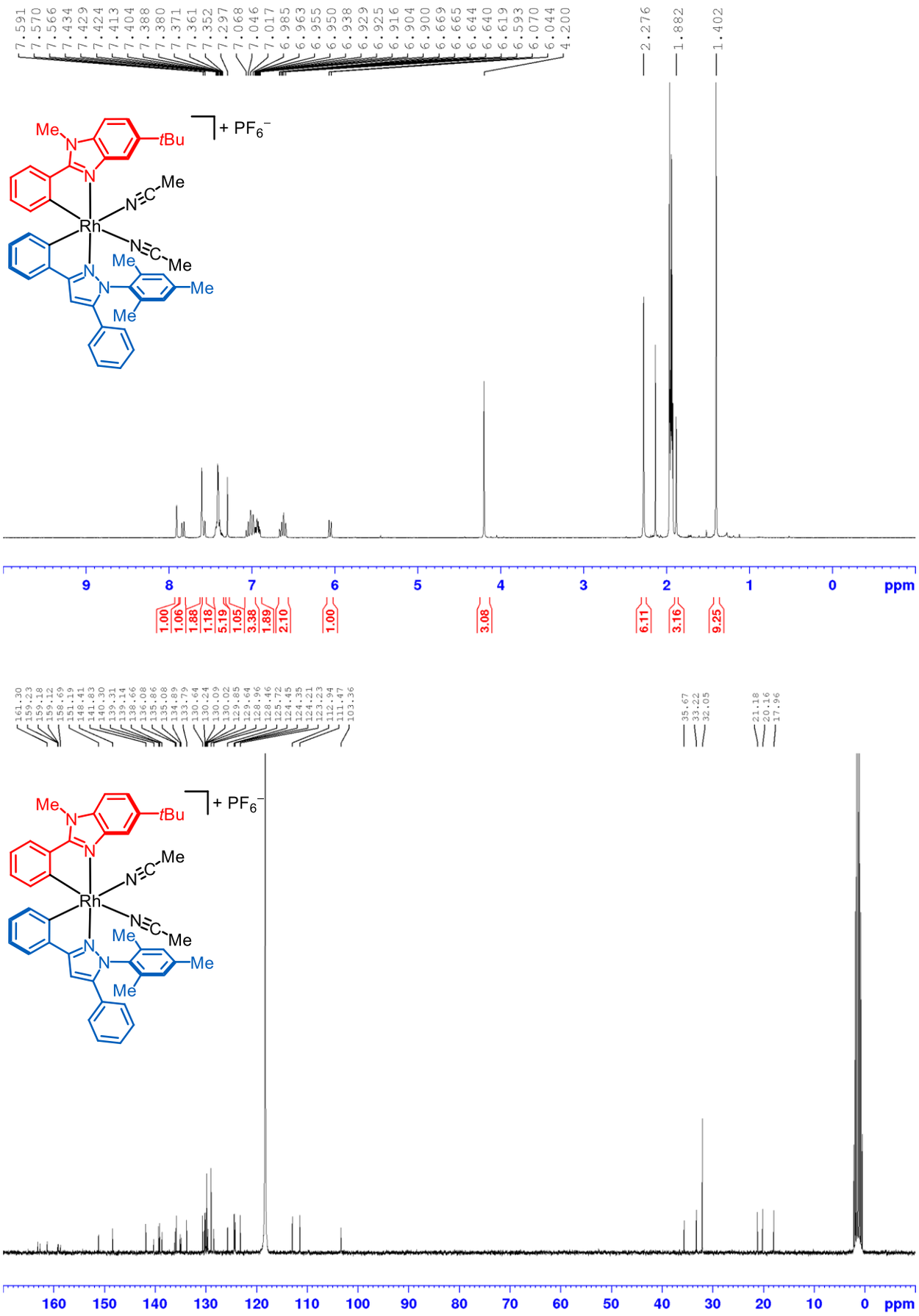

Figure 82: ^{1}H NMR (300 MHz) and ^{13}C NMR (75 MHz) spectrum of *rac*-**RhNP2** in CD_3CN.

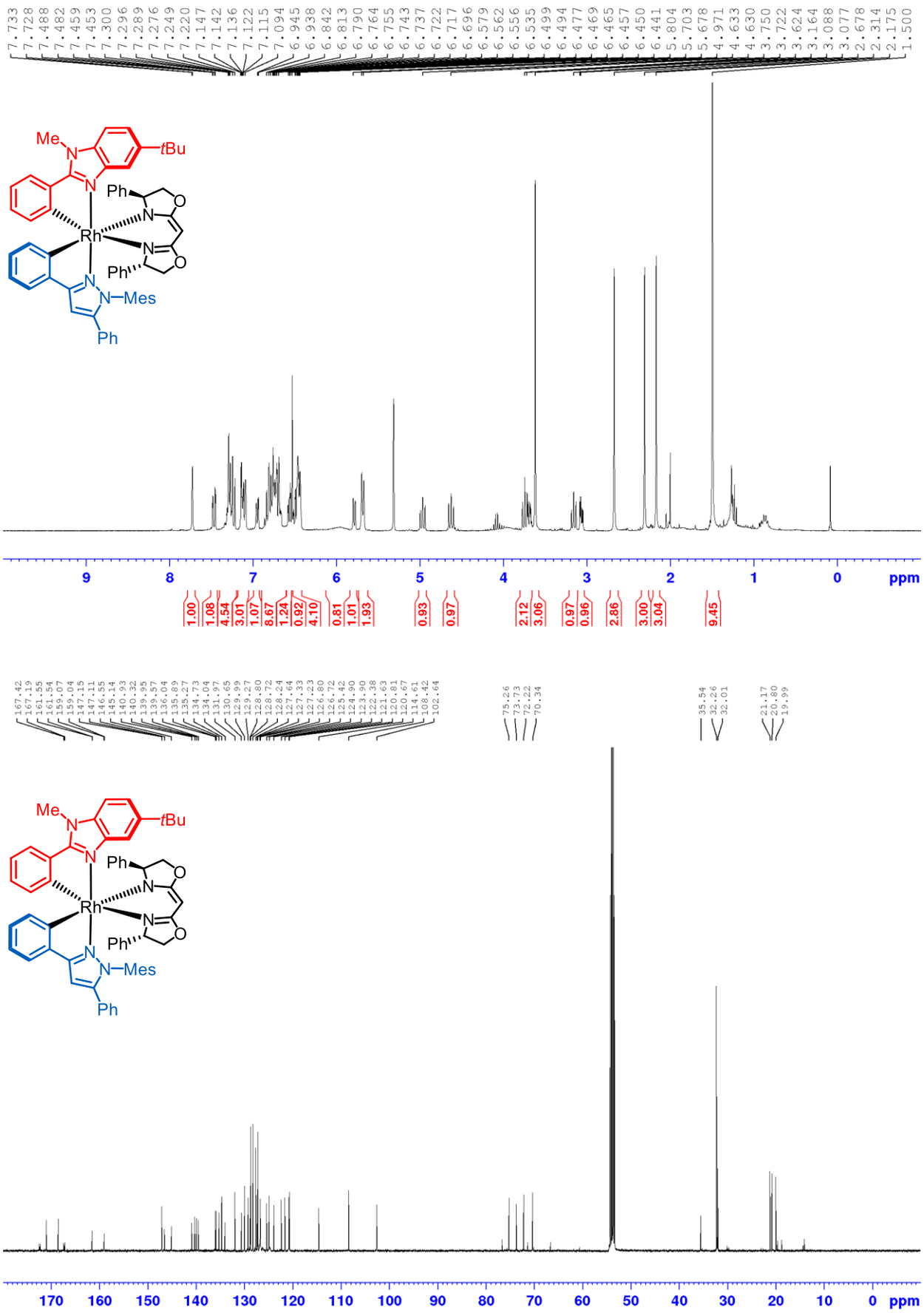

Figure 83: ^{1}H NMR (300 MHz) and ^{13}C NMR (126 MHz) spectrum of Λ-(*S*,*S*)-**79** in CD_2Cl_2.

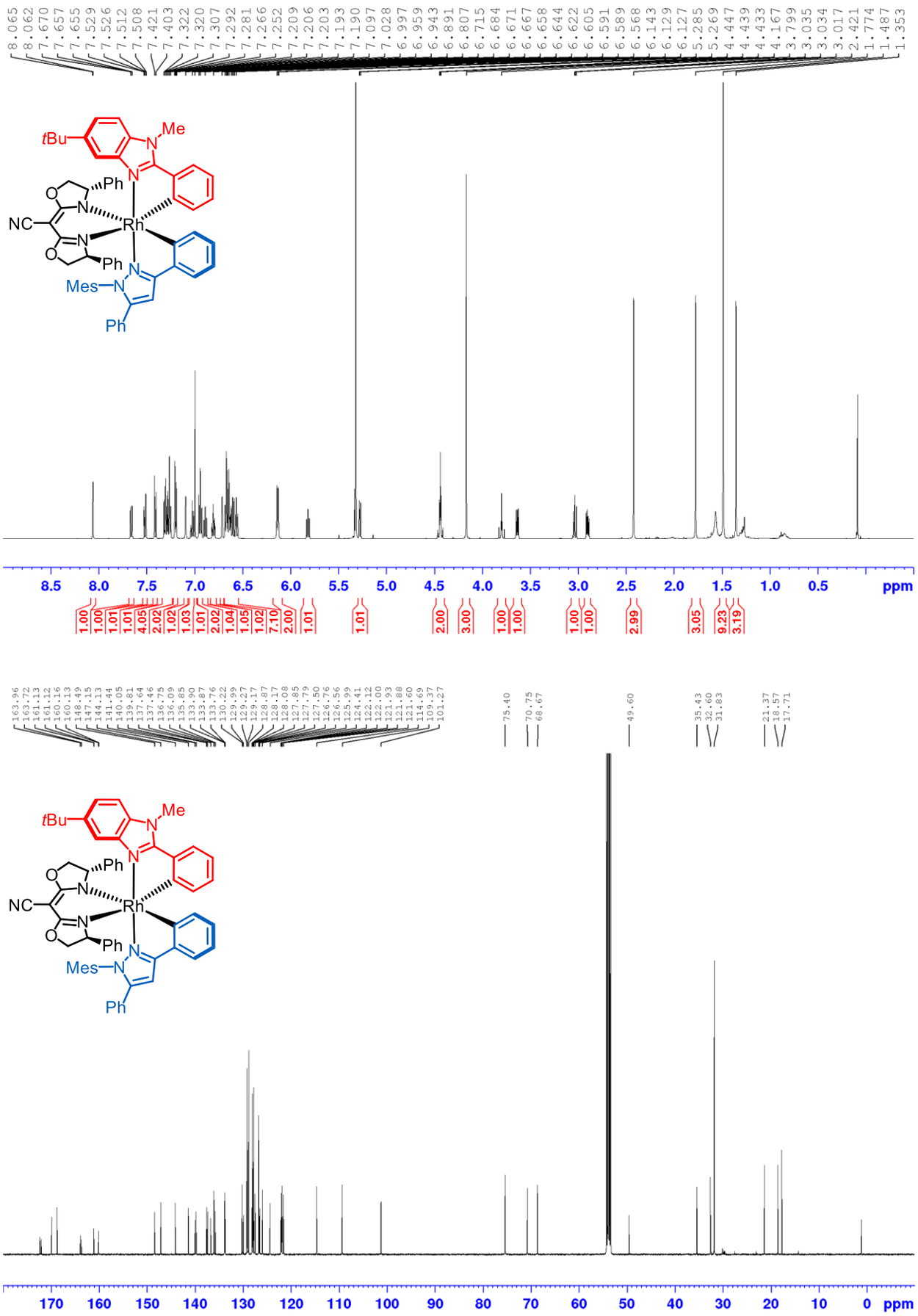

Figure 84: ^{1}H NMR (500 MHz) and ^{13}C NMR (126 MHz) spectrum of Δ-(*S*,*S*)-**80** in CD_2Cl_2.

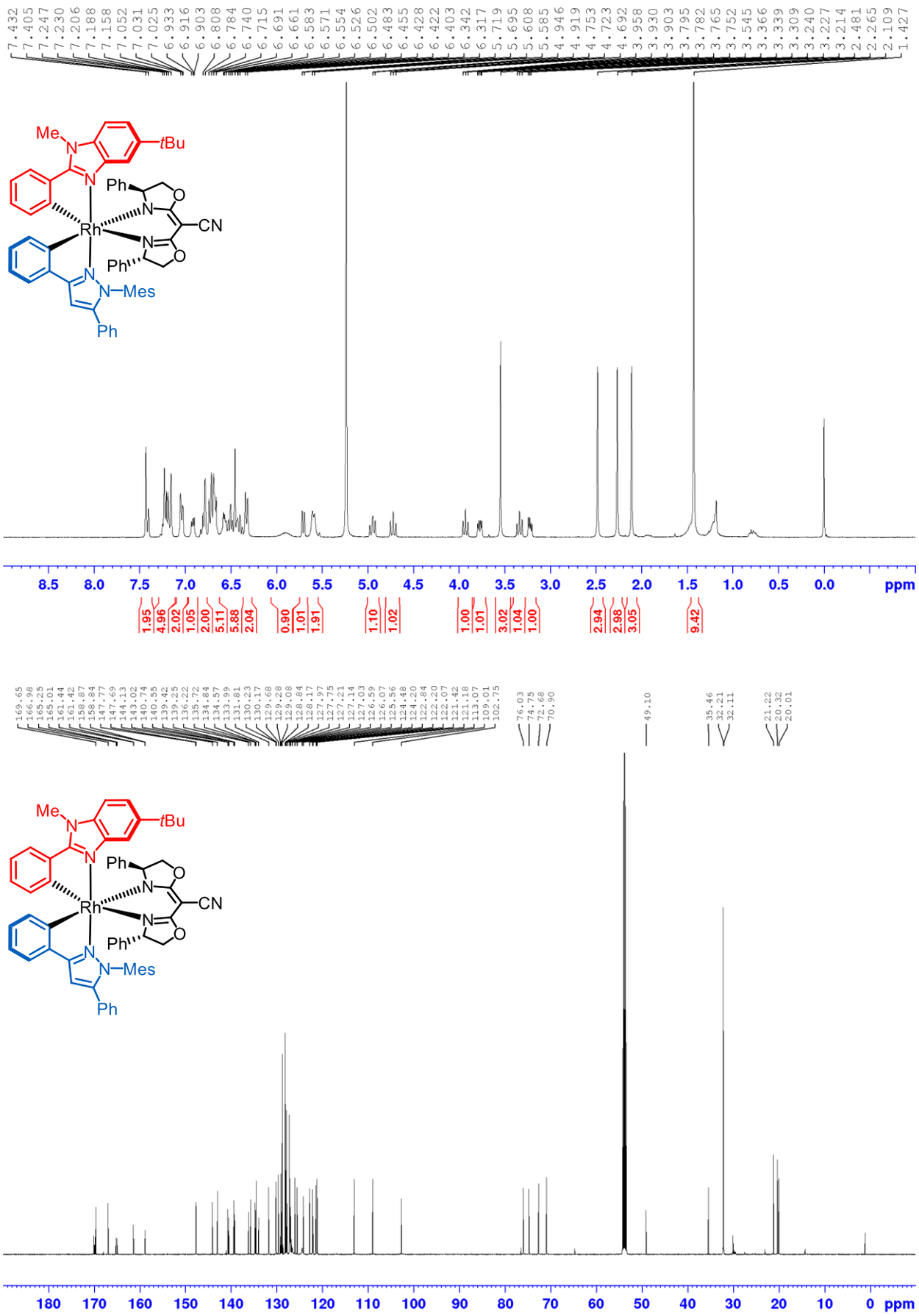

Figure 85: ^{1}H NMR (300 MHz) and ^{13}C NMR (126 MHz) spectrum of Λ-(*S*,*S*)-**80** in CD_2Cl_2.

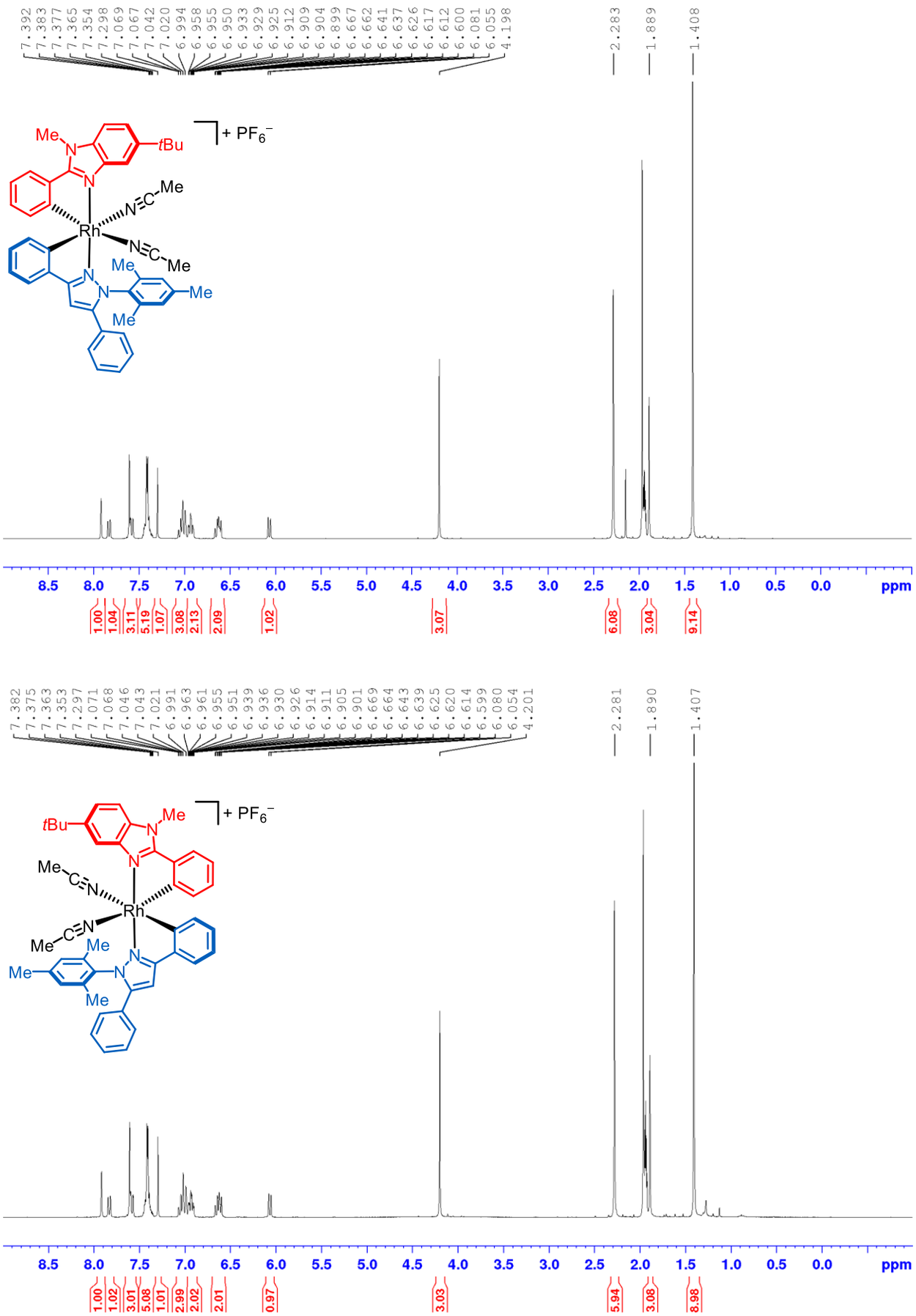

Figure 86: Representative ^{1}H NMR (300 MHz) spectra of enantiomerically pure Λ- (top) and Δ-**RhNP2** (bottom) in CD_3CN.

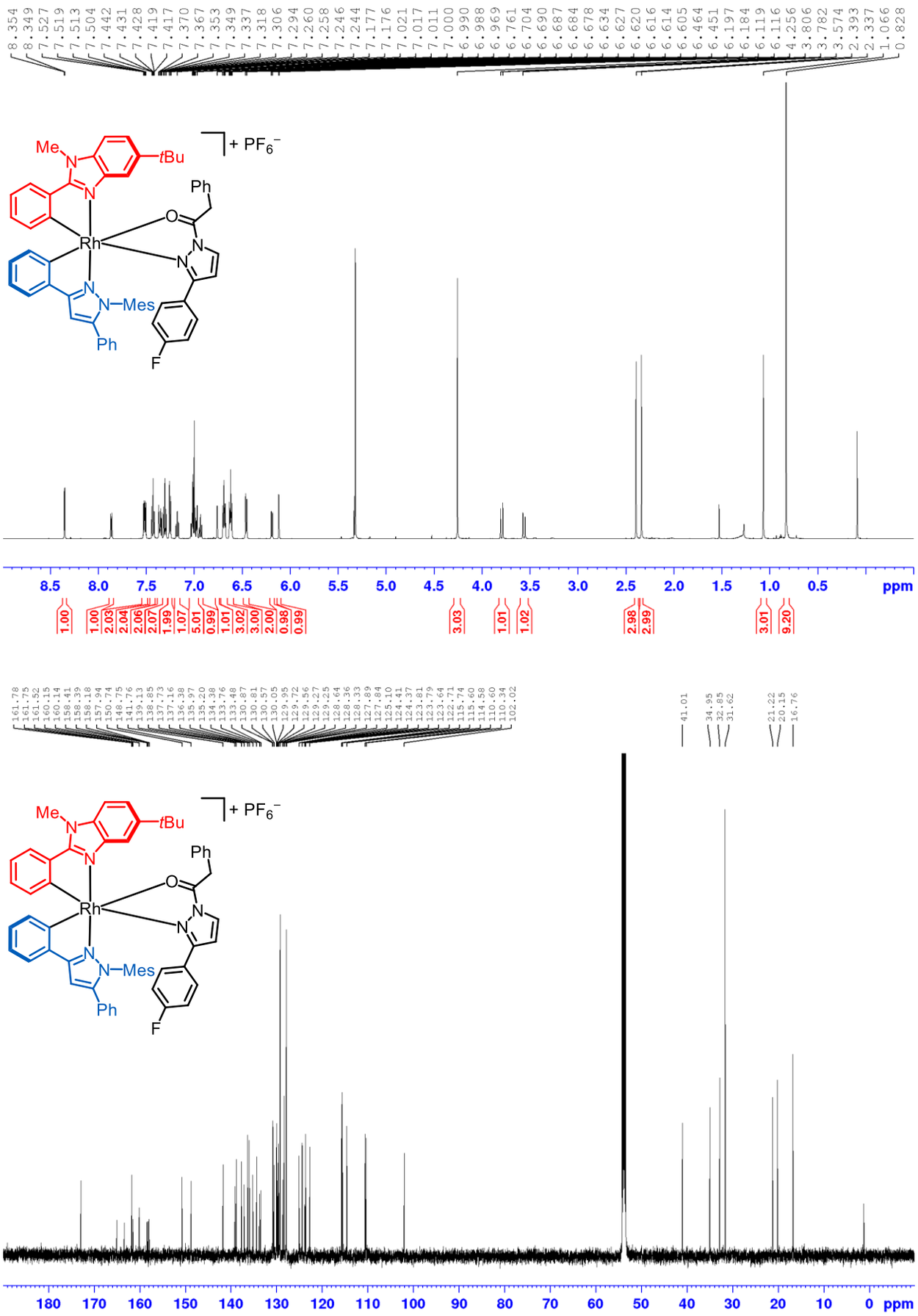

Figure 87: ^{1}H NMR (600 MHz) and ^{13}C NMR (151 MHz) spectrum of rhodium-substrate complex **95a** in CD_2Cl_2.

6.2 Chiral HPLC Traces

Chiral HPLC traces of the synthesized rhodium complexes are shown. HPLC chromatograms of the catalysis products from Chapter 3.2. and from Chapter 3.5 can be found in the corresponding Supporting Information in references [102] and [161], respectively.

Chiral HPLC Traces of Λ- and Δ-RhNS1:

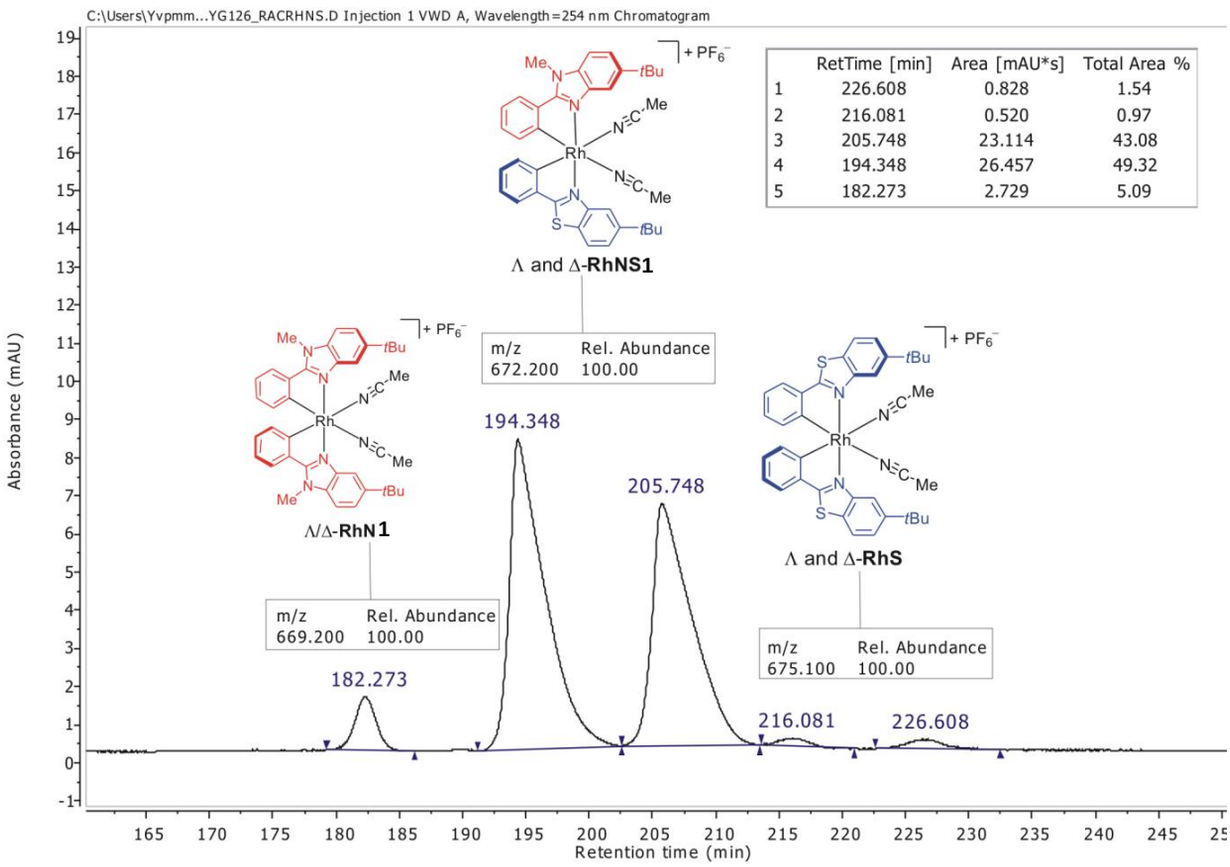

Figure 88: LC/MS trace of *rac*-**RhNS1**, which also shows the peaks of the bis-heteroleptic side products *rac*-**RhN1** and *rac*-**RhS**. HPLC conditions: Daicel Chiralpak® IB-N5 column, 250 x 4.6 mm, absorbance at 254 nm, H_2O + 0.1% TFA/MeCN = 60:40 to 50:50 in 180 min, 50:50 maintained until 240 min, gradient elution, flow rate 0.6 mL/min, 25 °C.

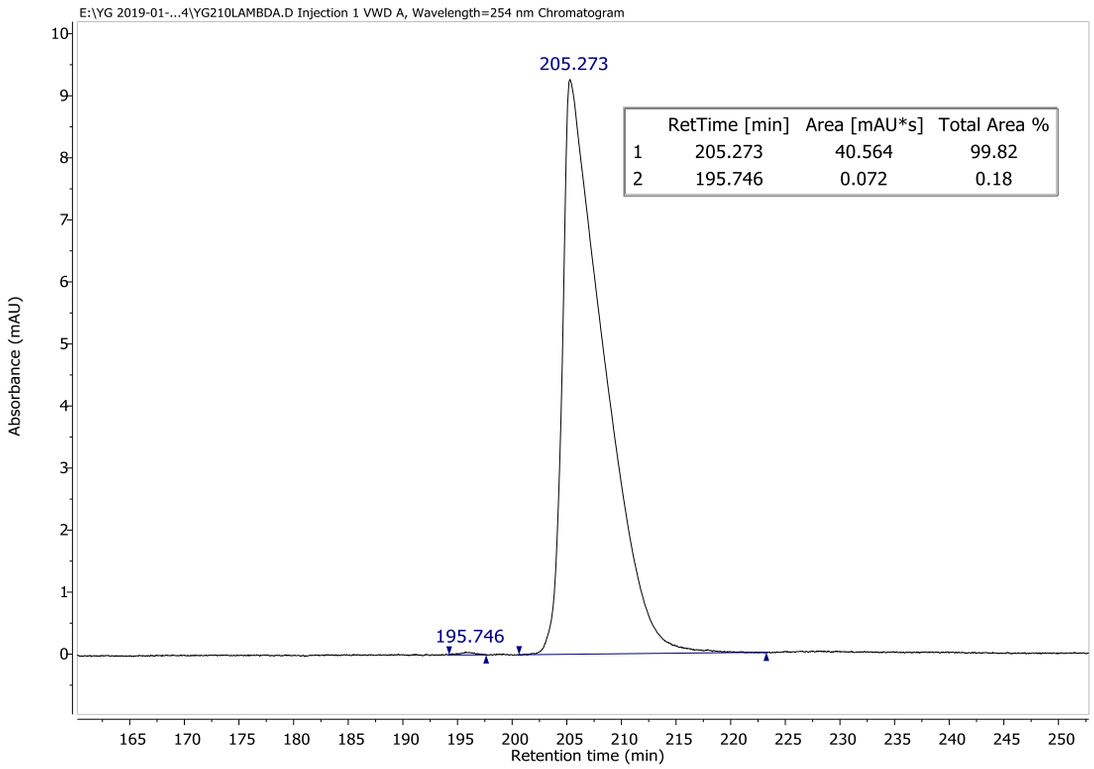

Figure 89: LC/MS trace of Λ-**RhNS1** (99.6% ee).

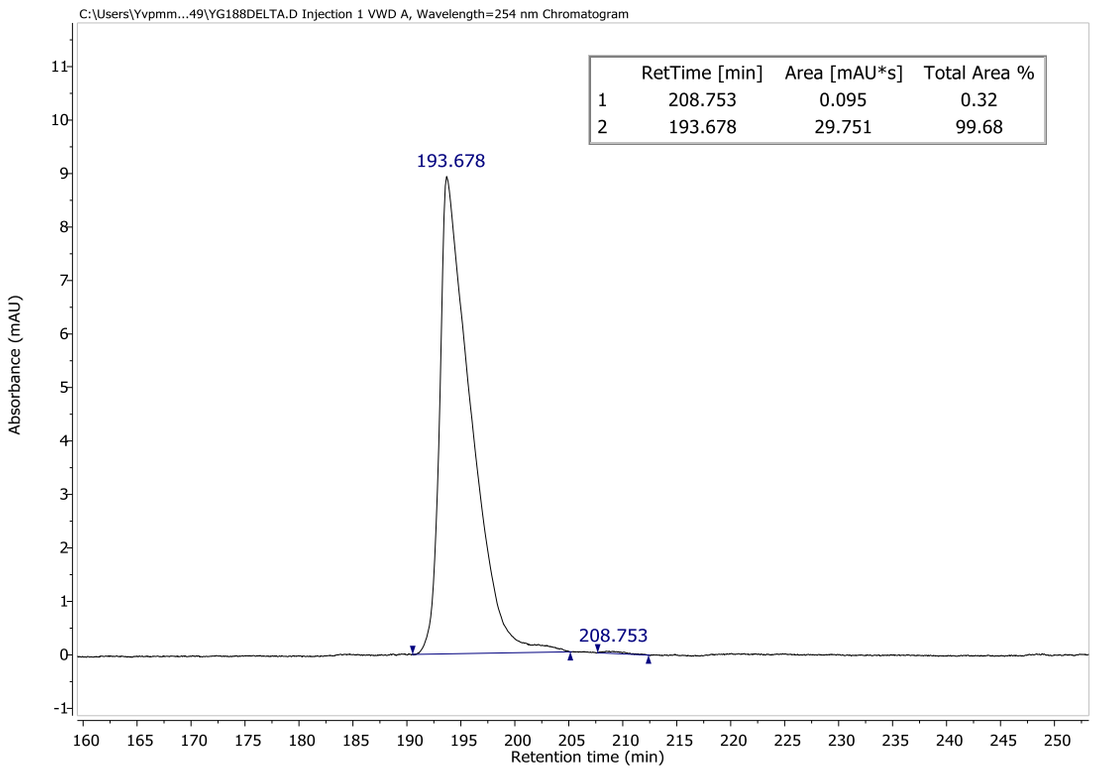

Figure 90: LC/MS trace of Δ-**RhNS1** (99.4% ee).

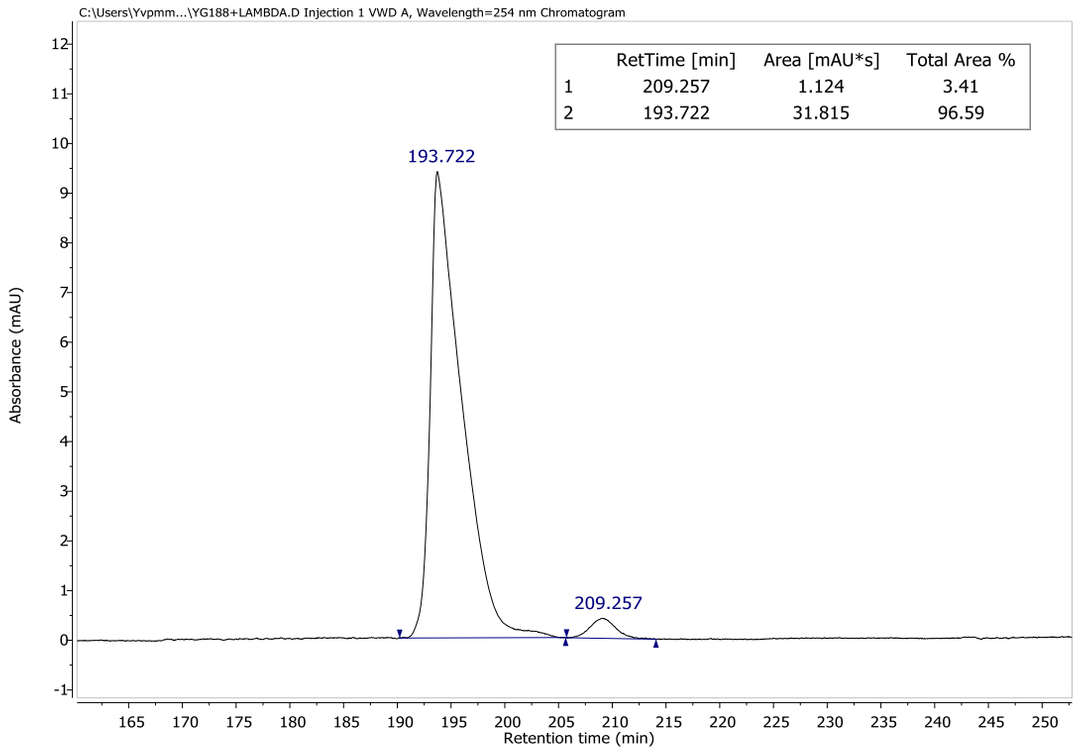

Figure 91: Spiking experiment: LC/MS trace of Δ-**RhNS1**, plus 2% Λ-**RhNS1** to verify that the peak at t_r = 209.3 min belongs to the Λ-enantiomer.

Chiral HPLC Traces of Λ- and Δ-RhS:

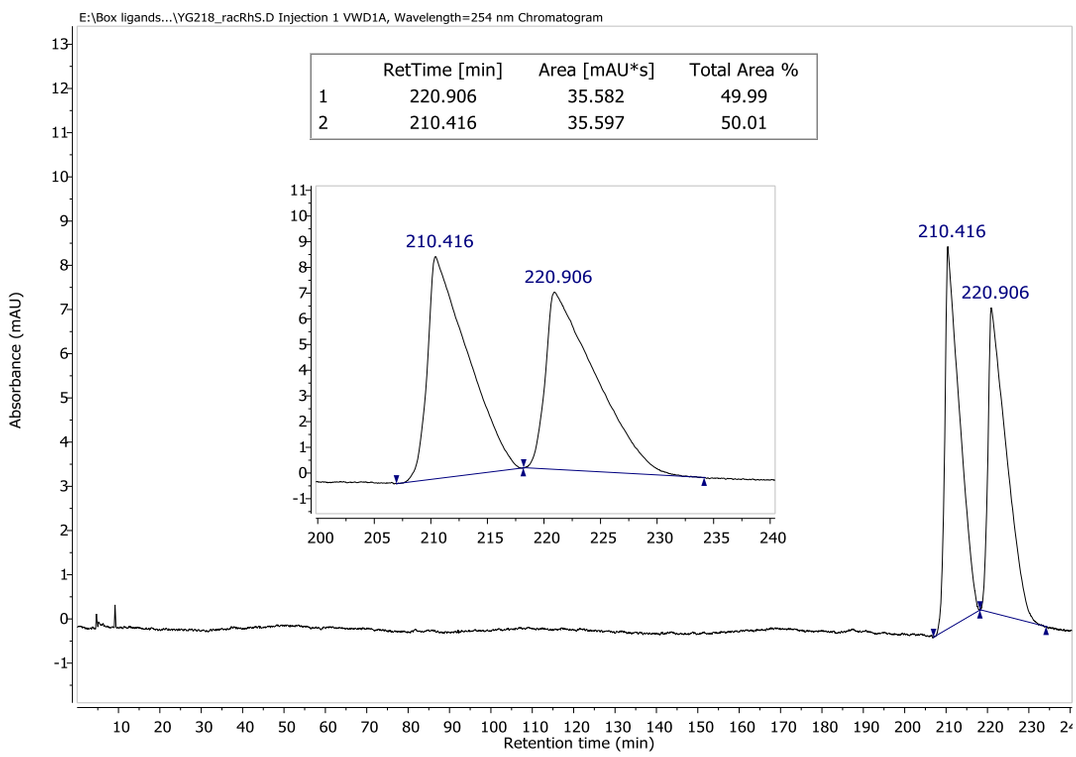

Figure 92: HPLC trace of *rac*-**RhS**. HPLC conditions: Daicel Chiralpak® IB-N5 column, 250 x 4.6 mm, absorbance at 254 nm, H_2O + 0.1% TFA/MeCN = 60:40 to 50:50 in 180 min, 50:50 maintained until 240 min, gradient elution, flow rate 0.6 mL/min, 25 °C.

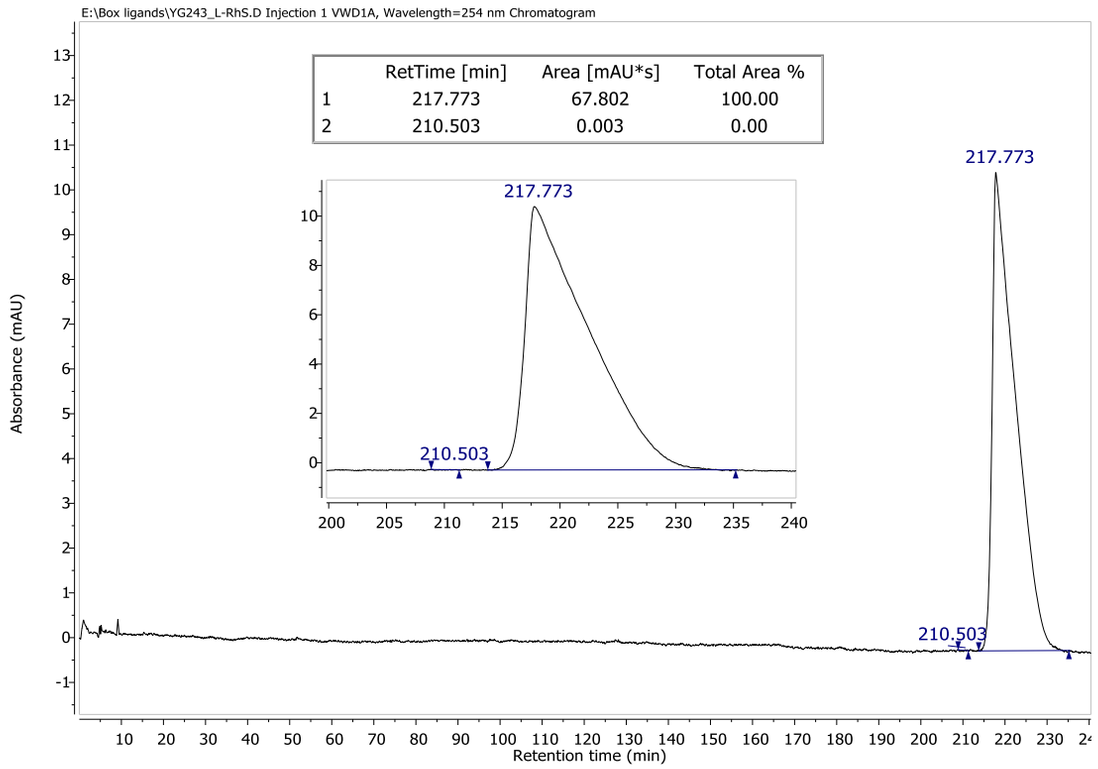

Figure 93: HPLC trace of Λ-**RhS** (>99.9% ee).

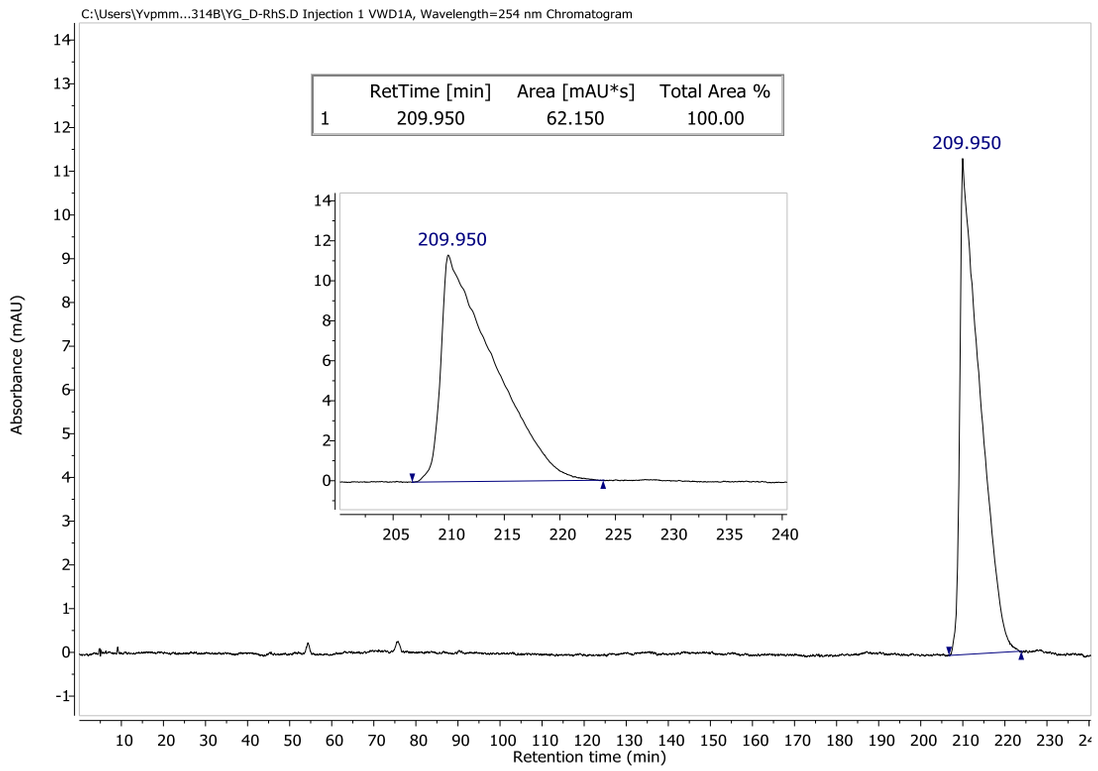

Figure 94: HPLC trace of Δ-**RhS** (>99% ee).

Chiral HPLC Traces of Λ- and Δ-RhNP1:

<Chromatogram>

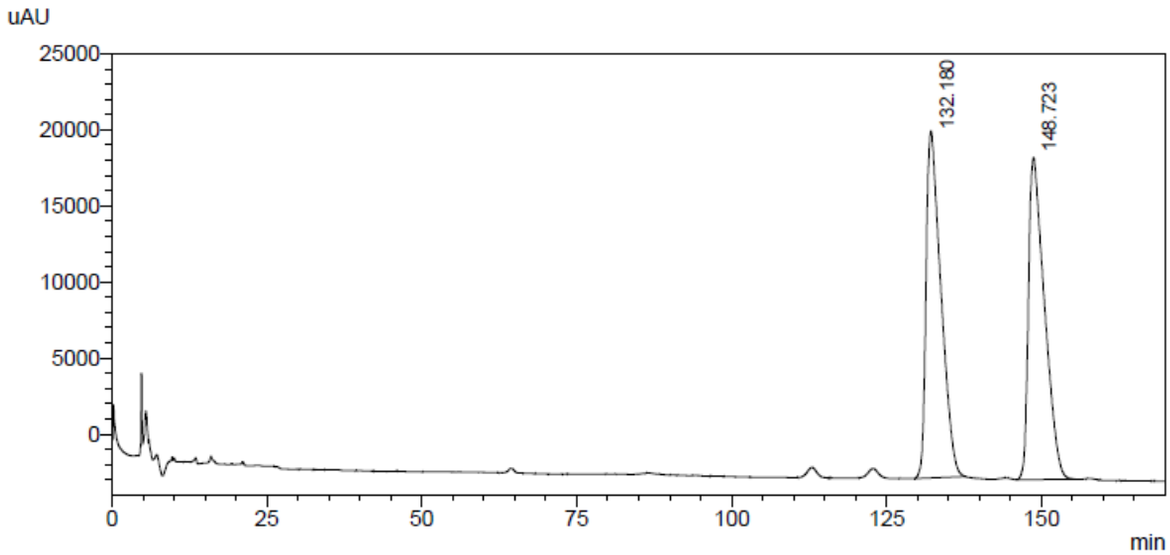

<Peak Table>

Detector A 254nm

Peak#	Ret. Time [min]	Area [mAU*s]	Total Area%
1	132.180	3787465	49.882
2	148.723	3805336	50.118
Total		7592801	100.000

Figure 95: HPLC trace of *rac*-**RhNP1**. HPLC conditions: Daicel Chiralpak® IB-N5 column, 250 x 4.6 mm, absorbance at 254 nm, H_2O + 0.1% TFA/MeCN = 60:40 to 50:50 in 180 min, 50:50 maintained until 190 min, gradient elution, flow rate 0.6 mL/min, 25 °C.

<Chromatogram>

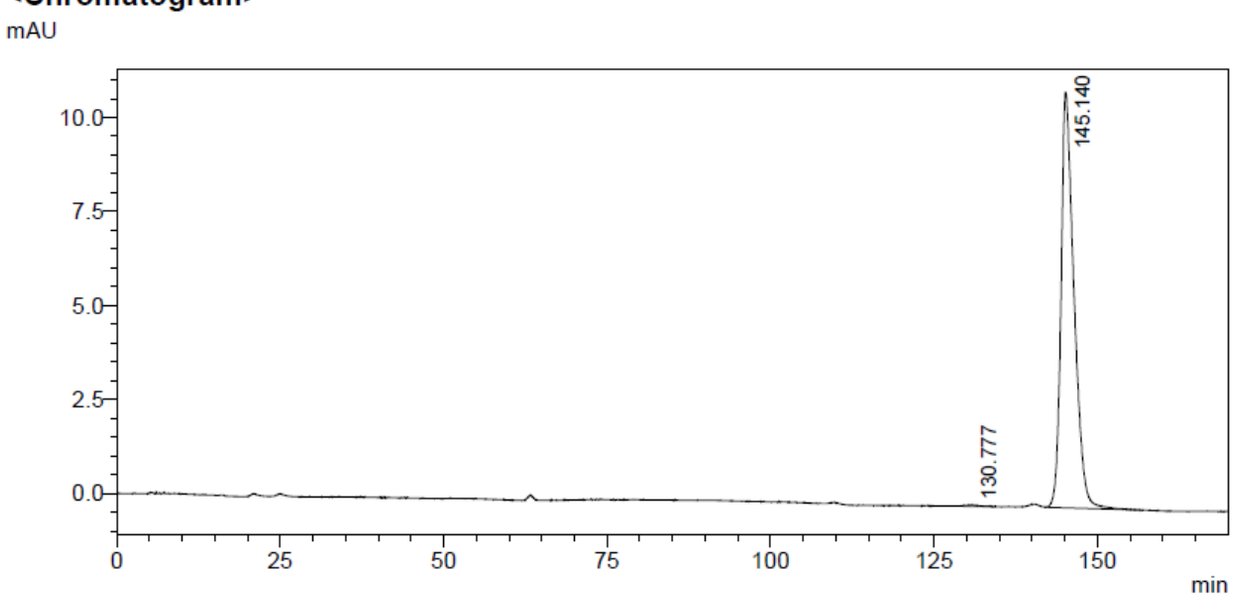

<Peak Table>

Detector A 254nm

Peak#	Ret. Time [min]	Area [mAU*s]	Total Area%
1	130.777	6085	0.398
2	145.140	1522591	99.602
Total		1528677	100.000

Figure 96: HPLC trace of Λ-**RhNP1** (99.2% ee).

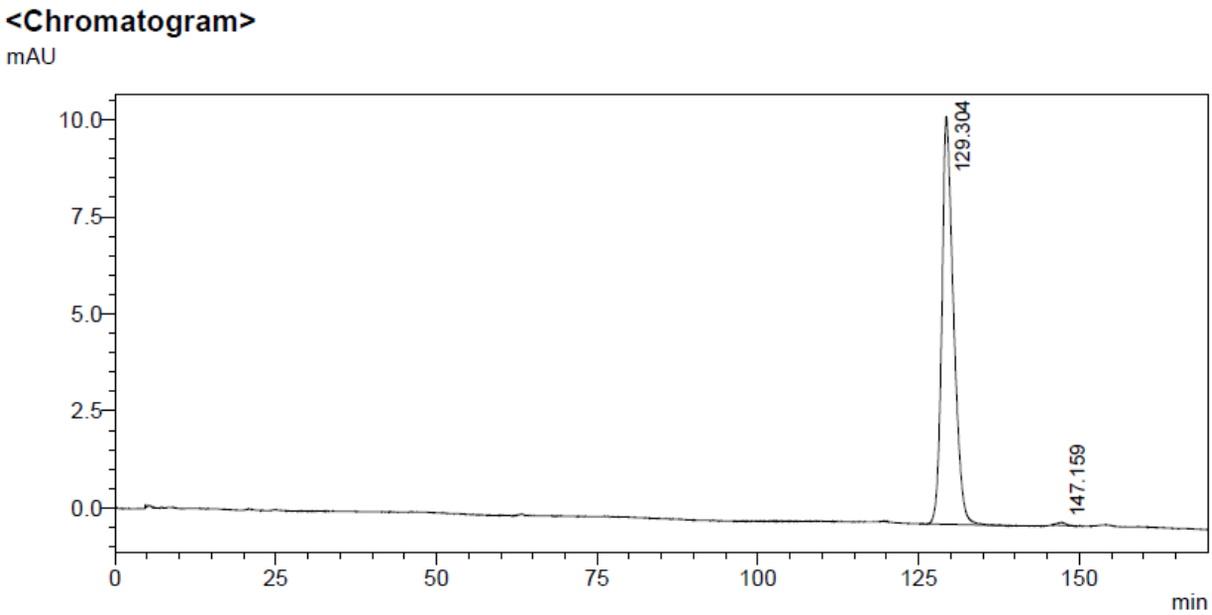

<Peak Table>

Detector A 254nm

Peak#	Ret. Time [min]	Area [mAU*s]	Total Area%
1	129.304	1332422	99.485
2	147.159	6896	0.515
Total		1339318	100.000

Figure 97: HPLC trace of Δ-**RhNP1** (99.0% ee).

Chiral HPLC Traces of Λ- and Δ-RhNP2:

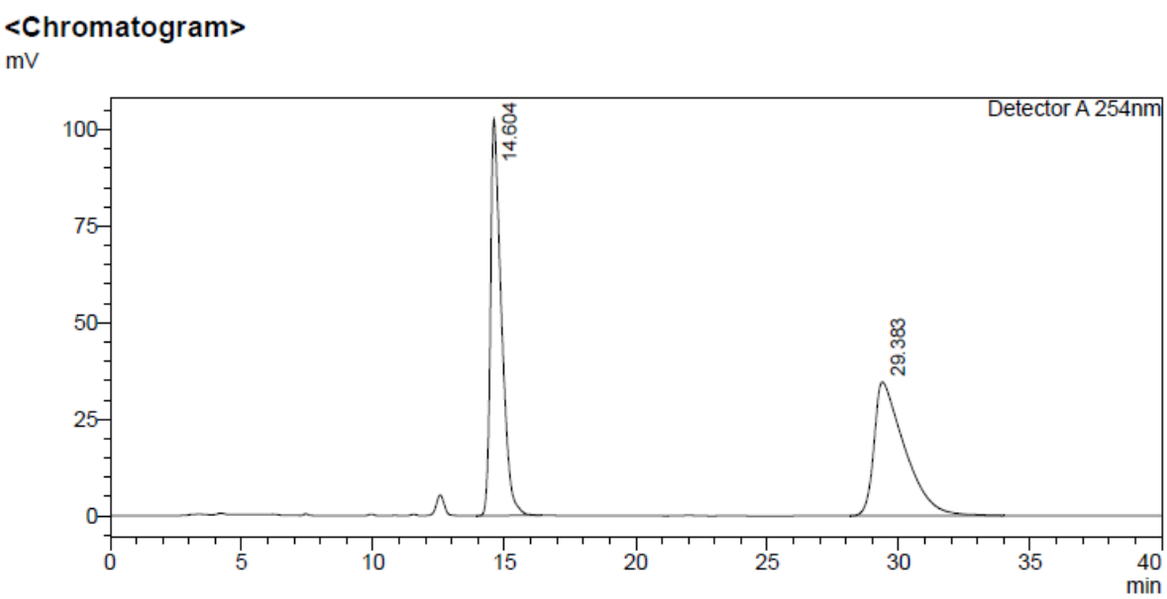

<Peak Table>

Detector A 254nm

Peak#	Ret. Time [min]	Area [mAU*s]	Total Area%
1	14.604	2956266	51.368
2	29.383	2798827	48.632
Total		5755093	100.000

Figure 98: HPLC trace of *rac*-**RhNP2**. HPLC conditions: Daicel Chiralpak® IB-N5 column, 250 x 4.6 mm, absorbance at 254 nm, H_2O + 0.1% TFA/MeCN = 30:70, isocratic flow, flow rate 0.6 mL/min, 25 °C.

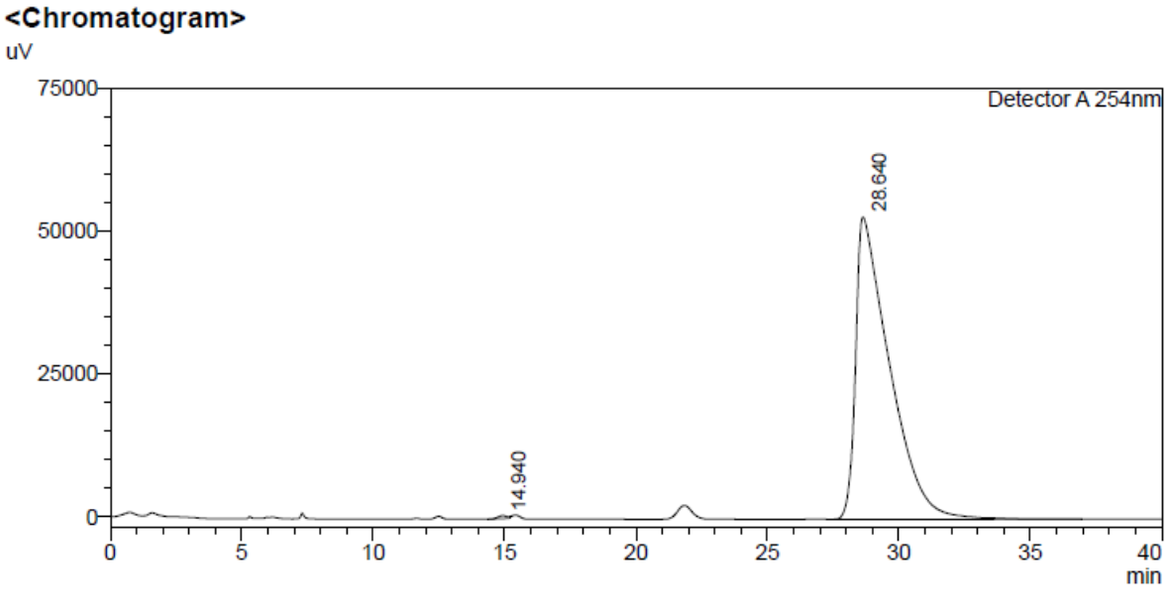

<Peak Table>

Detector A 254nm

Peak#	Ret. Time [min]	Area [mAU*s]	Total Area%
1	14.940	12777	0.268
2	28.640	4749862	99.732
Total		4762639	100.000

Figure 99: HPLC trace of Λ-**RhNP2** (99.5% ee).

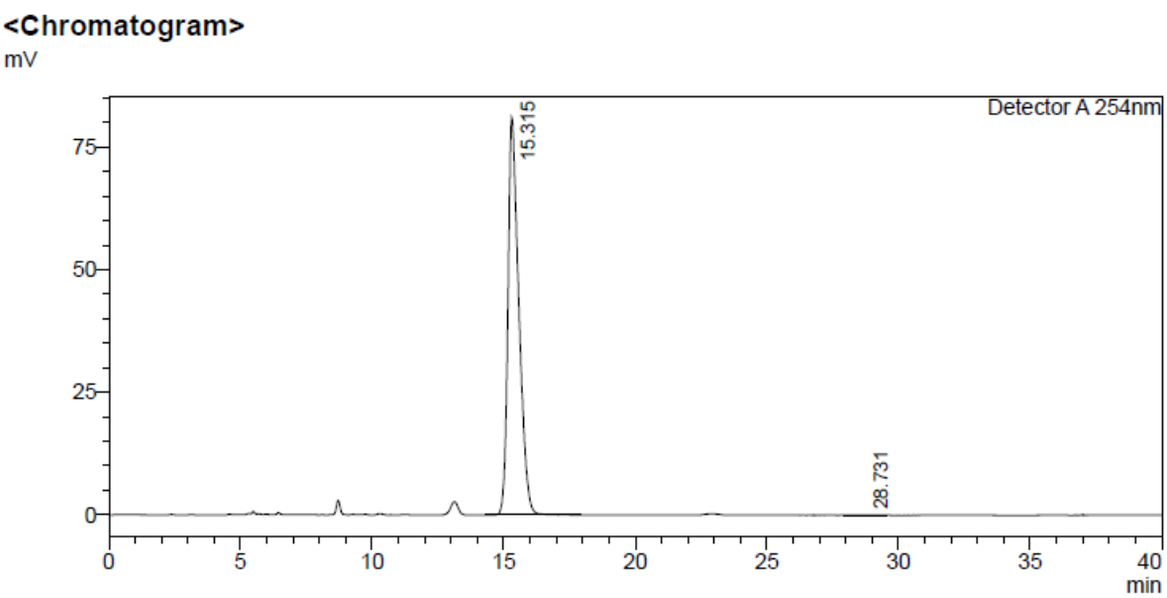

<Peak Table>

Detector A 254nm

Peak#	Ret. Time [min]	Area [mAU*s]	Total Area%
1	15.315	2337710	99.866
2	28.731	3131	0.134
Total		2340841	100.000

Figure 100: HPLC trace of Δ-**RhNP2** (99.7% ee).

6.3 CD Spectra

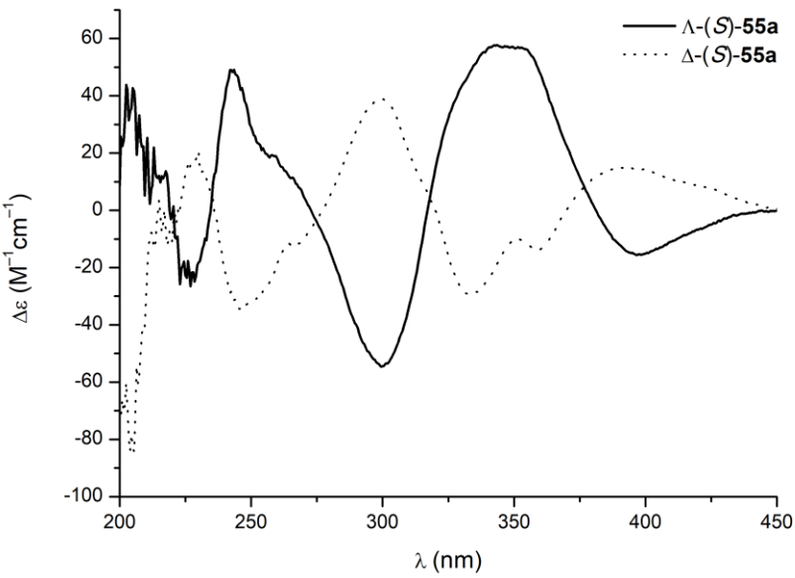

Figure 101: CD spectra (0.2 mM in MeOH) of Λ- and Δ-(*S*)-**55a**.

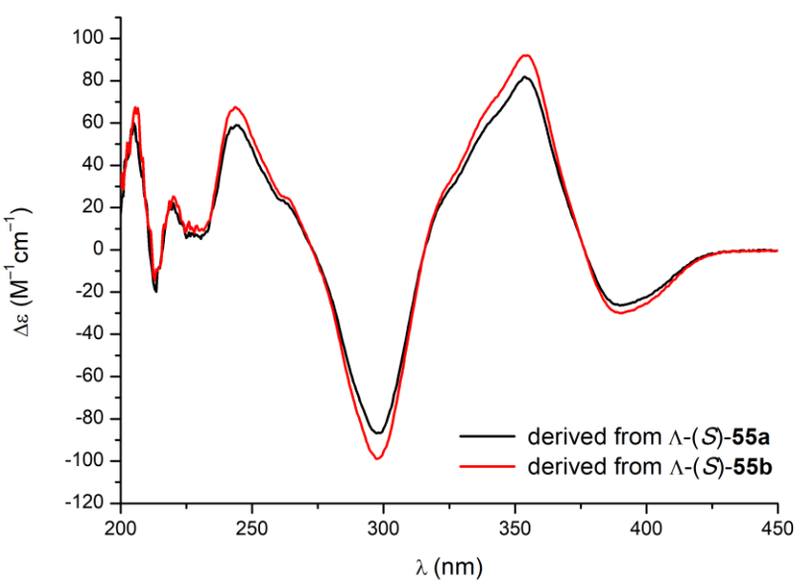

Figure 102: CD spectra (0.2 mM in MeOH) of Λ-(*S*)-**55a** and Λ-(*S*)-**55b** after cleavage of the chiral auxiliary showing that both diastereomers possess the same metal-centered configuration.

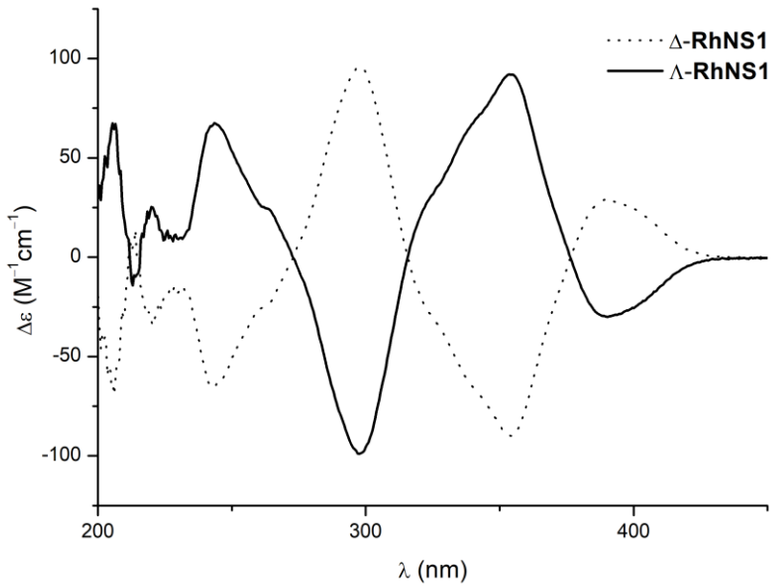

Figure 103: CD spectra (0.2 mM in MeOH) of Λ- and Δ-**RhNS1**.

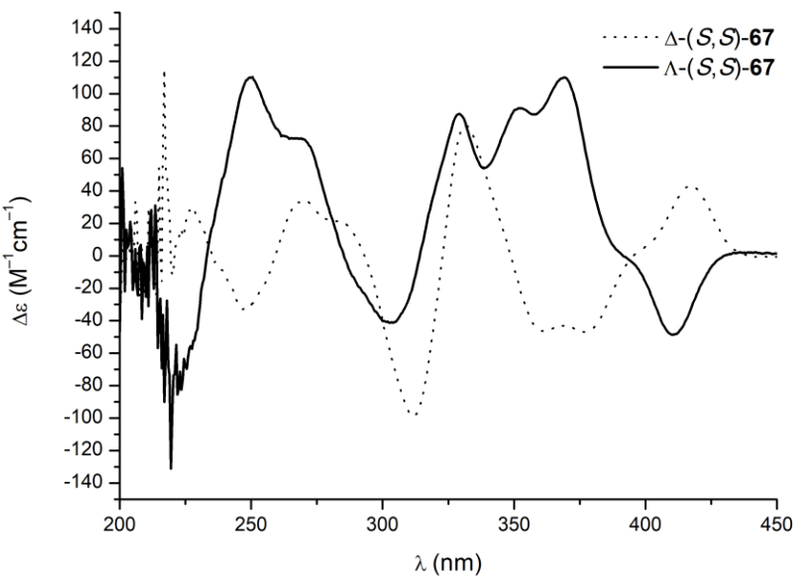

Figure 104: CD spectra (0.2 mM in CH_2Cl_2) of Λ- and Δ-(*S*,*S*)-**67**.

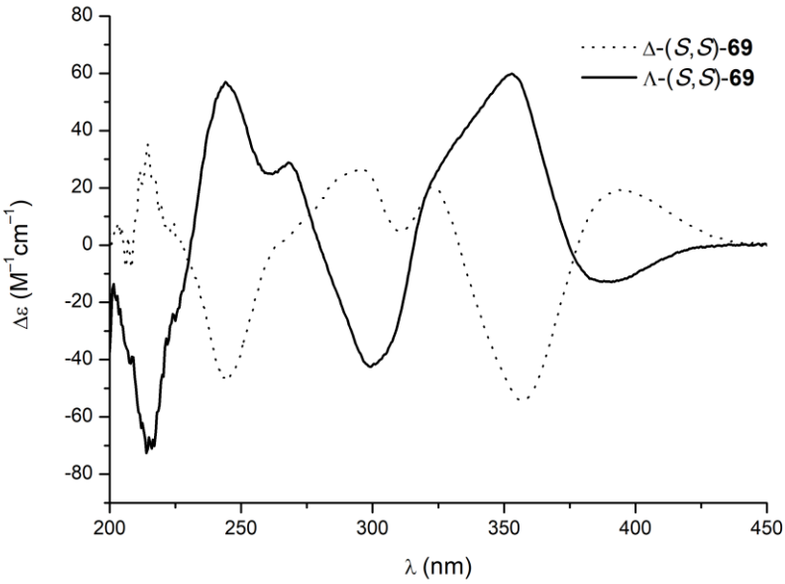

Figure 105: CD spectra (0.2 mM in MeOH) of Λ- and Δ-(*S*,*S*)-**69**.

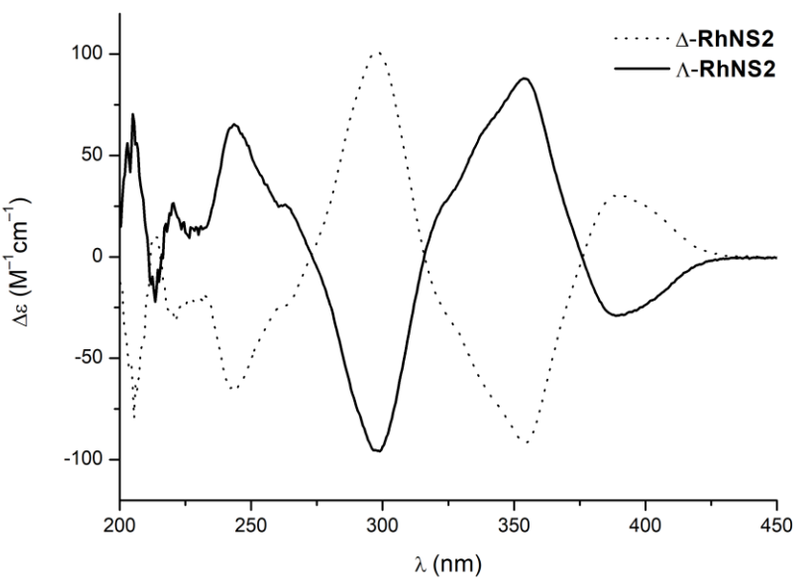

Figure 106: CD spectra (0.2 mM in MeOH) of Λ- and Δ-**RhNS2**.

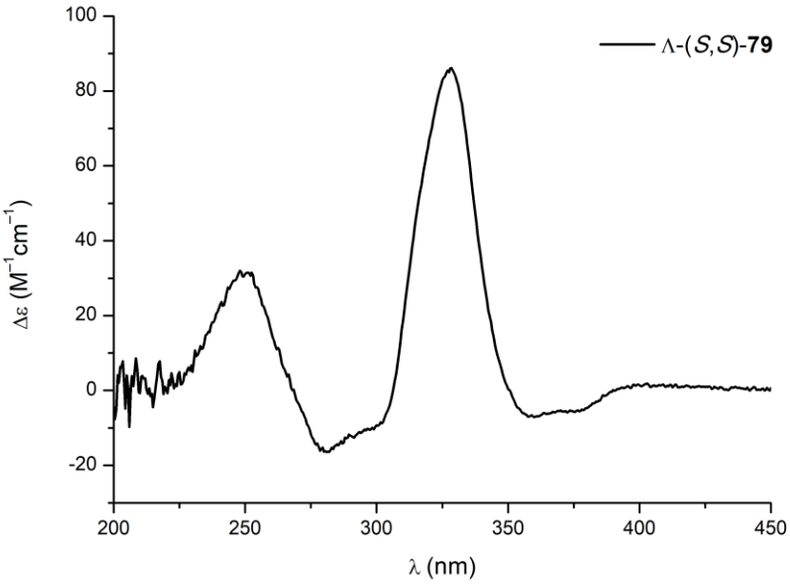

Figure 107: CD spectrum (0.2 mM in CH_2Cl_2) of Λ-(*S*,*S*)-**79**.

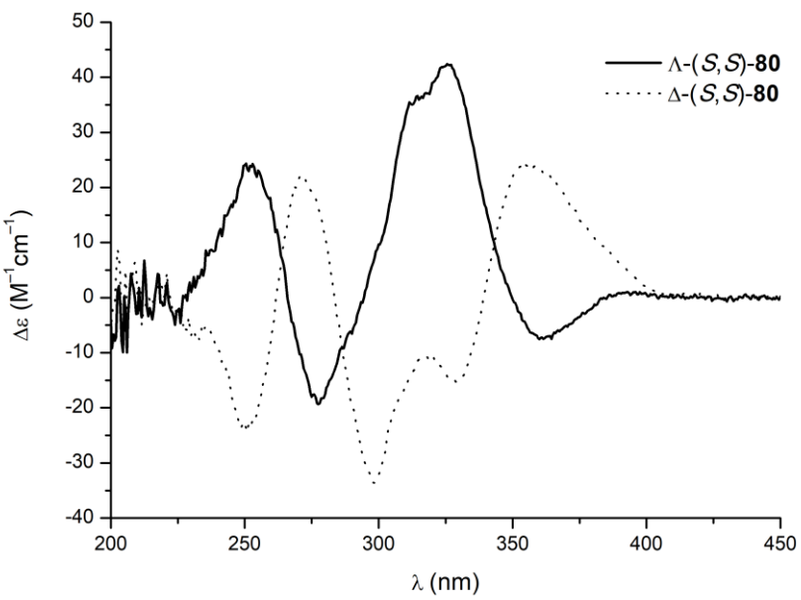

Figure 108: CD spectra (0.2 mM in CH_2Cl_2) of Λ- and Δ-(*S*,*S*)-**80**.

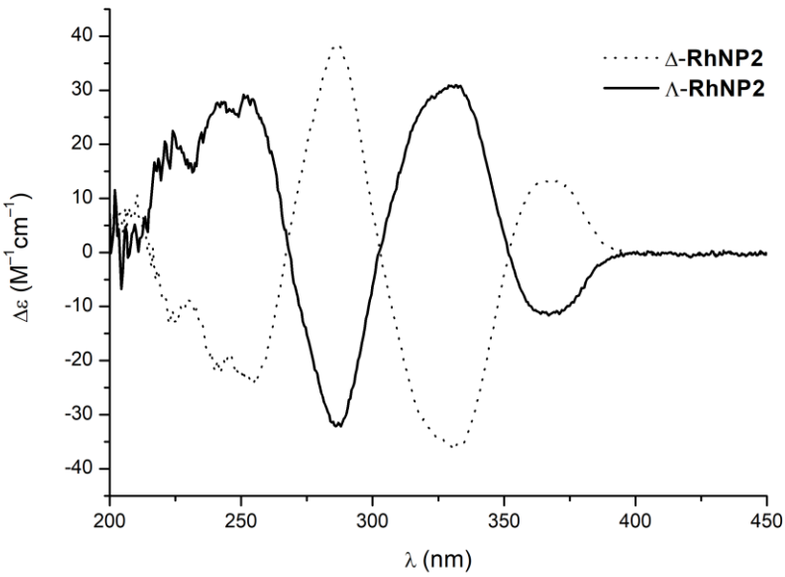

Figure 109: CD spectra (0.2 mM in MeOH) of Λ- and Δ-**RhNP2**.

6.4 Crystallographic Data

General Remarks

Single crystal X-ray diffraction measurements were performed by the members of the department for crystal structure analysis at the Philipps-Universität Marburg. Crystal structures of mono-cyclometalated rhodium complexes **48a** and **48c**, Δ-(*S*)-**55a**, Δ-**RhNS1**, cyclobutane **61**, Λ-(*S*,*S*)-**67** and Λ-(*S*,*S*)-**69**, *rac*-**RhNP1**. were evaluated by **Dr. Klaus Harms**, the former head of the X-ray service department. For all these structures, diffraction data were collected and structures were solved and refined as follows:

Data were collected[218] with a STOE STADIVARI diffractometer equipped with Cu-Kα radiation, a graded multilayer mirror monochromator (λ = 1.54186 Å) and a DECTRIS PILATUS 300K detector using an oil-coated shock-cooled crystal at 100(2) K. Absorption effects were corrected semi-empirical using multi-scanned reflections (STOE LANA, absorption correction by scaling of reflection intensities[219]). The number of observed reflections of the data collection, which was used to refine the cell constants, is given in the corresponding crystal data tables under "Cell determination".[220] Structures were solved by direct methods by using the program XT V2014/1 (Bruker AXS Inc., 2014)[221] and refined by full matrix least squares procedures on F^2 using SHELXL-2018/1 (Sheldrick, 2018)[222]. The non-hydrogen atoms have been refined anisotropically, carbon bonded hydrogen atoms were included at calculated positions and refined using the 'riding model' with isotropic temperature factors at 1.2 times (for CH_3 groups 1.5 times) that of the preceding carbon atom. CH_3 groups were allowed to rotate about the bond to their next atom to fit the electron density. Further details and deviations from the procedure described here are given for each crystal structure individually in the corresponding section.

Published structures have been deposited in the Cambridge Structural Database. The supplementary crystallographic data can be obtained free of charge from The Cambridge Crystallographic Data Centre via www.ccdc.cam.ac.uk/structures.

Single Crystal X-Ray Diffraction Data of Complex 48a

Single crystals of mono-cyclometalated rhodium(III) complex **48a** suitable for X-ray diffraction were obtained by adding a few drops of Et_2O to a saturated solution of complex **48a** (20 mg) in acetonitrile in a 10 mL vial. Crystals were obtained after two days at room temperature. The crystal structure is shown in Figure 110. Crystal data and details of the structure determination are presented in Table 10.

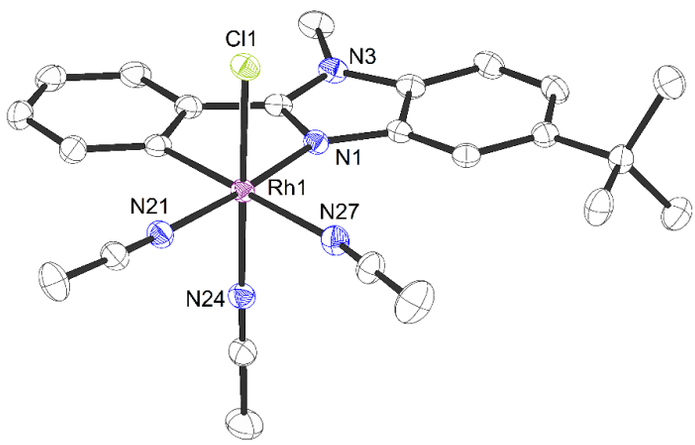

Figure 110: Crystal structure of mono-cyclometalated rhodium complex **48a** as an ORTEP drawing with 50% probability thermal ellipsoids. The PF_6^- counterion and solvent molecules are omitted for clarity.

Table 10: Crystal Data and Details of the Structure Determination for Complex **48a**.

Crystal Data:

Identification code	YG025	
Habitus, colour	needle, colorless	
Crystal size	0.18 x 0.07 x 0.05 mm^3	
Crystal system	Triclinic	
Space group	P-1	Z = 2
Unit cell dimensions	a = 9.9111(2) Å	α = 77.173(1)°
	b = 12.4199(2) Å	β = 77.673(1)°
	c = 14.0725(2) Å	γ = 88.433(1)°
Volume	1649.72(5) $Å^3$	
Cell determination	44470 peaks with Theta 3.7 to 76.1°	
Empirical formula	C_{28} H_{34} Cl F_6 N_7 P Rh	
Moiety formula	C_{24} H_{28} Cl N_5 Rh, F_6 P, 2(C_2 H_3 N)	
Formula weight	751.95	
Density (calculated)	1.514 Mg/m^3	
Absorption coefficient	5.960 mm^{-1}	
F(000)	764	

Data collection:

Diffractometer type	STOE STADIVARI
Wavelength	1.54178 Å
Temperature	100(2) K
Theta range for data collection	3.651 to 75.268°
Index ranges	–12<=h<=12, –15<=k<=9, –17<=l<=17
Data collection software	X-Area Pilatus3_SV 1.31.127.0 (STOE, 2016)[218]
Cell refinement software	X-Area Recipe 1.33.0.0 (STOE, 2015)[220]
Data reduction software	X-Area Integrate 1.71.0.0 (STOE, 2016)[223] X-Area LANA 1.68.2.0 (STOE, 2016)[219]

Solution and refinement:

Reflections collected	33864
Independent reflections	6705 [R(int) = 0.0352]
Completeness to theta = 67.679°	99.4%
Observed reflections	6035[I > 2σ(I)]
Reflections used for refinement	6705
Absorption correction	Semi-empirical from equivalents[219]
Max. and min. transmission	0.2721 and 0.0784
Largest diff. peak and hole	0.691 and –0.564 e·Å^{-3}
Solution	intrinsic phases[221]
Refinement	Full-matrix least-squares on F^2[222]
Treatment of hydrogen atoms	Calculated positions, constr. ref.
Programs used	XT V2014/1 (Bruker AXS Inc., 2014)[221] SHELXL-2017/1 (Sheldrick, 2017)[222] DIAMOND (Crystal Impact)[224] ShelXle (Hübschle, Sheldrick, Dittrich, 2011)[225]
Data / restraints / parameters	6705 / 465 / 470
Goodness-of-fit on F^2	0.984
R index (all data)	wR2 = 0.0620
R index conventional [I >2 σ(I)]	R1 = 0.0237
CCDC	1892283

Single Crystal X-Ray Diffraction Data of Complex 48c

Single crystals of mono-cyclometalated rhodium(III) complex **48c** suitable for X-ray diffraction were obtained by adding a few drops of Et_2O to a saturated solution of complex **48c** (20 mg) in acetonitrile in a 10 mL vial. Crystals were obtained after several days at room temperature. The crystal structure is shown in Figure 111. Crystal data and details of the structure determination are presented in Table 11.

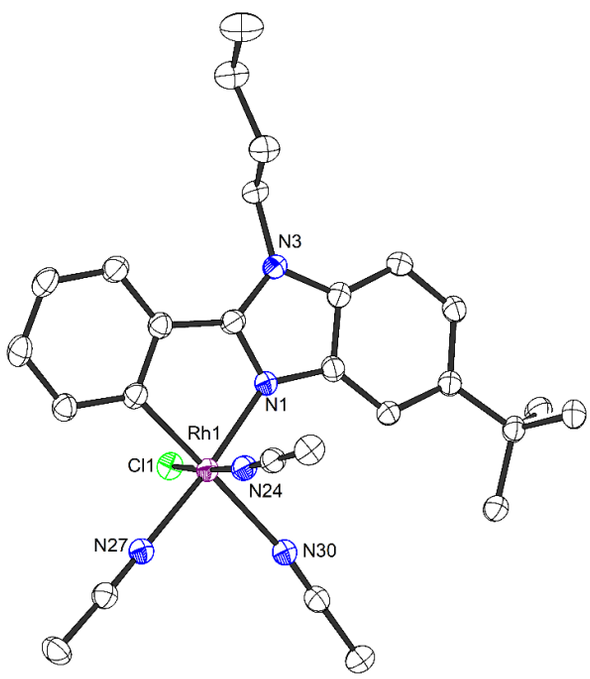

Figure 111: Crystal structure of mono-cyclometalated rhodium complex **48c** as an ORTEP drawing with 50% probability thermal ellipsoids. The PF_6^- counterion and solvent molecules are omitted for clarity.

Table 11: Crystal Data and Details of the Structure Determination for Complex **48c**.

Crystal data:

Identification code	PS020	
Habitus, color	block, yellow	
Crystal size	0.30 x 0.24 x 0.15 mm^3	
Crystal system	Monoclinic	
Space group	$P2_1/c$	Z = 4
Unit cell dimensions	a = 16.4855(2) Å	α = 90°
	b = 9.2164(2) Å	β = 104.205(1)°
	c = 20.9490(4) Å	γ = 90°
Volume	3085.61(10) $Å^3$	
Cell determination	37958 peaks with Theta 2.8 to 76.5°	

Empirical formula	C_{27} H_{34} Cl F_6 N_5 P Rh
Moiety formula	C_{27} H_{34} Cl N_5 Rh, F_6 P
Formula weight	711.92
Density (calculated)	1.532 Mg/m^3
Absorption coefficient	6.316 mm^{-1}
F(000)	1448

Data collection:

Diffractometer type	STOE STADIVARI
Wavelength	1.54186 Å
Temperature	100(2) K
Theta range for data collection	2.765 to 76.204°
Index ranges	–20<=h<=20, –11<=k<=9, –26<=l<=18
Data collection software	X-Area Pilatus3_SV 1.31.127.0 (STOE, 2016)[218]
Cell refinement software	X-Area Recipe 1.33.0.0 (STOE, 2015)[220]
Data reduction software	X-Area Integrate 1.71.0.0 (STOE, 2016)[223]
	X-Area LANA 1.68.2.0 (STOE, 2016)[219]

Solution and refinement:

Reflections collected	29163
Independent reflections	6342 [R(int) = 0.0248]
Completeness to theta = 67.686°	99.9%
Observed reflections	5958[I > 2σ(I)]
Reflections used for refinement	6342
Absorption correction	Semi-empirical from equivalents[219]
Max. and min. transmission	0.0904 and 0.0040
Largest diff. peak and hole	0.537 and –1.094 $e \cdot Å^{-3}$
Solution	intrinsic phases[221]
Refinement	Full-matrix least-squares on F^2[222]
Treatment of hydrogen atoms	Calculated positions, constr. ref.
Programs used	XT V2014/1 (Bruker AXS Inc., 2014)[221]
	SHELXL-2018/3 (Sheldrick, 2018)[222]
	DIAMOND (Crystal Impact)[224]
	ShelXle (Hübschle, Sheldrick, Dittrich, 2011)[225]
Data / restraints / parameters	6342 / 117 / 414
Goodness-of-fit on F^2	1.032
R index (all data)	wR2 = 0.0735
R index conventional [I > 2σ(I)]	R1 = 0.0275

Single Crystal X-Ray Diffraction Data of Δ-(*S*)-55a

Single crystals of Δ-(*S*)-**55a** were obtained by slow diffusion of *n*-hexane into a THF solution of Δ-(*S*)-**55a** (5 mg) in an NMR tube. The tube was stored at room temperature for several days. For Δ-(*S*)-**55a** disordered solvent could not be modelled and has been treated by using the PLATON/SQUEEZE procedure. The absolute configuration has been determined. The crystal structure is shown in Figure 112. Crystal data and details of the structure determination are presented in Table 12.

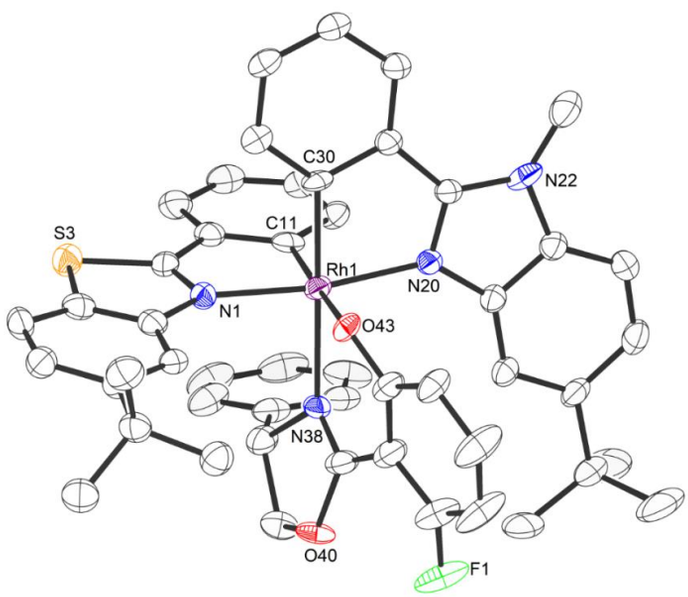

Figure 112: Crystal structure of auxiliary complex Δ-(*S*)-**55a** as an ORTEP drawing with 50% probability thermal ellipsoids. Solvent molecules are omitted for clarity.

Table 12: Crystal Data and Details of the Structure Determination for Δ-(*S*)-**55a**.

Crystal data:		
Identification code	YGauxD2	
Habitus, color	elongated plate, light yellow	
Crystal size	0.20 x 0.05 x 0.02 mm^3	
Crystal system	Monoclinic	
Space group	C2	Z = 4
Unit cell dimensions	a = 34.1885(15) Å	α = 90°
	b = 13.2574(4) Å	β = 105.243(3)°
	c = 11.0731(5) Å	γ = 90°
Volume	4842.3(3) $Å^3$	
Cell determination	75744 peaks with Theta 2.7 to 74.8°	
Empirical formula	C_{50} H_{46} F N_4 O_2 Rh S	

Moiety formula	C_{50} H_{46} F N_4 O_2 Rh S
Formula weight	888.88
Density (calculated)	1.219 Mg/m^3
Absorption coefficient	3.601 mm^{-1}
F(000)	1840

Data collection:

Diffractometer type	STOE STADIVARI
Wavelength	1.54186 Å
Temperature	100(2) K
Theta range for data collection	2.679 to 74.079°
Index ranges	–42<=h<=31, –15<=k<=16, –13<=l<=13
Data collection software	X-Area Pilatus3_SV 1.31.127.0 (STOE, 2016)[218]
Cell refinement software	X-Area Recipe 1.33.0.0 (STOE, 2015)[220]
Data reduction software	X-Area Integrate 1.71.0.0 (STOE, 2016)[223] X-Area LANA 1.68.2.0 (STOE, 2016)[219]

Solution and refinement:

Reflections collected	63788
Independent reflections	9544 [R(int) = 0.0995]
Completeness to theta = 67.686°	100.0%
Observed reflections	7480[I > 2σ(I)]
Reflections used for refinement	9544
Absorption correction	Semi-empirical from equivalents[219]
Max. and min. transmission	0.7651 and 0.0811
Flack parameter (absolute struct.)	–0.039(14)[226]
Largest diff. peak and hole	1.369 and –0.967 $e \cdot Å^{-3}$
Solution	intrinsic phases[221]
Refinement	Full-matrix least-squares on F^2[222]
Treatment of hydrogen atoms	Calculated positions, constr. ref.
Programs used	XT V2014/1 (Bruker AXS Inc., 2014)[221] SHELXL-2018/1 (Sheldrick, 2018)[222] DIAMOND (Crystal Impact)[224] ShelXle (Hübschle, Sheldrick, Dittrich, 2011)[225] PLATON/SQUEEZE (Spek, 2015)[227,228]
Data / restraints / parameters	9544 / 566 / 646
Goodness-of-fit on F^2	0.972
R index (all data)	wR2 = 0.1491
R index conventional [I > 2σ(I)]	R1 = 0.0620
CCDC	1892282

Single Crystal X-Ray Diffraction Data of Δ-RhNS1

Single crystals of Δ-**RhNS1** were obtained by slow diffusion of *n*-hexane into a THF/ acetonitrile solution of Δ-**RhNS1** (5 mg) in an NMR tube. The tube was stored at room temperature for several days. Data was collected with a STOE STADIVARI diffractometer equipped with Mo-Kα radiation, a graded multilayer mirror monochromator (λ = 0.71073 Å) and DECTRIS PILATUS 300K detector using an oil-coated shock-cooled crystal at 100(2) K. Disorder of ligands, anions, and solvent molecules has been refined using restraints for geometrical and anisotropic displacement parameters. A lot of reflections did not perfectly fit. The diffraction pattern showed superstructure effects that have not been taken into account. Some disordered solvent could not be modelled and has been treated using the PLATON/SQUEEZE procedure. The absolute configuration has been determined. The crystal structure is shown in Figure 113. Crystal data and details of the structure determination are presented in Table 13.

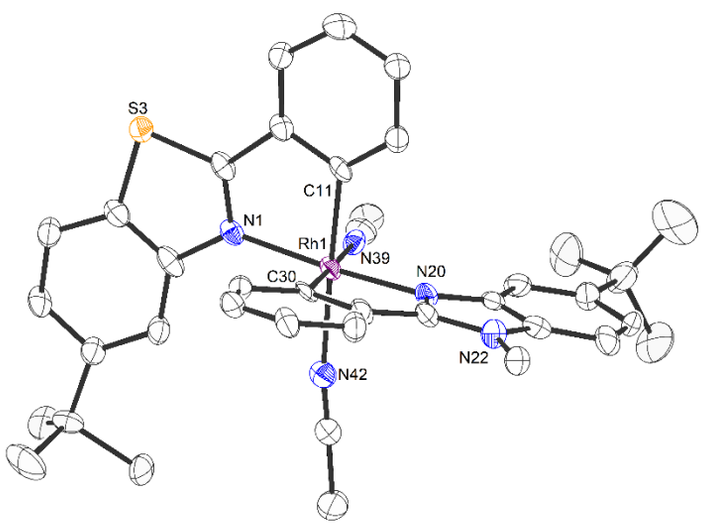

Figure 113: Crystal structure of Δ-**RhNS1** as an ORTEP drawing with 50% probability thermal ellipsoids. The PF_6^- counterion and solvent molecules are omitted for clarity.

Table 13: Crystal Data and Details of the Structure Determination for Δ-**RhNS1**.

Crystal data:	
Identification code	YG175D2
Habitus, color	elongated plate, colorless
Crystal size	0.55 x 0.13 x 0.08 mm^3
Crystal system	Triclinic
Space group	P1 Z = 2

Unit cell dimensions	a = 13.3149(6) Å	α = 96.082(3)°
	b = 13.9264(6) Å	β = 102.692(3)°
	c = 14.8787(7) Å	γ = 118.444(3)°
Volume	2294.17(19) $Å^3$	
Cell determination	28700 peaks with Theta 2.4 to 32.2°	
Empirical formula	$C_{43.85}$ $H_{50.28}$ F_6 $N_{5.43}$ O P Rh S	
Moiety formula	C_{39} H_{41} N_5 Rh S, F_6 P, C_4 H_8 O, 0.425(C_2 H_3 N)	
Formula weight	949.26	
Density (calculated)	1.374 Mg/m^3	
Absorption coefficient	0.516 mm^{-1}	
F(000)	979	

Data collection:

Diffractometer type	STOE STADIVARI
Wavelength	0.71073 Å
Temperature	100(2) K
Theta range for data collection	2.360 to 25.249°
Index ranges	–15<=h<=15, –16<=k<=16, –17<=l<=17
Data collection software	X-Area Pilatus3_SV 1.31.127.0 (STOE, 2016)[218]
Cell refinement software	X-Area Recipe 1.33.0.0 (STOE, 2015)[220]
Data reduction software	X-Area Integrate 1.71.0.0 (STOE, 2016)[223]
	X-Area LANA 1.68.2.0 (STOE, 2016)[219]

Solution and refinement:

Reflections collected	43220
Independent reflections	15622 [R(int) = 0.0817]
Completeness to theta = 25.242°	99.7%
Observed reflections	12615[I > 2σ(I)]
Reflections used for refinement	15622
Absorption correction	Semi-empirical from equivalents[219]
Max. and min. transmission	0.0707 and 0.0058
Flack parameter (absolute struct.)	0.02(3)[226]
Largest diff. peak and hole	2.955 and –0.674 $e \cdot Å^{-3}$
Solution	intrinsic phases[221]
Refinement	Full-matrix least-squares on F^2[222]
Treatment of hydrogen atoms	calculated positions, constr. ref.
Programs used	XT V2014/1 (Bruker AXS Inc., 2014)[221]
	SHELXL-2018/1 (Sheldrick, 2018)[222]
	DIAMOND (Crystal Impact)[224]
	ShelXle (Hübschle, Sheldrick, Dittrich, 2011)[225]
	PLATON/SQUEEZE (Spek, 2015)[227,228]
Data / restraints / parameters	15622 / 1630 / 1162
Goodness-of-fit on F^2	1.024
R index (all data)	wR2 = 0.1759
R index conventional [I > 2σ(I)]	R1 = 0.0589
CCDC	1892284

Single Crystal X-Ray Diffraction Data of Cyclobutane 61

Single crystals of compound **61** suitable for X-ray diffraction were obtained by slow diffusion of *n*-hexane into a solution of **61** (15 mg) in Et_2O and CH_2Cl_2 (only a few drops) in a 1 mL vial. Crystals were obtained after three days at room temperature. Nitrogen or oxygen bonded hydrogen atoms were located and allowed to refine isotropically. The absolute configuration of the molecule has been determined. The crystal structure is shown in Figure 114. Crystal data and details of the structure determination are presented in Table 14.

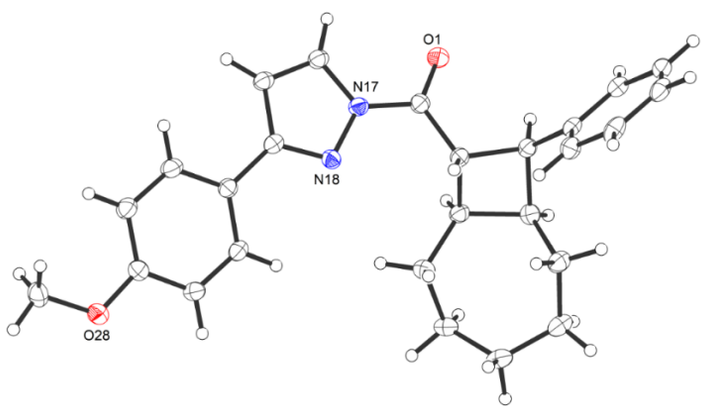

Figure 114: Crystal structure of **61** as an ORTEP drawing with 50% probability thermal ellipsoids.

Table 14: Crystal Data and Details of the Structure Determination for Compound **61**.

Crystal data:		
Identification code	YG212	
Habitus, color	nugget, colorless	
Crystal size	0.26 x 0.14 x 0.11 mm^3	
Crystal system	Monoclinic	
Space group	$P2_1$	Z = 2
Unit cell dimensions	a = 11.4060(6) Å	α = 90°
	b = 5.3747(2) Å	β = 106.822(4)°
	c = 17.5904(8) Å	γ = 90°
Volume	1032.21(8) $Å^3$	
Cell determination	29563 peaks with Theta 4.1 to 76.2°	
Empirical formula	$C_{26}H_{28}N_2O_2$	
Moiety formula	$C_{26}H_{28}N_2O_2$	
Formula weight	400.50	
Density (calculated)	1.289 Mg/m^3	
Absorption coefficient	0.641 mm^{-1}	
F(000)	428	

Data collection:

Diffractometer type	STOE STADIVARI
Wavelength	1.54186 Å
Temperature	100(2) K
Theta range for data collection	4.049 to 75.169°
Index ranges	–10<=h<=14, –6<=k<=6, –21<=l<=21
Data collection software	X-Area Pilatus3_SV 1.31.127.0 (STOE, 2016)[218]
Cell refinement software	X-Area Recipe 1.33.0.0 (STOE, 2015)[220]
Data reduction software	X-Area Integrate 1.71.0.0 (STOE, 2016)[223] X-Area LANA 1.68.2.0 (STOE, 2016)[219]

Solution and refinement:

Reflections collected	18034
Independent reflections	4042 [R(int) = 0.0264]
Completeness to theta = 67.686°	99.8%
Observed reflections	3861[I > 2σ(I)]
Reflections used for refinement	4042
Absorption correction	Semi-empirical from equivalents[219]
Max. and min. transmission	0.8287 and 0.2837
Flack parameter (absolute struct.)	0.09(8)[226]
Largest diff. peak and hole	0.248 and –0.234 e·Å^{-3}
Solution	intrinsic phases[221]
Refinement	Full-matrix least-squares on F^2[222]
Treatment of hydrogen atoms	Calculated positions, constr. ref.
Programs used	XT V2014/1 (Bruker AXS Inc., 2014)[221] SHELXL-2018/3 (Sheldrick, 2018)[222] DIAMOND (Crystal Impact)[224] ShelXle (Hübschle, Sheldrick, Dittrich, 2011)[225]
Data / restraints / parameters	4042 / 1 / 272
Goodness-of-fit on F^2	1.084
R index (all data)	wR2 = 0.0922
R index conventional [I > 2σ(I)]	R1 = 0.0343
CCDC	1892281

Single Crystal X-Ray Diffraction Data of Λ-(*S*,*S*)-67

Single crystals of Λ-(*S*,*S*)-**67** suitable for X-ray diffraction were obtained by slow diffusion of *n*-hexane into a CH_2Cl_2 solution of Λ-(*S*,*S*)-**67** (5 mg) in an NMR tube. Crystals were obtained after two days at room temperature. The absolute structure of this crystal has been established. The crystal structure is shown in Figure 115. Crystal data and details of the structure determination are presented in Table 15.

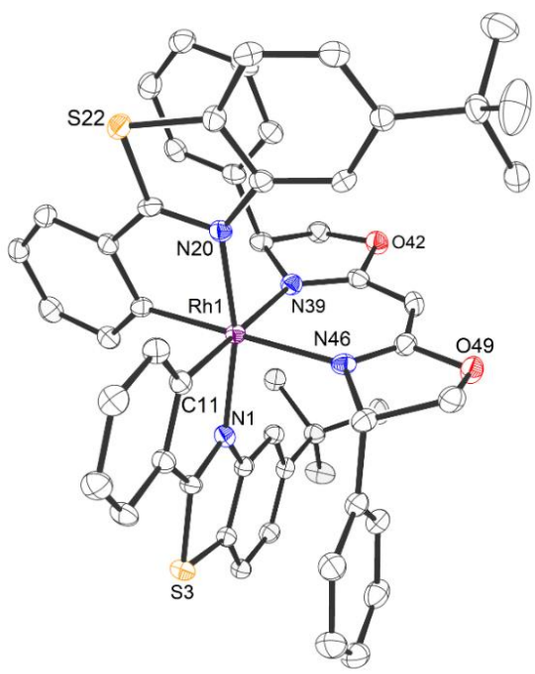

Figure 115: Crystal structure of auxiliary complex Λ-(*S*,*S*)-**67** as an ORTEP drawing with 50% probability thermal ellipsoids. Solvent molecules are omitted for clarity.

Table 15: Crystal Data and Details of the Structure Determination for Λ-(*S*,*S*)-**67**.

Crystal data:		
Identification code	YG236D1	
Habitus, color	needle, orange	
Crystal size	0.32 x 0.04 x 0.04 mm^3	
Crystal system	Orthorhombic	
Space group	$P2_12_12_1$	Z = 4
Unit cell dimensions	a = 10.2316(1) Å	α = 90°
	b = 13.2702(2) Å	β = 90°
	c = 32.2303(5) Å	γ = 90°
Volume	4376.08(10) $Å^3$	
Cell determination	38212 peaks with Theta 3.6 to 76.4°	

Empirical formula	C_{53} H_{49} N_4 O_2 Rh S_2
Moiety formula	C_{53} H_{49} N_4 O_2 Rh S_2
Formula weight	940.99
Density (calculated)	1.428 Mg/m^3
Absorption coefficient	4.418 mm^{-1}
F(000)	1952

Data collection:

Diffractometer type	STOE STADIVARI
Wavelength	1.54186 Å
Temperature	100(2) K
Theta range for data collection	3.602 to 76.103°
Index ranges	–11<=h<=12, –10<=k<=16, –39<=l<=37
Data collection software	X-Area Pilatus3_SV 1.31.127.0 (STOE, 2016)[218]
Cell refinement software	X-Area Recipe 1.33.0.0 (STOE, 2015)[220]
Data reduction software	X-Area Integrate 1.71.0.0 (STOE, 2016)[223] X-Area LANA 1.68.2.0 (STOE, 2016)[219]

Solution and refinement:

Reflections collected	46624
Independent reflections	8989 [R(int) = 0.0537]
Completeness to theta = 67.686°	99.8%
Observed reflections	8418[I > 2σ(I)]
Reflections used for refinement	8989
Absorption correction	Semi-empirical from equivalents[219]
Max. and min. transmission	0.3384 and 0.0958
Flack parameter (absolute struct.)	–0.021(3)[226]
Largest diff. peak and hole	0.409 and -0.616 $e \cdot Å^{-3}$
Solution	intrinsic phases[221]
Refinement	Full-matrix least-squares on F^2[222]
Treatment of hydrogen atoms	Calculated positions, constr ref
Programs used	XT V2014/1 (Bruker AXS Inc., 2014)[221] SHELXL-2018/3 (Sheldrick, 2018)[222] DIAMOND (Crystal Impact)[224] ShelXle (Hübschle, Sheldrick, Dittrich, 2011)[225]
Data / restraints / parameters	8989 / 0 / 565
Goodness-of-fit on F^2	0.997
R index (all data)	wR2 = 0.0684
R index conventional [I > 2σ(I)]	R1 = 0.0283
CCDC	1939489

Single Crystal X-Ray Diffraction Data of Λ-(*S*,*S*)-69

Single crystals of Λ-(*S*,*S*)-**69** suitable for X-ray diffraction were obtained by chance. After column chromatographic separation of the stereoisomers, the solvent (mixture of *n*-pentane/ EtOAc, plus 1% Et_3N) was reduced to approximately 5 mL under reduced pressure, then the corresponding 500 mL round bottom flask was left open to air for 30 min at room temperature. The absolute configuration has been determined. The crystal structure is shown in Figure 116. Crystal data and details of the structure determination are presented in Table 16.

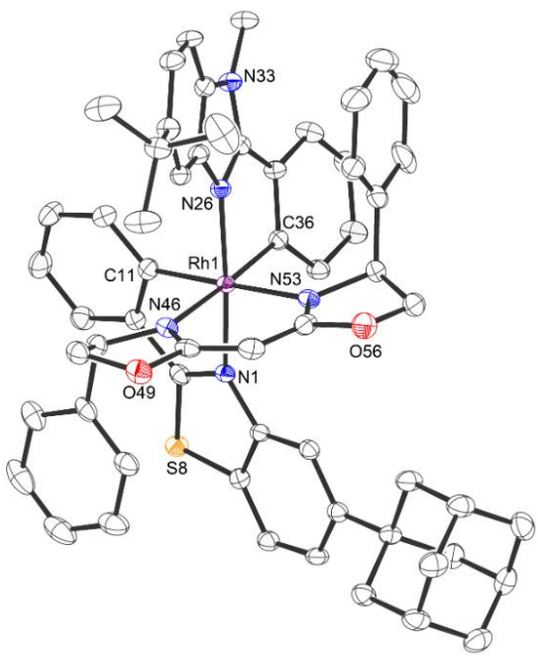

Figure 116: Crystal structure of auxiliary complex Λ-(*S*,*S*)-**69** as an ORTEP drawing with 50% probability thermal ellipsoids. Solvent molecules are omitted for clarity.

Table 16: Crystal Data and Details of the Structure Determination for Λ-(*S*,*S*)-**69**.

Crystal data:		
Identification code	ND223D1	
Habitus, color	prism, yellow	
Crystal size	0.41 x 0.30 x 0.24 mm^3	
Crystal system	Monoclinic	
Space group	$P2_1$	Z = 4
Unit cell dimensions	a = 17.2246(2) Å	α = 90°
	b = 13.1588(1) Å	β = 105.458(1)°
	c = 28.1023(3) Å	γ = 90°

Volume	6139.12(11) $Å^3$
Cell determination	146263 peaks with Theta 2.7 to 76.4°
Empirical formula	C_{70} H_{78} N_5 O_7 Rh S
Moiety formula	C_{60} H_{58} N_5 O_2 Rh S, 2.5(C_4 H_8 O_2)
Formula weight	1236.34
Density (calculated)	1.338 Mg/m^3
Absorption coefficient	3.037 mm^{-1}
F(000)	2600

Data collection:

Diffractometer type	STOE STADIVARI
Wavelength	1.54186 Å
Temperature	100(2) K
Theta range for data collection	2.662 to 75.677°
Index ranges	–18<=h<=21, –16<=k<=15, –33<=l<=35
Data collection software	X-Area Pilatus3_SV 1.31.127.0 (STOE, 2016)[218]
Cell refinement software	X-Area Recipe 1.33.0.0 (STOE, 2015)[220]
Data reduction software	X-Area Integrate 1.71.0.0 (STOE, 2016)[223]
	X-Area LANA 1.68.2.0 (STOE, 2016)[219]

Solution and refinement:

Reflections collected	124754
Independent reflections	24544 [R(int) = 0.0261]
Completeness to theta = 67.686°	99.9%
Observed reflections	23803[I > 2σ(I)]
Reflections used for refinement	24544
Absorption correction	Semi-empirical from equivalents[219]
Max. and min. transmission	0.2751 and 0.0900
Flack parameter (absolute struct.)	–0.013(2)[226]
Largest diff. peak and hole	0.957 and -0.718 $e \cdot Å^{-3}$
Solution	intrinsic phases[221]
Refinement	Full-matrix least-squares on F^2[222]
Treatment of hydrogen atoms	Calculated positions, constr. ref.
Programs used	XT V2014/1 (Bruker AXS Inc., 2014)[221]
	SHELXL-2018/3 (Sheldrick, 2018)[222]
	DIAMOND (Crystal Impact)[224]
	ShelXle (Hübschle, Sheldrick, Dittrich, 2011)[225]
Data / restraints / parameters	24544 / 1596 / 1772
Goodness-of-fit on F^2	1.043
R index (all data)	wR2 = 0.0874
R index conventional [I > 2σ(I)]	R1 = 0.0326
CCDC	1939490

Single Crystal X-Ray Diffraction Data of *rac*-RhNP1

Single crystals of *rac*-**RhNP1** suitable for X-ray diffraction were obtained by slow diffusion of *n*-hexane into a solution of *rac*-**RhNP1** (about 15 to 20 mg) in CH_2Cl_2 in a 1 mL vial. Crystals were obtained after several days at room temperature. The nitrogen hydrogen atom was located and allowed to refine isotropically. The crystal structure is shown in Figure 117. Crystal data and details of the structure determination are presented in Table 17.

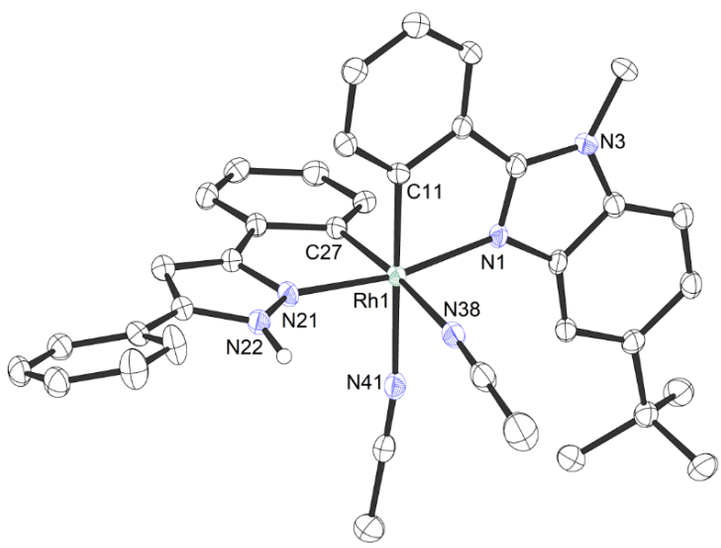

Figure 117: Crystal structure of *rac*-**RhNP1** as an ORTEP drawing with 50% probability thermal ellipsoids. The PF_6^- counterion and solvent molecules are omitted for clarity.

Table 17: Crystal Data and Details of the Structure Determination for *rac*-**RhNP1**.

Crystal data:		
Identification code	YG286	
Habitus, color	nugget, orange	
Crystal size	0.20 x 0.10 x 0.05 mm^3	
Crystal system	Triclinic	
Space group	P-1	Z = 2
Unit cell dimensions	a = 9.1813(3) Å	α = 101.846(3)°
	b = 13.3518(5) Å	β = 99.603(3)°
	c = 17.2012(5) Å	γ = 106.915(3)°
Volume	1915.79(12) $Å^3$	
Cell determination	48309 peaks with Theta 3.6 to 76.2°	
Empirical formula	C_{38} H_{38} Cl_2 F_6 N_6 P Rh	
Moiety formula	C_{37} H_{36} N_6 Rh, F_6 P, C H_2 Cl_2	
Formula weight	897.52	
Density (calculated)	1.556 Mg/m^3	

Absorption coefficient	5.859 mm^{-1}
F(000)	912

Data collection:

Diffractometer type	STOE STADIVARI
Wavelength	1.54186 Å
Temperature	100(2) K
Theta range for data collection	3.593 to 75.407°
Index ranges	–11<=h<=11, –11<=k<=16, –20<=l<=21
Data collection software	X-Area Pilatus3_SV 1.31.127.0 (STOE, 2016)[218]
Cell refinement software	X-Area Recipe 1.33.0.0 (STOE, 2015)[220]
Data reduction software	X-Area Integrate 1.71.0.0 (STOE, 2016)[223]
	X-Area LANA 1.68.2.0 (STOE, 2016)[219]

Solution and refinement:

Reflections collected	37060
Independent reflections	7720 [R(int) = 0.0780]
Completeness to theta = 67.686°	99.1%
Observed reflections	6913[I > 2σ(I)]
Reflections used for refinement	7720
Absorption correction	Semi-empirical from equivalents[219]
Max. and min. transmission	0.0757 and 0.0079
Largest diff. peak and hole	2.830 and –1.137 $e \cdot Å^{-3}$
Solution	Intrinsic phases[221]
Refinement	Full-matrix least-squares on F^2[222]
Treatment of hydrogen atoms	CH calc. pos., constr., NH located, isotr. ref.
Programs used	XT V2014/1 (Bruker AXS Inc., 2014)[221]
	SHELXL-2018/3 (Sheldrick, 2018)[222]
	DIAMOND (Crystal Impact)[224]
	ShelXle (Hübschle, Sheldrick, Dittrich, 2011)[225]
Data / restraints / parameters	7720 / 201 / 560
Goodness-of-fit on F^2	1.056
R index (all data)	wR2 = 0.1370
R index conventional [I > 2σ(I)]	R1 = 0.0520

General Remarks

Single crystal X-ray diffraction measurements were performed by the members of the department for crystal structure analysis at the Philipps-Universität Marburg. Crystal structures of complex **49**, *rac*-**RhNP2** and Δ-(*S*,*S*)-**80** were evaluated by **Dr. (RUS) Sergei Ivlev**, the current head of the X-ray service department. For all these structures, diffraction data were collected and structures were solved and refined as follows:

Suitable crystals of the indicated compounds were selected under inert oil and mounted using a MiTeGen loop. Intensity data of the crystals were recorded with a D8 Quest diffractometer (Bruker AXS). The instrument was operated with Mo-Kα radiation (0.71073 Å, microfocus source) and equipped with a PHOTON 100 detector. Evaluation, integration and reduction of the diffraction data was carried out using the Bruker APEX 3 software suite.[229] Multi-scan and numerical absorption corrections were applied using the SADABS program.[230,231] Structures were solved using dual-space methods (SHELXT-2014/5) and refined against F^2 (SHELXL-2018/3 using ShelXle interface).[225,222,221] All non-hydrogen atoms were refined with anisotropic displacement parameters. The hydrogen atoms were refined using the "riding model" approach with isotropic displacement parameters 1.2 times (1.5 for methyl groups) of that of the preceding carbon atom. Further details and deviations from the procedure described here are given for each crystal structure individually in the corresponding section.

Published structures have been deposited in the Cambridge Structural Database. The supplementary crystallographic data can be obtained free of charge from The Cambridge Crystallographic Data Centre via www.ccdc.cam.ac.uk/structures.

Single Crystal X-Ray Diffraction Data of Tetra-Acetonitrile Complex 49

Single crystals of complex **49** ($C_{26}H_{31}N_6Rh(PF_6)_2$) suitable for X-ray diffraction were obtained by slow diffusion of Et_2O into an acetonitrile solution of complex **49** (about 3 mg) in an NMR tube. Crystals were obtained after several days at room temperature. Intensity data of the crystal were recorded with a STADIVARI diffractometer (Stoe & Cie). The diffractometer was operated with Cu-Kα radiation (1.54186 Å, microfocus source) and equipped with a Dectris PILATUS 300K detector. Evaluation, integration and reduction of the diffraction data was carried out using the X Area software suite.[232] Multi-scan and numerical absorption corrections were applied with the X-Red32 and LANA modules of the X-Area software suite.[233,234] Two of the four PF_6^- anions showed signs of mild disorder. Introduction of the disorder into the refinement did not improve the model, therefore, the anions were safely refined as they are. The crystal structure contains solvent accessible channels. It was not possible to find an adequate model for the disordered solvent molecules in the channels. The corresponding residual electron density was eliminated using the SQUEEZE algorithm implemented in the PLATON software (92 electrons per 521 $Å^3$).[228,235] The crystal structure is shown in Figure 118. Selected crystallographic data and details of the structure determination are presented in Table 18.

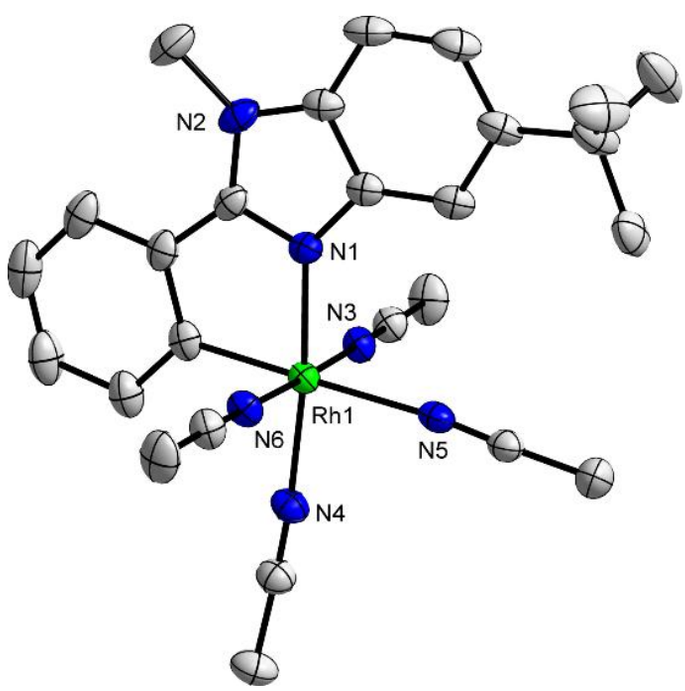

Figure 118: Crystal structure of complex **49**. The PF_6^- counterions and the hydrogen atoms are omitted for clarity. One of the two crystallographically independent cations is shown. Displacement ellipsoids are shown at 50% probability level at 100 K.

Table 18: Crystal Data and Details of the Structure Determination for Complex **49**.

Identification code	**YG410**
Empirical formula	$C_{26}H_{31}F_{12}N_6P_2Rh$
Molar mass / g·mol^{-1}	820.42
Space group (No.)	$I4_1$ (80)
***a* / Å**	33.5264(3)
***c* / Å**	13.1136(2)
***V* / Å^3**	14739.9(3)
Z	16
$\rho_{calc.}$ **/ g·cm^{-3}**	1.479
μ **/ mm^{-1}**	5.366
Color	colorless
Crystal habitus	needle
Crystal size / mm^3	0.385 x 0.095 x 0.070
***T* / K**	100
λ **/ Å**	1.54186 (Cu-K_α)
θ **range / °**	3.619 to 75.791
Range of Miller indices	$-42 \leq h \leq 38$
	$-34 \leq k \leq 41$
	$-16 \leq l \leq 14$
Absorption correction	multi-scan and numerical
T_{min}, T_{max}	0.1475, 0.5208
R_{int}, R_σ	0.0429, 0.0285
Completeness of the data set	0.999
No. of measured reflections	83005
No. of independent reflections	14778
No. of parameters	865
No. of restrains	1
***S* (all data)**	1.083
$R(F)$ $(I \geq 2\sigma(I)$**, all data)**	0.0364, 0.0389
$wR(F^2)$ $(I \geq 2\sigma(I)$**, all data)**	0.0950, 0.0962
Flack parameter *x*	0.000(6)
Extinction coefficient	not refined
$\Delta\rho_{max}$, $\Delta\rho_{min}$ **/ e·Å^{-3}**	0.565, –0.757

Single Crystal X-Ray Diffraction Data of *rac*-RhNP2

Single crystals of *rac*-**RhNP2** ($C_{46}H_{46}N_6Rh(PF_6)$) suitable for X-ray diffraction were obtained by slow diffusion of *n*-hexane into a CH_2Cl_2 solution of *rac*-**RhNP2** (about 3 mg) in an NMR tube. Crystals were obtained after several days at room temperature. The terminal *tert*-butyl group was rotationally disordered between two positions and was refined using the DSR plugin.[236] The structure contains solvent accessible voids filled primarily with CH_2Cl_2 molecules. However, a good refinement of the solvent was not possible, therefore, it was decided to remove the corresponding electron density using the SQUEEZE algorithm in the PLATON software.[228] The crystal structure is shown in Figure 119. Selected crystallographic data and details of the structure determination are presented in Table 19.

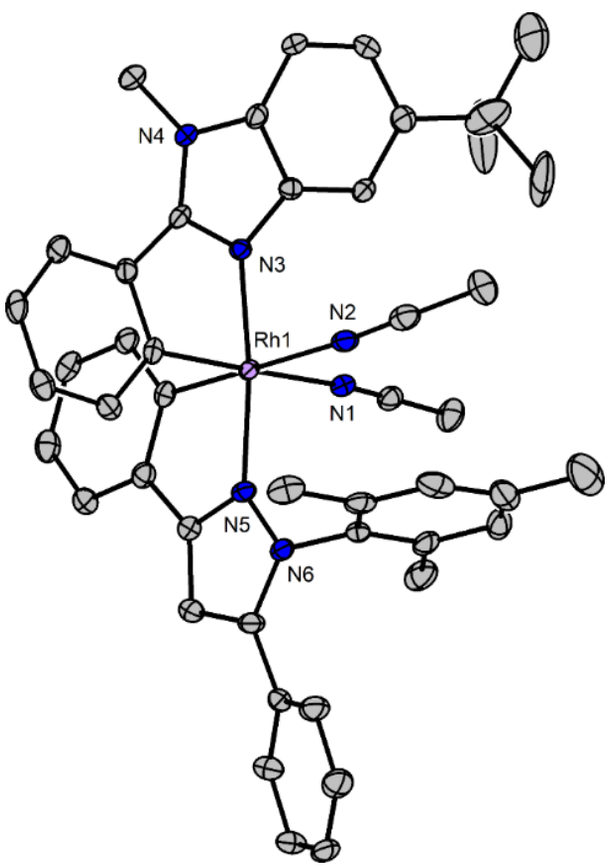

Figure 119: Crystal structure of *rac*-**RhNP2**. The PF_6^- counterion and the hydrogen atoms are omitted for clarity. Only one disordered *tert*-butyl group is shown. Displacement ellipsoids are shown at 50% probability level at 100 K.

Table 19: Crystal Data and Details of the Structure Determination for *rac*-**RhNP2**.

Identification code	**YG392**
Empirical formula	$C_{46}H_{46}F_6N_6PRh$
Molar mass / g·mol^{-1}	930.77
Space group (No.)	$P2_1/n$ (14)
***a* / Å**	8.7967(5)
***b* / Å**	23.7327(15)
***c* / Å**	22.4247(14)
***β* / °**	95.521(2)
***V* / Å^3**	4659.9(5)
Z	4
$\rho_{calc.}$ **/ g·cm^{-3}**	1.327
***μ* / mm^{-1}**	0.462
Color	colorless
Crystal habitus	needle
Crystal size / mm^3	0.359 x 0.067 x 0.056
***T* / K**	100
***λ* / Å**	0.71073 (Mo-K_α)
***θ* range / °**	1.944 to 28.350
Range of Miller indices	$-11 \leq h \leq 11$ $-24 \leq k \leq 31$ $-28 \leq l \leq 29$
Absorption correction	multi-scan and numerical
T_{min}, T_{max}	0.8712, 0.9867
R_{int}, R_σ	0.0669, 0.0611
Completeness of the data set	0.999
No. of measured reflections	72282
No. of independent reflections	11612
No. of parameters	591
No. of restrains	78
***S* (all data)**	1.020
***R*(*F*) (*I* ≥ 2*σ*(*I*), all data)**	0.0475, 0.0781
***wR*(*F*^{2}) (*I* ≥ 2*σ*(*I*), all data)**	0.0871, 0.0954
Extinction coefficient	not refined
$\Delta\rho_{max}$, $\Delta\rho_{min}$ **/ e·Å^{-3}**	0.674, –0.848
CCDC	2090827

Single Crystal X-Ray Diffraction Data of Δ-(*S*,*S*)-80

Single crystals of Δ-(*S*,*S*)-**80** ($C_{62}H_{56}N_7O_2Rh \cdot 2CH_2Cl_2$) suitable for X-ray diffraction were obtained by slow diffusion of *n*-hexane into a CH_2Cl_2 solution of Δ-(*S*,*S*)-**80** (about 3 mg) in an NMR tube. Crystals were obtained after several days at room temperature. All non-hydrogen atoms with the exception of one carbon atom (see below) were refined with anisotropic displacement parameters. The CH_2Cl_2 solvent molecules exhibit complicated disorder in the solvent accessible voids. Although the observed electron density was well resolved, in total six disordered species had to be employed to sufficiently model the disorder with the help of the DSR plugin[236] and the SUMP command in SHELXL. The refinement led to a good model quality and to good R-factors, though one carbon atom in one of the solvent molecules was refined with negative displacement parameter (which was then constrained). The overall occupancy of the CH_2Cl_2 molecules was restrained to eight molecules per unit cell, which matched very well the electron number per void obtained using the SQUEEZE algorithm in PLATON.[228] The absolute configuration of Δ-(*S*,*S*)-**80** has been determined. The crystal structure is shown in Figure 120. Selected crystallographic data and details of the structure determination are presented in Table 20.

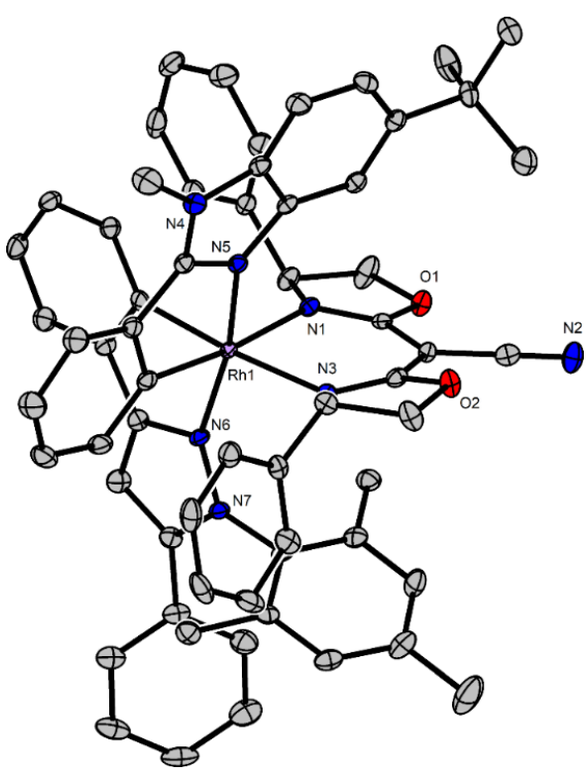

Figure 120: Crystal structure of auxiliary complex Δ-(*S*,*S*)-**80**. Solvent molecules and the hydrogen atoms are omitted for clarity. Displacement ellipsoids are shown at 50% probability level at 100 K.

Table 20: Crystal Data and Details of the Structure Determination for Δ-(*S*,*S*)-**80**.

Sample ID	**YG416D2**
Empirical formula	$C_{64}H_{60}Cl_4N_7O_2Rh$
Molar mass / g·mol^{-1}	1203.90
Space group (No.)	$P2_12_12_1$ (19)
***a* / Å**	11.9513(9)
***b* / Å**	16.5866(13)
***c* / Å**	30.088(2)
***V* / Å^3**	5964.3(8)
Z	4
$\rho_{calc.}$ **/ g·cm^{-3}**	1.341
μ **/ mm^{-1}**	0.515
Color	colorless
Crystal habitus	needle
Crystal size / mm^3	0. 304 x 0.093 x 0.063
***T* / K**	100
λ **/ Å**	0.71073 (Mo-K_α)
θ **range / °**	2.176 to 27.921
Range of Miller indices	$-15 \leq h \leq 15$ $-21 \leq k \leq 21$ $-39 \leq l \leq 39$
Absorption correction	multi-scan and numerical
T_{min}, T_{max}	0.9146, 0.9906
R_{int}, R_σ	0.0418, 0.0336
Completeness of the data set	0.999
No. of measured reflections	87649
No. of independent reflections	14242
No. of parameters	819
No. of restrains	207
***S* (all data)**	1.082
***R*(*F*) (*I* ≥ 2σ(*I*), all data)**	0.0307, 0.0362
***wR*(*F*^{2}) (*I* ≥ 2σ(*I*), all data)**	0.0639, 0.0655
Extinction coefficient	0.00096(14)
Flack parameter *x*	–0.023(5)
$\Delta\rho_{max}$, $\Delta\rho_{min}$ **/ e·Å^{-3}**	0.756, –0.479
CCDC	2090828

7. Abbreviations and Symbols

$\{^1H\}$	proton decoupled
δ	chemical shift
$\Delta\varepsilon$	molar absorptivity
λ	wavelength
Λ/Δ	absolute stereochemical descriptors: left- (Λ) and right- (Δ) handed propeller
$\tilde{\nu}$	wave number
θ	ellipticity
σ	mirror plane
AcOH	acetic acid
APCI	atmospheric pressure chemical ionization
BINAP	2,2'-bis(diphenylphosphino)-1,1'-binaphthyl
BINOL	1,1'-bi-2-naphthol
BINPO	(2-diphenylphosphino-2'-diphenylphosphineoxide)-binaphthyl
Boc	*tert*-butyloxycarbonyl
BOX	bis(oxazoline)
Bu	butyl
BuLi	butyllithium
calcd.	calculated
cat.	catalytic or catalyst
CCDC	Cambridge Crystallographic Data Centre
CD	circular dichroism
COD	1,5-cyclooctadiene
conv.	conversion
Cp*	1,2,3,4,5-pentamethylcyclopentadienyl ($C_5Me_5^-$)
Cy	cyclohexyl
de	diastereomeric excess
DIOP	*O*-isopropylidene-2,3-dihydroxy-1,4-bis(diphenylphosphino)butane
DiPAMP	1,2-bis[(2-methoxyphenyl)(phenyl)phosphaneyl]ethane
DMAP	4-(dimethylamino)pyridine
DMBA	2,2-dimethylbutanoic acid
DMF	*N*,*N*-dimethylformamide
DMSO	dimethyl sulfoxide
DOPA	3,4-dihydroxyphenylalanine
DQF-COSY	double-quantum filtered correlation spectroscopy
d.r.	diastereomeric ratio
EDC	1-ethyl-3-(3-dimethylaminopropyl) carbodiimide
ee	enantiomeric excess
e.g.	for example
EI	electron impact ionization
equiv.	equivalents
ESI	electrospray ionization
Et	ethyl
et al.	*et alii* (and others)
Et_2O	diethyl ether
EtOAc	ethyl acetate
EtOH	ethanol
FT-IR	Fourier transform infrared spectroscopy
·HCl	hydrochloride
HFIP	hexafluoroisopropanol
HMBC	heteronuclear multiple bond correlation

HOBt	1-hydroxybenzotriazole
$\cdot H_2O$	hydrate
HPLC	high-performance liquid chromatography
HRMS	high resolution mass spectrometry
HSQC	heteronuclear single quantum coherence
i	*iso*
J	coupling constant
K	Kelvin
KO*t*Bu	potassium *tert*-butoxide
LED	light-emitting diode
m-	*meta*-
M	molar mass; molar (mol/L)
*m*CPBA	*meta*-chloroperoxybenzoic acid
Me	methyl
MeCN	acetonitrile
MeOH	methanol
Mes	2,4,6-trimethylphenyl (mesityl)
mol%	molar percentage
m.p.	melting point
MS	molecular sieve
MsOH	methanesulfonic acid
m/z	mass-to-charge ratio
NCS	*N*-chlorosuccinimide
n.f.	not formed
n.i.	not isolated
NMM	*N*-methylmorpholine
NMR	nuclear magnetic resonance
NOE	nuclear Overhauser effect
NOESY	nuclear Overhauser enhancement spectroscopy
Nu	nucleophile
o-	*ortho*-
OAc	acetate
Oxone®	potassium peroxymonosulfate, sold as triple salt ($2\ KHSO_5 \cdot KHSO_4 \cdot K_2SO_4$)
p-	*para*-
Ph	phenyl
PHOX	phosphinooxazoline
ppm	parts per million
Pr	propyl
quant.	quantitative
R	rest, residue
R_f	retardation factor
r_t	retention time
r.t.	room temperature
sat.	saturated
S_NAr	nucleophilic aromatic substitution
t	*tert*
TBS	*tert*-butyldimethylsilyl
TFA	trifluoroacetic acid
TfCl	trifluoromethanesulfonyl chloride
TfOH	trifluoromethanesulfonic acid
THF	tetrahydrofuran
TLC	thin layer chromatography
TMEDA	*N,N,N',N'*-tetramethylethylenediamine
TMS	tetramethylsilane
Tos	toluenesulfonyl (tosyl)
UV	ultraviolet

8. References

[1] J. Halpern, B. M. Trost, *Proc. Natl. Acad. Sci. U.S.A.* **2004**, *101*, 5347.

[2] P. J. Walsh, M. C. Kozlowski, *Fundamentals of asymmetric catalysis*, University Science Books, Sausalito, Calif., **2009**.

[3] H. Huo, C. Fu, K. Harms, E. Meggers, *J. Am. Chem. Soc.* **2014**, *136*, 2990–2993.

[4] A. Pfaltz, W. J. Drury, *Proc. Natl. Acad. Sci. U.S.A.* **2004**, *101*, 5723–5726.

[5] C. Moberg, *Isr. J. Chem.* **2012**, *52*, 653–662.

[6] Oligomeric structures may possess rotational symmetry; for example, see: B. Wörsdörfer, L. M. Henning, R. Obexer, D. Hilvert, *ACS Catal.* **2012**, *2*, 982–985.

[7] C. E. Housecroft, A. G. Sharpe, *Inorganic chemistry*, 2nd Edition, Prentice Hall, Harlow, U.K., **2005**.

[8] C. Moberg, *Angew. Chem. Int. Ed.* **1998**, *37*, 248–268.

[9] J. K. Whitesell, *Chem. Rev.* **1989**, *89*, 1581–1590.

[10] A. Pfaltz, *Chimia* **2001**, *55*, 708–714.

[11] T. P. Yoon, E. N. Jacobsen, *Science* **2003**, *299*, 1691–1693.

[12] W. Sommer, D. Weibel, *Aldrich ChemFiles* **2008**, *8.2*, 2.

[13] Q.-L. Zhou (Ed.), *Privileged chiral ligands and catalysts*, Wiley-VCH, Weinheim, Germany, **2011**.

[14] T. P. Dang, H. B. Kagan, *J. Chem. Soc. D: Chem. Commun.* **1971**, 481.

[15] W. S. Knowles, *Angew. Chem. Int. Ed.* **2002**, *41*, 1998–2007.

[16] W. S. Knowles, *Acc. Chem. Res.* **1983**, *16*, 106–112.

[17] P. Ahlberg, *Advanced Information on the Nobel Prize in Chemistry 2001*, The Royal Swedish Academy of Sciences, Stockholm, Sweden, **2001**.

[18] A. Miyashita, A. Yasuda, H. Takaya, K. Toriumi, T. Ito, T. Souchi, R. Noyori, *J. Am. Chem. Soc.* **1980**, *102*, 7932–7934.

[19] T. Ohta, H. Takaya, M. Kitamura, K. Nagai, R. Noyori, *J. Org. Chem.* **1987**, *52*, 3174–3176.

[20] M. Kitamura, T. Ohkuma, S. Inoue, N. Sayo, H. Kumobayashi, S. Akutagawa, T. Ohta, H. Takaya, R. Noyori, *J. Am. Chem. Soc.* **1988**, *110*, 629–631.

[21] R. Noyori, T. Ikeda, T. Ohkuma, M. Widhalm, M. Kitamura, H. Takaya, S. Akutagawa, N. Sayo, T. Saito, T. Taketomi, H. Kumobayashi, *J. Am. Chem. Soc.* **1989**, *111*, 9134–9135.

[22] T. Ohkuma, H. Ooka, S. Hashiguchi, T. Ikariya, R. Noyori, *J. Am. Chem. Soc.* **1995**, *117*, 2675–2676.

[23] T. Ohkuma, H. Ooka, T. Ikariya, R. Noyori, *J. Am. Chem. Soc.* **1995**, *117*, 10417–10418.

[24] R. Noyori, *Angew. Chem. Int. Ed.* **2002**, *41*, 2008–2022.

[25] K. B. Sharpless, *Angew. Chem. Int. Ed.* **2002**, *41*, 2024–2032.

[26] K. Inoguchi, S. Sakuraba, K. Achiwa, *Synlett* **1992**, *1992*, 169–178.

[27] M. Chiba, H. Takahashi, H. Takahashi, T. Morimoto, K. Achiwa, *Tet. Lett.* **1987**, *28*, 3675–3678.

[28] G. Helmchen, A. Pfaltz, *Acc. Chem. Res.* **2000**, *33*, 336–345.

[29] G. J. Dawson, C. G. Frost, J. M. J. Williams, S. J. Coote, *Tet. Lett.* **1993**, *34*, 3149–3150.

[30] P. von Matt, A. Pfaltz, *Angew. Chem. Int. Ed.* **1993**, *32*, 566–568.

[31] J. Sprinz, G. Helmchen, *Tet. Lett.* **1993**, *34*, 1769–1772.

[32] I. Sagasser, G. Helmchen, *Tet. Lett.* **1998**, *39*, 261–264.

[33] Y. Uozumi, K. Kato, T. Hayashi, *Tetrahedron: Asymmetry* **1998**, *9*, 1065–1072.

[34] A. Pfaltz, J. Blankenstein, R. Hilgraf, E. Hörmann, S. McIntyre, F. Menges, M. Schönleber, S. P. Smidt, B. Wüstenberg, N. Zimmermann, *Adv. Synth. Catal.* **2003**, *345*, 33–43.

[35] J. W. Faller, B. J. Grimmond, D. G. D'Alliessi, *J. Am. Chem. Soc.* **2001**, *123*, 2525–2529.

[36] P. Kocovský, S. Vyskocil, M. Smrcina, *Chem. Rev.* **2003**, *103*, 3213–3246.

[37] M. T. Reetz, J.-A. Ma, R. Goddard, *Angew. Chem. Int. Ed.* **2005**, *44*, 412–415.

[38] M. Shibasaki, S. Matsunaga, *Chem. Soc. Rev.* **2006**, *35*, 269–279.

[39] X.-B. Yang, J. Feng, J. Zhang, N. Wang, L. Wang, J.-L. Liu, X.-Q. Yu, *Org. Lett.* **2008**, *10*, 1299–1302.

[40] B. M. Trost, D. A. Bringley, S. M. Silverman, *J. Am. Chem. Soc.* **2011**, *133*, 7664–7667.

[41] K. Endo, S. Yakeishi, D. Hamada, T. Shibata, *Chem. Lett.* **2013**, *42*, 547–549.

[42] S.-Y. Yan, Y.-Q. Han, Q.-J. Yao, X.-L. Nie, L. Liu, B.-F. Shi, *Angew. Chem. Int. Ed.* **2018**, *57*, 9093–9097.

[43] J.-M. Tian, A.-F. Wang, J.-S. Yang, X.-J. Zhao, Y.-Q. Tu, S.-Y. Zhang, Z.-M. Chen, *Angew. Chem. Int. Ed.* **2019**, *58*, 11023–11027.

[44] K. Endo, D. Hamada, S. Yakeishi, T. Shibata, *Angew. Chem. Int. Ed.* **2013**, *52*, 606–610.

[45] T. Ohshima, T. Kawabata, Y. Takeuchi, T. Kakinuma, T. Iwasaki, T. Yonezawa, H. Murakami, H. Nishiyama, K. Mashima, *Angew. Chem. Int. Ed.* **2011**, *50*, 6296–6300.

[46] V. Coeffard, M. Aylward, P. J. Guiry, *Angew. Chem. Int. Ed.* **2009**, *48*, 9152–9155.

[47] S. O'Reilly, P. J. Guiry, *Synthesis* **2014**, *46*, 722–739.

[48] H. A. McManus, P. J. Guiry, *J. Org. Chem.* **2002**, *67*, 8566–8573.

[49] H. A. McManus, P. G. Cozzi, P. J. Guiry, *Adv. Synth. Catal.* **2006**, *348*, 551–558.

[50] G. C. Hargaden, H. A. McManus, P. G. Cozzi, P. J. Guiry, *Org. Biomol. Chem.* **2007**, *5*, 763–766.

[51] G. C. Hargaden, T. P. O'Sullivan, P. J. Guiry, *Org. Biomol. Chem.* **2008**, *6*, 562–566.

[52] M. Inoue, M. Nakada, *Org. Lett.* **2004**, *6*, 2977–2980.

[53] M. Inoue, T. Suzuki, A. Kinoshita, M. Nakada, *Chem. Rec.* **2008**, *8*, 169–181.

[54] B. Qiu, D. Xu, Q. Sun, C. Miao, Y.-M. Lee, X.-X. Li, W. Nam, W. Sun, *ACS Catal.* **2018**, *8*, 2479–2487.

[55] W. Sun, Q. Sun, *Acc. Chem. Res.* **2019**, *52*, 2370–2381.

[56] D. Shen, C. Miao, S. Wang, C. Xia, W. Sun, *Eur. J. Inorg. Chem.* **2014**, *2014*, 5777–5782.

[57] A. Fujii, S. Hashiguchi, N. Uematsu, T. Ikariya, R. Noyori, *J. Am. Chem. Soc.* **1996**, *118*, 2521–2522.

[58] M. Langner, C. Bolm, *Angew. Chem. Int. Ed.* **2004**, *43*, 5984–5987.

[59] J. M. Fraile, J. I. García, A. Gissibl, J. A. Mayoral, E. Pires, O. Reiser, M. Roldán, I. Villalba, *Chem. Eur. J.* **2007**, *13*, 8830–8839.

[60] V. A. Pavlov, *Tetrahedron* **2008**, *64*, 1147–1179.

[61] K. Matsumoto, T. Oguma, T. Katsuki, *Angew. Chem. Int. Ed.* **2009**, *48*, 7432–7435.

[62] W. Chen, F. Spindler, B. Pugin, U. Nettekoven, *Angew. Chem. Int. Ed.* **2013**, *52*, 8652–8656.

[63] B. M. Trost, E. J. Donckele, D. A. Thaisrivongs, M. Osipov, J. T. Masters, *J. Am. Chem. Soc.* **2015**, *137*, 2776–2784.

[64] A. R. Keeri, I. Justyniak, J. Jurczak, J. Lewiński, *Adv. Synth. Catal.* **2016**, *358*, 864–868.

[65] P. J. Czerwiński, M. Michalak, *Synthesis* **2019**, *51*, 1689–1714.

[66] C. Lepori, R. Guillot, J. Hannedouche, *Adv. Synth. Catal.* **2019**, *361*, 714–719.

[67] G. Xu, C. H. Senanayake, W. Tang, *Acc. Chem. Res.* **2019**, *52*, 1101–1112.

[68] Z. Zhou, S. Chen, Y. Hong, E. Winterling, Y. Tan, M. Hemming, K. Harms, K. N. Houk, E. Meggers, *J. Am. Chem. Soc.* **2019**, *141*, 19048–19057.

[69] M. Fontecave, O. Hamelin, S. Ménage, *Top. Organomet. Chem.* **2005**, *15*, 271–288.

[70] Z.-Y. Cao, W. D. G. Brittain, J. S. Fossey, F. Zhou, *Catal. Sci. Technol.* **2015**, *5*, 3441–3451.

[71] L. Zhang, E. Meggers, *Chem. Asian J.* **2017**, *12*, 2335–2342.

[72] X. Shen, H. Huo, C. Wang, B. Zhang, K. Harms, E. Meggers, *Chem. Eur. J.* **2015**, *21*, 9720–9726.

[73] T. Deng, G. K. Thota, Y. Li, Q. Kang, *Org. Chem. Front.* **2017**, *4*, 573–577.

[74] K. Li, Q. Wan, Q. Kang, *Org. Lett.* **2017**, *19*, 3299–3302.

[75] S.-W. Li, J. Gong, Q. Kang, *Org. Lett.* **2017**, *19*, 1350–1353.

[76] Y. Tan, W. Yuan, L. Gong, E. Meggers, *Angew. Chem. Int. Ed.* **2015**, *54*, 13045–13048.

[77] C. Wang, L.-A. Chen, H. Huo, X. Shen, K. Harms, L. Gong, E. Meggers, *Chem. Sci.* **2015**, *6*, 1094–1100.

[78] G.-Q. Xu, H. Liang, J. Fang, Z.-L. Jia, J.-Q. Chen, P.-F. Xu, *Chem. Asian J.* **2016**, *11*, 3355–3358.

[79] C. Tian, L. Gong, E. Meggers, *Chem. Commun.* **2016**, *52*, 4207–4210.

[80] H. Huo, X. Shen, C. Wang, L. Zhang, P. Röse, L.-A. Chen, K. Harms, M. Marsch, G. Hilt, E. Meggers, *Nature* **2014**, *515*, 100–103.

[81] S.-X. Lin, G.-J. Sun, Q. Kang, *Chem. Commun.* **2017**, *53*, 7665–7668.

[82] X. Huang, E. Meggers, *Acc. Chem. Res.* **2019**, *52*, 833–847.

[83] H. Liang, G.-Q. Xu, Z.-T. Feng, Z.-Y. Wang, P.-F. Xu, *J. Org. Chem.* **2019**, *84*, 60–72.

[84] H. Brunner, *Angew. Chem. Int. Ed.* **1999**, *38*, 1194–1208.

[85] U. Knof, A. von Zelewsky, *Angew. Chem. Int. Ed.* **1999**, *38*, 302–322.

[86] H. Amouri, M. Gruselle, *Chirality in transition metal chemistry*, Wiley, Chichester, U.K., **2008**.

[87] E. Meggers, *Eur. J. Inorg. Chem.* **2011**, *2011*, 2911–2926.

[88] L. Zhang, E. Meggers, *Acc. Chem. Res.* **2017**, *50*, 320–330.

[89] C. Wang, Y. Zheng, H. Huo, P. Röse, L. Zhang, K. Harms, G. Hilt, E. Meggers, *Chem. Eur. J.* **2015**, *21*, 7355–7359.

[90] H. Huo, C. Wang, K. Harms, E. Meggers, *J. Am. Chem. Soc.* **2015**, *137*, 9551–9554.

[91] C. Wang, J. Qin, X. Shen, R. Riedel, K. Harms, E. Meggers, *Angew. Chem. Int. Ed.* **2016**, *55*, 685–688.

[92] H. Huo, K. Harms, E. Meggers, *J. Am. Chem. Soc.* **2016**, *138*, 6936–6939.

[93] J. Ma, X. Shen, K. Harms, E. Meggers, *Dalton Trans.* **2016**, *45*, 8320–8323.

[94] X. Huang, R. D. Webster, K. Harms, E. Meggers, *J. Am. Chem. Soc.* **2016**, *138*, 12636–12642.

[95] X. Shen, K. Harms, M. Marsch, E. Meggers, *Chem. Eur. J.* **2016**, *22*, 9102–9105.

[96] X. Huang, T. R. Quinn, K. Harms, R. D. Webster, L. Zhang, O. Wiest, E. Meggers, *J. Am. Chem. Soc.* **2017**, *139*, 9120–9123.

[97] L. Gong, S. P. Mulcahy, K. Harms, E. Meggers, *J. Am. Chem. Soc.* **2009**, *131*, 9602–9603.

[98] E. Meggers, *Chem. Eur. J.* **2010**, *16*, 752–758.

[99] L. Gong, M. Wenzel, E. Meggers, *Acc. Chem. Res.* **2013**, *46*, 2635–2644.

[100] J. Ma, X. Zhang, X. Huang, S. Luo, E. Meggers, *Nat. Protoc.* **2018**, *13*, 605–632.

[101] E. Marchi, R. Sinisi, G. Bergamini, M. Tragni, M. Monari, M. Bandini, P. Ceroni, *Chem. Eur. J.* **2012**, *18*, 8765–8773.

[102] Y. Grell, Y. Hong, X. Huang, T. Mochizuki, X. Xie, K. Harms, E. Meggers, *Organometallics* **2019**, *38*, 3948–3954.

[103] P. Beaulieu, B. Haché, E. von Moos, *Synthesis* **2003**, 1683–1692.

[104] S. Brunen, Y. Grell, P. S. Steinlandt, K. Harms, E. Meggers, *Molecules* **2021**, *26*, 1822.

[105] M. Nonoyama, *Bull. Chem. Soc. Jpn.* **1974**, *47*, 767–768.

[106] M. Felici, P. Contreras-Carballada, J. M. M. Smits, R. J. M. Nolte, R. M. Williams, L. de Cola, M. C. Feiters, *Molecules* **2010**, *15*, 2039–2059.

[107] R. M. Edkins, A. Wriglesworth, K. Fucke, S. L. Bettington, A. Beeby, *Dalton Trans.* **2011**, *40*, 9672–9678.

[108] E. Baranoff, B. F. E. Curchod, J. Frey, R. Scopelliti, F. Kessler, I. Tavernelli, U. Rothlisberger, M. Grätzel, M. K. Nazeeruddin, *Inorg. Chem.* **2012**, *51*, 215–224.

[109] M. Lepeltier, F. Dumur, B. Graff, P. Xiao, D. Gigmes, J. Lalevée, C. R. Mayer, *Helv. Chim. Acta* **2014**, *97*, 939–956.

[110] X. Xu, X. Yang, J. Dang, G. Zhou, Y. Wu, H. Li, W.-Y. Wong, *Chem. Commun.* **2014**, *50*, 2473–2476.

[111] X. Xu, X. Yang, Y. Wu, G. Zhou, C. Wu, W.-Y. Wong, *Chem. Asian J.* **2015**, *10*, 252–262.

[112] Y. Cudré, F. Franco de Carvalho, G. R. Burgess, L. Male, S. J. A. Pope, I. Tavernelli, E. Baranoff, *Inorg. Chem.* **2017**, *56*, 11565–11576.

[113] Y. Hisamatsu, S. Kumar, S. Aoki, *Inorg. Chem.* **2017**, *56*, 886–899.

[114] Y. Tamura, Y. Hisamatsu, S. Kumar, T. Itoh, K. Sato, R. Kuroda, S. Aoki, *Inorg. Chem.* **2017**, *56*, 812–833.

[115] V. Adamovich, S. Bajo, P.-L. T. Boudreault, M. A. Esteruelas, A. M. López, J. Martín, M. Oliván, E. Oñate, A. U. Palacios, A. San-Torcuato, J.-Y. Tsai, C. Xia, *Inorg. Chem.* **2018**, *57*, 10744–10760.

[116] T. B. Nguyen, L. Ermolenko, P. Retailleau, A. Al-Mourabit, *Angew. Chem. Int. Ed.* **2014**, *53*, 13808–13812.

[117] O. Chepelin, J. Ujma, X. Wu, A. M. Z. Slawin, M. B. Pitak, S. J. Coles, J. Michel, A. C. Jones, P. E. Barran, P. J. Lusby, *J. Am. Chem. Soc.* **2012**, *134*, 19334–19337.

[118] L.-A. Chen, W. Xu, B. Huang, J. Ma, L. Wang, J. Xi, K. Harms, L. Gong, E. Meggers, *J. Am. Chem. Soc.* **2013**, *135*, 10598–10601.

[119] D. L. Davies, K. Singh, S. Singh, B. Villa-Marcos, *Chem. Commun.* **2013**, *49*, 6546–6548.

[120] M. Helms, Z. Lin, L. Gong, K. Harms, E. Meggers, *Eur. J. Inorg. Chem.* **2013**, *2013*, 4164–4172.

[121] X. Huang, X. Li, X. Xie, K. Harms, R. Riedel, E. Meggers, *Nat. Commun.* **2017**, *8*, 2245.

[122] N. Hu, H. Jung, Y. Zheng, J. Lee, L. Zhang, Z. Ullah, X. Xie, K. Harms, M.-H. Baik, E. Meggers, *Angew. Chem. Int. Ed.* **2018**, *57*, 6242–6246.

[123] A. Werner, *On the constitution and configuration of compounds of a higher order*, From Nobel Lectures, Chemistry 1901–1921, Elsevier Publishing Company: Amsterdam, The Netherlands, **1966**.

[124] E. C. Constable, *Chem. Soc. Rev.* **2013**, *42*, 1637–1651.

[125] L.-J. Chen, H.-B. Yang, M. Shionoya, *Chem. Soc. Rev.* **2017**, *46*, 2555–2576.

[126] S.-Y. Yao, Y.-L. Ou, B.-H. Ye, *Inorg. Chem.* **2016**, *55*, 6018–6026.

[127] L.-P. Li, S.-Y. Yao, Y.-L. Ou, L.-Q. Wei, B.-H. Ye, *Organometallics* **2017**, *36*, 3257–3265.

[128] Y. Grell, N. Demirel, K. Harms, E. Meggers, *Organometallics* **2019**, *38*, 3852–3859.

[129] A. K. Ghosh, P. Mathivanan, J. Cappiello, *Tetrahedron: Asymmetry* **1998**, *9*, 1–45.

[130] J. S. Johnson, D. A. Evans, *Acc. Chem. Res.* **2000**, *33*, 325–335.

[131] T. P. Yoon, E. N. Jacobsen, *Science* **2003**, *299*, 1691–1693.

[132] G. Desimoni, G. Faita, K. A. Jørgensen, *Chem. Rev.* **2006**, *106*, 3561–3651.

[133] S. Dagorne, S. Bellemin-Laponnaz, A. Maisse-François, *Eur. J. Inorg. Chem.* **2007**, *2007*, 913–925.

[134] R. Rasappan, D. Laventine, O. Reiser, *Coord. Chem. Rev.* **2008**, *252*, 702–714.

[135] G. C. Hargaden, P. J. Guiry, *Chem. Rev.* **2009**, *109*, 2505–2550.

[136] G. Desimoni, G. Faita, K. A. Jørgensen, *Chem. Rev.* **2011**, *111*, PR284-PR437.

[137] L. Wang, J. Zhou, Y. Tang, *Chin. J. Chem.* **2018**, *36*, 1123–1129.

[138] S. E. Denmark, C. M. Stiff, *J. Org. Chem.* **2000**, *65*, 5875–5878.

[139] S. Luo, X. Zhang, Y. Zheng, K. Harms, L. Zhang, E. Meggers, *J. Org. Chem.* **2017**, *82*, 8995–9005.

[140] Y. Huang, L. Song, L. Gong, E. Meggers, *Chem. Asian J.* **2015**, *10*, 2738–2743.

[141] L. Song, L. Gong, E. Meggers, *Chem. Commun.* **2016**, *52*, 7699–7702.

[142] H. Lin, Z. Zhou, J. Cai, B. Han, L. Gong, E. Meggers, *J. Org. Chem.* **2017**, *82*, 6457–6467.

[143] G.-J. Sun, J. Gong, Q. Kang, *J. Org. Chem.* **2017**, *82*, 796–803.

[144] J. Gong, Q. Wan, Q. Kang, *Adv. Synth. Catal.* **2018**, *360*, 4031–4036.

[145] S.-W. Li, Q. Wan, Q. Kang, *Org. Lett.* **2018**, *20*, 1312–1315.

[146] T. Mietke, T. Cruchter, V. A. Larionov, T. Faber, K. Harms, E. Meggers, *Adv. Synth. Catal.* **2018**, *360*, 2093–2100.

[147] X. Huang, Q. Zhang, J. Lin, K. Harms, E. Meggers, *Nat. Catal.* **2019**, *2*, 34–40.

[148] S. Qurban, Y. Du, J. Gong, S.-X. Lin, Q. Kang, *Chem. Commun.* **2019**, *55*, 249–252.

[149] Q. Wan, S. Li, Q. Kang, Y. Yuan, Y. Du, *J. Org. Chem.* **2019**, *84*, 15201–15211.

[150] Q. Wan, L. Chen, S. Li, Q. Kang, Y. Yuan, Y. Du, *Org. Lett.* **2020**, *22*, 9539–9544.

[151] L.-A. Chen, X. Tang, J. Xi, W. Xu, L. Gong, E. Meggers, *Angew. Chem. Int. Ed.* **2013**, *52*, 14021–14025.

[152] L.-A. Chen, W. Xu, B. Huang, J. Ma, L. Wang, J. Xi, K. Harms, L. Gong, E. Meggers, *J. Am. Chem. Soc.* **2013**, *135*, 10598–10601.

[153] J. Ma, X. Ding, Y. Hu, Y. Huang, L. Gong, E. Meggers, *Nat. Commun.* **2014**, *5*, 4531.

[154] X. Ding, C. Tian, Y. Hu, L. Gong, E. Meggers, *Eur. J. Org. Chem.* **2016**, *2016*, 887–890.

[155] W. Xu, M. Arieno, H. Löw, K. Huang, X. Xie, T. Cruchter, Q. Ma, J. Xi, B. Huang, O. Wiest, L. Gong, E. Meggers, *J. Am. Chem. Soc.* **2016**, *138*, 8774–8780.

[156] L. Gong, L.-A. Chen, E. Meggers, *Angew. Chem. Int. Ed.* **2014**, *53*, 10868–10874.

[157] Y. Kashiwame, S. Kuwata, T. Ikariya, *Chem. Eur. J.* **2010**, *16*, 766–770.

[158] S. Kuwata, T. Ikariya, *Chem. Eur. J.* **2011**, *17*, 3542–3556.

[159] E. J. Corey, W. Zhe, *Tet. Lett.* **1993**, *34*, 4001–4004.

[160] L. Gong, S. P. Mulcahy, D. Devarajan, K. Harms, G. Frenking, E. Meggers, *Inorg. Chem.* **2010**, *49*, 7692–7699.

[161] Y. Grell, X. Xie, S. I. Ivlev, E. Meggers, *ACS Catal.* **2021**, *11*, 11396–11406.

[162] Z. Gonda, Z. Novák, *Chem. Eur. J.* **2015**, *21*, 16801–16806.

[163] H.-J. Böhm, D. Banner, S. Bendels, M. Kansy, B. Kuhn, K. Müller, U. Obst-Sander, M. Stahl, *ChemBioChem* **2004**, *5*, 637–643.

[164] J. Wang, M. Sánchez-Roselló, J. L. Aceña, C. Del Pozo, A. E. Sorochinsky, S. Fustero, V. A. Soloshonok, H. Liu, *Chem. Rev.* **2014**, *114*, 2432–2506.

[165] E. P. Gillis, K. J. Eastman, M. D. Hill, D. J. Donnelly, N. A. Meanwell, *J. Med. Chem.* **2015**, *58*, 8315–8359.

[166] M. Oestreich, *Angew. Chem. Int. Ed.* **2005**, *44*, 2324–2327.

[167] M. Ueda, T. Kano, K. Maruoka, *Org. Biomol. Chem.* **2009**, *7*, 2005–2012.

[168] A. M. R. Smith, K. K. Hii, *Chem. Rev.* **2011**, *111*, 1637–1656.

[169] J.-A. Ma, D. Cahard, *Chem. Rev.* **2008**, *108*, PR1–PR43.

[170] S. Lectard, Y. Hamashima, M. Sodeoka, *Adv. Synth. Catal.* **2010**, *352*, 2708–2732.

[171] K. Shibatomi, A. Narayama, *Asian J. Org. Chem.* **2013**, *2*, 812–823.

[172] X. Yang, T. Wu, R. J. Phipps, F. D. Toste, *Chem. Rev.* **2015**, *115*, 826–870.

[173] M. Gómez-Martínez, D. A. Alonso, I. M. Pastor, G. Guillena, A. Baeza, *Asian J. Org. Chem.* **2016**, *5*, 1428–1437.

[174] M. P. Brochu, S. P. Brown, D. W. C. MacMillan, *J. Am. Chem. Soc.* **2004**, *126*, 4108–4109.

[175] N. Halland, A. Braunton, S. Bachmann, M. Marigo, K. A. Jørgensen, *J. Am. Chem. Soc.* **2004**, *126*, 4790–4791.

[176] T. D. Beeson, D. W. C. MacMillan, *J. Am. Chem. Soc.* **2005**, *127*, 8826–8828.

[177] M. Marigo, D. Fielenbach, A. Braunton, A. Kjærsgaard, K. A. Jørgensen, *Angew. Chem. Int. Ed.* **2005**, *44*, 3703–3706.

[178] M. Marigo, S. Bachmann, N. Halland, A. Braunton, K. A. Jørgensen, *Angew. Chem. Int. Ed.* **2004**, *43*, 5507–5510.

[179] P. Kwiatkowski, T. D. Beeson, J. C. Conrad, D. W. C. MacMillan, *J. Am. Chem. Soc.* **2011**, *133*, 1738–1741.

[180] L. Hintermann, A. Togni, *Helv. Chim. Acta* **2000**, *83*, 2425–2435.

[181] L. Hintermann, A. Togni, *Angew. Chem. Int. Ed.* **2000**, *39*, 4359–4362.

[182] Y. Hamashima, K. Yagi, H. Takano, L. Tamás, M. Sodeoka, *J. Am. Chem. Soc.* **2002**, *124*, 14530–14531.

[183] K. Shibatomi, Y. Soga, A. Narayama, I. Fujisawa, S. Iwasa, *J. Am. Chem. Soc.* **2012**, *134*, 9836–9839.

[184] X. Gu, Y. Zhang, Z.-J. Xu, C.-M. Che, *Chem. Commun.* **2014**, *50*, 7870–7873.

[185] Y. Naganawa, T. Aoyama, K. Kato, H. Nishiyama, *ChemistrySelect* **2016**, *1*, 1938–1942.

[186] Y. Hamashima, T. Suzuki, H. Takano, Y. Shimura, M. Sodeoka, *J. Am. Chem. Soc.* **2005**, *127*, 10164–10165.

[187] W. Zheng, Z. Zhang, M. J. Kaplan, J. C. Antilla, *J. Am. Chem. Soc.* **2011**, *133*, 3339–3341.

[188] T. Suzuki, Y. Hamashima, M. Sodeoka, *Angew. Chem. Int. Ed.* **2007**, *46*, 5435–5439.

[189] T. Ishimaru, N. Shibata, D. S. Reddy, T. Horikawa, S. Nakamura, T. Toru, *Beilstein J. Org. Chem.* **2008**, *4*, 16.

[190] D. H. Paull, M. T. Scerba, E. Alden-Danforth, L. R. Widger, T. Lectka, *J. Am. Chem. Soc.* **2008**, *130*, 17260–17261.

[191] D. S. Reddy, N. Shibata, T. Horikawa, S. Suzuki, S. Nakamura, T. Toru, M. Shiro, *Chem. Asian J.* **2009**, *4*, 1411–1415.

[192] J. Erb, D. H. Paull, T. Dudding, L. Belding, T. Lectka, *J. Am. Chem. Soc.* **2011**, *133*, 7536–7546.

[193] G.-Q. Xu, H. Liang, J. Fang, Z.-L. Jia, J.-Q. Chen, P.-F. Xu, *Chem. Asian J.* **2016**, *11*, 3355–3358.

[194] S. Yuan, C. Liao, W.-H. Zheng, *Org. Lett.* **2021**, *23*, 4142–4146.

[195] H. Wack, A. E. Taggi, A. M. Hafez, W. J. Drury, T. Lectka, *J. Am. Chem. Soc.* **2001**, *123*, 1531–1532.

[196] S. France, H. Wack, A. E. Taggi, A. M. Hafez, T. R. Wagerle, M. H. Shah, C. L. Dusich, T. Lectka, *J. Am. Chem. Soc.* **2004**, *126*, 4245–4255.

[197] E. C. Lee, K. M. McCauley, G. C. Fu, *Angew. Chem. Int. Ed.* **2007**, *46*, 977–979.

[198] J. Douglas, K. B. Ling, C. Concellón, G. Churchill, A. M. Z. Slawin, A. D. Smith, *Eur. J. Org. Chem.* **2010**, *2010*, 5863–5869.

[199] Y. Hamashima, T. Nagi, R. Shimizu, T. Tsuchimoto, M. Sodeoka, *Eur. J. Org. Chem.* **2011**, *2011*, 3675–3678.

[200] K. Ishihara, K. Nishimura, K. Yamakawa, *Angew. Chem. Int. Ed.* **2020**, *132*, 17794–17800.

[201] S. Meninno, F. Franco, M. Benaglia, A. Lattanzi, *Adv. Synth. Catal.* **2021**, *363*, 3380–3410.

[202] D. Aubert, C. Ferrand, J.-P. Maffrand, *Thieno [3,2-c] pyridine derivatives and their therapeutic application*, U.S. Patent 4.529.596, **1985**.

[203] Y. Li, W. Bi, X. Zhang, H. Song, B. Lv, *Method of preparing clopidogrel and its sulfate*, Chinese Patent CN102250114 A, **2011**.

[204] P. Helmut, *Method of Converting Alcohol to Halide*, WO Patent 2016/202894, **2016**.

[205] L. Li, F. Han, X. Nie, Y. Hong, S. Ivlev, E. Meggers, *Angew. Chem. Int. Ed.* **2020**, *59*, 12392–12395.

[206] G. R. Fulmer, A. J. M. Miller, N. H. Sherden, H. E. Gottlieb, A. Nudelman, B. M. Stoltz, J. E. Bercaw, K. I. Goldberg, *Organometallics* **2010**, *29*, 2176–2179.

[207] H. A. Wegner, H. Reisch, K. Rauch, A. Demeter, K. A. Zachariasse, A. de Meijere, L. T. Scott, *J. Org. Chem.* **2006**, *71*, 9080–9087.

[208] X. Xie, S. P. Mulcahy, E. Meggers, *Inorg. Chem.* **2009**, *48*, 1053–1061.

[209] A. V. Stepakov, A. P. Molchanov, R. R. Kostikov, *Russ. J. Org. Chem.* **2007**, *43*, 538–543.

[210] V. A. Osyanin, E. A. Ivleva, Y. N. Klimochkin, *Synth. Commun.* **2012**, *42*, 1832–1847.

[211] M. Marinova, M. Torres-Werlé, G. Taupier, A. Maisse-François, T. Achard, A. Boeglin, K. D. H. Dorkenoo, S. Bellemin-Laponnaz, *ACS Omega* **2019**, *4*, 2676–2683.

[212] K. A. Nolin, R. W. Ahn, Y. Kobayashi, J. J. Kennedy-Smith, F. D. Toste, *Chem. Eur. J.* **2010**, *16*, 9555–9562.

[213] H.-J. Zhang, C.-Y. Shi, F. Zhong, L. Yin, *J. Am. Chem. Soc.* **2017**, *139*, 2196–2199.

[214] S. Niwayama, H. Cho, C. Lin, *Tet. Lett.* **2008**, *49*, 4434–4436.

[215] S. Knör, A. V. Khrenov, B. Laufer, E. L. Saenko, C. A. E. Hauser, H. Kessler, *J. Med. Chem.* **2007**, *50*, 4329–4339.

[216] K. Tokumasu, R. Yazaki, T. Ohshima, *J. Am. Chem. Soc.* **2016**, *138*, 2664–2669.

[217] K. Miyamoto, S. Tsuchiya, H. Ohta, *J. Fluor. Chem.* **1992**, *59*, 225–232.

[218] *X-Area Pilatus3_SV*, STOE & Cie GmbH, Darmstadt, Germany, **2016**.

[219] *X-Area LANA*, STOE & Cie GmbH, Darmstadt, Germany, **2016**.

[220] *X-Area Recipe*, STOE & Cie GmbH, Darmstadt, Germany, **2015**.

[221] G. M. Sheldrick, *Acta Cryst. A* **2015**, *71*, 3–8.

[222] G. M. Sheldrick, *Acta Cryst. C* **2015**, *71*, 3–8.

[223] *X-Area Integrate*, STOE & Cie GmbH, Darmstadt, Germany, **2016**.

[224] K. Brandenburg, *Diamond - Crystal and Molecular Structure Visualization*, Crystal Impact, H. Putz & K. Brandenburg GbR, Bonn, Germany, **2014**.

[225] C. B. Hübschle, G. M. Sheldrick, B. Dittrich, *J. Appl. Cryst.* **2011**, *44*, 1281–1284.

[226] S. Parsons, H. D. Flack, T. Wagner, *Acta Cryst. B* **2013**, *69*, 249–259.

[227] P. Van der Sluis, A. L. Spek, *Acta Cryst. A* **1990**, *46*, 194–201.

[228] A. L. Spek, *Acta Cryst. C* **2015**, *71*, 9–18.

[229] *APEX3*, Bruker AXS Inc., Madison, Wisconsin, USA, **2018**.

[230] L. Krause, R. Herbst-Irmer, G. M. Sheldrick, D. Stalke, *J. Appl. Cryst.* **2015**, *48*, 3–10.

[231] *SADABS*, Bruker AXS Inc., Madison, Wisconsin, USA, **2016**.

[232] *X-Area*, STOE & Cie GmbH, Darmstadt, Germany, **2018**.

[233] *X-RED32*, STOE & Cie GmbH, Darmstadt, Germany, **2018**.

[234] *LANA - Laue Analyzer*, STOE & Cie GmbH, Darmstadt, Germany, **2019**.

[235] A. L. Spek, *PLATON - A Multipurpose Crystallographic Tool*, Utrecht University, Utrecht, The Netherlands, **2019**.

[236] D. Kratzert, I. Krossing, *J. Appl. Cryst.* **2018**, *51*, 928–934.

Erklärung

Ich erkläre, dass eine Promotion noch an keiner anderen Hochschule als der Philipps-Universität Marburg, Fachbereich Chemie, versucht wurde.

Hiermit versichere ich, dass ich die vorliegende Dissertation

„***Design and Synthesis of Tris-Heteroleptic Bis-Cyclometalated Chiral-at-Rhodium Catalysts for Application in Asymmetric Catalysis***“

selbstständig, ohne unerlaubte Hilfe Dritter angefertigt und andere als die in der Dissertation angegebenen Hilfsmittel nicht benutzt habe. Alle Stellen, die wörtlich oder sinngemäß aus veröffentlichten oder unveröffentlichten Schriften entnommen sind, habe ich als solche kenntlich gemacht. Dritte waren an der inhaltlich-materiellen Erstellung der Dissertation nicht beteiligt; insbesondere habe ich hierfür nicht die Hilfe eines Promotionsberaters in Anspruch genommen. Kein Teil dieser Arbeit ist in einem anderen Promotions- oder Habilitationsverfahren verwendet worden. Mit dem Einsatz von Software zur Erkennung von Plagiaten bin ich einverstanden.

_____ _____

Ort/Datum Unterschrift